Flexible AC Transmission Systems Modelling in Optimal Power Flows Using Newton's Method

by

Hugo Ambriz Pérez

A Thesis submitted to the
Department of Electronics and Electrical Engineering of
The University of Glasgow
for the degree of Doctor of Philosophy

December 1998

To my parents, Marcelina Pérez and Elias Ambriz, whose love, help and encouragement have sustained me throughout my life.

Abstract

This research project is related to the modelling of the new generation of power electronics-based plant components presently emerging as a result of the recently developed concept of Flexible AC Transmission Systems (FACTS). These new power network technologies represent the application of power electronics in AC power systems to provide adaptive power flow control under both steady state and emergency conditions. These technologies may have a profound impact on the electricity supply industry world wide over the next decade.

The economical and operational benefits afforded by this form of electronic control are many, however, this is at the expense of a sharp increase in network planning and operational complexity. As the various controls present in the network interact with each other, good power system tools are required in order to carry out power system studies. In a secure operating environment, the operation of these devices would have to be well co-ordinated and advanced computational tools, such as Optimal Power Flows are required in order to aid planning and control engineers to achieve this task.

This research addresses the issue of FACTS models suitable for steady state solutions of large-scale power networks. Considerable progress has been made in Load Flow studies which include realistic FACTS device models. However, very little work has been done in tackling the more complex issue of OPF solutions where FACTS devices are included. Nevertheless, it is this application tool that needs to be well developed if the value of the FACTS technology is to be demonstrated from the power system economics and security viewpoints.

The aim of this research work is to develop FACTS device models suitable for large-scale Optimal Power Flow studies. The models represent the various steady state operating control features of the FACTS devices using generalised nodal admittances. Models are developed for the following FACTS devices: Phase-Shifting Transformer, Load Tap-Changing Transformer, Static Var Compensator, Thyristor Controlled Series Capacitor, Interphase Power Controller, Unified Power Flow Controller and High Voltage DC link. The FACTS models are integrated into an efficient Newton Optimal Power Flow program.

The robustness of the convergence of the various steady-state FACTS device models has been thoroughly investigated. The newly developed FACTS OPF* computer program has been used to study several electrical power networks, some of the them corresponding to test networks available in the open literature, and a number of other real-life electric networks where hundreds of variables are to be optimised.

* A computer program user's manual was written. It includes documented listings and flow diagrams.

Acknowledgements

I wish to convey my deep sense of gratitude to my supervisor Dr. Enrique Acha for his technical support, encouragement, valuable suggestions and sincere friendship during the past three years of this research.

I would like to thank all my postgraduate colleagues. Thanks to Claudio Fuerte-Esquivel who made valuable suggestions and gave me insight into many theoretical aspects associated with my research. I wish also to extend my gratitude to John Parle for his many suggestions in the preparation of the thesis.

Thanks to Armando de la Torre and Marcelino Madrigal for helping me to increase my understanding in important aspects of this research. I also wish to express my gratitude to my mentors and colleagues in Comisión Federal de Electricidad (CFE), México.

I gratefully acknowledge the financial assistance given to me by the Consejo Nacional de Ciencia y Tecnología (CONACYT), México, during my doctoral studies. I also wish to express my appreciation to Comisión Federal de Electricidad (CFE), México, for granting me study leave to carry out PhD studies at the University of Glasgow.

I would like to thank my sisters and brothers for their love, encouragement and unconditional support through my academic career.

Finally, my heartiest thanks go to Aida and Carolina for their sacrifices and patience during the past three years of my research.

Contents

List of Figures

List of Tables

Abbreviations

FACTS	Flexible AC Transmission Systems.
AC	Alternating Current.
TCSC	Thyristor Controller Series Capacitor.
PS	Phase Shifter.
PST	Phase-Shifting Transformer.
IPC	Interphase Power Controller.
SVC	Static Var Compensator.
LTC	Load Tap Changer.
UPFC	Unified Power Flow Controller.
HVDC	High Voltage Direct Current.
OPF	Optimal Power Flow.
MW	MegaWatts.
MVAR	Mega Volt Ampere Reactives.
pu	per unit.

$\boldsymbol{V_p, I_p, Z_p}$	Voltage, current and impedance in bold type represent complex quatities.

The word processor used for the typesetting of this thesis was Microsoft Word 97, and the drawing program used for graphs was Axum TriMetrix, Inc.

Chapter 1

Introduction

1.1 Why Flexible Alternating Current Transmission Systems ?

The lack of fast load flow control in electric power systems is one of the crucial factors that has affected the way power systems have evolved. Traditionally AC power systems have been controlled with electro-mechanical devices, with their slow response times. The ensuing slow speed control has rendered the AC transmission systems to be inflexible and over-designed. In meshed AC power systems, the power flows are largely distributed as a function of the transmission line impedance: a transmission line with a low impedance will take larger power flows across it than a transmission line with high impedance. This is a problem beyond the control of operation engineers or one which can only be contained with great difficulty. Examples of operating problems which the unregulated flow of active and reactive power give rise to are: loss of stability, loop flows, voltage limit violations, thermal limit violations and high short circuit levels [1-3]. In the long-term these problems could in principle be solved by building new power plants and transmission facilities, but during actual operation, load shedding becomes a last resort option.

The electricity supply industry world-wide is facing a great many challenges in its program of expansion; a variety of economic and environmental pressures are some of the difficulties which prevent licensing and building new transmission lines and electric power plants. Additionally, the use of transmission facilities by bulk supply users and deregulation of the electricity supply industry, requires maintaining acceptable levels of network reliability and stability. As a result of these circumstances, high performance control of the power system is becoming imperative. As explained above, the electro-mechanical devices with their slow responses may no longer be the preferred option. The industry is currently looking at ways of maximising power flows while enhancing network security by employing power electronics-based controllers in the high-voltage side of the power network.

Flexible Alternating Current Transmission Systems (FACTS) is a title used to encompass all the newly emerging devices [4-24]. FACTS can be defined as AC transmission systems incorporating power electronics-based equipment into the high voltage side of the network so as to make it electronically controllable. 'High Power Electronics and Flexible AC Transmission System' was the topic of a speech delivered by N.G. Hingorani on 19 April, 1988 at the American Power Conference's 50th Annual Meeting in Chicago [8]

There is widespread agreement that power electronics-based equipment is potential substitutes for conventional electro-mechanical solutions. Although they are, in general

more expensive, they offer a number of unique functions which cannot be achieved with conventional equipment. FACTS controllers make use of the latest high-current, high-power electronics technology to ensure effective power flow and voltage control. Of course, advanced control techniques and software will be needed to plan and operate FACTS-upgraded networks.

FACTS devices have the ability to control, in an adaptive fashion, key network parameters that have a direct bearing on the operation of the power system. They are designed to control one or more of the following power system parameters: voltage magnitude, line impedance, phase angle, active power flow and reactive power flow. The ability to control the line impedance and the nodal voltage magnitudes and angles at both the sending and receiving ends of key transmission lines with almost no delay will increase significantly the transmission capabilities. For instance, series FACTS controllers may be used to increase the power transfer capability of transmission networks and to provide direct control of power flows over designated transmission routes.

1.2 Inherent Limitations of Transmission Systems

The characteristics of a system will change over time as the load grows and new generation is added. If the transmission facilities are not upgraded sufficiently the power system may become susceptible to both steady-state and transient stability problems as stability limits are approached.

The ability of the transmission system to transmit power becomes impaired by one or more of the following steady-state limitations [1,2]:

- Angular stability limits.
- Voltage magnitude limits.
- Thermal limits.

and the following dynamic limitations:

- Transient stability.
- Dynamic stability.

These parameters define the maximum electric power that can be transmitted without causing damage to transmission lines and electric equipment. In principle, limitations on power transfer can always be relieved by the addition of new transmission and generation facilities. Alternatively, FACTS devices should allow the same objectives to be met with a minimum of system changes. The potential benefits brought about by FACTS devices include a reduction of operation and transmission investment costs, increased system security and reliability, and an increase of power transfer capabilities [1,2].

1.3 FACTS Controllers

Power flow control has traditionally relied on generator control, transmission line and reactive compensation switching, and voltage regulation via tap-changing and phase-shifting transformers. Phase-shifting transformers have been used for the purpose of regulating active power in AC transmission networks [4-9]. Some of them are permanently operated with fixed angles, but in most cases they are fitted with variable tapping facilities. Another kind of controller is the series reactor which is used to reduce

power flow and short circuit levels in a given line or node of the network. Series capacitors, on the other hand, are used to shorten the electrical distance of the line, hence, increasing power flow [13-17]. Series compensators may be installed in several locations of the power network, and are switched on and off according to both load and voltage conditions. For instance, in longitudinal power systems, which are identified by a low degree of interconnection and long transmission lines between major generation and load centres, series capacitive compensators are bypassed during minimum loading in order to avoid transmission line overvoltages due to excessive capacitive effects in the system. Conversely, during maximum loading, series capacitive compensators are fully utilised in order to increase the transfer of power from generating sites to load centres, without subjecting transmission lines to overloads.

Until recently these solutions served the requirements of the electricity supply industry well. However, deregulation of the industry and difficulties in securing new rights-of-way have created the need for newer and more advanced technological developments based on high-voltage, high-current solid state devices. In partnership with manufacturers and research organisations, the Supply Industry has embarked on an ambitious program to develop a new generation of power electronic-based plant components. The impact of these developments is beginning to be felt in all three areas of the business: generation, transmission and distribution.

High-Voltage Direct Current power converters, Thyristor Controlled Reactors and Shunt-connected Thyristor Switched Capacitors have been in existence for many years although their operational characteristics resemble those of FACTS devices [1,2,61-64]. Power electronics-based versions of phase-shifting and tap-changing transformers were embraced at an early stage by the proponents of FACTS technology [4-9]. These devices together with the electronically controlled series compensator, can be considered to belong to the first generation of FACTS devices. The Unified Power Flow Controller, Static Compensator and Interphase Power Controller are more recent developments [10-13,18-24]. Their control capabilities and intended function are much more sophisticated than those of the first wave of FACTS devices. They are said to belong to a second generation of FACTS devices.

Most of the FACTS devices perform useful roles during both steady-state and transient conditions, however, there are FACTS devices which are specifically designed to operate only under transient power system conditions, e.g. Hingorani's SSR Damper [3]. The applications of FACTS controllers to the solution of the steady-state operating problems are presented in Table 1.1 [2], and a brief description of their operation, as given by IEEE [1,2], is reproduced below for completeness:

Thyristor Controlled Reactor (TCR). This is a shunt-connected, thyristor controlled reactor whose effective reactance is varied in a continuous manner by partial conduction control of the thyristor valve.

Load Tap-Changing Transformer (LTCT). This controller can be considered a FACTS device if tap changes are controlled by thyristors. The LTCT provides a rapidly varying output voltage.

Thyristor Controlled Phase-Shifting Transformer (TCPST). This controller is a phase-shifting transformer adjusted by thyristor switches to provide a rapidly varying phase angle.

Thyristor Controlled Series Capacitor (TCSC). This FACTS controller is a capacitive reactance compensator which consists of series capacitor banks shunted by a

thyristor controlled reactor in order to provide a smoothly variable series capacitive compensation.

Table 1.1. FACTS controller applications to overcome operating problems [2].

Issue	Operating Problem	Corrective Action	FACTS device
Voltage Limits	Low voltage at heavy load	Supply reactive power	TCSC, STATCOM
	High voltage at high load	Remove reactive power supply	TCSC,TCR
		Absorb reactive power	TCR, STATCOM
	High voltage following outage	Absorb reactive power	TCR
	Low voltage following outage	Supply reactive power	STATCOM, TCSC
		Prevent overload	IPC, TCSC
	Load voltage and overload	Supply reactive power and limit overload	IPC, TCSC, UPFC STATCOM
Thermal Limits	Line/transformer overload	Reduce overload	TCSC, UPFC
			TCR, IPC
	Tripping of parallel circuit	Limit circuit loading	IPC, UPFC, TCR
Loop flows	Parallel line load sharing	Adjust series reactance	IPC, UPFC, TCSC
	Post-fault sharing	Rearrange network or use thermal limit actions	IPC, TCSC, UPFC TCR
	Flow direction reversal	Adjust phase angle	IPC, UPFC

Interphase Power Controller (IPC). This controller is a series connected power controller consisting of inductive and capacitive branches subjected to separate phase shifted voltage magnitudes. The active power transfer is set by adjusting the phase shifters and/or the impedances. The reactive power can be controlled independently from the active power.

Static Synchronous Compensator (STATCOM). This controller is a static synchronous condenser operated without an external electric energy source as a shunt-connected static var compensator whose capacitive or inductive output current can be controlled independently of the AC system voltage magnitude. The output current is adjusted to control a specific parameter of the electrical power system. The node voltage magnitude is usually controlled but reactive power injection may also be used.

Unified Power Flow Controller (UPFC). The UPFC is a combination of a Static Synchronous Compensator and a Static Synchronous Series Compensator which are coupled via a common dc link, to allow bi-directional flow of real power between the series output terminals of the SSSC and shunt output terminals of the STATCOM. The UPFC, by means of an angularly unconstrained, series voltage injection, is able to control, concurrently or selectively, the transmission line impedance, nodal voltage magnitude and the real and reactive power flow in the line. The UPFC may also provide independently controllable shunt reactive compensation.

Power electronics and control technologies have been applied to electric power systems for many years. The first devices were High Voltage DC Transmission (HVDC) converters and Static Var Compensators (SVC), which are already well established [1,2,61-64]:

High Voltage DC Transmission (HVDC) Converter. It is a controller whose objectives are: a) to transmit large block of electrical energy with minimum losses; b) to

control all DC parameters with sufficient accuracy and speed of response; c) to ensure stable converter operation in the presence of small system disturbances; d) to connect systems with different operational frequency.

Static Var Compensator (SVC). This is a shunt-connected static var generator/absorber whose output is adjusted to exchange capacitive or inductive current so as to maintain or control specific parameters of the electrical power system.

1.4 Background of Optimal Power Flow

Electric power systems have experienced continuous growth in all three sectors of the industry, namely generation, transmission and distribution. In the past, transmission systems contained only a low degree of interconnection, hence, it was not complicated to share the load among several generating units. The increase in both the load size and complexity of the power networks, brought about by the widespread interconnection of transmission systems, some of them encompassing continental distances, introduced major difficulties into the operation of electrical power networks. It became necessary for many electrical utilities to operate their systems closer to the system operating capacity. It became impractical to diagnose the existing network conditions and to determine appropriate operating strategies based on observation and experience of the operator. The operating philosophy had to be revised and new concepts based on economic considerations were adopted. The possibility of using computational resources as a basic tool in the operation of the system was deemed not just desirable but essential. This is the background from where Optimal Power Flows arose in power systems [25-52].

Optimal Power flows can be understood if one thinks in terms of conventional power flows, where the objective is to determine the steady-state operating conditions of the network [53-56,58-60]. Voltage magnitudes and angles at all nodes of the network corresponding to specified levels of load and generation are determined first. Power flows throughout the network are calculated afterwards. It is most likely that this solution, while feasible will not yield the most economic generating schedule or an operating point where minimum losses are incurred [25,47]. The optimal power flow solution, on the other hand, includes an objective function which is optimised without violating the system operating constraints. These include the network equations, loading conditions and physical limits on the active and reactive power generation [26,27]. The choice of the objective function depends on the operating philosophy of each power system. The most common objective function is the active power generation cost. The Economic Dispatch is a particular case of the Optimal Power Flow problem.

1.5 Why Newton's Method ?

The optimal operation of the power network gives rise to a non-linear set of equations which are normally solved by iteration. The method used in this research is Newton's method. It should be noted that if simplifying assumptions are made in the operation of the power system then linear programming techniques can be used instead. The latter have been used extensively for solving conventional Optimal Power Flow problems. They are highly developed, leading to fast and reliable solutions. However, FACTS devices are highly non-linear and their inclusion in linear programming-based algorithms becomes difficult without sacrificing model fidelity. Hence, Newton's method has been adopted in this research as the vehicle for solving the FACTS Optimal Power Flow problem. So far, the result obtained using this method have been very encouraging [37,38,48,50].

The main benefits of having active powers optimally scheduled are related to economic factors [27]. However, additional advantages could be:

- To establish limits for complying with stability considerations and with thermal ratings of transmission lines [2].
- To model accurately the active power losses as given by the power balance equations. Reactive power mismatches are also readily available [28,29].

On the other hand, the distribution of generated reactive power is directly related to the quality of service which the power company can deliver. The following items can be potential benefits:

- Good voltage magnitude profile.
- Stability enhancement by avoiding low voltage levels in the transmission system [2].
- Decreased active power generation costs by minimising active power transmission losses [28,29].

The economic aspect is a matter of paramount importance to electricity companies. The price of fuel and its strategic importance motivates them to operate electric plants with maximum efficiency. By doing so, the cost per kilowatt-hour to customers can be reduced. Even small reductions in the amount of fuel and transmission losses represent large amounts of money to be saved if one considers that network operation takes place over a long time horizon.

1.6 Motivation Behind this Research

In order to determine the usefulness of this new generation of power system devices on a network-wide basis, it will become necessary to upgrade most of the analysis tools which power engineers rely upon to plan and to operate their systems. Before meaningful results can be obtained from application studies, realistic models for the transmission systems and relevant FACTS controllers need to be created, verified and implemented in existing or newly developed power system software. Some of the tools which require immediate attention are:

For steady-state studies:

- Load Flows.
- Optimal Power Flows.
- State Estimation.
- Harmonic Analysis.

And for transient studies:

- Transient Stability.
- Small Signal Stability.
- Electro-Magnetic Transients.

This research is concerned with FACTS models suitable for steady state solutions of large scale power networks. Considerable progress has been made in this field and an extensive program of research which addresses realistic FACTS device models suitable for conventional load flows studies has just been completed [24]. However, very little work has been done world-wide in tackling the very pressing issue of OPF solutions

where FACTS devices are included. So far, only one reference can be found in open literature where the series compensator and the phase-shifting transformer have been modelled. Linear programming techniques were used in that work and the authors have reported extreme complexity in carrying out their task, particularly in the case of the phase-shifting transformer. The reason is that the phase-shifting transformer is a non-linear device that cannot be accommodated easily within the frame [57] of reference offered by linear programming. In contrast, no such difficulties are experienced when incorporating these or other more complex devices in Newton's method. For instance, the UPFC is a far more sophisticated device than the phase-shifting transformer. The realisation and computer implementation of the UPFC model is much more challenging than the phase-shifting transformer.

1.7 Purposes and Objectives of the Present Work

The objectives of the research carried out in this thesis were as follows:

- To develop a robust and efficient algorithm for the solution of Optimal Power Flows capable of solving large-scale electrical power networks. Newton's method was used as the main numerical algorithm and the equal incremental cost criterion is used to provide starting conditions to the OPF solution, which eliminates the need for using a load flow solution.
- To develop FACTS device models suitable for large-scale power system studies. The models must represent the various steady state operating control features of the device. For example, the Unified Power Flow Controller must be able to maintain active and reactive power flows at the target values chosen by either the OPF algorithm or the user. The models to be developed are:
  - Phase-Shifting Transformer.
  - Load Tap-Changing Transformer.
  - Static Var Compensator.
  - Thyristor Controlled Series Compensator.
  - Interphase Power Controller .
  - Unified Power Flow Controller.
  - High Voltage DC link.
- To integrate the various FACTS models into a Newton Optimal Power Flow program. The program must maintain efficiency without compromising the strong convergence characteristics of Newton's method.
- To compare answers provided by the Optimal Power Flow program with those of a leading software vendor by solving a wide range of networks. The PSS/OPF module of the Power Technologies Inc. (PTI) package is used for this purpose. This software is highly reliable and used throughout the world, however, it should be mentioned that the package does not have FACTS device modelling capabilities.
- To compare the results given by the Optimal Power Flow program and a 'conventional' FACTS load flow program [24]. The latter is supplied with scheduled generating powers and generating voltages as given by the OPF solution
- To investigate the robustness of the convergence by using the newly developed digital program to solve several types of electrical networks corresponding to test

networks available in the open literature, and real life electric networks with hundreds of variables to be optimised.

1.8 Publications

The following publications were generated during the course of the present research:

1.8.1 Transaction-graded Papers

- Ambriz-Pérez H., Acha E., Fuerte-Esquivel C.R. and De la Torre A.: 'Incorporation of a UPFC model in an Optimal Power Flow using Newton's Method', IEE Proceedings on Generation, Transmission and Distribution. Vol. 145, No. 3, May 1998, pp. 336-344.
- Ambriz-Pérez H., Acha E. and Fuerte-Esquivel C.R.: 'Advanced SVC Models for Newton-Raphson Load Flow and Newton Optimal Power Flow Studies', Accepted for publication in IEEE Transactions on Power Systems, 1998.
- Fuerte-Esquivel C.R., Acha E. and Ambriz-Pérez H.: 'A Comprehensive Newton-Raphson UPFC for the Quadratic Power Flow Solution of Practical Power Networks', Accepted for publication in IEEE Transactions on Power Systems, 1998.
- Acha E., Ambriz-Pérez H. and Fuerte-Esquivel C.R.: 'Advanced Transformer Control Modelling in an Optimal Power Flow Using Newton's Method', Accepted for publication in IEEE Transactions on Power Delivery, 1998.
- Ambriz-Pérez H., Acha E. and Fuerte-Esquivel C.R.: 'TCSC-Firing Angle Model for Optimal Power Flow Solutions Using Newton's Method', Submitted to IEEE Transactions on Power Delivery, 1998.
- Fuerte-Esquivel C.R., Acha E. and Ambriz-Pérez H.: 'A Thyristor Controlled Series Compensator Model for the Power Flow Solution of Practical Power Networks', Accepted for publication in IEEE Transactions on Power Systems, 1998.

1.8.2 Conference Papers

- Acha E., Ambriz-Pérez H., Tan S.G. and Fuerte-Esquivel C.R.: 'A New Generation of Power System Software Based on the OOP Paradigm', Proceedings of the International Power Engineering Conference 1997 (IPEC 97), Singapore 22-24 May 1997, pp. 68-73.
- Acha E., Ambriz-Pérez H., Fuerte-Esquivel C.R. and Chua C.S.: 'On the Auditing of Individual Generator Contributions to Optimal Power Flows, Losses and Costs in Large, Interconnected Power Networks', Proceedings of the International Power Engineering Conference 1997 (IPEC 97), Singapore 22-24 May 1997, pp. 513-518.
- Acha E. and Ambriz-Pérez H.: 'FACTS Devices Modelling in Optimal Power Flows Using Newton's Method', Accepted for presentation at the 13th Power System Computation Conference (PSCC), Norway June 28-July 2nd, 1999.

1.9 Contributions

The main contributions of the research work are summarised below:

- A complete methodology for developing efficient and reliable Optimal Power Flow programs using Newton's method has been presented. A digital computer program has been written in C++, which is able to solve large-scale power networks.

- Efficient handling of inequality constraints has been implemented. The Multipliers method is used to handle all the state variables of FACTS devices, leading to highly efficient Optimal Power Flow solutions of constrained power networks. The method does not require structural changes in the linearised system of equations during the iterative solution of the Newton Optimal Power Flow. On the other hand, the inequality constraints on functions of variables, such as controllable sources of reactive power, are handled efficiently by using quadratic penalty functions.

- A general framework of reference for unified iterative solutions is presented. The power flow equations for modelling the FACTS devices are incorporated directly into the set of linearised system equations to be solved in the Optimal Power Flow.

- A complete three-winding transformer model with tap ratios in all three windings has been developed. The two-winding transformer model and the classic phase-shifting and load tap-changing transformer models have shown to be particular cases of the complete three-winding transformer model. The models were developed to be very flexible by having a complex tap changer in each winding. In addition, it is possible to represent primary, secondary and tertiary complex impedances. The model proved to be very robust indeed.

- New, efficient Static Var Compensator models are proposed and incorporated into the Newton Optimal Power Flow. Both SVC models are considered as variable susceptances which use only one node to represent SVCs operating inside and outside limits. This contrasts with current IEEE and CIGRÉ recommended models, which require of two or three nodes. Computational disadvantages are given in Section 4.3.

- A Thyristor Controlled Series Compensator firing angle model is a new model which introduces the thyristor's firing angle as a control variable. The optimal compensation level is achieved by regulating the firing angle. The model is able to manage either constrained or unconstrained active power flow across the compensated branch. The model compares favourably with the TCSC Controllable Reactance model whose controllable reactance is the device's control variable.

- An IPC load flow model based on the Phase-Shifting Transformer and TCSC Controllable Reactance models has been implemented. The IPC technology may be used to increase steady-state Phase-Shifting Transformer capabilities.

- A comprehensive and robust steady-state model for the Unified Power Flow Controller is developed for Optimal Power Flow studies. The model is very flexible and allows the control of active and reactive powers and voltage magnitude simultaneously, or any other control combination.

- Implementation of a High Voltage Direct Current link model.

- The newly developed FACTS device models add a great deal to software flexibility and are amenable to more realistic electric energy studies.

1.10 Outline of the Thesis

The thesis is organised as follows:

- Chapter 2 deals with the general formulation for the Optimal Power Flow problem based on Newton's method. The Chapter also includes a detailed mathematical model for 'conventional' power system elements, such as transmission lines, shunt

elements and generating units. Handling of inequality constraints is also described in detail. Several test cases are carried out with the newly developed OPF.

- Chapter 3 presents the new three-winding transformer model, which is a general case of an the existing two-winding transformer model. The classic phase-shifting and load tap-changing transformer models are particular instances of the two-winding transformer model. These models are implemented in an Optimal Power Flow by extending the system of equations used in solving the basic OPF problem. The robustness of the method is illustrated by numerical examples.

- Chapter 4 addresses two advanced Static VAR Compensator load flow models which are based on the variable shunt susceptance concept. The first one is named the Static VAR Compensator firing angle model and the second one the Static VAR Compensator Controllable susceptance model. By using numerical examples, both models have shown their robustness towards the convergence.

- Chapter 5 proposes two models suitable for the Thyristor Controlled Series Compensator. The state variables are taken to be the firing angle and the susceptance, respectively. The robustness of both model is fully discussed.

- Chapter 6 presents a load flow model for the Interphase Power Controller. The implemented model uses the Phase-Shifting Transformer and Thyristor Controlled Series Compensator models. The model is very flexible and allows the control of active power very efficiently, under different operating conditions. Case studies are presented to show the effectiveness of the algorithm.

- Chapter 7 presents a Unified Power Flow Controller model within the context of the Optimal Power Flow. The model is validated against a simpler model, which makes use of load flow concepts [23]. A limitation of the latter model is that all the control facilities of the UPFC need to be active at the same time.

- Chapter 8 describes a methodology for implementing a HVDC transmission link in an existing Optimal Power Flow. The converter equations are incorporated directly into the system of equations used to solve the Optimal Power Flow. The behaviour of HVDC links is illustrated by numerical examples. A 2172-node network is used to show the prowess of the Optimal Power Flow when several FACTS devices of various kinds are embedded in a large-scale real power network.

- Chapter 9 presents the conclusions and discusses areas that require further investigation and research effort.

1.11 References

[1] IEEE/CIGRE: 'FACTS Overview', Special Issue, 95TP108, IEEE Service Center, Piscataway, N.J., 1995.

[2] IEEE Power Engineering Society: 'FACTS Applications', Special Issue 96TP116-0, IEEE Service Center, Piscataway, N.J., 1996.

[3] Hingorani N.G.: 'Flexible AC Transmission Systems', IEEE Spectrum, April 1993, pp. 40-45.

[4] Han Z.X.: 'Phase Shifter and Power Flow Control', IEEE Transactions on Power Apparatus and Systems, Vol. PAS-101, No. 10, October 1982, pp. 3790-3795.

[5] Mihalic R. and Zunko P.: 'Phase-Shifting transformer with fixed phase between terminal voltage and voltage boost: tool for transient stability margin enhancement', IEE Proceedings Generation, Transmission and Distribution, Vol. 142, No. 3, May 1995, pp. 257-262.

[6] Ooi B.T., Dai S.Z. and Galiana F.D.: 'A Solid-State PWM Phase-Shifter', IEEE Transactions on Power Delivery, Vol. 8, No. 2, April 1993, pp. 573-579.

[7] Iravani M.R., Dandeno P.L., Nguyen K.H. and Maratukulam D.: 'Applications of Static Phase Shifters in Power Systems', IEEE Transactions on Power Delivery, Vol. 9, No. 3, July 1994, pp. 1600-1608.

[8] Hingorani N.G.: 'High Power Electronics and Flexible AC Transmission System', IEEE Power Engineering Review, July 1988, pp. 3-4.

[9] Kappenman J.: 'Static Phase Shifter Applications and Concepts for the Minnesota-Ontario Interconnection', Flexible AC Transmission Systems (FACTS) Conference, EPRI, Boston Massachusetts, 18-20 May, 1992.

[10] Gyugyi L.: 'Power Electronics in Electric Utilities: Static Var Compensators', Proceedings of the IEEE, Vol. 76, No. 4, April 1988, pp. 483-494.

[11] Tenório A.R.M., Jenkins N. and Bollen M.H.J.: 'A TCSC Model for Electromagnetic Transient Studies', IEEE/KTH Stockholm Power Tech Conference, Stockholm, Sweden, June 18-22, 1995, pp. 130-135.

[12] Enrinmez I.A., Ed.: 'Static Var Compensators', Working Group 38-01, Task Force No.2 on SVC, CIGRÉ, 1986.

[13] Brochu J., Pelletier P., Beauregard F. and Morin G.: 'The Interphase Power Controller a New Concept for Managing Power Flow within AC Networks', IEEE Transactions on Power Delivery, Vol. 9, No. 2, April 1994, pp. 883-841.

[14] Larsen E.V., Clark K., Miske S.S. and Urbanek J.: 'Characteristics and Rating Considerations of Thyristor Controlled Series Compensation', IEEE Transactions on Power Delivery, Vol. 9, No. 2, April 1994, pp. 992-1000.

[15] Larsen E., Bowler C., Damsky B. and Nilsson S.: 'Benefits of Thyristor Controlled Series Compensation', International Conference on Large High Voltage Electric Systems (CIGRÉ), paper 14/37/38-04, Paris, September 1992.

[16] Christl N., Hedin R., Sadek K., Lützelberger P., Krause P.E., McKenna S.M., Montoya A.H. and Togerson D.: 'Advanced Series Compensation (ASC) with Thyristor Controlled Impedance', International Conference on Large High Voltage Electric Systems (CIGRÉ), paper 14/37/38-05, Paris, September 1992.

[17] Helbing S.G. and Karady G.G.: 'Investigations of an Advanced Form of Series Compensation', IEEE Transactions on Power Delivery, Vol. 9, No. 2, April 1994, pp. 939-947.

[18] Noroozian M, Ängquist L., Ghandhari M. and Anderson G.; 'Use of UPFC for Optimal Power Flow Control', IEEE/KTH Stockholm Power Tech Conference, Stockholm, Sweden, June 1995, pp. 506-511.

[19] Gyugyi L., Schauder C.D., Williams S.L., Rietman T.R., Torgerson D.R. and Edris A.: 'The Unified Power Flow Controller: A new Approach to Power Tranmission Control', IEEE Transactions on Power Delivery, Vol. 10, No. 2, April 1995, pp. 1085-1097.

[20] Mihalic R., Zunko P. and Povh D.: 'Improvement of Transient Stability Using Unified Power Flow Controller', IEEE Transactions on Power Delivery, Vol. 11, No. 1, Janauary 1996, pp. 485-490.

[21] Gyugyi L.: 'A Unified Power Flow Control Concept for Flexible AC Transmission Systems', IEE Proceedings-C, Vol. 139, No. 4, July 1992, pp. 323-331.

[22] Schauder C.D., Gyugyi L., Lund M.R.., Hamai D.M., Rietman T.R., Torgerson D.R. and Edris A.: 'Operation of the Unified Power Flow Controller (UPFC) Under Practical Constraints', PE-511-PWRD-0-11-1996, To be published in IEEE Transactions on Power Delivery, 1996.

[23] Nabavi-Niaki A. and Iravani M.R.: 'Steady-State and Dynamic Models of Unified Power Flow Controller (UPFC) for Power System Studies', presented at 1996 IEEE/PES Winter Meeting, 96 WM 257-6 PWRS, Baltimore, MD, January 1996.

[24] Fuerte-Esquivel C.R.: 'Steady State Modelling and Analysis of Flexible AC Transmission Systems' , PhD Thesis, University of Glasgow, August 1997.

[25] Happ H.H.: 'Optimal Power dispatch -A Comprehensive Surrey', IEEE Transactions on Power Apparatus and Systems, Vol. PAS-96, No. 3, May/June 1977, pp. 841-854.

[26] Sasson A.M.: 'Combined use of the Powell and Fletcher-Powell Non-linear Programming Methods for Optimal Load Flows', IEEE Transactions on Power Apparatus and Systems, Vol. PAS-88, No. 10, October1969, pp. 1530-1537.

[27] Sun D.I., Ashley B., Brewer B., Hughes A. and Tinney W.F.: 'Optimal Power Flow By Newton Approach', IEEE Transactions on Power Apparatus and Systems, Vol. PAS-103, No. 10, October 1984, pp. 2864-2880.

[28] Wollenberg B., Wood A. J., 'Power Generation, Operation and Control', John Wiley & Sons Inc., Second Edition, 1984.

[29] Franchi L., Innorta M., Marannino P. and Sabelli C.: 'Evaluation of Economy and/or Security Functions for Reactive Power Scheduling in Large Scale Power Systems', IEEE Transactions on Power Apparatus and Systems, Vol. PAS-102, No. 10, October 1983, pp. 3481-3488.

[30] Wu Q.H. and Ma J.Y.: 'Power system optimal reactive power dispatch using evolutionary programming', IEEE Transactions on Power Apparatus and Systems, Vol. 10, No. 3, August 1995, pp. 1243-1249.

[31] Sasson A.M., Viloria F. and Aboytes F.: 'Optimal Load Flow Solution Using the Hessian Matrix', IEEE Transactions on Power Apparatus and Systems, Vol. PAS-92, No. 1, January/February 1973, pp. 31-41.

[32] Divi R. and Kesavan J.A.: 'A Shifted Penalty Function Approach for Optimal Load-Flow', IEEE Transactions on Power Apparatus and Systems, Vol. PAS-101, No. 9, September 1982, pp. 3502-3512.

[33] Gamal A.M. and Findlay J.A.: 'A Newton Optimal Power Flow Program for Ontario Hydro EMS', IEEE Transactions on Power Systems, Vol. PWRS-2, No. 3, August 1987, pp. 536-584.

[34] Sasson A.M. and Merrill H.M.: 'Some Applications of Optimization Techniques to Power System Problems', Proceedings of the IEEE, Vol. 62, No. 7, July 1974, pp. 959-972.

[35] Hong Y.Y.: 'Enhanced Newton Optimal Power Flow Approach Experiences in Taiwan Power System', IEE Proceedings-C, Vol. 139, No. 3, May 1992, pp. 205-210.

[36] Dommel H.W. and Tinney W.F.: 'Optimal Power Flow Solutions', IEEE Transactions on Power Apparatus and Systems, Vol. PAS-87, No. 10, October 1968, pp. 1866-1876.

[37] Monticelli A. and Liu W.-H.E.: 'Adaptive Movement Penalty Method for the Newton Optimal Power Flow', IEEE Transactions on Power Systems, Vol. 7, No. 1, February 1992, pp. 334-342.

[38] Sun D.I., Hu T.-I., Lin G.-S., Lin C.-J. and Chen C.-M.: 'Experiences with Implementing Optimal Power Flow for Reactive Scheduling in the in Taiwan Power System', IEEE Transactions on Power Systems, Vol. 3, No. 3, August 1988, pp. 1193-1200.

[39] Burchett R.C., Happ H.H. and Wirgau K.A.: 'Large Scale Optimal Power Flow', IEEE Transactions on Power Apparatus and Systems, Vol. PAS-101, No. 10, October 1982, pp. 3722-3732.

[40] El-Abiad A.H. and Jaimes F.J.: 'A Method for optimum Scheduling of Power and Voltage Magnitude, IEEE Transactions on Power Apparatus and Systems, Vol. PAS-88, No. 4, April 1969, pp. 413-422.

[41] Sasson A.M.: 'Nonlinear Programming Solutions for Load-Flow, Minimum-Loss, and Economic Dispatching Problems', IEEE Transactions on Power Apparatus and Systems, Vol. PAS-88, No. 4, April 1969, pp. 399-409.

[42] Qiu J. and Shahidehpour S.M.: 'A new Approach for Minimizing Power Losses and Improving Voltage Profile', IEEE Transactions on Power Systems, Vol. PWRS-2, No. 2, May 1987, pp. 287-297.

[43] Alsac O., Bright J., Prais M. and Stott B.: 'Further Developments in LP-Based Optimal Power Flow', IEEE Transactions on Power Systems, Vol. 5, No. 3, August 1990, pp. 697-711.

[44] Gribik P.R., Shirmohammadi D., Hao S. and Tomas C. L.: 'Optimal Power Flow Sensitivity Analysis', IEEE Transactions on Power Systems, Vol. PWRS-5, No. 3, August 1990, pp. 969-976.

[45] Burchett R.C., Happ H.H. and Vierath D.R.: 'Quadratically Convergent Optimal Power Flow', IEEE Transactions on Power Apparatus and Systems, Vol. PAS-103, No. 11, November 1984, pp. 3267-3275.

[46] Tinney W.F., Bright J.M., Demaree K.D. and Hughes B.A.: 'Some Deficiencies in Optimal Power Flow', IEEE Transactions on Power Systems, Vol. PWRS-3, No. 2, May 1988, pp. 696-683.

[47] El-Hawary M.E. and Tsang D.H.: 'The Hydro-Thermal Optimal Power Flow, A Practical Formulation and Solution Technique using Newton's Approach', IEEE Transactions on Power Systems, Vol. PWRS-1, No. 3, August 1986, pp. 157-167.

[48] Santos Jr. A., Dackmann D. and Soares S.: 'A Dual Augmented Lagrangian Approach for Optimal Power Flows', IEEE Transactions on Power Systems, Vol. 3, No. 3, August 1988, pp. 1020-1025.

[49] Huneault M.. and Galiana F.D.: 'A Survey of the Optimal Power Flow Literature', IEEE Transactions on Power Systems, Vol. 6, No. 2, May 1991, pp. 762-770.

[50] Luenberger, D.G.: 'Introduction to Linear and Nonlinear Programming', Addison-Wesley Publishing Co., Second Edition, 1984.

[51] Gill P.E., Murray W. and Wright M.: 'Practical Optimisation', Academic Press 1981

[52] Tinney W.F. and Hart C.E.: 'Power Flow Solution by Newton's Method', IEEE Transactions on Power Apparatus and Systems, Vol. PAS-96, No. 11, November 1977, pp. 1449-1460.

[53] Maria G.A., Yuen A.H. and Findlay J.A.: 'Control Variable Adjustment in Load Flow', IEEE Transactions on Power Apparatus and Systems, Vol. 3, No. 3, August 1988, pp. 858-864.

[54] Stott B.: 'Review of Load-Flow Calculations Methods', IEEE Proceedings, Vol. 62, July 1974, pp. 916-929.

[55] Stott B.: 'Effective Starting Process for Newton-Raphson Load Flows', IEE Proceedings, Vol. 118, No. 8, August 1971, pp. 983-987.

[56] Freris L.L. and Sasson A.M.: 'Investigation of the Load-Flow Problem', IEE Proceedings, Vol. 115, No. 10, October 1968, pp. 1459-1470.

[57] Taranto G.N., Pinto L.M.V. and Pereira M.V.F.: 'Representation of FACTS Devices in Power System Economic Dispatch', Vol. 7, No. 2, May 1992, pp. 572-576.

[58] Stagg G.W. and El-Abiad A.H.: 'Computer Methods in Power Systems Analysis', McGraw-Hill 1968.

[59] Elgerd O.I.: 'Electric Energy System Theory: An introduction', McGraw-Hill, Second Edition, 1983

[60] Chang S.K. and Brandwajn V.: 'Adjusted Solutions in Fast Decoupled Load Flow', IEEE Transactions on Power Systems, Vol. 3, No. 2, May 1988, pp. 726-733.

[61] Kimbark E.: 'Direct current Transmission', Vol. I, Wiley- Interscince, New-York, 1971.

[62] Rissik H. and Donaldson J.M.: 'Mercury-Arc Current Convertors', Sir Isaac Pitman and Sons Ltd, London, 1935.

[63] Friedlander E.: 'Transient Effects in Static Shunt Compensators for Long AC Lines' IEEE Transactions on Power Apparatus and Systems, Vol. PAS-95, No. 10, October 1976, pp. 1669-1680.

[64] Miller T.J.E.: 'Reactive Power Control in Electric Systems', Wiley Interscience, 1982, ISBN 0-471-86933-3.

Chapter 2

Optimal Power Flow by Newton's Method

This Chapter summarises the Optimal Power Flow (OPF) knowledge available in the open literature [1-21]. Arguably, Load Flow is still the analysis tool most widely used by power engineers today [22-24], but conventional OPF is rapidly becoming the preferred choice, particularly in network planning and operation. The conventional OPF formulation presented in this thesis is stated as a static non-linear programming problem, which is solved by Newton's method. In fact, a Newton-Raphson load flow has been extended to become a Newton-based OPF. In general the OPF algorithm addresses the issue of minimisation of active power generation, while satisfying system constraints. Inequality constraints on variables are handled efficiently by the Multipliers method overcoming the long standing problem of identifying the binding set*. The complete set of OPF equations are given for transmission lines, conventional transformers, shunt elements (capacitors and inductors), and generators. Furthermore, different size test networks, ranging from 5 to 118 nodes, are solved with the newly developed OPF program and the solutions compared favourably with a commercial software, used in many electric power companies throughout the world.

2.1 General Formulation

Optimal Power Flow solutions are carried out to determine the optimum operating state of the power network subject to physical and operational constraints. The objective function to be optimised may involve economic, security or environmental aspects. The constraints are physical laws that govern power generation and transmission system availability, design limits of electrical equipment and operating strategies. This kind of problem is usually expressed as a static, non-linear programming problem, with the objective function represented as a non-linear function, and the constraints represented as non-linear or linear equations.

In this research, the objective function is taken to be the cost of generation, reflecting the economic aspects of the electrical power system [1-7]. The mathematical formulation consists of minimising active power generation costs by adjusting suitable control parameters. Reactive power does not have a production cost in itself, however, it indirectly affects the generation cost as well as active and reactive power losses.

* The binding set is the set of inequality constraints that must be active at the optimum.

The OPF problem can be formulated as follows:

$$\begin{aligned} &\textbf{\textit{Minimise}} \quad f(\boldsymbol{x}) \\ &\textbf{\textit{Subject to}}\ h(\boldsymbol{x}) = 0 \\ &\textbf{\textit{and}} \quad g(\boldsymbol{x}) \leq 0 \end{aligned} \tag{2.1}$$

where $\boldsymbol{x}$ is the vector of state variables, $f(\boldsymbol{x})$ is the objective function to be optimised, $h(\boldsymbol{x})$ represents the power flow equations and $g(\boldsymbol{x})$ consists of state variable limits as well as functional operating constraints.

2.1.1 Variables

The variables which can be adjusted in pursuit of the optimal solution are named control variables. Examples of such variables are active power generation, taps and phase angles in tap-changing and phase-shifting transformers, respectively and; voltage magnitudes at the generating units, synchronous compensators and Static VAR Compensator nodes [2-4]. The control parameters may be considered to be either continuous or discrete quantities. The former representation is better handled in the OPF formulation, and provides a good approximation to model discrete controls in cases where sufficiently small discrete steps are involved.

The dependent variables are those variables which depend on the control variables. They can take any value, within the limits, as dictated by the solution algorithm. Examples of dependent variables are voltage phase angles at all nodes, except the slack node; voltage magnitudes at all load nodes; reactive power at all generation nodes; active power generation cost; and active and reactive power flows (network losses) in transmission lines, transformers and FACTS series devices.

In addition to those variables, active and reactive power loads and the network topology and parameters form a set of fixed parameters which must be specified at the beginning of the study.

2.1.2 Objective Function

The main aim of the OPF solution is to determine the control settings and system state that optimises the value of the objective function. The selection of the objective function should be based on careful analysis of the power system security and economy. However, power generation cost is the most popular objective function in OPF studies, i.e. the objective is to minimise active power generation cost. It incorporates the economic aspects of the electrical network by including the thermal generation unit costs, generally represented by the following non-linear, second order function [2,35],

$$F_T = \sum_{i=1}^{N_g} F_i(P_{gi}) \tag{2.2}$$

where F_i is the fuel cost at unit i, P_{gi} is the active power generated at unit i and N_g is the number of generators in the system including the slack generator. Also,

$$F_i(P_{gi}) = a_i + b_i P_{gi} + c_i P_{gi}^2 \tag{2.3}$$

where a_i, b_i and c_i are the cost coefficients of unit i.

It should be noted that it is crucial to include the slack generator contribution in the OPF formulation, equations (2.2) and (2.3), otherwise the minimisation process will dispatch

all the generating units at their minimum capacity while assigning the rest of the required generation to the slack generator.

2.1.3 Equality Constraints

The power flow equations provide a means for calculating the power balance that exists in the network during steady-state operation. They must be satisfied, unconditionally, if a feasible solution is to exist [1-4,22]. If the network equations are not satisfied, the OPF problem is said to be infeasible; attempts can be made then to find a limited but still useful solution by relaxing some of the network constraints. The power flows injected at the nodes can be obtained either by real measurements or using a state estimator.

The power flow equations represent the link between the control variables and the dependent variables,

$$P_i(V,\theta) + P_{di} - P_{gi} = 0 \tag{2.4}$$

$$Q_i(V,\theta) + Q_{di} - Q_{gi} = 0 \tag{2.5}$$

where $P_i(V,\theta)$ and $Q_i(V,\theta)$ are active and reactive power injections at node i, respectively. P_{di} and Q_{di} are active and reactive power loads at node i, respectively. P_{gi} and Q_{gi} are scheduled active and reactive power generations at node i, respectively, V and θ are the voltage magnitudes and angles, respectively.

A generic node including generation, load and a transmission line is shown in Figure 2.1.

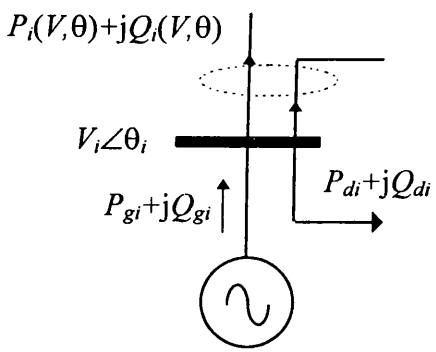

Figure 2.1. A node of the electric network.

It should be noted that all equality constraints in the power network are non-linear. However, as will be shown in Sections 2.4-2.6, they are incorporated in a linearised form within the OPF formulation [19].

2.1.4 Inequality Constraints

All variables have upper and lower limits which must be satisfied in the optimal solution. Control variable constraints reflect bounds on the operating conditions of the equipment used for power dispatch. Limits on generated active power and voltage magnitude at generating units are the most important of such bounds. If these limits are unknown, typical values can be used, for instance the voltage magnitude limits could be 0.95 an 1.05 pu.

Functional constraints result from the application of limits on control variables. Constraints on the voltage magnitude at a load node, generated reactive power and active power flows across transmission lines are the most common. Functional

constraints can be relaxed under emergency conditions in order to obtain sub-optimal but still technically feasible solutions.

The main inequality constraints are:

- Upper and lower bounds on the active power generation at all the generation nodes:

$$P_{gi}^{\min} \le P_{gi} \le P_{gi}^{\max} \quad i = 1,\ldots,N_g \tag{2.6}$$

- Upper and lower limits on the voltage magnitudes at all the nodes:

$$V_i^{\min} \le V_i \le V_i^{\max} \quad i = 1,\ldots,N_b \tag{2.7}$$

- The reactive power at the generation nodes is constrained as follows:

$$Q_{gi}^{\min} \le Q_{gi} \le Q_{gi}^{\max} \quad i = 1,\ldots,N_g \tag{2.8}$$

where

$$Q_{gi} = Q_i(V,\theta) + Q_{di} \tag{2.9}$$

N_b is the number of total nodes and N_g is the number of total generation nodes.

If there is a violation of reactive power at a generating node, the node is changed to a load node with the corresponding voltage constraints.

2.2 Newton's Method

From a mathematical viewpoint, the Optimal Power Flow is a non-linear programming problem, with the objective function represented by a non-linear function and the constraints represented by either non-linear or linearised equations. In Newton's method, the objective function and constraints have to be twice differentiable because the solution process makes use of the Hessian and Jacobian matrices. If this is not the case, matrix $\boldsymbol{W}$ will be singular and Newton's method is not longer applicable; in practice, the matrix $\boldsymbol{W}$ could have small numbers, (due to some round-off error), as consequence, the corrections for the control variables would be big numbers. The non-linear problem is solved by a sequence of quadratic approximations [36-38], moving from one static point $\boldsymbol{x}^j$ to the next $\boldsymbol{x}^{j+1}$, in such a way that a reduction in the value of the objective function is achieved. If the correct binding inequalities are known and the penalty weighting factors are adequate, Newton's method will converge quasi-quadratically. However, the binding inequality set is not known a-priori and this degrades convergence.

In non-linear programming, the first necessary condition for the optimum solution to exist is that the vector of first derivatives of the objective function must be zero at the minimum point. If the objective function is not quadratic, the solution of the equations corresponding to this condition may be difficult. Moreover, there is no guarantee that the solution obtained is a global minimum, since the derivative can also vanish at a point that is either a local minimum or the maximum [36-38].

Algebraically, the method is derived from the Taylor series expansion of a function in the neighbourhood of an operating point $\boldsymbol{x}^0$. The point $\boldsymbol{x}$ is taken to be the point where the derivative of $f(\boldsymbol{x})$ equals zero, i.e.,

$$\frac{df(\boldsymbol{x})}{d\boldsymbol{x}} = \boldsymbol{F}(\boldsymbol{x}) = \boldsymbol{0} \tag{2.10}$$

where

$$f(\boldsymbol{x}) = \begin{bmatrix} f(x_1) & f(x_2) & \cdots & \cdots & f(x_N) \end{bmatrix}^t \tag{2.11}$$

The Taylor series expansion of $\boldsymbol{F}(\boldsymbol{x})$ is,

$$\boldsymbol{F}(\boldsymbol{x}+\Delta\boldsymbol{x}) = \boldsymbol{F}(\boldsymbol{x}^0) + \frac{d\boldsymbol{F}(\boldsymbol{x}^0)}{d\boldsymbol{x}}\Delta\boldsymbol{x} + \frac{1}{2}\frac{d^2\boldsymbol{F}(\boldsymbol{x}^0)}{d\boldsymbol{x}^2}\Delta\boldsymbol{x}^2 + \cdots \tag{2.12}$$

If the higher order terms in (2.12) are neglected, then equation (2.12) can be approximated by,

$$\boldsymbol{F}(\boldsymbol{x}+\Delta\boldsymbol{x}) = \boldsymbol{F}(\boldsymbol{x}^0) + \frac{d\boldsymbol{F}(\boldsymbol{x}^0)}{d\boldsymbol{x}}\Delta\boldsymbol{x} = \boldsymbol{0} \tag{2.13}$$

or

$$\frac{d\boldsymbol{F}(\boldsymbol{x}^0)}{d\boldsymbol{x}}\Delta\boldsymbol{x} = -\boldsymbol{F}(\boldsymbol{x}^0) \tag{2.14}$$

Newton's iterative method replaces $\boldsymbol{x}^0$ by $\boldsymbol{x}^j$,

$$\frac{d\boldsymbol{F}(\boldsymbol{x}^j)}{d\boldsymbol{x}}\Delta\boldsymbol{x}^{j+1} = -\boldsymbol{F}(\boldsymbol{x}^j) \tag{2.15}$$

where j is an iteration counter.

If equation (2.15) is expressed in terms of $f(\boldsymbol{x})$, the following expression is obtained,

$$\frac{d^2 f(\boldsymbol{x}^j)}{d^2\boldsymbol{x}}\Delta\boldsymbol{x}^{j+1} = -\frac{df(\boldsymbol{x}^j)}{d\boldsymbol{x}} \tag{2.16}$$

It should be noted that there is only one stationary point that can be found by setting the first derivative equal to zero and solving the linear equation (2.16). The solution is found by resorting to an iterative process because the first derivative of the objective function is non-linear.

The minimum can be verified by checking that the following conditions are satisfied [36-38]:

$$\frac{\partial f(\boldsymbol{x}^{j+1})}{\partial\boldsymbol{x}} = \boldsymbol{0} \tag{2.17}$$

$$\frac{\partial^2 f(\boldsymbol{x}^{j+1})}{\partial^2\boldsymbol{x}} > \boldsymbol{0} \tag{2.18}$$

2.3 Application of Newton's Method to Optimal Power Flow

In the general optimisation problem, the aim is to optimise an objective function but the solution has to satisfy a number of equality and inequality constraints. Any solution point that satisfies the constraints is said to be a feasible solution. A local minimum is a feasible point that minimises the objective function within a neighbourhood. The global minimum is a local minimum with the lowest value in the complete feasible region.

The first step in solving the constrained optimisation problem via Newton's method is to convert the problem into an unconstrained optimisation problem. This is achieved by constructing an augmented Lagrangian function for equation (2.1). This is given as [36-38],

$$L(\boldsymbol{x},\lambda) = f(\boldsymbol{x}) + \lambda^t h(\boldsymbol{x}) + \psi\big(g(\boldsymbol{x}),\mu\big) \tag{2.19}$$

where λ and μ are Lagrange multiplier vectors for equality and inequality constraints, respectively; $\psi(g(\boldsymbol{x}), \mu)$ is the penalty function of the inequality constraints. There are as many Lagrange multipliers as the number of active constraints; the problem is to find $\boldsymbol{x}^{opt}$ and λ^{opt} at the global optimum. The technique for handling the functional inequality constraints is presented in Section 2.7.

The Lagrangian function corresponding to the power flow mismatch equations is explicitly modelled in the OPF Newton's method as an equality constraint given by the following equation [1-7,36-38],

$$L_{system}(\boldsymbol{x},\lambda) = F_T + \sum_{i=1}^{N_b} \lambda_{pi}(P_i(V,\theta) + P_{di} - P_{gi}) + \sum_{i=1}^{N_b} \lambda_{qi}(Q_i(V,\theta) + Q_{di} - Q_{gi}) \tag{2.20}$$

where F_T is the objective function.

The summations are taken over all the nodes whose active and reactive power injections are specified in the study. λ_{pi} and λ_{qi} are the Lagrange multipliers for active and reactive power equations, respectively.

2.4 Equation System

The efficient solution of the Lagrangian function, equations (2.19)-(2.20), is achieved by solving the following equation,

$$\boldsymbol{W}\Delta\mathbf{z} = -\boldsymbol{g} \tag{2.21}$$

This equation (2.21) can be written as,

$$\begin{bmatrix} \boldsymbol{W} \end{bmatrix} \begin{bmatrix} \Delta\boldsymbol{x} \\ \Delta\lambda \end{bmatrix} = -\begin{bmatrix} \nabla\boldsymbol{x} \\ \nabla\lambda \end{bmatrix} \tag{2.22}$$

where

$$\boldsymbol{W} = \begin{bmatrix} \boldsymbol{H} & \boldsymbol{J}^t \\ \boldsymbol{J} & \mathbf{0} \end{bmatrix} \tag{2.23}$$

$$\nabla\boldsymbol{x} = \begin{bmatrix} \nabla\boldsymbol{P}_g & \nabla\theta & \nabla\boldsymbol{V} \end{bmatrix}^t \tag{2.24}$$

$$\nabla\lambda = \begin{bmatrix} \nabla\lambda_p & \nabla\lambda_q \end{bmatrix}^t \tag{2.25}$$

$$\Delta x = \begin{bmatrix} \Delta\boldsymbol{P}_g & \Delta\theta & \Delta\boldsymbol{V} \end{bmatrix}^t \tag{2.26}$$

$$\Delta\lambda = \begin{bmatrix} \Delta\lambda_p & \Delta\lambda_q \end{bmatrix}^t \tag{2.27}$$

Partial derivatives are used to assemble the matrix $\boldsymbol{W}$. The matrix $\boldsymbol{W}$ contains the second partial derivatives of the Lagrangian function $L(\boldsymbol{x},\lambda)$ with respect to the state variables $\boldsymbol{x}$ and Lagrange multipliers λ. The matrix $\boldsymbol{W}$ is symmetric and it has a null matrix at its

lower right hand corner because the second partial derivatives of the form $\partial^2 L(\boldsymbol{x},\lambda)/\partial\lambda_i\partial\lambda_j$ do not exist. The gradient vector $\boldsymbol{g}$ is $\nabla L(\boldsymbol{x},\lambda)$. The first partial derivatives of $\nabla L(\boldsymbol{x},\lambda)$ are the second partial derivatives of the Lagrangian function $L(\boldsymbol{x},\lambda)$. $\Delta\mathbf{z}$ is the vector of correction terms. The state variables are the active power generations, the nodal voltage magnitudes and angles, P_g, V and θ, respectively. The Lagrange multipliers are the incremental costs for active and reactive powers, λ_p and λ_q, respectively.

Some derivative terms give rise to the Hessian matrix $\boldsymbol{H}$ while others give rise to the Jacobian matrix $\boldsymbol{J}$ or its transpose $\boldsymbol{J}^t$. The matrix $\mathbf{0}$ is the null matrix.

The derivative terms associated with the inequality constraints, $\psi(g(\boldsymbol{x}),\mu)$, are omitted at the beginning of the solution since they are introduced into the matrix equation only after limits are enforced. Hence, the new Hessian and Jacobian terms are:

$$\boldsymbol{H} = \frac{\partial^2 L(\boldsymbol{x},\lambda)}{\partial \boldsymbol{x}^2} = \frac{\partial^2 f(\boldsymbol{x})}{\partial \boldsymbol{x}^2} + \left(\frac{\partial^2 h(\boldsymbol{x})}{\partial \boldsymbol{x}^2}\right)^t \lambda \tag{2.28}$$

$$\boldsymbol{J} = \frac{\partial^2 L(\boldsymbol{x},\lambda)}{\partial \boldsymbol{x}\partial\lambda} = \frac{\partial h(\boldsymbol{x})}{\partial \boldsymbol{x}} \tag{2.29}$$

It is observed that submatrices $\boldsymbol{H}$, $\boldsymbol{J}$ and $\boldsymbol{J}^t$ have the same sparsity structure as the nodal admittance matrix.

2.5 Optimality Conditions for Newton's Method

The conditions for $(\boldsymbol{x}^{opt}, \lambda^{opt})$ to be a global minimum are intrinsically linked to the properties of the matrix $\boldsymbol{W}$. However, it is difficult to verify that the matrix $\boldsymbol{W}$ is positive definite for large scale problems, such as OPF, because it would be computationally too expensive to carry out this test, therefore it is skipped in practical problems. The only optimality tests performed are to check whether or not the gradient vector is zero and that the Lagrange multipliers for the binding inequalities pass their sign test. However, the practical conditions for an Optimal Power Flow are [2,7]:

- The mismatches of all power flow equations are within a prescribed tolerance.
- The inequality constraints are satisfied.
- The vector gradient is zero.
- A further reduction in the objective function can only be achieved if the constraints are violated.

In general optimisation problems, it is not sufficient to optimise an objective function, but the solution has to satisfy a number of constraints, in the form of equalities and inequalities. The inequality constraints are made active by changing them to equality constraints. Thus, the general optimisation problem is to find the optimum of a function subject to satisfying a set of equality constraints.

2.6 Power Plant Modelling in OPF

Superposition is used to construct the linearised equation (2.21) at each iterative step. The plant components of the power system can be modelled independently, their individual entries being placed in $\boldsymbol{W}$ and $\boldsymbol{g}$. The node number determines the location of

the individual Hessian and Jacobian terms in the overall W structure. An example of the superposition application is presented in Section 2.6.5.

2.6.1 Transmission Line Representation

The circuit shown in Figure 2.2 is used to derive the transmission line power flow equations and the linearised equations required by Newton's method. The same power flow equations may be used to represent conventional transformers, but the elements of the admittance matrix are calculated in a different way, as will be shown in Chapter 3.

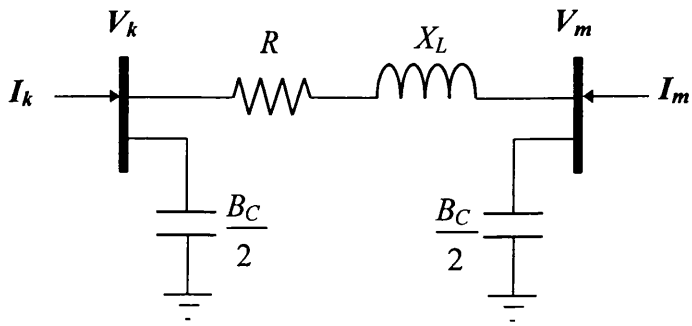

Figure 2.2. Nominal π representation of the transmission line.

The transfer admittance matrix of the transmission line circuit shown in Figure 2.2 is given by the following equation [39,40],

$$\begin{bmatrix} I_k \\ I_m \end{bmatrix} = \begin{bmatrix} G_{kk} + jB_{kk} & G_{km} + jB_{km} \\ G_{mk} + jB_{mk} & G_{mm} + jB_{mm} \end{bmatrix} \begin{bmatrix} V_k \\ V_m \end{bmatrix} \tag{2.30}$$

where

$$G_{kk} = G_{mm} = \frac{R}{R^2 + X_L^2} \tag{2.31}$$

$$B_{kk} = B_{mm} = \frac{B_C}{2} - \frac{X_L}{R^2 + X_L^2} \tag{2.32}$$

$$G_{km} = G_{mk} = -\frac{R}{R^2 + X_L^2} \tag{2.33}$$

$$B_{km} = B_{mk} = \frac{X_L}{R^2 + X_L^2} \tag{2.34}$$

The nodal power flow equations provide a means for calculating the power balance that exists in the network during steady-state operation. To simplify the notation, P_k and Q_k will be used instead of $P_k(V,\theta)$ and $Q_k(V,\theta)$, and similarly for P_m and Q_m. The active and reactive power equations at nodes k and m are given as:

$$P_k = V_k^2 G_{kk} + V_k V_m \left(G_{km} \cos(\theta_k - \theta_m) + B_{km} \sin(\theta_k - \theta_m) \right) \tag{2.35}$$

$$Q_k = -V_k^2 B_{kk} + V_k V_m \left(G_{km} \sin(\theta_k - \theta_m) - B_{km} \cos(\theta_k - \theta_m) \right) \tag{2.36}$$

$$P_m = V_m^2 G_{mm} + V_m V_k \left(G_{mk} \cos(\theta_m - \theta_k) + B_{mk} \sin(\theta_m - \theta_k) \right) \tag{2.37}$$

$$Q_m = -V_m^2 B_{mm} + V_m V_k \left(G_{mk} \sin(\theta_m - \theta_k) - B_{mk} \cos(\theta_m - \theta_k) \right) \tag{2.38}$$

For a single transmission line, the Lagrangian function corresponding to the power mismatch equations at nodes k and m are explicitly modelled in the OPF formulation as:

$$\begin{aligned} L_{trans.line}(\boldsymbol{x},\lambda) = L = \lambda_{pk}(P_k + P_{dk} - P_{gk}) + \lambda_{qk}(Q_k + Q_{dk} - Q_{gk}) \\ + \lambda_{pm}(P_m + P_{dm} - P_{gm}) + \lambda_{qm}(Q_m + Q_{dm} - Q_{gm}) \end{aligned} \tag{2.39}$$

The gradient vector, $\boldsymbol{g}$, is formed with the first partial derivatives of the Lagrangian function with respect to all the variables and Lagrange multipliers involved.
The first derivatives with respect to all the state variables, at node k, are:

$$\frac{\partial L}{\partial \theta_k} = \lambda_{pk}\frac{\partial P_k}{\partial \theta_k} + \lambda_{qk}\frac{\partial Q_k}{\partial \theta_k} + \lambda_{pm}\frac{\partial P_m}{\partial \theta_k} + \lambda_{qm}\frac{\partial Q_m}{\partial \theta_k} \tag{2.40}$$

$$\frac{\partial L}{\partial V_k} = \lambda_{pk}\frac{\partial P_k}{\partial V_k} + \lambda_{qk}\frac{\partial Q_k}{\partial V_k} + \lambda_{pm}\frac{\partial P_m}{\partial V_k} + \lambda_{qm}\frac{\partial Q_m}{\partial V_k} \tag{2.41}$$

$$\frac{\partial L}{\partial \lambda_{pk}} = P_k + P_{dk} - P_{gk} \tag{2.42}$$

$$\frac{\partial L}{\partial \lambda_{qk}} = Q_k + Q_{dk} - Q_{gk} \tag{2.43}$$

The first derivatives with respect to all the state variables, at node m, are:

$$\frac{\partial L}{\partial \theta_m} = \lambda_{pk}\frac{\partial P_k}{\partial \theta_m} + \lambda_{qk}\frac{\partial Q_k}{\partial \theta_m} + \lambda_{pm}\frac{\partial P_m}{\partial \theta_m} + \lambda_{qm}\frac{\partial Q_m}{\partial \theta_m} \tag{2.44}$$

$$\frac{\partial L}{\partial V_m} = \lambda_{pk}\frac{\partial P_k}{\partial V_m} + \lambda_{qk}\frac{\partial Q_k}{\partial V_m} + \lambda_{pm}\frac{\partial P_m}{\partial V_m} + \lambda_{qm}\frac{\partial Q_m}{\partial V_m} \tag{2.45}$$

$$\frac{\partial L}{\partial \lambda_{pm}} = P_m + P_{dm} - P_{gm} \tag{2.46}$$

$$\frac{\partial L}{\partial \lambda_{qm}} = Q_m + Q_{dm} - Q_{gm} \tag{2.47}$$

The matrix $\boldsymbol{W}$ is made up of submatrices $\boldsymbol{J}$ and $\boldsymbol{H}$, where $\boldsymbol{J}$ is the Jacobian used in power flows and $\boldsymbol{H}$ is the Hessian of the Lagrangian function given by (2.19) or (2.20). The elements of the matrix $\boldsymbol{W}$ are the second derivative terms of the Lagrangian function with respect to all the variables and Lagrange multipliers involved.

The second derivatives with respect to all the state variables at node k are (diagonal block):

$$\frac{\partial^2 L}{\partial \theta_k^2} = \lambda_{pk}\frac{\partial^2 P_k}{\partial \theta_k^2} + \lambda_{qk}\frac{\partial^2 Q_k}{\partial \theta_k^2} + \lambda_{pm}\frac{\partial^2 P_m}{\partial \theta_k^2} + \lambda_{qm}\frac{\partial^2 Q_m}{\partial \theta_k^2} \tag{2.48}$$

$$\frac{\partial^2 L}{\partial \theta_k \partial V_k} = \frac{\partial^2 L}{\partial V_k \partial \theta_k} = \lambda_{pk}\frac{\partial^2 P_k}{\partial \theta_k \partial V_k} + \lambda_{qk}\frac{\partial^2 Q_k}{\partial \theta_k \partial V_k} + \lambda_{pm}\frac{\partial^2 P_m}{\partial \theta_k \partial V_k} + \lambda_{qm}\frac{\partial^2 Q_m}{\partial \theta_k \partial V_k} \tag{2.49}$$

$$\frac{\partial^2 L}{\partial \theta_k \partial \lambda_{pk}} = \frac{\partial^2 L}{\partial \lambda_{pk} \partial \theta_k} = \frac{\partial P_k}{\partial \theta_k} \tag{2.50}$$

$$\frac{\partial^2 L}{\partial \theta_k \partial \lambda_{qk}} = \frac{\partial^2 L}{\partial \lambda_{qk} \partial \theta_k} = \frac{\partial Q_k}{\partial \theta_k} \tag{2.51}$$

$$\frac{\partial^2 L}{\partial V_k^2} = \lambda_{pk} \frac{\partial^2 P_k}{\partial V_k^2} + \lambda_{qk} \frac{\partial^2 Q_k}{\partial V_k^2} + \lambda_{pm} \frac{\partial^2 P_m}{\partial V_k^2} + \lambda_{qm} \frac{\partial^2 Q_m}{\partial V_k^2} \tag{2.52}$$

$$\frac{\partial^2 L}{\partial V_k \partial \lambda_{pk}} = \frac{\partial^2 L}{\partial \lambda_{pk} \partial V_k} = \frac{\partial P_k}{\partial V_k} \tag{2.53}$$

$$\frac{\partial^2 L}{\partial V_k \partial \lambda_{qk}} = \frac{\partial^2 L}{\partial \lambda_{qk} \partial V_k} = \frac{\partial Q_k}{\partial V_k} \tag{2.54}$$

The second derivatives with respect to all the state variables at nodes *k* and *m* are (non-diagonal block):

$$\frac{\partial^2 L}{\partial \theta_k \partial \theta_m} = \frac{\partial^2 L}{\partial \theta_m \partial \theta_k} = \lambda_{pk} \frac{\partial^2 P_k}{\partial \theta_k \partial \theta_m} + \lambda_{qk} \frac{\partial^2 Q_k}{\partial \theta_k \partial \theta_m} + \lambda_{pm} \frac{\partial^2 P_m}{\partial \theta_k \partial \theta_m} + \lambda_{qm} \frac{\partial^2 Q_m}{\partial \theta_k \partial \theta_m} \tag{2.55}$$

$$\frac{\partial^2 L}{\partial \theta_k \partial V_m} = \frac{\partial^2 L}{\partial V_m \partial \theta_k} = \lambda_{pk} \frac{\partial^2 P_k}{\partial \theta_k \partial V_m} + \lambda_{qk} \frac{\partial^2 Q_k}{\partial \theta_k \partial V_m} + \lambda_{pm} \frac{\partial^2 P_m}{\partial \theta_k \partial V_m} + \lambda_{qm} \frac{\partial^2 Q_m}{\partial \theta_k \partial V_m} \tag{2.56}$$

$$\frac{\partial^2 L}{\partial \theta_k \partial \lambda_{pm}} = \frac{\partial^2 L}{\partial \lambda_{pm} \partial \theta_k} = \frac{\partial P_m}{\partial \theta_k} \tag{2.57}$$

$$\frac{\partial^2 L}{\partial \theta_k \partial \lambda_{qm}} = \frac{\partial^2 L}{\partial \lambda_{qm} \partial \theta_k} = \frac{\partial Q_m}{\partial \theta_k} \tag{2.58}$$

$$\frac{\partial^2 L}{\partial V_k \partial \theta_m} = \frac{\partial^2 L}{\partial \theta_m \partial V_k} = \lambda_{pk} \frac{\partial^2 P_k}{\partial V_k \partial \theta_m} + \lambda_{qk} \frac{\partial^2 Q_k}{\partial V_k \partial \theta_m} + \lambda_{pm} \frac{\partial^2 P_m}{\partial V_k \partial \theta_m} + \lambda_{qm} \frac{\partial^2 Q_m}{\partial V_k \partial \theta_m} \tag{2.59}$$

$$\frac{\partial^2 L}{\partial V_k \partial V_m} = \frac{\partial^2 L}{\partial V_m \partial V_k} = \lambda_{pk} \frac{\partial^2 P_k}{\partial V_k \partial V_m} + \lambda_{qk} \frac{\partial^2 Q_k}{\partial V_k \partial V_m} + \lambda_{pm} \frac{\partial^2 P_m}{\partial V_k \partial V_m} + \lambda_{qm} \frac{\partial^2 Q_m}{\partial V_k \partial V_m} \tag{2.60}$$

$$\frac{\partial^2 L}{\partial V_k \partial \lambda_{pm}} = \frac{\partial^2 L}{\partial \lambda_{pm} \partial V_k} = \frac{\partial P_m}{\partial V_k} \tag{2.61}$$

$$\frac{\partial^2 L}{\partial V_k \partial \lambda_{qm}} = \frac{\partial^2 L}{\partial \lambda_{qm} \partial V_k} = \frac{\partial Q_m}{\partial V_k} \tag{2.62}$$

$$\frac{\partial^2 L}{\partial \lambda_{pk} \partial \theta_m} = \frac{\partial^2 L}{\partial \theta_m \partial \lambda_{pk}} = \frac{\partial P_k}{\partial \theta_m} \tag{2.63}$$

$$\frac{\partial^2 L}{\partial \lambda_{pk} \partial V_m} = \frac{\partial^2 L}{\partial V_m \partial \lambda_{pk}} = \frac{\partial P_k}{\partial V_m} \tag{2.64}$$

$$\frac{\partial^2 L}{\partial \lambda_{qk} \partial \theta_m} = \frac{\partial^2 L}{\partial \theta_m \partial \lambda_{qk}} = \frac{\partial Q_k}{\partial \theta_m} \tag{2.65}$$

$$\frac{\partial^2 L}{\partial \lambda_{qk} \partial V_m} = \frac{\partial^2 L}{\partial V_m \partial \lambda_{qk}} = \frac{\partial Q_k}{\partial V_m} \tag{2.66}$$

The second derivatives with respect to all the state variables at node m are (diagonal block):

$$\frac{\partial^2 L}{\partial \theta_m^2} = \lambda_{pk}\frac{\partial^2 P_k}{\partial \theta_m^2} + \lambda_{qk}\frac{\partial^2 Q_k}{\partial \theta_m^2} + \lambda_{pm}\frac{\partial^2 P_m}{\partial \theta_m^2} + \lambda_{qm}\frac{\partial^2 Q_m}{\partial \theta_m^2} \tag{2.67}$$

$$\frac{\partial^2 L}{\partial \theta_m \partial V_m} = \frac{\partial^2 L}{\partial V_m \partial \theta_m} = \lambda_{pk}\frac{\partial^2 P_k}{\partial \theta_m \partial V_m} + \lambda_{qk}\frac{\partial^2 Q_k}{\partial \theta_m \partial V_m} + \lambda_{pm}\frac{\partial^2 P_m}{\partial \theta_m \partial V_m} + \lambda_{qm}\frac{\partial^2 Q_m}{\partial \theta_m \partial V_m} \tag{2.68}$$

$$\frac{\partial^2 L}{\partial \theta_m \partial \lambda_{pm}} = \frac{\partial^2 L}{\partial \lambda_{pm} \partial \theta_m} = \frac{\partial P_m}{\partial \theta_m} \tag{2.69}$$

$$\frac{\partial^2 L}{\partial \theta_m \partial \lambda_{qm}} = \frac{\partial^2 L}{\partial \lambda_{qm} \partial \theta_m} = \frac{\partial Q_m}{\partial \theta_m} \tag{2.70}$$

$$\frac{\partial^2 L}{\partial V_m^2} = \lambda_{pk}\frac{\partial^2 P_k}{\partial V_m^2} + \lambda_{qk}\frac{\partial^2 Q_k}{\partial V_m^2} + \lambda_{pm}\frac{\partial^2 P_m}{\partial V_m^2} + \lambda_{qm}\frac{\partial^2 Q_m}{\partial V_m^2} \tag{2.71}$$

$$\frac{\partial^2 L}{\partial V_m \partial \lambda_{pm}} = \frac{\partial^2 L}{\partial \lambda_{pm} \partial V_m} = \frac{\partial P_m}{\partial V_m} \tag{2.72}$$

$$\frac{\partial^2 L}{\partial V_m \partial \lambda_{qm}} = \frac{\partial^2 L}{\partial \lambda_{qm} \partial V_m} = \frac{\partial Q_m}{\partial V_m} \tag{2.73}$$

The expressions (2.40) through (2.73) are the transmission line terms of the linearised system of equations required for the solution of the OPF using Newton's method. These terms are systematically placed into $\boldsymbol{W}$ and $\boldsymbol{g}$ to make them correspond with the locations of nodes k and m:

$$\begin{bmatrix}
\frac{\partial^2 L}{\partial \theta_k^2} & \frac{\partial^2 L}{\partial \theta_k \partial V_k} & \frac{\partial P_k}{\partial \theta_k} & \frac{\partial Q_k}{\partial \theta_k} & \frac{\partial^2 L}{\partial \theta_k \partial \theta_m} & \frac{\partial^2 L}{\partial \theta_k \partial V_m} & \frac{\partial P_m}{\partial \theta_k} & \frac{\partial Q_m}{\partial \theta_k} \\
\frac{\partial^2 L}{\partial V_k \partial \theta_k} & \frac{\partial^2 L}{\partial V_k^2} & \frac{\partial P_k}{\partial V_k} & \frac{\partial Q_k}{\partial V_k} & \frac{\partial^2 L}{\partial V_k \partial \theta_m} & \frac{\partial^2 L}{\partial V_k \partial V_m} & \frac{\partial P_m}{\partial V_k} & \frac{\partial Q_m}{\partial V_k} \\
\frac{\partial P_k}{\partial \theta_k} & \frac{\partial P_k}{\partial V_k} & & & \frac{\partial P_k}{\partial \theta_m} & \frac{\partial P_k}{\partial V_m} & & \\
\frac{\partial Q_k}{\partial \theta_k} & \frac{\partial Q_k}{\partial V_k} & & & \frac{\partial Q_k}{\partial \theta_m} & \frac{\partial Q_k}{\partial V_m} & & \\
\hdashline
\frac{\partial^2 L}{\partial \theta_m \partial \theta_k} & \frac{\partial^2 L}{\partial \theta_m \partial V_k} & \frac{\partial P_k}{\partial \theta_m} & \frac{\partial Q_k}{\partial \theta_m} & \frac{\partial^2 L}{\partial \theta_m^2} & \frac{\partial^2 L}{\partial \theta_m \partial V_m} & \frac{\partial P_m}{\partial \theta_m} & \frac{\partial Q_m}{\partial \theta_m} \\
\frac{\partial^2 L}{\partial V_m \partial \theta_k} & \frac{\partial^2 L}{\partial V_m \partial V_k} & \frac{\partial P_k}{\partial V_m} & \frac{\partial Q_k}{\partial V_m} & \frac{\partial^2 L}{\partial V_m \partial \theta_m} & \frac{\partial^2 L}{\partial V_m^2} & \frac{\partial P_m}{\partial V_m} & \frac{\partial Q_m}{\partial V_m} \\
\frac{\partial P_m}{\partial \theta_k} & \frac{\partial P_m}{\partial V_k} & & & \frac{\partial P_m}{\partial \theta_m} & \frac{\partial P_m}{\partial V_m} & & \\
\frac{\partial Q_m}{\partial \theta_k} & \frac{\partial Q_m}{\partial \theta_k} & & & \frac{\partial Q_m}{\partial \theta_m} & \frac{\partial Q_m}{\partial V_m} & &
\end{bmatrix}
\begin{bmatrix}
\Delta\theta_k \\ \Delta V_k \\ \Delta\lambda_{pk} \\ \Delta\lambda_{qk} \\ \Delta\theta_m \\ \Delta V_m \\ \Delta\lambda_{pm} \\ \Delta\lambda_{qm}
\end{bmatrix}
= -
\begin{bmatrix}
\frac{\partial L}{\partial \theta_k} \\ \frac{\partial L}{\partial V_k} \\ \frac{\partial L}{\partial \lambda_{pk}} \\ \frac{\partial L}{\partial \lambda_{qk}} \\ \frac{\partial L}{\partial \theta_m} \\ \frac{\partial L}{\partial V_m} \\ \frac{\partial L}{\partial \lambda_{pm}} \\ \frac{\partial L}{\partial \lambda_{qm}}
\end{bmatrix} \tag{2.74}$$

2.6.2 Hessian and Jacobian Elements for the Transmission Line Power Flow Equations at Node *k*

The active and reactive power equations at nodes *k* and *m* for the transmission line and conventional transformer were given by equations (2.35)-(2.38). The first partial derivatives of the active power flow equations are:

$$\frac{\partial P_k}{\partial \theta_k} = -V_k V_m \left(G_{km} \sin(\theta_k - \theta_m) - B_{km} \cos(\theta_k - \theta_m) \right) \tag{2.75}$$

$$\frac{\partial P_k}{\partial \theta_m} = V_k V_m \left(G_{km} \sin(\theta_k - \theta_m) - B_{km} \cos(\theta_k - \theta_m) \right) \tag{2.76}$$

$$\frac{\partial P_k}{\partial V_k} = 2V_k G_{kk} + V_m \left(G_{km} \cos(\theta_k - \theta_m) + B_{km} \sin(\theta_k - \theta_m) \right) \tag{2.77}$$

$$\frac{\partial P_k}{\partial V_m} = V_k \left(G_{km} \cos(\theta_k - \theta_m) + B_{km} \sin(\theta_k - \theta_m) \right) \tag{2.78}$$

$$\frac{\partial Q_k}{\partial \theta_k} = V_k V_m \left(G_{km} \cos(\theta_k - \theta_m) + B_{km} \sin(\theta_k - \theta_m) \right) \tag{2.79}$$

$$\frac{\partial Q_k}{\partial \theta_m} = -V_k V_m \left(G_{km} \cos(\theta_k - \theta_m) + B_{km} \sin(\theta_k - \theta_m) \right) \tag{2.80}$$

$$\frac{\partial Q_k}{\partial V_k} = -2V_k B_{kk} + V_m \left(G_{km} \sin(\theta_k - \theta_m) - B_{km} \cos(\theta_k - \theta_m) \right) \tag{2.81}$$

$$\frac{\partial Q_k}{\partial V_m} = V_k \left(G_{km} \sin(\theta_k - \theta_m) - B_{km} \cos(\theta_k - \theta_m) \right) \tag{2.82}$$

The second partial derivatives of the active power flow equations are:

$$\frac{\partial^2 P_k}{\partial \theta_m \partial \theta_k} = V_k V_m \left(G_{km} \cos(\theta_k - \theta_m) + B_{km} \sin(\theta_k - \theta_m) \right) \tag{2.83}$$

$$\frac{\partial^2 P_k}{\partial \theta_m \partial V_k} = V_m \left(G_{km} \sin(\theta_k - \theta_m) - B_{km} \cos(\theta_k - \theta_m) \right) \tag{2.84}$$

$$\frac{\partial^2 P_k}{\partial \theta_m \partial V_m} = V_k \left(G_{km} \sin(\theta_k - \theta_m) - B_{km} \cos(\theta_k - \theta_m) \right) \tag{2.85}$$

$$\frac{\partial^2 P_k}{\partial \theta_k \partial V_k} = -V_m \left(G_{km} \sin(\theta_k - \theta_m) - B_{km} \cos(\theta_k - \theta_m) \right) \tag{2.86}$$

$$\frac{\partial^2 P_k}{\partial \theta_k \partial V_m} = -V_k \left(G_{km} \sin(\theta_k - \theta_m) - B_{km} \cos(\theta_k - \theta_m) \right) \tag{2.87}$$

$$\frac{\partial^2 P_k}{\partial V_k \partial V_m} = \left(G_{km} \cos(\theta_k - \theta_m) + B_{km} \sin(\theta_k - \theta_m) \right) \tag{2.88}$$

$$\frac{\partial^2 P_k}{\partial \theta_m^2} = -V_k V_m \left(G_{km} \cos(\theta_k - \theta_m) + B_{km} \sin(\theta_k - \theta_m) \right) \tag{2.89}$$

$$\frac{\partial^2 P_k}{\partial \theta_k^2} = -V_k V_m \left(G_{km} \cos(\theta_k - \theta_m) + B_{km} \sin(\theta_k - \theta_m) \right) \tag{2.90}$$

$$\frac{\partial^2 P_k}{\partial V_k^2} = 2G_{kk} \tag{2.91}$$

$$\frac{\partial^2 P_k}{\partial V_m^2} = 0 \tag{2.92}$$

The second partial derivatives of the reactive power flow equations are:

$$\frac{\partial^2 Q_k}{\partial \theta_m \partial \theta_k} = V_k V_m \left(G_{km} \sin(\theta_k - \theta_m) - B_{km} \cos(\theta_k - \theta_m) \right) \tag{2.93}$$

$$\frac{\partial^2 Q_k}{\partial \theta_m \partial V_k} = -V_m \left(G_{km} \cos(\theta_k - \theta_m) + B_{km} \sin(\theta_k - \theta_m) \right) \tag{2.94}$$

$$\frac{\partial^2 Q_k}{\partial \theta_m \partial V_m} = -V_k \left(G_{km} \cos(\theta_k - \theta_m) + B_{km} \sin(\theta_k - \theta_m) \right) \tag{2.95}$$

$$\frac{\partial^2 Q_k}{\partial \theta_k \partial V_k} = V_m \left(G_{km} \cos(\theta_k - \theta_m) + B_{km} \sin(\theta_k - \theta_m) \right) \tag{2.96}$$

$$\frac{\partial^2 Q_k}{\partial \theta_k \partial V_m} = V_k \left(G_{km} \cos(\theta_k - \theta_m) + B_{km} \sin(\theta_k - \theta_m) \right) \tag{2.97}$$

$$\frac{\partial^2 Q_k}{\partial V_k \partial V_m} = \left(G_{km} \sin(\theta_k - \theta_m) - B_{km} \cos(\theta_k - \theta_m) \right) \tag{2.98}$$

$$\frac{\partial^2 Q_k}{\partial \theta_m^2} = -V_k V_m \left(G_{km} \sin(\theta_k - \theta_m) - B_{km} \sin(\theta_k - \theta_m) \right) \tag{2.99}$$

$$\frac{\partial^2 Q_k}{\partial \theta_k^2} = -V_k V_m \left(G_{km} \sin(\theta_k - \theta_m) - B_{km} \cos(\theta_k - \theta_m) \right) \tag{2.100}$$

$$\frac{\partial^2 Q_k}{\partial V_k^2} = -2B_{kk} \tag{2.101}$$

$$\frac{\partial^2 Q_k}{\partial V_m^2} = 0 \tag{2.102}$$

To obtain the partial derivatives of P_m and Q_m it is only necessary to exchange k by m in equations (2.75)-(2.102).

2.6.3 Shunt Element Representation

In electric power systems, nodal voltages are affected by load variations and by network topology changes. The voltage drops when the network is operating under heavy loading, and when the load level in the system is low, over-voltages can arise due to the capacitive effect of the transmission lines. Voltage regulation is achieved by controlling the production and absorption of reactive power. Shunt capacitors and shunt reactors are

used for this purpose. Shunt compensators are either permanently connected to the network, or switched on and off according to requirements.

The shunt elements are included in the OPF formulation as shown below. If the element is connected at node k, its Lagrangian function is given by,

$$L_{shunt}(\boldsymbol{x},\lambda) = L = \lambda_{qk}(Q_{k,shunt}) = \lambda_{qk}(-V_k^2 B_{shunt}) \tag{2.103}$$

In this case the shunt element's contribution to the linearised system of equations is,

$$\begin{bmatrix} 0 & 0 & 0 & 0 \\ 0 & \frac{\partial^2 L}{\partial V_k^2} & 0 & \frac{\partial Q_{k,shunt}}{\partial V_k} \\ 0 & 0 & 0 & 0 \\ 0 & \frac{\partial Q_{k,shunt}}{\partial V_k} & 0 & 0 \end{bmatrix} \begin{bmatrix} 0 \\ \Delta V_k \\ 0 \\ \Delta\lambda_{qk} \end{bmatrix} = -\begin{bmatrix} 0 \\ \frac{\partial L}{\partial V_k} \\ 0 \\ \frac{\partial L}{\partial \lambda_{qk}} \end{bmatrix} \tag{2.104}$$

where

$$\frac{\partial L}{\partial V_k} = -2\lambda_{qk} V_k B_{shunt} \tag{2.105}$$

$$\frac{\partial^2 L}{\partial V_k^2} = -2\lambda_{qk} B_{shunt} \tag{2.106}$$

$$\frac{\partial Q_{k,shunt}}{\partial V_k} = -2V_k B_{shunt} \tag{2.107}$$

$$\frac{\partial L}{\partial \lambda_{qk}} = Q_{k,shunt} = -V_k^2 B_{shunt} \tag{2.108}$$

2.6.4 Generator Representation

Generators are an essential component of the power system. They provide the active power demanded by the system. Also, they control the production and absorption of reactive power aiming at maintaining a fixed voltage magnitude at their terminals. In OPF, the steam generators are included in the problem formulation, hydro generators are assumed to have fixed active power generation but contributing to the production and absorption of reactive power.

The procedure for incorporating the generator contributions in the OPF formulation is similar to the case of shunt compensation. Its Lagrangian function is given by:

$$L_{gen}(\boldsymbol{x},\lambda) = L = a_i + b_i P_{gi} + c_i P_{gi}^2 \tag{2.109}$$

Its contribution to the linearised system of equations is:

$$\frac{\partial L}{\partial P_{gi}} = b_i + 2c_i P_{gi} - \lambda_{pi} \tag{2.110}$$

$$\frac{\partial^2 L}{\partial P_{gi}^2} = 2c_i \tag{2.111}$$

2.6.5 Example of a Complete OPF Linearised Structure

By way of example, the complete OPF linearised structure corresponding to the 3-node network of Figure 2.3, is shown below. The matrix equation is shown as if all the node mismatch equations were active and all the variables were free. It should be noted that in reality this situation never occurs simultaneously during the solution process.

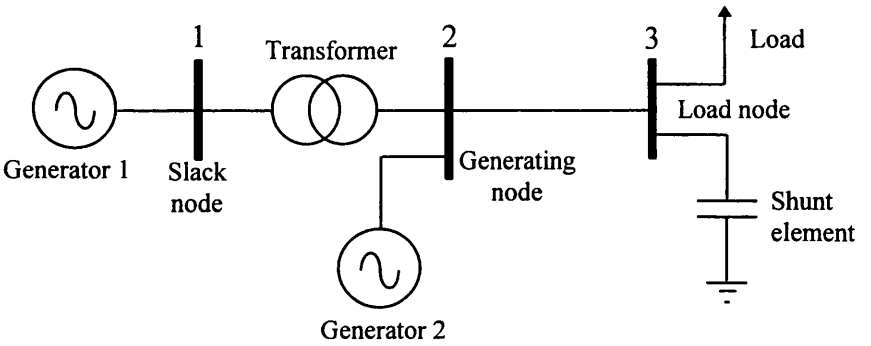

Figure 2.3. 3-node network.

$$
\left[\begin{array}{cccc:cccc:cccc:cc}
H_{11}^{1} & H_{11}^{2} & J_{11}^{1} & J_{11}^{3} & H_{12}^{1} & H_{12}^{2} & J_{12}^{1} & J_{12}^{3} & & & & & & \\
H_{11}^{3} & H_{11}^{4} & J_{11}^{2} & J_{11}^{4} & H_{12}^{3} & H_{12}^{4} & J_{12}^{2} & J_{12}^{4} & & & & & & \\
J_{11}^{1} & J_{11}^{2} & & & J_{12}^{1} & J_{12}^{2} & & & & & & & -1 & \\
J_{11}^{3} & J_{11}^{4} & & & J_{12}^{3} & J_{12}^{4} & & & & & & & & \\
\hdashline
H_{21}^{1} & H_{21}^{2} & J_{21}^{1} & J_{21}^{3} & H_{22}^{1} & H_{22}^{2} & J_{22}^{1} & J_{22}^{3} & H_{23}^{1} & H_{23}^{2} & J_{23}^{1} & J_{23}^{3} & & \\
H_{21}^{3} & H_{21}^{4} & J_{21}^{2} & J_{21}^{4} & H_{22}^{3} & H_{22}^{4} & J_{22}^{2} & J_{22}^{4} & H_{23}^{4} & H_{23}^{4} & J_{23}^{2} & J_{23}^{4} & & \\
J_{21}^{1} & J_{21}^{2} & & & J_{22}^{1} & J_{22}^{2} & & & J_{23}^{1} & J_{23}^{2} & & & & -1 \\
J_{21}^{3} & J_{21}^{4} & & & J_{22}^{3} & J_{22}^{4} & & & J_{23}^{3} & J_{23}^{4} & & & & \\
\hdashline
 & & & & H_{32}^{1} & H_{32}^{2} & J_{32}^{1} & J_{32}^{3} & H_{33}^{1} & H_{33}^{2} & J_{33}^{1} & J_{33}^{3} & & \\
 & & & & H_{32}^{3} & H_{32}^{4} & J_{32}^{2} & J_{32}^{4} & H_{33}^{3} & H_{33}^{4} & J_{33}^{2} & J_{33}^{4} & & \\
 & & & & J_{32}^{1} & J_{32}^{2} & & & J_{33}^{1} & J_{33}^{2} & & & & \\
 & & & & J_{32}^{3} & J_{32}^{4} & & & J_{33}^{3} & J_{33}^{4} & & & & \\
\hdashline
 & & -1 & & & & & & & & & & 2c_1 & \\
 & & & & & & -1 & & & & & & & 2c_2
\end{array}\right]
\tag{2.112}
$$

The incremental vectors of state variables and gradients are,

$$
\left[\begin{array}{cccc:cccc:cccc:cc}
\Delta\theta_1 & \Delta V_1 & \Delta\lambda_{p1} & \Delta\lambda_{q1} & \Delta\theta_2 & \Delta V_2 & \Delta\lambda_{p2} & \Delta\lambda_{q2} & \Delta\theta_3 & \Delta V_3 & \Delta\lambda_{p3} & \Delta\lambda_{q3} & \Delta P_1 & \Delta P_2
\end{array}\right]^t
\tag{2.113}
$$

$$
\left[\begin{array}{cccc:cccc:cccc:cc}
\nabla\theta_1 & \nabla V_1 & \nabla\lambda_{p1} & \nabla\lambda_{q1} & \nabla\theta_2 & \nabla V_2 & \nabla\lambda_{p2} & \nabla\lambda_{q2} & \nabla\theta_3 & \nabla V_3 & \nabla\lambda_{p3} & \nabla\lambda_{q3} & \nabla P_1 & \nabla P_2
\end{array}\right]^t
\tag{2.114}
$$

As pointed out above, the submatrices $\boldsymbol{H}$, $\boldsymbol{J}$ and $\boldsymbol{J}^t$ have the same structure as the nodal admittance matrix.

2.7 Handling Inequality Constraints

The set of equality constraints that are included in the Lagrangian function at any stage of the iterative process is called the active set. The set of inequality constraints that must be active at the optimum is called the binding set; the optimal solution will not necessarily require all the inequality constraints to be binding. The binding set is not known a priori and it is the task of the optimisation algorithm to determine it as well as to enforce it. The inequalities that become active during the solution process are changed to equalities and included in the active set. The problem is then to minimise the Lagrangian function for the new active set.

2.7.1 Handling the Inequality Constraints on Variables

The inequality constraints are handled in the OPF formulation by means of the Multipliers method as opposed to the Penalty Function method [36-38]. The inequality constraints when made active are changed to equality constraints. This has the effect of a restraining force which pulls the inadmissible points back into the admissible region. In the Multipliers method a penalty term is added to the Lagrangian function $L(x,\lambda)$, thus forming the Augmented Lagrangian function, as given by equation (2.19). The minimisation of the Lagrangian function is carried out using Newton's method only for the primal variables (state variables). The dual variables, μs, are updated at the end of each global iteration. Multipliers (dual variables) are checked for limit violations and variables within bound limits are ignored.

The inequality constraints are handled by using the following generic form of the function $\psi\,(g(x),\mu)$ [38]:

$$\psi_i(g_i(x),\mu_i)=\begin{cases}\mu_i(g_i(x)-\bar{g}_i)+\dfrac{c}{2}(g_i(x)-\bar{g}_i)^2 & \text{if} \quad \mu_i+c(g_i(x)-\bar{g}_i)\geq 0\\ \mu_i(g_i(x)-\underline{g}_i)+\dfrac{c}{2}(g_i(x)-\underline{g}_i)^2 & \text{if} \quad \mu_i+c(g_i(x)-\underline{g}_i)\leq 0\\ 0 \quad \text{otherwise}\end{cases} \tag{2.115}$$

where $\bar{g}$ and $\underline{g}$ are the limits on the state variables as well as functional constraints.

The multipliers are adjusted as follows:

$$\mu_i^{\,j+1}=\begin{cases}\mu_i^{\,j}+c^j(g_i(x^j)-\bar{g}_i) & \text{if} \quad \mu_i^{\,j}+c^j(g_i(x^j)-\bar{g}_i)\geq 0\\ \mu_i^{\,j}+c^j(g_i(x^j)-\underline{g}_i) & \text{if} \quad \mu_i^{\,k}+c^j(g_i(x^j)-\underline{g}_i)\leq 0\\ 0 \quad \text{otherwise}\end{cases} \tag{2.116}$$

where $$0<c^j<c^{j+1}$$

In Reference [38] it is demonstrated that upon convergence, μ satisfies the optimality conditions as given by Kuhn and Tucker. In this situation, all the state variable increments are smaller than a pre-specified tolerance and no limit violations occur.

The Multipliers method provides an efficient way to handle the binding and non-binding constraints. After moving the variable to one of its limits, the algorithm holds it there as long as it is needed, otherwise the variable can be freed [39]. Equation (2.115) satisfies the Kuhn and Tucker conditions [36-38]:

$$\mu g(x) = 0;\ \mu \geq 0 \tag{2.117}$$

For any given constraint, if the product $\mu g(x)$ is equal to zero, either μ is equal to zero or $g(x)$ is non-binding; if $\mu>0$, then $g(x)$ must be zero. Equation (2.115) provides a means to indicate whether or not a constraint is a binding constraint.

The inequality constraints are assumed to be inactive during the initial evaluation. At the end of each iteration, all variables are checked according to equation (2.115) and updated according to equation (2.116). Equation (2.115) is used for evaluating the gradient vector and matrix $\boldsymbol{W}$. Hence, first and second derivatives of equation (2.115) are required. The first derivative is added to the gradient vector and the second derivative to matrix $\boldsymbol{W}$. It should be noted that when a variable is within limits, the derivatives are null.

The penalty parameter c^j should observe the following practical conditions:

- The initial parameter c^0 should not be so large, to the point that the unconstrained minimisation becomes ill-conditioned.
- The parameter c^j should not be increased too fast, to the point that the unconstrained minimisation becomes numerically unstable.
- The parameter c^j should not be increased too slowly, to extent that the multiplier iterations have a poor convergence rate.

It is difficult to determinate a suitable values for the penalty parameter. A scheme that usually works well is one where a moderate value of c^0 is chosen by trial and error and subsequent values of c^j are monotonically increased according $c^{j+1} = \beta\, c^j$, where β is a scalar greater than 1.

The Multipliers method fulfils the requirements of inequality constraints enforcement in Newton's method. It provides a means for shifting a variable to the appropriate limit together with the simultaneous appropriate correction of all the other variables.

2.7.2 Handling Inequality Constraints on Functions of Variables

Arguably, the most important functional inequality constraints are those corresponding to controllable sources of reactive power. Reactive power generator limits are checked at the end of each global iteration. It should be pointed out that the reactive power equation of each generator is placed in the matrix $\boldsymbol{W}$, however, when the generator is within limits, the method places a large number in the diagonal element associated to λ_q. Hence, the corresponding equation is deactivated and its effects nullified. The functional inequality constraints are activated only when it becomes necessary to enforce either upper or lower limits on reactive power. This is done by removing the large number from the corresponding diagonal element. Penalty function techniques are used to either activate or deactivate the equations corresponding to generation nodes.

Quadratic penalty functions are used since they have first and second derivatives. The form of the penalty function for reactive power constraint at generation node k is [36-38],

$$E_{qi} = \frac{1}{2} S \lambda_{qi}^2 \tag{2.118}$$

and its first and second derivatives are,

$$\frac{dE_{qi}}{d\lambda_{qi}} = S\lambda_{qi} \tag{2.119}$$

$$\frac{d^2E_{qi}}{d^2\lambda_{qi}} = S \tag{2.120}$$

where S is a positive large, penalty weighting factor.

Adding the first and second derivatives to the corresponding gradient and diagonal element in matrix $\boldsymbol{W}$ associated with λ_{qi}, deactivates the reactive power flow equations of the generation node i. In this situation λ_{qi} has a zero value. When a reactive power limit is violated, the derivatives are removed and the node changes from being a generation node to a load node, then λ_{qi} changes its value from zero to nonzero. The sign of λ_{qi} indicates whether or not the reactive power has returned to be within limits.

Table 2.1. Constraints on reactive power injections

Limit	$\lambda_{qi} < 0$	$\lambda_{qi} > 0$
Upper	to add penalty term	to remove penalty term
Lower	to remove penalty term	to add penalty term

2.8 Implementation of OPF Using Newton's Method

The mathematical formulation for the active power optimisation has been presented in some detail in the previous Sections. This Section deals with aspects concerning its practical implementation. The main steps are shown in Figure 2.4 and key additional aspects are explained below. Three main process can be seen from the flow diagram: the initialisation of all the control variables, the main iteration loop and the inner iteration loop corresponding to the Newton process.

The initialisation of the variables includes a lossless economic dispatch, the generators operate within limits at the beginning of the two loops. The OPF initialisation is presented in detail in the following Section.

In the main iterative loop, the state variables $\boldsymbol{x}$ are checked. Here the inequality constraints are either activated or deactivated according to equation (2.115); the multipliers are updated by using (2.116), similarly the penalty weighting factors. If at the end of a main iterative loop there are no changes in the inequality constraint set then the process terminates.

The iterative Newton process is characterised by the fixed values of the multipliers and penalty weighting factors. The linearised system of equations for minimising the active power generation cost is solved. Once the linearised system of equations has been assembled then a sparsity-oriented solution is carried out. This process is repeated until a small, pre-specified tolerance is reached. In the OPF algorithm implemented in this research a tight convergence criterion was adopted for the mismatch gradient vector, i.e 10^{-12}.

An important practical detail is that the matrix $\boldsymbol{W}$ is modified to nullify the increments of the slack angle. This is achieved by placing a large penalty weighting factor in the diagonal element associated with θ_{slack}. Very small increments may still exist but their effect on the rest of the variables is negligible. For practical purposes, the increment $\Delta\theta_{slack}$ is made 0 in every iteration.

2.8.1 Initial Conditions in OPF Solutions

All the state variables x, and all the Lagrange multipliers λ, must be given an initial value at the beginning of the solution procedure. The initial values should be selected by following a engineering judgement in order to ensure a good rate of convergence. Details are given below.

Nodal Voltage Magnitudes and Angles

State variables are initialised similarly to load flow problems, i.e. 1 pu voltage magnitudes and 0 voltage angles for all nodes. This provides a suitable starting condition. Engineering experience indicates that, for most problems, the variation of voltage magnitude and voltage angle from the 1 and 0 initial conditions is relatively small, i.e. $0.95 \leq V_k \leq 1.05$ and $-15^0 \leq \theta_k \leq 15^0$.

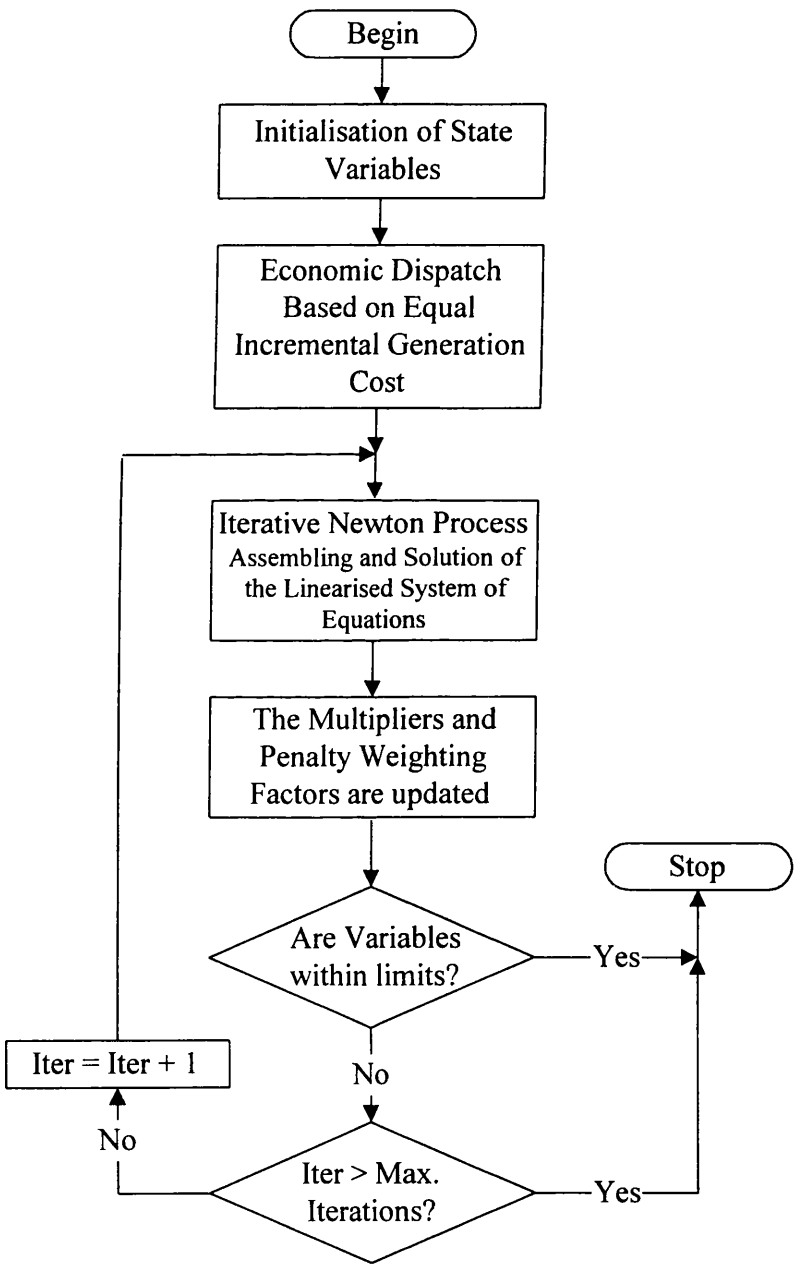

Figure 2.4. Flow chart for active power optimisation.

Active Power Schedule

A lossless economic dispatch as opposed to a load flow solution is used to provide good starting conditions for the full OPF solution. The equal incremental cost criterion is used for this purpose [35]. Different variants of this method are available in the open literature but the one adopted here takes generator limits into consideration, hence, providing more realistic starting conditions.

The Lagrange function is given as,

$$L_{gen}(\boldsymbol{x},\lambda) = L = F_T + \lambda\left(P_d - \sum_{i=1}^{Ng} P_{gi}\right) \tag{2.121}$$

The necessary conditions to minimise active power generation cost are met when the first derivatives with respect to each one of the variable involved is zero:

$$\frac{\partial L}{\partial P_{gi}} = \frac{dF_i(P_{gi})}{dP_{gi}} - \lambda_{pi} = 0 \tag{2.122}$$

It can be seen that the necessary condition for the existence of a minimum generation cost solution is that an equal incremental cost rate exists for all generators. Also, the balance between the generation and the demand has to be met.

$$\sum_{i=1}^{Ng} P_{gi} = P_d \tag{2.123}$$

Moreover, the inequality constraints given by (2.6) have to be satisfied. If this is not the case, an economic dispatch is carried out using Newton's method and the inequality constraints are handled by means of the Multipliers method. The matrix $\boldsymbol{W}$ is built and the set of equations to be solved is:

$$\begin{bmatrix} \frac{d^2F_1}{dP_1^2} & 0 & 0 & 0 & 0 & -1 \\ 0 & \frac{d^2F_2}{dP_2^2} & 0 & 0 & 0 & -1 \\ 0 & 0 & \frac{d^2F_3}{dP_3^2} & 0 & 0 & -1 \\ 0 & 0 & 0 & \ddots & 0 & \vdots \\ 0 & 0 & 0 & 0 & \frac{d^2F_{Ng}}{dP_{Ng}^2} & -1 \\ -1 & -1 & -1 & \cdots & -1 & 0 \end{bmatrix} \begin{bmatrix} \Delta P_1 \\ \Delta P_2 \\ \Delta P_3 \\ \vdots \\ \Delta P_{Ng} \\ \Delta\lambda \end{bmatrix} = -\begin{bmatrix} \frac{\partial L}{\partial P_{g1}} \\ \frac{\partial L}{\partial P_{g2}} \\ \frac{\partial L}{\partial P_{g3}} \\ \vdots \\ \frac{\partial L}{\partial P_{Ng}} \\ P_d - \sum_{i=1}^{Ng} P_{gi} \end{bmatrix} \tag{2.124}$$

When Newton's method is applied to solve the lossless economic dispatch using the quadratic cost function and no violations exist, the optimal solution is reached in one step. Otherwise, generation limits are enforced in order to start the solution of the complete OPF problem from a feasible operating condition.

Lagrange Multipliers

The Lagrange multipliers for active and reactive power flow mismatch equations are initialised at the λ_p given by the lossless economic dispatch and 0, respectively. These values give rise to very robust iterative solutions.

Penalty Weighting Factors

The Multipliers method has been found to be more effective than the better known penalty function method. The former is a less empirical method, where the weighting parameter c is selected according to the following guidelines:

- Values of c^o within the range 10^2 - 10^5 have proved effective starting conditions. Larger values of c^o have led to numeric difficulties during the factorisation process of matrix $\boldsymbol{W}$. For all the tested cases, a value of c^o = 1000 was chosen for voltages magnitude constraints, whereas for active power constraints, the value chosen was the largest quadratic coefficient of the cost curves multiplied by 1000.
- In subsequent iterations, the parameter c is increased by a constant factor β. Values of β = 1.3 produce very reliable solutions. Larger values of β led to ill-conditioned situations whereas smaller values of β led to a slow rate of convergence.

The weighting factor S, in equation (2.118)-(2.120), is a positive parameter as large as 10^{10}. It provides an effective enforcement on the functional inequality constraints for a controllable sources of reactive power. No numerical problems have been encountered with this value of S.

2.8.2 Conjugated Variables

The voltage magnitude and MVAR generation at a given node are strongly interlinked. If a pair of these variables are simultaneously outside limits during the solution process, only one of them will be made active in the first instance, not both of them at the same time. The voltage magnitude is bounded first, i.e. the MVAR generation is not made active if its associated voltage magnitude is outside limits. If these variables are bounded and they are about to be released at the end of a main iteration, only one of them will be released at the time.

2.8.3 Sparsity Techniques

In the OPF using Newton's method the major computational effort lies on forming and solving a sparse, large system of linear equations [25]. Therefore the efficiency of the algorithm depends on the efficiency of its sparsity operations. The efficiency of the algorithm is greatly improved if the reactive power equations of each generator are incorporated in the matrix $\boldsymbol{W}$. The advantage of this approach stems from the fact that the ordering is done only once in the whole iterative procedure.

Depending on the system conditions and parameters, some diagonal terms may have a very small absolute value. Numerical problems may therefore be found in the process of solving the linear set of equations. The following procedure has been implemented to overcome these kind of problems, which make the solution process more stable [6,7]: At each pivoted term, if the absolute value of the pivoted term is smaller than the value of a chosen absolute threshold, e.g. 10^{-7}, then, it is replaced by the absolute value of the threshold, e.g. 10^{-3}, with the corresponding sign.

2.8.4 Programming

The OPF computer program has been written in C++ under a UNIX environment [26-30,41]. The development of the program follows the algorithm described in previous sections. C++ has become one of industry's computer language of choice owing to its accelerated production cycles and its close association with C. C++ is an enhanced version of C. It retains the efficient programming capabilities of C. Solutions obtained with newly developed software in C++, for example load flows, have shown to be almost as fast as the solutions given by a load flow program written in FORTRAN [28,29,30].

2.9 Optimal Power Flow Test Cases

To illustrate the robustness of the OPF Newton program towards the convergence, it has been applied to the solution of a large number of power networks of different sizes and varying degrees of operational complexity. System sizes range from 5 to 166 nodes [31-34,39,42]. Most of these systems are available in open literature, except the 166-node system, which corresponds to a real life power network. In this Chapter, only the test networks available in the open literature are studied [31-33,39,42].

The inequality constraints considered are maximum and minimum generator active and reactive power limits, and the maximum and minimum node voltage magnitudes. The objective function is the minimisation of active power generation cost. The network data, which are also required by conventional load flows were mainly taken from Reference [33]. The additional data required by the optimisation procedure, such as fuel cost curves, and upper and lower limits for variables, were given typical values when not available in the open literature.

In order to validate the solutions given by the OPF program written by this author, several test systems, including no FACTS devices were also solved with commercial software. The PSS/OPF module of the Power Technologies Inc. (PTI) package was used for this purpose. This software is highly reliable and used throughout the world, however, it has no FACTS device modelling capabilities.

The Optimal Power Flow is solved by iteration, and the tolerances used for the detection of the various types of constraint violations should be properly co-ordinated to prevent the solution process from entering into endless loops. The tolerance for the mismatch gradient vector components was 10^{-12}, whereas for the voltage magnitudes and active powers it was 10^{-6}.

2.9.1 5-node Test System

The solution vector $\boldsymbol{x}^{opt}$ for all the control variables for this system is given in Tables 2.2 to 2.4 while the power flow results are shown in Figure 2.5. These tables also show the voltage magnitude limits at each node, the cost coefficients of the generating units, the maximum and minimum generator active and reactive power limits. In Table 2.2, columns 4 to 6 correspond to the PTI solution and columns 7 to 9 correspond to the solution given by the OPF algorithm developed by the author. During the iterative process there were violations, but the Multipliers method handled the violations very efficiently. For example, the voltage magnitude in node South was suitably bounded at its upper limit at the end of the solution process. Tables 2.3 to 2.4 show the active and reactive power dispatch of all generators and their operation cost. Finally, Table 2.5 summarises the most important quantities where it can be seen that the active power

generation cost for this test network is 747.98 $/hour and the active power losses are 3.050 MW. It can also be observed that the solution given by the OPF algorithm agrees very well with the results given by the PTI program.

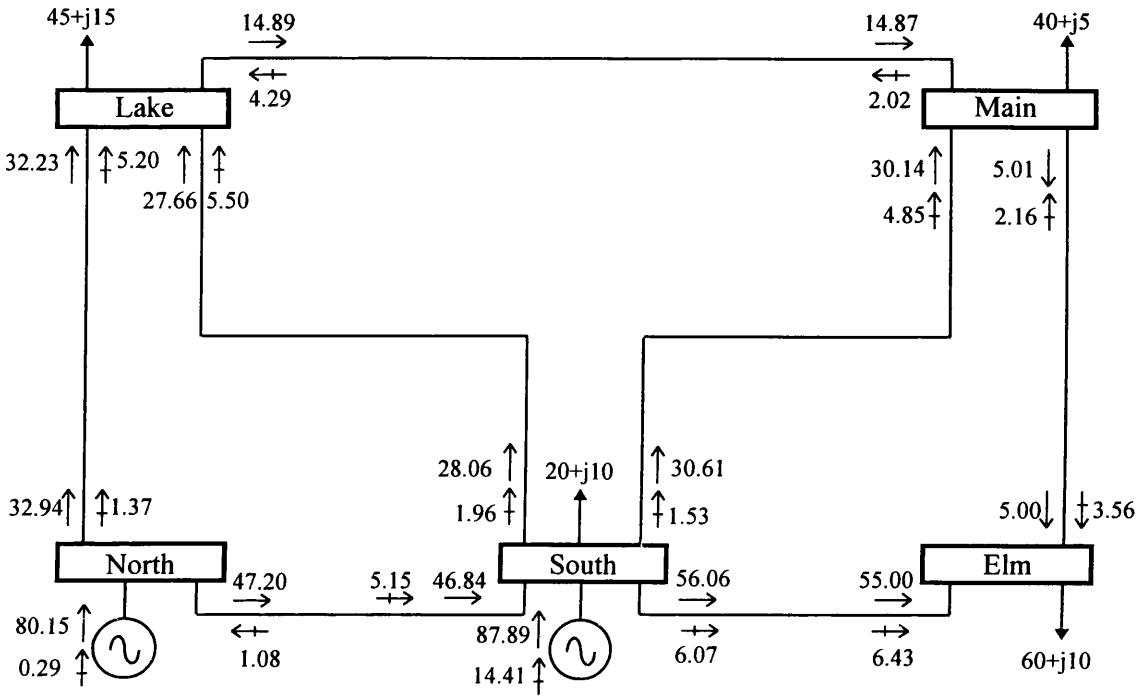

Figure 2.5. Five-node test network and optimal load flow results.

Table 2.2. Limits and nodal information for 5-node system.

Node	Voltage Limits		PTI Power System Simulator			OPF Program Developed		
	Min (pu)	Max (pu)	Voltage (pu)	Angle (degrees)	λ_p ($/MWhr)	Voltage (pu)	Angle (degrees)	λ_p ($/MWhr)
Elm	0.90	1.10	1.0726	-4.42	4.2639	1.0726	-4.42	4.2639
Main	0.90	1.10	1.0779	-3.85	4.2341	1.0779	-3.85	4.2341
Lake	0.90	1.10	1.0784	-3.62	4.2232	1.0784	-3.62	4.2232
South	0.90	1.10	1.1000	-1.31	4.1032	1.1000	-1.31	4.1032
North	0.90	1.50	1.1096	0.00	4.0412	1.1096	0.00	4.0412

Table 2.3. Limits on active power generation and optimal solution for 5-node system.

Node	Cost Coefficients			Active Power Limits		PTI	OPF
	a ($/hr)	*b* ($/MWhr)	*c* ($/MW^{2}hr)	Min (MW)	Max (MW)	(MW)	(MW)
South	60.0	3.40	0.0040	30.00	200.0	87.90	87.90
North	60.0	3.40	0.0040	30.00	200.0	80.15	80.15

Table 2.4. Limits on reactive power generation and optimal solution for 5-node system.

Node	Reactive Power Limits		PTI	OPF
	Min (MVAR)	Max (MVAR)	(MVAR)	(MVAR)
South	-300.00	300.00	14.41	14.41
North	-300.00	300.00	0.30	0.30

Table 2.5. Summary of optimal solution for 5-node system.

Results	PTI	OPF
Active power generation cost ($/hr)	747.98	747.98
Active power losses (MW)	3.050	3.050
Active power generation (MW)	168.05	168.05
Reactive power generation (MVAR)	14.70	14.71

To compare the different type of results given by Load Flow and OPF programs, the 5-node test network was solved by using a Newton-Raphson Load Flow program. The voltage magnitude to be maintained by the generators South and North were 1.00 and 1.06 pu, respectively, and the active power generated at node South was assumed equal to 40 MW. It should be noted that these operating conditions correspond to those given in Reference [39], and they are not associated in any way with an optimal operation of the network.

The network and the power flow results are shown in Figure 2.6 while the final nodal complex voltages are given in Table 2.6. A summary of the most important quantities is shown in Table 2.7.

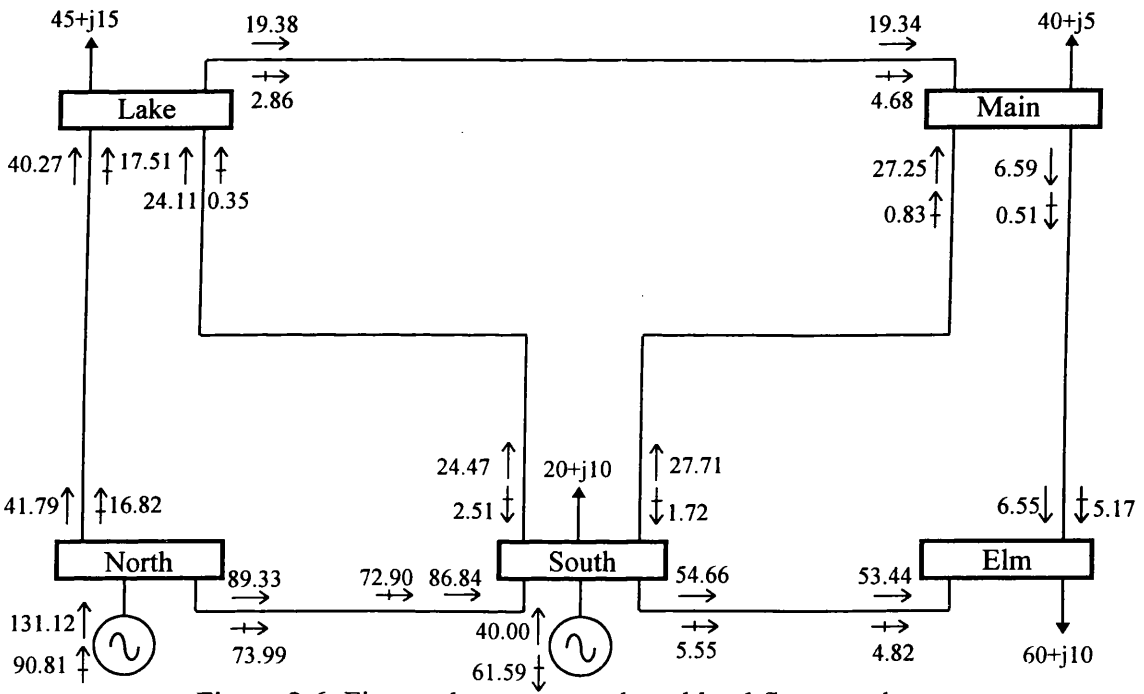

Figure 2.6. Five-node test network and load flow results.

Table 2.6. Nodal complex voltages for the 5-node system.

Complex Voltage	Nodes				
	Elm	Main	Lake	South	North
Voltage Magnitude (pu)	0.9717	0.9841	0.9872	1.0000	1.0600
Phase Angle (degrees)	-5.77	-4.96	-4.64	-2.06	0.00

Table 2.7. Summary of load flow solution for 5-node system.

Results	Load Flow	OPF
Active power generation cost ($/hr)	776.99	747.98
Active power losses (MW)	6.122	3.050
Active power generation (MW)	171.12	168.05
Reactive power generation (MVAR)	29.22	14.71

It can be observed in Figures 2.5 and 2.6 that the flow distribution is more regular when OPF is applied to this system. For example in Figure 2.6, a large active power travels from North to South. It is distributed almost in the same proportion as in Figure 2.5. The reactive power distribution is also irregular in Figure 2.6 where is shown that the generator at node North injects reactive power to the network which is mostly absorbed by generator at node South. Moreover, the voltage magnitudes in the three nodes of type PQ are below 1.0 pu. As a consequence of such irregular power distributions, the generation cost increases by 3.8% and the network losses increase by 100.72% with respect to the OPF solution. If the system were to be operated under the conditions given by the load flow, the total generation is 3.071 MW greater than the conditions given by OPF.

2.9.2 Lagrange Multipliers Meaning

The incorporation of the power flow equations (equality constraints) in the global optimisation problem implicitly requires the computation of the network losses. From the transmission viewpoint, network losses are responsible for increasing the active power generation, and as consequence, the Lagrange multipliers λ_p obtained by the OPF vary at each node. These multipliers are normally greater than the Lagrange multiplier $\lambda_{p\text{-}lossless}$ given by the lossless economic dispatch solution. Figure 2.7 depicts the Lagrange multiplier profile for the 5-node system. It should be noted that only the slack node multiplier is smaller than $\lambda_{p\text{-}lossless}$.

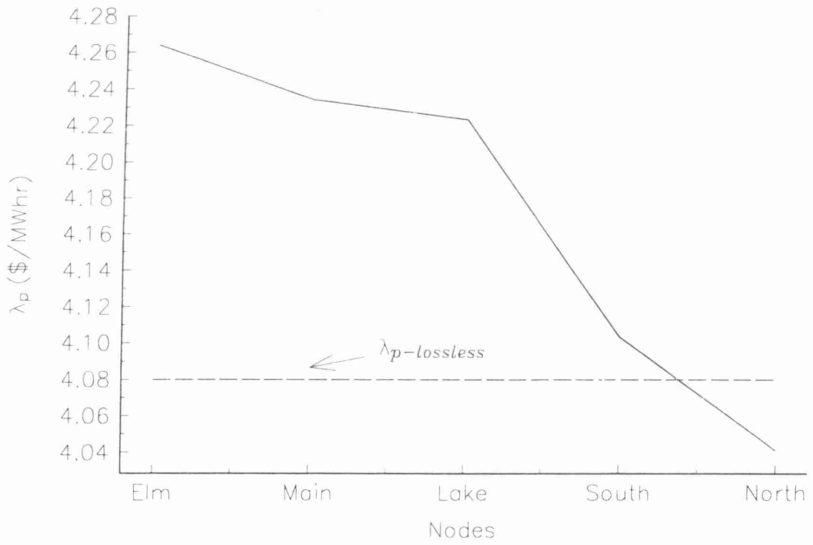

Figure 2.7. Lagrange multiplier profile for the 5-node system.

Important economic information can be derived from λ. Each Lagrange multiplier measures the sensitivity of the objective function to changes in the active power equality constraints at the optimum point [43]. At node *k* the relation is,

$$\lambda_k = \frac{\partial f(\boldsymbol{x}^*)}{\partial h_k(\boldsymbol{x}^*)} \tag{2.125}$$

For example, if the active power load at Main is increased by 1 MW, the total generation cost of the system, which is 747.98 $/hour, would be increased to 752.2141 $/hour, i.e. 747.98 + (4.2341 x 1) = 752.2141. It should be noted that λ_p at Main is 4.2341 $/MWhr.

The Lagrange multipliers associated with the reactive power balance, λ_q, also provide information similar to that of λ_p. In a lossless economic dispatch solution, they are all zero at each node. They measure the sensitivity of the objective function to changes in the reactive power equality constraints. Their effect on the objective function is practically null in most cases. However, the active power generation cost is affected indirectly by the network losses because they are susceptible to changes in generator reactive power injections. If λ_{qk} is large, then node k should be provided with a bank of capacitors aiming at reducing network losses. If the generator connected at node k is operating within reactive power limits the λ_{qk} is equal to 0. This means that an increment in the reactive load at node k is supplied locally by the generator, and network losses are not increased as a result of such increment. Table 2.8 gives the λ_q for the 5-node test system.

Table 2.8. Lagrange multipliers, λ_q, associated with the 5-node system.

OPF	Nodes				
	Elm	Main	Lake	South	North
λ_q ($/MWhr)	0.0228	0.0185	0.0209	0.0000	0.0000

If the reactive power load at Main is increased by 1 MVAR, the total generation cost of the system would be increased to 748.0985 $/hour, i.e. 747.98 + (0.0185x 1) = 748.0985 since λ_q at Main is 0.0185 $/MWhr.

2.9.3 9-node Test System

The main active and reactive power results for the 9-node test system are given in Table 2.9, where all the variables are inside the limits. During the iterative process it could be observed that there were voltage violations in Nod_1, Nod_6 and Nod_8, however, they were bounded at the end of the solution process. There were no violations in the variables of the generating units. The OPF converged in 5 iterations. Unfortunately, no such information was possible to obtain for the PTI solution.

Table 2.9. Summary of the optimal power flow solution for 9-node system.

Node	PTI Power System Simulator			OPF		
	Act. Power (MW)	Reac. Power (MVAR)	Cost ($/hr)	Act. Power (MW)	Reac. Power (MVAR)	Cost ($/hr)
Nod_1	89.80	12.96	1486.01	89.80	12.96	1486.01
Nod_2	134.32	0.03	2294.76	134.32	0.03	2294.76
Nod_3	94.19	-22.63	1515.92	94.19	-22.63	1515.92
Totals	318.31	-9.63	5296.69	318.31	-9.63	5296.69
Losses	3.307 (MW)			3.307 (MW)		

2.9.4 11-node Test System

Table 2.10 shows the main results of the minimisation process for this test system. Converge was obtained in 4 iterations. The final active power generation cost is 1253.69 $/hour and the active power losses are 10.265 MW. The active set was made up by the voltage magnitude at Nod_6. There were no violations in the variables of the generating units. It should be noted that the reactive power generated at Nod_3 is almost at its lower limit. However, the tolerances used in the algorithm allow to control (to activate or to deactivate) of all the variables involved in the process.

Table 2.10. Summary of the optimal power flow solution for 11-node system.

Node	PTI Power System Simulator			OPF		
	Act. Power (MW)	Reac. Power (MVAR)	Cost ($/hr)	Act. Power (MW)	Reac. Power (MVAR)	Cost ($/hr)
Nod_1	47.36	26.31	221.71	47.35	26.23	221.67
Nod_2	74.70	43.63	336.31	74.70	43.56	336.27
Nod_3	48.54	0.20	234.46	48.54	0.08	234.44
Nod_4	47.60	14.13	226.79	47.60	14.31	226.83
Nod_5	52.07	13.38	234.43	52.08	13.48	234.49
Totals	270.26	97.65	1253.69	270.26	97.66	1253.69
Losses	10.260 (MW)			10.265 (MW)		

2.9.5 30-node Test System

The key points of the active and reactive power dispatch solution for this system are given in Table 2.11. The OPF converged in 6 iterations. The solution shows that all the variables are inside the limits. During the iterative process it could be observed that there were violations but the Multipliers method handled these violations rather well. For example, the voltage magnitudes in Nod_9 and Nod_12, and the active power generation at Nod_8 and Nod_11 were bounded at the end of the solution process. Furthermore, the quadratic penalty function enforced the reactive power generated at Nod_8 at its lower limit. It should be noted that the Multipliers method and the Penalty function allow to handle inequality constraints on variables and inequality constraints on functions of variables at the same node without conflict. As in previous cases, the solution given by the OPF algorithm developed in this research agrees very well with the results given by the PTI program.

Table 2.11. Summary of the optimal power flow solution for 30-node system.

Node	PTI Power System Simulator			OPF		
	Act. Power (MW)	Reac. Power (MVAR)	Cost ($/hr)	Act. Power (MW)	Reac. Power (MVAR)	Cost ($/hr)
Nod_1	61.76	2.56	199.81	61.76	2.47	199.80
Nod_2	79.26	20.12	248.63	79.26	19.96	248.63
Nod_5	30.04	26.97	86.43	30.04	26.90	86.43
Nod_8	55.00	40.00	203.86	55.00	40.00	203.86
Nod_11	30.00	2.74	112.50	30.00	2.92	112.50
Nod_13	31.37	-7.09	118.70	31.37	-6.95	118.70
Totals	287.42	85.30	969.91	287.42	85.30	969.91
Losses	4.021 (MW)			4.020 (MW)		

2.9.6 57-node Test System

Table 2.12 shows the main results of the minimisation process for this test system. Convergence was obtained in 6 iterations. The active power generation cost is 3176.39 $/hour, and the active power losses are 19.060 MW. The binding set at the optimum included the voltage magnitude at Nod_46, four active power generations at their upper limit and two reactive power generations at their upper limit.

Table 2.12. Summary of the optimal power flow solution for 57-node system.

Node	PTI Power System Simulator			OPF		
	Act. Power (MW)	Reac. Power (MVAR)	Cost ($/hr)	Act. Power (MW)	Reac. Power (MVAR)	Cost ($/hr)
Nod_1	265.33	72.73	783.78	265.35	73.30	783.91
Nod_2	100.00	50.00	130.20	100.00	50.000	130.20
Nod_3	140.00	36.74	238.20	140.00	37.01	238.20
Nod_6	100.00	6.37	130.20	100.00	5.78	130.20
Nod_8	276.97	55.79	850.42	276.93	54.67	850.19
Nod_9	100.00	9.000	130.20	100.00	9.00	130.20
Nod_12	287.56	48.250	913.39	287.58	49.04	913.49
Totals	1269.86	278.90	3176.39	1269.86	278.90	3176.39
Losses	19.060 (MW)			19.060 (MW)		

2.9.7 118-node Test System

Key details of active and reactive power generation are given in Table 2.13. Convergence was obtained in 10 iterations. In this test system there are 54 active power and 54 reactive power generators inside limits. The binding set at the optimum solution consists of eight voltage magnitudes at their upper limit and 6 reactive powers, four at their lower limit and two at their upper limit. The final active power generation cost is 4717.08 $/hour and the active power losses are 47.46 MW. It can be seen that the solution given by OPF algorithm compares very well with the results given by the PTI program.

Table 2.13. Summary of the optimal power flow solution for 118-node system.

Node	PTI Power System Simulator			OPF		
	Act. Power (MW)	Reac. Power (MVAR)	Cost ($/hr)	Act. Power (MW)	Reac. Power (MVAR)	Cost ($/hr)
Nod_1	79.04	15.00	86.38	79.04	15.00	86.38
Nod_4	78.31	45.94	85.01	78.31	45.73	85.01
Nod_6	78.72	26.71	85.78	78.72	26.66	85.78
Nod_8	78.32	-136.88	85.03	78.32	-136.53	85.03
Nod_10	77.67	-130.86	83.82	77.67	-130.83	83.83
Nod_12	79.48	46.84	87.21	79.48	46.77	87.21
Nod_15	79.10	10.89	86.49	79.10	11.01	86.49
Nod_18	78.33	14.89	85.05	78.33	14.98	85.06
Nod_19	78.64	24.00	85.63	78.64	24.00	85.63
Nod_24	75.76	-24.07	80.32	75.75	-24.05	80.31
Nod_25	76.19	-47.00	81.10	76.19	-47.00	81.10
Nod_26	76.52	-28.01	81.70	76.52	-28.04	81.71
Nod_27	77.07	6.03	82.71	77.07	6.04	82.72
Nod_31	77.19	22.53	82.94	77.19	22.56	82.93
Nod_32	76.95	9.42	82.49	76.95	9.42	82.49
Nod_34	81.07	-28.42	90.24	81.07	-27.05	90.25
Nod_36	80.88	16.03	89.88	80.88	16.28	89.88
Nod_40	84.00	29.31	95.96	84.00	29.44	95.96
Nod_42	85.57	11.38	99.09	85.57	11.52	99.10
Nod_46	85.01	-5.94	97.97	85.00	-6.03	97.96
Nod_49	85.88	0.66	99.71	85.88	0.18	99.71
Nod_54	87.81	28.08	103.64	87.82	27.94	103.67
Nod_55	87.56	17.53	103.13	87.57	17.45	103.15
Nod_56	87.75	13.65	103.52	87.75	13.45	103.53

Table 2.13. Summary of the optimal power flow solution for 118-node system (continuation).

Node	PTI Power System Simulator			OPF		
	Act. Power (MW)	Reac. Power (MVAR)	Cost ($/hr)	Act. Power (MW)	Reac. Power (MVAR)	Cost ($/hr)
Nod_59	87.13	74.56	102.25	87.14	74.33	102.27
Nod_61	85.37	30.26	98.69	85.36	29.20	98.68
Nod_62	85.36	9.50	98.67	85.36	9.26	98.67
Nod_65	84.11	17.27	96.17	84.11	16.79	96.18
Nod_66	84.35	-67.00	96.65	84.35	-67.00	96.66
Nod_69	83.24	-131.65	94.46	83.23	-129.63	94.45
Nod_70	78.62	19.11	85.59	78.62	19.34	85.60
Nod_72	74.10	-4.71	77.33	74.10	-4.62	77.33
Nod_73	75.94	-14.99	80.65	75.94	-14.56	80.65
Nod_74	81.34	20.10	90.76	81.34	20.05	90.77
Nod_76	83.18	42.32	94.34	83.17	42.25	94.33
Nod_77	84.14	45.25	96.23	84.14	45.15	96.23
Nod_80	83.95	-24.14	95.86	83.95	-22.93	95.86
Nod_85	78.44	22.68	85.26	78.44	22.54	85.27
Nod_87	72.22	1.12	74.02	72.22	1.25	74.02
Nod_89	78.60	-10.45	85.56	78.60	-10.55	85.55
Nod_90	79.60	34.61	87.44	79.60	34.56	87.45
Nod_91	77.60	-0.95	83.69	77.60	-1.00	83.69
Nod_92	78.82	24.56	85.97	78.82	24.38	85.98
Nod_99	78.62	3.71	85.59	78.62	3.64	85.59
Nod_100	77.64	58.18	83.77	77.65	58.17	83.79
Nod_103	74.34	22.11	77.76	74.34	22.45	77.77
Nod_104	73.89	12.35	76.96	73.92	14.79	77.01
Nod_105	73.56	-8.00	76.37	73.59	-8.00	76.44
Nod_107	73.20	-0.18	75.74	73.23	0.53	75.80
Nod_110	70.12	-8.00	70.40	70.10	-8.00	70.38
Nod_111	67.96	1.80	66.77	67.94	0.67	66.74
Nod_112	70.05	9.45	70.28	70.03	8.48	70.25
Nod_113	77.26	-26.70	83.06	77.26	-26.59	83.07
Nod_116	83.89	47.80	95.74	83.89	45.00	95.75
Totals	4289.46	137.68	4717.09	4289.46	138.86	4717.08
Losses	47.460 (MW)			47.463 (MW)		

2.10 Conclusions

The OPF algorithm presented in this Chapter is a direct application of Newton's method for the minimisation of a multivariable non-linear function. An iteration of the OPF algorithm consists of the simultaneous solution of all the unknown variables in the problem via Lagrange functions. Second partial derivatives of the Lagrange function with respect to all the variables and the Lagrange multipliers are determined and the resultant terms are suitably accommodated in matrix W. This matrix has a block matrix structure where each block stores 12 non-zero elements per node. In the formulation presented in this Chapter, all the variables are processed identically in the simultaneous solution.

An OPF solution can be thought of as finding the operating state of the power network which optimises a specific objective when the network is subjected to physical and

operating constraints. Active power generation cost is the most popular objective function used today.

Six test systems, containing no FACTS devices ranging from 5 to 118 nodes, were used to demonstrate the numerical performance of the OPF algorithm developed in this research. The solutions for all test systems were achieved in 3 to 9 iterations. In all cases, the solution given by the OPF algorithm compared very well with the results given by a commercial OPF used widely throughout the world, i.e., the PTI program. At the optimum solution, the gradient vector satisfies a pre-specified tolerance of 10^{-12} for all the variables. This comparison exercise should give potential users of the OPF program, sufficient confidence about the fidelity of the results.

An OPF program is an effective tool for power systems analysis. It provides a realistic and effective way to obtain the minimisation of production cost of active power dispatch within the specified plant and transmission network operating limits. The optimal redistribution of generated active power results in a significant reduction in the active power generation cost and active power transmission losses.

2.11 References

[1] Dommel H.W. and Tinney W.F.: 'Optimal Power Flow Solutions', IEEE Transactions on Power Apparatus and Systems, Vol. PAS-87, No. 10, October 1968, pp. 1866-1876.

[2] Sun D.I., Ashley B., Brewer B., Hughes A. and Tinney W.F.: 'Optimal Power Flow By Newton Approach', IEEE Transactions on Power Apparatus and Systems, Vol. PAS-103, No. 10, October 1984, pp. 2864-2880.

[3] Sun D.I., Hu T.I., Lin G.S., Lin C.J. and Chen C.H.: 'Experiences with Implementing Optimal Power Flow for Reactive Scheduling in the Taiwan Power System', IEEE Transactions on Power Systems, Vol. 3, No. 3, August 1988, pp. 1193-1200.

[4] Hong Y.Y.: 'Enhanced Newton Optimal Power Flow Approach Experiences in Taiwan Power System', IEE Proceedings-C, Vol. 139, No. 3, May 1992, pp. 205-210.

[5] Santos Jr. A., Dackmann D. and Soares S.: 'A Dual Augmented Lagrangian Approach for Optimal Power Flows', IEEE Transactions on Power Systems, Vol. 3, No. 3, August 1988, pp. 1020-1025.

[6] Monticelli A. and Liu W.H.E.: 'Adaptive Movement Penalty Method for the Newton Optimal Power Flow', IEEE Transactions on Power Systems, Vol. 7, No. 1, February 1992, pp. 334-342.

[7] Maria G.A. and Findlay J.A.: 'A Newton Optimal Power Flow Program for Ontario Hydro EMS', IEEE Transactions on Power Systems, Vol. PWRS-2, No. 3, August 1987, pp. 576-584.

[8] El-Abiad A.H. and Jaimes F.J.: 'A Method for optimum Scheduling of Power and Voltage Magnitude, IEEE Transactions on Power Apparatus and Systems, Vol. PAS-88, No. 4, April 1969, pp. 413-422.

[9] Sasson A.M.: 'Nonlinear Programming Solutions for Load-Flow, Minimum-Loss, and Economic Dispatching Problems', IEEE Transactions on Power Apparatus and Systems, Vol. PAS-88, No. 4, April 1969, pp. 399-409.

[10] Sasson A.M.: 'Combined use of the Powell and Fletcher-Powell Non-linear Programming Methods for Optimal Load Flows', IEEE Transactions on Power Apparatus and Systems, Vol. PAS-88, No. 10, October1969, pp. 1530-1537.

[11] Sasson A.M., Viloria F. and Aboytes F.: 'Optimal Load Flow Solution Using the Hessian Matrix', IEEE Transactions on Power Apparatus and Systems, Vol. PAS-92, No. 1, January/February 1973, pp. 31-41.

[12] Sasson A.M. and Merrill H.M.: 'Some Applications of Optimization Techniques to Power System Problems', Proceedings of the IEEE, Vol. 62, No. 7, July 1974, pp. 959-972.

[13] Happ H.H.: 'Optimal Power dispatch - A Comprehensive Surrey', IEEE Transactions on Power Apparatus and Systems, Vol. PAS-96, No. 3, pp. 841-854, May/June 1977.

[14] Burchett R.C., Happ H.H. and Wirgau K.A.: 'Large Scale Optimal Power Flow', IEEE Transactions on Power Apparatus and Systems, Vol. PAS-101, No. 10, October 1982, pp. 3722-3732.

[15] Franchi L., Innorta M., Marannino P. and Sabelli C.: 'Evaluation of Economy and/or Security Functions for Reactive Power Scheduling in Large Scale Power Systems', IEEE Transactions on Power Apparatus and Systems, Vol. PAS-102, No. 10, October 1983, pp. 3481-3488.

[16] Burchett R.C., Happ H.H. and Vierath D.R.: 'Quadratically Convergent Optimal Power Flow', IEEE Transactions on Power Apparatus and Systems, Vol. PAS-103, No. 11, November 1984, pp. 3267-3275.

[17] El-Hawary M.E. and Tsang D.H.: 'The Hydro-Thermal Optimal Power Flow, A Practical Formulation and Solution Technique using Newton's Approach', IEEE Transactions on Power Systems, Vol. PWRS-1, No. 3, August 1986, pp. 157-167.

[18] Qiu J. and Shahidehpour S.M.: 'A new Approach for Minimizing Power Losses and Improving Voltage Profile', IEEE Transactions on Power Systems, Vol. PWRS-2, No. 2, pp. 287-297, May 1987.

[19] Alsac O., Bright J., Prais M. and Stott B.: 'Further Developments in LP-Based Optimal Power Flow', IEEE Transactions on Power Systems, Vol. 5, No. 3, August 1990, pp. 697-711.

[20] Gribik P.R., Shirmohammadi D., Hao S. and Tomas C. L.: 'Optimal Power Flow Sensitivity Analysis', IEEE Transactions on Power Systems, Vol. PWRS-5, No. 3, August 1990, pp. 969-976.

[21] Huneault M. and Galiana F.D.: 'A Survey of the Optimal Power Flow Literature', IEEE Transactions on Power Systems, Vol. 6, No. 2, May 1991, pp. 762-770.

[22] Tinney W.F. and Hart C.E.: 'Power Flow Solution by Newton's Method', IEEE Transactions on Power Apparatus and Systems, Vol. PAS-96, No. 11, November 1967, pp. 1449-1460.

[23] Stott B.: 'Review of Load-Flow Calculations Methods', IEEE Proceedings, Vol. 62, July 1974, pp. 916-929.

[24] Stott B.: 'Effective Starting Process for Newton-Raphson Load Flows', IEE Proceedings, Vol. 118, No. 8, August 1971, pp. 983-987.

[25] Tinney W.F. and Walker J.M.: 'Direct Solutions of Sparse Network Equations by Optimally Ordered Triangular Factorization', Proceedings of IEEE, Vol. 55, November 1967, pp. 1801-1809.

[26] Foley M., Bose A., Mitchell W. and Faustini A.: 'An Object Based Graphical User Interface for Power Systems', IEEE Transactions on Power Systems, Vol. 8, No. 1, February 1993, pp. 97-104.

[27] Neyer A.F., Wu F.F. and Imhof K.: 'Object Oriented Programming for Flexible Software: Example of a Load Flow', IEEE Transactions on Power Systems, Vol. 5, No. 3, August 1990, pp. 689-696.

[28] Hakavik B. and Holen A.T.: 'Power System Modelling and Sparse Matrix Operations Using Object Oriented Programming', IEEE Transactions on Power Systems, Vol. 9, No. 2 , May 1994, pp. 1045-1051.

[29] Foley M. and Bose A.: 'Object-Oriented On-Line Network Analysis', IEEE Transactions on Power Systems, Vol. 10, No. 1, February 1995, pp. 125-132.

[30] Fuerte-Esquivel C.R., Acha E., Tan S.G. and Rico J.J.: 'Efficient Object Oriented Power System Software for the Analysis of Large-Scale Networks Containing FACTS-Controlled Branches', IEEE Transactions on Power Systems, Vol. 13, No. 2, May 1998, pp. 464-472.

[31] Wu Q.H. and Ma J.Y.: 'Power system optimal reactive power dispatch using evolutionary programming', IEEE Transactions on Power Apparatus and Systems, Vol. 10, No. 3, August 1995, pp. 1243-1249.

[32] Divi R. and Kesavan J.A.: 'A Shifted Penalty Function Approach for Optimal Load-Flow', IEEE Transactions on Power Apparatus and Systems, Vol. PAS-101, No. 9, September 1982, pp. 3502-3512.

[33] Freris L.L. and Sasson A.M.: 'Investigation of the Load-Flow Problem', IEE Proceedings, Vol. 115, No. 10, October 1968, pp. 1459-1470.

[34] Aboytes F. and Arroyo G.: 'Security Assessment in the Operation of Longitudinal Power Systems', IEEE Transactions on Power Apparatus and Systems, Vol. PWRS-1, No. 2, May 1986, pp. 225-232.

[35] Wollenberg B. and Wood A. J., 'Power Generation, Operation and Control', John Wiley & Sons Inc., Second Edition, 1984.

[36] Luenberger D.G.: 'Introduction to Linear and Nonlinear Programming', Addison-Wesley Publishing Co., Second Edition, 1984.

[37] Gill P.E., Murray W. and Wright M.: 'Practical Optimisation', Academic Press 1981.

[38] Bertsekas D.P.: 'Constrained Optimization and Lagrange Multiplier Methods', Academic Press, 1982.

[39] Stagg G.W. and El-Abiad A.H.: 'Computer Methods in Power Systems Analysis', McGraw-Hill, 1968.

[40] Elgerd O.I.: 'Electric Energy System Theory: An Introduction', McGraw-Hill, Second Edition, 1983.

[41] Buzzi-Ferraris G.: 'Scientific C++, Building Numerical Libraries the Object Oriented Way', Addison-Wesley, 1994.

[42] Anderson P.M. and Fouad A.A.: 'Power System Control and Stability', The Iowa State University Press, 1986.

[43] Shen C.M. and Laughton M.A.: 'Determination of Optimum Power-System Operating Conditions Under Constraints', IEE Proceedings, Vol. 116, No. 2, February 1969, pp. 225-239.

Chapter 3

Advanced Transformer Control Modelling in an Optimal Power Flow

This Chapter reports on advanced transformer modelling facilities suitable for large-scale OPF studies. The new, more comprehensive transformer models are developed from first principles and incorporated into an existing Newton-based Optimal Power Flow computer program for highly robust iterative solutions. A three-winding transformer model with tap ratios in all three windings is shown to be a general case for existing two-winding transformer models and the classic phase-shifting transformer and load tap-changing transformer models. The newly developed transformer models add a great deal to software flexibility and are amenable to more realistic electric energy studies. This is partly due to the transformer models being fitted with complex tap changers in each winding and a non-linear representation of the magnetising branch. The OPF strong convergence characteristics are demonstrated using test networks of different size.

3.1 Introduction

Power system transformer models for studies at the fundamental frequency have been in existence for many years [1,2,15,16,20,21]. These transformer representations incorporate Load Tap-Changing (LTC) and Phase-Shifting control modelling facilities and are suitable for large-scale Load Flows [1,15,16] and Optimal Power Flows (OPF) [2,3,4] studies. However, there is growing concern among practising engineers that these transformer models may have various shortcomings [5] including model inflexibility and a lack of magnetising branch representation. These models were developed bearing in mind the structure of high-voltage transmission circuits, e.g. the tap-changing facilities are assumed to be on the primary side of the transformer [1-3,15,16,20,21].

Over the years there have been repeated calls by experienced engineers that the transformer magnetising branch be modelled in power flow algorithms in order to conduct more realistic electric energy studies [5]. Good progress has been achieved in this direction and a two-winding transformer model, developed within the context of load flow solutions [5,6,7], is in daily use in most UK distribution companies. However, three-winding transformer models for load flow studies do not seem to be

highly developed and with the growing interest in the use of FACTS devices at the transmission and distribution levels [8,9], it is most important that fully fledged three-winding transformer models be made available in the open literature.

This Chapter now reports on more advanced transformer models than the ones currently available in the open literature [1-3,5-7,15,16,20,21]. Comprehensiveness and flexibility have been the over-riding concerns while developing these new models. Considering the need to conduct realistic energy studies in a de-regulated environment, these models have been developed within the context of optimal power flows; a subject of considerably more engineering and mathematical complexity than load flows.

A generalised, three-winding transformer model is developed from first principles, which caters for both Load Tap-Changing (LTC) transformers and Phase-Shifting Transformers (PST). The combined model takes the form of a nodal admittance matrix equation where complex tap ratios on the primary, secondary and tertiary windings of the transformer are represented explicitly. The magnetising branch, which under saturated conditions is non-linear, is included to account for the saturation effects. The generalised transformer model has been incorporated in an Optimal Power Flow algorithm, leading to very robust iterative solutions since the optimisation process is carried out via Newton's method. The model is very flexible and can be set to simulate different operating modes with ease, and in a highly efficient fashion. For instance, in order to realise the power flow control exerted by a phase-shifting transformer, it is only necessary to add the second derivative term of a large penalty weighting factor at the appropriate locations in the linearised system of equations. The efficiency of the solution stems from the fact that the system dimensions remain unchanged throughout the iterative solution; there is no need to re-calculate the elimination sequence in the Gaussian elimination process, regardless of the control requirements. It is shown in the Chapter that more realistic studies of active and reactive power losses at the system level are possible with the use of the new optimal power flow transformer models. Several power networks are used for this purpose.

3.2 Advanced Transformer Model

The advanced transformer model presented in this Chapter addresses from the transmission network point of view, and is based on the physical representation of the three-winding transformer shown in Figure 3.1. Each winding is represented as the series combination of a resistance, leakage reactance and ideal transformer. Furthermore, each winding is provided with a complex tap changing mechanism to allow for tap changing and phase shifting facilities. The magnetising branch of the transformer is included to account for the saturation effects, whereas the core losses are presented by adding a resistive element in parallel with the magnetising branch. Figure 3.1(b) shows the equivalent circuit of the three-winding transformer shown in Figure 3.1(a).

The primary winding is represented as an ideal transformer having complex tap ratios $\boldsymbol{T_v}$ **: 1** and $\boldsymbol{T_i}$ **: 1** in series with the impedance $\boldsymbol{Z_p}$, where $\boldsymbol{T_v} = \boldsymbol{T_i}^* = t+j\alpha = T_v \angle\phi_{tv}$. The * denotes the conjugate operation. The secondary winding is represented as an ideal transformer having complex tap ratios $\boldsymbol{U_v}$ **: 1** and $\boldsymbol{U_i}$ **: 1** in series with the impedance $\boldsymbol{Z_s}$, where $\boldsymbol{U_v} = \boldsymbol{U_i}^* = u+j\beta = U_v \angle\phi_{uv}$. Similarly, the ideal transformer in the tertiary winding has complex ratios $\boldsymbol{W_v}$ **: 1** and $\boldsymbol{W_i}$ **: 1** in series with an impedance $\boldsymbol{Z_t}$, where $\boldsymbol{W_v} = \boldsymbol{W_i}^* = w+j\gamma = W_v \angle\phi_{wv}$. The core losses and the magnetising branch of the transformer are represented by the admittance $\boldsymbol{Y_0} = G_0 + jB_0$.

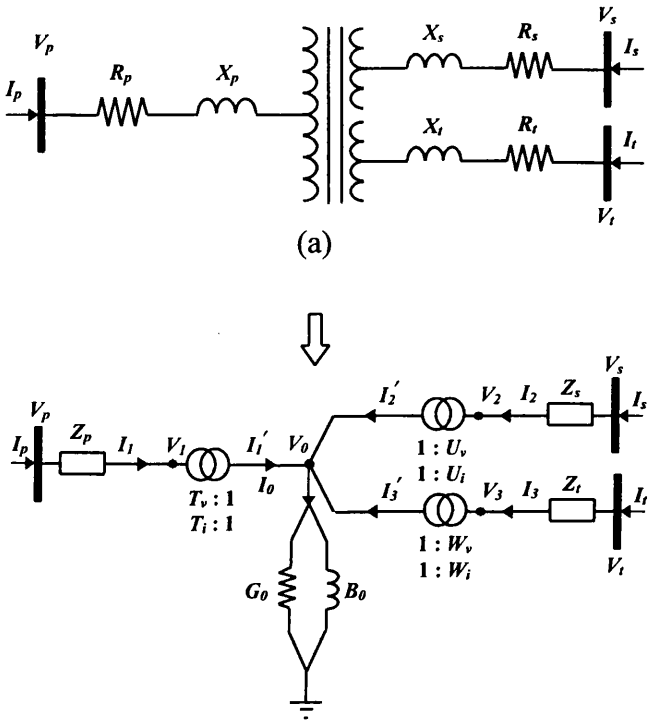

Figure 3.1. Schematic representation and equivalent circuit of the three winding transformer.

The resistive path of the admittance Y_0 is directly related to the iron losses and its conductance G_0 draws a current that varies linearly with the voltage across the magnetising branch. However, in the inductive path the relationship between the current and the voltage is dictated by the RMS *V-I* characteristic, which under saturating conditions becomes non-linear.

The following relationships exist in the ideal primary and secondary transformers,

$$\frac{V_1}{V_0} = \frac{T_v}{1} \quad \text{and} \quad \frac{T_i}{1} = \frac{I_1'}{I_1} \tag{3.1}$$

$$\frac{V_2}{V_0} = \frac{U_v}{1} \quad \text{and} \quad \frac{U_i}{1} = \frac{I_2'}{I_2} \tag{3.2}$$

$$\frac{V_3}{V_0} = \frac{W_v}{1} \quad \text{and} \quad \frac{W_i}{1} = \frac{I_3'}{I_3} \tag{3.3}$$

The currents across the impedances Z_p, Z_s and Z_t are:

$$I_1 = \frac{V_p - V_1}{Z_p} = \frac{V_p - T_v V_0}{Z_p} = I_p \tag{3.4}$$

$$I_2 = \frac{V_s - V_2}{Z_s} = \frac{V_s - U_v V_0}{Z_s} = I_s \tag{3.5}$$

$$I_3 = \frac{V_t - V_3}{Z_t} = \frac{V_t - W_v V_0}{Z_t} = I_t \tag{3.6}$$

while at the centre of the transformer the following relationship holds:

$$0 = I_1' + I_2' + I_3' - I_0 = T_i I_1 + U_i I_2 + W_i I_3 - I_0 \tag{3.7}$$

Substituting equations (3.4), (3.5) and (3.6) into (3.7) gives:

$$0 = -\frac{T_v^* V_p}{Z_p} - \frac{U_v^* V_s}{Z_s} - \frac{W_v^* V_t}{Z_t} + \left(\frac{T_v^2}{Z_p} + \frac{U_v^2}{Z_s} + \frac{W_v^2}{Z_t} + Y_0\right) V_0 \tag{3.8}$$

Putting equations (3.4), (3.5), (3.6) and (3.8) in matrix form gives:

$$\begin{bmatrix} I_p \\ I_s \\ I_t \\ 0 \end{bmatrix} = \begin{bmatrix} \frac{1}{Z_p} & 0 & 0 & -\frac{T_v}{Z_p} \\ 0 & \frac{1}{Z_s} & 0 & -\frac{U_v}{Z_s} \\ 0 & 0 & \frac{1}{Z_t} & -\frac{W_v}{Z_t} \\ -\frac{T_v^*}{Z_p} & -\frac{U_v^*}{Z_s} & -\frac{W_v^*}{Z_t} & \frac{T_v^2}{Z_p} + \frac{U_v^2}{Z_s} + \frac{W_v^2}{Z_t} + Y_0 \end{bmatrix} \begin{bmatrix} V_p \\ V_s \\ V_t \\ V_0 \end{bmatrix} \tag{3.9}$$

Equation (3.9) represents the transformer shown in Figure 3.1. However, it is possible to find a reduced equivalent matrix that still models the transformer correctly whilst retaining only the external nodes *p*, *s* and *t*. This is done by means of a Gaussian elimination:

$$\begin{bmatrix} I_p \\ I_s \\ I_t \end{bmatrix} = \frac{1}{\Delta} \begin{bmatrix} U_v^2 Z_t + W_v^2 Z_s + Z_s Z_t Y_0 & -T_v U_v^* Z_t & -T_v W_v^* Z_s \\ -T_v^* U_v Z_t & T_v^2 Z_t + W_v^2 Z_p + Z_p Z_t Y_0 & -U_v W_v^* Z_p \\ -T_v^* W_v Z_s & -U_v^* W_v Z_p & T_v^2 Z_s + U_v^2 Z_p + Z_p Z_s Y_0 \end{bmatrix} \begin{bmatrix} V_p \\ V_s \\ V_t \end{bmatrix} \tag{3.10}$$

where $$\Delta = T_v^2 Z_s Z_t + U_v^2 Z_p Z_t + W_v^2 Z_p Z_s + Z_p Z_s Z_t Y_0$$

3.2.1 The Two-Winding Transformer Model

The nodal admittance representation of a two-winding transformer can be easily obtained by introducing simplifying assumptions in equation (3.10). For instance, when the tertiary winding does not exist, the row and column corresponding to this node become redundant and they are removed from equation (3.10). Moreover, the tap ratios W_v and W_i become zero and the impedance Z_t takes an infinite value. Hence, applying the L'Hospital differentiation rule, the nodal admittance matrix equation representing the two-winding transformer is arrived at:

$$\begin{bmatrix} I_p \\ I_s \end{bmatrix} = \frac{1}{\Delta} \begin{bmatrix} U_v^2 + Z_s Y_0 & -T_v U_v^* \\ -T_v^* U_v & T_v^2 + Z_p Y_0 \end{bmatrix} \begin{bmatrix} V_p \\ V_s \end{bmatrix} \tag{3.11}$$

where $$\Delta = T_v^2 Z_s + U_v^2 Z_p + Z_p Z_s Y_0$$

The above equation can be expressed in a more compact form as,

$$\begin{bmatrix} \boldsymbol{I_p} \\ \boldsymbol{I_s} \end{bmatrix} = \begin{bmatrix} \boldsymbol{Y_{pp}} & \boldsymbol{Y_{ps}} \\ \boldsymbol{Y_{sp}} & \boldsymbol{Y_{ss}} \end{bmatrix} \begin{bmatrix} \boldsymbol{V_p} \\ \boldsymbol{V_s} \end{bmatrix} \tag{3.12}$$

where

$$\boldsymbol{Y_{pp}} = \frac{U_v^2 + \boldsymbol{Z_s Y_0}}{\Delta} \tag{3.13}$$

$$\boldsymbol{Y_{ps}} = \frac{-\boldsymbol{T_v U_v^*}}{\Delta} \tag{3.14}$$

$$\boldsymbol{Y_{sp}} = \frac{-\boldsymbol{T_v^* U_v}}{\Delta} \tag{3.15}$$

$$\boldsymbol{Y_{ss}} = \frac{T_v^2 + \boldsymbol{Z_p Y_0}}{\Delta} \tag{3.16}$$

where the Y-bus admittance matrix is calculated by using the following expression:

$$G_{pp} = \frac{F_1(U_v^2 + R_1) + F_2 R_2}{A_2} \tag{3.17}$$

$$B_{pp} = \frac{F_1 R_2 - F_2(U_v^2 + R_1)}{A_2} \tag{3.18}$$

$$G_{ss} = \frac{F_1(T_v^2 + R_3) + F_2 R_4}{A_2} \tag{3.19}$$

$$B_{ss} = \frac{F_1 R_4 - F_2(T_v^2 + R_3)}{A_2} \tag{3.20}$$

$$G_{ps} = \frac{-T_v U_v(F_1 \cos\phi_1 + F_2 \sin\phi_1)}{A_2} \tag{3.21}$$

$$B_{ps} = \frac{T_v U_v(F_2 \cos\phi_1 - F_1 \sin\phi_1)}{A_2} \tag{3.22}$$

$$G_{sp} = \frac{-T_v U_v(F_1 \cos\phi_2 + F_2 \sin\phi_2)}{A_2} \tag{3.23}$$

$$B_{sp} = \frac{T_v U_v(F_2 \cos\phi_2 - F_1 \sin\phi_2)}{A_2} \tag{3.24}$$

$$F_1 = T^2 R_s + U_v^2 R_p + R_{eq1} \tag{3.25}$$

$$F_2 = T_v^2 X_s + U_v^2 X_p + X_{eq1} \tag{3.26}$$

$$A_2 = F_1^2 + F_2^2 \tag{3.27}$$

$$R_{eq1} = (R_p R_s - X_p X_s) G_o - (R_p X_s + R_s X_p) B_o \tag{3.28}$$

$$X_{eq1} = (R_p R_s - X_p X_s) B_o + (R_p X_s + R_s X_p) G_o \tag{3.29}$$

$$R_1 = R_s G_o - X_s B_o \tag{3.30}$$

$$R_2 = R_s B_o + X_s G_o \tag{3.31}$$

$$R_3 = R_p G_o - X_p B_o \tag{3.32}$$

$$R_4 = R_p B_o + X_p G_o \tag{3.33}$$

$$\phi_1 = \phi_{tv} - \phi_{uv} \tag{3.34}$$

$$\phi_2 = \phi_{uv} - \phi_{tv} \tag{3.35}$$

$$\delta_1 = \theta_p - \theta_s \tag{3.36}$$

$$\delta_2 = \theta_s - \theta_p \tag{3.37}$$

It must be noted that owing to the flexibility of the two-winding transformer model in equation (3.11), it is possible to assemble a transformer model that represents the transformer circuit shown in Figure 3.1(b) by using three of these two-winding transformer models. An example of how this can be achieved is given below, where suitable parameter selection is used for each one of the two-winding transformer models involved.

Transformer 1: $\boldsymbol{U}_{v,1} = \boldsymbol{U}^*_{i,1} = 1+j0$, $\boldsymbol{Z}_{s,1} = \boldsymbol{0}$, and $\boldsymbol{Y}_{0,1} = \boldsymbol{Y}_0$:

$$\begin{bmatrix} \boldsymbol{I}_{p,1} \\ \hline \boldsymbol{I}_{s,1} \end{bmatrix} = \frac{1}{\boldsymbol{Z}_{p,1}} \left[\begin{array}{c|c} 1 & -\boldsymbol{T}_{v,1} \\ \hline -\boldsymbol{T}^*_{v,1} & \boldsymbol{T}^2_{v,1} + \boldsymbol{Z}_{p,1}\boldsymbol{Y}_0 \end{array}\right] \begin{bmatrix} \boldsymbol{V}_{p,1} \\ \hline \boldsymbol{V}_{s,1} \end{bmatrix} \tag{3.38}$$

Transformer 2: $\boldsymbol{U}_{v,2} = \boldsymbol{U}^*_{i,2} = 1+j0$, $\boldsymbol{Z}_{s,2} = \boldsymbol{0}$, and $\boldsymbol{Y}_{0,2} = 0$:

$$\begin{bmatrix} \boldsymbol{I}_{p,2} \\ \hline \boldsymbol{I}_{s,2} \end{bmatrix} = \frac{1}{\boldsymbol{Z}_{p,2}} \left[\begin{array}{c|c} 1 & -\boldsymbol{T}_{v,2} \\ \hline -\boldsymbol{T}^*_{v,2} & \boldsymbol{T}^2_{v,2} + \boldsymbol{Z}_{p,2}\boldsymbol{Y}_0 \end{array}\right] \begin{bmatrix} \boldsymbol{V}_{p,2} \\ \hline \boldsymbol{V}_{s,2} \end{bmatrix} \tag{3.39}$$

Transformer 3: $\boldsymbol{U}_{v,3} = \boldsymbol{U}^*_{i,3} = 1+j0$, $\boldsymbol{Z}_{s,3} = \boldsymbol{0}$, and $\boldsymbol{Y}_{0,3} = 0$:

$$\begin{bmatrix} \boldsymbol{I}_{p,3} \\ \hline \boldsymbol{I}_{s,3} \end{bmatrix} = \frac{1}{\boldsymbol{Z}_{p,3}} \left[\begin{array}{c|c} 1 & -\boldsymbol{T}_{v,3} \\ \hline -\boldsymbol{T}^*_{v,3} & \boldsymbol{T}^2_{v,3} + \boldsymbol{Z}_{p,3}\boldsymbol{Y}_0 \end{array}\right] \begin{bmatrix} \boldsymbol{V}_{p,3} \\ \hline \boldsymbol{V}_{s,3} \end{bmatrix} \tag{3.40}$$

Furthermore, by selecting the following topology constraints:

$$\boldsymbol{I}_{s,1} + \boldsymbol{I}_{s,2} + \boldsymbol{I}_{s,3} = \boldsymbol{0} \qquad\qquad \boldsymbol{V}_{s,1} = \boldsymbol{V}_{s,2} = \boldsymbol{V}_{s,3} = \boldsymbol{V}_{s,0}$$

A nodal admittance matrix representation that is fully equivalent to the nodal admittance model of the three-winding transformer is obtained:

$$\begin{bmatrix} \boldsymbol{I}_{p,1} \\ \boldsymbol{I}_{p,2} \\ \boldsymbol{I}_{p,3} \\ \boldsymbol{0} \end{bmatrix} = \begin{bmatrix} \frac{1}{\boldsymbol{Z}_{p,1}} & \boldsymbol{0} & \boldsymbol{0} & -\frac{\boldsymbol{T}_{v,1}}{\boldsymbol{Z}_{p,1}} \\ \boldsymbol{0} & \frac{1}{\boldsymbol{Z}_{p,2}} & \boldsymbol{0} & -\frac{\boldsymbol{T}_{v,2}}{\boldsymbol{Z}_{p,2}} \\ \boldsymbol{0} & \boldsymbol{0} & \frac{1}{\boldsymbol{Z}_{p,3}} & -\frac{\boldsymbol{T}_{v,3}}{\boldsymbol{Z}_{p,3}} \\ -\frac{\boldsymbol{T}^*_{v,1}}{\boldsymbol{Z}_{p,1}} & -\frac{\boldsymbol{T}^*_{v,2}}{\boldsymbol{Z}_{p,2}} & -\frac{\boldsymbol{T}^*_{v,3}}{\boldsymbol{Z}_{p,3}} & \frac{\boldsymbol{T}^2_{v,1}}{\boldsymbol{Z}_{p,1}} + \frac{\boldsymbol{T}^2_{v,2}}{\boldsymbol{Z}_{p,2}} + \frac{\boldsymbol{T}^2_{v,3}}{\boldsymbol{Z}_{p,3}} + \boldsymbol{Y}_0 \end{bmatrix} \begin{bmatrix} \boldsymbol{V}_{p,1} \\ \boldsymbol{V}_{p,2} \\ \boldsymbol{V}_{p,3} \\ \boldsymbol{V}_{s,0} \end{bmatrix} \tag{3.41}$$

The load tap-changing and phase-shifting transformer models are particular cases of the two-winding transformer model and they are introduced in the following Sections.

3.3 Phase-Shifting Transformer

The growth of electric power consumption in most countries is certain to continue unabated in the foreseeable future and the problems faced by the Electric Utilities in delivering the demanded power are increasing. The phase-shifting transformer is one special application of transformers that will help utilities to better utilise existing transmission corridors and to improve on the operation of the system [10].

A schematic representation of the PST is shown in Figure 3.2 [11]. The PST is capable of redirecting power flows by locally altering the voltage angle difference imposed on the device by network conditions.

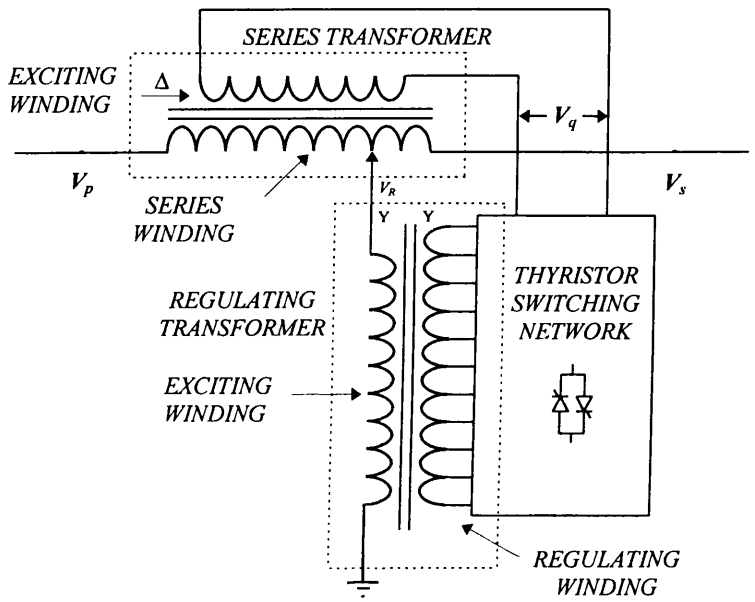

Figure 3.2. Thyristor Controlled Phase-Shifting Transformer.

When power flows between two nodes, there is a voltage drop and a phase angle shift between the sending node and receiving node, which depend on the magnitude and angle of the load current. Figure 3.3 shows a transmission line representation and its phase diagram, where it is assumed that the line current I_{ps} is in phase with the voltage magnitude V_p.

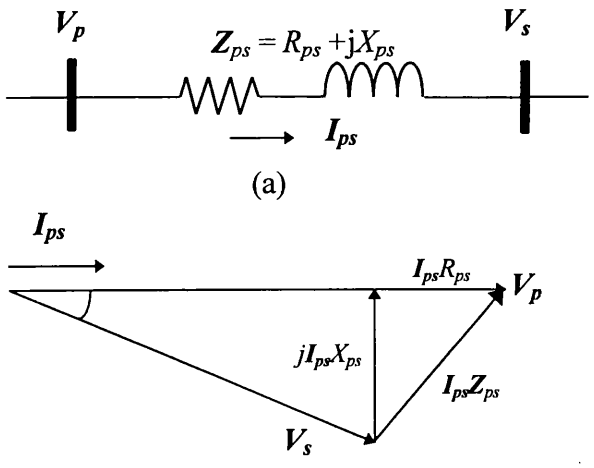

Figure 3.3. Transmission line representation.

Figure 3.3 (b) shows the voltage drop $jI_{ps}X_{ps}$ in quadrature with the system line-to-ground voltage V_p. The PST compensates for the $jI_{ps}X_{ps}$ drop by inserting, between its sending and its receiving nodes, a series voltage in quadrature with the line-to-ground voltage. This quadrature voltage produces, between the PST terminals, a phase shift whose magnitude varies with the magnitude of the quadrature voltage, hence, the term phase-shifting transformer. The quadrature voltage is obtained from the shunt connected three phase transformer, called exciting transformer. It is inserted into the PST terminals via the series connected transformer, called the booster transformer.

Some significant benefits obtained by using the PST are: (a) Reduction of active power losses by eliminating circulating currents; (b) Improvement in of transmission line capability through proper division of the power flow; (c) Control of power flow.

3.3.1 The Classical Phase-Shifting Transformer Model

In open literature [1-3,15,16] it is common to represent the phase-shifting transformer as an impedance connected in series with an ideal transformer having a complex turns ratio. Figure 3.4 shows the equivalent circuit of the PST connected between nodes p and s. The transformer phase shifting capabilities are taken to be on node p.

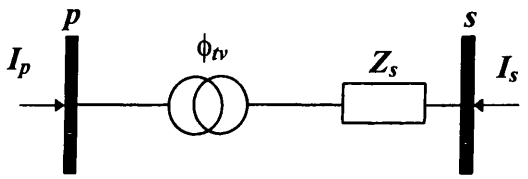

Figure 3.4. Equivalent circuit to PST.

The classical PST model can be obtained by introducing simplifying assumptions in the two-winding transformer model given by equation (3.11). If $T_v=T_i^*$ $=\cos\phi_{tv}+j\sin\phi_{tv}=a+jb$, $U_v= U_i^* = 1$, $Y_o= 0$ and $Z_p= 0$, a nodal transfer admittance model for the PST shown in Figure 3.4 can be obtained,

$$\begin{bmatrix} I_p \\ I_s \end{bmatrix} = \frac{1}{(a^2+b^2)Z_s} \left[\begin{array}{c:c} 1 & -(a+jb) \\ \hdashline -(a-jb) & (a^2+b^2) \end{array}\right] \begin{bmatrix} V_p \\ V_s \end{bmatrix} \tag{3.42}$$

or in the form shown in Reference [15]

$$\begin{bmatrix} I_p \\ \cdots \\ I_s \end{bmatrix} = \frac{1}{Z_s} \left[\begin{array}{c:c} \dfrac{1}{(a^2+b^2)} & -\dfrac{1}{(a-jb)} \\ \hdashline -\dfrac{1}{(a+jb)} & 1 \end{array}\right] \begin{bmatrix} V_p \\ \cdots \\ V_s \end{bmatrix} \tag{3.43}$$

3.3.2 Power Flow Equations

Based on the nodal admittance matrix equation of the two-winding transformer, equation (3.11) or (3.12), the following active and reactive power equations can be written for a two-winding transformer connected between node p and node s:

At node p:

$$P_p = V_p^2 G_{pp} + V_p V_s \left(G_{ps}\cos(\theta_p - \theta_s) + B_{ps}\sin(\theta_p - \theta_s)\right) \tag{3.44}$$

$$Q_p = -V_p^2 B_{pp} + V_p V_s \left(G_{ps} \sin(\theta_p - \theta_s) - B_{ps} \cos(\theta_p - \theta_s)\right) \quad (3.45)$$

At node *s*:

$$P_s = V_s^2 G_{ss} + V_s V_p \left(G_{sp} \cos(\theta_s - \theta_p) + B_{sp} \sin(\theta_s - \theta_p)\right) \quad (3.46)$$

$$Q_s = -V_s^2 B_{ss} + V_s V_p \left(G_{sp} \sin(\theta_s - \theta_p) - B_{sp} \cos(\theta_s - \theta_p)\right) \quad (3.47)$$

where P_p, P_s, Q_p, Q_s are the active and reactive power flow injections at nodes p and s. V_p, V_s, θ_p, θ_s are the voltage magnitudes and phase angles at nodes p and s, respectively.

3.3.3 PST-OPF Formulation

The mathematical formulation consists of minimising the active power generation cost in the power system by adjusting suitable controllable parameters. For the PST model having phase shifting facilities only in the primary winding, the OPF formulation is as follows [3,4,17]:

$$\begin{aligned} &\textbf{\textit{Minimise}} \quad f(P_g) \\ &\textbf{\textit{Subject to}} \quad h(P_g, V, \theta, \phi_{tv}) = 0 \\ &\textbf{\textit{and}} \qquad\quad g(P_g, V, \theta, \phi_{tv}) \le 0 \end{aligned} \quad (3.48)$$

where P_g, V, θ and ϕ_{tv} are the active power generations, voltage magnitudes, phase angles and phase shifter angles, respectively. $f(P_g)$ is the objective function to be optimised, $h(P_g, V, \theta, \phi_{tv})$ represents the power flow equations and $g(P_g, V, \theta, \phi_{tv})$ represents state variable limits as well as functional operating constraints.

The constrained optimisation problem is converted to an unconstrained optimisation problem by constructing the Lagrangian function corresponding to equation (3.48). This is given as,

$$L(\boldsymbol{x}, \lambda) = f(P_g) + \lambda^t h(P_g, V, \theta, \phi_{tv}) \quad (3.49)$$

where $\boldsymbol{x}$ is a vector of state variables and λ is the Lagrange multipliers vector for equality constraints. The inequality constraints are not shown because they are only included when there are variables outside limits. The superscript t indicates transposition.

3.3.4 Lagrangian Function

The phase-shifting transformer state variables are combined with the network nodal voltage magnitudes and phase angles in a single frame of reference for a unified optimal solution via Newton's method. Phase-shifting transformers state variables are adjusted automatically so as to satisfy specified power flows, voltage magnitudes and optimality conditions as given by Kuhn and Tucker [17].

The Lagrangian function corresponding to the power flow mismatch equations at nodes p and s is explicitly modelled in the OPF formulation as an equality constraint given by the following equation:

$$\begin{aligned} L_{ps}(\boldsymbol{x}, \lambda) = {} & \lambda_{pp}(P_p + P_{dp} - P_{gp}) + \lambda_{qp}(Q_p + Q_{dp} - Q_{gp}) \\ & + \lambda_{ps}(P_s + P_{ds} - P_{gs}) + \lambda_{qs}(Q_s + Q_{ds} - Q_{gs}) \end{aligned} \quad (3.50)$$

where P_{dp}, P_{ds}, Q_{dp}, Q_{ds} are active and reactive power loads at nodes p and s, respectively. P_{gp}, P_{gs}, Q_{gp}, Q_{gs} are scheduled active and reactive power generations at

nodes p and s, respectively. λ_{pp}, λ_{ps}, λ_{qp}, λ_{qs} are Lagrange multipliers at nodes p and s, respectively.

3.3.5 PST Power Flow Constraint

The active power P_{ps} flowing from node p to s, can be regulated by a phase-shifting transformer. In the OPF formulation this condition is expressed as an equality constraint which remains active throughout the iterative process unless one wishes this constraint to be deactivated. The operating condition is represented by the following Lagrangian function,

$$L_{flow}(\boldsymbol{x},\lambda) = \lambda_{flow-ps}(P_{ps} - P_{specified}) \tag{3.51}$$

where $\lambda_{flow\text{-}ps}$ is the Lagrange multiplier associated with the active power flowing from node p to s. $P_{specified}$ is the required value of active power flow across the transformer.

The PST Lagrangian function encompassing the individual contributions presented above is:

$$L = L_{pst}(\boldsymbol{x},\lambda) = L_{ps}(\boldsymbol{x},\lambda) + L_{flow}(\boldsymbol{x},\lambda) \tag{3.52}$$

3.3.6 Linearised System of Equations

The representation of the PST in the OPF algorithm requires the matrix $\boldsymbol{W}$ to be augmented by one row and one column per transformer. Under this condition either ϕ_{tv} or ϕ_{uv} are extra state variables which become incorporated in the OPF formulation. Furthermore, if the PST is controlling active power flow then the dimensions of the matrix $\boldsymbol{W}$ are increased further, because one row and one column is required for each phase shifter controlling power flow.

When the two-winding transformer has phase shifting facilities only in the primary winding, i.e. $\boldsymbol{U}_v = \boldsymbol{U}_i^* = u+j\beta = 1\angle 0^0$, the linearised system of equations for minimising the Lagrangian function via Newton's method is given by equation (3.53).

$$\begin{bmatrix}
\frac{\partial^2 L}{\partial \theta_p^2} & \frac{\partial^2 L}{\partial \theta_p \partial V_p} & \frac{\partial P_p}{\partial \theta_p} & \frac{\partial Q_p}{\partial \theta_p} & \frac{\partial^2 L}{\partial \theta_p \partial \theta_s} & \frac{\partial^2 L}{\partial \theta_p \partial V_s} & \frac{\partial P_s}{\partial \theta_p} & \frac{\partial Q_s}{\partial \theta_p} & \frac{\partial^2 L}{\partial \theta_p \partial \phi_{tv}} & \frac{\partial^2 L}{\partial \theta_p \partial \lambda_\phi} \\
\frac{\partial^2 L}{\partial V_p \partial \theta_p} & \frac{\partial^2 L}{\partial V_p^2} & \frac{\partial P_p}{\partial V_p} & \frac{\partial Q_p}{\partial V_p} & \frac{\partial^2 L}{\partial V_p \partial \theta_s} & \frac{\partial^2 L}{\partial V_p \partial V_s} & \frac{\partial P_s}{\partial V_p} & \frac{\partial Q_s}{\partial V_p} & \frac{\partial^2 L}{\partial V_p \partial \phi_{tv}} & \frac{\partial^2 L}{\partial V_p \partial \lambda_\phi} \\
\frac{\partial P_p}{\partial \theta_p} & \frac{\partial P_p}{\partial V_p} & & & \frac{\partial P_p}{\partial \theta_s} & \frac{\partial P_p}{\partial V_s} & & & \frac{\partial P_p}{\partial \phi_{tv}} & \\
\frac{\partial Q_p}{\partial \theta_p} & \frac{\partial Q_p}{\partial V_p} & & & \frac{\partial Q_p}{\partial \theta_s} & \frac{\partial Q_p}{\partial V_s} & & & \frac{\partial Q_p}{\partial \phi_{tv}} & \\
\frac{\partial^2 L}{\partial \theta_s \partial \theta_p} & \frac{\partial^2 L}{\partial \theta_s \partial V_p} & \frac{\partial P_p}{\partial \theta_s} & \frac{\partial Q_p}{\partial \theta_s} & \frac{\partial^2 L}{\partial \theta_s^2} & \frac{\partial^2 L}{\partial \theta_s \partial V_s} & \frac{\partial P_s}{\partial \theta_s} & \frac{\partial Q_s}{\partial \theta_s} & \frac{\partial^2 L}{\partial \theta_s \partial \phi_{tv}} & \frac{\partial^2 L}{\partial \theta_s \partial \lambda_\phi} \\
\frac{\partial^2 L}{\partial V_s \partial \theta_p} & \frac{\partial^2 L}{\partial V_s \partial V_p} & \frac{\partial P_p}{\partial V_s} & \frac{\partial Q_p}{\partial V_s} & \frac{\partial^2 L}{\partial V_s \partial \theta_s} & \frac{\partial^2 L}{\partial V_s^2} & \frac{\partial P_s}{\partial V_s} & \frac{\partial Q_s}{\partial V_s} & \frac{\partial^2 L}{\partial V_s \partial \phi_{tv}} & \frac{\partial^2 L}{\partial V_s \partial \lambda_\phi} \\
\frac{\partial P_s}{\partial \theta_p} & \frac{\partial P_s}{\partial V_p} & & & \frac{\partial P_s}{\partial \theta_s} & \frac{\partial P_s}{\partial V_s} & & & \frac{\partial P_s}{\partial \phi_{tv}} & \\
\frac{\partial Q_s}{\partial \theta_p} & \frac{\partial Q_s}{\partial V_p} & & & \frac{\partial Q_s}{\partial \theta_s} & \frac{\partial Q_s}{\partial V_s} & & & \frac{\partial Q_s}{\partial \phi_{tv}} & \\
\frac{\partial^2 L}{\partial \phi_{tv} \partial \theta_p} & \frac{\partial^2 L}{\partial \phi_{tv} \partial V_p} & \frac{\partial P_p}{\partial \phi_{tv}} & \frac{\partial Q_p}{\partial \phi_{tv}} & \frac{\partial^2 L}{\partial \phi_{tv} \partial \theta_s} & \frac{\partial^2 L}{\partial \phi_{tv} \partial V_s} & \frac{\partial P_s}{\partial \phi_{tv}} & \frac{\partial Q_s}{\partial \phi_{tv}} & \frac{\partial^2 L}{\partial \phi_{tv}^2} & \frac{\partial^2 L}{\partial \phi_{tv} \partial \lambda_\phi} \\
\frac{\partial^2 L}{\partial \lambda_\phi \partial \theta_p} & \frac{\partial^2 L}{\partial \lambda_\phi \partial V_p} & & & \frac{\partial^2 L}{\partial \lambda_\phi \partial \theta_s} & \frac{\partial^2 L}{\partial \lambda_\phi \partial V_s} & & & \frac{\partial^2 L}{\partial \lambda_\phi \partial \phi_{tv}} &
\end{bmatrix}
\begin{bmatrix} \Delta\theta_p \\ \Delta V_p \\ \Delta\lambda_{pp} \\ \Delta\lambda_{qp} \\ \Delta\theta_s \\ \Delta V_s \\ \Delta\lambda_{ps} \\ \Delta\lambda_{qs} \\ \Delta\phi_{tv} \\ \Delta\lambda_{ps} \end{bmatrix}
=
\begin{bmatrix}
-\frac{\partial L}{\partial \theta_p} \\
-\frac{\partial L}{\partial V_p} \\
-\frac{\partial L}{\partial \lambda_{pp}} \\
-\frac{\partial L}{\partial \lambda_{qp}} \\
-\frac{\partial L}{\partial \theta_s} \\
-\frac{\partial L}{\partial V_s} \\
-\frac{\partial L}{\partial \lambda_{ps}} \\
-\frac{\partial L}{\partial \lambda_{qs}} \\
-\frac{\partial L}{\partial \phi_{tv}} \\
-\frac{\partial L}{\partial \lambda_\phi}
\end{bmatrix} \tag{3.53}$$

The first and second derivative expression for all the terms used in equation (3.53) are given in Appendix I. The derivative terms corresponding to inequality constraints are placed into matrix $\boldsymbol{W}$ only if limits need to be enforced, owing to a state variable having violated one of its limits.

If the phase shifting facilities of the two-winding transformer are on the secondary winding rather than the primary winding, i.e. $\boldsymbol{T}_v = \boldsymbol{T}_i^* = t+j\alpha = 1\angle 0^0$, then the tapping variable ϕ_{tv} will be replaced by ϕ_{tv} in equation (3.53).

The equation (3.53) is incorporated into matrix $\boldsymbol{W}$ and gradient vector $\boldsymbol{g}$ of the entire network and the solution is carried out. This procedure corresponds to cases in which the PST is operated in standard control mode. The PST is set to control active power flowing from node p to s.

In OPF solutions, PST variables are normally adjusted automatically during the solution process in order to reach the best operating point of the electrical power system. In this case the PST is not set to control a fixed amount of active power flowing from nodes p to s, and the matrix $\boldsymbol{W}$ is suitably modified to reflect this operating condition. This is done by adding the second partial derivative term of a large (infinite), quadratic penalty function to the diagonal element corresponding to the Lagrange multiplier λ_{ps}. The first derivative term of the function is added to the corresponding gradient element.

3.3.7 Handling Limits of PST Variables

The handling of PST inequality constraints was carried out using the Multipliers method [18]. The phase shifter angles inside bounds are ignored whilst binding inequality constraints become part of the Lagrangian function and, hence, become enforced.

If one considers that the phase shifting facilities are on the primary winding, the handling of this variable can be carried out by using the following function,

$$\psi_i(\phi_{tv,i}^j, \mu_i^j) = \begin{cases} \mu_i^j(\phi_{tv,i}^j - \phi_{tv,i}^{\max}) + \dfrac{c}{2}(\phi_{tv,i}^j - \phi_{tv,i}^{\max})^2 & \text{if} \quad \mu_i^j + c(\phi_{tv,i}^j - \phi_{tv,i}^{\max}) \geq 0 \\ \mu_i^j(\phi_{tv,i}^j - \phi_{tv,i}^{\min}) + \dfrac{c}{2}(\phi_{tv,i}^j - \phi_{tv,i}^{\min})^2 & \text{if} \quad \mu_i^j + c(\phi_{tv,i}^j - \phi_{tv,i}^{\min}) \leq 0 \\ 0 \quad \text{otherwise} \end{cases} \tag{3.54}$$

where i is the phase shifter number and j is an iteration counter associated with the actual value of ϕ_{tv}; $\phi_{tv,i}^{\max}$ and $\phi_{tv,i}^{\min}$ are the upper and lower limits for the phase shifter angle.

3.3.8 Initial Conditions

Initial conditions have an important impact on convergence. Computational experience has show that the PST model is very robust when the phase shifting angle is initialised at 0^0. The following initial conditions are also required.

Nodal Voltage Magnitudes, Phase Angles and Complex Taps

State variables are initialised similarly to load flow problems, i.e. 1 pu voltage magnitudes and 0 voltage angles for all nodes. The primary and secondary complex taps

are set with a magnitude of one and phase angle of zero, i.e. the phase shifter angles are initialised at 0. It is shown in Section 3.3.10 that the algorithm is very robust if the phase shifter angle is initialised within the range of $\pm 10^0$.

Lagrange Multipliers

The Lagrange multipliers for active and reactive power flow mismatch equations are initialised at the λ_p given by the lossless economic dispatch and 0, respectively. The Lagrange multiplier for the power flow constraint, $\lambda_{flow\text{-}ps}$, is set to zero. This value gives rise to very robust iterative solutions.

3.3.9 Phase-Shifting Transformer Test Cases

The OPF Newton algorithm has been applied to the solution of a large number of power networks. It has shown to be a powerful tool to solve PST upgraded networks very reliably. In this section, the 5-node system, the AEP 14-node system and a real life power network are used to show the prowess of the newly developed algorithm.

The 5-node system is used to illustrate how the PST would perform when installed in a power system with these or similar characteristics [15]. The phase-shifting transformer was included in series with the transmission line connected between nodes Lake and Main. An additional node, termed LakePST is used for this purpose, as shown in Figure 3.5.

The PST is used in two different operating modes:

A) To optimise the active power transfer from Lake to Main.

B) To maintain the active power flow from LakePST to Main at 25 MW.

The primary and secondary winding impedances contain no resistance. The primary and secondary inductive reactances were set to 0.0 pu and 0.05 pu, respectively. The complex tap ratios were $\boldsymbol{T}_v = \boldsymbol{U}_v = 1.0\angle 0^0$. The control of active power flow is carried out with the primary phase angle control. The phase shifter angle limits were set at $\pm 10^0$. Convergence was obtained in 4 iterations for both cases to a tolerance of 10^{-9}.

The power flow results for Case A are shown in Figure 3.5. The voltage magnitude, phase angle, active and reactive power dispatch and Lagrange multipliers are given in Table 3.1 and Table 3.2 for both cases. The phase shifter angles, at each iteration, are shown in Table 3.3.

Table 3.1. Nodal complex voltages of modified network for Case A.

Node	Voltage Magnitude (pu)	Phase Angle (degrees)	Active Power (MW)	Reactive Power (MVAR)	λ_p ($/MWhr)
LakePST	1.079	-3.632	0	0	4.2234
Elm	1.072	-4.424	0	0	4.2639
Main	1.078	-3.864	0	0	4.2342
Lake	1.077	-3.610	0	0	4.2232
South	1.100	-1.306	87.90	14.42	4.1032
North	1.109	0.000	80.15	0.38	4.0412

The PST was used to optimise the active power flow level in transmission line Lake-Main (Case A), i.e. 14.92 MW, which is amenable to minimum active power generation cost and active power losses, i.e. 747.980 $/hour and 3.052 MW, respectively. In Case B as expected, if the PST is set to control active power flow at a level different from the optimal, then the active power generation cost and network losses will increase. The solution given by the algorithm in Case B leads to an active power generation cost of 748.330 $/hour and the transmission losses are 3.143 MW.

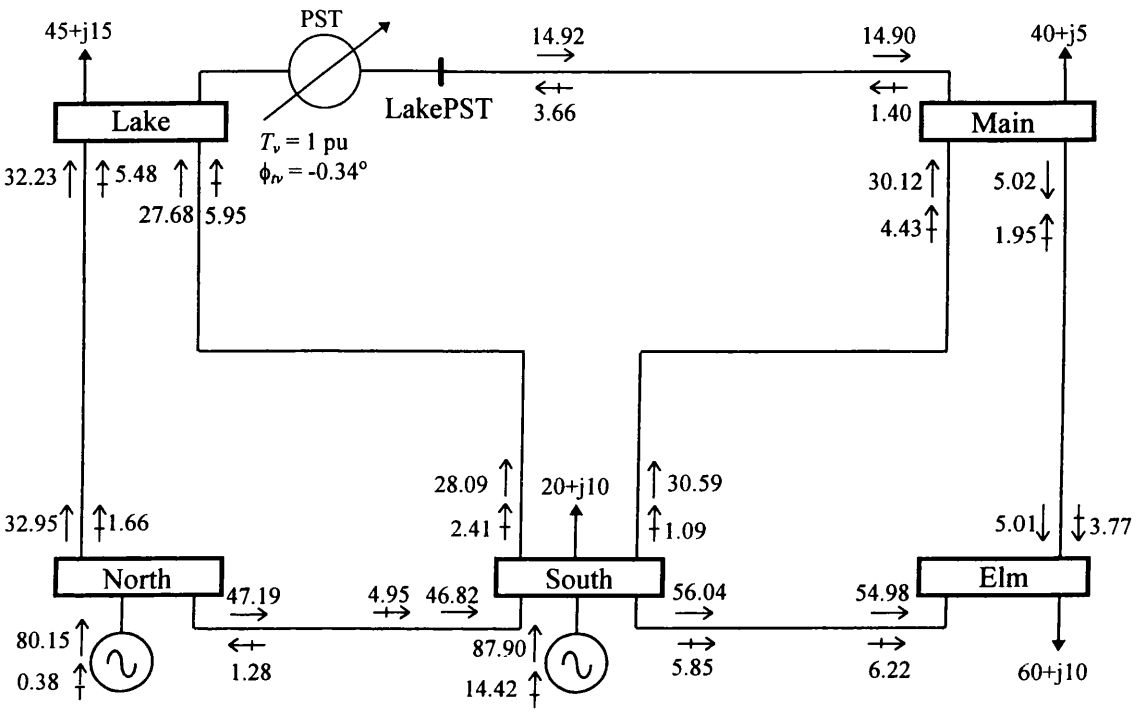

Figure 3.5. Modified 5-node network and OPF results.

Table 3.2. Nodal complex voltages of modified network for Case B.

Node	Voltage Magnitude (pu)	Phase Angle (degrees)	Active Power (MW)	Reactive Power (MVA)	λ_p ($/MWhr)
LakePST	1.079	-2.705	0	0	4.1819
Elm	1.073	-4.097	0	0	4.2509
Main	1.079	-3.102	0	0	4.2005
Lake	1.076	-4.098	0	0	4.2509
South	1.100	-1.193	87.61	14.32	4.1009
North	1.109	0.000	80.52	0.93	4.0442

Table 3.3. Phase shifter angles for the 5-node test system.

Iterations	Case A ϕ_{tv} (degrees)	Case B ϕ_{tv} (degrees)
0	0.000	0.000
1	-0.325	-1.874
2	-0.363	-2.122
3	-0.346	-2.009
4	-0.346	-2.010

To show the effect of the phase shifter angle on the control of active power flow in different locations of the power system the following cases were simulated.

C) PST in series with the transmission line connected between Lake and Main.

D) PST in series with the transmission line connected between South and Lake.

E) PST in series with the transmission line connected between North and Lake.

Figure 3.6 depicts the variations in percent of the active power flow as function of the phase shifter angle. The power flows across those branches with no PST were taken as the base values in order to calculate the increments in per cent. Figure 3.6 shows a linear relationship between the two PST quantities. The PST's ability to control active power flow in both directions is clearly shown in this figure.

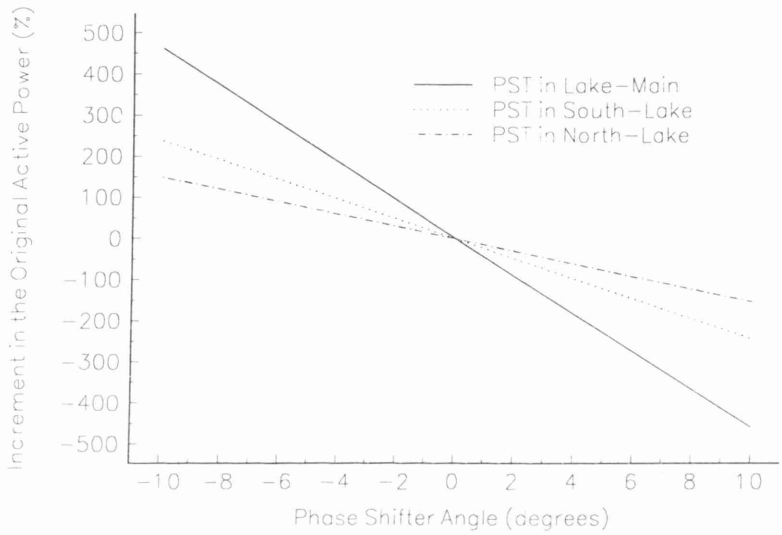

Figure 3.6. Effect of the phase shifter angle on the control of active power flow.

3.3.10 Effect of the Initial Phase Shifter Angle

The standard AEP 14-node system [12] has been modified and used to show the ability of the OPF algorithm to converge to very tight tolerances, regardless of the initial condition given to the phase shifter angle. One conventional transformer was modified to be a PST and a second transformer was embedded in the power system in the location shown in Figure 3.7. The PSTs were not set to maintain a fixed amount of active power flowing across them. The active power flows across the two branches in the original system were 1.68 MW and 26.89 MW, respectively. The active power generation cost and network losses were 215.457 $/hour and 1.901 MW, respectively.

The parameters of both PSTs are given in Table 3.4. The resistance of both windings were set to zero. The limits of the phase shifter angles were set at $\pm 15^0$. The active power control is carried out with the primary phase angle control.

Table 3.4. Phase-Shifting Transformers parameters for the AEP 14-node system.

Phase Shifting Transformer	Primary Tap			Secondary Tap		
	T_v (pu)	ϕ_{tv} (degrees)	X_p (pu)	U_u (pu)	ϕ_{uv} (degrees)	X_s (pu)
Nod_4-Nod_9	0.969	0.000	0.000	1.000	0.000	0.556
Nod_5-Nod_5PST	0.969	0.000	0.000	1.000	0.000	0.556

In order to asses the impact of the phase shifter angle initial conditions, several simulations were carried out. The first iterative solution was carried out with an initial phase shifter angle of $+10^0$. Subsequent simulations were performed with 5^0 decrements. In each case, both PSTs were initialised at the same value, i.e.:

A) $\phi_{tv} = +10^0$.

B) $\phi_{tv} = +5^0$.

C) $\phi_{tv} = 0^0$.

D) $\phi_{tv} = -5^0$.

E) $\phi_{tv} = -10^0$.

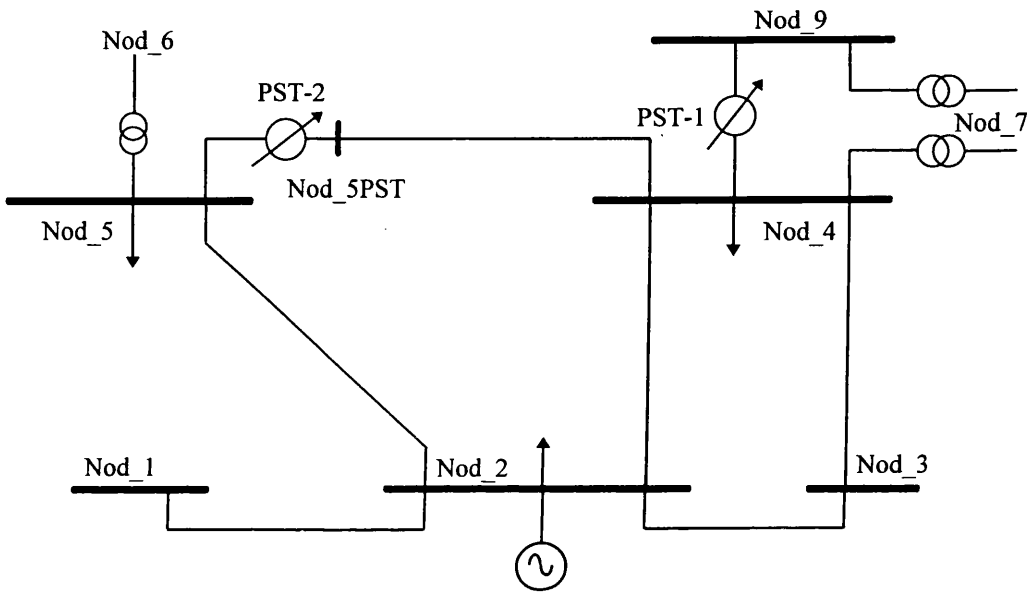

Figure 3.7. Relevant part of the AEP 14-node system with two PSTs.

Table 3.5 shows the phase shifter angles at the end of each iteration during the solution process; it corresponds to the case when ϕ_{tv} was initialised at 0^0. In each case, all the inequality constraints were satisfied, and only the voltage magnitude at Nod_7 required enforcement. The number of iterations taken by the algorithm to converge was 3 in all the five cases. The same active power generation cost and active power losses were arrived at, i.e. 215.440 $/hour and 1.889 MW. Similarly, the same phase shifter angles were arrived at.

Figures 3.8 and 3.9 show the convergence pattern of the the Lagrangian function gradient with respect to the phase shifter angles PST-1 and PST-2, respectively. The overshootings in iterations 1 and 2 show that the Lagrangian function gradients are very sensitive to changes in the set of active constraints, and changes in the penalty weighting factor, which vary from iteration to iteration.

Table 3.5. Final phase shifter angles of the AEP 14-node system.

Iterations	PST-1 ϕ_{tv} (degrees)	PST-2 ϕ_{tv} (degrees)
0	0.000	0.000
1	-8.216	-9.081
2	-7.642	-9.105
3	-7.929	-9.114

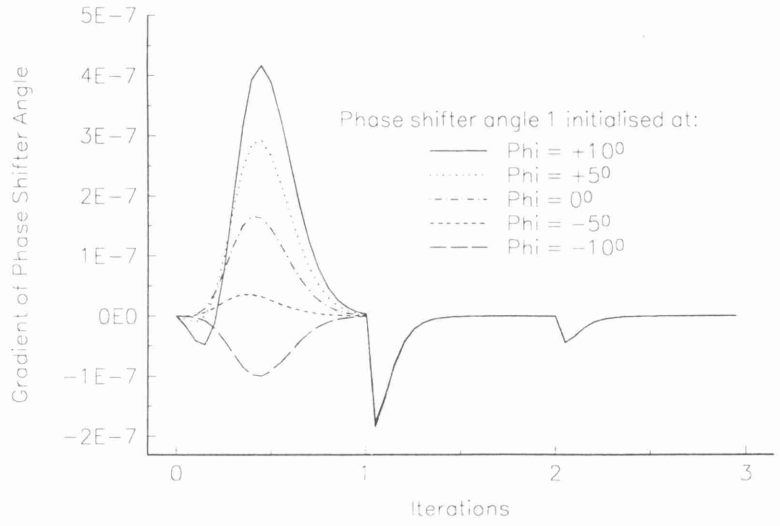

Figure 3.8. Gradient of the Lagrangian function with respect to ϕ_{tv} (PST-1).

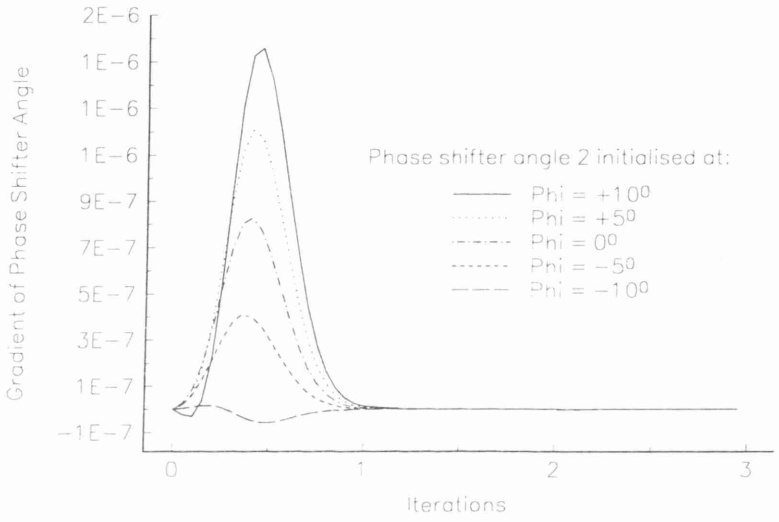

Figure 3.9. Gradient of the Lagrangian function with respect to ϕ_{tv} (PST-2).

Figures 3.10 and 3.11 depict the profiles of the phase shifter angles PST-1 and PST-2 as a function of the iteration number. After the first iteration, both profiles follow a smooth pattern, which demonstrates the very strong convergence characteristics of the PST model. Furthermore, the algorithm shows to be very resilient to changes in the penalty weighting factor and to interactions with other PSTs.

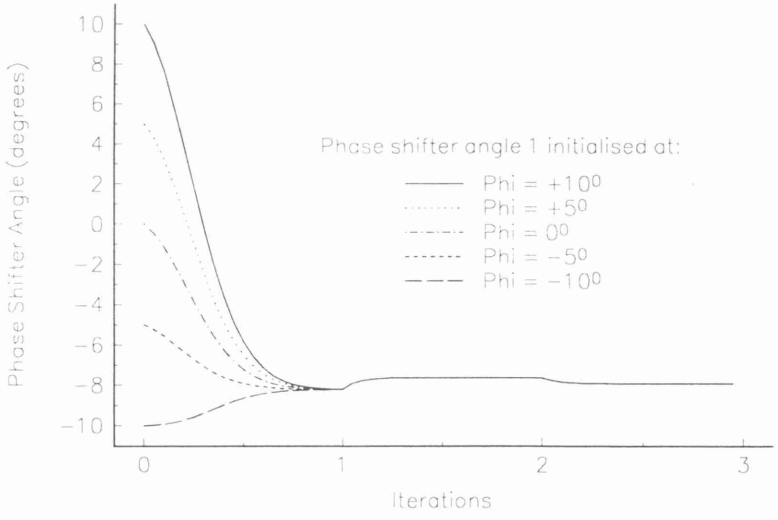

Figure 3.10. Phase shifter angle profile for PST-1.

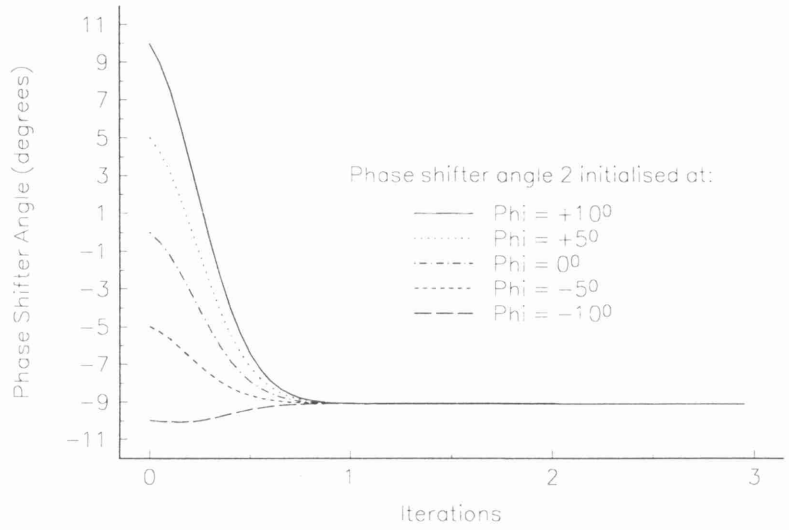

Figure 3.11. Phase shifter angle profile for PST-2.

Figures 3.12 and 3.13 depict active power flows through the phase-shifting transformers Nod_4-Nod_9 and Nod_5-Nod_5PST, respectively. The patterns of convergence exhibit slight oscillations in the first and second iterations due to changes in the active set and penalty weighting factors.

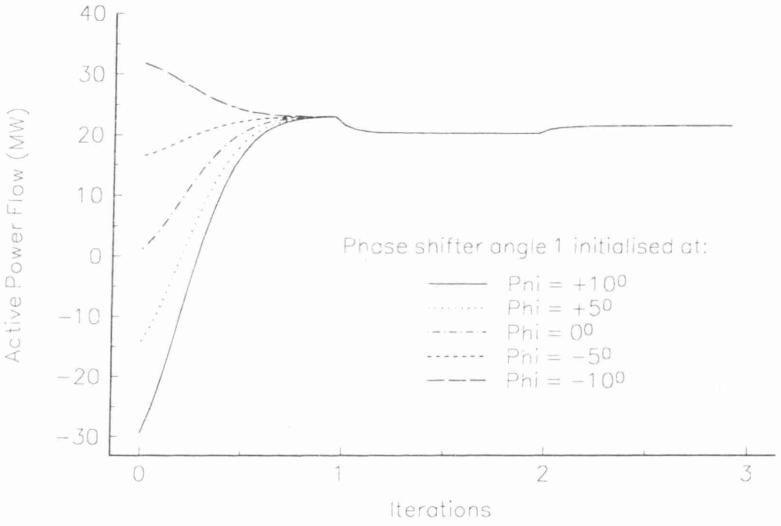

Figure 3.12. Active power flow across PST-1.

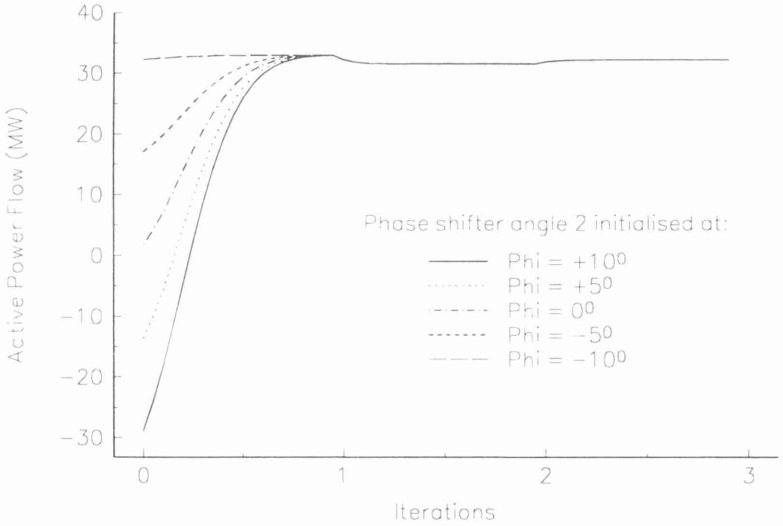

Figure 3.13. Active power flow across PST-2.

In order to asses the behaviour of the PST when used to regulate active power flow, the active power flows to be controlled by the PST-1 and PST-2 have been specified at 30 MW and 40 MW, respectively. Three different initial phase shifting angles were used in this study:

A) $\phi_{tv} = +10^0$.

B) $\phi_{tv} = 0^0$.

C) $\phi_{tv} = -10^0$.

Figures 3.14 and 3.15 depict the profiles of the phase shifter angles PST-1 and PST-2 as a function of the number of iterations. As expected, if the PST is set to regulate active power flow at a level different from the optimal value given by the OPF algorithm, the generation cost will rise. This case leads to an active power generation cost of 215.496 $/hour and to active power losses of 1.934 MW. Once again after the first iteration, the profiles follow a very smooth pattern, confirming the very strong convergence characteristics of the PST model. Furthermore, the algorithm seems to be insensitive to changes in the penalty weighting factor.

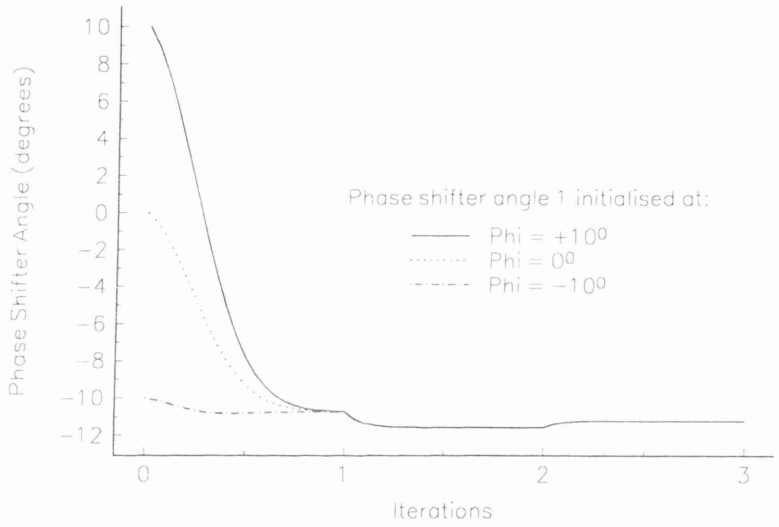

Figure 3.14. Phase shifter angle profile for PST-1 maintaining a fixed power flow.

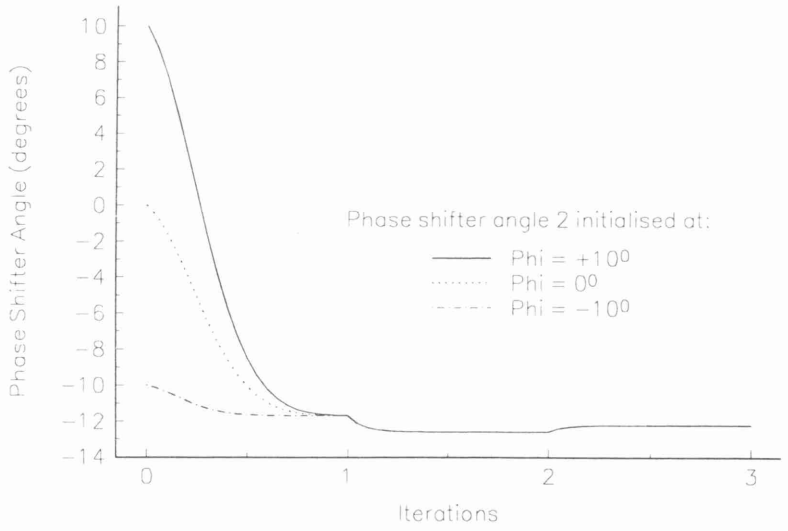

Figure 3.15. Phase shifter angle profile for PST-2 maintaining a fixed power flow.

The active power flows across both PSTs as function of the number of iterations are shown in Figures 3.16 and 3.17. Practically no oscillations are observed. The algorithm reaches its target value after the first iteration, reaching convergence in 3 iterations.

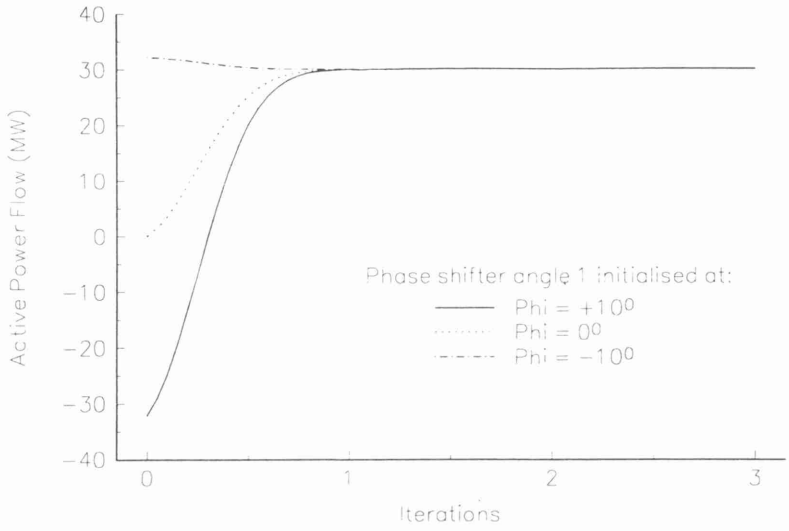

Figure 3.16. Active power flow across PST-1 maintaining a fixed power flow.

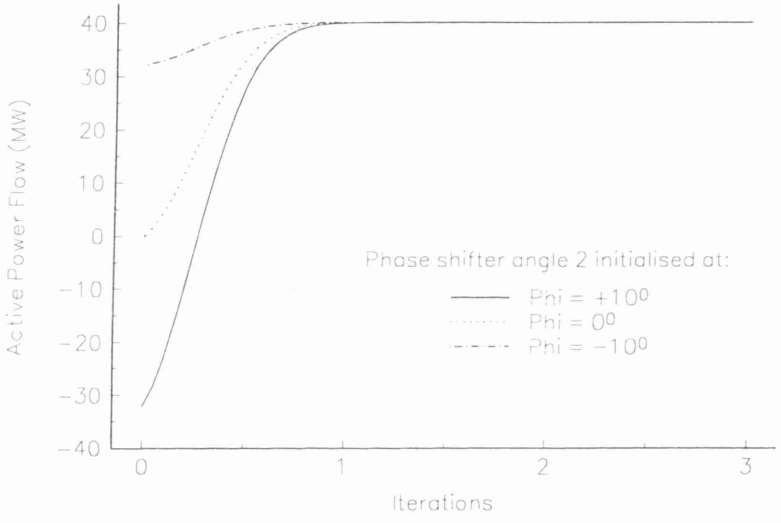

Figure 3.17. Active power flow across PST-2 maintaining a fixed power flow.

3.3.11 Active Power Flow Control in a Real Power System

To show the behaviour of the phase-shifting transformer model in an OPF algorithm, a real life power system consisting of 166 nodes, 108 transmission lines and 128 transformers was used [13]. This network is actually part of a much larger interconnected system which consists of 160 power plants (76 hydro and 84 thermal) with 579 generating units, 2172 nodes, 2294 transmission lines and 768 transformers. For the 166-node power system, the active power generation and demand are 2096 MW and 2076 MW, respectively. Table 3.6 gives the general characteristics of the system.

Table 3.6. General characteristics of test system.

Network	Nodes			Total
	Total	APG	RPG	Branches
166-node	166	22	24	236

where APG are nodes with active power generation and RPG are nodes with reactive power generation.

In order to show the robustness of the OPP algorithm when a large number of PSTs are embedded in the network, 11 conventional transformers were assumed to be PSTs. The parameters of the phase-shifting transformers embedded in the network are presented in Table 3.7. The transformer impedances are assumed to be on the secondary windings. The phase-shifting angle limits were set at $\pm 15^0$. The active power control is carried out with primary phase angle control. The PSTs were not set to control a fixed amount of active power flowing across them.

Table 3.7. Phase-shifting transformer parameters for the 166-node system.

Phase Shifting Transformer	Primary Tap			Secondary Tap		
	T_v (pu)	ϕ_{tv} (degrees)	X_p (pu)	U_u (pu)	ϕ_{uv} (degrees)	X_s (pu)
PAH-PAL	1.000	0.000	0.000	1.000	0.000	0.05226
MRH-MTL	1.000	0.000	0.000	1.000	0.000	0.05226
RUH-RUL	1.000	0.000	0.000	1.000	0.000	0.05517
TJH-TJL1	1.000	0.000	0.000	1.000	0.000	0.05226
TJH-TJL2	1.000	0.000	0.000	1.000	0.000	0.05146
MXH-MXL1	1.000	0.000	0.000	1.000	0.000	0.05356
MXH-MXL2	1.000	0.000	0.000	1.000	0.000	0.05356
CTH-CTL	1.000	0.000	0.000	1.000	0.000	0.11498
CIH-CIL1	1.000	0.000	0.000	1.000	0.000	0.18616
CIH-CIL2	1.000	0.000	0.000	1.000	0.000	0.06237
CIH-CIL3	1.000	0.000	0.000	1.000	0.000	0.05806

The actual power system was solved in 5 iterations. The second and third columns of Table 3.8 show the active power flowing across each transformer when they are modelled as conventional transformers. The fourth and fifth columns of Table 3.8 show the phase shifter angles and the active power flowing through the PSTs. This table shows the largest phase shifter angle increment to be -4.805^0. The active power flows are not greatly affected by the PSTs. However, phase-shifting transformers reduce active power generation cost and active power losses. The former were reduced from 293.643 to 293.625 $/hour, and the latter from 20.117 to 20.043 MW. In contrast, PSTs demand additional reactive power from the system. The total reactive power generated is approximately 1 MVAR more than the original case, where the PSTs are not operating.

Table 3.8. Phase-shifting transformer results for the 166-node system.

Phase Shifting Transformer	Conventional Transformers		PST operating	
	Phase angle ϕ_{tv} (degrees)	Active power flow (MW)	Phase angle ϕ_{tv} (degrees)	Active power flow (MW)
PAH-PAL	0	62.750	-1.144	77.714
MRH-MTL	0	50.884	-0.252	52.223
RUH-RUL	0	20.000	-4.805	19.991
TJH-TJL1	0	42.293	0.128	35.561
TJH-TJL2	0	42.951	0.144	35.565
MXH-MXL1	0	-82.025	0.000	-85.286
MXH-MXL2	0	-82.025	0.000	-85.286
CTH-CTL	0	-29.081	-0.871	-19.747
CIH-CIL1	0	6.513	-1.791	-0.200
CIH-CIL2	0	19.555	-2.927	32.172
CIH-CIL3	0	9.560	-0.243	5.320
CIH-CIL3	0	9.560	-0.243	5.320

3.4 Load Tap-Changing Transformer

Load tap changers (LTC) regulate nodal voltage magnitudes by varying the transformer tap ratio under load, without interruption. A schematic representation of a LTC transformer is shown in Figure 3.18 [11].

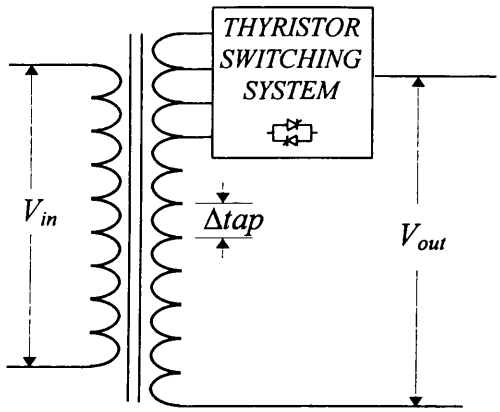

Figure 3.18. Thyristor Controlled Load-Tap Changing Transformer.

The voltage magnitude control at the output winding is achieved by injecting a small variable voltage magnitude in phase (added or subtracted) with the voltage magnitude at the output winding.

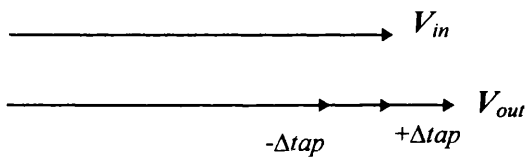

Figure 3.19. LTC transformer voltage vector diagrams.

Traditionally, a mechanical-based mechanism has been used to exert this change in voltage between two-winding, where the tap-changing operation was carried out by a motor drive unit. If the mechanical-based mechanism were to be replaced by a thyristor switching system then the output voltage magnitude adjustment would be carried out with almost no delay. However, independently of the mechanism used to switch between tap positions, the LTC transformer can only influence the relative voltage magnitude at the transformer nodes; they do not generate active or reactive power by themselves.

3.4.1 LTC Transformer Model for the Control of Nodal Voltage Magnitude

The LTC transformer model is derived from the two-winding single phase transformer model with complex taps on both the primary and secondary windings. The magnetising branch is also included to account for the core losses.

The transformer model introduced in Section 3.2, relating the primary voltage and current to the secondary voltage and current can also be expressed as,

$$\begin{bmatrix} I_p \\ I_s \end{bmatrix} = \begin{bmatrix} Y_{pp} & Y_{ps} \\ Y_{sp} & Y_{ss} \end{bmatrix} \begin{bmatrix} V_p \\ V_s \end{bmatrix} \tag{3.55}$$

where

$$Y_{pp} = \frac{U_v^2 + Z_s Y_0}{\Delta} \tag{3.56}$$

$$Y_{ps} = \frac{-T_v U_v^*}{\Delta} \tag{3.57}$$

$$Y_{sp} = \frac{-T_v^* U_v}{\Delta} \tag{3.58}$$

$$Y_{ss} = \frac{T_v^2 + Z_p Y_0}{\Delta} \tag{3.59}$$

3.4.2 The Classical Load Tap-Changing Transformer Model

In the open literature it is common practice to represent the Load Tap-Changing transformer as an impedance connected in series with an ideal transformer of tap ratio t:1. Figure 3.20 shows the equivalent circuit of a LTC connected between nodes p and s. The transformer tap-changing capabilities are taken to be on the tap connected to node p [1-3,15,16].

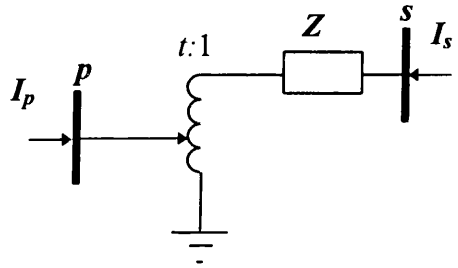

Figure 3.20. Equivalent circuit of a LTC transformer.

The classical LTC model can be obtained by introducing simplifications in the two-winding transformer model given by equation (3.55). If $T_v = T_i^* = t+j0$, $U_v = U_i^* = 1+j0$, $Y_o = \mathbf{0}$, $Z_p = \mathbf{0}$ and $Z_s = Z$, a nodal transfer admittance model for the LTC corresponding to Figure 3.20 can be obtained, as reference [1-3,15,16],

$$\begin{bmatrix} I_p \\ \hline I_s \end{bmatrix} = \frac{1}{T_v^2 Z_s} \begin{bmatrix} U_v^2 & -T_v U_v^* \\ \hline -T_v^* U_v & T_v^2 \end{bmatrix} \begin{bmatrix} V_p \\ \hline V_s \end{bmatrix} \tag{3.60}$$

Finally, the values of T_v and Z_s are substituted in equation (3.55) which gives,

$$\begin{bmatrix} I_p \\ \hline I_s \end{bmatrix} = \frac{1}{Z} \begin{bmatrix} 1/t^2 & -1/t \\ \hline -1/t & 1 \end{bmatrix} \begin{bmatrix} V_p \\ \hline V_s \end{bmatrix} \tag{3.61}$$

3.4.3 Lagrangian Function

The power flow equations are the same as those given for the PST model. The Lagrangian function incorporating the power flow mismatch equations at nodes p and s can be expressed as an equality constraint given by the following equation:

$$\begin{aligned} L_{ltc}(\boldsymbol{x},\lambda) = {} & \lambda_{pp}(P_p + P_{dp} - P_{gp}) + \lambda_{qp}(Q_p + Q_{dp} - Q_{gp}) \\ & + \lambda_{ps}(P_s + P_{ds} - P_{gs}) + \lambda_{qs}(Q_s + Q_{ds} - Q_{gs}) \end{aligned} \tag{3.62}$$

where $\boldsymbol{x}$ includes P_g, V, θ and T_v if the tapping facilities are on the primary winding. Otherwise, U_v replaces T_v. λ is the Lagrange multipliers vector for equality constraints.

3.4.4 Linearised System of Equations

The representation of the LTC in the OPF algorithm requires the matrix $\boldsymbol{W}$ to be augmented by one row and one column per transformer. Under this condition either T_v or U_v are extra state variables which become incorporated in the OPF formulation.

When the two-winding transformer has tap changing facilities only on the primary winding, i.e. $\boldsymbol{T_v}$:$1\angle 0^0$, the linearised system of equations for minimising the Lagrangian function via Newton's method is given by,

$$\begin{bmatrix}
\frac{\partial^2 L}{\partial \theta_p^2} & \frac{\partial^2 L}{\partial \theta_p \partial V_p} & \frac{\partial P_p}{\partial \theta_p} & \frac{\partial Q_p}{\partial \theta_p} & \frac{\partial^2 L}{\partial \theta_p \partial \theta_s} & \frac{\partial^2 L}{\partial \theta_p \partial V_s} & \frac{\partial P_s}{\partial \theta_p} & \frac{\partial Q_s}{\partial \theta_p} & \frac{\partial^2 L}{\partial \theta_p \partial T_v} \\
\frac{\partial^2 L}{\partial V_p \partial \theta_p} & \frac{\partial^2 L}{\partial V_p^2} & \frac{\partial P_p}{\partial V_p} & \frac{\partial Q_p}{\partial V_p} & \frac{\partial^2 L}{\partial V_p \partial \theta_s} & \frac{\partial^2 L}{\partial V_p \partial V_s} & \frac{\partial P_s}{\partial V_p} & \frac{\partial Q_s}{\partial V_p} & \frac{\partial^2 L}{\partial V_p \partial T_v} \\
\frac{\partial P_p}{\partial \theta_p} & \frac{\partial P_p}{\partial V_p} & & & \frac{\partial P_p}{\partial \theta_s} & \frac{\partial P_p}{\partial V_s} & & & \frac{\partial P_p}{\partial T_v} \\
\frac{\partial Q_p}{\partial \theta_p} & \frac{\partial Q_p}{\partial V_p} & & & \frac{\partial Q_p}{\partial \theta_s} & \frac{\partial Q_p}{\partial V_s} & & & \frac{\partial Q_p}{\partial T_v} \\
\frac{\partial^2 L}{\partial \theta_s \partial \theta_p} & \frac{\partial^2 L}{\partial \theta_s \partial V_p} & \frac{\partial P_p}{\partial \theta_s} & \frac{\partial Q_p}{\partial \theta_s} & \frac{\partial^2 L}{\partial \theta_s^2} & \frac{\partial^2 L}{\partial \theta_s \partial V_s} & \frac{\partial P_s}{\partial \theta_s} & \frac{\partial Q_s}{\partial \theta_s} & \frac{\partial^2 L}{\partial \theta_s \partial T_v} \\
\frac{\partial^2 L}{\partial V_s \partial \theta_p} & \frac{\partial^2 L}{\partial V_s \partial V_p} & \frac{\partial P_p}{\partial V_s} & \frac{\partial Q_p}{\partial V_s} & \frac{\partial^2 L}{\partial V_s \partial \theta_s} & \frac{\partial^2 L}{\partial V_s^2} & \frac{\partial P_s}{\partial V_s} & \frac{\partial Q_s}{\partial V_s} & \frac{\partial^2 L}{\partial V_s \partial T_v} \\
\frac{\partial P_s}{\partial \theta_p} & \frac{\partial P_s}{\partial V_p} & & & \frac{\partial P_s}{\partial \theta_s} & \frac{\partial P_s}{\partial V_s} & & & \frac{\partial P_s}{\partial T_v} \\
\frac{\partial Q_s}{\partial \theta_p} & \frac{\partial Q_s}{\partial V_p} & & & \frac{\partial Q_s}{\partial \theta_s} & \frac{\partial Q_s}{\partial V_s} & & & \frac{\partial Q_s}{\partial T_v} \\
\frac{\partial^2 L}{\partial T_v \partial \theta_p} & \frac{\partial^2 L}{\partial T_v \partial V_p} & \frac{\partial P_p}{\partial T_v} & \frac{\partial Q_p}{\partial T_v} & \frac{\partial^2 L}{\partial T_v \partial \theta_s} & \frac{\partial^2 L}{\partial T_v \partial V_s} & \frac{\partial P_s}{\partial T_v} & \frac{\partial Q_s}{\partial T_v} & \frac{\partial^2 L}{\partial T_v^2}
\end{bmatrix}
\begin{bmatrix} \Delta\theta_p \\ \Delta V_p \\ \Delta\lambda_{pp} \\ \Delta\lambda_{qp} \\ \Delta\theta_p \\ \Delta V_p \\ \Delta\lambda_{ps} \\ \Delta\lambda_{qs} \\ \Delta T_v \end{bmatrix}
=
\begin{bmatrix}
-\frac{\partial L}{\partial \theta_p} \\ -\frac{\partial L}{\partial V_p} \\ -\frac{\partial L}{\partial \lambda_{pp}} \\ -\frac{\partial L}{\partial \lambda_{qp}} \\ -\frac{\partial L}{\partial \theta_s} \\ -\frac{\partial L}{\partial V_s} \\ -\frac{\partial L}{\partial \lambda_{ps}} \\ -\frac{\partial L}{\partial \lambda_{qs}} \\ -\frac{\partial L}{\partial T_v}
\end{bmatrix}
\tag{3.63}$$

where L=L_{ltc}. The first and second derivative expressions for all the terms used in equation (3.63) are given in Appendix II.

If the tap changing facilities of the two-winding transformer are on the secondary winding rather than on the primary, i.e. $\boldsymbol{U_v}$:$1\angle 0^0$, then the variable U_v will replace the variable T_v in equation (3.63). The other elements of equations (3.63) remain unchanged.

If the LTC transformer is controlling the voltage magnitude at a specified value, either p or s, the matrix $\boldsymbol{W}$ is modified by adding the second derivative term of a large quadratic penalty function to the diagonal element corresponding to either p or s. The first derivative term of the quadratic penalty function is also added to the corresponding gradient element.

3.4.5 Handling Limits of LTC Transformer Variables

The handling of LTC transformers inequality constraints was also carried out by using the Multipliers method [18]. Tap changer positions inside bounds are ignored whilst binding inequality constraints become enforced by the function given by (3.54). The variable T_v replaces ϕ_{tv} if the tapping facilities are on the primary winding.

3.4.6 Initial Conditions

Complex Taps

The initial condition of the primary and secondary complex taps are set with a magnitude of one and phase angle of zero. It was observed that for initial conditions at T_v=0.9$\angle 0^0$ or T_v=1.1$\angle 0^0$ the algorithm is still very reliable towards the convergence.

3.4.7 Practical Implementation

The voltage magnitude and the tap position of the tap changer, at the same node, are strongly interrelated. If a pair of these variables are outside limits, simultaneously, during the solution process, the voltage magnitude is bounded first. The tap changer limits are not made active if its associated voltage magnitude is not inside limits. If these variables are bounded and they are about to be released at the end of a main iteration, only one of them will be released. The sequence is reversed with respect to the sequence of the binding procedure.

3.4.8 LTC Transformer Test Cases

The original 5-node system [15] presented previously in Section 3.3.9 is now modified to include a LTC transformer in series with the transmission line connected between Lake and Main, and two parallel connected transformers in series with transmission line Elm-Main. Two additional dummy nodes, LakeLTC and ElmLTC are used. The configuration of the upgraded network is shown in Figure 3.21. The LTCs are not maintaining voltage magnitude at a specified value. The primary and secondary complex taps of the three LTC transformers were initialised at $1\angle 0^0$. The transformer impedances are taken to be on the secondary winding, where the resistance are 0 and the inductive reactance are 0.05 pu. The tap in the primary winding is used to regulate the voltage magnitudes at both LTC transformer terminals. The OPF algorithm takes 4 iterations to converge. The power flow results are shown in Figure 3.21. The nodal complex voltages, active and reactive power dispatch and Lagrange multiplier at each node are given in Table 3.9.

Table 3.9. Nodal complex voltages of modified system with an LTC.

Node	Voltage Magnitude (pu)	Phase Angle (degrees)	Active Power (MW)	Reactive Power (MVA)	λ_p ($/MWhr)
LakeLTC	1.077	-3.815	0	0	4.2247
ElmLTC	1.072	-4.457	0	0	4.2640
Elm	1.072	-4.508	0	0	4.2645
Main	1.077	-4.013	0	0	4.2352
Lake	1.078	-3.505	0	0	4.2222
South	1.100	-1.332	87.91	14.55	4.1033
North	1.109	0.000	80.14	0.24	4.0411

The adjustment of tap changers operating in parallel was achieved with no problem. Table 3.10 shows the tap changer position as a function of the iteration number. The OPF using Newton's method updates the taps of both parallel tap changers identically if the transformer parameters are also identical.

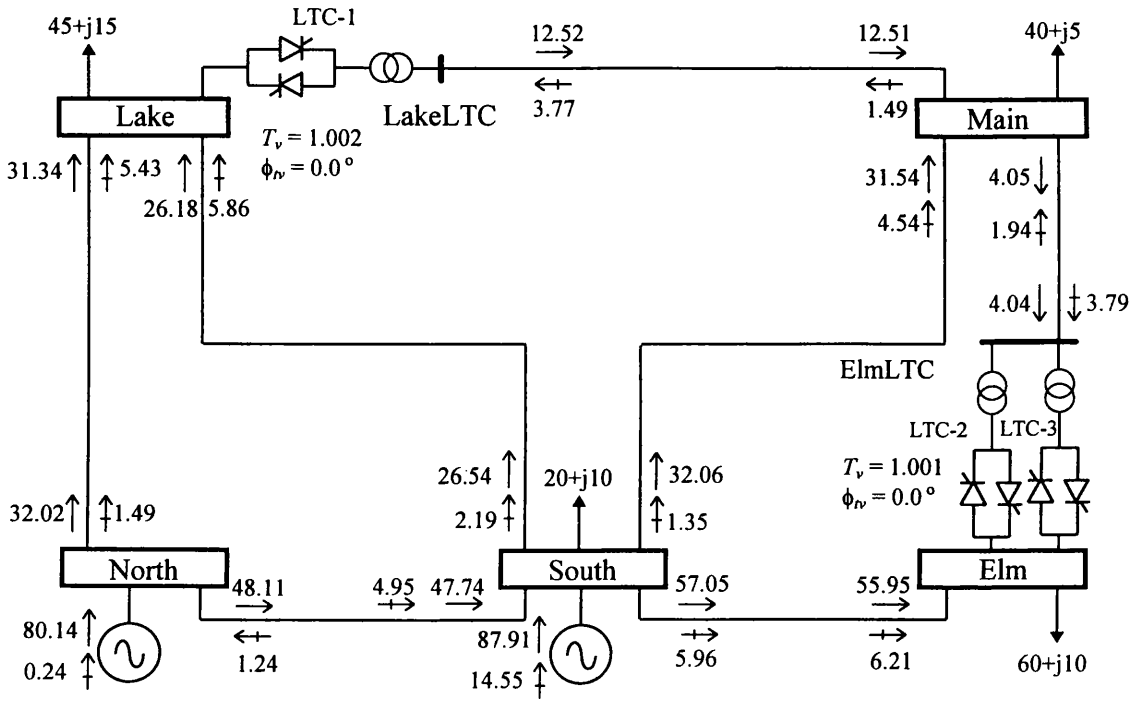

Figure 3.21. Modified 5-node system with LTCs and OPF solution.

Extensive tests have shown that the OPF using Newton's method can handle parallel transformer configurations with ease. This applies whether or not the transformers have different parameters or tap position limits. If a LTC hits one of its limits, then the Multipliers Method is used to enforce the offending limit.

Table 3.10. Tap position in tap changers for the 5-node test system.

Iterations	LTC-1 T_v	LTC-2	LTC-3 T_v
0	1.000	1.000	1.000
1	1.007	1.007	1.007
2	1.001	0.998	0.998
3	1.003	1.001	1.001
4	1.002	1.001	1.001

3.4.9 Effect of the Initial Tap Position

This Section investigates the robustness of the OPF algorithm as function of the initial tap positions. The AEP 14-node system [12] was modified to this effect, the conventional transformers connected at nodes Nod_5-Nod_6 and Nod_4-Nod_9 were taken to be LTC transformers as shown in Figure 3.22. The LTC transformers are set free to regulate voltage magnitudes optimally. The transformer reactances [12] were assumed to be on the secondary winding. The tap capabilities were placed on the primary side.

Five different simulations were carried out. The first one was started from an initial tap position of 0.9 for both transformers. Subsequent simulations were 0.95, 1.00, 1.05 and 1.1. The number of iterations taken to obtain the solution was 5 for all cases. The case when there are no LTC transformers in the network yields the following solution: the

active power generation cost is 215.457 $/hour and the active power losses are 1.901 MW. LTC transformers benefit the operation of the network, with the algorithm giving the following solution: 215.374 $/hour and 1.840 MW.

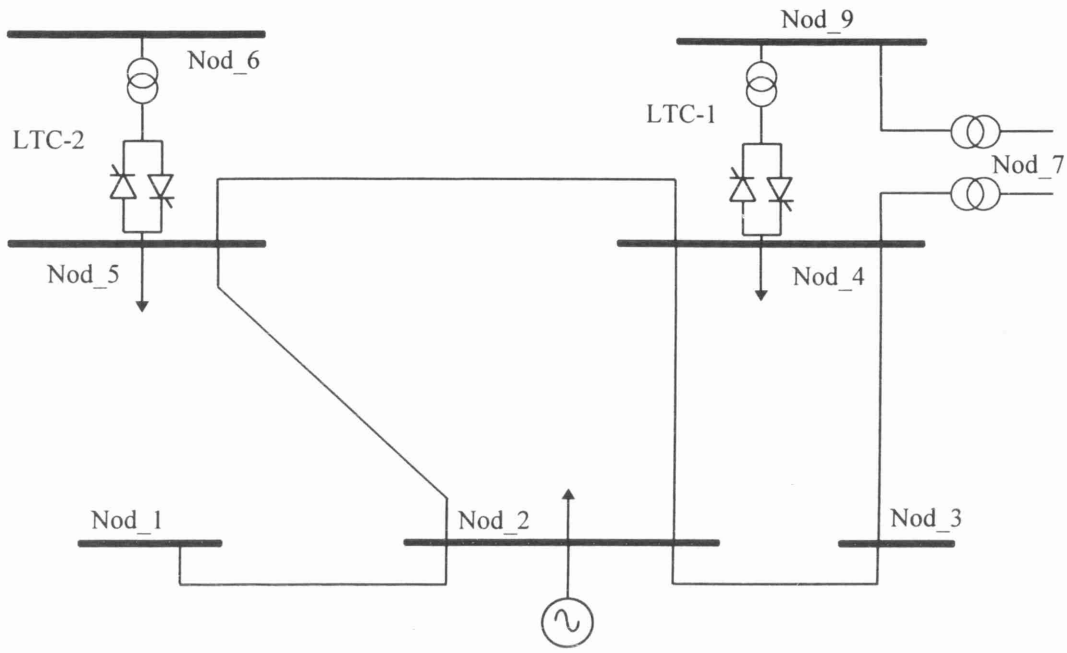

Figure 3.22. Relevant part of AEP 14-node system with two LTCs embedded.

Figures 3.23 and 3.24 show the tap position profiles for LTC-1 and LTC-2 as a function of the iteration number. The tap changers are shown to be very sensitive to changes in the set of active constraint of voltage magnitudes and the penalty weighting factor. However, the results show the robustness of the OPF algorithm towards the convergence regardless of the initial condition.

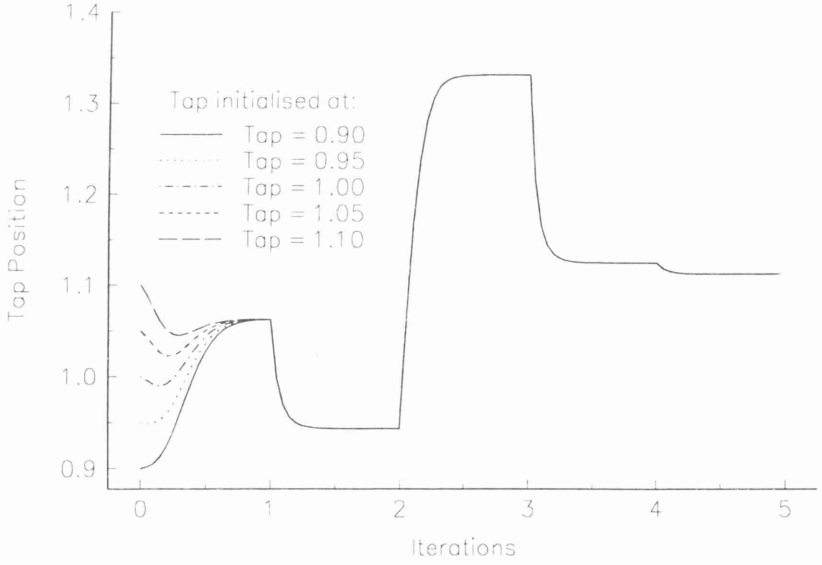

Figure 3.23. Tap position profile for LTC-1.

Figure 3.25 depicts the nodal voltage profiles as a function of the number of iterations. Significant differences can be observed during the five iterations, due to the interaction between the voltage magnitudes and the tap changers. During the iterative process, three nodes, Nod_4, Nod_5 and Nod_7, were enforced by means of the Multipliers Method,

leading to large tap position variations. By way of example, at the beginning of the first iteration, the nodal voltage magnitudes at Nod_4 and Nod_5 were enforced affecting greatly the tap position of LTC-1 and LTC-2, as shown in Figures 3.23 and 3.24. In fact, the tap changer drove the voltage magnitudes towards their top values, and hence, producing large variations in the rest of the network.

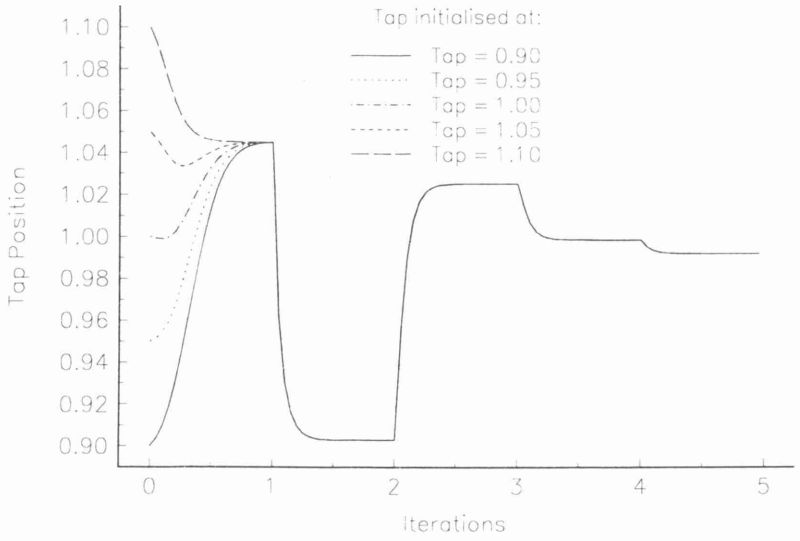

Figure 3.24. Tap position profile for LTC-2.

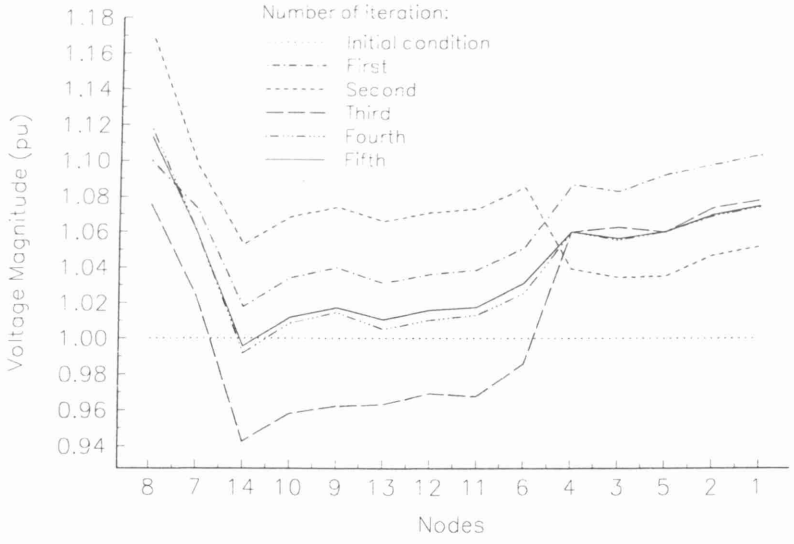

Figure 3.25. Nodal voltage profiles for the AEP 14-node system upgraded with two LTCs.

In contrast, Figure 3.26 depicts the nodal voltage profiles for the case with no LTCs. As it can be observed, the profiles at each iteration are more regular than those in Figure 3.25, where smaller voltage variations take place during the iterative process. Here, only the voltage at Nod_7 was enforced by the algorithm.

In order to show the versatility of the algorithm the LTC transformers were used to maintain the Nod_5 and Nod_4 voltage magnitudes at 1.05 pu. The initial conditions and the control facilities were the same as those used above. Converge was obtained in 4 iterations to a tolerance of 10^{-9}. The nodes Nod_5 and Nod_4 upheld their target value.

Figure 3.26. Nodal voltage profiles for the AEP 14-node system.

Figure 3.27 depicts the tap position profiles for LTC-1 and LTC-2 as a function of the iteration number. It can be observed that the increments in the tap changer were smaller than the case where the voltage magnitudes were not maintained at a specified value. Furthermore, the iteration number taken to converge was reduced from 5 to 4. The OPF algorithm seems to be more robust under this operating condition.

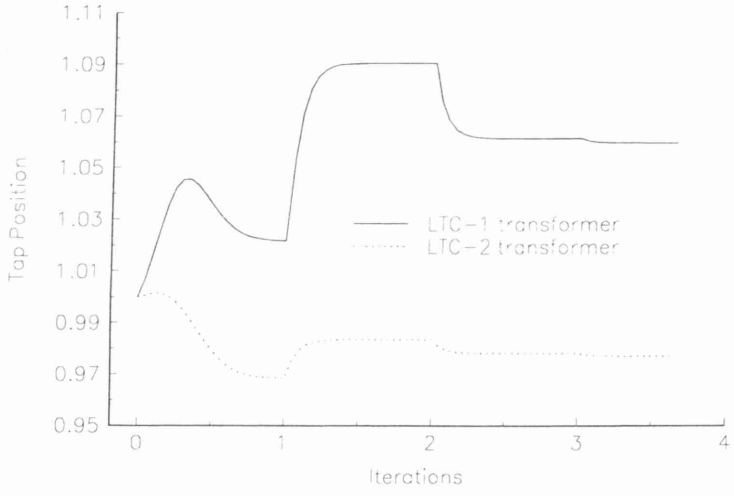

Figure 3.27. Tap position profile for LTC-1 and LTC-2.

3.4.10 LTC Transformers in a Real Power System

The power system used in Section 3.3.11 was suitably modified to incorporate LTC transformer devices [13]. In order to show the robustness of the OPF algorithm when a large number of LTCs are embedded in the network, the 11 conventional transformers were substituted by LTCs.

The parameters of the LTC are presented in Table 3.7. The impedances of the transformers are taken to be in the secondary winding. The upper and lower LTC transformer limits were 0.95 and 1.05, respectively, for all the transformers. The voltage magnitude control is carried out with the primary tap changing facilities. The LTCs were set free to regulate voltage magnitude.

The actual power system was solved by using the Newton OPF algorithm. The number of iterations taken to converge was 13. Table 3.11 shows the initial tap changer positions for all the LTC transformers. The nodal voltage magnitude at the primary and

secondary nodes of all the transformers are also shown. The last three columns of Table 3.11 show the tap changer positions and nodal voltage magnitudes at both terminal nodes. As can be observed, the voltage magnitude at the LTC's terminals were slightly increased, which benefited the operational conditions of the power system by reducing the active power cost and network losses.

Table 3.11. Tap changer positions for the transformers in the 166-node system.

Transformer	Original conditions			LTC is operating		
	Tap	Voltage Mag. (pu)		Tap	Voltage Mag.(pu)	
		primary	secondary		primary	secondary
PAH-PAL	1.000	1.0140	1.0133	1.0207	1.0322	1.0124
MTH-MTL	1.000	1.0133	1.0114	1.0164	1.0317	1.0121
RUH-RUL	1.000	1.0147	1.0109	1.0174	1.0269	1.0056
TJH-TJL1	1.000	1.0141	1.0119	1.0202	1.0320	1.0107
TJH-TJL2	1.000	1.0141	1.0119	1.0202	1.0320	1.0107
MXH-MXL1	1.000	1.0183	1.0061	0.9618	1.0262	1.0386
MXH-MXL2	1.000	1.0183	1.0061	0.9618	1.0262	1.0386
CTH-CTL	1.000	1.0216	1.0057	0.9500	1.0257	1.0404
CIH-CIL1	1.000	1.0135	1.0143	1.0088	1.0292	1.0198
CIH-CIL2	1.000	1.0135	1.0143	1.0102	1.0292	1.0198
CIH-CIL3	1.000	1.0135	1.0101	1.0128	1.0292	1.0113

Table 3.12 summarises the active power generation cost, network losses and active and reactive power generations. As pointed out above, the LTC transformers are suitable for reducing active power generation cost and active power losses. Furthermore, a re-distribution of reactive power flows throughout the network was produced by changing the LTC transformer taps, which benefited the operational condition of the power system. The total reactive power generated is smaller than in the case when no LTCs where in operation.

Table 3.12. Final results for 166-node system.

Results	Original conditions	LTC operating
Active power generation cost ($/hr)	293.64	293.25
Active power losses (MW)	20.117	20.064
Active power generation (MW)	2095.92	2095.86
Reactive power generation (MVAR)	512.39	501.24

3.5 Effect of the Transformer Magnetising Branch

The transformer magnetising branch in the transformer model has been implemented for completeness. The magnetising branch of the transformer is non-linear in order to account for possible saturation effects. This procedure also allows for the inclusion of the transformer iron losses, hence providing a method for conducting accurate electric energy loss studies. An experimental magnetising characteristic corresponding to a practical transformer was used in this study [14]. The following expression was found to approximate well the experimental magnetising characteristics.

$$I = 0.0034202V + 0.0025818V^{19} \tag{3.64}$$

The value of B_0 can be derived from (3.64). The following expression exists if the tap is located on the primary winding and the impedance is on the secondary side of the transformer,

$$B_0 = -\left[0.0034202\frac{1}{T_v} + 0.049054\left(\frac{V_p}{T_v}\right)^{18} \right] \tag{3.65}$$

The effect of the magnetising branch on network losses is illustrated below.

3.5.1 Effect of the Magnetising Branch in LTC Transformers

The test system reported in this section is the 166-node system [13]. Firstly, the 11 transformers are assumed to have no voltage regulating capabilities. However, the voltage magnitudes are constrained between upper and lower limits. The transformer impedances were assumed to be on the secondary windings and the tap changers were assumed to be on the primary winding. The initial complex taps were set at $\boldsymbol{T}_v = 1\angle 0^0$.

Unregulated Transformers

In order to compare the effect of the magnetising branch, Table 3.13 presents three different cases where the controllable transformers were not in operation, i.e. the transformers were modelled as conventional transformers. The three cases were: (A) No Magnetising Branch (NMB), (B) Linear Magnetising Branch (LMB), and (C) Non-linear Magnetising Branch (NLMB). Table 3.13 shows that the active power generation cost and active power losses are very similar in all three cases. However, some differences are observed in the reactive power generated by the system, the largest increment is reached when the non-linear magnetising branch is taken into account. Also, in the NLMB case, the iteration number is increased by 1.

Table 3.13. Effect of magnetising branch in the 166-node system.

Results	Conventional Transformers		
	NMB	LMB	NLMB
Active power generation cost ($/hr)	293.643	293.697	293.632
Active power losses (MW)	20.117	20.331	20.431
Active power generation (MW)	2095.92	2096.13	2096.23
Reactive power generation (MVAR)	512.386	512.893	521.549
Iterations	5	5	6

Regulated Transformers

The 166-node system with LTC transformers was solved taking the effects of the magnetising branch into account. Three cases were solved (a) NMB, (b) LMB, and (c) NLMB. Table 3.14 shows the final position of the tap changers. The final values are not greatly affected by the magnetising branch.

Table 3.15 shows the results for these cases. As expected, there were increments in the reactive power demanded from the system. However, they are smaller than those shown in Table 3.13. The reason is that in this case additional control variables become available, which minimise the reactive power losses by regulating nodal voltage magnitudes in an optimal fashion. Hence, the reactive power for each case are smaller than those values presented in Table 3.13.

Table 3.14. Effect of the magnetising branch in the position of tap changers for 166-node system.

LTC Transformer	Tap position of tap-changers		
	NMB	LMB	NLMB
PAH-PAL	1.0207	1.0231	1.0245
MTH-MTL	1.0164	1.0165	1.0179
RUH-RUL	1.0174	1.0174	1.0194
TJH-TJL1	1.0202	1.0204	1.0217
TJH-TJL2	1.0202	1.0204	1.0217
MXH-MXL1	0.9618	0.9618	0.9643
MXH-MXL2	0.9618	0.9618	0.9643
CTH-CTL	0.9500	0.9500	0.9500
CIH-CIL1	1.0088	1.0088	1.0104
CIH-CIL2	1.0102	1.0102	1.0118
CIH-CIL3	1.0128	1.0129	1.0146

Table 3.15. Effect of magnetising branch in the 166-node system (LTC transformers in operation).

Results	Conventional Transformers		
	NMB	LMB	NLMB
Active power generation cost ($/hr)	293.255	293.308	293.297
Active power losses (MW)	20.0643	20.278	20.245
Active power generation (MW)	2095.86	2096.08	2096.05
Reactive power generation (MVAR)	501.236	501.875	505.511
Iterations	13	13	14

3.5.2 Effect of the Magnetising Branch in PS Transformers

In this case, the active power flowing from node p to s is not maintained at a fixed active power flow. The phase shifter facilities were considered to be on the primary winding. The taps changers on both sides of the transformer were fixed at 1 pu, and all initial phase angles were set at 0^0. Table 3.16 shows the final position of the phase shifters. Similarly to the LTC cases presented above, the final values of the transformer parameters were not greatly affected by the presence of the magnetising branch.

Table 3.17 presents results where it can be observed that the phase shifters reduce both active power generation cost and active power losses. In contrast, phase shifters demand quite a substantial amount of reactive power from the system. Table 3.17 shows that the total reactive power generated by the system is larger than the case in which the phase shifters are not operating (Table 3.13).

It can be observed in the last three cases presented above that the inclusion of the magnetising branch in the study does not affect the generation costs by much. However, the magnetising branch is responsible for increasing the active power losses and the reactive power generated by the system. As far as active power losses are concerned, the linear and non-linear representation of the magnetising branch yield identical results. However, the non-linear representation becomes important when assessing system reactive power generation.

Table 3.16. Effect of the magnetising branch in the position of phase shifters for 166-node system

PS transformer	Phase shifter angle (degrees)		
	NMB	LMB	NLMB
PAH-PAL	-1.1438	-1.1443	-1.1345
MTH-MTL	-0.2526	-0.2523	-0.2480
RUH-RUL	-4.8025	-4.8061	-4.6898
TJH-TJL1	0.1280	0.1284	0.1278
TJH-TJL2	0.1439	0.1443	0.1437
MXH-MXL1	0.0000	0.0000	0.0000
MXH-MXL2	0.0000	0.0000	0.0000
CTH-CTL	-0.8711	-0.8714	-0.8360
CIH-CIL1	-1.7911	-1.7911	-1.7811
CIH-CIL2	-2.9273	-2.9275	-2.9082
CIH-CIL3	-0.2429	-0.2424	-0.2392

Table 3.17. Effect of magnetising branch in the 166-node system (phase shifters in operation).

Results	Conventional Transformers		
	NMB	LMB	NLMB
Active power generation cost ($/hr)	293.625	293.678	293.501
Active power losses (MW)	20.0439	20.2577	20.3890
Active power generation (MW)	2095.84	2096.06	2096.19
Reactive power generation (MVAR)	513.268	513.776	521.857
Iterations	5	5	7

3.6 Conclusions

This Chapter has introduced advanced transformer control modelling facilities within the context of optimal power flow solutions within the context of transmission networks. The OPF algorithm uses Newton's method to solve the linearised system of equations, leading to very robust iterative solutions for networks of any size. Moreover, the Multipliers method is used to handle the LTC and phase-shifting transformer control variables, leading to highly flexible and efficient, constrained OPF solutions. The algorithm has been used to solve a large number of standard and non-standard networks of various sizes. Its prowess has been illustrated by numeric examples. In general, the solution of networks containing LTCs and phase-shifting transformers is achieved in the same number of iterations as networks with no controllable transformers i.e. 5-7 iterations. Furthermore, extensive computational testing has indicated that the OPF algorithm is not really affected by the initial condition given to both PS and LTC transformers.

A new and generalised three-winding transformer model with complex tap ratios in each winding has been developed from first principles. Only two and three-winding transformer models have received attention in this work since transformers with a higher number of windings are not common in high voltage AC transmission. The model is shown to be a general case for the existing two-winding transformer models and the classic LTC and phase-shifting transformer models. The model includes the effect of the magnetising branch of the transformer, which under saturating conditions becomes non-linear. This allows for more realistic electric energy studies, where the non-linear

magnetising branch is shown to be responsible for increasing active power losses and reactive power system requirements by 1-2% and 2-3%, respectively. However, the magnetising branch does not have a great effect on the total generation cost.

3.7 References

[1] Peterson N.M. and Scott-Meyer W.: 'Automatic Adjustment of Transformer and Phase Shifter Taps in the Newton Power Flow', IEEE Transactions on Power Apparatus and Systems, Vol. PAS-90, No. 1, January/February 1971, pp. 103-108.

[2] Shen C.M. and Laughton M.: 'Determination of Optimum Power-System Operating Conditions Under Constraints', Proceedings of IEE, Vol. 116, No. 2, February 1969, pp. 225-239.

[3] Sun D.I., Ashley B., Brewer B., Hughes A. and Tinney W.F.: 'Optimal Power Flow By Newton Approach', IEEE Transactions on Power Apparatus and Systems, Vol. PAS-103, No 10, October 1984, pp. 2864-2880.

[4] Sun D.I., Hu T.I., Lin G.S., Lin C.J. and Chen C.H.: 'Experiences with Implementing Optimal Power Flow for Reactive Scheduling in the Taiwan Power System', IEEE Transactions on Power Systems, Vol. 3, No. 3, August. 1988, pp. 1193-1200.

[5] Electricity-DINIS (E): 'Technical Information for Engineers,' International Computers Limited, Leeds, UK, July 1993.

[6] Fuerte-Esquivel C.R. and Acha E.: 'Newton-Raphson Algorithm for the Reliable Solution of Large Power Networks With Embedded FACTS Devices', IEE Proceedings Genereration, Transmission and Distribution, Vol. 143, No. 5, September 1996, pp. 447-454.

[7] Fuerte-Esquivel C.R. and Acha E.: 'A Newton-Type Algorithm for the Control of Power Flow in Electrical Power Networks', IEEE Transactions on Power Systems, Vol. 12, No. 4, November 1997, pp. 1474-1480.

[8] Hingorani N.G.: 'Flexibly AC Transmission Systems', IEEE Spectrum, April 1993, pp. 40-45.

[9] Hingorani N.G.: 'Introducing CUSTOM POWER', IEEE Spectrum, June 1995, pp. 41-48.

[10] Kappenman J.: 'Static Phase Shifter Applications and Concepts for the Minnesota-Ontario Interconnection', Flexible AC Transmission Systems (FACTS) Conference, EPRI, Boston Massachusetts, 18-20 May, 1992.

[11] IEEE/CIGRE: 'FACTS Overview', Special Issue, 95TP108, IEEE Service Center, Piscataway, N.J., 1995.

[12] Freris L.L. and Sasson A.M.: 'Investigation of the Load-Flow Problem', Proceedings of IEE, Vol. 115, No. 10, October 1968, pp. 1459-1470.

[13] Aboytes F. and Arroyo G.: 'Security Assessment in the Operation of Longitudinal Power Systems', IEEE Transactions on Power Apparatus and Systems, Vol. PWRS-1, No. 2, May 1986, pp. 225-232

[14] Dommel H.W., Yan A. and De Marcano, R.J.O.: 'Case Studies for Electromagnetic Transients', Internal Report, Department of Electrical Engineering, University of British Columbia, Vancouver, Canada, 1983.

[15] Stagg G.W. and El-Abiad A.H.: 'Computer Methods in Power Systems Analysis', McGraw-Hill, 1968.

[16] Elgerd O.: 'Electric Energy Systems Theory: An Introduction', McGraw-Hill, 1971.

[17] Luenberger D.G.: 'Introduction to Linear and Nonlinear Programming', Addison Wesley Publishing Co., 1984.

[18] Bertsekas D.P.: 'Constrained Optimization Lagrange Multiplier Methods', Academic Press, 1992.

[19] Wollenberg B. and Wood A. J., 'Power Generation, Operation and Control', John Wiley & Sons Inc., Second Edition, 1984.

[20] Shen C.M. and Laughton M. A.: 'Determination of Optimum Power-System Operating Conditions Under Constraints', IEE Proceedings, Vol. 116, No. 2, February 1969, pp. 225-239.

[21] Brameller A. and Pandey R.S.: 'General Fault Analysis Using Phase Frame of Reference', Proceedings of IEE, Vol. 121, No. 5, May 1974, pp. 366-368.

Chapter 4

Advanced SVC Models for Optimal Power Flow

Advanced load flow models for the Static VAR Compensator (SVC) are presented in this Chapter. The models are incorporated in an existing Optimal Power Flow (OPF) algorithm. Unlike SVC models available in open literature, the new models depart from the *generator* representation of the SVC and are based instead on the variable shunt susceptance concept. In particular, a SVC model which uses the firing angle as the state variable provides key information for cases when the load flow solution is used to initialise other power system applications, e.g. harmonic analysis. The SVC state variables are combined with the nodal voltage magnitudes and angles of the network in a single frame-of-reference for a unified, iterative solution through Newton's method. The OPF algorithm exhibits very strong convergence characteristics, regardless of network size and the number of controllable devices. Results are presented which demonstrate the prowess of the new SVC models.

4.1 Introduction

In electric power systems, one of the objectives is to supply electric energy at the lowest possible cost and in a continuous way. Moreover, the frequency and voltage magnitude throughout the power system must be kept within limits. It is well known that operational problems are likely to occur if the voltage magnitude in parts of the network deviates significantly from its nominal value. For example, if the load level in the system is low, over-voltages can arise due to the Ferranti effect, mainly at the 400 KV level and above. Over-voltages can cause equipment failures due to insulation breakdown and produce magnetic saturation in transformers, resulting in harmonic generation. Capacitive over-compensation and over-excitation of synchronous machines can also occur [1]. The complexity of power systems has grown relentlessly due to the large interconnection programs directed at making better use of generation capacity between countries. As a consequence, to maintain good voltage and frequency regulation is not a straight-forward issue.

The production and absorption of reactive power allows the nodal voltage magnitude to be regulated. Sources and sinks of reactive power, such as shunt capacitors, shunt reactors, synchronous condensers and SVCs are used for this purpose. Shunt capacitors and shunt reactors are either permanently connected to the network, or switched on and

off according to daily requirements. They only provide passive compensation since their production/absorption of reactive power depends on their ratings and local bus voltage level. Conversely, the reactive power supplied/absorbed by synchronous condensers and SVCs is automatically adjusted, attempting to regulate the voltage magnitude at the connection point in an adaptive fashion.

This Chapter focuses on the development of new SVC models and their implementation in an Optimal Power Flow computer program. The SVC is assumed to be a continuous, variable shunt susceptance, which is adjusted in order to achieve a specified voltage magnitude while satisfying network constraint conditions.

Two models are presented in this Chapter:

- The SVC Controllable susceptance model. A changing susceptance B_{svc} represents the fundamental frequency equivalent susceptance of all shunt modules making up the SVC. This model is an improved version of SVC models currently available in open literature.
- The SVC firing angle model. The equivalent susceptance of the SVC which is function of a changing firing angle α, is made up of the parallel combination of a Thyristor Controlled Reactor (TCR) equivalent admittance and a fixed capacitive susceptance. This is a new and more advanced SVC representation than those which are currently available in the open literature. This model provides information on the SVC firing angle required to achieve a given level of compensation, which is useful to initialise other power system applications.

The SVC models have been tested in a wide range of power networks of varying sizes. In this Chapter, three power systems, consisting of 5, 14 and 166 nodes are used to demonstrate the prowess of the new SVC models. The 166-node network corresponds to a portion of a large utility power network.

4.2 Static VAR Compensator's Equivalent Susceptance

Power electronics technology, together with sophisticated control methods, made the development of fast SVCs in the early 1970s possible. The SVC consists of a group of shunt connected capacitors and reactor banks with fast control action by means of thyristor switching. Usually a purpose-built transformer is employed between the high-voltage bus and the low-voltage bus. However, the tertiary winding of an existing transformer is also a popular option. From the operational point of view, the SVC can be seen as a variable shunt reactance with automatic adjustment in response to changing system operating conditions. Depending on the nature of the equivalent SVC's reactance, i.e. capacitive or inductive, the SVC either draws capacitive or inductive current from the network. Suitable control of this equivalent reactance allows voltage magnitude regulation at the SVC point of connection. SVCs achieve their main operating characteristic at the expense of generating harmonic currents and filters are employed with them.

SVCs may consist of a combination of mechanically controlled and thyristor controlled shunt capacitors and reactors [1,2]. The most popular configurations for continuously controlled SVCs are the combination of either fixed capacitor and thyristor controlled reactor or thyristor switched capacitor and thyristor controlled reactor [3,4]. As far as positive sequence steady-state analysis is concerned, both configurations can be modelled along similar lines. The SVC structure shown in Figure 4.1 is used to derive a SVC model which considers the TCR firing angle α as a state variable. This is a new

and more advanced SVC load flow representation than what is currently available in the open literature.

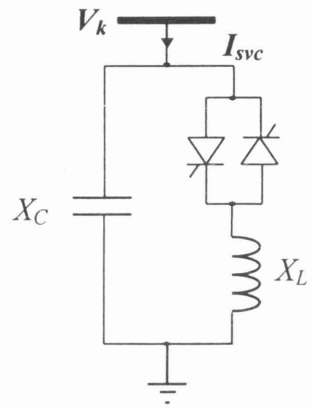

Figure 4.1. SVC structure used to derive the model based on the firing angle.

The variable TCR equivalent reactance, X_{Leq}, at the fundamental frequency, is given by [3],

$$X_{Leq} = X_L \frac{\pi}{2(\pi - \alpha) + \sin(2\alpha)} \tag{4.1}$$

where α is the thyristor's firing angle.

The SVC effective reactance X_{svc} is determined by the parallel combination of X_C and X_{Leq},

$$X_{svc} = \frac{X_C \, X_L}{\frac{X_C}{\pi}\left(2(\pi - \alpha) + \sin(2\alpha)\right) - X_L} \tag{4.2}$$

Depending on the ratio X_C/X_L there is a value of firing angle that causes a fundamental frequency resonance to occur. Figure 4.2 shows the SVC equivalent impedance at the fundamental frequency, as a function of the firing angle. It corresponds to a capacitive reactance of 15 Ω and a variable inductive reactance of 2.6 Ω.

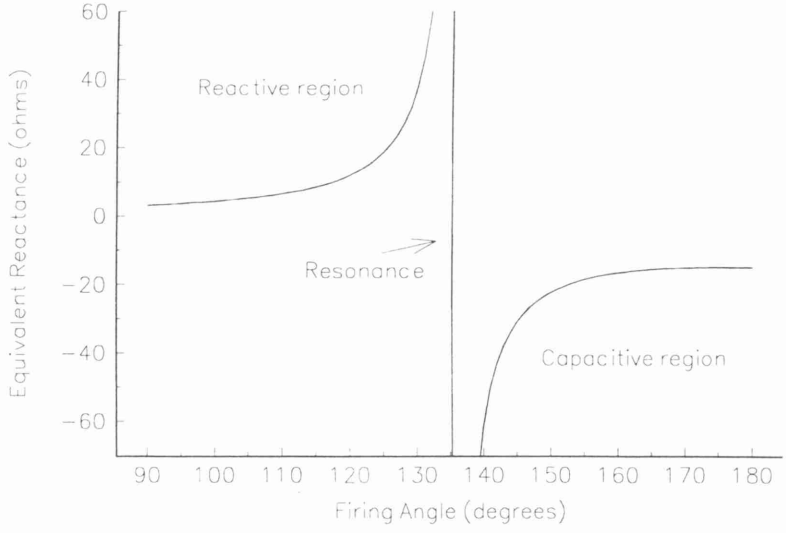

Figure 4.2. SVC equivalent reactance as a function of the firing angle.

The SVC equivalent susceptance is given by equation (4.3) whilst its profile, as a function of the firing angle, is given in Figure 4.3.

$$B_{svc} = -\frac{X_L - \frac{X_C}{\pi}\left(2(\pi-\alpha)+\sin(2\alpha)\right)}{X_C X_L} \tag{4.3}$$

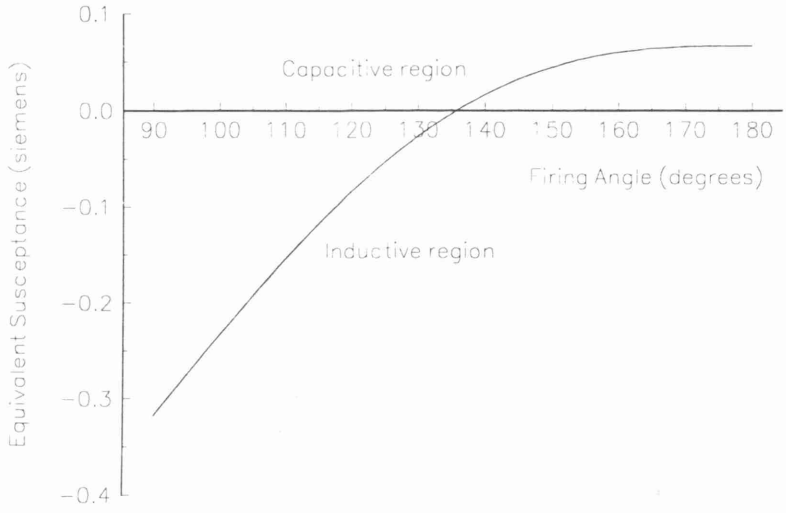

Figure 4.3. SVC equivalent susceptance as a function of the firing angle.

It is shown in Figure 4.3 that the SVC equivalent susceptance profile, as a function of the firing angle, does not present discontinuities. B_{svc} varies smoothly in both operative regions. Hence, linearisation of the SVC power flow equations, based on B_{svc}, with respect to the firing angle, should exhibit a better numerical behaviour than the linearised model based on X_{svc}.

4.3 Established SVC Load Flow Models

The SVC models for load flow analysis recommended by CIGRÉ [1] and IEEE [4] are widely used. The SVC is treated as a *generator* behind an inductive reactance when the SVC is operating within limits. This reactance represents the SVC voltage regulation characteristic, i.e. SVC's slope, X_{SL}.

A simpler representation assumes that the SVC slope, which accounts for voltage regulation, is zero. This assumption may be acceptable as long as the SVC is operating well within limits, but may lead to gross errors if the SVC is operating close to its reactive limits [1,4]. Firstly, let us assume that the power system characteristic *V/I* may be determined by representing the power system by its Thevenin equivalent, as seen from the node whose voltage magnitude is being controlled. The voltage at the controlled node decreases with an inductive load and increases with a capacitive load, as illustrated in Figure 4.4. It should be noted that at point A there is maximum absorption of inductive current by the load system. Conversely, in point B, the opposite effect takes place. It corresponds to a point of maximum capacitive current injection by the load system.

The characteristic (1) in Figure 4.5 corresponds to the case when the SVC output current is zero. Now, let us consider the characteristic (2), which results from the system operating under minimum inductive loading condition. As a consequence, under this condition, there is an increase in system voltage (point A). If the SVC slope, X_{SL}, were to be zero, then the *generator* would violate its inductive reactive limit, point $A_{XSL=0}$. However, the *generator* would operate well within limits if the SVC slope was taken into account, point A. The slope X_{SL} is a function of the regulation voltage. In most applications, this slope is used to prevent the SVC from reaching the end positions too

frequently. The SVC current is measured and a proportional voltage signal is added to the voltage regulator. This signal has a different sign for leading and lagging current in such a way that it corresponds to a decrease or an increase of the reference voltage for leading or lagging current.

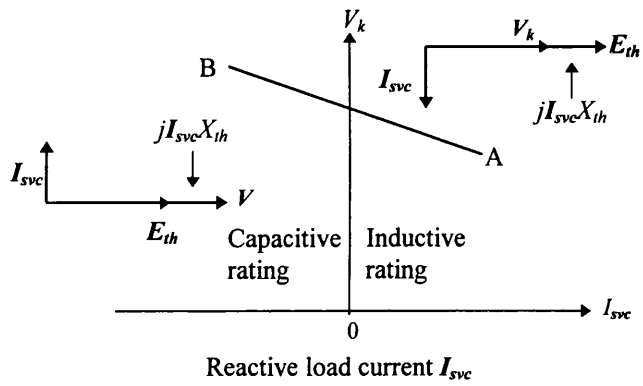

Figure 4.4. Voltage-current characteristics for power systems.

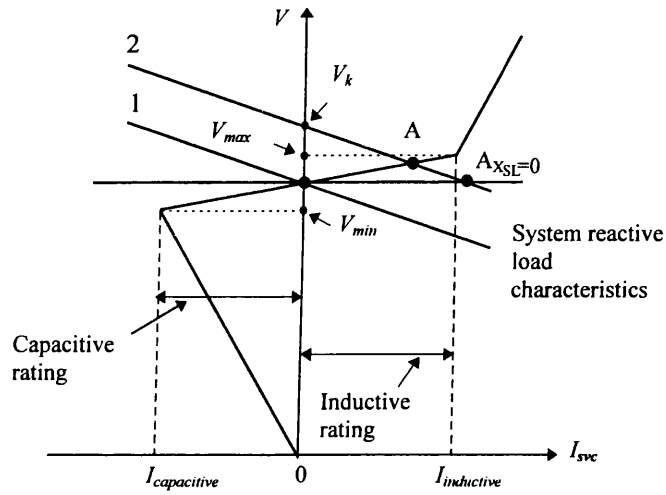

Figure 4.5. Comparison between actual and idealised SVC voltage-current characteristics.

The SVC characteristic shown above is well represented by connecting the *generator* to a dummy bus coupled to the high-voltage node via an inductive reactance whose value, on the SVC base, is equal to the per unit slope [1,4]. From the load flow theory viewpoint, the dummy bus is represented as a *PV*-type node whereas the high-voltage node is represented as a *PQ*-type node.

For operation outside limits, the *generator* representation is no longer valid [1]. In such cases, CIGRÉ recommends changing the SVC representation to a fixed reactive susceptance. This combined model yields accurate results. However, both representations employ a different number of nodes. The *generator* uses two or three nodes [4] whereas the fixed susceptance uses only one node [1]. In Newton-Raphson load flow implementations this requirement may result in Jacobian re-ordering and re-dimensioning during the iterative solution. Also, extensive checking becomes necessary in order to verify whether or not the SVC can return to operation inside limits.

It must be remarked that for operation outside limits, it is important to model the SVC as a susceptance and not as a *generator* set at its violated limit, $Q_{violated}$. Ignoring this point will lead to inaccurate results. The reason is that the amount of reactive power

drawn or supplied by the SVC is given by the product of the fixed susceptance, B_{fixed}, and the nodal voltage magnitude, V_k. Since V_k is a function of the network operating conditions, the amount of reactive power drawn or supplied by the fixed susceptance model may differ from the reactive power drawn by the *generator* model, i.e.,

$$Q_{violated} \neq -B_{fixed} V_k^2 \tag{4.4}$$

This point is exemplified in Figure 4.6 where the reactive power output of the *generator* was set at 100 MVAR. This value is constant as it is voltage independent. The result given by the constant susceptance model varies with nodal voltage magnitude. A voltage range of 0.95-1.05 was considered. A susceptance value of 1 pu on a 100 MVA base was used.

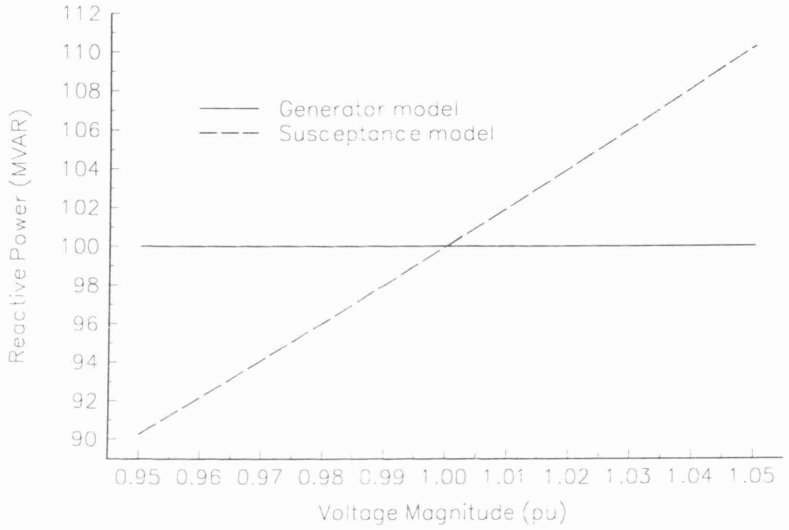

Figure 4.6. Comparative analysis of reactive power injected by *generator* and susceptance models.

4.4 Power Flow Equations

The SVC model presented above, based on the *generator* and fixed susceptance representations, is better handled as a susceptance model only. It takes the form of a variable susceptance when the SVC is operating within reactive limits and it takes the form of a fixed susceptance otherwise. This representation is a more realistic one because the SVC regulates the voltage magnitude at the point of connection by varying its adjustable susceptance in either the capacitive or the inductive ranges.

Moreover, a new and more advanced SVC representation then becomes possible, where the thyristor firing angle mechanism is represented explicitly as a function of network operating conditions. Both representations, the total susceptance and the firing angle models, are presented below.

In practice the SVC can be seen as an adjustable reactance with either firing angle limits or reactance limits. The circuit shown in Figure 4.7 is used to derive the SVC's non-linear power equations and the linearised equations required by Newton's method. B_{eq} is the SVC's susceptance value, which may be a function of the firing angle.

The transfer admittance equation for the variable-shunt compensator is,

$$\boldsymbol{I} = jB_{eq}\ \boldsymbol{V}_k \tag{4.5}$$

and the reactive power equation is,

$$Q_k = -V_k^2 B_{svc} \tag{4.6}$$

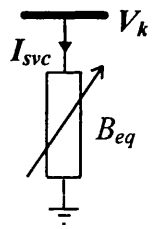

Figure 4.7. Variable shunt susceptance.

A linearised, positive sequence SVC model suitable for OPF solutions are described in the following Section. The SVC state variables, B_{svc} or α, are combined with the AC network nodal state variables for a unified, optimal solution via Newton's method. The SVC state variables are adjusted automatically so as to satisfy specified power flows, voltage magnitudes and optimality conditions [9].

4.5 SVC-OPF Formulation

The mathematical formulation consists of minimising active power generation cost in the power system by adjusting suitable controllable parameters. For the SVC controllable susceptance model, the OPF problem can be formulated as follows [5,6,9]:

$$\begin{aligned} &\textbf{\textit{Minimise}} \quad f(P_g) \\ &\textbf{\textit{Subject to}} \quad h(P_g, V, \theta, B_{svc}) = 0 \\ &\textbf{\textit{and}} \qquad\quad g(P_g, V, \theta, B_{svc}) \le 0 \end{aligned} \tag{4.7}$$

where P_g, V, θ, and B_{svc} are active power generation, voltage magnitude, phase angle and susceptance value, respectively. $f(P_g)$ is the objective function to be optimised, $h(P_g, V, \theta, B_{svc})$ represents the power flow equations and $g(P_g, V, \theta, B_{svc})$ consists of state variable limits as well as functional operating constraints.

The constrained optimisation problem is converted to an unconstrained optimisation problem by constructing an Lagrangian function corresponding to equation (4.7). This is given as,

$$L(\boldsymbol{x}, \lambda) = f(P_g) + \lambda^t h(P_g, V, \theta, B_{svc}) \tag{4.8}$$

where $\boldsymbol{x}$ is the vector of state variables and λ is vector of Lagrange multipliers for equality constraints. The inequality constraints are not shown because they are only included when there are variables outside limits. The superscript t indicates transposition.

4.5.1 Lagrangian Function

The contribution of the SVC to the Lagrangian function is explicitly modelled in the OPF Newton's method as an equality constraint given by the following equation:

$$L_{svc}(\boldsymbol{x}, \lambda) = \lambda_{qk} Q_k \tag{4.9}$$

where $\boldsymbol{x}=[V_k \;\; B]^t$, Q_k is the reactive power injected by the SVC at node k as defined in equation (4.6). $\lambda=[\lambda_{qk}]$ where λ_{qk} is the Lagrange multiplier at node k associated with

the reactive power balance equation. The variable B is either B_{svc} or α, depending on the SVC model used in the OPF study.

The SVC linearised system of equations for minimising the Lagrangian function via Newton's method is given by,

$$\boldsymbol{W}\Delta\mathbf{z} = -\boldsymbol{g} \tag{4.10}$$

where matrix $\boldsymbol{W}$ contains second partial derivatives of the Lagrangian function $L_{svc}(\boldsymbol{x}, \lambda)$ with respect to state variables V_k, B and λ_{qk}. The gradient vector $\boldsymbol{g}$ is $[\nabla V_k \; \nabla B \; \nabla\lambda_{qk}]^t$. It consists of first partial derivative terms. $\Delta\mathbf{z}$ is the vector of correction terms, given by $[\Delta V_k \; \Delta B \; \Delta\lambda_{qk}]^t$.

Once equation (4.10) is assembled and combined with matrix $\boldsymbol{W}$ and gradient vector $\boldsymbol{g}$ of the entire network, then a sparsity-oriented solution is carried out. This process is repeated until the optimally conditions stated in Chapter 2 are reached.

4.5.2 SVC Firing Angle Model

In this case, equation (4.10) takes the following form,

$$\begin{bmatrix} 0 & 0 & 0 & 0 & 0 \\ 0 & \dfrac{\partial^2 L}{\partial V_k^2} & 0 & \dfrac{\partial Q_k}{\partial V_k} & \dfrac{\partial^2 L}{\partial V_k \partial \alpha} \\ 0 & 0 & 0 & 0 & 0 \\ 0 & \dfrac{\partial Q_k}{\partial V_k} & 0 & 0 & \dfrac{\partial Q_k}{\partial \alpha} \\ 0 & \dfrac{\partial^2 L}{\partial \alpha \partial V_k} & 0 & \dfrac{\partial Q_k}{\partial \alpha} & \dfrac{\partial^2 L}{\partial \alpha^2} \end{bmatrix} \begin{bmatrix} 0 \\ \Delta V_k \\ 0 \\ \Delta\lambda_{qk} \\ \Delta\alpha \end{bmatrix} = \begin{bmatrix} 0 \\ -\dfrac{\partial L}{\partial V_k} \\ 0 \\ -\dfrac{\partial L}{\partial \lambda_{qk}} \\ -\dfrac{\partial L}{\partial \alpha} \end{bmatrix} \tag{4.11}$$

The relevant partial derivative terms can be found from equations (4.3), (4.6) and (4.9). The derivative terms corresponding to inequality constraints are not required at the beginning of the iterative solution, they are introduced into matrix equations (4.11) only after limits are enforced.

In OPF studies it is normal to assume that voltage magnitudes at the SVC are controlled within certain limits, e.g. 0.95-1.10 pu. However, if the voltage magnitude is to be controlled at a fixed value, then matrix $\boldsymbol{W}$ is suitably modified to reflect this operational constraint. This is done by adding the second derivative term of a large, quadratic penalty factor to the second derivative term (with respect to the voltage magnitude V_k) of the Lagrangian function. Also, the first derivative term of the quadratic penalty function is added to the corresponding gradient element. Hence, the diagonal element corresponding to voltage magnitude V_k will have a very large value, resulting in a null voltage increment, ΔV_k. This is equivalent to de-activating the equation of partial derivatives of the Lagrangian function with respect to V_k from matrix $\boldsymbol{W}$.

4.5.3 Hessian and Jacobian Elements for the SVC Firing Angle Model

The first and second partial derivative terms corresponding to node k are found from equations (4.3) and (4.6) with respect to the firing angle:

$$\frac{\partial Q_k}{\partial V_k} = 2V_k\left(\frac{X_L - \frac{X_C}{\pi}\left(2(\pi-\alpha)+\sin(2\alpha)\right)}{X_C X_L}\right) \tag{4.12}$$

$$\frac{\partial Q_k}{\partial \alpha} = \frac{2V_k^2(\cos(2\alpha)-1)}{\pi X_L} \tag{4.13}$$

$$\frac{\partial^2 Q_k}{\partial V_k^2} = 2\left(\frac{X_L - \frac{X_C}{\pi}\left(2(\pi-\alpha)+\sin(2\alpha)\right)}{X_C X_L}\right) \tag{4.14}$$

$$\frac{\partial^2 Q_k}{\partial \alpha^2} = -\frac{4V_k\ \sin(2\alpha)}{\pi X_L} \tag{4.15}$$

$$\frac{\partial^2 Q_k}{\partial \alpha \partial V_k} = \frac{4V_k\ (\cos(2\alpha)-1)}{\pi X_L} \tag{4.16}$$

4.5.4 SVC Controllable Susceptance Model

Similarly to the case presented above, equation (4.10) would be given as,

$$\begin{bmatrix} 0 & 0 & 0 & 0 & 0 \\ 0 & \frac{\partial^2 L}{\partial V_k^2} & 0 & \frac{\partial Q_k}{\partial V_k} & \frac{\partial^2 L}{\partial V_k \partial B_{svc}} \\ 0 & 0 & 0 & 0 & 0 \\ 0 & \frac{\partial Q_k}{\partial V_k} & 0 & 0 & \frac{\partial Q_k}{\partial B_{svc}} \\ 0 & \frac{\partial^2 L}{\partial B_{svc} \partial V_k} & 0 & \frac{\partial Q_k}{\partial B_{svc}} & 0 \end{bmatrix} \begin{bmatrix} 0 \\ \Delta V_k \\ 0 \\ \Delta \lambda_{qk} \\ \Delta B_{svc} \end{bmatrix} = \begin{bmatrix} 0 \\ -\frac{\partial L}{\partial V_k} \\ 0 \\ -\frac{\partial L}{\partial \lambda_{qk}} \\ -\frac{\partial L}{\partial B_{svc}} \end{bmatrix} \tag{4.17}$$

4.5.5 Hessian and Jacobian elements for the SVC Controllable Susceptance Model

The first and second partial derivative terms corresponding to the node k are found from equations (4.6) with respect to B_{svc}:

$$\frac{\partial Q_k}{\partial V_k} = -2V_k B_{svc} \tag{4.18}$$

$$\frac{\partial Q_k}{\partial B_{svc}} = -V_k^2 \tag{4.19}$$

$$\frac{\partial^2 Q_k}{\partial V_k^2} = -2B_{svc} \tag{4.20}$$

$$\frac{\partial^2 Q_k}{\partial V_k \partial B_{svc}} = -2V_k \tag{4.21}$$

4.5.6 Handling Limits of SVC Variables

The Multipliers method [10] is used to handle the inequality constraint set. Here, a penalty term is added to the Lagrangian function, which becomes the augmented Lagrangian function. Variables outside limits become part of the augmented Lagrangian function and, hence, become enforced.

The generic function ψ_i, presented in Chapter 2, is shown below in a modified form where the state variable to be constrained for the controllable susceptance model is B_{svc}. A similar representation exists for the firing angle model.

$$\psi_i(B^j_{svc,i},\mu^j_i)=\begin{cases}\mu^j_i(B^j_{svc,i}-B^{\max}_{svc,i})+\dfrac{c}{2}(B^j_{svc,i}-B^{\max}_{svc,i})^2 & \text{if} \quad \mu^j_i+c(B^j_{svc,i}-B^{\max}_{svc,i})\geq 0\\ \mu^j_i(B^j_{svc,i}-B^{\min}_{svc,i})+\dfrac{c}{2}(B^j_{svc,i}-B^{\min}_{svc,i})^2 & \text{if} \quad \mu^j_i+c(B^j_{svc,i}-B^{\min}_{svc,i})\leq 0\\ 0 \quad \text{otherwise}\end{cases} \tag{4.22}$$

where i is the SVC number and j is an iteration counter associated with the actual value of B_{svc}; $B^{\max}_{svc,i}$ and $B^{\min}_{svc,i}$ are the upper and lower limits for controllable susceptance; μ_i is a multiplier term and c is a penalty weighting term.

4.5.7 Initial Conditions

Nodal Voltage Magnitudes, Phase Angles and SVC Variables

The voltage magnitude, V_k, is initialised at 1 pu and a phase angle at 0, which correspond to the same conditions for load flow power studies.

On the other hand, the initial conditions for the SVC firing angle is selected within the range of ±8 electric degrees away from a zero susceptance, or its equivalent value for the controllable susceptance model. However, the best initial conditions could be chosen according to a good guess given by the user by taking into account the performance of the power system studied and the computational experience. If one expects to have the SVC working in the capacitive region, the user's best estimation in the capacitive region should be used as an initial condition for the SVC.

Lagrange Multipliers

For the SVC Lagrange multiplier, the initial value of λ_{qk} is set to 0. This value gives rise to very robust iterative solutions. It should be noted that this Lagrange multiplier λ_{qk} is the same multiplier used to represent the reactive power balance equation as in Chapter 2.

4.6 Test Cases for SVC Firing Angle Model

The 5-node system [11] used in Chapters 2 and 3 was modified to include a SVC connected at Main, as shown in Figure 4.8. The objective function to be minimised is active power generation cost. The reactances of the SVC are X_C = 0.9375 pu and X_L = 0.1625 pu and the upper and lower limits for the firing angle are 90^0 and 180^0 respectively. The SVC was modelled as a susceptance, which does not present

discontinuities in the range 90^0-180^0. The initial firing angle was given as $\alpha = 145^0$. Two cases are considered below:

A) The voltage magnitude at node Main is allowed to take any value within the range 0.95-1.1 pu.

B) The voltage magnitude at node Main is fixed at 1.1 pu.

Convergence was achieved in 4 iterations for Case A and 3 iterations for Case B. The tolerance used was 10^{-9}. The power flow results for Case A are shown in Figure 4.8. The voltage magnitude, phase angle, active and reactive power dispatch and Lagrange multiplier per node are given in Table 4.1 and Table 4.2 for Cases A and B, respectively. The SVC susceptance values and reactive power at each iteration are shown in Table 4.3.

The OPF solution for the case with no SVC was carried out in Section 2.9.1. For this study, the active power generation cost is 747.98 $/hour, the network losses are 3.050 MW and the reactive power generation is 14.71 MVAR. Similar results for Case A are 747.865 $/hour, 3.02381 MW and 2.4 MVAR. By comparing these results, it is seen that the SVC injects reactive power satisfying part of the reactive load where it is required, i.e. the reactive power injected by generators at North and South is either not flowing across all the branches or flowing in a low portion. As a consequence, the generation cost and network losses are reduced.

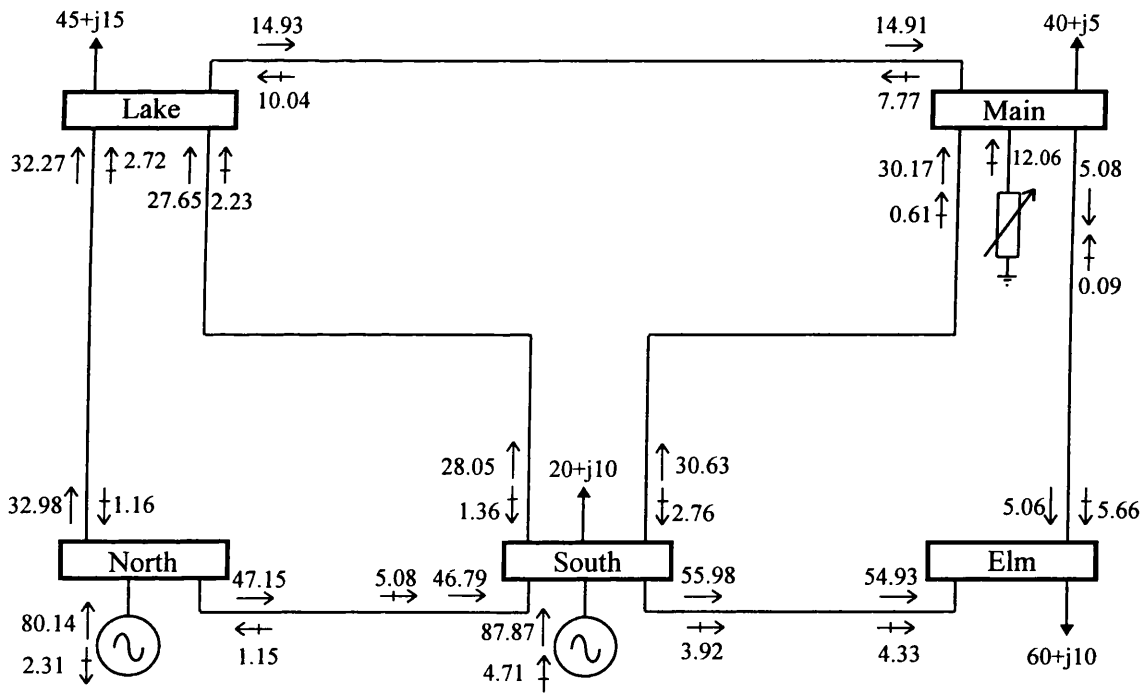

Figure 4.8. Modified 5-node network with a SVC and its OPF solution.

Table 4.1. Nodal complex voltages of modified network (Case A).

Node	Voltage Magnitude (pu)	Phase Angle (degrees)	Active Power (MW)	Reactive Power (MVA)	λ_p ($/MWhr)
Elm	1.075	-4.450	0	0	4.2625
Main	1.085	-3.962	0	0	4.2324
Lake	1.083	-3.701	0	0	4.2217
South	1.100	-1.304	87.87	4.71	4.1030
North	1.109	0.000	80.14	-2.31	4.0411

Table 4.2. Nodal complex voltages of modified network (Case B).

Node	Voltage Magnitude (pu)	Phase Angle (degrees)	Active Power (MW)	Reactive Power (MVA)	λ_p ($/MWhr)
Elm	1.080	-4.471	0	0	4.2650
Main	1.100	-4.148	0	0	4.2431
Lake	1.095	-3.836	0	0	4.2299
South	1.100	-1.2613	87.81	-20.37	4.1024
North	1.111	0.000	80.33	-2.33	4.0426

As expected, active power generation cost and active power losses are greater for Case B. The results for Case A are mentioned above, and for Case B are 748.339 $/hour and 3.14226 MW. However, Case B converged in one iteration less than Case A. In Case B, the constraint to be satisfied by the demands that the SVC injects 37.13 MVAR. This injection of reactive power flows from node Main to other nodes producing, as a consequence, an increment in network losses.

Table 4.3 indicates that in order to maintain the voltage magnitude of node Main at 1.1 pu, it is necessary for the SVC to inject more reactive power. For example, if one observes the Figure 4.8, the nodes Lake and Main absorb reactive power from the other nodes, it means that no reactive power is flowing from the SVC to nodes where the generators could supply the local or adjacent demand. It should be noted that the sign minus in Table 4.3 indicates injection of reactive power.

Table 4.3. Final parameters, Cases A and B, for SVC firing angle model.

Iterations	Case A			Case B		
	α (degrees)	B_{eq} (pu)	Q (MVAR)	α (degrees)	B_{eq} (pu)	Q (MVAR)
0	145.000	0.514	-51.420	145.000	0.514	-51.420
1	136.627	0.056	-7.231	136.598	0.054	-6.630
2	137.819	0.131	-14.534	144.712	0.501	-60.640
3	137.234	0.095	-11.213	140.832	0.306	-37.130
4	137.347	0.102	-12.061	-	-	-

4.7 Effect of the Initial Firing Angle

The same 5-node test system was used to show the ability of the OPF algorithm to converge to very tight tolerance. The simulations were carried out by assuming the two different operative conditions used in Section 4.6.

In order to asses the impact of firing angle initial conditions, various solutions were carried out, starting from different values of α. The first iterative solution was carried out with $\alpha = 140^0$. Subsequent initial firing angles were specified at 5^0 intervals. Five cases were solved:

A) $\alpha = 140^0$.

B) $\alpha = 145^0$.

C) $\alpha = 150^0$.

D) $\alpha = 155^0$.

E) $\alpha = 160^0$.

Figures 4.9 and 4.10 depict the firing angle profiles for the two operative conditions presented above (Case A and B, Section 4.6). It can be observed that the pattern of convergence is smooth during the iterative process. However, there was a slightly irregular performance after the first iteration due to the enforcement of the voltage magnitude at node South.

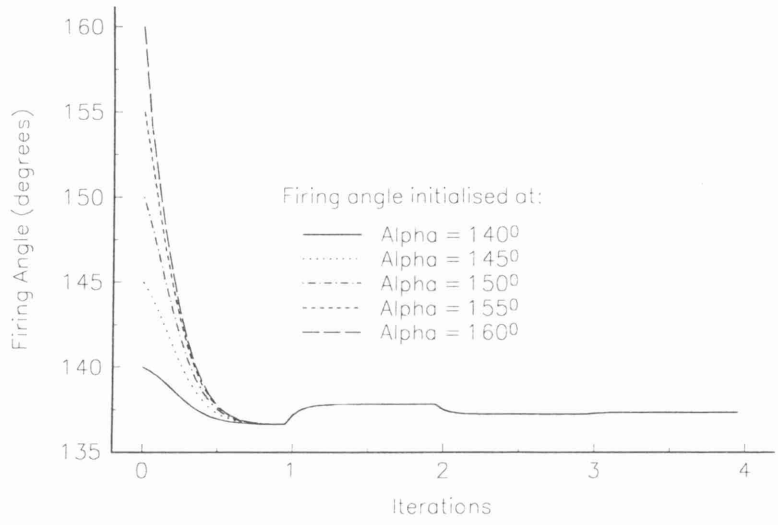

Figure 4.9. Firing angle profile for the SVC, Case A, Section 4.6.

The result in Figure 4.10 contrasts with the results in Figure 4.9, with the former being highly irregular after the first iteration. In the first iteration, the generator at South injects 10.79 MVAR and the losses were 2.91 MW while the SVC injected 6.63 MVAR. However, the voltage magnitude at that node is violating its upper limit. During the binding stage, the operating point of the 5-node test system was changed drastically. The generator at South absorbed 43.03 MVAR and the losses were 3.53 MW, while the SVC injected 60.64 MVAR. In spite of this irregular convergence pattern, the algorithm converged faster for the Case A, Section 4.6.

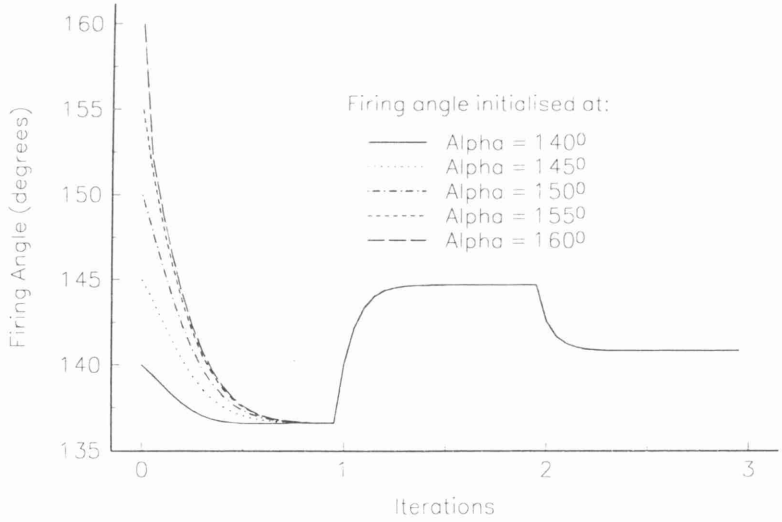

Figure 4.10. Firing angle profile for the SVC, Case B, Section 4.6.

4.8 Test Cases for SVC Controllable Susceptance Model

A comparative analysis of the reliability towards the convergence of both models is presented below. The modified 5-node test system is presented in this Section but the

SVC is modelled as a controllable susceptance (B_{svc}). The lower (inductive susceptance) and upper (capacitive susceptance) limits were -0.384 pu and 0.066 pu, respectively. The initial susceptance value was B_{svc} = 0.514 pu, which corresponds to $\alpha = 145^0$. Two cases are simulated:

A) The voltage magnitude at node Main is maintained within the values 0.95 and 1.1 pu.

B) The voltage magnitude at node Main is fixed at 1.1 pu.

Convergence was obtained in 4 and 3 iterations for the Case A and B, respectively. The solution for the voltage magnitudes, phase angles, active and reactive power generations and Lagrange multipliers are exactly the same as those presented in Table 4.1. The SVC susceptance values during the iterative process are show in Table 4.4. It can be observed from Tables 4.3 and 4.4 that the SVC susceptances for both models are exactly the same.

Table 4.4. Final parameters, Cases A and B, for SVC Controllable susceptance model.

Iterations	Case A		Case B	
	B_{svc} (pu)	Q (MVAR)	B_{svc} (pu)	Q (MVAR)
0	0.5140	-51.420	0.514	-51.420
1	0.056	-7.204	0.054	-6.594
2	0.131	-14.534	0.501	-60.641
3	0.095	-11.213	0.306	-37.130
4	0.102	-12.061	-	-

4.9 Effect of the Initial Conditions for SVC Controllable Susceptance Model

A similar analysis to the one presented in Section 4.7 was carried out for the 5-node test system. The minimum and maximum limits of the SVC electric parameters were -0.384 (90^0) and 0.066 (180^0), respectively. Similar simulations were carried as those presented in Section 4.8.

The initial values assigned to the susceptances correspond to the equivalent firing angles used in Section 4.7. The five cases studied were:

A) $B_{svc} = 0.260$.

B) $B_{svc} = 0.514$.

C) $B_{svc} = 0.711$.

D) $B_{svc} = 0.857$.

E) $B_{svc} = 0.958$.

Convergence was achieved in the same number of iterations as those given in Section 4.7. Figures 4.11 and 4.12 show that the patterns of convergence for the susceptance as a state variable follow exactly the same patterns as those presented in Figures 4.9 and 4.10. It can also be observed that no overshothings occur in the iterative process. Although two values were chosen as initial conditions for both models, i.e. $\alpha = 160^0$ and $B_{svc,}$= 0.958, the algorithm was very robust and converged in the same number of iterations.

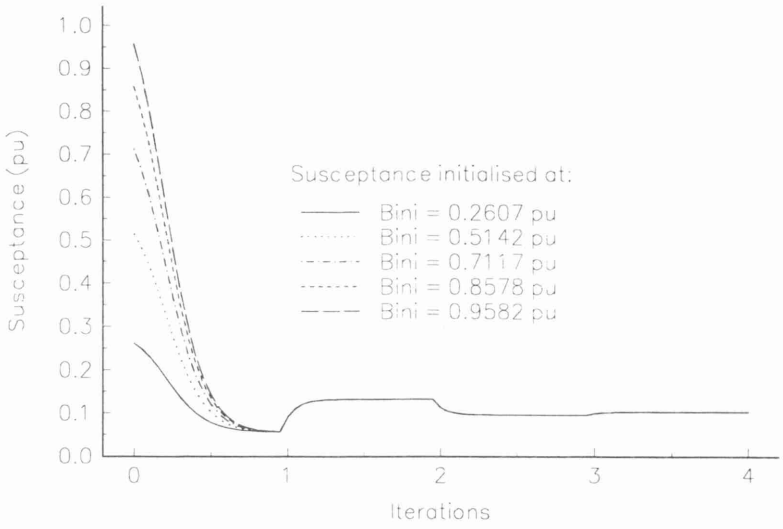

Figure 4.11. Susceptance profile for SVC, Case A, Section 4.6.

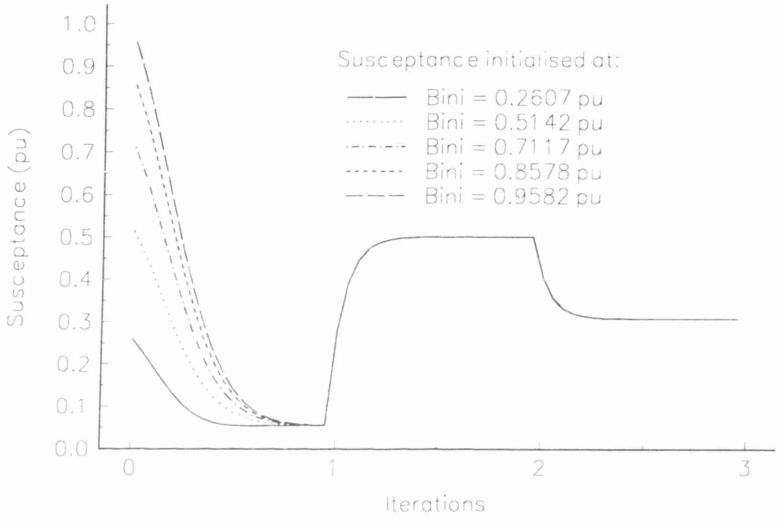

Figure 4.12. Susceptance profile for SVC, Case B, Section 4.6.

4.10 Control Voltage Magnitudes in a Real Power System

To test the robustness of the OPF algorithm when solving real networks, the company network described in Chapter 3 was used [7]. The optimal generation cost for both the base and modified cases (SVC upgraded) are given in Table 4.5, together with system losses. The SVC optimal susceptance values are given in Table 4.6 and the voltages at the connection point are given in Table 4.7. The SVCs were embedded in nodes with low voltage magnitude and nodes where SVCs are able to improve the voltage profile for a group of nodes. In reality, these nodes are compensated by a shunt capacitor. As expected, the SVCs improved the voltage magnitudes at connecting nodes and also in adjacent nodes. SVC voltage magnitudes were subjected to inequality constraints within the range 0.95-1.10 pu.

Table 4.5. Optimal generation cost and system losses.

Parameters	Base case	C. Susceptance Model	Firing Angle Model
Cost ($/hr)	293.643	293.596	293.596
Losses (MW)	20.1172	20.116	20.116

Table 4.6. Comparison of optimal susceptance values for both SVC models.

Static VAR Compensator	C. Susceptance Model	Firing Angle Model	
	B_{svc} (pu)	α (degrees)	B_{eq} (pu)
SVC-1	0.2410	136.355	0.2410
SVC-2	0.1273	136.184	0.1273
SVC-3	0.4132	136.616	0.4132

Table 4.7. Voltage magnitudes at the SVC connection point.

Static VAR Compensator	Voltage magnitude (pu)	
	Base case	Upgraded network
SVC-1	0.994	1.017
SVC-2	0.972	1.034
SVC-3	1.000	1.049

In all cases, solutions were achieved in 5 iterations. Figure 4.13 shows active power generation cost as a function of the iteration number whilst Figure 4.14 shows the active power losses as a function of the iteration number. It can be observed that the algorithm settles down quite rapidly to the solution.

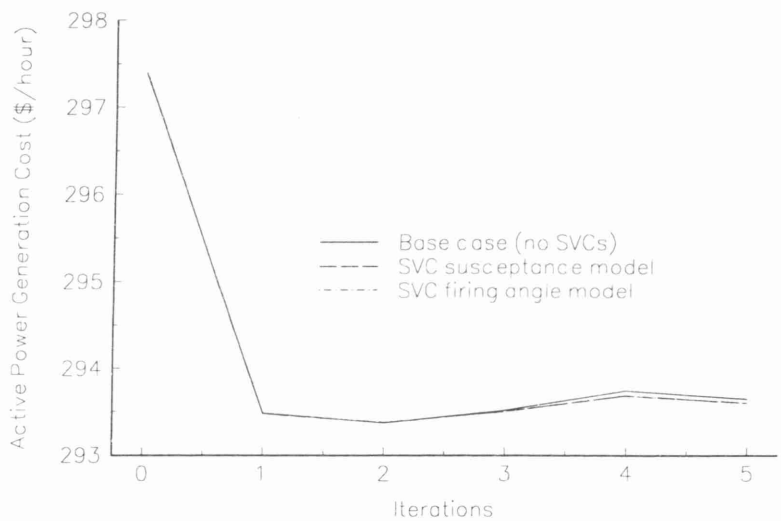

Figure 4.13. Active power generation cost profiles.

Figure 4.14. Active power losses profiles.

The SVC control option used above was changed in order to assess the SVC models capability to control voltage magnitude at fixed values. In this case the SVCs were set to control voltage magnitudes at 1 pu at their point of connection.

The optimal SVC state variable values for both models, i.e. susceptance and firing angle models, are shown in Table 4.8. As expected, these values differ from those given in Table 4.6.

Table 4.8. Comparison of optimal susceptance values for both SVC models.

Static VAR Compensator	C. Susceptance model	Firing angle model	
	B_{svc} (pu)	α (degrees)	B_{eq} (pu)
SVC-1	0.1780	136.26	0.1780
SVC-2	0.0725	136.10	0.0725
SVC-3	0.1361	136.19	0.1361

It was also observed that practically, there were no variations in the active power generation cost and active power losses for both SVC control conditions.

4.11 AEP 14-Node System with Three-Winding Transformers

The standard AEP 14-node system [8] is now used, in modified form, to include two three-winding transformers. Their location is shown in Figure 4.15. One of the transformers is connected at nodes Nod_4, Nod_8 and Nod_9. Tapping facilities exist in Nod_8 and a Synchronous Condenser is attached to the same node. The second transformer is connected between nodes Nod_5, Nod_6 and Nod_7. Tapping facilities exist in Nod_6 and a Static Var Compensator is connected at Nod_7. The parameters of both transformers are identical, and the windings contain no resistance. The voltage limits for controlled voltage nodes are 0.94 and 1.15, and for load nodes the range is 0.94-1.06.

In order to illustrate the impact of the SVCs and LTCs on system operation, three different scenarios were considered. The first one assumes that all three taps in both transformers remain fixed at their nominal position, e.g. $\boldsymbol{T_v}=\boldsymbol{U_v}=\boldsymbol{W_v}=1\angle 0^0$. The second scenario assumes that the tap changer in LTC-1 is active and that the tap changer in LTC-2 remains fixed at its nominal value. The third scenario considers the case when the tapping facilities in both LTCs are active.

The number of iterations taken by the OPF solution to converge to the specified tolerance, i.e. 10^{-9} for all variables, was 5 iterations for the first two cases and 7 iterations for the third case. Table 4.9 shows the active and reactive power generations, costs and losses for all three cases, whilst Table 4.10 shows results relating to LTC-1 and LTC-2. Improved solutions are obtained for the second and third cases compared to the first case, owing to the influence of the tap changers. For instance, for the last case the active power generation cost was reduced by 0.416 $/hour and the active power losses were reduced by 4.7%, with respect to the base case. However, the best operating solution demands more reactive power of the SVC and the Synchronous condenser, as Table 4.10 shows.

Figure 4.16 shows the nodal voltage profiles for the three cases under consideration. Significant differences can be observed between the three voltage profiles, due to the influence of the tap changers. The system voltage profile improves slightly when the first LTC is in operation. However, when the two LTCs are in operation, the system

voltage profile gets much improved, and the overall effect is an important reduction in active power losses, as well as a reduction in reactive power generation. It must be noted that large voltage variations exist at the transformer nodes.

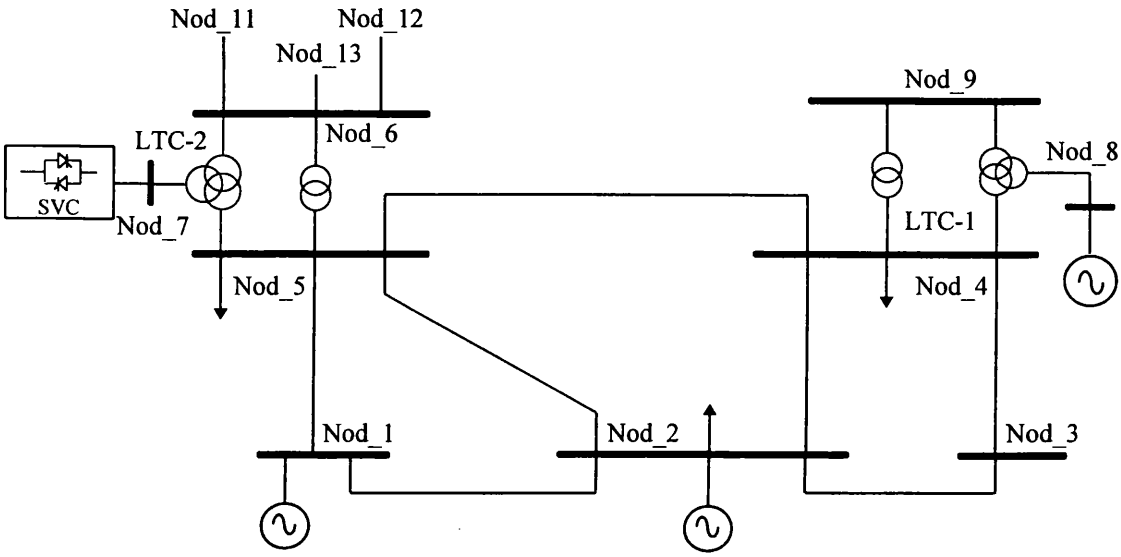

Figure 4.15. Modified AEP 14-node system with two three winding transformers.

Table 4.9. Results for the AEP 14-node system.

Case	Active Power Generation (MW)	Reactive Power Generation* (MVAR)	Active Power Generation Cost ($/hour)	Active Power Losses (MW)
1	263.274	65.650	310.684	4.273
2	263.230	73.500	310.594	4.229
3	263.073	61.506	310.268	4.072

* The reactive power injection of Nod_8 is taken into account.

Table 4.10. Results for the AEP 14-node system at connection nodes.

Case	Nod_7			Nod_8	
	SVC parameters		LTC-2	Synchronous Cond.	LTC-1
	α (degrees)	Q (MVAR)	Tap position	(MVAR)	Tap position
1	135.959	-1.440	1.000	30.970	1.000
2	135.607	1.140	1.000	35.448	0.900
3	136.541	-6.298	0.949	35.112	0.900

Table 4.11 gives examples of voltage control interactions between the transformer tapping facilities and two kinds of VAR compensating plants. When the voltage magnitude is set to 1.0 pu at node Nod_7, reactive power is drawn from the system and the tap position is moved down to 0.949. The SVC operates in the inductive region, i.e. firing angle is 135.662^0. To maintain a voltage magnitude of 1 pu at Nod_8 requires that the synchronous condenser supplies 26.130 MVAR while the transformer tap hits its lower tap position, i.e. 0.9. If higher voltage magnitudes are required at these nodes, e.g. 1.05, then the SVC continues to operate in the inductive region and additional reactive power is demanded from the synchronous condenser. In fact, the synchronous condenser hits the upper reactive limit and the transformer tap moves down from its nominal tap position.

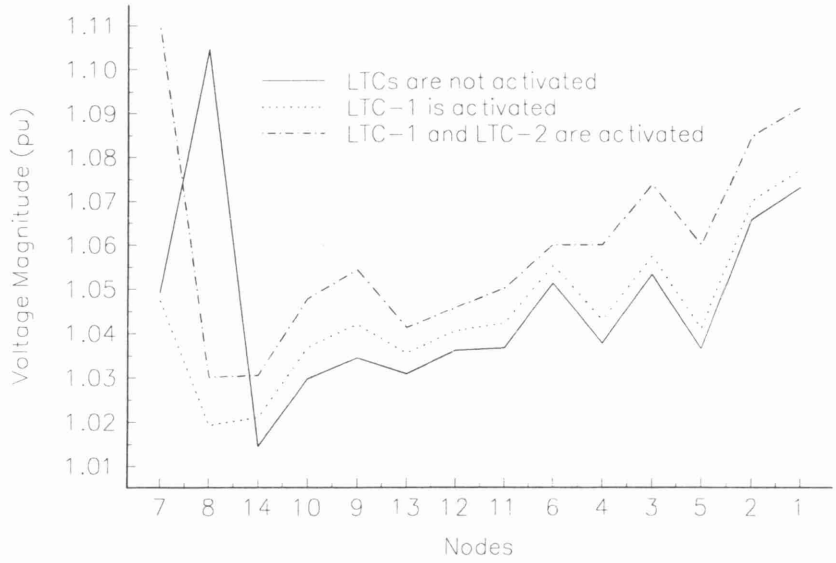

Figure 4.16. Nodal voltage profile for three different scenarios.

Table 4.11. Results for the AEP 14-node system at connection nodes for fixed voltages.

Voltage Mag. (pu)	Nod_7			Nod_8	
	SVC parameters		LTC-2	Synchronous	LTC-1
	α (deg.)	Q (MVAR)	Tap position	Cond. (MVAR)	Tap position
1.00	135.662	0.670	0.949	26.130	0.900
1.05	134.586	8.812	1.014	40.000	0.912
1.10	134.626	8.916	1.061	40.000	0.961

An additional study is carried out below. For this study, the tap positions of both LTCs are fixed at 0.9, 1.0 and 1.1 and the voltage magnitude at nodes Nod_7 and Nod_8 are freed. Tables 4.12 and 4.13 show the results of this study. The interaction between the transformer tapping facilities and the VAR compensating plants is similar between voltage magnitudes and taps. For example, by observing Tables 4.11 and 4.13, one can see that a low tap position gives a low voltage magnitude, and that a high tap position gives a high voltage magnitude. The VAR compensating plants regulate the amount of reactive power to move the system to the best operating condition. Some trade offs take place in this study when the taps are at 0.9, the active power generation cost and network losses are the lowest, even though the consumption of reactive power is highest, but the voltage magnitude at Nod_7 is poor. The opposite behaviour is observed when the taps are set at 1.1; the active power generation cost, network losses and voltages at Nod_7 and Nod_8 are the highest. For this scenario, a balance is reached when tap positions are set at 1.0, because the voltage solution is close to 1.0 pu and the generation of reactive power is not the highest, leaving an emergency margin.

Table 4.12. Results for the AEP 14-node system when the taps are fixed.

Tap position	Active Power Generation (MW)	Reactive Power Generation* (MVAR)	Active Power Generation Cost ($/hour)	Active Power Losses (MW)
0.9	263.188	71.313	310.507	4.188
1.0	263.274	65.650	310.684	4.273
1.1	263.431	65.388	311.006	4.430

* The reactive power injection of Nod_8 is taken into account.

Table 4.13. Results for the AEP 14-node system at connection nodes when the taps are fixed.

Tap position	Nod_7 SVC parameters α (deg.)	Nod_7 SVC parameters Q (MVAR)	Nod_7 Voltage Mag. (pu)	Nod_8 Synchronous Cond. (MVAR)	Nod_8 Voltage Mag. (pu)
0.9	135.131	3.756	0.940	38.514	1.031
1.0	135.959	-1.440	1.049	30.970	1.104
1.1	135.843	-0.700	1.150	10.085	1.150

4.12 Conclusions

Comprehensive SVC models suitable for conventional and optimal power flow analysis have been presented in this Chapter, namely the SVC Controllable susceptance model and the SVC firing angle model. In contrast to SVC models reported in open literature, the proposed models do not make use of the *generator* concept employed for the SVC representation. Instead, they use the variable shunt susceptance concept. Arguably, this has the advantage of representing actual SVC operation more realistically. Moreover, since SVC shunt susceptance models only make use of one node to represent SVCs operating inside and outside ranges then Newton based power flow solutions become more efficient, compared to cases when *generator* based models of SVCs are used in Newton algorithms. A SVC model which uses the thyristor firing angle as the state variable has shown to provide fuller information that existing SVC models. The firing angle required to achieve a specified level of compensation becomes readily available from the optimal power flow solution which can be used to initialise other power system applications, such as harmonic analysis. A Newton's OPF algorithm has been upgraded to incorporate the new SVC models. Also, the SVC models interface easily with the three-winding transformer model, leading to optimal co-ordination between these two plant components. Two standard test networks, and a real-life, bulk transmission system have been used as test cases. Optimal solutions were obtained in 7 or less iterations.

4.13 References

[1] Enrinmez I.A., Ed.: 'Static VAR Compensators', Working Group 38-01, Task Force No. 2 on SVC, CIGRÉ, 1986.

[2] Gyugyi L.: 'Power Electronics in Electric Utilities: Static VAR Compensators', Proceedings of the IEEE, Vol. 76, No. 4, April 1988, pp. 483-494.

[3] Miller T.J.E.: 'Reactive Power Control in Electric Systems', Wiley Interscience, 1982, ISBN 0-471-86933-3.

[4] IEEE Special Stability Controls Working Group.: 'Static VAR Compensator Models for Power Flow and Dynamic Performance Simulation', IEEE Transactions on Power Systems, Vol. 9, No. 1, February 1995, pp. 229-240.

[5] Sun D.I., Ashley B., Brewer B., Hughes A. and Tinney W.F.: 'Optimal Power Flow By Newton Approach', IEEE Transactions on Power Apparatus and Systems, Vol. PAS-103, No 10, October 1984, pp. 2864-2880.

[6] Sun D.I., Hu T.I., Lin G.S., Lin C.J. and Chen C.H.: 'Experiences with Implementing Optimal Power Flow for Reactive Scheduling in the Taiwan Power System', IEEE Transactions on Power Systems, Vol. 3, No. 3, August 1988, pp. 1193-1200.

[7] Aboytes F. and Arroyo G.: 'Security Assessment in the Operation of Longitudinal Power Systems', IEEE Transactions on Power Systems, Vol. PWRS-1, No. 2, May 1986, pp. 225-232.

[8] Freris L.L. and Sasson A.M.: 'Investigation of the Load-Flow Problem', Proceedings of IEE, Vol. 115, No. 10, October 1968, pp. 1459-1470.

[9] Luenberger D.G.: 'Introduction to Linear and Nonlinear Programming', Addison-Wesley Publishing Co., Second Edition, 1984.

[10] Bertsekas D.P.: 'Constrained Optimization Lagrange Multiplier Methods', Academic Press, 1992.

[11] Stagg G.W. and El-Abiad A.H.: 'Computer Methods in Power System Analysis', McGraw-Hill, 1968.

Chapter 5

TCSC Models in an Optimal Power Flow

A novel power flow model for the Thyristor-Controlled Series Compensator (TCSC) is presented in this Chapter. The model takes the form of a firing angle-dependent, nodal admittance matrix that is incorporated in the Optimal Power Flow (OPF) algorithm. Comprehensive OPF solutions of TCSC-upgraded power networks are achieved via Newton's method. The thyristor's firing angle, a newly introduced state variable in OPF formulations, is combined with the nodal voltage magnitudes and angles of the power network in a single frame of reference for unified, iterative solutions. Compensation regions lying outside the TCSC resonant bands are considered by the OPF solution. This new model is a more efficient counterpart than an existing TCSC controllable reactance model which is also presented in this Chapter for completeness. The robustness of convergence is studied for both TCSC models.

5.1 Introduction

The TCSC is a key member of the FACTS family used to enhance the performance of the power network [1,2]. It allows rapid and continuous changes of the transmission line impedance [3,4]. Active power flow across the compensated transmission line can be maintained at a specified level under a wide range of operating conditions. A schematic representation of the TCSC is shown in Figure 5.1. It consists of a capacitor bank in parallel with a Thyristor Controlled Reactor (TCR). The controlling elements are the two anti-parallel thyristors, connected in series with the linear reactor.

One TCSC configuration, which has shown to be very effective is where the TCSC comprises a large number of series connected TCSC modules [3]. This TCSC configuration is termed an Advanced Series Compensator (ASC); and it is reported to exert control with minimum losses and minimum harmonic distortion [3]. Indeed, the harmonic studies that have been conducted indicate that the harmonic currents tend to circulate within the individual *LC* modules rather than escape into the transmission system [3]. An alternative arrangement consists of a conventional capacitor bank of large rating in series with a TCSC of small rating at each end of the capacitor bank [4]. No harmonic studies have been reported for this TCSC configuration but it is reasonable to expect that the harmonic currents generated by the two small rating TCRs will also be confined to the individual *LC* modules.

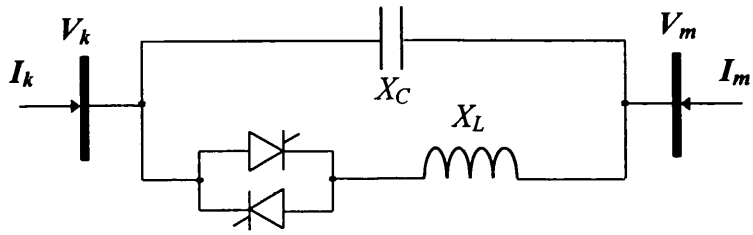

Figure 5.1. TCSC module.

A considerable amount of work relating to the TCSC has been published in the following areas: experiences of commercial operation [3,4]; performance and test models for Electro Magnetic Transient (EMTP) and SSR mitigation studies [5,6] and power systems stability [4,7,8]. However, little progress has been reported on models and tools suitable for assessing the impact of TCSC devices on improving the steady state security and economic performance of the power network. In fact, a pioneering but limited work [9] based on linear programming and a controllable reactance may be the only publication available in open literature that addresses these two very important issues of the TCSC technology. That work, however, failed to address the very important issue of the TCSC impedance characteristic and accompanying resonant points.

This has provided the motivation for extending the Newton OPF program to encompass more advanced TCSC models. Two possible ways of representing a TCSC module exist in the program; by means of a controllable reactance, and by means of the newly implemented firing-angle-dependent impedance. The former model uses the reactance as the control parameter in the OPF solution whereas the latter uses the thyristor's firing angle. The Newton OPF algorithm shows equal reliability towards convergence with either TCSC models.

5.2 Basic Characteristics

The main operational advantage of the TCSC is that it allows smooth continuous control of the transmission line compensation level. Series capacitors do not allow such a fine control. Series capacitive compensation is bypassed during minimum loading in order to avoid transmission line overvoltages resulting from excessive capacitive effects in the system. Conversely, series capacitive compensation is fully utilised during maximum loading. The purpose of this operating strategy is to increase the transfer of power from generating sites to load centres, without overloading transmission lines. The TCSC is an improvement on the series capacitors technology, which incorporate power electronics in order to make the high voltage side of the network electronically controllable.

Basically, the TCSC uses a Thyristor-controlled reactor (TCR) and a capacitor in parallel with the TCR, as shown in Figure 5.1. Its three fundamental modes of operation are: (a) thyristor-blocked mode, (b) thyristor-bypassed mode and (c) thyristor operating in phase controlled mode [10].

In the thyristor-blocked mode, the thyristor current is zero and, consequently, the TCSC functions as a capacitive reactance. This operating mode is illustrated in Figure 5.2. The arrow thickness represents the amount of electric current flowing across each component.

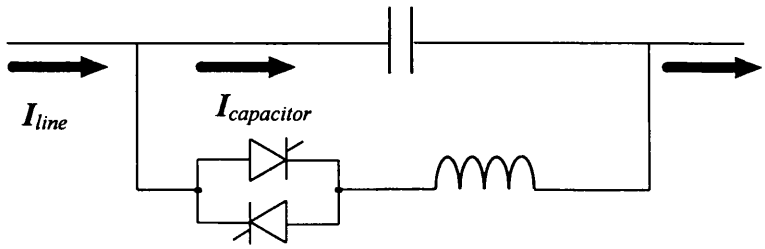

Figure 5.2. Thyristor-blocked mode.

In the thyristor bypassed mode, the thyristor valves are fired with no delay and the TCSC has a small inductive impedance. Figure 5.3 shows this mode of operation.

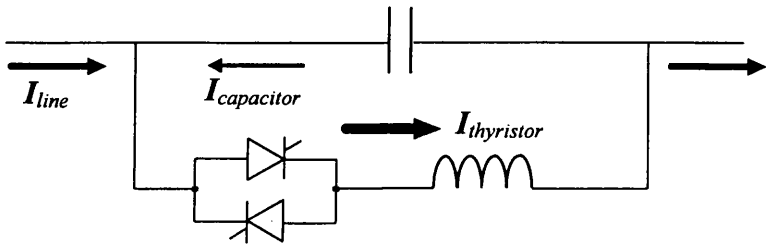

Figure 5.3. Thyristor-bypassed mode.

When the thyristor operates in phase-controlled mode, the thyristor valves operate with control of the firing angle. The TCSC can work as either a capacitive or an inductive reactance. But, basically, during this operating mode the thyristor firing mechanism is controlled to vary the amount of effective capacitance, as shown in Figure 5.4.

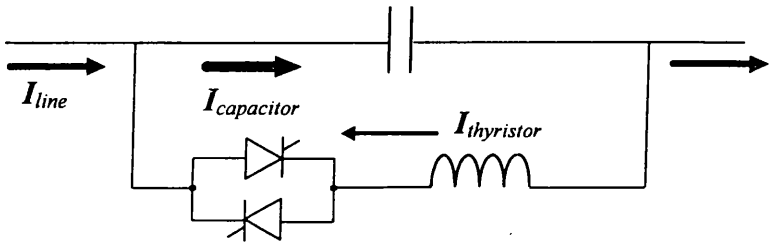

Figure 5.4. Thyristor operating in phase controlled capacitive mode.

Figures 5.5 and 5.6 show a fundamental frequency period of the voltage and current in the TCSC inductor and capacitor when the firing angle is 155^0. The inductance and capacitor parameters are taken to be 2.6 Ω and 15 Ω, respectively. These parameters correspond to the Kayenta scheme, which operates at a frequency of 60 Hz [3,5]. During the conduction period, the voltages across the inductive and capacitive reactances are identical. However, when there is no conduction in the thyristor, the voltage across the inductor is null and the only TCSC impedance is due to the capacitor. The firing instant can be controlled by applying a controlled firing signal at a desired angle, called firing angle and denoted by α. The firing angle is measured from the voltage zero crossing.

Figure 5.6 (a) shows that once conduction starts, the current flows through the thyristor, reaches a peak and returns to zero. The current appears again when another control pulse is applied to the thyristor gate. The period during which the thyristor is conducting is defined as the conduction angle and is given by $\sigma=2(\pi-\alpha)$. As α increases, σ decreases and therefore the current through the thyristor is also reduced. Full conduction is obtained with a firing angle of 90^0, which means that the TCSC behaves like a small inductive impedance. No conduction is obtained with a firing angle of 180^0, which means that the TCSC is a capacitive reactance. Figure 5.6 (b) shows the resulting current flowing from node *k* to *m*.

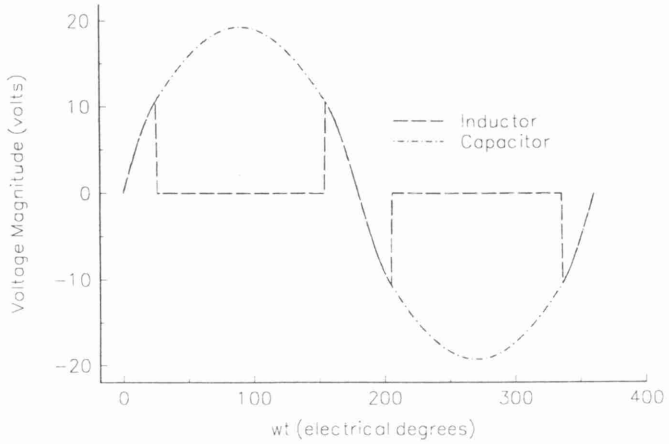

Figure 5.5. Voltage waveshapes in the TCSC inductor and capacitor.

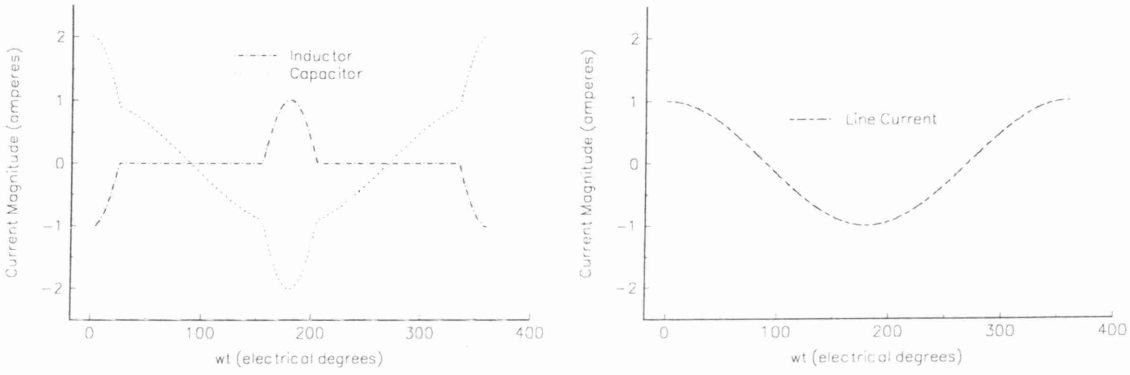

(a) For inductor and capacitor (b) Resulting current

Figure 5.6. TCSC currents when $\alpha = 155^0$.

5.3 TCSC Firing Angle Model

5.3.1 TCSC Fundamental Frequency Impedance

The expression for the fundamental frequency TCSC impedance, as a function of the thyristor's firing angle (TCSC-FA), is given as [3,5]:

$$\begin{aligned} X_{TCSC} = &- X_C + C_1 \left(2(\pi - \alpha) + \sin(2(\pi - \alpha))\right) \\ &- C_2 \cos^2(\pi - \alpha)\left(\varpi \tan(\varpi(\pi - \alpha)) - \tan(\pi - \alpha)\right) \end{aligned} \tag{5.1}$$

where

$$X_{LC} = \frac{X_C X_L}{X_C - X_L} \tag{5.2}$$

$$C_1 = \frac{X_C + X_{LC}}{\pi} \tag{5.3}$$

$$C_2 = \frac{4 X_{LC}^2}{X_L \pi} \tag{5.4}$$

and $X_C = 1/\omega C$ is the reactance of the capacitor bank; $X_L = \omega L$ is the reactance of the linear inductor; α is the firing angle after voltage zero crossing; $\varpi = \omega_0/\omega$; $\omega_0 = 1/(LC)^{1/2}$ and $\omega = 2\pi f$.

Figure 5.7 shows a typical, 60 Hz TCSC impedance-firing angle characteristic. The inductive and capacitive reactances are taken to be 2.6 Ω and 15 Ω, respectively. These parameters correspond to the Kayenta TCSC scheme [3,5]. TCSCs are operated in the range of 90°-180°. It can be observed that a resonant condition takes place when the firing angle approaches a value of 143°. In fact, for this characteristic, firing angles in the range of 140°-145° would lead to high impedance operations. Realistic TCSC-OPF models should avoid using such resonant regions as part of their solution space. Maximum and minimum TCSC firing angles in the capacitive and inductive regions are carefully established at the design stage in order to prevent the TCSC operating in high impedance regions, as this would result in high voltage drops across the TCSC [3,5]. In addition, careful selection of inductive and capacitive elements should avoid the presence of multiple resonant points.

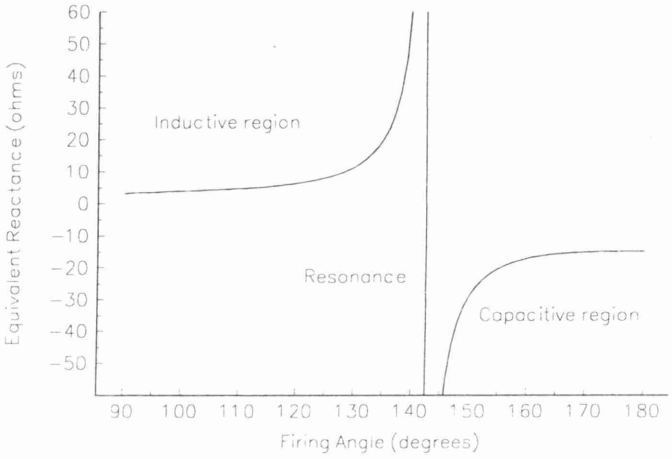

Figure 5.7. TCSC steady state impedance characteristic.

In the range of 90°-180°, the TCSC resonant points are given by the following expression,

$$\alpha = \pi\left(1 - \frac{(2n-1)\,\omega\sqrt{LC}}{2}\right) \qquad n = 1,2,3.... \tag{5.5}$$

From the numerical viewpoint, multiple resonant impedance points pose difficulties to the OPF solution. Furthermore, the likelihood of the OPF algorithm finding a sub-optimal solution is quite real, owing to the multiple peaks and valleys exhibited by the TCSC impedance. In these situations, the thyristor's firing angle α would have to be constrained in several small regions. This issue will be addressed in greater detail in Section 5.3.8.

5.3.2 TCSC Nodal Power Equations

The nodal power equations for the firing angle-based TCSC module are presented in this Section. The derivation is based on the transfer admittance matrix of the TCSC module shown in Figure 5.1,

$$\begin{bmatrix} \boldsymbol{I}_k \\ \boldsymbol{I}_m \end{bmatrix} = \begin{bmatrix} jB_{kk} & jB_{km} \\ jB_{mk} & jB_{mm} \end{bmatrix} \begin{bmatrix} \boldsymbol{V}_k \\ \boldsymbol{V}_m \end{bmatrix} \tag{5.6}$$

where

$$B_{kk} = B_{mm} = B_{TCSC} = -\frac{1}{X_{TCSC}} \tag{5.7}$$

$$B_{km} = B_{mk} = -B_{TCSC} = \frac{1}{X_{TCSC}} \quad (5.8)$$

In the absence of resistive elements in the TCSC module, the active and reactive power equations at node k and node m may be written as follows:

$$P_k = -V_k V_m B_{TCSC} \sin(\theta_k - \theta_m) \quad (5.9)$$

$$Q_k = -V_k^2 B_{TCSC} + V_k V_m B_{TCSC} \cos(\theta_k - \theta_m) \quad (5.10)$$

$$P_m = -V_m V_k B_{TCSC} \sin(\theta_m - \theta_k) \quad (5.11)$$

$$Q_m = -V_m^2 B_{TCSC} + V_m V_k B_{TCSC} \cos(\theta_m - \theta_k) \quad (5.12)$$

where P_k, P_m, Q_k and Q_m are the active and reactive power injections at nodes k and m, respectively. V_k, V_m, θ_k and θ_m are the voltage magnitude and phase angle at nodes k and m, respectively.

5.3.3 TCSC-OPF Formulation

The mathematical formulation consists of minimising the active power generation cost in the power system by adjusting suitable controllable parameters. For the TCSC-FA model, the OPF formulation is as follows [11,12,16]:

$$\begin{aligned} &\textbf{\textit{Minimise}} \quad f(P_g) \\ &\textbf{\textit{Subject to}} \quad h(P_g, V, \theta, \alpha) = 0 \\ &\textbf{\textit{and}} \qquad\quad g(P_g, V, \theta, \alpha) \le 0 \end{aligned} \quad (5.13)$$

where P_g, V, θ and α are the active power generations, voltage magnitudes, phase angles and thyristor's firing angles, respectively. $f(P_g)$ is the objective function to be optimised, $h(P_g, V, \theta, \alpha)$ represents the power flow equations and $g(P_g, V, \theta, \alpha)$ represents the state variable limits as well as functional operating constraints.

The constrained optimisation problem is converted to an unconstrained optimisation problem by constructing a Lagrangian function corresponding to equation (5.13). This is given as,

$$L(\boldsymbol{x}, \lambda) = f(P_g) + \lambda^t h(P_g, V, \theta, \alpha) \quad (5.14)$$

where $\boldsymbol{x}$ is a vector of state variables and λ is the Lagrange multipliers vector for equality constraints. The inequality constraints are not shown because they are only included when there are variables outside limits. The superscript t indicates transposition.

5.3.4 TCSC Lagrangian Function

The incorporation of the TCSC power equations into an OPF algorithm using Newton's method requires that for each TCSC present in the network, the matrix $\boldsymbol{W}$ be augmented by two rows and two columns in cases when the TCSC is exerting active power flow control. However, if the TCSC is not controlling active power flow, then matrix $\boldsymbol{W}$ is only augmented by one row and one column. α is an extra state variable which enters into the OPF formulation. In the former case a new Lagrange multiplier is added to account for the contribution of the power flow across the branch.

The TCSC state variables are combined with the network nodal voltage magnitudes and phase angles in a single frame-of-reference for a unified optimal solution via Newton's method. The TCSC state variables are adjusted automatically so as to satisfy specified power flows, voltage magnitudes and optimality conditions as given by Kuhn and Tucker [16].

The power flow mismatch equations at nodes k and m are explicitly modelled in the Lagrangian function as an equality constraint given by the following equation:

$$\begin{aligned} L_{tcsc}(\boldsymbol{x},\lambda) &= \lambda_{pk}(P_k + P_{dk} - P_{gk}) + \lambda_{qk}(Q_k + Q_{dk} - Q_{gk}) \\ &+ \lambda_{pm}(P_m + P_{dm} - P_{gm}) + \lambda_{qm}(Q_m + Q_{dm} - Q_{gm}) \end{aligned} \tag{5.15}$$

where P_{dk}, P_{dm}, Q_{dk}, Q_{dm} are active and reactive power loads at nodes k and m, respectively. P_{gk}, P_{gm}, Q_{gk}, Q_{gm} are scheduled active and reactive power generations at nodes k and m, respectively. λ_{pk}, λ_{pm}, λ_{qk}, λ_{qm} are Lagrange multipliers at nodes k and m, respectively.

5.3.5 Transmission Line Loading

As shown in Figure 5.8, the active power flow across branch m-l, P_{ml}, is controlled by the TCSC connected between nodes k and m. In the OPF formulation this operating condition is expressed as an equality constraint which remains active throughout the iterative process unless one expressly wishes this constraint to be deactivated.

The operating condition is represented by the following equation,

$$L_{flow}(\boldsymbol{x},\lambda) = \lambda_{ml}(P_{ml} - P_{specified}) \tag{5.16}$$

where λ_{ml} is the Lagrange multiplier associated with the active power flowing from node m to node l, and $P_{specified}$ is the target value of active power flow across the TCSC component.

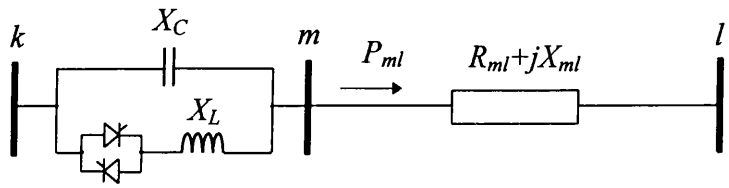

Figure 5.8. Compensated transmission line.

5.3.6 Linearised System of Equations

First and second order derivative terms obtained from equations (5.15) and (5.16) are placed in matrix $\boldsymbol{W}$ and gradient vector $\boldsymbol{g}$. The linearised system of equations for minimising the Lagrangian function via Newton's method is given by,

$$\boldsymbol{W}\Delta\mathbf{z} = -\boldsymbol{g} \tag{5.17}$$

where matrix $\boldsymbol{W}$ contains second partial derivatives of the Lagrangian function $L(\boldsymbol{x},\lambda)$ with respect to state variables $\boldsymbol{x}$ and Lagrange multipliers λ. The gradient vector $\boldsymbol{g}$ is $[\nabla\boldsymbol{x}\ \nabla\lambda]^t$. It consists of first partial derivative terms. $\Delta\mathbf{z}$ is the vector of correction terms, given by $[\Delta\boldsymbol{x}\ \Delta\lambda]^t$.

An expanded version of equation (5.17), as applied to the TCSC circuit of Figure 5.8 is given by equation (5.18). It must be noted that the Lagrangian function, L, of the

compensated branch *k-l*, consists of the sum of equations (5.15) and (5.16), i.e. $L = L_{tcsc}(\boldsymbol{x},\lambda) + L_{flow}(\boldsymbol{x},\lambda)$.

The first and second derivative expressions for all the terms used in equation (5.18) are given in Section 5.3.7. The derivative terms corresponding to inequality constraints are incorporated in matrix $\boldsymbol{W}$ only after state variables outside limits are detected.

$$
\begin{bmatrix}
\frac{\partial^2 L}{\partial \theta_k^2} & \frac{\partial^2 L}{\partial \theta_k \partial V_k} & \frac{\partial P_k}{\partial \theta_k} & \frac{\partial Q_k}{\partial \theta_k} & \frac{\partial^2 L}{\partial \theta_k \partial \theta_m} & \frac{\partial^2 L}{\partial \theta_k \partial V_m} & \frac{\partial P_m}{\partial \theta_k} & \frac{\partial Q_m}{\partial \theta_k} & & & & & \frac{\partial^2 L}{\partial \theta_k \partial \alpha} & \\
\frac{\partial L}{\partial V_k \partial \theta_k} & \frac{\partial^2 L}{\partial V_k^2} & \frac{\partial P_k}{\partial V_k} & \frac{\partial Q_k}{\partial V_k} & \frac{\partial^2 L}{\partial V_k \partial \theta_m} & \frac{\partial^2 L}{\partial V_k \partial V_m} & \frac{\partial P_m}{\partial V_k} & \frac{\partial Q_m}{\partial V_k} & & & & & \frac{\partial^2 L}{\partial V_k \partial \alpha} & \\
\frac{\partial P_k}{\partial \theta_k} & \frac{\partial P_k}{\partial V_k} & & & \frac{\partial P_k}{\partial \theta_m} & \frac{\partial P_k}{\partial V_m} & & & & & & & \frac{\partial P_k}{\partial \alpha} & \\
\frac{\partial Q_k}{\partial \theta_k} & \frac{\partial Q_k}{\partial V_k} & & & \frac{\partial Q_k}{\partial \theta_m} & \frac{\partial Q_k}{\partial V_m} & & & & & & & \frac{\partial Q_k}{\partial \alpha} & \\
\frac{\partial^2 L}{\partial \theta_m \partial \theta_k} & \frac{\partial^2 L}{\partial \theta_m \partial V_k} & \frac{\partial P_k}{\partial \theta_m} & \frac{\partial Q_k}{\partial \theta_m} & \frac{\partial^2 L}{\partial \theta_m^2} & \frac{\partial^2 L}{\partial \theta_m \partial V_m} & \frac{\partial P_m}{\partial \theta_m} & \frac{\partial Q_m}{\partial \theta_m} & \frac{\partial^2 L}{\partial \theta_m \partial \theta_l} & \frac{\partial^2 L}{\partial \theta_m \partial V_l} & \frac{\partial P_l}{\partial \theta_m} & \frac{\partial Q_l}{\partial \theta_m} & \frac{\partial^2 L}{\partial \theta_m \partial \alpha} & \frac{\partial P_{ml}}{\partial \theta_m} \\
\frac{\partial^2 L}{\partial V_m \partial \theta_k} & \frac{\partial^2 L}{\partial V_m \partial V_k} & \frac{\partial P_k}{\partial V_m} & \frac{\partial Q_k}{\partial V_m} & \frac{\partial L}{\partial V_m \partial \theta_m} & \frac{\partial^2 L}{\partial V_m^2} & \frac{\partial P_m}{\partial V_m} & \frac{\partial Q_m}{\partial V_m} & \frac{\partial^2 L}{\partial V_m \partial \theta_l} & \frac{\partial^2 L}{\partial V_m \partial V_l} & \frac{\partial P_l}{\partial V_m} & \frac{\partial Q_l}{\partial V_m} & \frac{\partial^2 L}{\partial V_m \partial \alpha} & \frac{\partial P_{ml}}{\partial V_m} \\
\frac{\partial P_m}{\partial \theta_k} & \frac{\partial P_m}{\partial V_k} & & & \frac{\partial P_m}{\partial \theta_m} & \frac{\partial P_m}{\partial V_m} & & & \frac{\partial P_m}{\partial \theta_l} & \frac{\partial P_m}{\partial V_l} & & & \frac{\partial P_m}{\partial \alpha} & \\
\frac{\partial Q_m}{\partial \theta_k} & \frac{\partial Q_m}{\partial V_k} & & & \frac{\partial Q_m}{\partial \theta_m} & \frac{\partial Q_m}{\partial V_m} & & & \frac{\partial Q_m}{\partial \theta_l} & \frac{\partial Q_m}{\partial V_l} & & & \frac{\partial Q_m}{\partial \alpha} & \\
 & & & & \frac{\partial^2 L}{\partial \theta_l \partial \theta_m} & \frac{\partial^2 L}{\partial \theta_l \partial V_m} & \frac{\partial P_m}{\partial \theta_l} & \frac{\partial Q_m}{\partial \theta_l} & \frac{\partial^2 L}{\partial \theta_l^2} & \frac{\partial^2 L}{\partial \theta_l \partial V_l} & \frac{\partial P_l}{\partial \theta_l} & \frac{\partial Q_l}{\partial \theta_l} & & \frac{\partial P_{ml}}{\partial \theta_l} \\
 & & & & \frac{\partial^2 L}{\partial V_l \partial \theta_m} & \frac{\partial^2 L}{\partial V_l \partial V_m} & \frac{\partial P_m}{\partial V_l} & \frac{\partial Q_m}{\partial V_l} & \frac{\partial L}{\partial V_l \partial \theta_l} & \frac{\partial^2 L}{\partial V_l^2} & \frac{\partial P_l}{\partial V_l} & \frac{\partial Q_l}{\partial V_l} & & \frac{\partial P_{ml}}{\partial V_l} \\
 & & & & \frac{\partial P_l}{\partial \theta_m} & \frac{\partial P_l}{\partial V_m} & & & \frac{\partial P_l}{\partial \theta_l} & \frac{\partial P_l}{\partial V_l} & & & & \\
 & & & & \frac{\partial Q_l}{\partial \theta_m} & \frac{\partial Q_l}{\partial V_m} & & & \frac{\partial Q_l}{\partial \theta_l} & \frac{\partial Q_l}{\partial V_l} & & & & \\
\frac{\partial^2 L}{\partial \alpha \partial \theta_k} & \frac{\partial^2 L}{\partial \alpha \partial V_k} & \frac{\partial P_k}{\partial \alpha} & \frac{\partial Q_k}{\partial \alpha} & \frac{\partial^2 L}{\partial \alpha \partial \theta_m} & \frac{\partial^2 L}{\partial \alpha \partial V_m} & \frac{\partial P_m}{\partial \alpha} & \frac{\partial Q_m}{\partial \alpha} & & & & & \frac{\partial^2 L}{\partial \alpha^2} & \\
 & & & & \frac{\partial P_{ml}}{\partial \theta_m} & \frac{\partial P_{ml}}{\partial V_m} & & & \frac{\partial P_{ml}}{\partial \theta_l} & \frac{\partial P_{ml}}{\partial V_l} & & & &
\end{bmatrix}
\begin{bmatrix}
\Delta\theta_k \\ \Delta V_k \\ \Delta\lambda_{pk} \\ \Delta\lambda_{qk} \\ \Delta\theta_m \\ \Delta V_m \\ \Delta\lambda_{pm} \\ \Delta\lambda_{qm} \\ \Delta\theta_l \\ \Delta V_l \\ \Delta\lambda_{pl} \\ \Delta\lambda_{ql} \\ \Delta\alpha \\ \Delta\lambda_{ml}
\end{bmatrix}
=
\begin{bmatrix}
-\frac{\partial L}{\partial \theta_k} \\ -\frac{\partial L}{\partial V_k} \\ -\frac{\partial L}{\partial \lambda_{pk}} \\ -\frac{\partial L}{\partial \lambda_{qk}} \\ -\frac{\partial L}{\partial \theta_m} \\ -\frac{\partial L}{\partial V_m} \\ -\frac{\partial L}{\partial \lambda_{pm}} \\ -\frac{\partial L}{\partial \lambda_{qm}} \\ -\frac{\partial L}{\partial \theta_l} \\ -\frac{\partial L}{\partial V_l} \\ -\frac{\partial L}{\partial \lambda_{pl}} \\ -\frac{\partial L}{\partial \lambda_{ql}} \\ -\frac{\partial L}{\partial \alpha} \\ -\frac{\partial L_{flow}}{\partial \lambda_{ml}}
\end{bmatrix}
\tag{5.18}
$$

Once equation (5.18) has been assembled and combined with both matrix $\boldsymbol{W}$ and gradient vector $\boldsymbol{g}$ of the entire network, a sparsity-oriented solution is carried out. This process is repeated until a small, pre-specified tolerance is reached for all the variables involved. It should be noted that this procedure only corresponds to the case in which the TCSC is being operated in standard control mode, i.e. the TCSC is controlling active power flow from nodes *m* to *l*.

In OPF applications lower cost solutions are obtained when the OPF algorithm itself selects the optimum level of power flow across the TCSC. However, any change in the TCSC operating mode is easily accommodated in the general OPF formulation given in equation (5.18). For instance, if the TCSC is not controlling active power flow then matrix $\boldsymbol{W}$ is suitably modified to reflect this operating mode. This can be achieved by adding the second derivative term of a large (infinite) quadratic penalty factor to the diagonal element corresponding to multipliers λ_{ml}, thus forcing these multipliers to be zero for the whole iterative process. The first derivative term of the quadratic Penalty Function is evaluated and added to the corresponding gradient element.

5.3.7 Hessian and Jacobian Elements of the TCSC Sending Node for the Firing Angle Model

The first and second partial derivative terms corresponding to the sending end of the TCSC are derived explicitly. They are obtained by deriving equations (5.9) and (5.10)

with respect to the firing angle. The first and second partial derivative terms for the receiving node are obtained by exchanging subscripts k and m in (5.19)-(5.33).

$$\frac{\partial P_k}{\partial \alpha} = -V_k V_m \sin(\theta_k - \theta_m) B_{TCSC}^2 \frac{\partial X_{TCSC(1)}}{\partial \alpha} \tag{5.19}$$

$$\frac{\partial Q_k}{\partial \alpha} = \left(-V_k^2 + V_k V_m \cos(\theta_k - \theta_m)\right) B_{TCSC}^2 \frac{\partial X_{TCSC(1)}}{\partial \alpha} \tag{5.20}$$

where

$$\frac{\partial B_{TCSC}}{\partial \alpha} = B_{TCSC}^2 \frac{\partial X_{TCSC(1)}}{\partial \alpha} \tag{5.21}$$

$$\begin{aligned} \frac{\partial X_{TCSC}}{\partial \alpha} = & -2C_1\left(1+\cos(2(\pi-\alpha))\right) \\ & + C_2 \sin\left(2(\pi-\alpha)\right)\left(\tan(\pi-\alpha) - \varpi \tan(\varpi(\pi-\alpha))\right) \\ & + C_2\left(\varpi^2 \frac{\cos^2(\pi-\alpha)}{\cos^2(\varpi(\pi-\alpha))} - 1\right) \end{aligned} \tag{5.22}$$

The equations presented above can be simplified by making use of the following relationships,

$$\cos\left(2(\pi-\alpha)\right) = \cos(2\alpha) \text{ and } \sin\left(2(\pi-\alpha)\right) = -\sin(2\alpha) \tag{5.23}$$

The second partial derivative terms of the power equations with respect to the firing angle are,

$$\frac{\partial^2 P_k}{\partial \alpha \partial V_k} = -V_m \sin(\theta_k - \theta_m) B_{TCSC}^2 \frac{\partial X_{TCSC}}{\partial \alpha} \tag{5.24}$$

$$\frac{\partial^2 P_k}{\partial \alpha \partial V_m} = -V_k \sin(\theta_k - \theta_m) B_{TCSC}^2 \frac{\partial X_{TCSC}}{\partial \alpha} \tag{5.25}$$

$$\frac{\partial^2 Q_k}{\partial \alpha \partial V_k} = \left(-2V_k + V_m \cos(\theta_k - \theta_m)\right) B_{TCSC}^2 \frac{\partial X_{TCSC}}{\partial \alpha} \tag{5.26}$$

$$\frac{\partial^2 Q_k}{\partial \alpha \partial V_m} = V_k \cos(\theta_k - \theta_m) B_{TCSC}^2 \frac{\partial X_{TCSC}}{\partial \alpha} \tag{5.27}$$

$$\frac{\partial^2 P_k}{\partial \alpha \partial \theta_k} = -V_k V_m \cos(\theta_k - \theta_m) B_{TCSC}^2 \frac{\partial X_{TCSC}}{\partial \alpha} \tag{5.28}$$

$$\frac{\partial^2 P_k}{\partial \alpha \partial \theta_m} = V_k V_m \cos(\theta_k - \theta_m) B_{TCSC}^2 \frac{\partial X_{TCSC}}{\partial \alpha} \tag{5.29}$$

$$\frac{\partial^2 Q_k}{\partial \alpha \partial \theta_k} = -V_k V_m \sin(\theta_k - \theta_m) B_{TCSC}^2 \frac{\partial X_{TCSC}}{\partial \alpha} \tag{5.30}$$

$$\frac{\partial^2 Q_k}{\partial \alpha \partial \theta_m} = V_k V_m \sin(\theta_k - \theta_m) B_{TCSC}^2 \frac{\partial X_{TCSC}}{\partial \alpha} \tag{5.31}$$

$$\frac{\partial^2 P_k}{\partial \alpha^2} = -V_k V_m \sin(\theta_k - \theta_m)\left(B_{TCSC}^2 \frac{\partial^2 X_{TCSC}}{\partial \alpha^2} + \frac{\partial X_{TCSC}}{\partial \alpha}\frac{\partial B_{TCSC}^2}{\partial \alpha} \right) \tag{5.32}$$

$$\frac{\partial Q_k}{\partial \alpha} = \left(-V_k^2 + V_k V_m \cos(\theta_k - \theta_m) \right)\left(B_{TCSC}^2 \frac{\partial^2 X_{TCSC}}{\partial \alpha^2} + \frac{\partial X_{TCSC}}{\partial \alpha}\frac{\partial B_{TCSC}^2}{\partial \alpha} \right) \tag{5.33}$$

$$\frac{\partial^2 B_{TCSC}}{\partial \alpha^2} = B_{TCSC}^2 \frac{\partial^2 X_{TCSC}}{\partial \alpha^2} + \frac{\partial X_{TCSC}}{\partial \alpha}\frac{\partial B_{TCSC}^2}{\partial \alpha} \tag{5.34}$$

$$\frac{\partial B_{TCSC}^2}{\partial \alpha} = -\frac{2}{X_{TCSC}^3}\frac{\partial X_{TCSC}}{\partial \alpha} \tag{5.35}$$

$$\begin{aligned}\frac{\partial^2 X_{TCSC}}{\partial \alpha^2} = & -4C_1 \sin(2(\pi-\alpha)) \\ & + C_2 \varpi^2 \left(\frac{2\cos^2(\varpi(\pi-\alpha))\cos(\pi-\alpha)\sin(\pi-\alpha)}{\cos^4(\varpi(\pi-\alpha))} \right) \\ & - C_2 \varpi^2 \left(\frac{2\varpi\cos^2(\pi-\alpha)\cos(\varpi(\pi-\alpha))\sin(\varpi(\pi-\alpha))}{\cos^4(\varpi(\pi-\alpha))} \right) \\ & + C_2 \varpi \left(2\tan(\varpi(\pi-\alpha))\cos(2(\pi-\alpha)) + \frac{\varpi\sin(2(\pi-\alpha))}{\cos^2(\varpi(\pi-\alpha))} \right) \\ & - C_2 \left(2\tan(\pi-\alpha)\cos(2(\pi-\alpha)) + \frac{\sin(2(\pi-\alpha))}{\cos^2(\pi-\alpha)} \right)\end{aligned} \tag{5.36}$$

5.3.8 Handling Limits of TCSC-FA Variables

In the OPF formulation, firing angle limits are included in the inequality constraints set. The Multipliers method [17] is used to handle this set. Firing angle values inside bounds are ignored whilst binding inequality constraints become part of the augmented Lagrangian function and, hence, become enforced.

The handling of the TCSC firing angle can be carried out by using the expressions given in Chapter 2,

$$\psi_i(\alpha_i^j, \mu_i^j) = \begin{cases} \mu_i^j(\alpha_i^j - \alpha_i^{max}) + \frac{c}{2}(\alpha_i^j - \alpha_i^{max})^2 & \text{if} \quad \mu_i^j + c(\alpha_i^j - \alpha_i^{max}) \geq 0 \\ \mu_i^j(\alpha_i^j - \alpha_i^{min}) + \frac{c}{2}(\alpha_i^j - \alpha_i^{min})^2 & \text{if} \quad \mu_i^j + c(\alpha_i^j - \alpha_i^{min}) \leq 0 \\ 0 \quad \text{otherwise} \end{cases} \tag{5.37}$$

where i is the number of the variable α and j is an iteration counter; α_i^{max} and α_i^{min} are the upper and lower limits for the firing angle; μ_i is a multiplier term and c is a penalty weighting term.

Firing angle values close to a resonant point give rise to large impedance increments which would adversely affect the mathematical properties of equation (5.17). The OPF algorithm avoids incorporating resonant bands as part its solution space. The firing angle varies in the range 90^0 to α^{max} in the inductive region and in the range α^{min} to 180^0 in the capacitive region. The range α^{max} to α^{min} is a non-operational region.

5.3.9 Initial Conditions

The solution process is started by assuming that the following initial conditions are used in the OPF algorithm.

Nodal Voltage Magnitudes and Phase Angles

The variables in vector **z** must be given initial values in order to start the iterative process. State variables for all nodes are initialised at 1 pu voltage magnitude and 0^0 voltage angle.

Lagrange Multipliers

The Lagrange multipliers for active and reactive power flow mismatch equations are initialised at λ_p given by the lossless economic dispatch and 0, respectively [18]. For TCSC Lagrange multipliers the initial values of λ_{ml} are set to zero. It is my experience that these values give rise to very robust iterative solutions.

TCSC's Firing Angle

The main factor affecting the OPF rate of convergence of TCSC-upgraded networks is the initial firing angle, α. Good starting conditions are required to prevent the solution diverging or arriving at some anomalous value. The initial condition for the TCSC firing angle is selected within the range of ±8 electric degrees from the resonant point given by equation (5.5). Experience has shown that the capacitive region is the normal operating region, and the region in which most OPF solutions lie. Hence initialisation in the capacitive region rather than in the inductive region invariably leads to good OPF solutions for TCSC-upgraded networks.

5.3.10 Practical Implementation of Active Power Flow Constraint

The implementation of the active power flow constraint requires careful consideration. Large variations in $\Delta\alpha$ occur in the early stages of the iterative process if the TCSC is not set to maintain active power flow across the branch *k-m* at a specified value. In this situation, the increments in the TCSC-FA are extremely large, leading to sudden changes from the capacitive to the inductive regions, causing the solution to diverge.

It has been found that the OPF algorithm performs much more reliably when the active power flow is constrained at the sending node, *m*, of the compensated transmission line, *m-l*, i.e. the state variable α does not form part of equation (5.16).

It should be noted that the TCSC control is only activated after the first internal iteration. If it is activated earlier, convergence will never be reached because a large overshooting will occur during the first global iteration. It should also be noted that the revision of limits takes place after the second iteration. Experimentation has shown that this revision scheme yields good iterative solutions.

It is difficult to know a priori the best step size to use in order to improve the rate convergence in OPF algorithms. In the scheme chosen in this work, the vector of correction terms $\Delta \mathbf{z}$ is multiplied by a step size of 0.05 during the first global iteration, and in subsequent iterations, it is increased by a constant factor of 0.05 during the first ten internal iterations until it reaches a value of 0.5. This leads to a slow rate of convergence, but ill-conditioned situations are overcome.

5.3.11 Numerical Problems of TCSC Firing Angle

Extensive testing has been carried out to identify some of the intrinsic numerical problems in the TCSC firing angle implementation. It has been found that in most cases the solution lies approximately 5 degrees away of the resonant point. However, this is also the area in which the TCSC exhibits the largest capacitive reactance increments. Figure 5.7 shows the normal operating area for the Kayenta TCSC scheme: between 145^0 and 180^0, reactance values are more uniform. Close to the resonant point, the numerical properties of the first and second partial derivatives of X_{TCSC} and B_{TCSC} with respect to the firing angle, are ill-conditioned. Figures 5.9 (a) and 5.9 (b) show the $\frac{\partial X_{TCSC}}{\partial \alpha}$ and $\frac{\partial B_{TCSC}}{\partial \alpha}$ profiles as a function of TCSC firing angles for the Kayenta TCSC scheme.

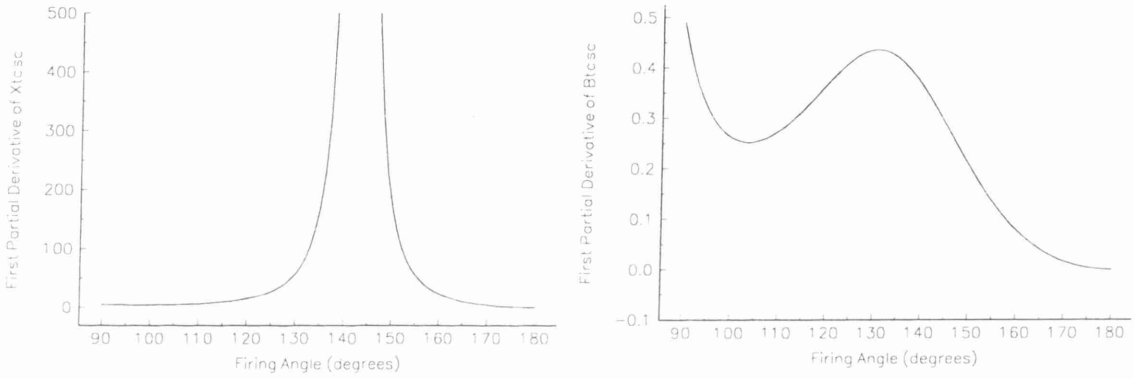

(a) $\frac{\partial X_{TCSC}}{\partial \alpha}$ (b) $\frac{\partial B_{TCSC}}{\partial \alpha}$

Figure 5.9. First partial derivatives of TCSC reactance.

From these figures, it can be observed that for angles near the resonant point, the variations of X_{TCSC} with respect to the firing angle are large in magnitude even for small variations in the firing angle. It should be noted that the curve follows similar patterns in both regions. This derivative term may introduce perturbations in the matrix $\boldsymbol{W}$, leading to large increments in firing angle corrections. Conversely, the variations of B_{TCSC} with respect to the firing angle are extremely small, but these variations show different performances in the inductive and capacitive regions. In fact, the numerical problems increase in the inductive region with some problems converging to infeasible solutions and others not converging at all.

Figures 5.10 (a) and 5.10 (b) show $\frac{\partial^2 X_{TCSC}}{\partial \alpha^2}$ and $\frac{\partial^2 B_{TCSC}}{\partial \alpha^2}$ profiles as a function of TCSC firing angles. From these figures it can be seen that the second partial derivatives of X_{TCSC} with respect to the firing angle are also large near the resonant point. This derivative may introduce the same type of perturbations in the matrix $\boldsymbol{W}$ as the first

partial derivative. In this case, the second partial derivative of B_{TCSC} with respect to the firing angle, has similar performance in both operating regions.

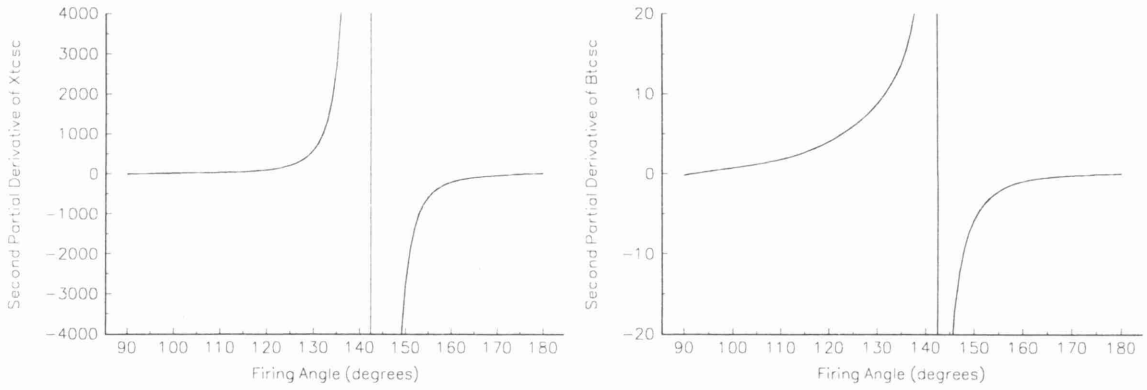

(a) $\frac{\partial^2 X_{TCSC}}{\partial \alpha^2}$ (b) $\frac{\partial^2 B_{TCSC}}{\partial \alpha^2}$

Figure 5.10. Second partial derivatives of TCSC reactance.

The results presented above show that the TCSC impedance and first and second derivatives are strongly non-linear. The capacitive region is the normal operating region of the TCSC under steady-state conditions.

5.3.12 TCSC-FA Active Power Flow Control Test Cases

The 5-node system is used to show how the TCSC performs when installed in a power system [19]. For this particular application, the inductive reactance of the transmission line Lake-Main was increased from 0.03 to 0.04 pu in order to allow larger compensating ratios. The OPF solution is given in Table 5.1 where the relevant variables are shown. Convergence was obtained in 4 iterations to the specified tolerance of 10^{-9}. The active power generation cost is 747.977 \$/hour and the active power losses are 3.051 MW.

Table 5.1. Nodal complex voltages of modified network.

Node	Voltage Magnitude (pu)	Phase Angle (degrees)	Active Power (MW)	Reactive Power (MVAR)	λ_p (\$/MWhr)
Elm	1.072	-4.437	0.00	0.00	4.2639
Main	1.078	-3.892	0.00	0.00	4.2342
Lake	1.078	-3.594	0.00	0.00	4.2231
South	1.100	-1.311	87.899	14.436	4.1032
North	1.109	0.000	80.151	0.290	4.0412

The 5-node system described above has been modified to include a TCSC which compensates the transmission line connected between nodes Lake and Main. The node LakeTCSC was added to the network, as shown in Figure 5.11. The TCSC firing angle model was used to optimise the active power flow level in transmission line Lake-Main, i.e. 14.97 MW, which is amenable to minimum active power generation cost and network losses, i.e. 747.975 \$/hour and 3.050 MW, respectively. The reactance values of the TCSC to achieve this result are X_C=0.9375% and X_L=0.1625%, with respect to a base voltage of 400 kV. The solution was achieved in 5 iterations, starting from an initial firing angle of 150°. The resultant power flows are shown in Figure 5.11 and the

nodal voltages, active and reactive generated powers and Lagrange multipliers are given in Table 5.2. The firing angle and the TCSC reactance at each iteration are given in Table 5.3.

Table 5.2. Nodal complex voltages of modified network.

Node	Voltage Magnitude (pu)	Phase Angle (degrees)	Active Power (MW)	Reactive Power (MVAR)	λ_p ($/MWhr)
LakeTCSC	1.078	-3.534	0.000	0.000	4.2232
Elm	1.072	-4.417	0.000	0.000	4.2639
Main	1.077	-3.846	0.000	0.000	4.2341
Lake	1.078	-3.622	0.000	0.000	4.2232
South	1.100	-1.303	87.898	14.400	4.1031
North	1.109	0.000	80.152	0.290	4.0412

Table 5.3. TCSC-FA parameters.

Iterations	TCSC-FA parameters	
	α (degrees)	X_{TCSC} (pu)
0	150.000	-0.0180
1	150.587	-0.0169
2	162.845	-0.0101
3	154.328	-0.0130
4	156.399	-0.0119
5	156.407	-0.0119

From Tables 5.1 and 5.2, some interesting observations can be made. For example, the λ_p associated with the North and Lake nodes are increased due to the increase in active power flowing from North-Lake. In the remaining nodes, their λ_ps were reduced. Now, it is more expensive to supply the load at the North and Lake nodes than previous to the installation of the TCSC. However, the total active power cost, active power losses, and even the reactive power were reduced due to the TCSC.

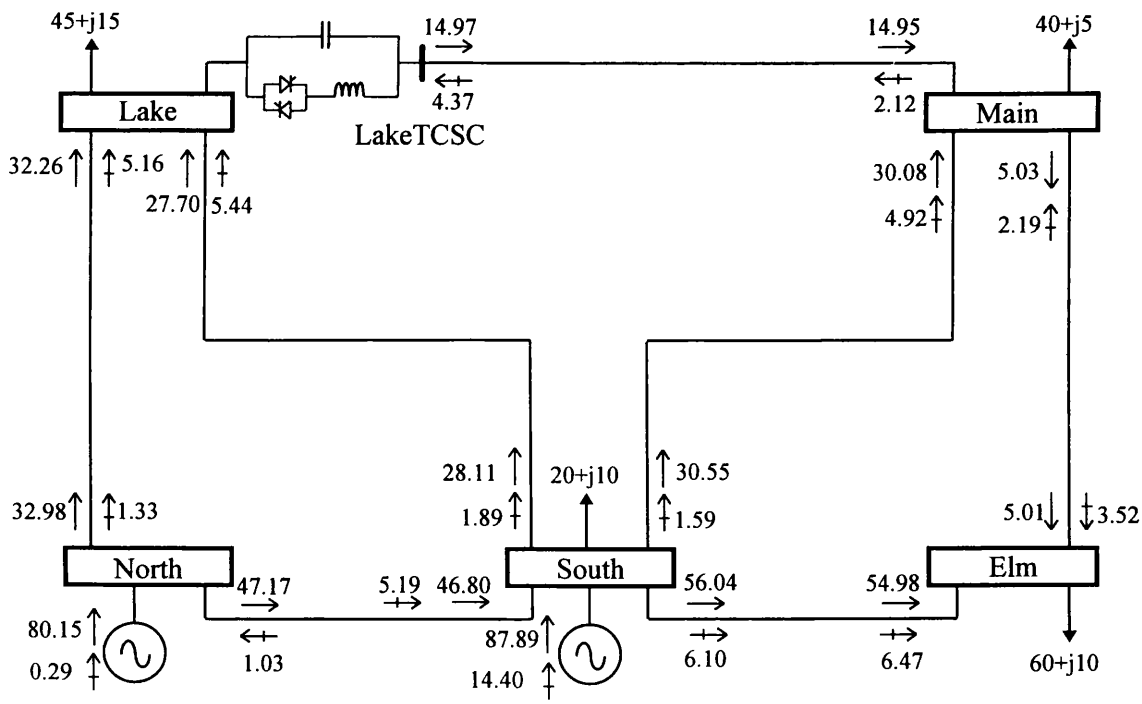

Figure 5.11. Modified 5-node system and OPF solution.

In a second case the TCSC is used to maintain the active power flow leaving LakeTCSC, at a specified power flow. The chosen value is 18.0 MW. The TCSC impedance and firing angles at each iteration are presented in Table 5.4 and the power flow results are shown in Figure 5.12. The TCSC-FA model upheld its target value. Convergence was obtained in 3 iterations. As expected, the generation cost and the network losses increased to 749.478 $/hour and 3.415 MW, respectively.

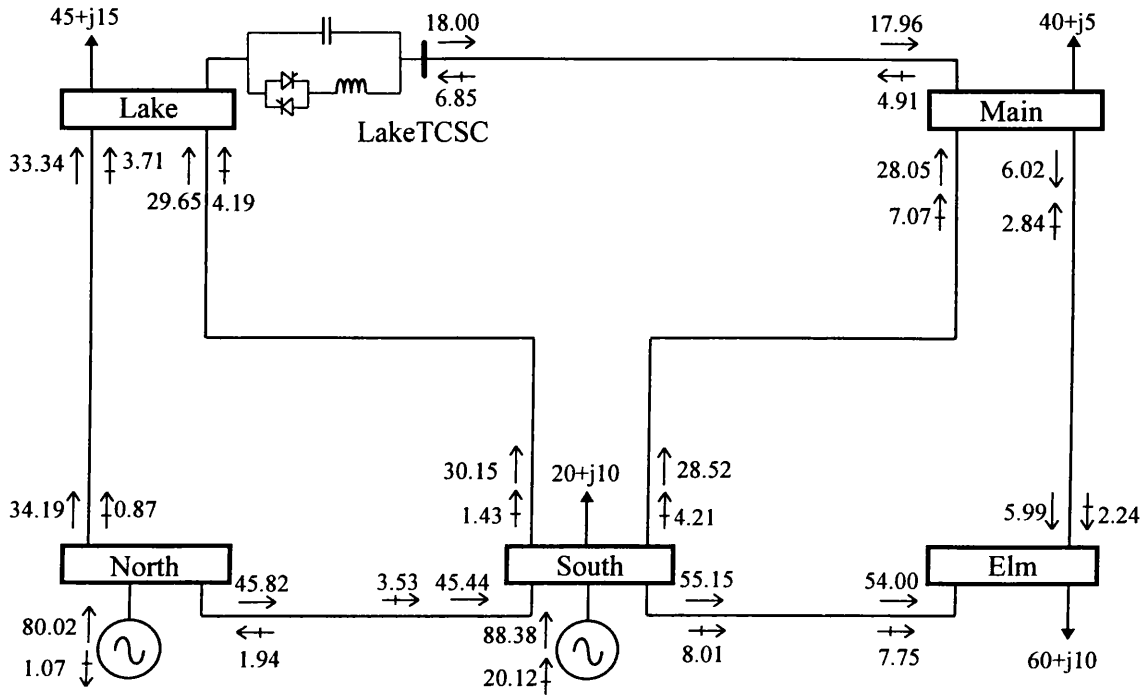

Figure 5.12. TCSC maintaining the active power flow at a specified power value.

Table 5.4. TCSC-FA parameters.

Iterations	TCSC-FA parameters	
	α (degrees)	X_{TCSC} (pu)
0	150.000	-0.0180
1	144.191	-0.0686
2	144.220	-0.0674
3	144.223	-0.0673

Figure 5.13 shows the convergence process of the active power flow across the transmission line Lake-Main when P_{ml} is operating under both constrained and unconstrained conditions. The pattern of convergence exhibits slight oscillations in the first and second iterations when P_{ml} is not constrained. This is due to changes in the active set during these iterations and changes in the penalty-weighting factors. Thereafter, the active power flow constraint converges smoothly to optimal operating condition. Several additional iterations are required to satisfy the very stringent convergence criterion, i.e. 10^{-9}. The iterative solution process is very sensitive and in some cases it will never reach convergence if P_{ml} is not regulating a fixed amount of active power flow. On the other hand, when P_{ml} is constrained at a specified flow, the process of convergence is more robust and changes in the penalty weighting factors do not distort the pattern of convergence.

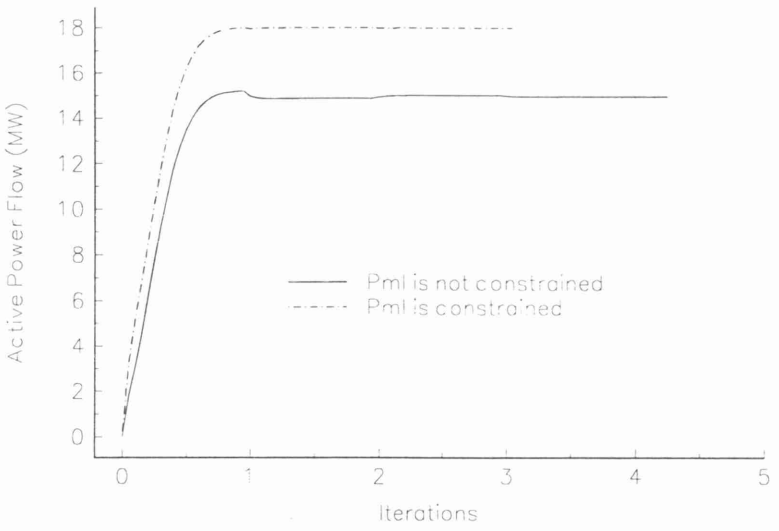

Figure 5.13. Active power flow in the transmission line Lake-Main.

Figure 5.14 shows the performance of the gradient of the Lagrangian function with respect to α for the two cases presented above. It can be observed that the constrained case shows a rather irregular pattern during the first iteration. Even though the gradient takes large values in the first iterations, its robustness is never lost during the iterative solution process.

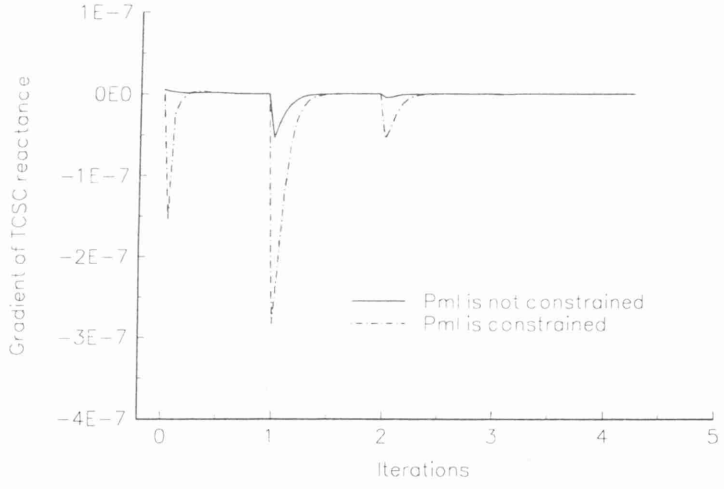

Figure 5.14. Gradient of Lagrangian function with respect α.

5.3.13 Effect of the Initial Firing Angle

The choice of TCSC firing angle initial value has an important bearing upon the iterative process. This is investigated in this Section.

Several initial firing angles were used to investigate their impact in the complete iterative process. The standard AEP 14-node system [13] was modified to incorporate two TCSCs aiming at controlling active power flow across branches Nod_5-Nod_4 and Nod_12-Nod_13 at 30 MW and 2 MW, respectively. Figure 5.15 shows the locations of these TCSCs. The inductive reactance of branch Nod_12-Nod_13 was increased from 0.19988 pu to 0.24 pu in order to observe better the TCSC effects in this branch. The power flows are 26.8 MW and 1.7 MW, respectively. For the purpose of this exercise all the synchronous condensers in the original network are assumed to be synchronous

generators, i.e. capable of generating active power. The data required by the optimisation algorithm, such as fuel cost curves, were given typical values.

In order to assess the impact of the firing angle initial guess, five different solutions were carried out. The first iterative solution was carried out with an initial firing angle of 144^0. Subsequent solutions were performed with 3^0 increases with respect to the initial firing angle. Both TCSCs were initialised equally in every case. The TCSCs reactances are X_C = 0.9375%. and X_L = 0.1625%. It should be noted that the negative sign of the capacitive reactance has already been taken into account in equation (5.1).

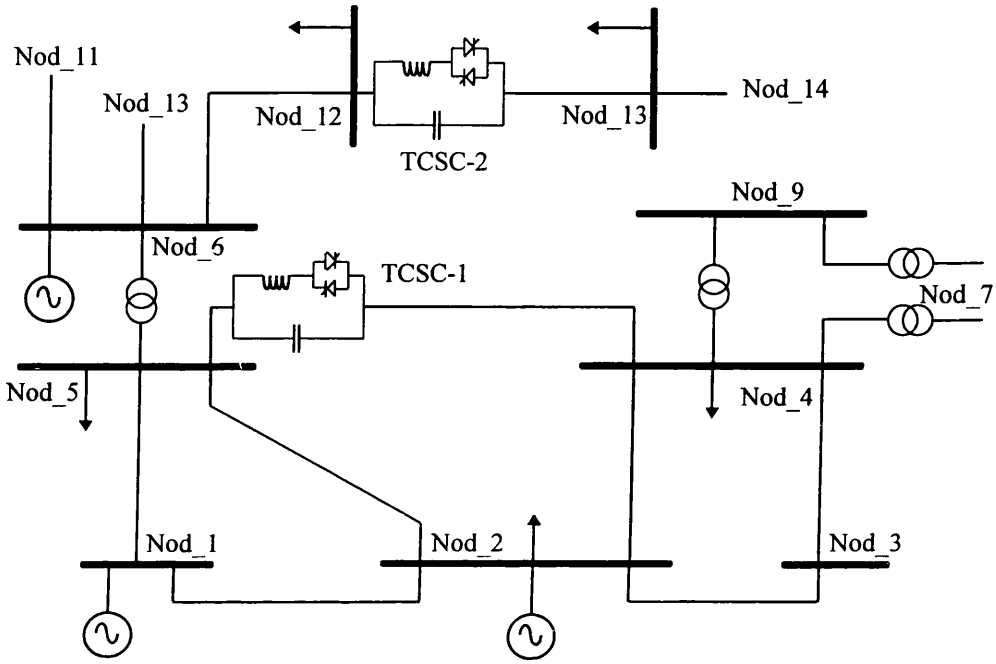

Figure 5.15. AEP 14-node system with two TCSC devices embedded.

Table 5.5 shows the values of the TCSC firing angle at the end of each iteration for the initial firing angle of 144^0. All the inequality constraints were satisfied, except for the voltage magnitude at node Nod_7 which was suitably enforced by means of the Multipliers method. The number of iterations taken by the algorithm to converge to the specified tolerance was 5 for the first four cases. Exactly the same active power generation cost and active power losses were arrived at, i.e. 215.453 $/hr and 1.899 MW. Similarly, the TCSC equivalent reactances were identical in all cases. The case when the firing angle was initialised at 156^0 converged in 4 iterations but it converged to an undesirable value. The final TCSC firing angle was very different than for the previous four cases. It settled down to 180^0, which clearly indicates an unrealistic solution. Furthermore, the power generation cost and active power losses were much larger.

Table 5.5. TCSC parameters when α starts at 144^0.

	TCSC-1 parameters		TCSC-2 parameters	
Iteration	α (degrees)	X_{TCSC} (pu)	α (degrees)	X_{TCSC} (pu)
0	144.000	-0.0771	144.000	-0.0771
1	147.488	-0.0251	144.212	-0.0677
2	147.783	-0.0239	144.028	-0.0757
3	146.698	-0.0292	146.011	-0.0343
4	147.277	-0.0261	144.479	-0.0588
5	147.164	-0.0266	144.656	-0.0542

Figures 5.16 and 5.17 show the firing angles profiles for both TCSCs as a function of the iteration number. It can be observed that the patterns of convergence are irregular during the first global iteration. The very pronounced overshooting due to the large variations taken place in the first and second derivatives of the TCSCs reactances with respect to the firing angles. It can also be seen that the perturbations diminish once the iterative process approaches the solution. Good initial conditions are amenable to small firing angle increments. Conversely, initial values far from the solution, may lead to unrealistic answers. A case in point is the situation when the firing angle settles to a firing angle value of 180^0 for both TCSCs. This case corresponds to an initial firing angle of 156^0. It must be noted that in this case, the firing angle tends towards 180^0.

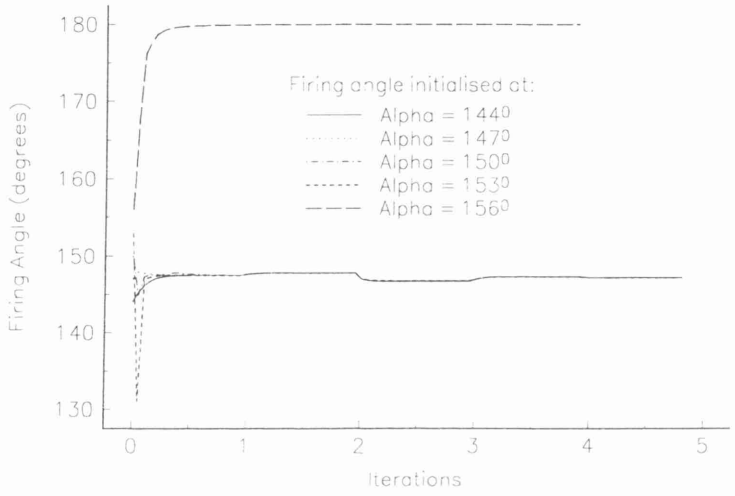

Figure 5.16. TCSC-1 firing angle profile.

The very large perturbations which take place during the first global iteration lead to TCSC limit violations. Here, fluctuations from the capacitive to the inductive regions take place in a rather unpredictable manner. Hence, no attempt is made to revise TCSC limits before the end of the second global iteration. At this point, nodal voltages and active and reactive nodal power are revised and, if required, suitably enforced. It is my experience that from the second iteration onwards, the TCSC firing angle moves in a continuous and smooth fashion. The results above show that the algorithm is very robust towards the convergence, however, if unsuitable initial conditions for the firing angle are used then the algorithm will converge to an unrealistic value.

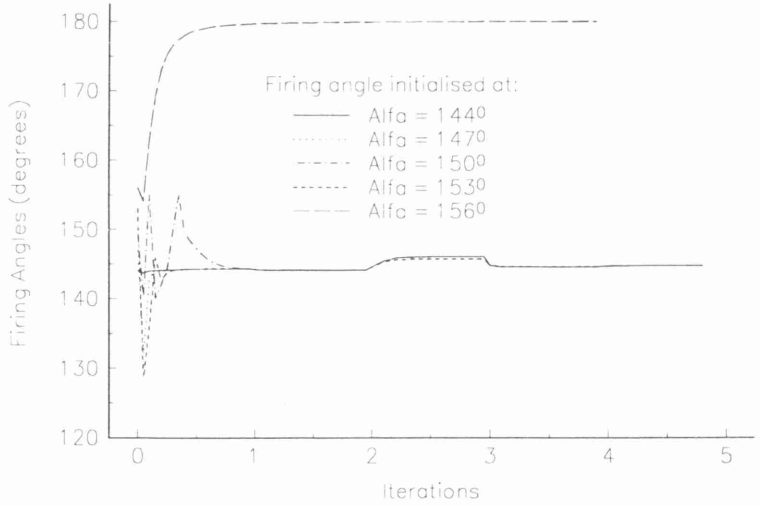

Figure 5.17. TCSC-2 firing angle profile.

The active power generation cost as a function of the iteration number is plotted in Figure 5.18, while the active power losses as a function of the iteration number are plotted in Figure 5.19. As expected differences in total cost and electric power losses for the case when the initial firing angle is set to 156^0 are due to the unrealistic solution. The initial cost and electric power losses are higher than subsequent values because the OPF algorithm starts the procedure from a lossless economic dispatch using the equal incremental cost criterion.

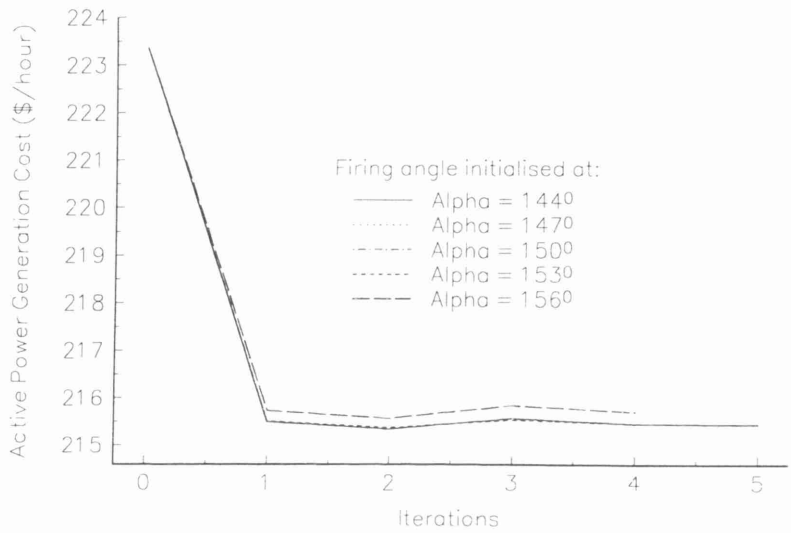

Figure 5.18. Active power generation cost profiles corresponding to AEP 14-node system.

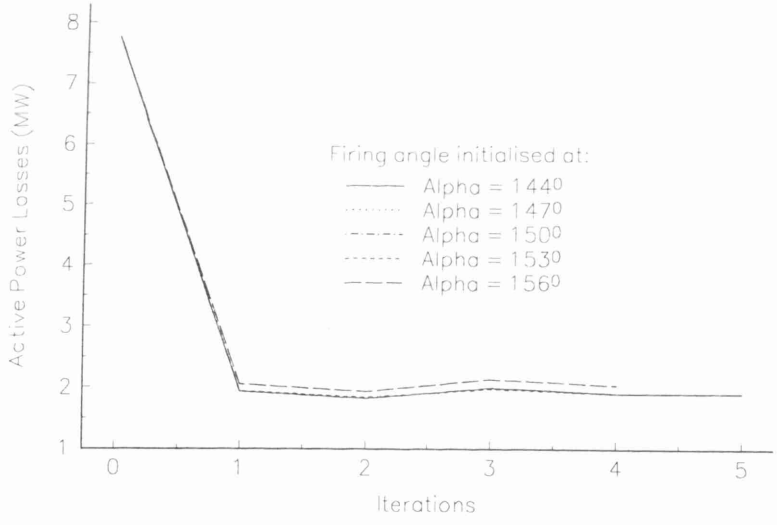

Figure 5.19. Active power losses profiles corresponding to AEP 14-node system.

5.3.14 TCSC-FA Control Near a Resonance Point

Figure 5.17 shows the performance of α that TCSC-2 requires to operate near the resonant point. There are large fluctuations in the firing angle of TCSC-2 during the early iterations. In general, the perturbations were larger than those exhibited by TCSC-1, which provides capacitive compensation at $\alpha = 147.164^0$, only four degrees away from the resonant point.

5.3.15 TCSC-FA Embedded in a Real Power System

This Section presents OPF results which relate to a large power network. The power system described in Section 3.3.11 was suitable modified to incorporate TCSCs. The relevant part of the upgraded network, with two TCSCs, is shown in Figure 5.20. Fuel cost curves and the upper and lower limits of all variables used in the optimisation procedure were given typical values.

In the original system during maximum demand, an active power flow of 60.42 MW is injected into node ROH through line RIH-ROH, and 87.22 MW is injected into node TJH through line MEH-TJH. Convergence was achieved in 5 iterations. The generation cost and network losses were 293.643 $/hour and 20.117 MW, respectively.

The TCSCs have been set to maintain active power flow injected into nodes ROH and TJH at 90 MW and 80 MW, respectively. The TCSCs' electric parameters are given in Table 5.6. TCSC-1 parameters are given on a base voltage of 230 KV. The TCSC-2 parameters are equal to a tenth of the TCSC-1 parameters. The firing angles of both TCSCs were initialised at 150^0. The mismatch tolerance was set at 10^{-9}. Table 5.7 shows the firing angle values and the equivalent impedances of both TCSCs at each iteration. These values are given in degrees and pu, respectively.

Table 5.6. TCSC's electric parameters.

TCSC	X_C (pu)	X_L (pu)
1	0.028355	0.004914
2	0.002835	0.000491

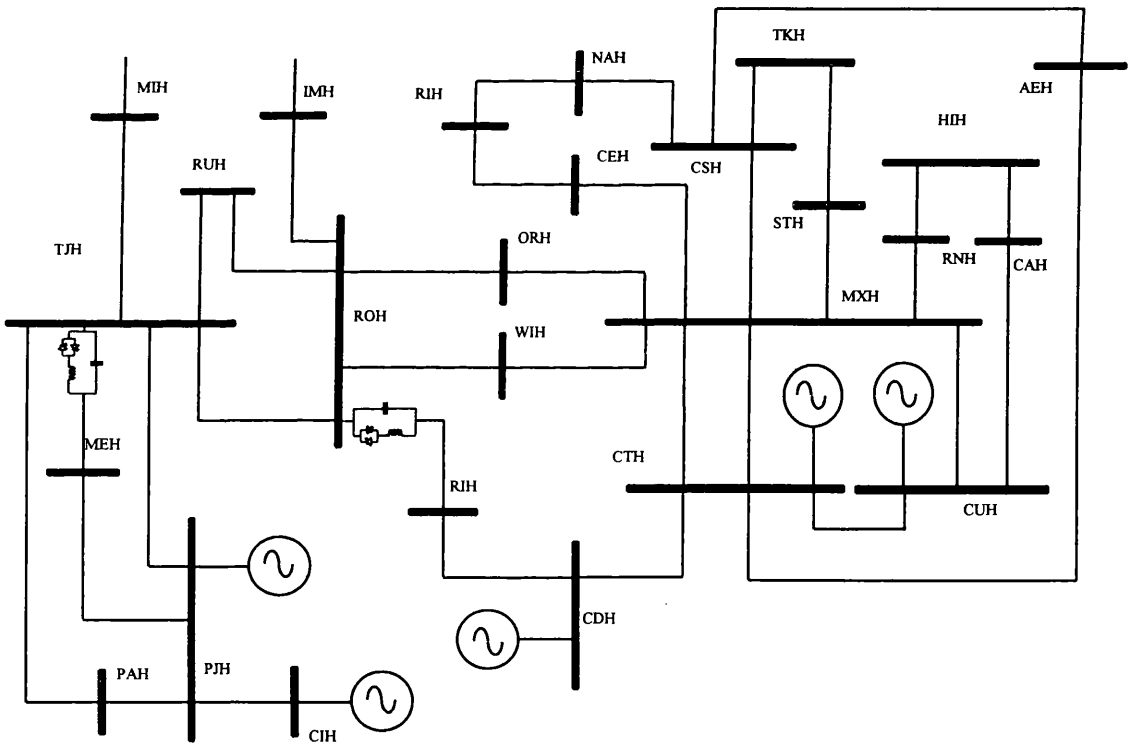

Figure 5.20. Relevant part of 166-node system with TCSCs.

Convergence was achieved in 10 iterations. The TCSCs were used to increase the active power flow across lines RIH-ROH and MEH-TJH and yet the overall performance was improved in terms of reduced production cost and active power losses. The generation cost was 293.36 $/hour and the electric power losses were 19.993 MW.

Table 5.7. Firing angle values for TCSCs.

Iteration	TCSC-1		TCSC-2	
	α (degrees)	X_{TCSC} (pu)	α (degrees)	X_{TCSC} (pu)
0	150.00	-0.0544	150.000	-0.00544
1	150.975	-0.0496	148.685	-0.00634
2	151.003	-0.0495	147.534	-0.00754
3	151.020	-0.0494	150.365	-0.00524
4	151.030	-0.0493	156.064	-0.00365
5	151.030	-0.0494	153.331	-0.00418
6	151.031	-0.0494	152.053	-0.00455
7	151.032	-0.0493	151.312	-0.00482
8	151.034	-0.0493	150.848	-0.00502
9	151.036	-0.0493	150.458	-0.00520
10	151.037	-0.0493	150.150	-0.00530

5.4 TCSC Controllable Reactance Model

In the controllable reactance model, the state variable is a reactance which is adjusted to allow the power flow across a branch to be maintained at a specified value [15]. The maximum and minimum values of the controllable reactance are determined by the total equivalent reactance of all the TCSC modules connected in series, irrespective of their operating mode. Once the level of compensation has been determined, the firing angle can be obtained from (5.1) by resorting to an iterative technique.

In this model, the TCSC power equations at node k are similar to equations (5.9) and (5.10), where B_{TCSC} is substituted by $-1/X_{TCSC}$:

$$P_k = \frac{V_k V_m}{X_{TCSC}} \sin(\theta_k - \theta_m) \tag{5.38}$$

$$Q_k = \frac{V_k^2}{X_{TCSC}} - \frac{V_k V_m}{X_{TCSC}} \cos(\theta_k - \theta_m) \tag{5.39}$$

First and second derivative terms for the equations (5.38) and (5.39) are given in the following Section. The new control variable is the controllable reactance X_{TCSC}. The Lagrangian function corresponding to the power flow mismatch equations at nodes k and m and the Lagrangian function used to control the active power across branch m-l are modelled in the same way as the TCSC-FA model, equations (5.15) and (5.16).

The linearised system of equations is similar to (5.18). The only difference is that the state variable α is substituted by X_{TCSC}, i.e. the vector x includes P_g, V, θ and X_{TCSC}. The initial condition guidelines given in Section 5.3.9 also apply to this model. The initial condition for X_{TCSC} is determined by computational experimentation with a view to increasing the rate of convergence of the system being tested.

5.4.1 Hessian and Jacobian Elements for the Controllable Reactance Model

The first partial derivatives of the power equations with respect to the controllable reactance are:

$$\frac{\partial P_k}{\partial X_{TCSC}} = -V_k V_m \sin(\theta_k - \theta_m)\frac{1}{X_{TCSC}^2} \tag{5.40}$$

$$\frac{\partial Q_k}{\partial X_{TCSC}} = \left(-V_k^2 + V_k V_m \cos(\theta_k - \theta_m)\right)\frac{1}{X_{TCSC}^2} \tag{5.41}$$

The second partial derivatives of the power equations with respect to the controllable reactance are:

$$\frac{\partial^2 P_k}{\partial X_{TCSC}\partial V_k} = -V_m \sin(\theta_k - \theta_m)\frac{1}{X_{TCSC}^2} \tag{5.42}$$

$$\frac{\partial^2 P_k}{\partial X_{TCSC}\partial V_m} = -V_m \sin(\theta_k - \theta_m)\frac{1}{X_{TCSC}^2} \tag{5.43}$$

$$\frac{\partial^2 Q_k}{\partial X_{TCSC}\partial V_k} = \left(-2V_k + V_m \cos(\theta_k - \theta_m)\right)\frac{1}{X_{TCSC}^2} \tag{5.44}$$

$$\frac{\partial^2 Q_k}{\partial X_{TCSC}\partial V_m} = V_k \cos(\theta_k - \theta_m)\frac{1}{X_{TCSC}^2} \tag{5.45}$$

$$\frac{\partial^2 P_k}{\partial X_{TCSC}\partial \theta_k} = -V_k V_m \cos(\theta_k - \theta_m)\frac{1}{X_{TCSC}^2} \tag{5.46}$$

$$\frac{\partial^2 P_k}{\partial X_{TCSC}\partial \theta_m} = V_k V_m \cos(\theta_k - \theta_m)\frac{1}{X_{TCSC}^2} \tag{5.47}$$

$$\frac{\partial^2 Q_k}{\partial X_{TCSC}\partial \theta_k} = -V_k V_m \sin(\theta_k - \theta_m)\frac{1}{X_{TCSC}^2} \tag{5.48}$$

$$\frac{\partial^2 Q_k}{\partial X_{TCSC}\partial \theta_m} = V_k V_m \sin(\theta_k - \theta_m)\frac{1}{X_{TCSC}^2} \tag{5.49}$$

$$\frac{\partial^2 P_k}{\partial X_{TCSC}^2} = V_k V_m \sin(\theta_k - \theta_m)\frac{2}{X_{TCSC}^3} \tag{5.50}$$

$$\frac{\partial^2 Q_k}{\partial X_{TCSC}^2} = \left(V_k^2 - V_k V_m \cos(\theta_k - \theta_m)\right)\frac{2}{X_{TCSC}^3} \tag{5.51}$$

The equations for node m are obtained by exchanging subscripts k and m in equations (5.42)-(5.51).

5.4.2 Comparison of the Controllable Reactance and the TCSC-FA Models

The two TCSC models are compared below in terms of their ability to converge. The 5-node, 14-node and 166-node systems used in Sections 5.3.12, 5.3.13 and 5.3.15 were solved with the controllable reactance TCSC model. The controllable reactance model was initialised at the reactance value corresponding to the equivalent firing angle used previously.

Two different scenarios are considered below, using the 5-node test system. In the first case, the power flow across branch Lake-Main was not specified a priori. The initial value of X_{TCSC} is set to -0.0180 (150^0). The TCSC reactance values throughout the iterative process are shown in Table 5.8. After convergence, the voltage magnitudes, phase angles and Lagrange multipliers corresponding to each node are exactly the same as those presented in Table 5.2.

Table 5.8. TCSC reactance.

Iterations	0	1	2	3	4
X_{TCSC} (pu)	-0.0180	-0.0169	-0.0101	-0.0130	-0.0119

Convergence was obtained in 4 iterations, one iteration less than the TCSC-FA model. The active power generation cost and the active power losses were 747.975 $/hour and 3.050 MW, respectively. Referring to Table 5.3, it can be seen that these values are the same as those obtained by the TCSC-FA model.

In the second case, the TCSC is used to maintain the active power flow leaving LakeTCSC at 18.0 MW. The algorithm converged in 4 iterations with the power flow maintaining its target value. The number of iterations and the TCSC reactance values given by both models are exactly the same. These are shown in Tables 5.4 and 5.9.

The convergence pattern of the Lagrangian function gradient with respect to X_{TCSC} is shown in Figure 5.21. It can be observed that during the first iteration the pattern of convergence is rather irregular. Figure 5.22 shows the convergence process of the active power flow across transmission line Lake-Main for the two operating conditions. Both figures show smaller variations than those exhibited by the TCSC-FA model. The controllable reactance TCSC model has shown to be quite resilient to changes in the penalty weighting factors. However, small perturbations can still be observed in the first iteration.

Table 5.9. TCSC reactance.

Iterations	0	1	2	3
X_{TCSC} (pu)	-0.0180	-0.0686	-0.0674	-0.0673

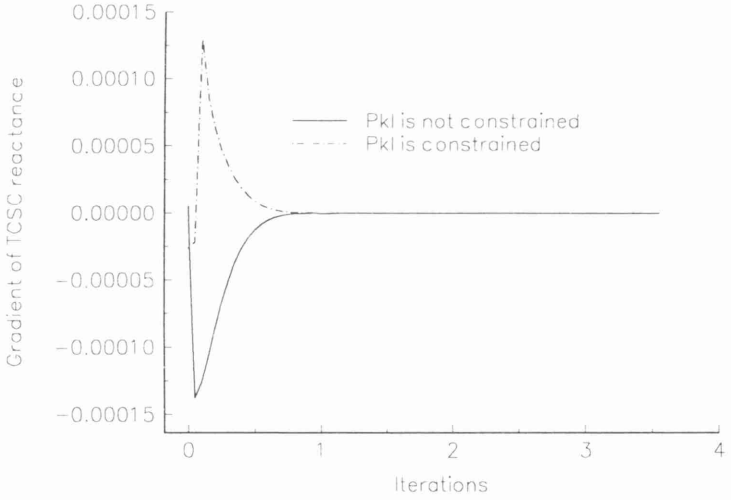

Figure 5.21. Derivative of the Lagrangian function with respect to X_{TCSC}.

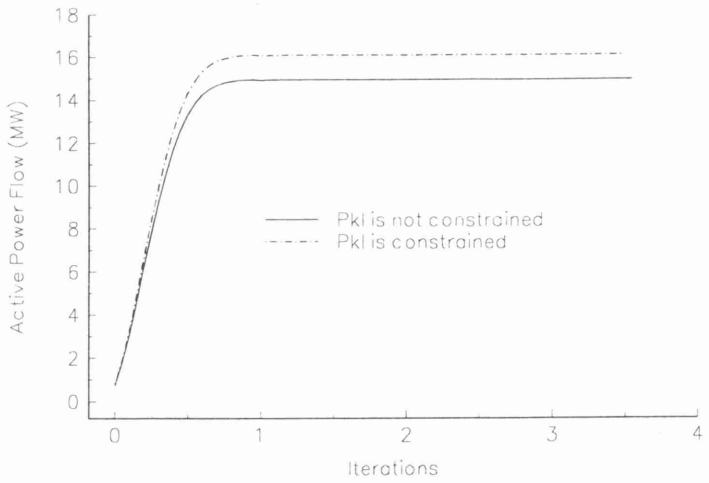

Figure 5.22. Active power flow in transmission line Lake-Main.

A similar analysis to the one presented in Section 5.3.13 was carried out for the 14-node system. An additional case considers the value of X_{TCSC} whose equivalent firing angle is 160^0, was analysed. The minimum and maximum limits of the TCSC parameters were set at -0.0093 pu and -0.0771 pu, respectively. Several cases, starting from different initial conditions were simulated to test the algorithm's ability to reach convergence,

A) Initial condition at X_{TCSC} = -0.0344 (146^0).

B) Initial condition at X_{TCSC} = -0.0275 (147^0).

C) Initial condition at X_{TCSC} = -0.0180 (150^0).

D) Initial condition at X_{TCSC} = -0.0141 (153^0).

E) Initial condition at X_{TCSC} = -0.0121 (156^0).

F) Initial condition at X_{TCSC} = -0.0107 (160^0).

In all cases, the algorithm found the optimal solution in three iterations, two fewer than the TCSC-FA model. Moreover, in all cases, the same TCSC equivalent reactance was obtained. Figures 5.23 and 5.24 show the TCSC equivalent reactance as a function of the iteration number for TCSC-1 and TCSC-2, respectively.

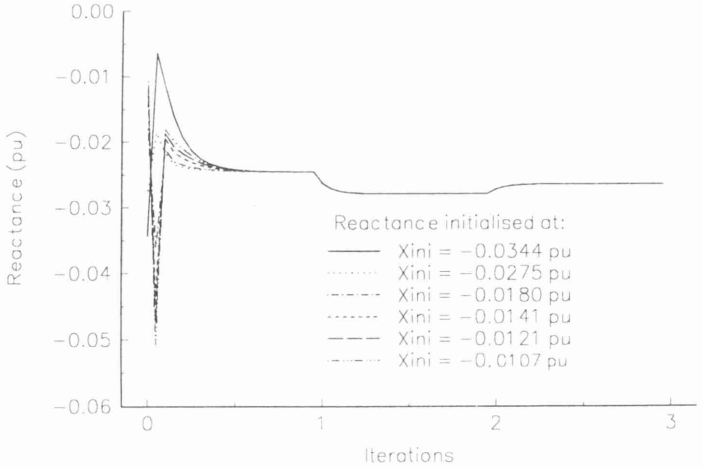

Figure 5.23. TCSC-1 reactance profile.

It can be observed in both figures that large overshootings occur in the first iteration. The overshootings decrease with better initial reactance guesses. When X_{TCSC} = -0.0107 was chosen as an initial condition, the algorithm converged in three iterations. The same result is obtained when X_{TCSC} = -0.0344. However, when X_{TCSC} = -0.0771 (maximum

limit) was used as an initial condition, the algorithm failed to convergence. This case is not shown.

Figures 5.25 and 5.26 show that the active power generation cost and the active power losses converged towards to the same optimum in every case. Both models yield the same solution. However, the controllable reactance model has shown to be more reliable towards the convergence.

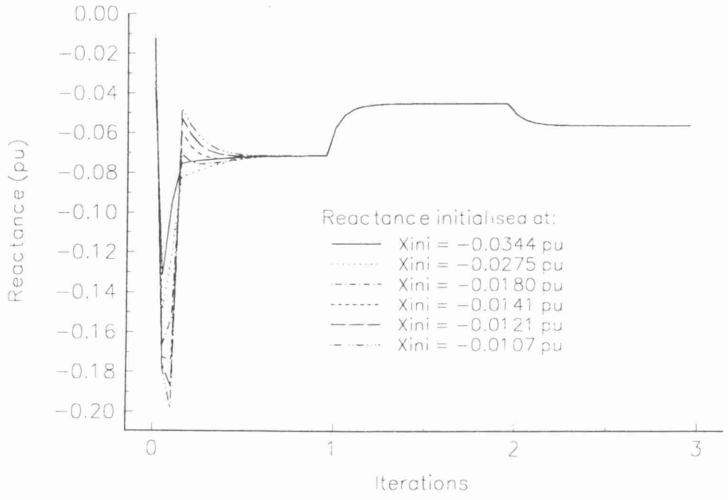

Figure 5.24. TCSC-2 reactance profile

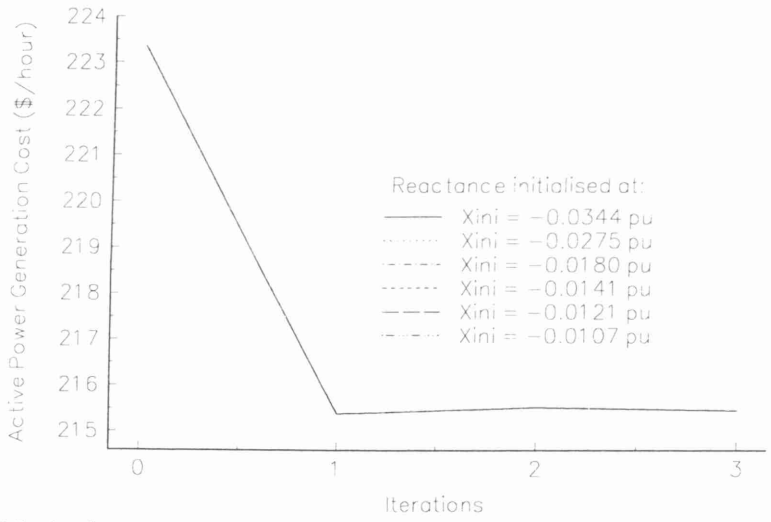

Figure 5.25. Active power generation cost profile for the AEP 14-node system.

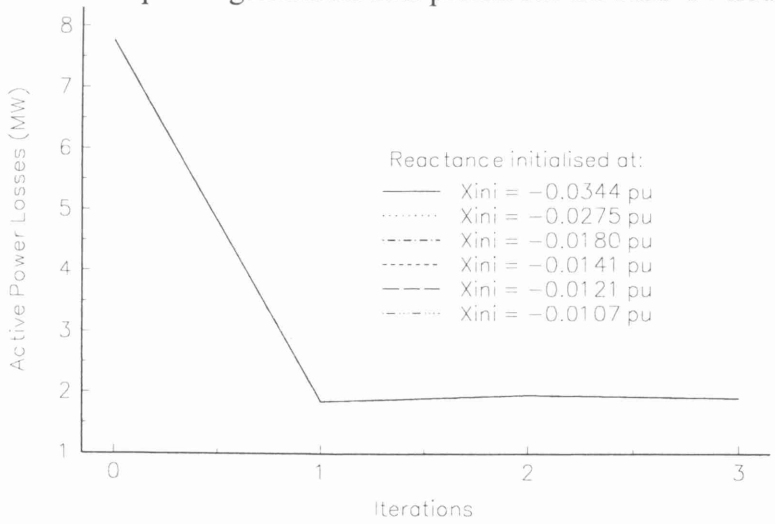

Figure 5.26. Active power losses profile for the AEP 14-node system.

5.4.3 Active Power Flow Control in a Real Power System

The TCSC controllable reactance model was also tested using the real power system described in Section 5.3.15. Two TCSCs were employed to maintain the active power flow at the sending end of nodes ROH and TJH at 90 MW and 80 MW, respectively. The upper and lower limits of the TCSC parameters are shown in Table 5.10. The mismatch tolerance was set at 10^{-9} and the TCSC reactances were initialised at -0.00544 pu (150°). Convergence was obtained in 9 iterations. Table 5.11 shows the TCSC reactance values at each iteration. The solution was practically the same as that obtained by the TCSC-FA model. However, the active power generation cost and the active power losses were slightly larger than for the TCSC-FA result, i.e. 293.4 $/hour and 20.0306 MW, respectively.

Table 5.10. Limits of Reactances.

TCSC	Minimum (pu)	Maximum (pu)
1	-0.028355	-0.233211
2	-0.002835	-0.023321

Table 5.11. Controllable reactance values.

Iteration	TCSC-1 X_{TCSC} (pu)	TCSC-2 X_{TCSC} (pu)
0	-0.0544	-0.00544
1	-0.0496	-0.00634
2	-0.0495	-0.00754
3	-0.0494	-0.00524
4	-0.0493	-0.00365
5	-0.0494	-0.00418
6	-0.0494	-0.00455
7	-0.0493	-0.00482
8	-0.0493	-0.00502
9	-0.0493	-0.00520

5.5 Conclusions

Two general TCSC power flow models have been presented in this chapter: the TCSC firing angle model and TCSC controllable reactance model.

The TCSC firing angle model is a newer TCSC-OPF model than those currently available in the open literature. The thyristor's firing angle, a newly introduced control variable in OPF formulations, is combined with the nodal voltage magnitudes and angles of the power network in a single frame-of-reference for unified iterative solutions via Newton's method. In this algorithm the thyristor's firing angle is regulated in order to achieve an optimal level of compensation under either constrained or unconstrained power flow across the compensated branch. In the latter case, the power flow and compensation level are selected by the algorithm, leading to more economic solutions than in cases when the power flow is set at a specified value.

The extended OPF Newton algorithm has proved to be a very powerful tool, capable of solving TCSC-upgraded power networks very reliably, using a minimum of iterative steps. The computational efficiency of the OPF Newton algorithm is further tightened by using the Multipliers Method to handle the binding set.

At first, providing suitable initial conditions for the thyristor's firing angle was found to be a troublesome issue. The TCSC slopes tend asymptotically to $\pm\infty$ at the resonant point and to zero at their maximum and minimum firing angle conduction points. As expected, initial conditions far from the optimal firing angle may lead to anomalous solutions or may even cause the algorithm to diverge. Extensive testing indicates that a TCSC firing angle of +8° away from the resonant point provides good initial conditions for solutions taking place in the capacitive region, whereas an angle of -8° away from the resonant point was suitable for solutions lying in the inductive region.

The efficiency of the algorithm has been illustrated by numeric examples. Networks of various sizes have been solved with the extended algorithm. Some of them correspond to large company networks. However, for the sake of presenting complete set of results, only two standard networks and one real life network are studied in the Chapter. The results clearly show the algorithm's flexibility and reliability towards the convergence.

The TCSC controllable reactance model has shown to be equally reliable. In this model, the state variable is a controllable reactance, which is combined with the nodal voltage magnitudes and phase angles of the power network. Small negative reactance values provide good initial conditions for optimal solutions taking place in the capacitive region.

The controllable reactance model implemented in the OPF algorithm has proved to be capable of solving large power networks. The same results were achieved with both the TCSC firing angle model and the TCSC controllable reactance model. However, the controllable reactance model has shown to be more robust towards the convergence than the TCSC-FA.

5.6 References

[1] Hingorani N.G.: 'Flexible AC Transmission Systems', IEEE Spectrum, April 1993, pp. 40-45.

[2] IEEE Power Engineering Society: 'FACTS Applications', Special Issue, 96TP116-0, IEEE Service Center, Piscataway, N.J., 1996.

[3] Christl N., Hedin R., Johnson R., Krause P. and Montoya A.: 'Power system studies and Modelling for the Kayenta 230 kV Substation Advance Series Compensation', Proceedings of the IEE 5th International Conference on AC and DC Power Transmission, London, 1991, pp. 33-37.

[4] Gama C., Salomao J.C.S., Gribel J.B. and Ping W.: 'Brazilian North-South Interconnection -Application of Thyristor Controlled Series Compesator (TCSC) to Damp Inter-area Oscillation Mode', EPRI Conference on the Future of Power Delivery in the 21st Century, Session 2-Grid Operation and Planning, November 18-20, 1997, La Jolla California.

[5] Tenorio A.R.M., Jenkins N. and Bollen M.H.J.: 'A TCSC Model for Electromagnetic Transient Studies', IEEE/KTH Stockholm Power Tech Conference, Stockholm , Sweden, June 18-22, 1995, pp. 130-135.

[6] Piwko R.J., Wegner C.A., Kinney S.J. and Eden J.D.: 'Subsynchronous Resonance Performance Tests of the Slatt Thyristor-Controlled Series Capacitor', IEEE Transaction on Power Delivery, Vol. 11, No. 2, April 1996, pp. 1112-1119.

[7] Wang H.F. and Swift F.J.: 'A Unified Model for the Analysis of FACTS Devices in Damping Power System Oscillations Part I: Single-Machine Infinite Bus Power

System', IEEE Transactions on Power Delivery, Vol. 12, No. 2, April 1997, pp. 941-946.

[8] Hedin R., Jalali S., Weiss S., Cope L., Johnson B., Mah D., Torgerson D. and Vossler B.: 'Improving System Stability Using an Advanced Series Compensation Scheme to Damp Power Swings', Proceedings of the IEE 6th International Conference on AC and DC Power Transmission, 29 April-3 May 1996, London, UK.

[9] Taranto G.N., Pinto L.M.V.G. and Pereira M.V.F.: 'Representation of FATCS devices in Power System Economic Dispatch', IEEE Transactions on Power Systems, Vol. 7, No. 2, May 1992, pp. 572-576.

[10] Larsen E.V., Clark K., Miske S.S. and Urbanek J.: 'Characteristics and Rating Considerations of Thyristor Controlled Series Compesator', IEEE Transactions on Power Delivery, Vol. 9, No. 2, April 1994, pp. 992-1000.

[11] Sun D.I., Ashley B., Brewer B., Hughes A. and Tinney W.F.: 'Optimal Power Flow By Newton Approach', IEEE Transactions on Power Apparatus and Systems, Vol. PAS-103, No. 10, October 1984, pp. 2864-2880.

[12] Sun D.I., Hu T.I., Lin G.S., Lin C.J. and Chen C.H.: 'Experiences with Implementing Optimal Power Flow for Reactive Scheduling in the Taiwan Power System', IEEE Transactions on Power Systems, Vol. 3, No. 3, August 1988, pp. 1193-1200.

[13] Freris L.L. and Sasson A.M.: 'Investigation of the Load-Flow Problem', Proceedings of IEE, Vol. 115, No. 10, October 1968, pp. 1459-1470.

[14] Aboytes F. and Arroyo G.: 'Security Assessment in the Operation of Longitudinal Power Systems', IEEE Transactions on Power Apparatus and Systems, Vol. PWRS-1, No. 2, May 1986, pp. 225-232.

[15] Fuerte-Esquivel C.R and Acha E.: 'A Newton-Type Algorithm for the control of Power Flow in Electrical Power Networks', IEEE Transactions on Power Systems, Vol. 12, No. 4, November 1997, pp. 1474-1480.

[16] Luenberger D.G.: 'Introduction to Linear and Nonlinear Programming', Addison-Wesley Publishing Co., Second Edition, 1984.

[17] Bertsekas D.P.: 'Constrained Optimization Lagrange Multiplier Methods', Academic Press, 1992.

[18] Wollenberg B. and Wood A.J.: 'Power Generation, Operation and Control', John Wiley & Sons Inc., Second Edition, 1984.

[19] Stagg G.W. and El-Abiad A.H.: 'Computer Methods in Power System Analysis', McGraw-Hill, 1968.

Chapter 6

Interphase Power Controller Modelling in an Optimal Power Flow

A comprehensive and versatile power flow model for the Interphase Power Controller (IPC) is presented in this Chapter. The new model is incorporated in an Optimal Power Flow (OPF) using Newton's Method. The state variables of the IPC are combined with the nodal voltage magnitudes and angles of the network in a single frame-of-reference for unified iterative solutions through Newton's method, leading to highly robust iterative solutions. The Phase Shifting Transformer (PST) and the TCSC Controllable Reactance models are used together to make up the IPC model. The model is very flexible, allowing the representation of anyone IPC structures with ease. The simulations carried out show that the IPC is very effective in controlling active power flow under a wide range of network operating conditions.

6.1 Introduction

The lack of fast power flow control in electric power systems is one of the main factors responsible which have dictated the way electric power systems have evolved. Traditionally, AC power systems have been controlled using electro-mechanical devices, which have slow response times. Slow speed control has led to AC transmission systems being inflexible and over-designed. In meshed AC power systems, the power flows are largely distributed as a function of transmission line impedances, i.e. a transmission line with a low impedance will take a larger power flow across it than a transmission line with a high impedance. This is a problem which has been beyond the control of operation engineers, or one which has only been addressed with great difficulty. Operational problems which arise from the unregulated flow of active and reactive powers include: loss of stability, loop flows, voltage limit violations, thermal limit violations and high short-circuit levels [1-3]. In the long-term, these problems can always be solved by building new power plants and transmission lines. However, during actual operation, load shedding becomes the last resort option. An alternative solution to these operating problems is to improve the characteristics of existing transmission corridors. For example, the Interphase Power Controller (IPC) is an emerging technology that could increase significantly the power transfer capabilities of Phase-shifting transformers [4]. The ability to increase power transfer provides the economic justification surrounding the developments of the new technology. IPC applications are

ideally suited for cases where power transfer is thermally limited by the phase-shifting transformer, or where a phase-shifting transformer is near an extreme tap position. Marketing research carried out in North America has shown that 29 out of 96 PSTs could incorporate IPC applications [4].

6.2 Basic Characteristics

As mentioned above, the IPC technology is a newly developed concept aimed at controlling power flows in AC networks. It is made up of individual single elements such as transformers, capacitors, reactors and circuit-breakers. For steady-state purposes, the IPC's main function is to provide near constant active power flow at its terminals. In its more general configuration, the IPC consists of two parallel reactive branches, one inductive and one capacitive. Each branch is subjected to separately phase-shifted voltages [5-7], as illustrated in Figure 6.1.

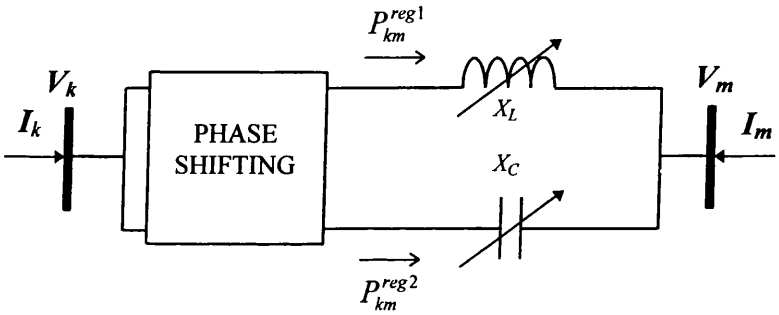

Figure 6.1. General IPC.

The IPC can take several forms depending on how the internal voltages are phase shifted [5-7]. For high-voltage applications, efficient IPCs are based on the use of phase-shifting transformers as shown in Figure 6.2 [8]. The transmitted power is controlled by changing either the internal phase-shifting angles or the reactance values.

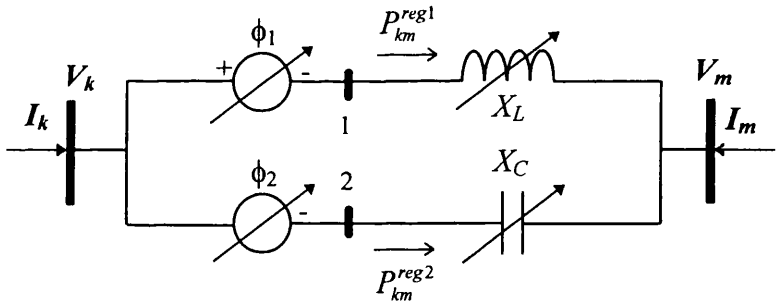

Figure 6.2. Schematic model of the IPC.

At least in one specific application, the IPC configuration consists of a single phase shifter connected in series with the inductive branch [8]. The schematic representation of this configuration is given in Figure 6.3. The capacitive branch can be either fixed or variable.

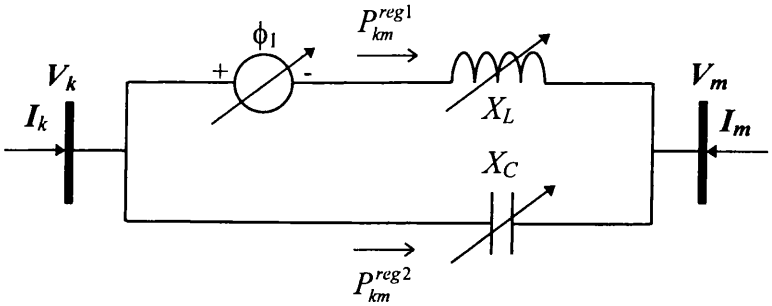

Figure 6.3. Schematic model of the IPC with one PS.

6.3 Integrated IPC Model

The IPC power flow model can be built by combining the TCSC Controllable Reactance model and the PST model presented in Chapters 3 and 5, respectively. Both controllers are connected through a dummy node, as shown in Figure 6.2. The attraction of modelling the IPC in this way is that existing models are used, taking advantage of the robustness and versatility afforded by the developed models. The IPC model uses the generalised transformer model with complex taps in both windings. In principle, this would allow to explore the use of IPCs in distribution networks. When the controller is embedded in a transmission network, the phase shifting is performed with the high-voltage side tap, normally on the secondary side. However, if the IPC were to be embedded in a distribution network, the control would be performed with the high-voltage side tap, which is normally located on the primary side of the transformer.

6.3.1 IPC-OPF Formulation

The mathematical formulation consists of minimising the active power generation cost in the power system by adjusting suitable controllable parameters. The OPF problem can be formulated as follows [9,10,12]:

$$\begin{aligned} &\textbf{\textit{Minimise}} \quad f(P_g) \\ &\textbf{\textit{Subject to}} \quad h(P_g, V, \theta, \phi, X_{TCSC}) = 0 \\ &\textbf{\textit{and}} \qquad\quad g(P_g, V, \theta, \phi, X_{TCSC}) \le 0 \end{aligned} \tag{6.1}$$

where P_g, V, θ, ϕ and X_{TCSC} are the active power generation, voltage magnitudes, phase angles, phase shifter angle and TCSC reactance, respectively. $f(P_g)$ is the objective function to be optimised, $h(P_g, V, \theta, \phi, X_{TCSC})$ represents the power flow equations and $g(P_g, V, \theta, \phi, X_{TCSC})$ represents state variable limits as well as functional operating constraints.

The constrained optimisation problem is converted to an unconstrained optimisation problem by constructing a Lagrangian function corresponding to equation (6.1). This is given as,

$$L(\boldsymbol{x}, \lambda) = f(P_g) + \lambda^t h(P_g, V, \theta, \phi, X_{TCSC}) \tag{6.2}$$

where $\boldsymbol{x}$ is the vector of state variables and λ is the Lagrange multipliers vectors for equality constraints. The inequality constraints are not shown because they are only included when there are variables outside limits.

6.3.2 Lagrangian Function

For the first phase-shifting transformer model in Figure 6.2, the Lagrangian function corresponding to the power flow mismatch equations at the primary and secondary nodes, i.e. node k and 1 is built in order to find the optimal solution. The mismatch equations are modelled in the OPF Newton's method as equality constraints given by the following equation:

$$\begin{aligned} L_{k1}(\boldsymbol{x}, \lambda) = {} & \lambda_{pk}(P_k + P_{dk} - P_{gk}) + \lambda_{qk}(Q_k + Q_{dk} - Q_{gk}) \\ & + \lambda_{p1}(P_1 + P_{d1} - P_{g1}) + \lambda_{q1}(Q_1 + Q_{d1} - Q_{g1}) \end{aligned} \tag{6.3}$$

where P_{dk}, P_{dl}, Q_{dk}, Q_{dl} are active and reactive power loads at nodes k and 1, respectively. P_{gk}, P_{gl}, Q_{gk}, Q_{gl} are scheduled active and reactive power generations at nodes k and 1, respectively. λ_{pk}, λ_{pl}, λ_{qk}, λ_{ql} are Lagrange multipliers at nodes k and 1, respectively. A similar expression for $L_{k2}(\boldsymbol{x}, \lambda)$ can be obtained.

On the other hand, the Lagrangian function associated with the Controllable Reactance model of the TCSC mismatch equations is given by equation (6.4). In this case, the power flow equations are different from the phase-shifting transformer equations because there is no conductance in TCSC model.

$$\begin{aligned} L_{1m}(\boldsymbol{x},\lambda) &= \lambda_{p1}(P_1 + P_{d1} - P_{g1}) + \lambda_{q1}(Q_1 + Q_{d1} - Q_{g1}) \\ &+ \lambda_{pm}(P_m + P_{dm} - P_{gm}) + \lambda_{qm}(Q_m + Q_{dm} - Q_{gm}) \end{aligned} \tag{6.4}$$

6.3.3 Transmission Line Loading

The active power flowing from node k to 1 can be controlled by using the phase-shifting transformer facilities. In the OPF formulation this condition is expressed as an equality constraint which remains active throughout the iterative process unless one wishes this constraint to be deactivated. The operating condition is represented by the following equation,

$$L_{flow-k1}(\boldsymbol{x},\lambda) = \lambda_{k1}(P_{k1} - P_{specified}) \tag{6.5}$$

where λ_{k1} is the Lagrange multiplier associated with the active power flowing from nodes k to 1. $P_{specified}$ is the required value of active power flow across the transformer. The above equation can be used to constrain the active power flow across each branch making up the IPC. Furthermore, the IPC model allows to constrain both active powers flowing in opposite directions.

Another operating condition is represented by incorporating equation (6.6) in the OPF formulation and shown in Figure 6.4. This is used if one wishes to constrain the total active power flowing in the IPC, i.e. P_{ml} represents the active flow given by P_{km}^{reg1} and P_{km}^{reg2}.

$$L_{flow-ml}(\boldsymbol{x},\lambda) = \lambda_{ml}(P_{ml} - P_{specified}) \tag{6.6}$$

where λ_{ml} is the Lagrange multiplier associated with the active power flowing from node m to l. $P_{specified}$ is the desired value of active power flow across the IPC component.

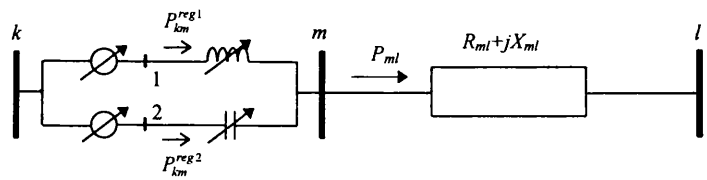

Figure 6.4. IPC constraining the active power flow.

The IPC Lagrangian function encompassing the individual contributions presented above including the capacitive branch effect is,

$$\begin{aligned} L = L_{k1}(\boldsymbol{x},\lambda) + L_{k2}(\boldsymbol{x},\lambda) + L_{1m}(\boldsymbol{x},\lambda) + L_{2m}(\boldsymbol{x},\lambda) + L_{flow-k1}(\boldsymbol{x},\lambda) \\ + L_{flow-k2}(\boldsymbol{x},\lambda) + L_{flow-ml}(\boldsymbol{x},\lambda) \end{aligned} \tag{6.7}$$

6.3.4 Linearised System of Equations

The linearised system of equations for minimising the Lagrangian function via Newton's method is given by,

$$W\Delta \mathbf{z} = -\boldsymbol{g} \tag{6.8}$$

To achieve the minimisation of active power generation cost by using IPC facilities, the following scheme is proposed: In cases when the active power flowing in both branches is only controlled with the phase-shifting mechanism, i.e. variable series compensation is fixed, the set of linearised power flow equations is given by equation (6.9). This is an expanded version of equation (6.8). The constrained active power flows in the PST and transmission line are also incorporated in equation (6.9).

$$\begin{bmatrix} W_{11} & W_{12} & W_{13} & 0 & W_{15} & W_{16} & 0 & 0 \\ W_{21} & W_{22} & 0 & W_{24} & W_{25} & 0 & 0 & 0 \\ W_{31} & 0 & W_{33} & W_{34} & 0 & W_{36} & 0 & 0 \\ 0 & W_{42} & W_{43} & W_{44} & 0 & 0 & W_{47} & W_{48} \\ W_{51} & W_{52} & 0 & 0 & W_{55} & 0 & 0 & 0 \\ W_{61} & 0 & W_{63} & 0 & 0 & W_{66} & 0 & 0 \\ 0 & 0 & 0 & W_{74} & 0 & 0 & W_{77} & W_{78} \\ 0 & 0 & 0 & W_{84} & 0 & 0 & W_{87} & 0 \end{bmatrix} \begin{bmatrix} \Delta \mathbf{z}_1 \\ \Delta \mathbf{z}_2 \\ \Delta \mathbf{z}_3 \\ \Delta \mathbf{z}_4 \\ \Delta \mathbf{z}_5 \\ \Delta \mathbf{z}_6 \\ \Delta \mathbf{z}_7 \\ \Delta \mathbf{z}_8 \end{bmatrix} = - \begin{bmatrix} \boldsymbol{g}_1 \\ \boldsymbol{g}_2 \\ \boldsymbol{g}_3 \\ \boldsymbol{g}_4 \\ \boldsymbol{g}_5 \\ \boldsymbol{g}_6 \\ \boldsymbol{g}_7 \\ \boldsymbol{g}_8 \end{bmatrix} \tag{6.9}$$

where:

$$W_{11} = \begin{bmatrix} \dfrac{\partial^2 L}{\partial \theta_k^2} & \dfrac{\partial^2 L}{\partial \theta_k \partial V_k} & \dfrac{\partial P_k}{\partial \theta_k} & \dfrac{\partial Q_k}{\partial \theta_k} \\ \dfrac{\partial^2 L}{\partial V_k \partial \theta_k} & \dfrac{\partial^2 L}{\partial V_k^2} & \dfrac{\partial P_k}{\partial V_k} & \dfrac{\partial Q_k}{\partial V_k} \\ \dfrac{\partial P_k}{\partial \theta_k} & \dfrac{\partial P_k}{\partial V_k} & 0 & 0 \\ \dfrac{\partial Q_k}{\partial \theta_k} & \dfrac{\partial Q_k}{\partial V_k} & 0 & 0 \end{bmatrix} \tag{6.10}$$

$$W_{12} = W_{21}' = \begin{bmatrix} \dfrac{\partial^2 L}{\partial \theta_k \partial \theta_l} & \dfrac{\partial^2 L}{\partial \theta_k \partial V_l} & \dfrac{\partial P_l}{\partial \theta_k} & \dfrac{\partial Q_l}{\partial \theta_k} \\ \dfrac{\partial^2 L}{\partial V_k \partial \theta_l} & \dfrac{\partial^2 L}{\partial V_k \partial V_l} & \dfrac{\partial P_l}{\partial V_k} & \dfrac{\partial Q_l}{\partial V_k} \\ \dfrac{\partial P_k}{\partial \theta_l} & \dfrac{\partial P_k}{\partial V_l} & 0 & 0 \\ \dfrac{\partial Q_k}{\partial \theta_l} & \dfrac{\partial Q_k}{\partial V_l} & 0 & 0 \end{bmatrix} \tag{6.11}$$

$$\boldsymbol{W}_{13} = \boldsymbol{W}_{31}^{t} = \begin{bmatrix} \dfrac{\partial^2 L}{\partial\theta_k \partial\theta_2} & \dfrac{\partial^2 L}{\partial\theta_k \partial V_2} & \dfrac{\partial P_2}{\partial\theta_k} & \dfrac{\partial Q_2}{\partial\theta_k} \\ \dfrac{\partial^2 L}{\partial V_k \partial\theta_2} & \dfrac{\partial^2 L}{\partial V_k \partial V_2} & \dfrac{\partial P_2}{\partial V_k} & \dfrac{\partial Q_2}{\partial V_k} \\ \dfrac{\partial P_k}{\partial\theta_2} & \dfrac{\partial P_k}{\partial V_2} & 0 & 0 \\ \dfrac{\partial Q_k}{\partial\theta_2} & \dfrac{\partial Q_k}{\partial V_2} & 0 & 0 \end{bmatrix} \tag{6.12}$$

$$\boldsymbol{W}_{51} = \boldsymbol{W}_{15}^{t} = \begin{bmatrix} \dfrac{\partial^2 L}{\partial\theta_k \partial\phi_1} & \dfrac{\partial^2 L}{\partial V_k \partial\phi_1} & \dfrac{\partial P_k}{\partial\phi_1} & \dfrac{\partial Q_k}{\partial\phi_1} \\ \dfrac{\partial P_{ps1}}{\partial\theta_k} & \dfrac{\partial P_{ps1}}{\partial V_k} & 0 & 0 \end{bmatrix} \tag{6.13}$$

$$\boldsymbol{W}_{61} = \boldsymbol{W}_{16}^{t} = \begin{bmatrix} \dfrac{\partial^2 L}{\partial\theta_k \partial\phi_2} & \dfrac{\partial^2 L}{\partial V_k \partial\phi_2} & \dfrac{\partial P_k}{\partial\phi_2} & \dfrac{\partial Q_k}{\partial\phi_2} \\ \dfrac{\partial P_{ps2}}{\partial\theta_k} & \dfrac{\partial P_{ps2}}{\partial V_k} & 0 & 0 \end{bmatrix} \tag{6.14}$$

$$\boldsymbol{W}_{22} = \begin{bmatrix} \dfrac{\partial^2 L}{\partial\theta_1^2} & \dfrac{\partial^2 L}{\partial\theta_1 \partial V_1} & \dfrac{\partial P_1}{\partial\theta_1} & \dfrac{\partial Q_1}{\partial\theta_1} \\ \dfrac{\partial^2 L}{\partial V_1 \partial\theta_1} & \dfrac{\partial^2 L}{\partial V_1^2} & \dfrac{\partial P_1}{\partial V_1} & \dfrac{\partial Q_1}{\partial V_1} \\ \dfrac{\partial P_1}{\partial\theta_1} & \dfrac{\partial P_1}{\partial V_1} & 0 & 0 \\ \dfrac{\partial Q_1}{\partial\theta_1} & \dfrac{\partial Q_1}{\partial V_1} & 0 & 0 \end{bmatrix} \tag{6.15}$$

$$\boldsymbol{W}_{24} = \boldsymbol{W}_{42}^{t} = \begin{bmatrix} \dfrac{\partial^2 L}{\partial\theta_1 \partial\theta_m} & \dfrac{\partial^2 L}{\partial\theta_1 \partial V_m} & \dfrac{\partial P_m}{\partial\theta_1} & \dfrac{\partial Q_m}{\partial\theta_1} \\ \dfrac{\partial^2 L}{\partial V_1 \partial\theta_m} & \dfrac{\partial^2 L}{\partial V_1 \partial V_m} & \dfrac{\partial P_m}{\partial V_1} & \dfrac{\partial Q_m}{\partial V_1} \\ \dfrac{\partial P_1}{\partial\theta_m} & \dfrac{\partial P_1}{\partial V_m} & 0 & 0 \\ \dfrac{\partial Q_1}{\partial\theta_m} & \dfrac{\partial Q_1}{\partial V_m} & 0 & 0 \end{bmatrix} \tag{6.16}$$

$$\boldsymbol{W}_{52} = \boldsymbol{W}_{25}^{t} = \begin{bmatrix} \dfrac{\partial^2 L}{\partial\theta_1 \partial\phi_1} & \dfrac{\partial^2 L}{\partial V_1 \partial\phi_1} & \dfrac{\partial P_1}{\partial\phi_1} & \dfrac{\partial Q_1}{\partial\phi_1} \\ \dfrac{\partial P_{ps1}}{\partial\theta_1} & \dfrac{\partial P_{ps1}}{\partial V_1} & 0 & 0 \end{bmatrix} \tag{6.17}$$

$$\boldsymbol{W}_{33} = \begin{bmatrix} \frac{\partial^2 L}{\partial \theta_2^2} & \frac{\partial^2 L}{\partial \theta_2 \partial V_2} & \frac{\partial P_2}{\partial \theta_2} & \frac{\partial Q_2}{\partial \theta_2} \\ \frac{\partial^2 L}{\partial V_2 \partial \theta_2} & \frac{\partial^2 L}{\partial V_2^2} & \frac{\partial P_2}{\partial V_2} & \frac{\partial Q_2}{\partial V_2} \\ \frac{\partial P_2}{\partial \theta_2} & \frac{\partial P_2}{\partial V_2} & 0 & 0 \\ \frac{\partial Q_2}{\partial \theta_2} & \frac{\partial Q_2}{\partial V_2} & 0 & 0 \end{bmatrix} \tag{6.18}$$

$$\boldsymbol{W}_{34} = \boldsymbol{W}_{43}^t = \begin{bmatrix} \frac{\partial^2 L}{\partial \theta_2 \partial \theta_m} & \frac{\partial^2 L}{\partial \theta_2 \partial V_m} & \frac{\partial P_m}{\partial \theta_2} & \frac{\partial Q_m}{\partial \theta_2} \\ \frac{\partial^2 L}{\partial V_2 \partial \theta_m} & \frac{\partial^2 L}{\partial V_2 \partial V_m} & \frac{\partial P_m}{\partial V_2} & \frac{\partial Q_m}{\partial V_2} \\ \frac{\partial P_2}{\partial \theta_m} & \frac{\partial P_2}{\partial V_m} & 0 & 0 \\ \frac{\partial Q_2}{\partial \theta_m} & \frac{\partial Q_2}{\partial V_m} & 0 & 0 \end{bmatrix} \tag{6.19}$$

$$\boldsymbol{W}_{63} = \boldsymbol{W}_{36}^t = \begin{bmatrix} \frac{\partial^2 L}{\partial \theta_2 \partial \phi_2} & \frac{\partial^2 L}{\partial V_2 \partial \phi_2} & \frac{\partial P_2}{\partial \phi_2} & \frac{\partial Q_2}{\partial \phi_2} \\ \frac{\partial P_{ps2}}{\partial \theta_2} & \frac{\partial P_{ps2}}{\partial V_2} & 0 & 0 \end{bmatrix} \tag{6.20}$$

$$\boldsymbol{W}_{44} = \begin{bmatrix} \frac{\partial^2 L}{\partial \theta_m^2} & \frac{\partial^2 L}{\partial \theta_m \partial V_m} & \frac{\partial P_m}{\partial \theta_m} & \frac{\partial Q_m}{\partial \theta_m} \\ \frac{\partial^2 L}{\partial V_m \partial \theta_m} & \frac{\partial^2 L}{\partial V_m^2} & \frac{\partial P_m}{\partial V_m} & \frac{\partial Q_m}{\partial V_m} \\ \frac{\partial P_m}{\partial \theta_m} & \frac{\partial P_m}{\partial V_m} & 0 & 0 \\ \frac{\partial Q_m}{\partial \theta_{in}} & \frac{\partial Q_m}{\partial V_m} & 0 & 0 \end{bmatrix} \tag{6.21}$$

$$\boldsymbol{W}_{47} = \boldsymbol{W}_{74}^t = \begin{bmatrix} \frac{\partial^2 L}{\partial \theta_m \partial \theta_l} & \frac{\partial^2 L}{\partial \theta_m \partial V_l} & \frac{\partial P_l}{\partial \theta_m} & \frac{\partial Q_l}{\partial \theta_m} \\ \frac{\partial^2 L}{\partial V_m \partial \theta_l} & \frac{\partial^2 L}{\partial V_m \partial V_l} & \frac{\partial P_l}{\partial V_m} & \frac{\partial Q_l}{\partial V_m} \\ \frac{\partial P_m}{\partial \theta_l} & \frac{\partial P_m}{\partial V_l} & 0 & 0 \\ \frac{\partial Q_m}{\partial \theta_l} & \frac{\partial Q_m}{\partial V_l} & 0 & 0 \end{bmatrix} \tag{6.22}$$

$$\boldsymbol{W}_{84} = \boldsymbol{W}_{48}^t = \begin{bmatrix} \frac{\partial P_{ml}}{\partial \theta_m} & \frac{\partial P_{ml}}{\partial V_m} & 0 & 0 \end{bmatrix} \tag{6.23}$$

$$\boldsymbol{W}_{55} = \begin{bmatrix} \frac{\partial^2 L}{\partial \phi_1^2} & 0 \\ 0 & 0 \end{bmatrix} \tag{6.24}$$

$$\boldsymbol{W}_{66}=\begin{bmatrix}\dfrac{\partial^2 L}{\partial\phi_2^2} & 0\\ 0 & 0\end{bmatrix} \tag{6.25}$$

$$\boldsymbol{W}_{77}=\begin{bmatrix}\dfrac{\partial^2 L}{\partial\theta_l^2} & \dfrac{\partial^2 L}{\partial\theta_l\partial V_l} & \dfrac{\partial P_l}{\partial\theta_l} & \dfrac{\partial Q_l}{\partial\theta_l}\\ \dfrac{\partial^2 L}{\partial V_l\partial\theta_l} & \dfrac{\partial^2 L}{\partial V_l^2} & \dfrac{\partial P_l}{\partial V_l} & \dfrac{\partial Q_l}{\partial V_l}\\ \dfrac{\partial P_l}{\partial\theta_l} & \dfrac{\partial P_l}{\partial V_l} & 0 & 0\\ \dfrac{\partial Q_l}{\partial\theta_l} & \dfrac{\partial Q_l}{\partial V_l} & 0 & 0\end{bmatrix} \tag{6.26}$$

$$\boldsymbol{W}_{87}=\boldsymbol{W}_{78}^{t}=\begin{bmatrix}\dfrac{\partial P_{ml}}{\partial\theta_l} & \dfrac{\partial P_{ml}}{\partial V_l} & 0 & 0\end{bmatrix} \tag{6.27}$$

$$\boldsymbol{g}_1=\begin{bmatrix}\dfrac{\partial L}{\partial\theta_k} & \dfrac{\partial L}{\partial V_k} & \dfrac{\partial L}{\partial\lambda_{pk}} & \dfrac{\partial L}{\partial\lambda_{qk}}\end{bmatrix}^t \tag{6.28}$$

$$\boldsymbol{g}_2=\begin{bmatrix}\dfrac{\partial L}{\partial\theta_1} & \dfrac{\partial L}{\partial V_1} & \dfrac{\partial L}{\partial\lambda_{p1}} & \dfrac{\partial L}{\partial\lambda_{q1}}\end{bmatrix}^t \tag{6.29}$$

$$\boldsymbol{g}_3=\begin{bmatrix}\dfrac{\partial L}{\partial\theta_2} & \dfrac{\partial L}{\partial V_2} & \dfrac{\partial L}{\partial\lambda_{p2}} & \dfrac{\partial L}{\partial\lambda_{q2}}\end{bmatrix}^t \tag{6.30}$$

$$\boldsymbol{g}_4=\begin{bmatrix}\dfrac{\partial L}{\partial\theta_m} & \dfrac{\partial L}{\partial V_m} & \dfrac{\partial L}{\partial\lambda_{pm}} & \dfrac{\partial L}{\partial\lambda_{qm}}\end{bmatrix}^t \tag{6.31}$$

$$\boldsymbol{g}_5=\begin{bmatrix}\dfrac{\partial L}{\partial\phi_1} & \dfrac{\partial L}{\partial\lambda_{ps1}}\end{bmatrix}^t \tag{6.32}$$

$$\boldsymbol{g}_6=\begin{bmatrix}\dfrac{\partial L}{\partial\phi_2} & \dfrac{\partial L}{\partial\lambda_{ps2}}\end{bmatrix}^t \tag{6.33}$$

$$\boldsymbol{g}_7=\begin{bmatrix}\dfrac{\partial L}{\partial\theta_l} & \dfrac{\partial L}{\partial V_l} & \dfrac{\partial L}{\partial\lambda_{pl}} & \dfrac{\partial L}{\partial\lambda_{ql}}\end{bmatrix}^t \tag{6.34}$$

$$\boldsymbol{g}_8=\begin{bmatrix}\dfrac{\partial L}{\partial\lambda_{ml}}\end{bmatrix} \tag{6.35}$$

$$\Delta\mathbf{z}_1=\begin{bmatrix}\Delta\theta_k & \Delta V_k & \Delta\lambda_{pk} & \Delta\lambda_{qk}\end{bmatrix}^t \tag{6.36}$$

$$\Delta\mathbf{z}_2=\begin{bmatrix}\Delta\theta_1 & \Delta V_1 & \Delta\lambda_{p1} & \Delta\lambda_{q1}\end{bmatrix}^t \tag{6.37}$$

$$\Delta \mathbf{z}_3 = \begin{bmatrix} \Delta\theta_2 & \Delta V_2 & \Delta\lambda_{p2} & \Delta\lambda_{q2} \end{bmatrix}^t \tag{6.38}$$

$$\Delta \mathbf{z}_4 = \begin{bmatrix} \Delta\theta_m & \Delta V_m & \Delta\lambda_{pm} & \Delta\lambda_{qm} \end{bmatrix}^t \tag{6.39}$$

$$\Delta \mathbf{z}_5 = \begin{bmatrix} \Delta\phi_1 \\ \Delta\lambda_{ps1} \end{bmatrix} \tag{6.40}$$

$$\Delta \mathbf{z}_6 = \begin{bmatrix} \Delta\phi_2 \\ \Delta\lambda_{ps2} \end{bmatrix} \tag{6.41}$$

$$\Delta \mathbf{z}_7 = \begin{bmatrix} \Delta\theta_l & \Delta V_l & \Delta\lambda_{pl} & \Delta\lambda_{ql} \end{bmatrix}^t \tag{6.42}$$

$$\Delta \mathbf{z}_8 = \begin{bmatrix} \lambda_{ml} \end{bmatrix} \tag{6.43}$$

The first and second derivative expressions for all the terms used in equation (6.9) are given in Appendix I and Chapters 5. The derivative terms corresponding to inequality constraints are entered in matrix $\boldsymbol{W}$ only after violated limits need to be enforced [13].

Once equation (6.9) has been assembled and combined with matrix $\boldsymbol{W}$ and the gradient vector $\boldsymbol{g}$ of the entire network, a sparsity-oriented solution is carried out. This process is repeated until a small, pre-specified tolerance is reached.

6.3.5 Handling Limits of IPC Variables

The handling of the IPC variables outside limits is efficiently carried out by using the Multipliers method [13]. For the IPC model, the new variables to be checked are the phase shifter angles for both phase-shifting transformers, ϕ_s, and the controllable reactances, X_{TCSCs}.

The phase shifter angle for the first transformer is checked by means of equation (6.44), where ϕ can be either ϕ_{tv} or ϕ_{uv}. A similar procedure is carried out to check the other three new variables,

$$\psi_i(\phi_i^j, \mu_i^j) = \begin{cases} \mu_i^j(\phi_i^j - \phi_i^{\max}) + \dfrac{c}{2}(\phi_i^j - \phi_i^{\max})^2 & \text{if} \quad \mu_i^j + c(\phi_i^j - \phi_i^{\max}) \geq 0 \\ \mu_i^j(\phi_i^j - \phi_i^{\min}) + \dfrac{c}{2}(\phi_i^j - \phi_i^{\min})^2 & \text{if} \quad \mu_i^j + c(\phi_i^j - \phi_i^{\min}) \leq 0 \\ 0 \quad \text{otherwise} \end{cases} \tag{6.44}$$

where i is the number of variable ϕ corresponding to the number of phase shifting transformers embedded into the network, and j is the iteration number associated with the actual value of ϕ; $\phi_i^{\max}$ and $\phi_i^{\min}$ are the upper and lower limits for the phase shifter angle; μ_i is a multiplier term and c is a penalty weighting term.

6.3.6 Initial Conditions

Providing no limit violations take place at the beginning of the iterative solution, the following initial conditions are taken into account.

Nodal Voltage Magnitudes, Phase Angles, Phase Shifter Angles and Controllable Reactance.

The variables in vector x must be given initial values in order to start the iterative process. State variables are initialised similarly to load flow problems, i.e. 1 pu voltage magnitudes and 0 voltage angles for all nodes. This provides a suitable starting condition. Engineering experience indicates that, for most problems, the variation of voltage magnitude and voltage angle from the 1 and 0 initial conditions is relatively small. The angles in PST are initialised at 0, and the tap position at 1.0. It should be pointed out that the reactance values are fixed in most practical IPC applications.

Lagrange Multipliers

The Lagrange multipliers for active and reactive power flow mismatch equations are initialised at λ_p given by the lossless economic dispatch and 0, respectively. For IPC Lagrange multipliers the initial values of λ_{k1}, λ_{k2}, and λ_{ml} are set equal to zero. These values give rise to very robust iterative solutions.

6.3.7 Practical Implementation of the IPC Model

It is possible to control active power flow in both branches of the IPC by using the TCSC model based on the Controllable Reactance model, with the phase-shifting mechanism fixed at a specified value. The set of linearised power flow equations is similar to equation (6.9) but large mismatch values in ΔP and ΔQ can take place in the early stages of the iterative process, resulting in poor convergence. The problem may not reach convergence if large increments in the level of compensation are required to maintain a specified active power flow. In such a case, large increments in the controllable reactance may cause the solution to oscillate.

To reduce the possibility of unwanted numerical problems, the OPF algorithm can constrain the active power flow by using the transmission line loading expression given in Chapter 5, Section 5.3.5. Furthermore, in Section 6.5 it will be shown the advantages of constraining the power flow leaving IPC at either node k or m.

In OPF algorithms, the various IPC operating modes are selected aiming at optimising the operation of the network. For example, if the IPC is not regulating active power flow, matrix W has to be suitably modified to reflect this operating mode. This can be done by adding the second derivative term of a large (infinite), quadratic penalty factor to the diagonal elements corresponding to Lagrange multipliers λ_{k1}, λ_{k2} and λ_{ml} for both PSTs, setting these multipliers to zero throughout the solution process. The first derivative terms of the quadratic penalty function are evaluated and added to the corresponding gradient elements.

6.4 IPC Active Power Flow Control Test Cases

The original 5-node power system described in previous Chapters was modified to show how the IPC would perform when installed in a power system [14]. The results given in Table 6.1 correspond to the case when no IPC was included in the test network.

Convergence was obtained in 4 iterations to satisfy the pre-specified tolerance of 10^{-9} for all the variables. The active power generation cost is 747.976 $/hour and the active power losses are 3.05096 MW.

Table 6.1. Nodal complex voltages of modified system and optimal active and reactive dispatch.

Node	Voltage Magnitude (pu)	Phase Angle (degrees)	Active Power (MW)	Reactive Power (MVAR)	λ_p ($/MWhr)
Elm	1.072	-4.420	0	0	4.2639
Main	1.077	-3.853	0	0	4.2341
Lake	1.078	-3.618	0	0	4.2232
South	1.100	-1.305	87.898	14.410	4.1032
North	1.109	0.000	80.152	0.292	4.0412

The 5-node system described above was modified to include an IPC in series with the transmission line connecting nodes Lake and Main. A dummy node LakeIPC was created, as shown in Figure 6.5. The IPC model is used to maximise the active power transference from Lake to Main by using the phase-shifting transformer facilities in the primary winding. The fixed inductive and capacitive reactances are assumed to be 0.01 and -0.01 pu. The initial conditions of both the primary and secondary complex taps are 1 pu and 0^0. The primary and secondary winding resistance are ignored in the model and the reactance is assumed to be on the secondary side. The inductive reactance in the secondary winding is set at 0.05 pu. The phase-shifting angle limits are assumed to be within the range $\pm 10^0$. Convergence was obtained in 3 iterations. The active power generation cost is 747.977 $/hour and the active power losses are 3.0510 MW. The power flow results are shown in Figure 6.5. The final voltage magnitude, phase angle, active and reactive power dispatch and Lagrange multiplier for each node are given in Table 6.2. The phase-shifting angles at each iteration of the solution process are shown in Table 6.3.

Table 6.2. Nodal complex voltages and optimal active and reactive dispatch for the modified 5-node test system upgraded with an IPC.

Node	Voltage Magnitude (pu)	Phase Angle (degrees)	Active Power (MW)	Reactive Power (MVAR)	λ_p ($/MWhr)
LakeIPC	1.078	-3.629	0	0	4.2230
Elm	1.072	-4.425	0	0	4.2637
Main	1.078	-3.862	0	0	4.2339
Lake	1.077	-3.615	0	0	4.2229
South	1.100	-1.308	87.90	14.650	4.1032
North	1.109	0.000	80.14	0.090	4.0411

Tables 6.1 and 6.2 show how the variables at each node change during the solution process. The Lagrange multipliers decreased for all nodes, except node South, which means that it is cheaper to supply additional network load. Even though this case includes four more elements (two phase-shifting transformers and two reactances), the active power cost and the active power losses are practically the same. The active flow across branch Lake-Main remains almost unchanged.

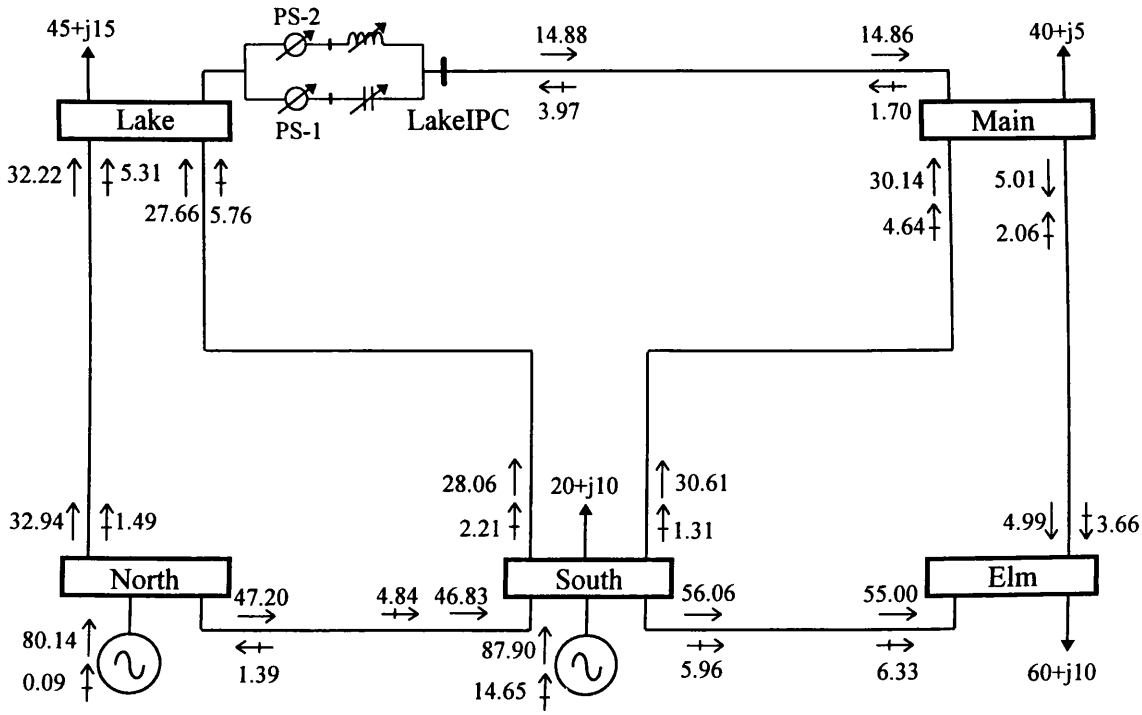

Figure 6.5. Modified 5-node system with an IPC and OPF solution.

Table 6.3. Phase shifter angles.

Iterations	ϕ_{PS-1} (degrees)	ϕ_{PS-2} (degrees)
0	0.000	0.000
1	-0.1553	-0.1589
2	-0.1653	-0.1648
3	-0.1619	-0.1621

Two different ways of using the IPC model are considered as follows. In Case A, active power flow is controlled using the transmission line loading equation. In this case several variables are involved in satisfying the specified active power flow. By way of example, the IPC is going to be used to maintain active power flow leaving LakeIPC towards Main at 25 MW. The power flows flowing across the IPC are shown in Figure 6.6. On the other hand, in Case B, a specified active power can be controlled by the phase-shifter in each branch, say 12.5 MW, these results are shown in Figure 6.7.

It can be observed that the active power generation cost was practically the same in both active power flow control cases. Furthermore, the active power losses and the reactive power generation are smaller in Case A than in Case B. For the test cases presented below, the option of controlling the active power flow in Case A will be used.

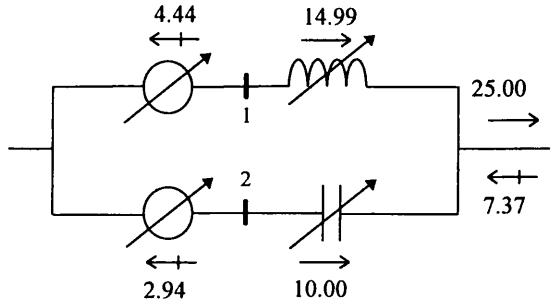

Figure 6.6. Power flow across IPC branches for Case A.

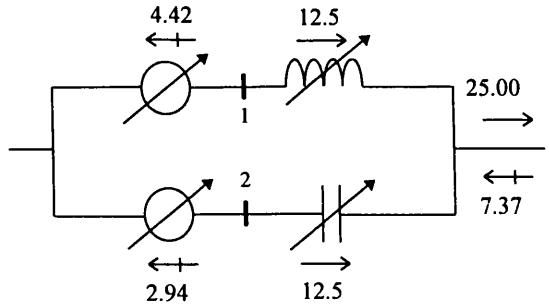

Figure 6.7. Power flow across IPC branches for Case B.

6.5 Active Power Across Reactances

The behaviour of the active power flow across the IPC reactances can be studied by using the standard AEP 14-node system [11]. The fixed inductive and capacitive reactances are assumed to be 0.1 and -0.1 pu. The primary and secondary complex taps initial conditions are 1 pu and 0^0. The primary and secondary winding resistance are ignored in the model, as well as the primary reactance. The inductive reactance in the secondary winding is set at 0.5 pu. The phase-shifting angle limits are assumed to be within the range $\pm 15^0$. This network was upgraded with one IPC included in branch Nod_5-Nod_4. The following cases were simulated:

A) No IPC.

B) IPC in branch Nod_5-Nod_4 with no power flow control.

C) IPC in branch Nod_5-Nod_4 with active power control set at 40 MW.

Table 6.4 gives the number of iterations taken to converge, the flow across branch Nod_5-Nod_4, active power generation cost and network losses. It can be observed from Cases A and B that the inclusion of a new component in the network will slightly increase the cost and the losses resulting from the reactances of the IPC. As a result of the new embedded device, the active power flow across branch Nod_5-Nod_4 will be larger. As expected, if the IPC is controlling active power flow at a level different from the optimal value (Case B), then the active power generation cost will increase. Electric power losses will also rise under these new operating conditions.

Table 6.4. Final Results for AEP 14-node system.

Case	Iterations	Flow in branch Nod_5-Nod_4 (MW)	Cost ($/hour)	Losses (MW)
A	3	26.891	215.457	1.9008
B	3	30.449	215.460	1.9061
C	3	40.000	215.538	1.9675

Figures 6.8 and 6.9 show the active power flow profile across both PSTs and the active power flow across branch Nod_5-Nod_4, at each iteration, for Cases B and C. These figures show that the patterns of convergence for the active power flow have a slight oscillation in the first iteration. Other than that, the power flows converge smoothly to the final value. Small variations occur at the end of each iteration due to changes in the set of active constraints and in the penalty weighting factors. In fact, the voltage magnitude at node Nod_7 was outwith limits in the first iteration, however, it was suitably enforced by using the Multipliers method.

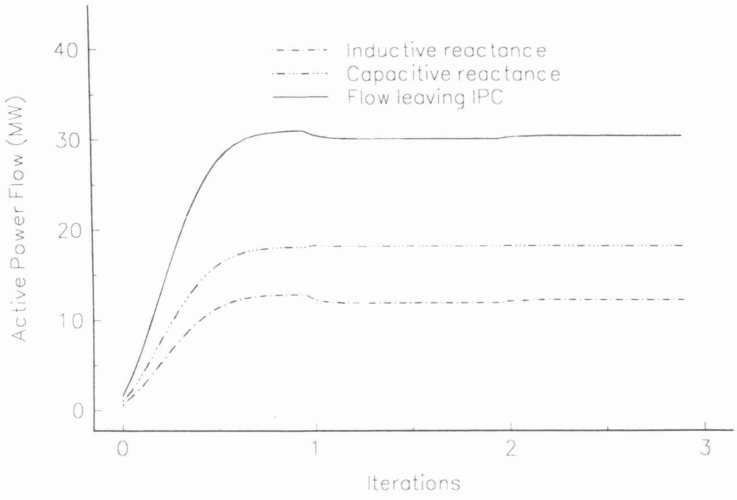

Figure 6.8. Unconstrained active power flow across branch Nod_5-Nod_4.

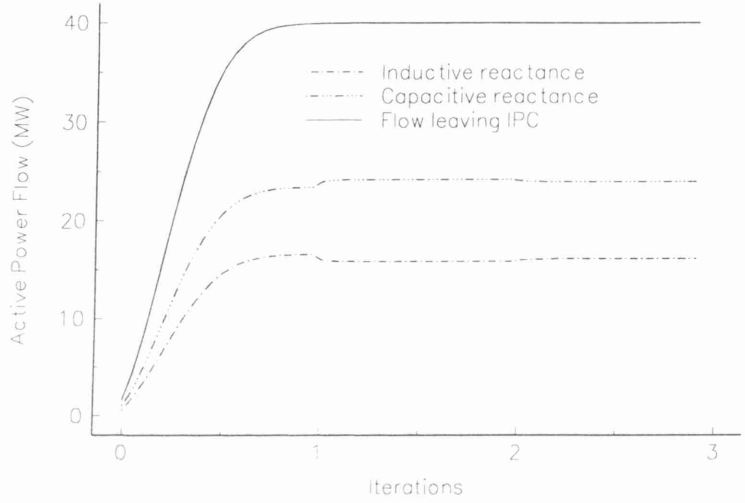

Figure 6.9. Constrained active power flow across branch Nod_5-Nod_4.

In Case C during iterations 1 and 2, a small power increment occurs in the inductive branch and a decrement of similar magnitude occurs in the capacitive branch, as shown in Figure 6.9. The reason is that the two controllers interact with each other. When the power flowing in the inductive branch increases, the power flowing in the capacitive branch decreases, and vice-versa. Consequently, the total power remains constant. In general, the feasible power flow control region of an IPC is a straight line, as shown in Figure 6.10.

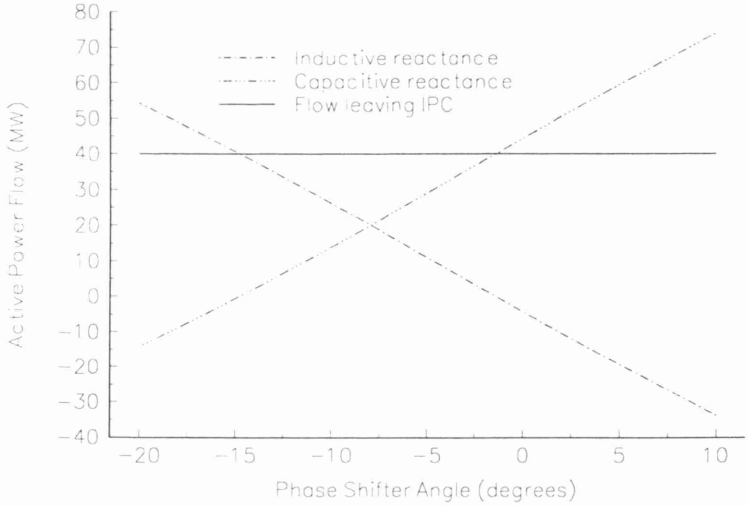

Figure 6.10. Active power flow across IPC's branches, Case C.

In order to demonstrate that the feasible power flow control region of an IPC is a straight line, the phase angle controlling power flow in the inductive branch was set between -20^0 and 10^0, and the total flow in line Nod_5-Nod_4 of the AEP 14-node system was set to 40 MW. The controller phase angle in the capacitive branch was determined by the algorithm.

6.6 Effect of IPC Reactances

The effect of the IPC inductive and capacitive reactances on the active power flow leaving the IPC is presented in this Section. The simulations were carried out as in the previous section. The IPC inductive and capacitive reactances were assumed to be conjugated, i.e. X_L=-X_C, with values between 0.01 and 0.2 pu and the IPC phase shifters were fixed at 0^0. The active power flow across transmission line Nod_5-Nod_4 was not constrained. Figure 6.11 shows the power flow across the inductive and capacitive branches and the total flow leaving the IPC. Figure 6.12 shows the active power generation cost as a function of the reactance values, whilst Figure 6.13 shows active power losses as a function of the reactance values.

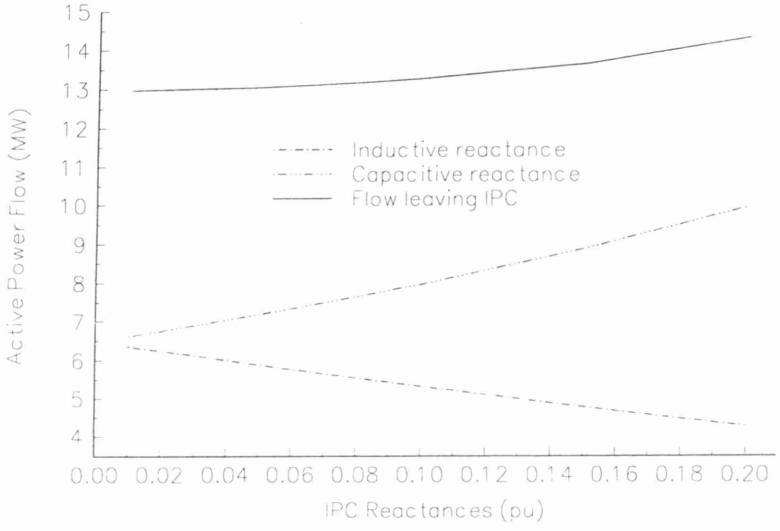

Figure 6.11. IPC power flow as a function of reactance values (X_L=-X_C).

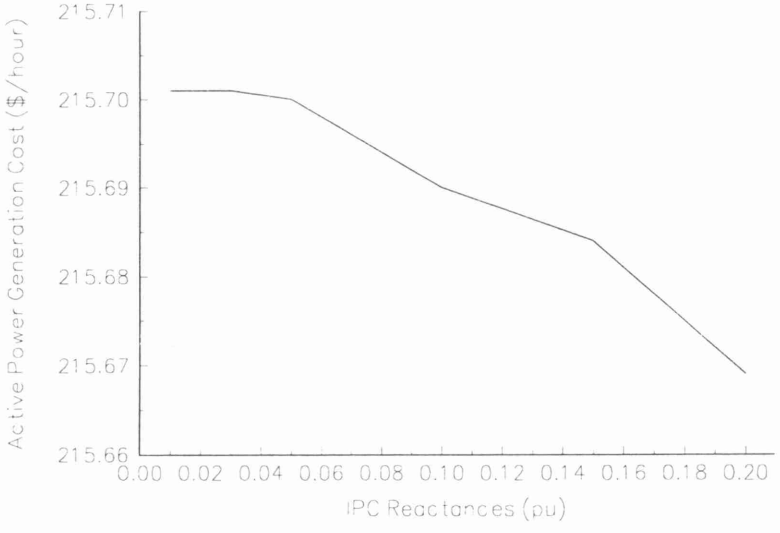

Figure 6.12. Active power generation cost as a function of reactance values.

It can be observed in Figure 6.11 that the active power flow across the inductive branch decreases as its reactance increases. Conversely, as the capacitive reactance increases,

the active power flow across this branch increases. In the former case, the electrical distance gets larger as the inductive reactance increases, and in latter case the branch gets electrically shorter. The total flow leaving the IPC increased slightly, but generally, it remains constant.

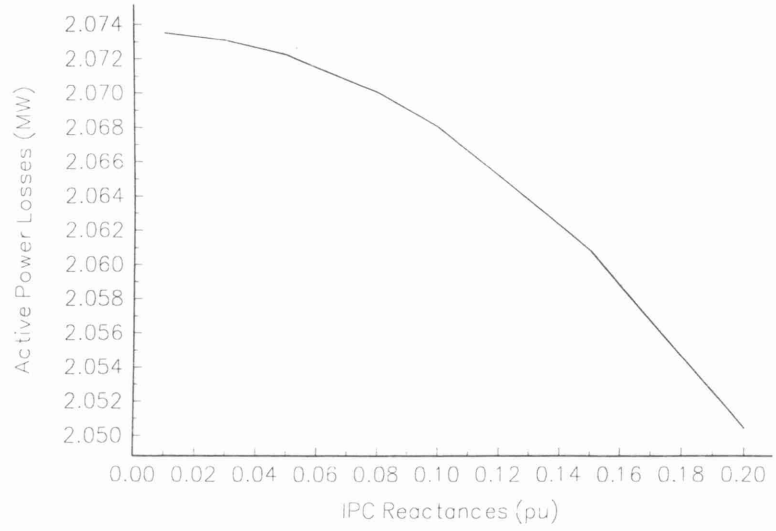

Figure 6.13. Active power losses as a function of reactances.

From Figures 6.12 and 6.13 it can be seen that the active power generation cost and the active power losses decreased as the reactive and capacitive reactances increased. The network is affected more by the capacitive branch increments because this branch is electrically shorter. The active power generation also decreases as shown in Figure 6.14. On the other hand, the generation of reactive power increased in this case, but this was not true for all the power systems tested. The reactive power may depend on the loading condition. When the power flow through a transmission line increases, reactive power should be injected at the sending and receiving nodes in order to compensate for the voltage drop. In a transmission line the load ability is penalised by the voltage drop, and in the case tested the generator compensates the voltage drop. This is depicted in Figure 6.15.

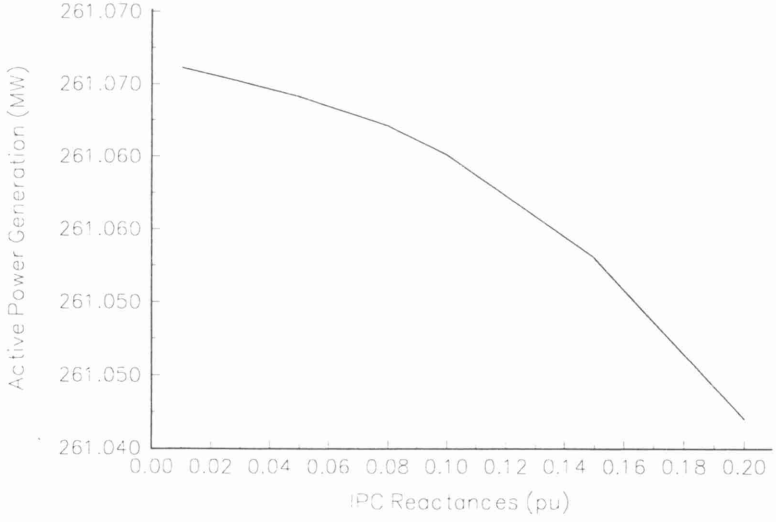

Figure 6.14. Active power generation as a function of reactance values.

The simulation described above was repeated with the IPC maintaining the active power flow in the transmission line Nod_5-Nod_4 at 40 MW. The IPC inductive and capacitive reactances were given values between 0.01 and to 0.2 pu. It was observed that while the convergence patterns were similar to those presented above (Figures 6.11-

6.14), the reactive power generation pattern was very different. The reactive power generation and the reactive power losses in the IPC as a function of the IPC reactances are plotted in Figures 6.16 and 6.17. It can be observed from these results that as a consequence of using different reactance values to maintain a fixed active power flow, both the reactive power losses in the IPC and the system reactive power generation decreased as the IPC reactance values increased.

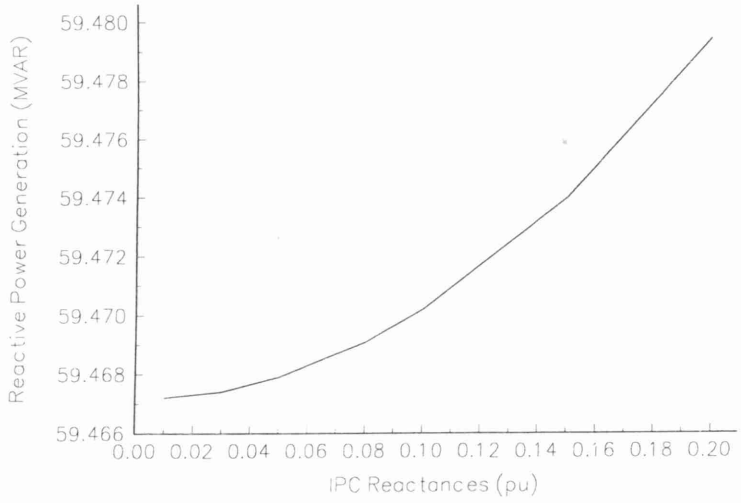

Figure 6.15. Reactive power generation as a function of reactance values.

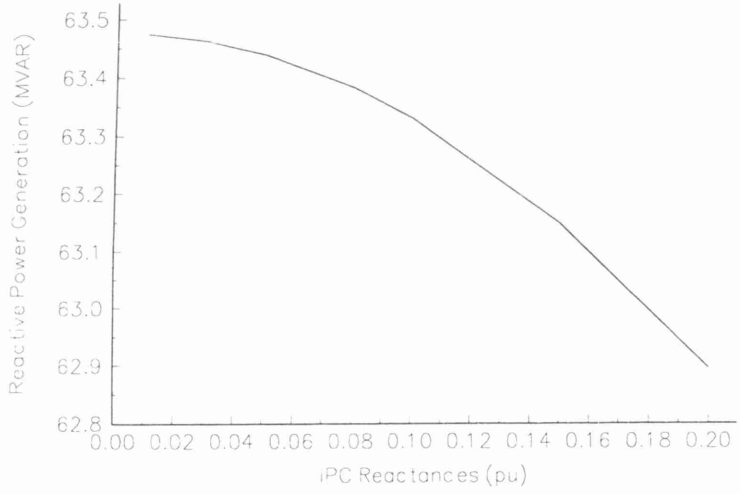

Figure 6.16. Reactive power generation as a function of reactance values.

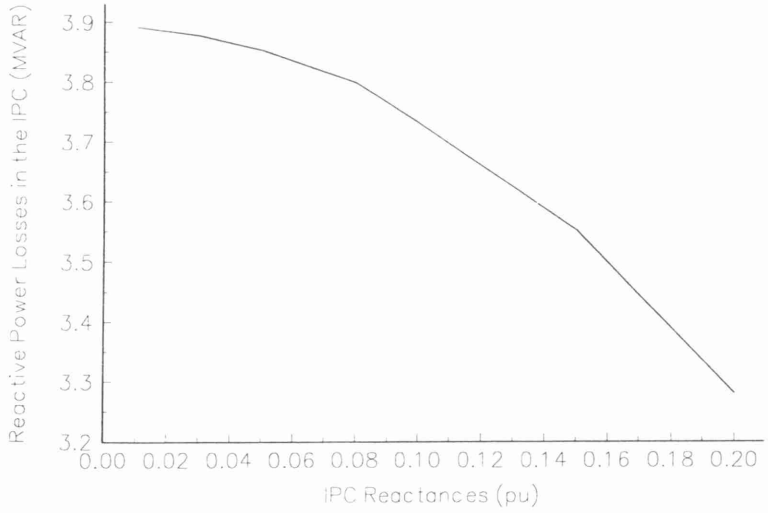

Figure 6.17. Reactive power losses of IPC as a function of reactance values.

6.7 Improving the PST Capabilities Through the Application of the IPC Concept

There are several ways in which IPC technology can be used to improve PST capabilities. In one configuration the phase shifting is only applied to one branch, generally the inductive one. The capacitive branch is either fixed or variable, and the inductive reactance is set to zero. The schematic representation of this configuration is shown in Figure 6.18, where X_{LEAK} is the leakage impedance of the PST. This IPC topology is useful in phase-shifting transformers, which are thermally limited or which are set too frequently at extreme tap positions.

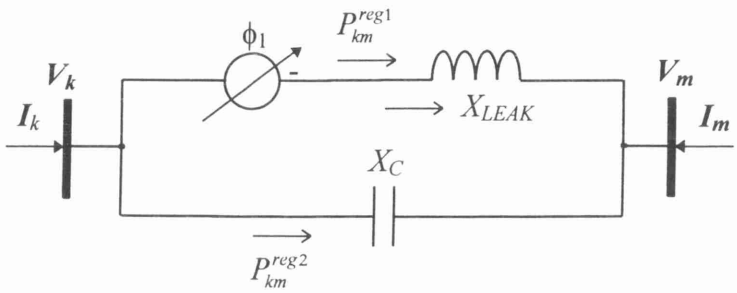

Figure 6.18. Schematic model of the IPC with one PST.

The configuration shown above can easily be implemented in the OPF algorithm, where each component is modelled independently and then linked together.

The case described in the previous section was modified to demonstrate more clearly the improvement on PST capabilities. The IPC capacitive reactance was given values between 0.01 and 0.35, and the IPC maintains active power flow in the transmission line connected between nodes Nod_5 and Nod_4 at 40 MW. No phase-shifting angle limits were taken into account. Figure 6.19 shows the IPC active power flow across the PST, the capacitive reactance, and the total IPC active power flow from nodes Nod_5 to Nod_4, as a function of capacitive reactance. Figure 6.20 shows the phase shifter angles as a function of capacitive reactance.

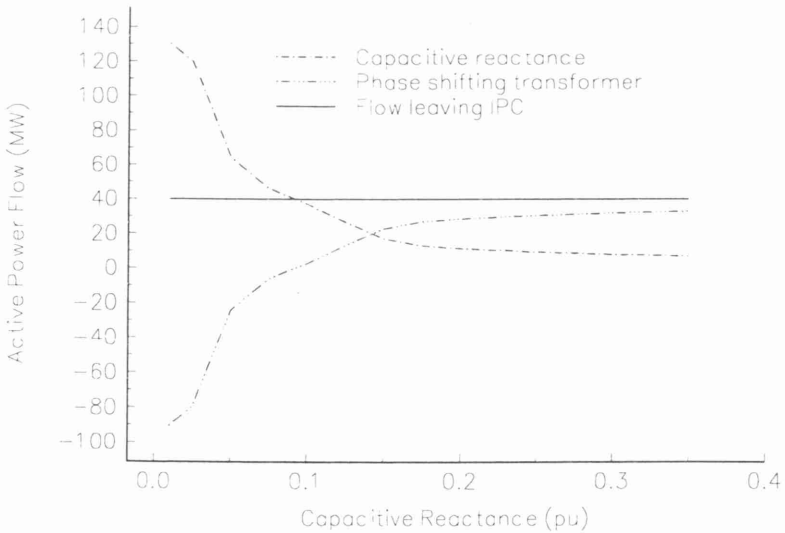

Figure 6.19. Active power flow across the IPC components as a function of capacitive reactance.

From Figures 6.19 and 6.20, it is clear that as the capacitive reactance increases the active power across the branch decreases. The active power flow was expected to increase since the electrical distance was shorter, however, unwanted loop flows can

appear in the IPC components, even under normal operating conditions, if the value of X_C is small. However, if the reactance is increased sufficiently such loops were eliminated. The PST capabilities increase greatly because the PST will be sharing the total active power flow with the capacitor. For example, the PST angle needs to be set at -12.38^0 to maintain the active power flow in transmission line Nod_5- Nod_4 at 40 MW. However, when a capacitor with a value of -0.25 pu is connected in parallel with the PST, the PST angle is set at -9.41^0 to maintain an active power flow of 30.58 MW across the PST. The remaining active power is transmitted through the capacitor. Under the configuration shown in Figure 6.18, the PST can transfer more power because it is sharing the total power flow with the capacitive reactance.

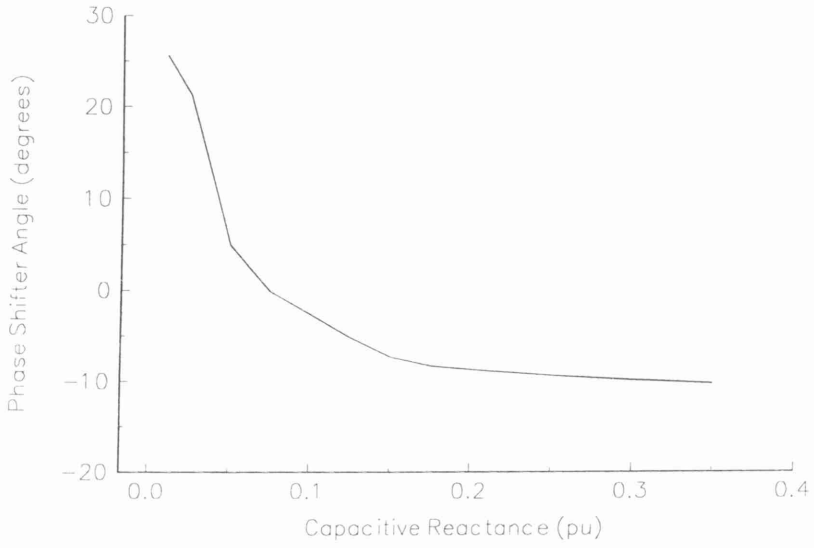

Figure 6.20. Phase shifter angles as a function of capacitive reactance.

6.8 Conclusions

Mathematical models suitable for assessing the steady state response of Interphase Power Controllers, which can be used to regulate active power flow across selected branches of a power network have been presented in this Chapter. The IPC power flow model was developed by combining the Controllable Reactance model of the TCSC and the PST model, taking advantage of the robustness and versatility afforded by those two models. The models have been linearised and included in the frame of reference afforded by using Newton's leading to very robust unified iterative solutions.

A method for increasing the steady-state transfer capabilities of an existing PST by using the IPC technology has also been presented. The addition of capacitors connected in parallel to the PST may lead to increase power transfer capabilities of the combined system. So far, transmission capacity enhancement has provided the economic justification for the application of this technology. Special care should be taken in the selection of the capacitor value to avoid undesirable operating conditions, such as active power flow loops.

The extended OPF Newton algorithm has proved to be very powerful tool, capable of solving IPC upgraded power networks very reliably.

6.9 References

[1] IEEE/CIGRE: 'FACTS Overview', Special Issue, 95TP108, IEEE Service Center, Piscataway, N.J., 1995.

[2] IEEE Power Engineering Society: 'FACTS Applications', Special Issue 96TP116-0, IEEE Service Center, Piscataway, N.J., 1996.

[3] Hingorani N.G.: 'Flexible AC Transmission Systems', IEEE Spectrum, April 1993, pp 40-45.

[4] Lemay J., Beauregard F., Brochu J., Pelletier P., Henderson M.I. Graham M.R., Kheir S., Habashi K.N., Kirby L.R. and Smith G.E.: 'Increasing the Capabilities of Phase-Shifting Transformers with the Interphase Power Controller Technology', EPRI Conference on the Future of Power Delivery in the 21st Century, Session 2-Grid Operation and Planning, November 18-20, 1997, La Jolla California.

[5] Brochu J., Pelletier P., Beauregard F. and Morin G.: 'The Interphase Power Controller a New Concept for Managing Power Flow within AC Networks', IEEE Transactions on Power Delivery, Vol. 9, No. 2, April 1994, pp. 883-841.

[6] Beauregard F., Brochu J., Morin G. and Pelletier P.: 'Interphase Power with Voltage Injection', IEEE Transsactions on Power Delivery, Vol. 9, No. 2, October 1994, pp. 1956-1962.

[7] Brochu J., Beauregard F., Morin G. and Pelletier P.: 'Interphase Power with Adapted to the Operating Conditions of Networks', 94 SM 475-4 PWRD, IEEE/PES Summer Meeting, San Francisco, CA, 24-28 July 1994.

[8] Sybille G., Haj-Maharsi Y., Morin G., Beauregard F., Brochu J., Lemay J. and Pelletier P.: 'Simulator Demonstration of the Interphase Power Controller Technology', 96 WM 119-8 PWRD, IEEE/PES Winter Meeting, Baltimore, MD, 21-25 January 1996.

[9] Sun D.I., Ashley B., Brewer B., Hughes A. and Tinney W.F.: 'Optimal Power Flow By Newton Approach', IEEE Transactions on Power Apparatus and Systems, Vol. PAS-103, No. 10, October 1984, pp. 2864-2880.

[10] Sun D.I., Hu T.I., Lin G.S., Lin C.J. and Chen C.H.: 'Experiences with Implementing Optimal Power Flow for Reactive Scheduling in the Taiwan Power System', IEEE Transactions on Power Systems, Vol. 3, No. 3, August 1988, pp. 1193-1200.

[11] Freris L.L. and Sasson A.M.: 'Investigation of the Load-Flow Problem', Proceedings of IEE, Vol. 115, No. 10, October 1968, pp. 1459-1470.

[12] Luenberger D.G.: 'Introduction to Linear and Nonlinear Programming', Addison-Wesley Publishing Co., Second Edition, 1984.

[13] Bertsekas D.P.: 'Constrained Optimization Lagrange Multiplier Methods', Academic Press, 1992.

[14] Stagg G.W. and El-Abiad A.H.: 'Computer Methods in Power System Analysis', McGraw-Hill, 1968.

Chapter 7

UPFC model in an Optimal Power Flow by Newton's Method

This Chapter addresses the issue of Unified Power Flow Controller (UPFC) modelling within the context of Optimal Power Flow (OPF) solutions. The non-linear optimisation problem is solved by Newton's method leading to highly robust iterative solutions even for cases of large-scale power networks, where hundreds of variables are to be optimised. It is shown in the Chapter that networks modified to include several UPFCs are solved with equal reliability. The UPFC model itself is very flexible, it allows the control of active and reactive powers and voltage magnitude simultaneously. It can also be set to control one or more of these parameters in any combination or to control none of them. Considerable progress has been achieved in UPFC modelling intended for conventional load flow studies but this is the first time that the more complex issue of UPFC modelling intended for OPF solutions has been addressed

7.1 Introduction

The UPFC is an advanced power systems device capable of providing simultaneous control of voltage magnitude and active and reactive power flows, all this in an adaptive fashion. Owing to its almost instantaneous speed of response and unrivalled functionality, it is well placed to solve most issues relating to power flow control while enhancing considerably transient and dynamic stability [1].

The basic principles of operation of the UPFC are presented in the following section [2]. This Chapter is concerned with UPFC models suitable for steady state solutions of large scale power networks. Considerable progress has been made in this direction [3,4] and a realistic UPFC model suitable for efficient load flow studies has been published very recently [5]. All these models, however, are only valid for the purpose of conventional load flow studies and no attempt has been made so far to tackle the more complex issue of OPF solutions of power networks where UPFCs are included. A comprehensive UPFC model suitable for OPF solutions has emanated from this research for the first time and it is now presented in this Chapter. It must be noted that the title of Reference [3] is misleading, since optimal solutions in that paper really refer to improved solutions

obtained by changing UPFC parameters on a trial and error basis as opposed to solutions where optimality conditions are fulfilled.

Using the UPFC-OPF model presented in this Chapter, very robust iterative solutions are achieved since the optimisation process is Carried out via Newton's method [6,7]. Hence, large-scale power networks are solved very reliably. The UPFC model has been developed to control active and reactive power flows at either the sending or receiving end nodes. Furthermore, the model can be set to simulate different UPFC operating modes very easily. For instance, in order to deactivate one or even two operational functions it is only necessary to add the second derivative term of a large, quadratic penalty weighting factor into the appropriate locations of the linearised system of equations. The dimensions of the system of equations remain unchanged and so does the elimination order in the gaussian elimination process, hence very efficient iterative solutions are achieved.

7.2 Basic Principles of UPFC Operation

The basic principles of operation of the UPFC are already well established in the open literature [2]. The schematic representation of the UPFC is shown in Figure 7.1. It consists of two back-to-back, self-commutated voltage source converters, sharing a shunt capacitor on the dc side. One converter is coupled to the ac system via a series transformer and the other is coupled to the ac system via a shunt transformer.

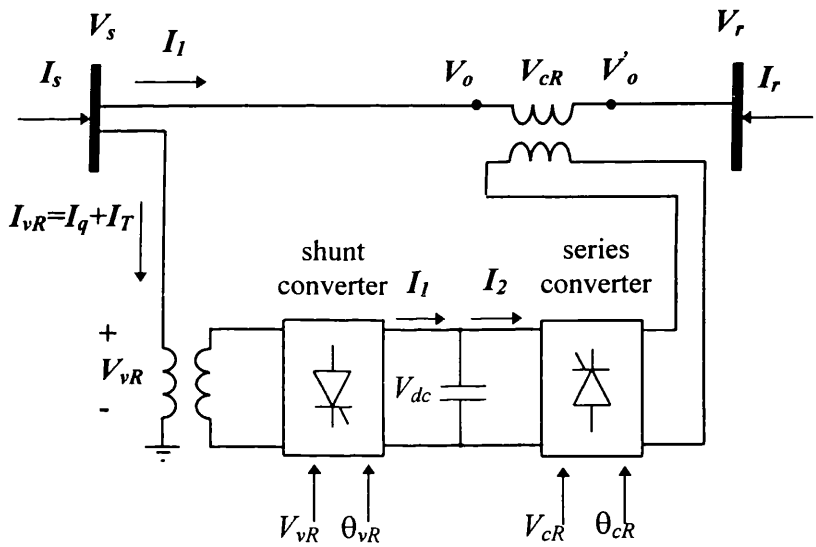

Figure 7.1. UPFC schematic diagram.

The output voltage of the series converter is added to the AC system terminal voltage V_o via the series connected coupling transformer. The injected voltage, V_{cR}, acts as an AC series voltage source, changing the effective sending-end voltage seen by the AC system at node r. The product of the transmission line current, I_r, and the series voltage source, V_{cR}, determines the active and reactive power exchanged between the series converter and the AC system.

The shunt converter supplies the real power demanded by the series converter at the common dc link from the AC power system, this real power is taken from the transmission lines connected at node s (current I_T). The shunt converter is able to generate or absorb controllable reactive power in both operating modes, i.e. rectifier and inverter (current I_q). The independently controlled shunt reactive compensation can be

used to maintain the shunt converter terminal AC voltage magnitude at a specified value.

Theoretically, the voltage magnitude V_{cR} can have any phase angle and a maximum magnitude of V_{cRmax}, confined to an operating area with a circle of radius V_{cRmax}. This voltage is added to V_o giving as a result that the phasors V_{cR} and V_o can take any position inside the circle as shown in Figure 7.2. The modified operating point can be changed at will. The component of V_{cR} in phase with the current I_r represents the active power injected at node r, and the component of V_{cR} in quadrature with the current I_r represents the reactive power injected at node r.

The UPFC has several functions by adding the injected voltage magnitude V_{cR} with the appropriate voltage magnitude and phase angle. (a) Terminal voltage regulation, the UPFC injects $V_{cR} = \Delta V$ in phase with V_o, the resulting function is similar to a LTC transformer with small tap steps. (b) Series compensation, the voltage $V_{cR} = V_c$ is injected in quadrature with the line current I_r, the effect is similar to that achieved with a capacitor. (c) Transmission angle regulation, the voltage $V_{cR} = V_\alpha$ is injected with the appropriate angle, shifting V_r by a phase angle with respect to V_o, as shown in Figure 7.2 (c), where α is the desired phase shifting angle. (d) Multifunction power flow control, the three previous functions described above are executed simultaneously, $V_{cR} = \Delta V + V_c + V_\alpha$. These operating functions are shown below.

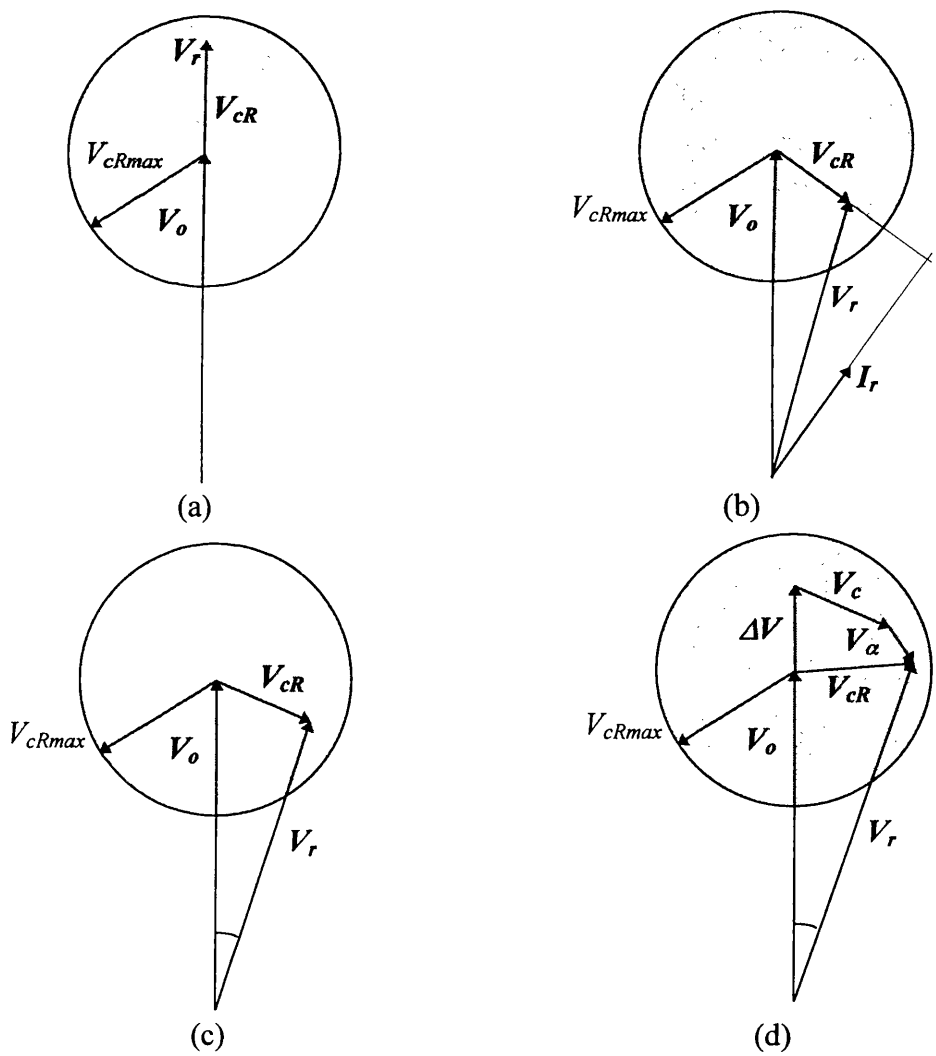

Figure 7.2. Vector diagrams of UPFC for different operating modes.

7.3 UPFC Equivalent Circuits

Two UPFC models are presented in this section. They are the voltage source-based model [5] and the model due to Navabi-Niaki and Iravani [4]. These models are used in Section 7.4 as the basis for the UPFC-OPF formulation.

7.3.1 Voltage Source-based Model

The UPFC equivalent circuit shown in Figure 7.1 [4,5] is used to derive a very flexible OPF-UPFC model. As far as power flow solutions is concerned, the only restriction which this model may have is that the UPFC converter valves are taken to be lossless. However, active power losses in the converter valves are expected to be negligible and this is expected to be a reasonable assumption. In this situation, the active power supplied to the shunt converter, $\mathrm{Re}\{V_{vR}\, I^{*}_{vR}\}$, satisfies the active power demanded by the series converter, $\mathrm{Re}\{V_{cR}\, I^{*}_{r}\}$.

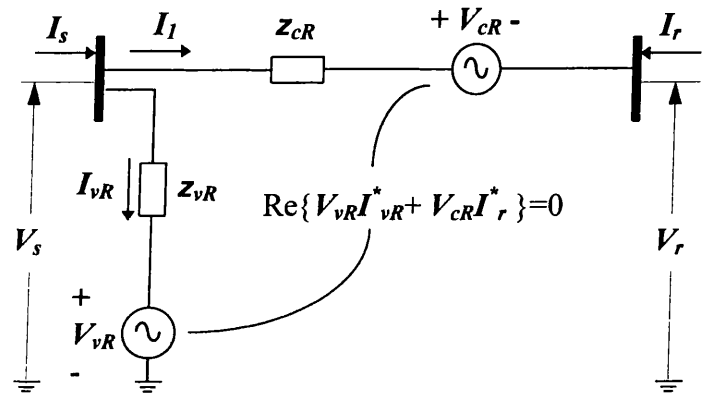

Figure 7.3. Equivalent circuit of the UPFC voltage source-based model.

The circuit is made up of two ideal voltage sources representing the fundamental Fourier series component of the switched voltage wave forms at the AC converter terminals. The impedance of the series and shunt transformers, z_{cR} and z_{vR} , are included explicitly in the model.

The ideal voltages sources are,

$$V_{vR} = V_{vR}\left(\cos\theta_{vR} + j\sin\theta_{vR}\right) \tag{7.1}$$

$$V_{cR} = V_{cR}\left(\cos\theta_{cR} + j\sin\theta_{cR}\right) \tag{7.2}$$

where V_{vR} and θ_{vR} are the controllable magnitude ($V_{vRmin} \le V_{vR} \le V_{vRmax}$) and angle ($0 \le \theta_{vR} \le 2\pi$) of the ideal voltage source representing the shunt converter. The magnitude V_{cR} and angle θ_{cR} of the ideal voltage source representing the series converter are controlled between limits ($V_{cRmin} \le V_{cR} \le V_{cRmax}$) and ($0 \le \theta_{cR} \le 2\pi$), respectively. Also, I_s, I_r are the currents entering nodes s and r, respectively; V_s, V_r are the voltages at nodes s and r, respectively; and I_l, I_{vR} are the currents flowing through both ideal voltage sources.

The Load Flow and OPF algorithms using this UPFC model are very flexible, since the UPFC can be set to control active and reactive powers and voltage magnitude simultaneously. It can also be set to control one or more of these parameters in any combination or to control none of them. Moreover, power losses in the transformer winding impedances are accounted for correctly.

7.3.2 Nabavi-Niaki and Iravani Model

Figure 7.4 (a) shows the schematic representation of a UPFC connected between nodes s and r and Figure 7.4 (b) shows its equivalent circuit representation using the load flow terminology. This equivalent circuit is due to Nabavi-Niaki and Iravani [4].

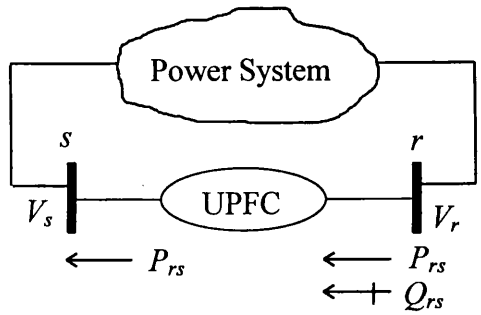

(a)

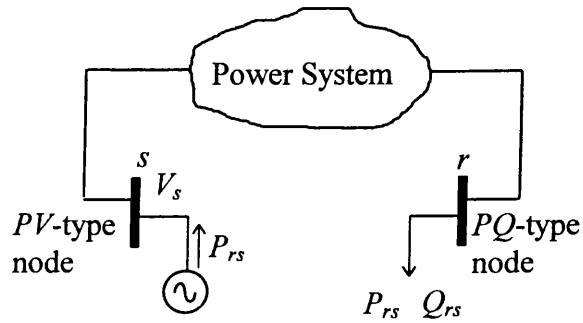

(b)

Figure 7.4. Nabavi-Niaki and Iravani model of the UPFC.

If the UPFC (converter valves plus transformers) is assumed to be lossless then the UPFC can be modelled by transforming node s into a PV-type node and node r into a PQ-type node. The UPFC active power flow is assigned to both the fictitious generator connected at node s and to the fictitious load connected at node r. The UPFC reactive power injected at node r is also assigned to the fictitious load. Furthermore, the UPFC voltage magnitude at node s is assigned to the newly created PV-type node.

This is a simple and elegant representation of the UPFC but, unfortunately, the model will only work if one wishes to exert simultaneous control of nodal voltage magnitude at node s, active power flowing from nodes r to s and reactive power injected at node r. Moreover, the model is no longer applicable if UPFC limits are violated. This model has been implemented in the UPFC-OPF algorithm and, where applicable, used for the purpose of comparing results with the voltage source-based model presented below.

7.4 UPFC Power Equations

The two UPFC models presented above have been implemented in the UPFC-OPF algorithm. The Nabavi-Niaki and Iravani model has been implemented in quite a direct manner by using standard OPF features. No cost function has been assigned to the generator and the PV node has been penalised so as to meet the specified voltage magnitude. The active and reactive power loads at the PQ node have required no special attention within the OPF algorithm. On the other hand, the voltage source-based model is far more flexible and sophisticated. Accordingly, the remaining of this section is dedicated to the derivation of the voltage source-based model equations as required by the OPF algorithm.

Based on the equivalent circuit shown in Figure 7.3, the following active and reactive power equations can be written:

At node *s*:

$$\begin{aligned} P_s = & V_s^2 G_{ss} + V_s V_r \left(G_{sr}\cos(\theta_s - \theta_r) + B_{sr}\sin(\theta_s - \theta_r)\right) \\ & + V_s V_{cR} \left(G_{sr}\cos(\theta_s - \theta_{cR}) + B_{sr}\sin(\theta_s - \theta_{cR})\right) \\ & + V_s V_{vR} \left(G_{vR}\cos(\theta_s - \theta_{vR}) + B_{vR}\sin(\theta_s - \theta_{vR})\right) \end{aligned} \tag{7.3}$$

$$\begin{aligned} Q_s = & -V_s^2 B_{ss} + V_s V_r \left(G_{sr}\sin(\theta_s - \theta_r) - B_{sr}\cos(\theta_s - \theta_r)\right) \\ & + V_s V_{cR} \left(G_{sr}\sin(\theta_s - \theta_{cR}) - B_{sr}\cos(\theta_s - \theta_{cR})\right) \\ & + V_s V_{vR} \left(G_{vR}\sin(\theta_s - \theta_{vR}) - B_{vR}\cos(\theta_s - \theta_{vR})\right) \end{aligned} \tag{7.4}$$

At node *r*:

$$\begin{aligned} P_r = & V_r^2 G_{rr} + V_r V_s \left(G_{rs}\cos(\theta_r - \theta_s) + B_{rs}\sin(\theta_r - \theta_s)\right) \\ & + V_r V_{cR} \left(G_{rr}\cos(\theta_r - \theta_{cR}) + B_{rr}\sin(\theta_r - \theta_{cR})\right) \end{aligned} \tag{7.5}$$

$$\begin{aligned} Q_r = & -V_r^2 B_{rr} + V_r V_s \left(G_{rs}\sin(\theta_r - \theta_s) - B_{rs}\cos(\theta_r - \theta_s)\right) \\ & + V_r V_{cR} \left(G_{rr}\sin(\theta_r - \theta_{cR}) - B_{rr}\cos(\theta_r - \theta_{cR})\right) \end{aligned} \tag{7.6}$$

Series converter:

$$\begin{aligned} P_{cR} = & V_{cR}^2 G_{rr} + V_{cR} V_s \left(G_{sr}\cos(\theta_{cR} - \theta_s) + B_{sr}\sin(\theta_{cR} - \theta_s)\right) \\ & + V_{cR} V_r \left(G_{rr}\cos(\theta_{cR} - \theta_r) + B_{rr}\sin(\theta_{cR} - \theta_r)\right) \end{aligned} \tag{7.7}$$

$$\begin{aligned} Q_{cR} = & -V_{cR}^2 B_{rr} + V_{cR} V_s \left(G_{sr}\sin(\theta_{cR} - \theta_s) - B_{sr}\cos(\theta_{cR} - \theta_s)\right) \\ & + V_{cR} V_r \left(G_{rr}\sin(\theta_{cR} - \theta_r) - B_{rr}\cos(\theta_{cR} - \theta_r)\right) \end{aligned} \tag{7.8}$$

Shunt converter:

$$P_{vR} = -V_{vR}^2 G_{vR} + V_{vR} V_s \left(G_{vR}\cos(\theta_{vR} - \theta_s) + B_{vR}\sin(\theta_{vR} - \theta_s)\right) \tag{7.9}$$

$$Q_{vR} = V_{vR}^2 B_{vR} + V_{vR} V_s \left(G_{vR}\sin(\theta_{vR} - \theta_s) - B_{vR}\cos(\theta_{vR} - \theta_s)\right) \tag{7.10}$$

where

$$G_{ss} = \mathrm{Re}\{\boldsymbol{z}_{cR}^{-1} + \boldsymbol{z}_{vR}^{-1}\} \tag{7.11}$$

$$B_{ss} = \mathrm{Im}\{\boldsymbol{z}_{cR}^{-1} + \boldsymbol{z}_{vR}^{-1}\} \tag{7.12}$$

$$G_{rr} = \mathrm{Re}\{\boldsymbol{z}_{cR}^{-1}\} \tag{7.13}$$

$$B_{rr} = \mathrm{Im}\{\boldsymbol{z}_{cR}^{-1}\} \tag{7.14}$$

$$G_{sr} = G_{rs} = \mathrm{Re}\{-\boldsymbol{z}_{cR}^{-1}\} \tag{7.15}$$

$$B_{sr} = B_{rs} = \mathrm{Im}\{-\boldsymbol{z}_{cR}^{-1}\} \tag{7.16}$$

$$G_{vR} = \mathrm{Re}\{-\boldsymbol{z}_{vR}^{-1}\} \tag{7.17}$$

$$B_{vR} = \mathrm{Im}\{-\boldsymbol{z}_{vR}^{-1}\} \tag{7.18}$$

Assuming a free loss converter operation, the UPFC neither absorbs nor injects active power with respect to the AC system. In this situation the active power supplied to the shunt converter, P_{vR} , must satisfy the active power demanded by the series converter, P_{cR}. Hence,

$$P_{vR} + P_{cR} = 0 \tag{7.19}$$

7.5 UPFC-OPF Formulation

The mathematical formulation consists of minimising the active power generation cost in the power system by adjusting suitable controllable parameters. The UPFC-OPF problem can be formulated as follows [6,7,10]:

$$\begin{aligned} &\textbf{\textit{Minimise}} \quad f(P_g) \\ &\textbf{\textit{Subject to}} \quad h(P_g, V, \theta, \theta_{cR}, V_{cR}, \theta_{vR}, V_{vR}) = 0 \\ &\textbf{\textit{and}} \qquad g(P_g, V, \theta, \theta_{cR}, V_{cR}, \theta_{vR}, V_{vR}) \le 0 \end{aligned} \tag{7.20}$$

where P_g, V, and θ are the active power generations, voltage magnitudes and phase angles, respectively. θ_{cR}, V_{cR}, θ_{vR} and V_{vR} are the UPFC's control variables. $f(P_g)$ is the objective function to be optimised, $h(P_g, V, \theta, \theta_{cR}, V_{cR}, \theta_{vR}, V_{vR})$ represents the power flow equations and $g(P_g, V, \theta, \theta_{cR}, V_{cR}, \theta_{vR}, V_{vR})$ represents state variable limits as well as functional operating constraints.

The constrained optimisation problem is converted to an unconstrained optimisation problem by constructing an Lagrangian function corresponding to equation (7.20). This is given as,

$$L(\boldsymbol{x}, \lambda) = f(P_g) + \lambda^t h(P_g, V, \theta, \theta_{cR}, V_{cR}, \theta_{vR}, V_{vR}) \tag{7.21}$$

where $\boldsymbol{x}$ is a vector of state variables and λ is the Lagrange multipliers vectors for equality constraints. The inequality constraints are not shown because they are only included when there are variables outside limits.

7.5.1 UPFC Lagrangian Function

The UPFC state variables are combined with the network nodal voltage magnitudes and angles in a single frame-of-reference for a unified, optimal solution via Newton's method. The UPFC state variables are adjusted automatically so as to satisfy specified power flows, voltage magnitudes and optimality conditions as given by Kuhn and Tucker [10].

The power flow equations provide a means for calculating the power balance existing in the network. They must be satisfied unconditionally, if a feasible solution is to exist. Otherwise, the OPF problem is said to be infeasible.

The Lagrangian function, $L_{sr}(\boldsymbol{x}, \lambda)$ corresponding to the power flow mismatch equations at nodes s and r, where $\boldsymbol{x}$ is the vector of state variables and λ is a Lagrange multiplier vector. They are explicitly modelled in the OPF Newton's method as an equality constraints given by the following equation:

$$\begin{aligned} L_{sr}(\boldsymbol{x}, \lambda) = {} & \lambda_{ps}(P_s + P_{ds} - P_{gs}) + \lambda_{qs}(Q_s + Q_{ds} - Q_{gs}) \\ & + \lambda_{pr}(P_r + P_{dr} - P_{gr}) + \lambda_{qr}(Q_r + Q_{dr} - Q_{gr}) \end{aligned} \tag{7.22}$$

where P_{ds}, P_{dr}, Q_{ds}, Q_{dr} are active and reactive power loads at nodes s and r, respectively. P_{gs}, P_{gr}, Q_{gs}, Q_{gr} are scheduled active and reactive power generations at nodes s and r, respectively. λ_{ps}, λ_{pr}, λ_{qs}, λ_{qr} are Lagrange multipliers at nodes s and r, respectively. The vector of state variables is $\boldsymbol{x} = [V\ \theta]^t$, where V and θ are the voltage magnitudes and angles, respectively. This voltage vector includes both nodal voltages and sources voltages. The superscript t indicates transposition.

7.5.2 DC link Lagrangian Function

A fundamental premise in our UPFC model is that the active power supplied to the shunt converter, P_{vR}, must satisfy the active power demanded by the series converter, P_{cR}. This condition must be met throughout the solution process. In the OPF formulation this condition is expressed as an equality constraint,

$$L_{sh-se}(\boldsymbol{x},\lambda) = \lambda_{sh-se}(P_{vR} + P_{cR}) \tag{7.23}$$

where $\lambda_{sh\text{-}se}$ is the Lagrange multiplier associated with the shunt and series power converters.

7.5.3 UPFC Power Flow Constraints

The power injected at node r can be formulated as a flow constraint across the branch connecting nodes s and r. In conventional OPF formulations, these kinds of constraints are enforced only if power flow limits have been exceeded. However, in this particular application this constraint remains active throughout the iterative solution unless one wishes this constraint to be deactivated. The normal operating condition is represented by the following equation when the UPFC is installed in the transmission line r-l, as it is shown in Figure 7.5,

$$L_{rl}(\boldsymbol{x},\lambda) = \lambda_{prl}(P_{rl} - P_{specified}) + \lambda_{qrl}(Q_{rl} - Q_{specified}) \tag{7.24}$$

where λ_{prl} is the Lagrange multiplier associated with active power injection at node r and λ_{qrl} is the Lagrange multiplier associated with reactive power injection at node r. $P_{specified}$ and $Q_{specified}$ are the specified active and reactive powers leaving node r.

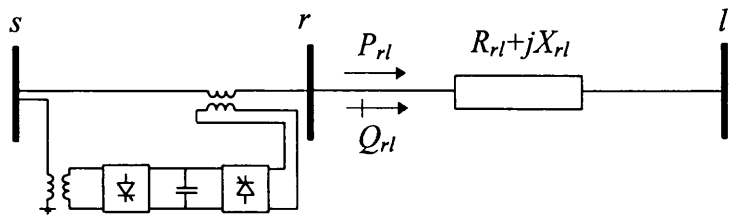

Figure 7.5. UPFC Power flow constraint at node r.

The UPFC Lagrangian function encompassing the individual contributions presented above is,

$$L_{upfc}(\boldsymbol{x},\lambda) = L_{sr}(\boldsymbol{x},\lambda) + L_{sh-se}(\boldsymbol{x},\lambda) + L_{rl}(\boldsymbol{x},\lambda) \tag{7.25}$$

where $L_{upfc}(\boldsymbol{x}, \lambda)$ is going to be substituted by $L(\boldsymbol{x},\lambda)$ in the following subsections.

7.5.4 Linearised Equations

As opposed to decoupled or linear programming-based methods, this formulation contains no simplifications. First and second order derivative terms are obtained and placed in matrix $\boldsymbol{W}$ and gradient vector $\boldsymbol{g}$ for a unified iterative solution via Newton's method.

The linearised system of equations for minimising the Lagrangian function via Newton's method is given by,

$$\boldsymbol{W}\Delta\mathbf{z} = -\boldsymbol{g} \tag{7.26}$$

where matrix $\boldsymbol{W}$ contains second partial derivatives of the Lagrangian function $L(\boldsymbol{x},\lambda)$ with respect to state variables $\boldsymbol{x}$ and Lagrange multipliers λ. The gradient vector $\boldsymbol{g}$ is $[\nabla\boldsymbol{x}\ \nabla\lambda]^t$. It consists of first partial derivative terms. $\Delta\mathbf{z}$ is the vector of correction terms, given by $[\Delta\boldsymbol{x}\ \Delta\lambda]^t$.

A more expanded version of equation (7.26) is,

$$\begin{bmatrix} \boldsymbol{W}_{11} & \boldsymbol{W}_{12} & \boldsymbol{W}_{13} & \boldsymbol{W}_{14} & \boldsymbol{W}_{15} & \mathbf{0} & \mathbf{0} \\ \boldsymbol{W}_{21} & \boldsymbol{W}_{22} & \boldsymbol{W}_{23} & \boldsymbol{W}_{24} & \boldsymbol{W}_{25} & \boldsymbol{W}_{26} & \boldsymbol{W}_{27} \\ \boldsymbol{W}_{31} & \boldsymbol{W}_{32} & \boldsymbol{W}_{33} & \boldsymbol{W}_{34} & \boldsymbol{W}_{35} & \mathbf{0} & \mathbf{0} \\ \boldsymbol{W}_{41} & \boldsymbol{W}_{42} & \boldsymbol{W}_{43} & \boldsymbol{W}_{44} & \boldsymbol{W}_{45} & \mathbf{0} & \mathbf{0} \\ \boldsymbol{W}_{51} & \boldsymbol{W}_{52} & \boldsymbol{W}_{53} & \boldsymbol{W}_{54} & \mathbf{0} & \mathbf{0} & \mathbf{0} \\ \mathbf{0} & \boldsymbol{W}_{62} & \mathbf{0} & \mathbf{0} & \mathbf{0} & \boldsymbol{W}_{66} & \boldsymbol{W}_{67} \\ \mathbf{0} & \boldsymbol{W}_{72} & \mathbf{0} & \mathbf{0} & \mathbf{0} & \boldsymbol{W}_{76} & \mathbf{0} \end{bmatrix} \begin{bmatrix} \Delta\mathbf{z}_1 \\ \Delta\mathbf{z}_2 \\ \Delta\mathbf{z}_3 \\ \Delta\mathbf{z}_4 \\ \Delta\mathbf{z}_5 \\ \Delta\mathbf{z}_6 \\ \Delta\mathbf{z}_7 \end{bmatrix} = \begin{bmatrix} -\boldsymbol{g}_1 \\ -\boldsymbol{g}_2 \\ -\boldsymbol{g}_3 \\ -\boldsymbol{g}_4 \\ -\boldsymbol{g}_5 \\ -\boldsymbol{g}_6 \\ -\boldsymbol{g}_7 \end{bmatrix} \tag{7.27}$$

where

$$\boldsymbol{W}_{11} = \begin{bmatrix} \dfrac{\partial^2 L}{\partial\theta_s^2} & \dfrac{\partial^2 L}{\partial\theta_s \partial V_s} & \dfrac{\partial P_s}{\partial\theta_s} & \dfrac{\partial Q_s}{\partial\theta_s} \\ \dfrac{\partial^2 L}{\partial V_s \partial\theta_s} & \dfrac{\partial^2 L}{\partial V_s^2} & \dfrac{\partial P_s}{\partial V_s} & \dfrac{\partial Q_s}{\partial V_s} \\ \dfrac{\partial P_s}{\partial\theta_s} & \dfrac{\partial P_s}{\partial V_s} & 0 & 0 \\ \dfrac{\partial Q_s}{\partial\theta_s} & \dfrac{\partial Q_s}{\partial V_s} & 0 & 0 \end{bmatrix} \tag{7.28}$$

$$\boldsymbol{W}_{12} = \boldsymbol{W}_{21}^t = \begin{bmatrix} \dfrac{\partial^2 L}{\partial\theta_s \partial\theta_r} & \dfrac{\partial^2 L}{\partial\theta_s \partial V_r} & \dfrac{\partial P_r}{\partial\theta_s} & \dfrac{\partial Q_r}{\partial\theta_s} \\ \dfrac{\partial^2 L}{\partial V_s \partial\theta_r} & \dfrac{\partial^2 L}{\partial V_s \partial V_r} & \dfrac{\partial P_r}{\partial V_s} & \dfrac{\partial Q_r}{\partial V_s} \\ \dfrac{\partial P_s}{\partial\theta_r} & \dfrac{\partial P_s}{\partial V_r} & 0 & 0 \\ \dfrac{\partial Q_s}{\partial\theta_r} & \dfrac{\partial Q_s}{\partial V_r} & 0 & 0 \end{bmatrix} \tag{7.29}$$

$$\boldsymbol{W}_{13} = \boldsymbol{W}_{31}^{t} = \begin{bmatrix} \dfrac{\partial^2 L}{\partial \theta_s \partial \theta_{cR}} & \dfrac{\partial^2 L}{\partial \theta_s \partial V_{cR}} \\ \dfrac{\partial^2 L}{\partial V_s \partial \theta_{cR}} & \dfrac{\partial^2 L}{\partial V_s \partial V_{cR}} \\ \dfrac{\partial P_s}{\partial \theta_{cR}} & \dfrac{\partial P_s}{\partial V_{cR}} \\ \dfrac{\partial Q_s}{\partial \theta_{cR}} & \dfrac{\partial Q_s}{\partial V_{cR}} \end{bmatrix} \tag{7.30}$$

$$\boldsymbol{W}_{14} = \boldsymbol{W}_{41}^{t} = \begin{bmatrix} \dfrac{\partial^2 L}{\partial \theta_s \partial \theta_{vR}} & \dfrac{\partial^2 L}{\partial \theta_s \partial V_{vR}} \\ \dfrac{\partial^2 L}{\partial V_s \partial \theta_{vR}} & \dfrac{\partial^2 L}{\partial V_s \partial V_{vR}} \\ \dfrac{\partial P_s}{\partial \theta_{vR}} & \dfrac{\partial P_s}{\partial V_{vR}} \\ \dfrac{\partial Q_s}{\partial \theta_{vR}} & \dfrac{\partial Q_s}{\partial V_{vR}} \end{bmatrix} \tag{7.31}$$

$$\boldsymbol{W}_{15} = \boldsymbol{W}_{51}^{t} = \begin{bmatrix} \dfrac{\partial P_{sh-se}}{\partial \theta_s} \\ \dfrac{\partial P_{sh-se}}{\partial V_s} \\ 0 \\ 0 \end{bmatrix} \tag{7.32}$$

$$\boldsymbol{W}_{22} = \begin{bmatrix} \dfrac{\partial^2 L}{\partial \theta_r^2} & \dfrac{\partial^2 L}{\partial \theta_r \partial V_r} & \dfrac{\partial P_r}{\partial \theta_r} & \dfrac{\partial Q_r}{\partial \theta_r} \\ \dfrac{\partial^2 L}{\partial V_r \partial \theta_r} & \dfrac{\partial^2 L}{\partial V_r^2} & \dfrac{\partial P_r}{\partial V_r} & \dfrac{\partial Q_r}{\partial V_r} \\ \dfrac{\partial P_r}{\partial \theta_r} & \dfrac{\partial P_r}{\partial V_r} & 0 & 0 \\ \dfrac{\partial Q_r}{\partial \theta_r} & \dfrac{\partial Q_r}{\partial V_r} & 0 & 0 \end{bmatrix} \tag{7.33}$$

$$\boldsymbol{W}_{23} = \boldsymbol{W}_{32}^{t} = \begin{bmatrix} \dfrac{\partial^2 L}{\partial \theta_r \partial \theta_{cR}} & \dfrac{\partial^2 L}{\partial \theta_r \partial V_{cR}} \\ \dfrac{\partial^2 L}{\partial V_r \partial \theta_{cR}} & \dfrac{\partial^2 L}{\partial V_r \partial V_{cR}} \\ \dfrac{\partial P_r}{\partial \theta_{cR}} & \dfrac{\partial P_r}{\partial V_{cR}} \\ \dfrac{\partial Q_r}{\partial \theta_{cR}} & \dfrac{\partial Q_r}{\partial V_{cR}} \end{bmatrix} \tag{7.34}$$

$$\boldsymbol{W}_{24} = \boldsymbol{W}_{42}^{t} = \begin{bmatrix} \dfrac{\partial^2 L}{\partial\theta_r \partial\theta_{vR}} & \dfrac{\partial^2 L}{\partial\theta_r \partial V_{vR}} \\ \dfrac{\partial^2 L}{\partial V_r \partial\theta_{vR}} & \dfrac{\partial^2 L}{\partial V_r \partial V_{vR}} \\ \dfrac{\partial P_r}{\partial\theta_{vR}} & \dfrac{\partial P_r}{\partial V_{vR}} \\ \dfrac{\partial Q_r}{\partial\theta_{vR}} & \dfrac{\partial Q_r}{\partial V_{vR}} \end{bmatrix} \tag{7.35}$$

$$\boldsymbol{W}_{25} = \boldsymbol{W}_{52}^{t} \begin{bmatrix} \dfrac{\partial P_{sh-se}}{\partial\theta_r} \\ \dfrac{\partial P_{sh-se}}{\partial V_r} \\ 0 \\ 0 \end{bmatrix} \tag{7.36}$$

$$\boldsymbol{W}_{26} = \boldsymbol{W}_{62}^{t} = \begin{bmatrix} \dfrac{\partial^2 L}{\partial\theta_r \partial\theta_l} & \dfrac{\partial^2 L}{\partial\theta_r \partial V_l} & \dfrac{\partial P_l}{\partial\theta_r} & \dfrac{\partial Q_l}{\partial\theta_r} \\ \dfrac{\partial^2 L}{\partial V_r \partial\theta_l} & \dfrac{\partial^2 L}{\partial V_r \partial V_l} & \dfrac{\partial P_l}{\partial V_r} & \dfrac{\partial Q_l}{\partial V_r} \\ \dfrac{\partial P_r}{\partial\theta_l} & \dfrac{\partial P_r}{\partial V_l} & 0 & 0 \\ \dfrac{\partial Q_r}{\partial\theta_l} & \dfrac{\partial Q_r}{\partial V_l} & 0 & 0 \end{bmatrix} \tag{7.37}$$

$$\boldsymbol{W}_{27} = \boldsymbol{W}_{72}^{t} = \begin{bmatrix} \dfrac{\partial P_{rl}}{\partial\theta_r} & \dfrac{\partial Q_{rl}}{\partial\theta_r} \\ \dfrac{\partial P_{rl}}{\partial V_r} & \dfrac{\partial Q_{rl}}{\partial V_r} \\ 0 & 0 \\ 0 & 0 \end{bmatrix} \tag{7.38}$$

$$\boldsymbol{W}_{33} = \begin{bmatrix} \dfrac{\partial^2 L}{\partial\theta_{cR}^2} & \dfrac{\partial^2 L}{\partial\theta_{cR} \partial V_{cR}} \\ \dfrac{\partial^2 L}{\partial V_{cR} \partial\theta_{cR}} & \dfrac{\partial^2 L}{\partial V_{cR}^2} \end{bmatrix} \tag{7.39}$$

$$\boldsymbol{W}_{34} = \boldsymbol{W}_{43}^{t} = \begin{bmatrix} \dfrac{\partial^2 L}{\partial\theta_{cR} \partial\theta_{vR}} & \dfrac{\partial^2 L}{\partial\theta_{cR} \partial V_{vR}} \\ \dfrac{\partial^2 L}{\partial V_{cR} \partial\theta_{vR}} & \dfrac{\partial^2 L}{\partial V_{cR} \partial V_{vR}} \end{bmatrix} \tag{7.40}$$

$$\boldsymbol{W}_{35} = \boldsymbol{W}_{53}^{t} = \begin{bmatrix} \dfrac{\partial P_{sh-se}}{\partial \theta_{cR}} \\ \dfrac{\partial P_{sh-se}}{\partial V_{cR}} \end{bmatrix} \tag{7.41}$$

$$\boldsymbol{W}_{44} = \begin{bmatrix} \dfrac{\partial^2 L}{\partial \theta_{vR}^2} & \dfrac{\partial^2 L}{\partial \theta_{vR} \partial V_{vR}} \\ \dfrac{\partial^2 L}{\partial V_{vR} \partial \theta_{vR}} & \dfrac{\partial^2 L}{\partial V_{vR}^2} \end{bmatrix} \tag{7.42}$$

$$\boldsymbol{W}_{45} = \boldsymbol{W}_{54}^{t} = \begin{bmatrix} \dfrac{\partial P_{sh-se}}{\partial \theta_{vR}} \\ \dfrac{\partial P_{sh-se}}{\partial V_{vR}} \end{bmatrix} \tag{7.43}$$

$$\boldsymbol{W}_{66} = \begin{bmatrix} \dfrac{\partial^2 L}{\partial \theta_l^2} & \dfrac{\partial^2 L}{\partial \theta_l \partial V_l} & \dfrac{\partial P_l}{\partial \theta_l} & \dfrac{\partial Q_l}{\partial \theta_l} \\ \dfrac{\partial^2 L}{\partial V_l \partial \theta_l} & \dfrac{\partial^2 L}{\partial V_l^2} & \dfrac{\partial P_l}{\partial V_l} & \dfrac{\partial Q_l}{\partial V_l} \\ \dfrac{\partial P_l}{\partial \theta_l} & \dfrac{\partial P_l}{\partial V_l} & 0 & 0 \\ \dfrac{\partial Q_l}{\partial \theta_l} & \dfrac{\partial Q_l}{\partial V_l} & 0 & 0 \end{bmatrix} \tag{7.44}$$

$$\boldsymbol{W}_{67} = \boldsymbol{W}_{67}^{t} = \begin{bmatrix} \dfrac{\partial P_{rl}}{\partial \theta_l} & \dfrac{\partial Q_{rl}}{\partial \theta_l} \\ \dfrac{\partial P_{rl}}{\partial V_l} & \dfrac{\partial Q_{rl}}{\partial V_l} \\ 0 & 0 \\ 0 & 0 \end{bmatrix} \tag{7.45}$$

$$\boldsymbol{g}_1 = \begin{bmatrix} \dfrac{\partial L}{\partial \theta_s} & \dfrac{\partial L}{\partial V_s} & \dfrac{\partial L}{\partial \lambda_{ps}} & \dfrac{\partial L}{\partial \lambda_{qs}} \end{bmatrix}^t \tag{7.46}$$

$$\boldsymbol{g}_2 = \begin{bmatrix} \dfrac{\partial L}{\partial \theta_r} & \dfrac{\partial L}{\partial V_r} & \dfrac{\partial L}{\partial \lambda_{pr}} & \dfrac{\partial L}{\partial \lambda_{qr}} \end{bmatrix}^t \tag{7.47}$$

$$\boldsymbol{g}_3 = \begin{bmatrix} \dfrac{\partial L}{\partial \theta_{cR}} & \dfrac{\partial L}{\partial V_{cR}} \end{bmatrix}^t \tag{7.48}$$

$$\boldsymbol{g}_4 = \begin{bmatrix} \dfrac{\partial L}{\partial \theta_{vR}} & \dfrac{\partial L}{\partial V_{vR}} \end{bmatrix}^t \tag{7.49}$$

$$\boldsymbol{g}_5 = \begin{bmatrix} \dfrac{\partial L}{\partial \lambda_{sh-se}} \end{bmatrix} \tag{7.50}$$

$$\boldsymbol{g}_6 = \left[\frac{\partial L}{\partial \theta_l} \quad \frac{\partial L}{\partial V_l} \quad \frac{\partial L}{\partial \lambda_{pl}} \quad \frac{\partial L}{\partial \lambda_{ql}} \right]^t \tag{7.51}$$

$$\boldsymbol{g}_7 = \left[\frac{\partial L_{rl}}{\partial \lambda_{prl}} \quad \frac{\partial L_{rl}}{\partial \lambda_{qrl}} \right]^t \tag{7.52}$$

$$\Delta \mathbf{z}_1 = \left[\Delta\theta_s \quad \Delta V_s \quad \Delta\lambda_{ps} \quad \Delta\lambda_{qs} \right]^t \tag{7.53}$$

$$\Delta \mathbf{z}_2 = \left[\Delta\theta_r \quad \Delta V_r \quad \Delta\lambda_{pr} \quad \Delta\lambda_{qr} \right]^t \tag{7.54}$$

$$\Delta \mathbf{z}_3 = \left[\Delta\theta_{cR} \quad \Delta V_{cR} \right]^t \tag{7.55}$$

$$\Delta \mathbf{z}_4 = \left[\Delta\theta_{vR} \quad \Delta V_{vR} \right]^t \tag{7.56}$$

$$\Delta \mathbf{z}_5 = \left[\Delta\lambda_{sh-se} \right] \tag{7.57}$$

$$\Delta \mathbf{z}_6 = \left[\Delta\theta_l \quad \Delta V_l \quad \Delta\lambda_{pl} \quad \Delta\lambda_{ql} \right]^t \tag{7.58}$$

$$\Delta \mathbf{z}_7 = \left[\Delta\lambda_{prl} \quad \Delta\lambda_{qrl} \right]^t \tag{7.59}$$

First and second order derivative terms in equations (7.28)-(7.52) are given explicitly in Appendix IV. The derivative terms corresponding to inequality constraints are not required at the beginning of the iterative solution, they are introduced into matrix equation (7.26) only after limits are enforced.

Once equations (7.28)-(7.52) have been assembled and combined with matrix $\boldsymbol{W}$ and gradient vector $\boldsymbol{g}$ of the entire network then a sparsity-oriented solution is carried out. This process is repeated until a small, pre-specified tolerance is reached. It must be noted that this procedure corresponds to the case in which the UPFC is being operated in standard control mode, i.e. it is controlling the nodal voltage magnitude at node *s*, active power flowing from nodes *r* to *l* and reactive power injected at node *r*.

However, if different UPFC operating modes are selected then matrix $\boldsymbol{W}$ and multipliers λ are suitably modified to reflect the new operating mode. For instance, if nodes *r* and *s* are PQ-type and the UPFC is not controlling active power flowing from nodes *r* to *l* and reactive power is not injected at node *r* then the matrix $\boldsymbol{W}$ and gradient vector $\boldsymbol{g}$ are suitably modified. This is done by adding the second derivative term of a large (infinite), quadratic penalty factor to the diagonal elements of matrix $\boldsymbol{W}$ corresponding to the multipliers λ_{prl} and λ_{qrl} and by setting these multipliers to zero. The first derivative terms of the quadratic penalty functions are evaluated and added to the corresponding gradient elements. Alternatively, if one chooses to free just one operating condition, e.g. reactive power injected at node *r*, then only the diagonal element of matrix $\boldsymbol{W}$

corresponding to multiplier λ_{qrl} is penalised. A similar procedure applies when the UPFC controls voltage magnitude at the AC shunt converter terminal.

7.5.5 Handling Limits of UPFC Controllable Variables

In the OPF formulation, the Multipliers method [11] is used to handle UPFC inequality constraints. Here, a penalty term is added to the Lagrangian function $L(\mathbf{x},\lambda)$ which then becomes the augmented Lagrangian function. Variables inside bounds are ignored whilst binding inequality constraints become part of the augmented Lagrangian function and, hence, become enforced.

The handling of UPFC inequality constraints can be carried out by equation (7.60). In this case, the equation is applied to the voltage magnitude at the shunt source at node *r*. A similar procedure is carried out for the remaining UPFC state variables.

$$\psi_i(V_{vR,i}^j,\mu_i^j)=\begin{cases}\mu_i^j(V_{vR,i}^j-V_{vR,i}^{\max})+\dfrac{c}{2}(V_{vR,i}^j-V_{vR,i}^{\max})^2 & \text{if} \quad \mu_i^j+c(V_{vR,i}^j-V_{vR,i}^{\max})\geq 0\\ \mu_i^j(V_{vR,i}^j-V_{vR,i}^{\min})+\dfrac{c}{2}(V_{vR,i}^j-V_{vR,i}^{\min})^2 & \text{if} \quad \mu_i^j+c(V_{vR,i}^j-V_{vR,i}^{\min})\leq 0\\ 0 \quad \text{otherwise}\end{cases} \tag{7.60}$$

where *i* is the number of UPFC associates with the variable V_{vR}, and the *j* is the iteration number associated with the actual value of V_{vR}; $V_{vR,i}^{\max}$ and $V_{vR,i}^{\min}$ are the upper and lower limits for voltage magnitude at the shunt source; μ_i is a multiplier term and *c* is a penalty weighting term.

7.5.6 UPFC Initial Conditions in OPF Solutions

Nodal Voltage Magnitudes and Angles

The variables in vector **z** must be given initial values in order to start the iterative process. State variables are initialised similarly to load flow problems, i.e. 1 pu voltage magnitudes and 0 voltage angles for all nodes. This provides a suitable starting condition. Engineering experience indicates that, for most problems, the variation of voltage magnitude and voltage angle from the 1 and 0 initial conditions is relatively small.

Lagrange Multipliers

The Lagrange multipliers for active and reactive power flow mismatch equations are initialised at λ_p given by the lossless economic dispatch [12] and 0, respectively. For UPFC Lagrange multipliers the initial value of $\lambda_{sh\text{-}se}$ is also set to λ_p and λ_{prl} and λ_{qrl} are set equal to zero. It is our experience that these values give rise to very robust iterative solutions.

Series Source

Equations for initialising the series source voltage magnitude and angle can be obtained from the solution of equations (7.5) and (7.6) for a specified nodal power at node *r*,

$$\theta_{cR}^{0} = arc\tan\left(\frac{P_{specified}}{|C1|}\right) \tag{7.61}$$

$$V_{cR}^{0} = \left(\frac{X_{cR}}{V_r^0}\right)\sqrt{P_{specified}^2 + C1^2} \tag{7.62}$$

where

$$C1 = Q_{specified} - \frac{V_r^0}{X_{cR}}(V_r^0 - V_s^0) \quad \text{if } V_r^0 \neq V_s^0 \tag{7.63}$$

$$C1 = Q_{specified} \quad \text{if } V_r^0 = V_s^0 \tag{7.64}$$

X_{cR} is the inductive reactance of the series source and the superscript 0 indicates initial value.

Shunt Source

An equation for initialising the shunt source angle can be obtained by substituting eqs. (7.7) and (7.9) into equation (7.11) and by performing simple operations,

$$\theta_{vR} = -\arcsin\left(\frac{(V_s^0 - V_r^0)V_{cR}^0 X_{vR}\sin\theta_{cR}^0}{V_{vR}^0 V_s^0 X_{cR}}\right) \tag{7.65}$$

where X_{vR} is the inductive reactance of the shunt source.

For the case in which the UPFC is set to regulate the nodal voltage magnitude, the initial value of the shunt source voltage magnitude is normally given as the target voltage. Then the voltage magnitude value is updated throughout the iterative process as given by the solution of equation (7.26). A large, quadratic penalty weighting factor is used to fix the nodal voltage magnitude at node *s*. For the case in which the UPFC is not regulating the nodal voltage magnitude, the shunt source voltage magnitude is initialised at 1 pu and no penalty weighting factor is used.

7.6 UPFC-OPF Test Cases

This Section presents OPF results which relate to large power networks, modified to include UPFC devices. The test systems reported in this section are the 5-node system, the AEP 14-node system and a portion of large, real life power network.

The original 5-node system was modified to include a UPFC in series with the transmission line connecting nodes Lake and Main [13]. A dummy node, LakeUPFC, was created as shown in Figure 7.6. The UPFC is used to maintain active power at 25 MW and reactive power at -6 MVAR leaving LakeUPFC towards Main. The UPFC's shunt converter is maintaining Lake's nodal voltage magnitude at 1 pu. The initial conditions of the UPFC voltage sources are computed by using the equations (7.61)-(7.65) which give V_{cR} = 0.025 pu, θ_{cR} = -76.50^0, V_{vR} = 1 pu, θ_{vR} = 0^0. The resistances of the coupling transformers are ignored and their inductive reactances are assumed to be $X_{cR} = X_{vR}$ = 0.1 pu. The voltage magnitude V_{cR} varies in the range 0.001 pu and 0.6 pu and V_{vR} in the range 0.9 pu and 1.1 pu. Convergence was achieved in 2 iterations to a power mismatch tolerance of 10^{-9}. Figure 7.6 shows the final power flow results.

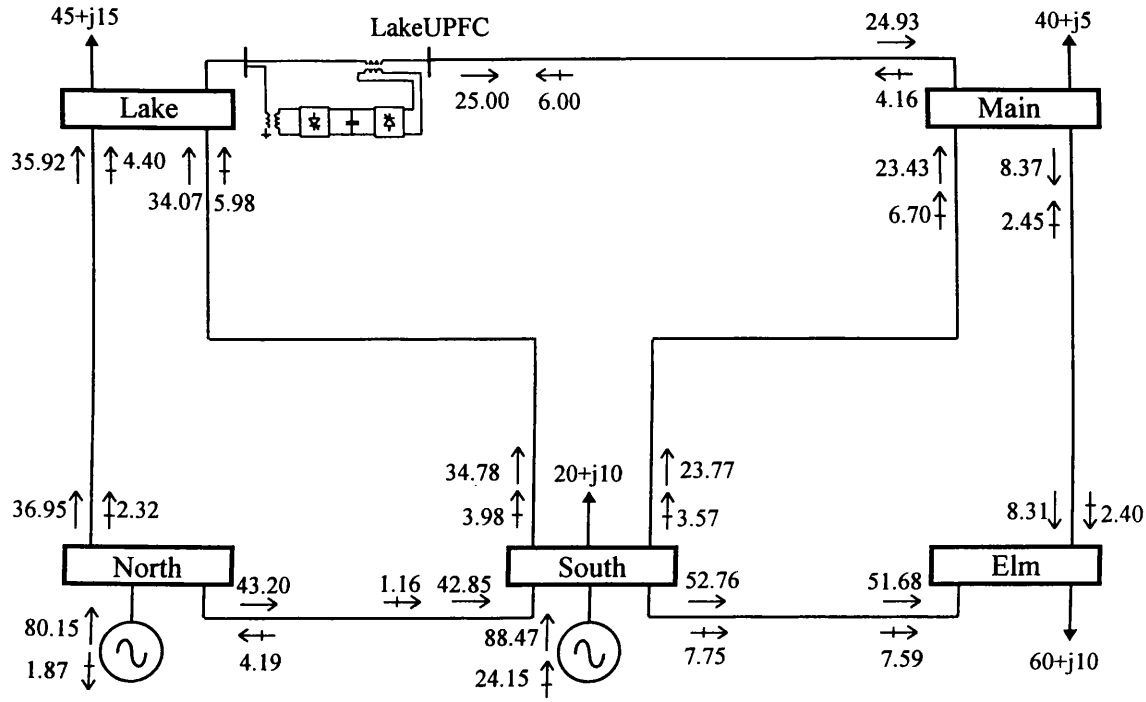

Figure 7.6. Modified 5-node system and OPF solution.

The final voltage magnitude, phase angle, active and reactive power generation and Lagrange Multiplier for each node are given in Table 7.1.

Table 7.1. Nodal complex voltages of modified network

Node	Voltage Magnitude (pu)	Phase Angle (degrees)	Active Power (MW)	Reactive Power (MVA)	λ_p ($/MWhr)
LakeUPFC	1.007	-3.128	0	0	4.2680
Elm	0.999	-4.722	0	0	4.2823
Main	1.006	-3.580	0	0	4.2246
Lake	1.000	-4.685	0	0	4.2680
South	1.029	-1.402	88.47	24.15	4.1077
North	1.036	0.000	80.15	-1.87	4.0412

Larger active power flowing in transmission lines North-Lake and South-Lake are observed in order to meet the power flow constraint imposed in the network. By comparing Tables 3.2 and 7.1, it can be observed that there were increments in the active power generation of 0.5 MW and 7.015 MVAR in the reactive power generation in this UPFC test case, i.e. 750.357 $/hour and 3.643 MW, respectively. Furthermore, the generation cost and the network losses were also increased by 2.027 $/hour and 0.5 MW, respectively. As expected, this case gave higher final results due there was not too freedom for the control variables because the UPFC met three operating conditions: to regulate active and reactive power flows, and voltage magnitude.

Table 7.2 shows the variation of the controllable voltage sources. It should be noted that the UPFC initial conditions obtained from equations (7.61)-(7.65) led to good estimates as indicated by the small changes in the parameters.

Table 7.2. Parameters of voltage sources.

Iteration	Series source		Shunt source	
	V_{cR} (pu)	θ_{cR} (degrees)	V_{vR} (pu)	θ_{vR} (degrees)
0	0.025	-76.500	1.000	0.000
1	0.052	-94.102	0.998	-4.718
2	0.052	-94.876	0.997	-4.705

The 5-node test system was also solved using the UPFC model presented in Section 7.3.2. This is the Nabavi-Niaki-Iravani conventional model. The representation is shown in Figure 7.7. The node Lake was transformed into a PV-type node and the node LakeUPFC into a PQ-type node.

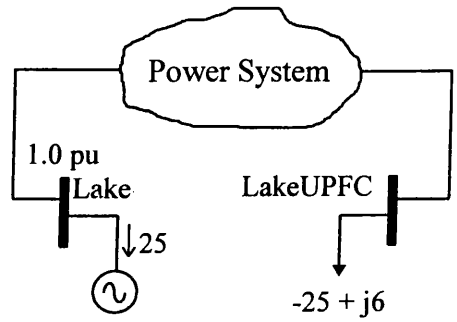

Figure 7.7. Nabavi-Niaki and Iravani model implemented into 5-node test system.

The number of iterations taken by the algorithm to converge was 2. This model provided identical results to those shown in Table 7.1. However, as mentioned above, the Nabavi-Niaki-Iravani conventional model will only work properly if one wishes to exert simultaneous control of the nodal voltage magnitude at node Lake, active and reactive power leaving the UPFC at node LakeUPFC.

Figure 7.8 shows active power generation cost as a function of iteration number whilst Figure 7.9 shows active power losses as a function of the iteration number. It can be observed from these figures that the pattern of convergence is regular during the iterative process. This is due to the fact that there is no bounded variables in the set of active constraints during the process and, as consequence, no penalty weighting factors were required. Small differences can be observed between the results given by the two UPFC models. Upon convergence both models give the same answer.

As it was pointed out in Section 7.3.2, the Nabavi-Niaki and Iravani model is assumed to be lossless, however, when the coupling transformer impedance losses are taking into account, the active power flowing at both system nodes where the UPFC is connected is different. For example, in the 5-node test system, the transformers coupling impedances were assumed to have a resistive part of $R_{cR} = R_{vR} = 0.05$ pu. Two more simulations were carried out by using the Generalised UPFC model and the Nabavi-Niaki and Iravani models. The active power flow injected at node Lake given by the simulation carried out with the former model was taken as input data for the later model. The results obtained from the Generalised UPFC model were used for the Nabavi-Niaki and Iravani model as shown in Figure 7.10.

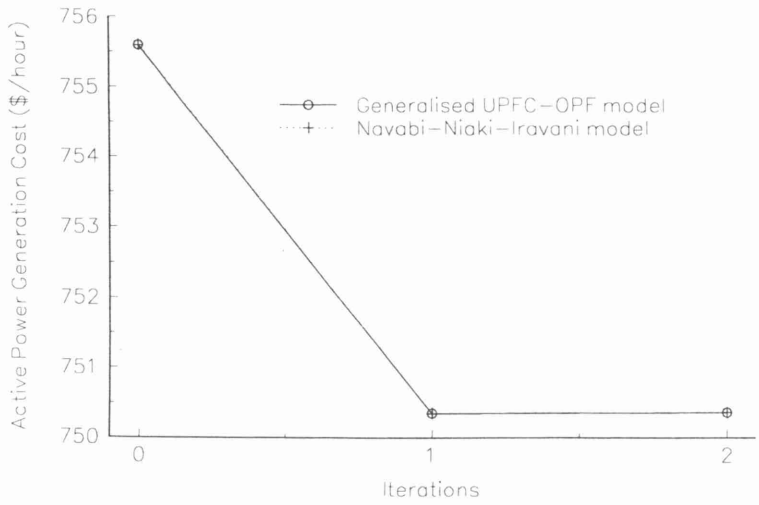

Figure 7.8. Active power generation cost profiles corresponding to two UPFC models in the 5-node test system

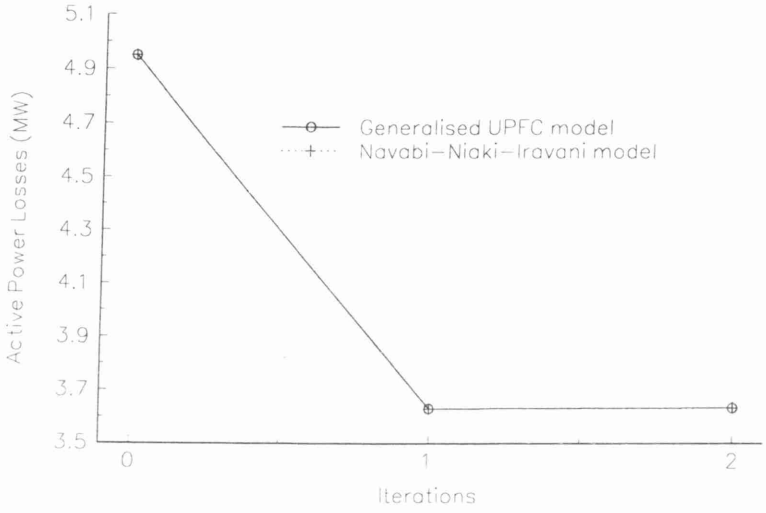

Figure 7.9. Active power losses profiles corresponding to two UPFC models in the 5-node test system

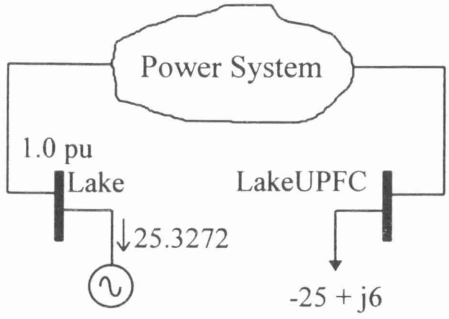

Figure 7.10. Nabavi-Niaki and Iravani model implemented into 5-node test system considering losses in the UPFC coupling transformers.

For the Generalised UPFC model, the solution converged in 2 iterations (as above). The UPFC upheld its target values. However, the active power generation cost increased to 751.755 $/hour and the active power losses to 3.974 MW due to the coupling transformer impedance losses. On the other hand, the Nabavi-Niaki and Iravani model gave different results, the generation cost was 751.754 $/hour and the network losses were 3.647 MW. As it can be seen, the Nabavi-Niaki and Iravani model is no longer applicable if losses in the UPFC coupling transformers are taken into account.

7.7 UPFC Operating Modes

In order to assess the behaviour of the various UPFC operating modes, its functional constraints were freed in sequence. These simulations were carried out with just one UPFC embedded in the 5-node test system in order to draw clearer conclusions from this study. These results are shown in Figure 7.11 where the normal UPFC operating mode (all constraints activated) is compared against cases where active and reactive power flows are freed and the voltage magnitude remains fixed, the voltage magnitude is freed and active and reactive power flows are fixed. The last simulation corresponds to the case when all three constraints are freed. Table 7.3 presents the relevant results for these tests.

Table 7.3. Final results corresponding to different UPFC operating modes in the 5-node test system.

Case	Iterations	Active Power (MW)	Reactive Power (MVAR)	Generation Cost ($/hour)	Network Losses (MW)
Normal UPFC operation	2	168.63	22.28	750.357	3.631
Fixed Voltage (node Lake)	2	168.52	14.19	749.928	3.519
Fixed P and Q injections	3	168.12	7.17	748.236	3.119
All constraints deactivated	3	168.06	0.98	747.828	3.015

As expected, the last case gives the minimum cost solution whereas the first case gives the most expensive solution. However, it can be argued that one of the main purposes of installing a UPFC is, in the first place, to have the ability to regulate power flows and voltage magnitude. In the last case, the reactive power generation seems to be small, however, the shunt converter injects 13.589 MVAR into the network.

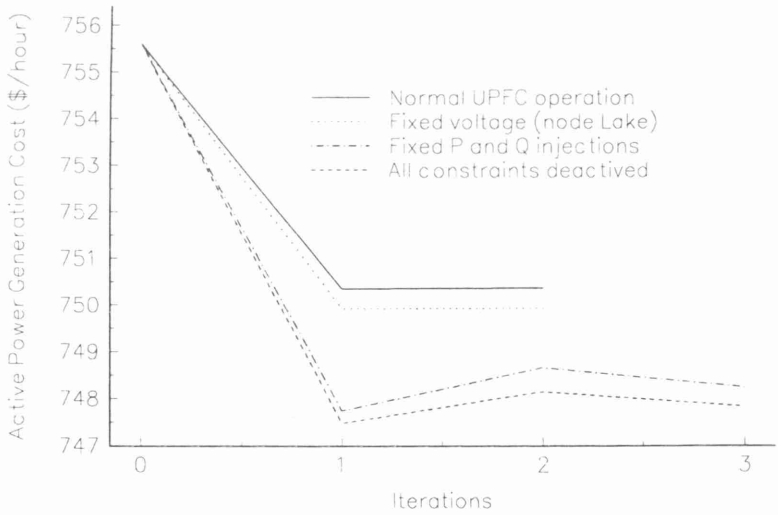

Figure 7.11. Active power generation cost profiles corresponding to different UPFC operating modes in the 5-node test system.

Table 7.4 shows the final parameters of the voltage sources for different UPFC operating modes. As it can be observed, θ_{cR} has the largest increments in the solution for all cases. However, as it was observed above, the case that satisfies the normal UPFC operating conditions converged in 2 iterations. It will be shown below that the extended OPF algorithm is more robust when solving cases where the UPFC meets all the operating conditions as opposed to cases where only one or two operating conditions are met.

Table 7.4. Parameters of voltage sources for different UPFC operating modes in the 5-node test system

Case	Series source		Shunt source	
	V_{cR} (pu)	θ_{cR} (degrees)	V_{vR} (pu)	θ_{vR} (degrees)
Normal UPFC operation	0.052	-94.876	0.997	-4.705
Fixed Voltage (node Lake)	0.021	-136.166	1.006	-4.249
Fixed P and Q injections	0.051	-84.250	1.089	-4.206
All constraints deactivated	0.013	-94.080	1.098	-3.738

7.8 Effect of the UPFC Initial Conditions

The impact of good UPFC initial conditions on convergence is shown by using different V_{cR} and θ_{cR} values. Bad initial conditions may degrade the convergence, or cause the solution to oscillate or even diverge.

The original standard AEP 14-node system has been modified and used to show the effect of the initial conditions for UPFC upgraded networks [8]. This FACTS device was connected in series with the transmission line connecting nodes Nod_5 and Nod_4. The node Nod_5UPFC was created as shown in Figure 7.12. The UPFC is used to maintain active power at 40 MW and reactive power at -2.5 MVAR leaving Nod_5UPFC towards Nod_4. The transformer parameters and voltage sources limits are identical to those given for the 5-node test system. In order to carry out this test, 6 cases were taken into account. The first one was carried out with initial conditions given by equations (7.61)-(7.65) (base case). Two subsequent solutions were carried out with decrements of 40% and 20% in the initial conditions of the base case. Another three solutions were tested with increments of 20%, 40% and 60% with respect to the base case. These cases are shown in Table 7.5. For all cases, the algorithm converged at the same active power generation cost and network losses, i.e. 215.6 $/hour and 2.010 MW, respectively.

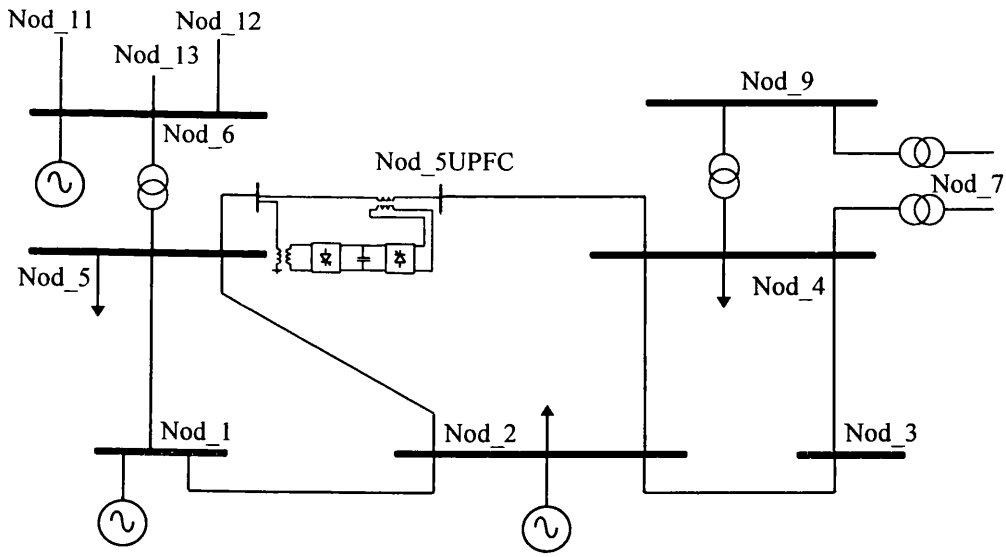

Figure 7.12. AEP 14-node system upgraded with a UPFC.

Figures 7.13 and 7.14 depict the series source voltage magnitudes and angles at each iteration of the solution process. It can be seen in both figures that the two variables display slight oscillations at the beginning of the iterative solution for each different initial condition. However, all the cases converged towards the same value at the beginning of iteration number one. Thereafter, the two variables followed the same

convergence patterns. As observed, the initial conditions do not degrade Newton's method convergence.

Table 7.5. Initial conditions for voltage sources.

Case	Series source	
	V_{cR} (pu)	θ_{cR} (degrees)
40 % of decrement	0.024	-51.852
20 % of decrement	0.032	-69.136
Initial conditions given by (7.61)-(7.65)	0.040	-86.420
20 % of increment	0.048	-103.704
40 % of increment	0.056	-120.988
60 % of increment	0.064	-138..272

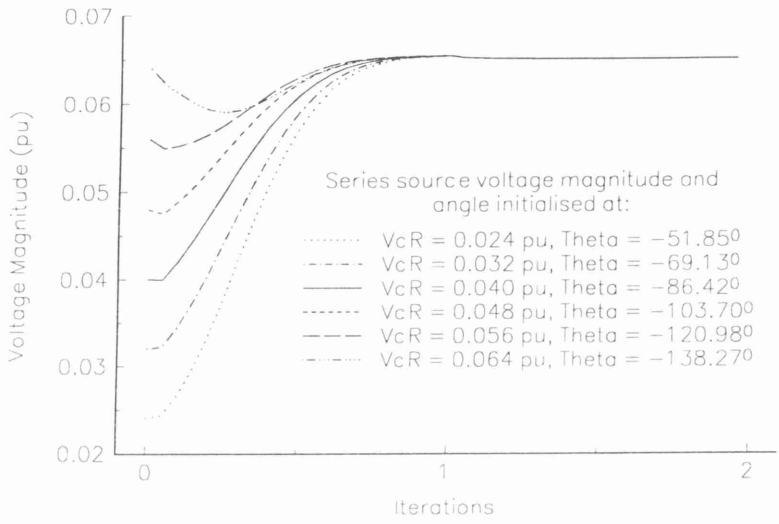

Figure 7.13. Series source voltage magnitude profiles as a function of the iteration number for normal UPFC mode.

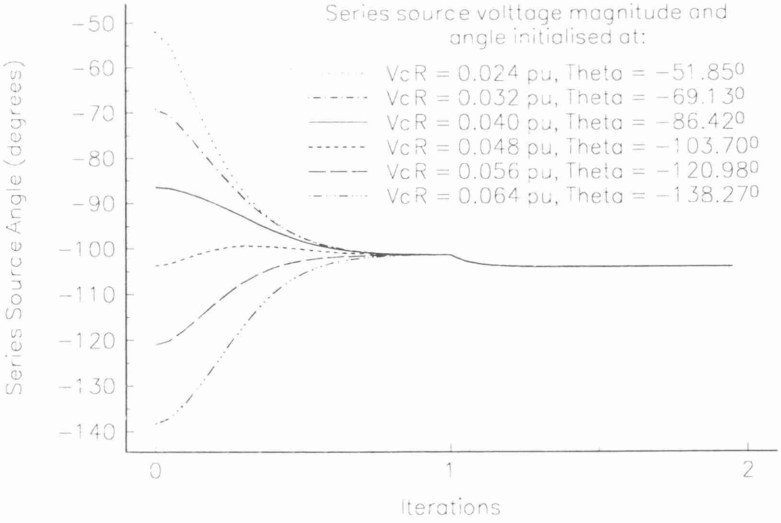

Figure 7.14. Series source voltage angle profiles as a function of the iteration number for normal UPFC mode.

An additional test case is presented in order to show the impact of UPFC initial conditions on convergence by freeing all 3 constraints. The initial condition for the series voltage source has been taken from the 14-node system assuming that the UPFC

was not incorporated in the test network. Under these conditions, the power flows across transmission line Nod_5-Nod_4 were 26.892 MW and -10.35 MVAR. The values of V_{cR} and θ_{cR} calculated with these values are shown in Table 7.6. Five additional simulations were carried out which are similar to those presented above.

Table 7.6. Initial conditions for voltage sources.

Case	Series source	
	V_{cR} (pu)	θ_{cR} (degrees)
40 % of decrement	0.017	-41.360
20 % of decrement	0.023	-55.152
Initial conditions given by (7.61)-(7.65)	0.028	-68.948
20 % of increment	0.034	-82.737
40 % of increment	0.040	-96.516
60 % of increment	0.046	-110.304

The number of iterations taken by the algorithm to converge was 5. This case gives a minimum cost solution whereas the case presented above gives the most expensive solution. The active power generation cost was reduced by 0.281 $/hour and the active power losses were reduced by 10.42% with respect to the case presented above. Figures 7.15 and 7.16 show the series source voltage magnitudes and angles at each iteration of the solution process. It can be observed that the magnitude of the voltage source is not as sensitive as the angle to changes in the set of active constraints and, as a consequence, to changes in the penalty weighting factors. The pattern of convergence for the angle of the voltage source is irregular in iterations 1 and 2. This is due to the voltage magnitude at Nod_7 violating its upper limit; furthermore, at the end of iteration number 2, Nod_5UPFC also violated its upper limit. However, the OPF algorithm enforced the offending variables by using the Multipliers method. After all the inequality constraints have been satisfied, the convergence pattern becomes smoother. A few additional iterations may then be required to satisfy the very stringent convergence criterion.

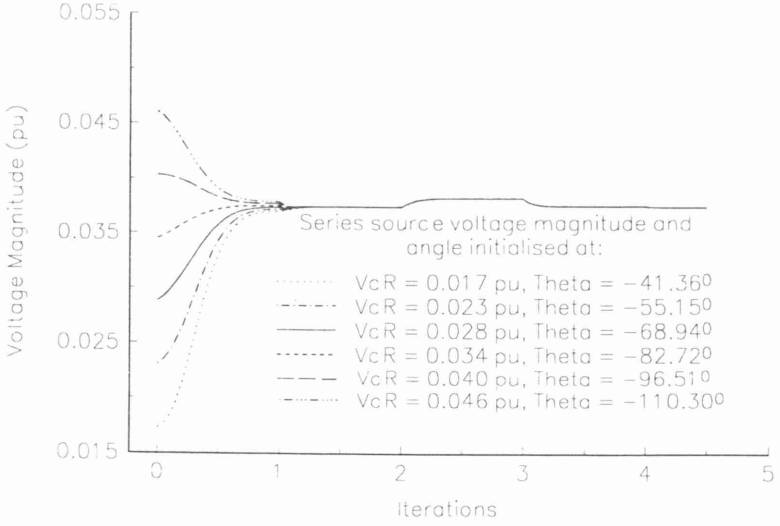

Figure 7.15. Series source voltage magnitude profiles as a function of the iteration number for all constraints deactivated.

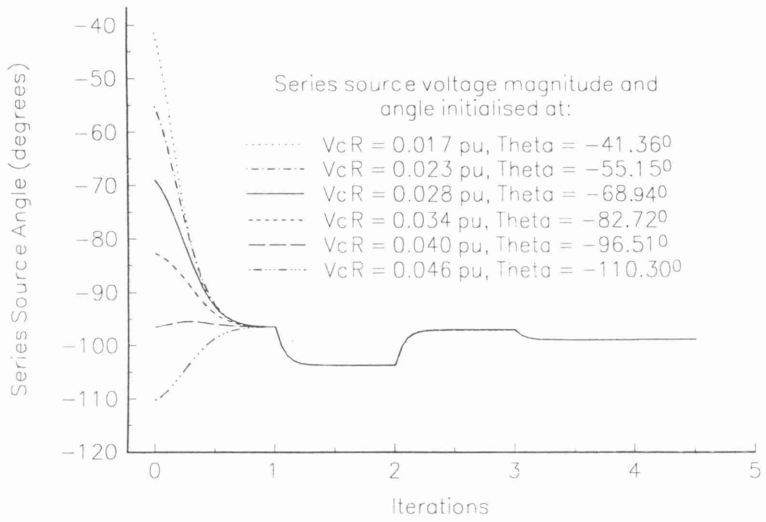

Figure 7.16. Series source voltage angle profiles as a function of the iteration number for all constraints deactivated.

7.9 Power Flow Control by Means of UPFC in a Real Power System

The minimum cost solution for the 166-node test system [9] was carried out in order to show the full capabilities of the generalised UPFC model. A critical part of the network is shown in Figure 7.17 where 3 UPFCs have been used. The active power transfer capability of the transmission lines ROH-RUM, AEH-CSH and PAH-TJH were increased by 10% with respect to the active power flow when the network has not been upgraded, and the reactive power is maintained at the original value. This new configuration of the network is shown in Figure 7.17. The UPFC initial conditions were calculated by using the equations given in Section 7.5.6.

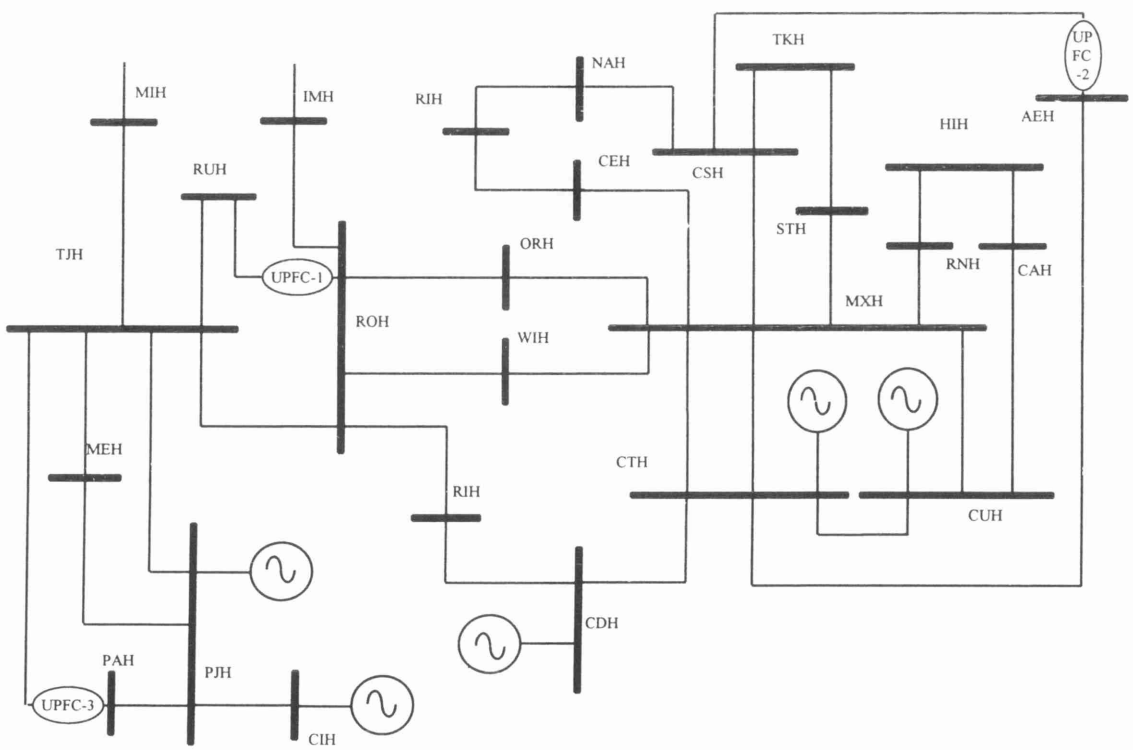

Figure 7.17. Relevant part of the 166-node test system upgraded with 3 UPFCs.

The solution was obtained in 5 iterations. Table 7.7 shows the final UPFC parameters. Figure 7.18 depicts the active power generation cost profile where it can be observed that the optimal solution for the modified and unmodified cases are almost the same. It is interesting to note that the UPFC has been used to introduce a significant change in the network operating conditions without affecting adversely the overall economic performance of the network.

Table 7.7. UPFCs parameters for the 166-node test system.

Device	Series source		Shunt source	
	V_{cR} (pu)	θ_{cR} (degrees)	V_{vR} (pu)	θ_{vR} (degrees)
UPFC-1	0.180	-126.709	1.008	-3.060
UPFC-2	0.132	-111.578	1.012	-1.944
UPFC-3	0.076	-124.137	1.011	-3.212

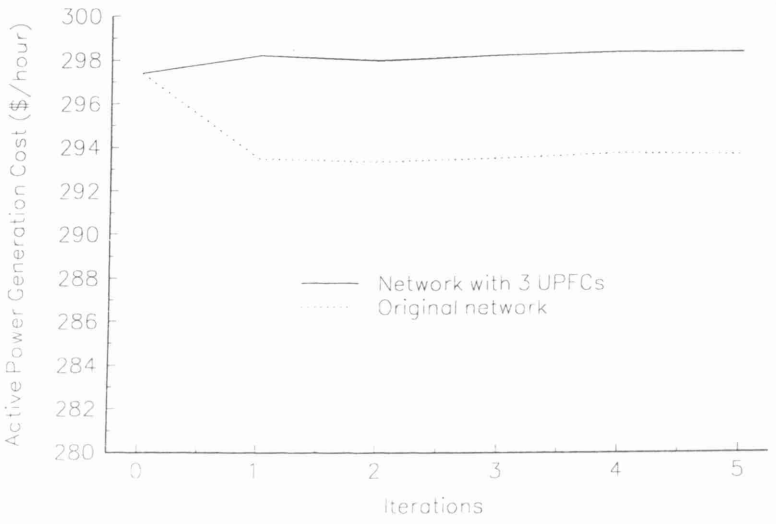

Figure 7.18. Active power generation cost profiles corresponding to the 166-node test system and the upgraded 166-node test system with 3 UPFCs.

7.10 Conclusions

A comprehensive UPFC model intended for OPF studies has been derived and implemented in a computer program. Newton's method has been used to solve the non-linear set of equations and the algorithm exhibits very strong convergence characteristics. Its prowess has been shown by numeric example. Both standard and non-standard test networks, containing UPFCs, have been used to verify accuracy and efficiency.

In this Chapter results pertaining to three networks have been presented. These networks have been suitably modified to include UPFCs in one or more locations in order to test the capabilities of the UPFC model. The UPFC model itself showed to be very flexible, it takes into account the various UPFC operating modes as well as its interaction with the network and other controllable plant components. Flexibility has been achieved without affecting adversely the efficiency of the solution. In general, the solution of networks containing no UPFCs and upgraded ones have been achieved in the same number of iterations. An alternative, more restrictive, UPFC model based on the concept of PV-PQ nodes has also been implemented in the OPF program and, where applicable, solutions given by the two UPFC models have been compared. However, this model will only work properly if one wishes to exert simultaneous control of nodal

voltage magnitude at node s, active power flowing from nodes r to s and reactive power injected at node r.

The effect of the UPFC initial conditions on convergence was studied. Improper selection of the initial condition may degrade the convergence, or more seriously, cause the solution to diverge. Extensive computational testing has shown that the OPF algorithm is robust and is not affected greatly by the initial conditions. However, it is advisable to initialise the iterative solution by the conditions presented in this Chapter.

7.11 References

[1] IEEE/CIGRE: 'FACTS Overview', Special Issue, 95TP108, IEEE Service Center, Piscataway, N.J., 1995.

[2] Gyugyi L.: 'A Unified Power Flow Control Concept for Flexible AC Transmission System', IEE Proceedings-C, Vol. 139, No. 4, July 1992, pp. 323-333.

[3] Noroozian M., Ängquist L., Ghandhari M. and Anderson G.; 'Use of UPFC for Optimal Power Flow Control', IEEE/KTH Stockholm Power Tech Conference, Stockholm, Sweden, June 18-22, 1995, pp. 506-511.

[4] Nabavi-Niaki A. and Iravani M.R.: 'Steady-State and Dynamic Models of Unified Power Flow Controller (UPFC) for Power System Studies', presented at 1996 IEEE/PES Winter Meeting, 96 WM 257-6 PWRS, January 21-25, 1996, Baltimore, MD.

[5] Fuerte-Esquivel C.R., Acha E.: 'The Unified Power Flow Controller: A Critical Comparison of Newton-Raphson UPFC Algorithms in Power Flow Studies', IEE Proceedings Generation Transmission and Distribution, Vol. 144, No. 5, September 1997, pp. 437-444.

[6] Sun D.I., Ashley B., Brewer B., Hughes A. and Tinney W.F.: 'Optimal Power Flow By Newton Approach', IEEE Transactions on Power Apparatus and Systems, Vol. PAS-103, No. 10, October 1984, pp. 2864-2880.

[7] Sun D.I., Hu T.I., Lin G.S., Lin C.J. and Chen C.H.: 'Experiences with Implementing Optimal Power Flow for Reactive Scheduling in the Taiwan Power System', IEEE Transactions on Power Systems, Vol. 3, No. 3, August 1988, pp. 1193-1200.

[8] Freris L.L. and Sasson A.M.: 'Investigation of the Load-Flow Problem', Proceedings of IEE, Vol. 115, No. 10, October 1968, pp. 1459-1270.

[9] Aboytes F. and Arroyo G.: 'Security Assessment in the Operation of Longitudinal Power Systems', IEEE Transactions on Power Apparatus and Systems, Vol. PWRS-1, No. 2, May 1986, pp. 225-232.

[10] Luenberger D.G.: 'Introduction to Linear and Nonlinear Programming', Addison-Wesley Publishing Co., Second Edition, 1984.

[11] Bertsekas D.P.: 'Constrained Optimization Lagrange Multiplier Methods', Academic Press, 1992.

[12] Wollenberg B. and Wood A. J.: 'Power Generation, Operation and Control', John Wiley & Sons Inc., Second Edition, 1984.

[13] Stagg G.W. and El-Abiad A.H.: 'Computer Methods in Power System Analysis', McGraw-Hill, 1968.

Chapter 8

High Voltage Direct Current Modelling in Optimal Power Flows

Two-terminal high-voltage direct current (HVDC) transmission links are in operation throughout the world. They are key elements in electrical power networks; their representation is oversimplified or ignored in most power system studies. This is particularly the case in OPF studies. Hence, the OPF has been extended to incorporate HVDC links, taking due account of overlapping and power transfer control characteristics. This is a new development in Newton Optimal Power Flows, where the converter equations are included directly in the matrix *W*. The method is indeed a unified one since the solution vector is extended to accommodate the DC variables. The HVDC link model correctly takes into account the relevant DC limit variables. The impact of HVDC links on Optimal Power Flow studies is illustrated by numeric examples, which includes a 5-node system, the AEP 14-node and a 166-node systems. Also, a real life 2172-node network is used to show the full capability of the algorithm.

8.1 Introduction

High Voltage Direct Current (HVDC) transmission constitutes a key application of the power electronics technology to electrical power networks. The economics of bulk power transmission by underground means is increasingly moving in favour of direct current. The HVDC links have the ability to exert instantaneous power control in neighbouring AC systems. Great many research efforts have been directed towards realising HVDC models for stability studies and power flows [1-10]. However, HVDC models for OPF studies have received limited attention and are underdeveloped [11,12]. De Martinis et al have developed a HVDC model but the solution algorithm is a sequential gradient restoration algorithm [11]. Lu at al also developed a HVDC model, which was incorporated in an sequential quadratic programming techniques [12]. These methods suffer from using a 'soft' solution methods, i.e. Newton's method is more robust. To circumvent these problem, the author of this thesis proposes a simultaneous solution in which the DC equations are combined with the AC equations in a single frame-of-reference for a unified iterative solution using Newton's method. In this Chapter, equations for the two-terminal HVDC link are developed and implemented in an OPF using Newton's method. The basic model of the HVDC link is based on the

formulation given in [13,18]. However, the incorporation of DC equations in the matrix W is a new development which leads to robust OPF solutions.

For the case of monopolar DC-links, 7 DC equations are involved for the DC side of the link. Limits on the DC control variables are checked and enforced during the iterative process because it has been found that these variables have a significant impact on active power generation costs. Numeric examples are presented to show the effectiveness of the proposed technique and to illustrate its features.

8.2 HVDC Configurations

The most common arguments put forward by the supporters of the HVDC technology are [18,19]:

- To transmit large blocks of energy, particularly in undersea transmission applications. In a long AC cable system, the cable capacitance will limit the maximum possible transmission distance. There is no such limitation in a DC cable system.
- To reduce active power losses. For the same power capacity, a HVDC has lower transmission losses than an AC transmission systems, even when converter losses are taken into account.
- To connect systems with different operational frequencies. There are HVDC links connecting networks with different nominal frequencies. Sometimes, HVDC links are used to connect systems which would be impossible to connect otherwise, e.g. due to stability problems.
- To control all DC parameters and neighbouring AC parameters with sufficient accuracy and speed of response. They can be used to exert constant power transfer and to redistribute power flow in the AC network. Also, owing to their fast speed of response, damping of power swings are also possible.
- To lower short circuit currents. HVDC transmission systems do not contribute to short circuit current to the AC system.

The three kinds of HVDC transmission schemes most currently favoured are [18,19]:

- Point to point HVDC transmission. This type of transmission uses overhead lines or submarine cables to connect the converter stations. Generally, the ground is used as a return path for the current. The highest voltage used today in DC transmission is 600 KV, and for submarine transmission is 450 KV.
- Back to back stations. In this kind of installation, the two converters are located in the same station and are used to connect two asynchronous AC systems.
- Multi-terminal system. This transmission system consists of more than two converter stations.

8.3 HVDC Link Steady State Model

The steady state analysis of the HVDC converters is significantly simplified if the following assumptions are made [18]:

- The AC source delivers, at the converter terminals, a sinusoidal voltage waveform with constant amplitude and frequency. Moreover, three phase voltages and currents are balanced.

- All harmonic voltages and currents produced by the converter are filtered out and are not passed on to the AC system.
- The converter transformers have no resistance and no magnetising impedance.
- The converter has no active power loss since the valves are ideal with no arc voltage drop.
- The DC voltage and current have no ripple.
- In a 6 pulse converter, the valves fire at 60° intervals. In a np-pulse converter the interval is $2\pi/np$.

A schematic representation of a HVDC link is shown in Figure 8.1 which consists of two converter stations and a DC transmission line. The converter stations perform the AC/DC/AC conversion process, and consist of valve bridges and LTC transformers. The thyristors switch each phase of the AC three phase system at the appropriate point of the voltage cycle to produce a direct current. The HVDC link uses one conductor if the ground is used as a return path. In submarine transmission the water is used as a return path. A metallic return is used only where the earth resistance is too high. The basic equations describing the two-terminal HVDC link are summarised as follows [13,18],

$$V_{dR} = \frac{3\sqrt{2}}{\pi} np_R a_R V_{tR} \cos\alpha_R - \frac{3}{\pi} X_{CR} np_R I_d \tag{8.1}$$

$$V_{dI} = \frac{3\sqrt{2}}{\pi} np_I a_I V_{tI} \cos\alpha_I - \frac{3}{\pi} X_{CI} np_I I_d \tag{8.2}$$

$$P_{dR} = V_{dR} I_d \tag{8.3}$$

$$P_{dI} = V_{dI} I_d \tag{8.4}$$

$$S_{dR} = k \frac{3\sqrt{2}}{\pi} a_R V_{tR} np_R I_d \tag{8.5}$$

$$S_{dI} = k \frac{3\sqrt{2}}{\pi} a_I V_{tI} np_I I_d \tag{8.6}$$

$$Q_{dR} = \sqrt{S_{dR}^2 - P_{dR}^2} \tag{8.7}$$

$$Q_{dI} = \sqrt{S_{dI}^2 - P_{dR}^2} \tag{8.8}$$

where k is given by [18]

$$k = \frac{\sqrt{\left[\cos 2\alpha - \cos 2(\alpha+\mu)\right]^2 + \left[2\mu + \sin 2\alpha - \sin 2(\alpha+\mu)\right]^2}}{4\left[\cos\alpha - \cos(\alpha+\mu)\right]} \tag{8.9}$$

for overlap values not exceeding 60°.

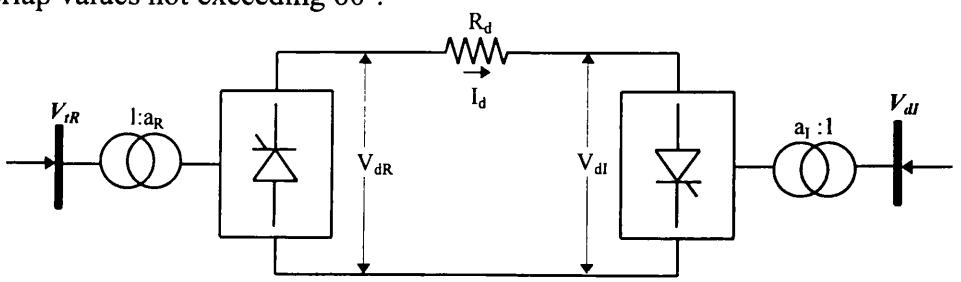

Figure 8.1. High Voltage DC Transmission.

V_{dR} and V_{dI} are the DC voltage magnitudes at the terminals of the rectifier and inverter stations, respectively. np_R and np_I are the numbers of series connected bridges in the rectifier and inverter, respectively. α_R and α_I are the control angles in the rectifier and inverter, respectively. X_{CR} and X_{CI} are the commutation resistances in the rectifier and inverter, respectively. V_{tR} and V_{tI} are the effective voltage magnitudes (line to line) at the AC terminals of the rectifier and inverter, respectively. I_d is the direct current.

In equation (8.9), α can be either α_R or α_I. If the commutation overlap is not taken into account, $\mu=0$ and $k=1$.

An increase in α_R leads to a reduction in DC voltage due to the term $\cos\alpha_R$. It also leads to an increase in the reactive power consumption since the current will lag the voltage. This is illustrated in Figures 8.2(a) and 8.3(a) where an idealised DC current I_d is shown. The fundamental current phasor I_{al} of I_d is shown in Figures 8.2(b) and 8.3(b) together with the voltage phasor E_a representing the line-neutral voltage.

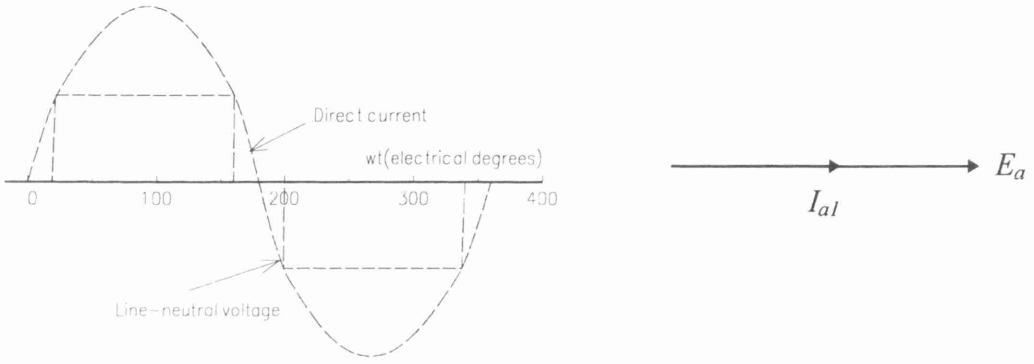

(a) (b)

Figure 8.2. Relation between ignition angle ($\alpha_R=0^0$) and phase displacements.

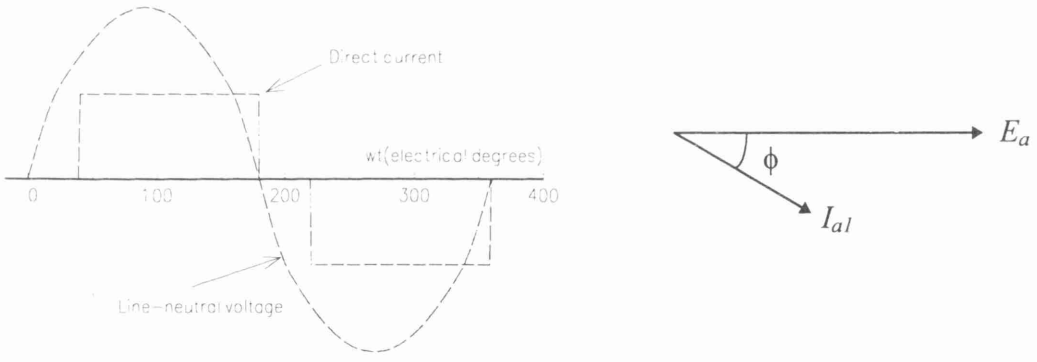

(a) (b)

Figure 8.3. Relation between ignition angle ($\alpha_R=30^0$) and phase displacements.

When the fundamental current I_{al} is in phase with the voltage E_a, $\phi = \alpha_R = 0$, the active power is maximum and the reactive power is null. An increase in α_R produces a decrease in active power and an increase in reactive power. Usually, the reactive power required by a converter station is 50% of the active power transmitted across the link [19].

During the rectification process, the phase currents cannot change instantly. The transfer of current from one phase to another requires a finite time which is called commutation time or overlap time. The result of this is a short-circuit of short duration between the

two commuting thyristors leading to a temporary voltage reduction. This effect does not explicitly appear in the set of equations presented above, but for the rectifier is given as,

$$\Delta V_d = \frac{3}{\pi} X_{CR}\, np_R I_d \tag{8.10}$$

A similar effect and representation exists for the inverter station.

One additional equation is required in the formulation, which is given by the DC system configuration. For the monopolar DC-link shown in Figure 8.1, the equation is,

$$V_{dR} = V_{dI} + R_d I_d \tag{8.11}$$

where R_d is the DC resistance.

8.4 HVDC Link-OPF Formulation

The mathematical formulation consists of minimising the active power generation cost in the power system by adjusting suitable controllable parameters. The HVDC-OPF problem can be formulated as follows [14,15,20]:

$$\begin{aligned} &\textbf{\textit{Minimise}} \quad f(P_g) \\ &\textbf{\textit{Subject to}} \quad h(P_g, V, \theta, \mathrm{V}, \mathrm{a}, \alpha, \mathrm{I}) = 0 \\ &\textbf{\textit{and}} \qquad\quad g(P_g, V, \theta, \mathrm{V}, \mathrm{a}, \alpha, \mathrm{I}) \le 0 \end{aligned} \tag{8.12}$$

where P_g, V, and θ are the active power generations, voltage magnitudes and phase angles, respectively. V, a, α and I are the DC state variables involved in the HVDC link model. $f(P_g)$ is the objective function to be optimised, $h(P_g, V, \theta, \mathrm{V}, \mathrm{a}, \alpha, \mathrm{I})$ represents the power flow equations in the DC side and $g(P_g, V, \theta, \mathrm{V}, \mathrm{a}, \alpha, \mathrm{I})$ represents state variable limits as well as functional operating constraints.

The constrained optimisation problem is converted to an unconstrained optimisation problem by constructing a Lagrangian function corresponding to equation (8.12). This is given as,

$$L(\boldsymbol{x}, \lambda) = f(P_g) + \lambda^t h(P_g, V, \theta, \mathrm{V}, \mathrm{a}, \alpha, \mathrm{I}) \tag{8.13}$$

where $\boldsymbol{x}$ is a vector of state variables and λ is the Lagrange multiplier vector for equality constraints. The inequality constraints are not shown because they are only included when there are variables outside limits.

8.4.1 HVDC link Lagrangian Function

The incorporation of the HVDC link equations in a Newton OPF algorithm requires that for each HVDC link present in the network, the matrix $\boldsymbol{W}$ be augmented by eight rows and eight columns. If the HVDC system is controlling active power flow, then the dimensions of matrix $\boldsymbol{W}$ are further augmented by one row and one column. Under this operating condition six extra state variables enter in the OPF formulation. Furthermore, three Lagrange multipliers are also used to incorporate the various equality constraints. The solution process satisfies the optimality conditions as given by Kuhn and Tucker [20].

The equations (8.1)-(8.8) and (8.11) are explicitly modelled in the Lagrangian function as an equality constraint given by the following equation:

$$\begin{aligned} L_{\mathrm{RI}}(\boldsymbol{x},\lambda) = {} & \lambda_{\mathrm{R}}\left(\mathrm{V_{dR}} - \frac{3\sqrt{2}}{\pi}\mathrm{np_R}\,\mathrm{a_R}V_{tR}\cos\alpha_{\mathrm{R}} + \frac{3}{\pi}\mathrm{X_{CR}}\,\mathrm{np_R}\,\frac{\mathrm{V_{dR}}-\mathrm{V_{dI}}}{\mathrm{R_d}}\right) \\ & + \lambda_{\mathrm{I}}\left(\mathrm{V_{dI}} - \frac{3\sqrt{2}}{\pi}\mathrm{np_I}\,\mathrm{a_I}V_{tI}\cos\alpha_{\mathrm{I}} + \frac{3}{\pi}\mathrm{X_{CI}}\,\mathrm{np_I}\,\frac{\mathrm{V_{dR}}-\mathrm{V_{dI}}}{\mathrm{R_d}}\right) \\ & + \lambda_{pR}(\mathrm{P_{dR}}) + \lambda_{qR}(\mathrm{Q_{dR}}) + \lambda_{pI}(-\mathrm{P_{dI}}) + \lambda_{qI}(\mathrm{Q_{dI}}) \end{aligned} \tag{8.14}$$

where λ_{R}, λ_{I}, $\lambda_{p\mathrm{R}}$, $\lambda_{q\mathrm{R}}$, $\lambda_{p\mathrm{I}}$, and $\lambda_{q\mathrm{I}}$ are Lagrange multipliers at the nodes where the rectifier and inverter stations are connected, respectively. It should be noted that $\lambda_{p\mathrm{R}}$, $\lambda_{q\mathrm{R}}$, $\lambda_{p\mathrm{I}}$, and $\lambda_{q\mathrm{I}}$ are the Lagrange multipliers corresponding to the Lagrangian function of the power flow mismatch equations as shown in Section 2.3. Vector $\boldsymbol{x}$ contains the following set of DC variables:

$$\boldsymbol{x} = \left[\begin{array}{ccc:ccc} \mathrm{V_{dR}} & \mathrm{a_R} & \cos\alpha_{\mathrm{R}} & \mathrm{V_{dI}} & \mathrm{a_I} & \cos\alpha_{\mathrm{I}} \end{array}\right]^t \tag{8.15}$$

$$\lambda = \left[\begin{array}{cc} \lambda_{\mathrm{R}} & \lambda_{\mathrm{I}} \end{array}\right]^t \tag{8.16}$$

where the superscript t indicates transposition.

8.4.2 DC Link Loading

The HVDC link variables are handled in the OPF solution in very much the same manner as AC variables. The DC link only has resistance and hence the DC voltage has no phase angle. The condition in which the DC line current is regulated may be represented in OPF formulations by using an equality constraint which remains active throughout the iterative process, unless one wishes to deactivate this constraint. The following equation represents this operating condition:

$$L_{\mathrm{dc}}(\boldsymbol{x},\lambda) = \lambda_{\mathrm{RI}}\left(\frac{\mathrm{V_{dR}}-\mathrm{V_{dI}}}{\mathrm{R_d}} - \mathrm{I_{specified}}\right) \tag{8.17}$$

where λ_{RI} is the Lagrange multiplier associated with the direct current flowing from the rectifier station to the inverter station. $\mathrm{I_{specified}}$ is the target value of direct current to be maintained across the link.

The HVDC link Lagrange function encompassing the individual contributions presented above is,

$$L_{hvdc}(\boldsymbol{x},\lambda) = L_{\mathrm{RI}}(\boldsymbol{x},\lambda) + L_{\mathrm{dc}}(\boldsymbol{x},\lambda) \tag{8.18}$$

8.4.3 Linearised System of Equations

The linearised system of equations for minimising the Lagrangian function using Newton's method is,

$$\boldsymbol{W}\Delta\mathbf{z} = -\boldsymbol{g} \tag{8.19}$$

where $\boldsymbol{W}$ contains second partial derivatives of the Lagrangian function $L(\boldsymbol{x}, \lambda)$ with respect to state variables $\boldsymbol{x}$ and Lagrange multiplier λ. The vector $\boldsymbol{g}$ consists of first partial derivative terms. $\Delta \mathbf{z}$ is the vector of increments obtained at the end of an iteration.

A more expanded version of the equation (8.19) applied to the Lagrangian function of the HVDC link, is given below,

$$\begin{bmatrix} \boldsymbol{W}_{11} & 0 & \boldsymbol{W}_{13} & \boldsymbol{W}_{14} & 0 \\ 0 & \boldsymbol{W}_{23} & \boldsymbol{W}_{24} & \boldsymbol{W}_{25} & 0 \\ \boldsymbol{W}_{31} & \boldsymbol{W}_{32} & \boldsymbol{W}_{33} & \boldsymbol{W}_{34} & \boldsymbol{W}_{35} \\ \boldsymbol{W}_{41} & \boldsymbol{W}_{42} & \boldsymbol{W}_{43} & \boldsymbol{W}_{44} & \boldsymbol{W}_{45} \\ 0 & 0 & \boldsymbol{W}_{53} & \boldsymbol{W}_{54} & 0 \end{bmatrix} \begin{bmatrix} \Delta \mathbf{z}_1 \\ \Delta \mathbf{z}_2 \\ \Delta \mathbf{z}_3 \\ \Delta \mathbf{z}_4 \\ \Delta \mathbf{z}_5 \end{bmatrix} = \begin{bmatrix} -\boldsymbol{g}_1 \\ -\boldsymbol{g}_2 \\ -\boldsymbol{g}_3 \\ -\boldsymbol{g}_4 \\ -\boldsymbol{g}_5 \end{bmatrix} \tag{8.20}$$

where

$$\boldsymbol{W}_{11} = \begin{bmatrix} 0 & 0 & 0 & 0 \\ 0 & \dfrac{\partial^2 L}{\partial V_{tR}^2} & 0 & \dfrac{\partial \mathrm{Q_{dR}}}{\partial V_{tR}} \\ 0 & 0 & 0 & 0 \\ 0 & \dfrac{\partial \mathrm{Q_{dR}}}{\partial V_{tR}} & 0 & 0 \end{bmatrix} \tag{8.21}$$

$$\boldsymbol{W}_{13} = \boldsymbol{W}_{31}^{t} = \begin{bmatrix} 0 & 0 & 0 & 0 \\ \dfrac{\partial^2 L}{\partial V_{tR} \partial \mathrm{V_{dR}}} & \dfrac{\partial^2 L}{\partial V_{tR} \partial \mathrm{a_R}} & \dfrac{\partial^2 L}{\partial V_{tR} \partial \cos\alpha_{\mathrm{R}}} & \dfrac{\partial \mathrm{R_I}}{\partial V_{tR}} \\ \dfrac{\partial \mathrm{P_{dR}}}{\partial \mathrm{V_{dR}}} & 0 & 0 & 0 \\ \dfrac{\partial \mathrm{Q_{dR}}}{\partial \mathrm{V_{dR}}} & \dfrac{\partial \mathrm{Q_{dR}}}{\partial \mathrm{a_R}} & 0 & 0 \end{bmatrix} \tag{8.22}$$

$$\boldsymbol{W}_{14} = \boldsymbol{W}_{41}^{t} = \begin{bmatrix} 0 & 0 & 0 & 0 \\ \dfrac{\partial^2 L}{\partial V_{tR} \partial \mathrm{V_{dI}}} & 0 & 0 & 0 \\ \dfrac{\partial \mathrm{P_{dR}}}{\partial \mathrm{V_{dI}}} & 0 & 0 & 0 \\ \dfrac{\partial \mathrm{Q_{dR}}}{\partial \mathrm{V_{dI}}} & 0 & 0 & 0 \end{bmatrix} \tag{8.23}$$

$$\boldsymbol{W}_{22} = \begin{bmatrix} 0 & 0 & 0 & 0 \\ 0 & \dfrac{\partial^2 L}{\partial V_{tI}^2} & 0 & \dfrac{\partial \mathrm{Q_{dI}}}{\partial V_{tI}} \\ 0 & 0 & 0 & 0 \\ 0 & \dfrac{\partial \mathrm{Q_{dI}}}{\partial V_{tI}^2} & 0 & 0 \end{bmatrix} \tag{8.24}$$

$$\boldsymbol{W}_{23} = \boldsymbol{W}_{32}^{t} = \begin{bmatrix} 0 & 0 & 0 & 0 \\ \dfrac{\partial^2 L}{\partial V_{tl}^2 \partial \mathrm{V_{dR}}} & 0 & 0 & 0 \\ \dfrac{\partial(-\mathrm{P_{dI}})}{\partial \mathrm{V_{dR}}} & 0 & 0 & 0 \\ \dfrac{\partial \mathrm{Q_{dI}}}{\partial \mathrm{V_{dR}}} & 0 & 0 & 0 \end{bmatrix} \tag{8.25}$$

$$\boldsymbol{W}_{24} = \boldsymbol{W}_{42}^{t} = \begin{bmatrix} 0 & 0 & 0 & 0 \\ \dfrac{\partial^2 L}{\partial V_{tl}^2 \partial \mathrm{V_{dI}}} & \dfrac{\partial^2 L}{\partial V_{tl}^2 \partial \mathrm{a_I}} & \dfrac{\partial^2 L}{\partial V_{tl}^2 \partial \cos\alpha_{\mathrm{I}}} & \dfrac{\partial \mathrm{R_2}}{\partial V_{tl}^2} \\ \dfrac{\partial(-\mathrm{P_{dI}})}{\partial \mathrm{V_{dI}}} & 0 & 0 & 0 \\ \dfrac{\partial \mathrm{Q_{dI}}}{\partial \mathrm{V_{dI}}} & \dfrac{\partial \mathrm{Q_{dI}}}{\partial \mathrm{a_I}} & 0 & 0 \end{bmatrix} \tag{8.26}$$

$$\boldsymbol{W}_{33} = \begin{bmatrix} \dfrac{\partial^2 L}{\partial \mathrm{V_{dR}^2}} & \dfrac{\partial^2 L}{\partial \mathrm{V_{dR}} \partial \mathrm{a_R}} & 0 & \dfrac{\partial \mathrm{R_1}}{\partial \mathrm{V_{dR}}} \\ \dfrac{\partial^2 L}{\partial \mathrm{a_R} \partial \mathrm{V_{dR}}} & \dfrac{\partial^2 L}{\partial \mathrm{a_R^2}} & \dfrac{\partial^2 L}{\partial \mathrm{a_R} \partial \cos\alpha_{\mathrm{R}}} & \dfrac{\partial \mathrm{R_1}}{\partial \mathrm{a_R}} \\ 0 & \dfrac{\partial^2 L}{\partial \cos\alpha_{\mathrm{R}} \partial \mathrm{a_R}} & 0 & \dfrac{\partial \mathrm{R_1}}{\partial \cos\alpha_{\mathrm{R}}} \\ \dfrac{\partial \mathrm{R_1}}{\partial \mathrm{V_{dR}}} & \dfrac{\partial \mathrm{R_1}}{\partial \mathrm{a_R}} & \dfrac{\partial \mathrm{R_1}}{\partial \cos\alpha_{\mathrm{R}}} & 0 \end{bmatrix} \tag{8.27}$$

$$\boldsymbol{W}_{34} = \boldsymbol{W}_{43}^{t} = \begin{bmatrix} \dfrac{\partial^2 L}{\partial \mathrm{V_{dR}} \partial \mathrm{V_{dI}}} & \dfrac{\partial^2 L}{\partial \mathrm{V_{dR}} \partial \mathrm{a_I}} & 0 & \dfrac{\partial \mathrm{R_2}}{\partial \mathrm{V_{dR}}} \\ \dfrac{\partial^2 L}{\partial \mathrm{a_R} \partial \mathrm{V_{dI}}} & 0 & 0 & 0 \\ 0 & 0 & 0 & 0 \\ \dfrac{\partial \mathrm{R_1}}{\partial \mathrm{V_{dI}}} & 0 & 0 & 0 \end{bmatrix} \tag{8.28}$$

$$\boldsymbol{W}_{53} = \boldsymbol{W}_{35}^{t} = \begin{bmatrix} \dfrac{\partial \mathrm{R_3}}{\partial \mathrm{V_{dR}}} & 0 & 0 & 0 \end{bmatrix} \tag{8.29}$$

$$\boldsymbol{W}_{44} = \begin{bmatrix} \dfrac{\partial^2 L}{\partial \mathrm{V_{dI}^2}} & \dfrac{\partial^2 L}{\partial \mathrm{V_{dI}} \partial \mathrm{a_I}} & 0 & \dfrac{\partial \mathrm{R_2}}{\partial \mathrm{V_{dI}}} \\ \dfrac{\partial^2 L}{\partial \mathrm{a_I} \partial \mathrm{V_{dI}}} & \dfrac{\partial^2 L}{\partial \mathrm{a_I^2}} & \dfrac{\partial^2 L}{\partial \mathrm{a_I} \partial \cos\alpha_{\mathrm{I}}} & \dfrac{\partial \mathrm{R_2}}{\partial \mathrm{a_I}} \\ 0 & \dfrac{\partial^2 L}{\partial \cos\alpha_{\mathrm{I}} \partial \mathrm{a_I}} & 0 & \dfrac{\partial \mathrm{R_2}}{\partial \cos\alpha_{\mathrm{I}}} \\ \dfrac{\partial \mathrm{R_2}}{\partial \mathrm{V_{dI}}} & \dfrac{\partial \mathrm{R_2}}{\partial \mathrm{a_I}} & \dfrac{\partial \mathrm{R_2}}{\partial \cos\alpha_{\mathrm{I}}} & 0 \end{bmatrix} \tag{8.30}$$

$$\boldsymbol{W}_{54} = \boldsymbol{W}_{45}^{t} = \begin{bmatrix} \dfrac{\partial \mathrm{R_3}}{\partial \mathrm{V_{dI}}} & 0 & 0 & 0 \end{bmatrix} \tag{8.31}$$

$$\boldsymbol{g}_1 = \left[0 \quad \frac{\partial^2 L}{\partial V_{tR}} \quad \mathrm{P_{dR}} \quad \mathrm{Q_{dR}} \right]^t \tag{8.32}$$

$$\boldsymbol{g}_2 = \left[0 \quad \frac{\partial^2 L}{\partial V_{tI}} \quad -\mathrm{P_{dI}} \quad \mathrm{Q_I} \right]^t \tag{8.33}$$

$$\boldsymbol{g}_3 = \left[\frac{\partial L}{\partial \mathrm{V_{dR}}} \quad \frac{\partial L}{\partial \mathrm{a_R}} \quad \frac{\partial L}{\partial \cos\alpha_{\mathrm{R}}} \quad \mathrm{R_1} \right]^t \tag{8.34}$$

$$\boldsymbol{g}_4 = \left[\frac{\partial L}{\partial \mathrm{V_{dI}}} \quad \frac{\partial L}{\partial \mathrm{a_I}} \quad \frac{\partial L}{\partial cos\alpha_{\mathrm{I}}} \quad R_2 \right]^t \tag{8.35}$$

$$\boldsymbol{g}_5 = \left[R_3 \right]^t \tag{8.36}$$

$$\Delta \mathbf{z}_1 = \left[0 \quad \Delta V_{tR} \quad \Delta\lambda_{pr} \quad \Delta\lambda_{qr} \right]^t \tag{8.37}$$

$$\Delta \mathbf{z}_2 = \left[0 \quad \Delta V_{tI} \quad \Delta\lambda_{pi} \quad \Delta\lambda_{qi} \right]^t \tag{8.38}$$

$$\Delta \mathbf{z}_3 = \left[\Delta \mathrm{V_{dR}} \quad \Delta \mathrm{a_R} \quad \Delta \cos\alpha_{\mathrm{R}} \quad \Delta\lambda_{\mathrm{R}} \right]^t \tag{8.39}$$

$$\Delta \mathbf{z}_4 = \left[\Delta \mathrm{V_{dI}} \quad \Delta \mathrm{a_I} \quad \Delta \cos\alpha_{\mathrm{I}} \quad \Delta\lambda_{\mathrm{I}} \right]^t \tag{8.40}$$

$$\Delta \mathbf{z}_5 = \left[\Delta\lambda_{\mathrm{RI}} \right]^t \tag{8.41}$$

where R_1, R_2 and R_3 are defined as

$$\mathrm{R_1} = \mathrm{V_{dR}} - \mathrm{k_1\, a_R} V_{tR} \cos\alpha_{\mathrm{R}} + \mathrm{k_2} \frac{\mathrm{V_{dR}} - \mathrm{V_{dI}}}{\mathrm{R_d}} = 0 \tag{8.42}$$

$$\mathrm{R_2} = \mathrm{V_{dI}} - \mathrm{k_3\, a_I} V_{tI} \cos\alpha_{\mathrm{I}} + \mathrm{k_4} \frac{\mathrm{V_{dR}} - \mathrm{V_{dI}}}{\mathrm{R_d}} = 0 \tag{8.43}$$

$$\mathrm{R_3} = \lambda_{\mathrm{RI}} \left(\frac{\mathrm{V_{dR}} - \mathrm{V_{dI}}}{\mathrm{R_d}} - \mathrm{I_{specified}} \right) \tag{8.44}$$

and $L_{hvdc}(\boldsymbol{x},\lambda)$ is substituted by $L(\boldsymbol{x}, \lambda)$.

First and second order derivative terms in equations (8.21)-(8.35) are given explicitly in Appendix V. It should be noted that the linearised system of equations presented above corresponds to the case where the HVDC link maintains direct current $\mathrm{I_d}$ at a specified value. The activation or deactivation of this constraint is carried out by removing or adding the second derivative term of a large quadratic penalty function factor to the diagonal element of matrix $\boldsymbol{W}$ corresponding to multiplier λ_{RI}.

8.4.4 Handling Limits of HVDC Link

Extensive testing of the HVDC-OPF algorithm has shown that limit violations in the iterative process occur rarely. However, for the few cases in which it is required, limits are enforced by means of the Multipliers method [21]. The generic function, given by equation (8.45) for V_{dR}, is used to handle the HVDC link inequality constraints, where a penalty term, involving the violated limit, is added to the Lagrangian function $L(\boldsymbol{x}, \lambda)$. Variables inside limits are ignored. The checking of limits is started at the second iteration.

$$\psi_i(V_{dR,i}^j, \mu_i^j) = \begin{cases} \mu_i^j (V_{dR,i}^j - V_{dR,i}^{max}) + \frac{c}{2}(V_{dR,i}^j - V_{dR,i}^{max})^2 & \text{if} \quad \mu_i^j + c(V_{dR,i}^j - V_{dR,i}^{max}) \geq 0 \\ \mu_i^j (V_{dR,i}^j - V_{dR,i}^{min}) + \frac{c}{2}(V_{dR,i}^j - V_{dR,i}^{min})^2 & \text{if} \quad \mu_i^j + c(V_{dR,i}^j - V_{dR,i}^{min}) \leq 0 \\ 0 \quad \text{otherwise} \end{cases} \tag{8.45}$$

8.4.5 HVDC Link Initial Conditions

Similarly to all the FACTS devices previously discussed in this work, good initial conditions are also required for the HVDC links to ensure smooth iterative solutions.

Nodal Voltage Magnitudes and Tap Positions

The nodal voltage magnitudes V_{tR} and V_{tI} are set at 1 pu, which lead to non-unity voltage values for V_{dR} and V_{dI}. These DC voltages are calculated by means of equations (8.1) and (8.2). The initial tap positions of the converter transformers are also set at 1.

Lagrange Multipliers

The HVDC Lagrange multiplier λ_R and λ_I are initialised at 0. These values have shown to yield robust iterative solutions.

Control Angles

A conventional rectifying terminal would typically have a value of α_R between 14^0 and 16^0, and as a minimum range 5^0-7^0. For the inverter, α_I is between 15^0 and 18^0 and maximum values will not exceed 22^0 [2]. In the OPF developed in this research, the initial conditions given to α_R and α_I are 15^0 and 18^0, respectively.

8.4.6 Practical Implementation

A key element of the algorithm which has demanded considerable attention is the implementation of the control modes in conventional power flow solutions. The OPF solution gives the best operative condition which satisfies equations (8.1)-(8.8). The algorithm selects the HVDC link control variables automatically [13]. However, one could easily change these variables to set values.

As pointed out above, if the initial conditions are not chosen carefully, the algorithm may run into difficulties due to large interchanges between active and reactive powers in the solution. It should be noted that no prioritisation of control modes in the HVDC link are required in the OPF algorithm in contrast to conventional load flow.

The implementation of limits checking required attention, even though no violations normally occur. They take place just after the third iteration, except for the AC voltage whose checking takes place from the first iteration. The control variables V_{dR}, a_R and α_R are affected if the voltage V_{tR} is binding. After the third iteration, four variables per node are checked if more than one variable violates its limits then, the first variable to be enforced is the variable with the largest violation. The following index is used [15]:

$$k_{vio} = \frac{\text{violation}}{\text{movement}} \tag{8.46}$$

where 'violation' is the amount by which the updated value of the inequality constraint violates its limit, and 'movement' is the updated amount given by the solution of (8.20). If these variables are released in subsequent iterations, the sequence is reversed with respect to the sequence of the binding but only one at a time.

8.5 HVDC Link Test Cases

The 5-node system [22] used in previous Chapters was modified to incorporate a HVDC link. The transmission line connected between nodes Lake and Main has been replaced with a HVDC link, as shown in Figure 8.4. The main characteristics, initial conditions and solution values of the HVDC link are given in Table 8.1 and 8.2. The algorithm was used to find the economic dispatch. The active power flow level across the HVDC link, is 13.716 MW. The solution was reached in 3 iterations. The power flow results are shown in Figure 8.4, and the active and reactive power at the converter stations are given in Table 8.3. The nodal voltages, active and reactive generated powers and Lagrange multipliers are given in Table 8.4.

Table 8.1. DC-Link characteristic

	Rectifier	Inverter
AC node	Lake	Main
Commutation reactance	0.01260	0.00728
DC-Link resistance	0.00334	

Table 8.2. DC-Link control parameters for the 5-node system.

DC Variable	Limits		Initial Condition	OPF Solution
	Min	Max		
V_{dR} (pu)	1.000	1.500	1.304	1.337
a_R	0.900	1.100	1.000	0.940
α_R (degrees)	10.000	20.000	15.000	10.839
V_{dI} (pu)	1.000	1.500	1.284	1.336
a_I	0.900	1.100	1.000	0.962
α_I (degrees)	15.000	25.000	18.000	16.735

Table 8.3. Power at the converters.

OPF Solution	P_{dR} (MW)	Q_{dR} (MVAR)	P_{dI} (MW)	Q_{dR} (MVAR)	I_d (pu)
DC Quantities	13.716	2.304	13.712	3.895	0.102

Table 8.4. Nodal complex voltages of modified network.

Node	Voltage Magnitude (pu)	Phase Angle (degrees)	Active Power (MW)	Reactive Power (MVAR)	λ_p ($/MWhr)
Elm	1.071	-4.447	0.000	0.000	4.2656
Main	1.075	-3.901	0.000	0.000	4.2378
Lake	1.071	-3.472	0.000	0.000	4.2225
South	1.100	-1.318	87.960	20.292	4.1036
North	1.109	0.000	80.135	3.150	4.0410

The active power generation cost for this test network is 748.156 $/hour and the active power losses in the AC network are 3.094 MW and in the HVDC link are 0.0035 MW.

In comparison with the results presented in Section 2.9.1, the following can be observed: A decrement in active power flow between node Lake and Main (i.e. a transmission line in Section 2.9.1 and HVDC link in this Section) is observed. Conversely, an increment in reactive power generated by the generators is also observed. This is due to the reactive power demanded by the rectification/inversion process of the converters. As a result of this, the active power generation cost is adversely affected due to an increase in network losses, owing to the generators having to inject the additional reactive power demanded by the power converters.

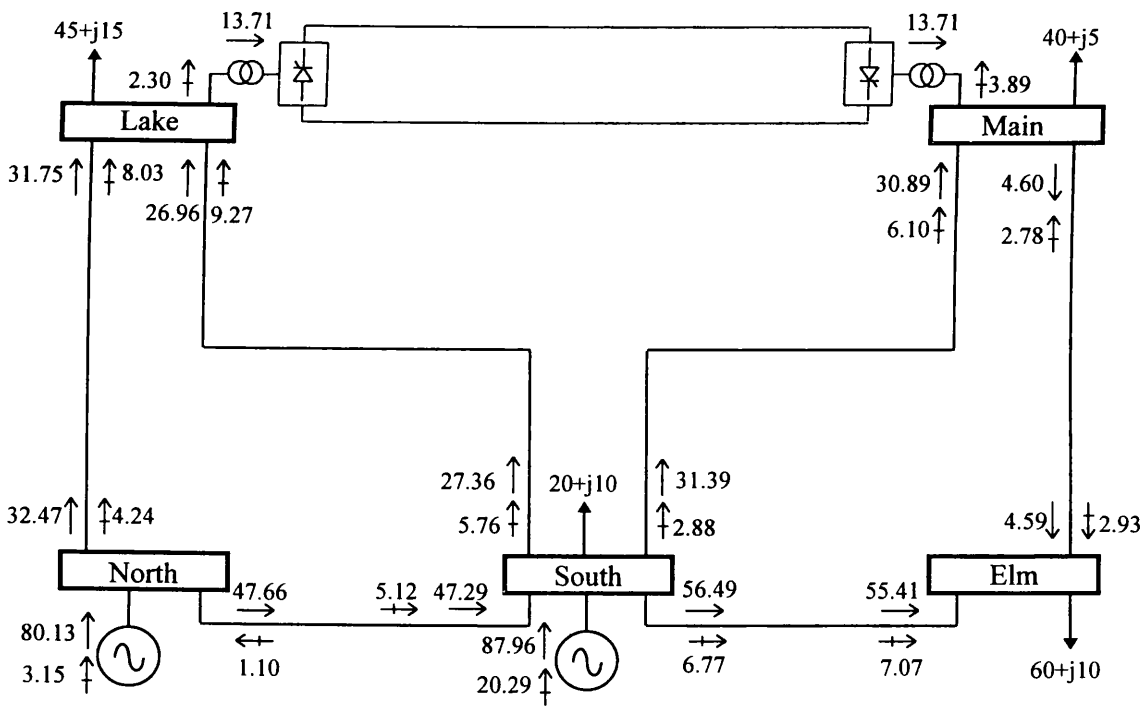

Figure 8.4. Modified 5-node system with a HVDC link and OPF solution.

A second test case was carried out in order to show the ability of the HVDC model to control active power across the HVDC links. The link is used to maintain the direct current leaving the rectifier (node Lake) at 0.15 pu. The HVDC link model upheld its target value. Convergence was obtained in 3 iterations. As expected, the generation cost and network losses increased, they are 748.451 $/hour and 3.168 MW, respectively. The losses in the HVDC link are 0.007 MW. It should be noted that the generation cost did not increase by much even though the power transfer across the HVDC link was increased. The reactive power generations showed the same behaviour, i.e. an increase

of 5.74 MW across the link required an additional generation of 4.675 MVAR. Table 8.5 and 8.6 summarise the results obtained for this case.

Table 8.5. Powers at the converters.

OPF Solution	P_{dR} (MW)	Q_{dR} (MVAR)	P_{dI} (MW)	Q_{dR} (MVAR)	I_d (pu)
DC Quantities	19.456	4.432	19.449	5.882	0.15

Table 8.6. Summary of load flow solution for 5-node system.

Results	OPF Solution
Active power generation Cost ($/hr)	748.451
Active power losses (MW)	3.168
Active power generation (MW)	168.168
Reactive power generation (MVAR)	28.116

8.6 Effect of the HVDC Link Initial Conditions

The impact of initial conditions on the HVDC-OPF algorithm link is addressed in this Section. It is shown that unsuitable initial conditions may cause the solution to diverge. The most common problem observed is that the active power could, under certain conditions, become larger than the apparent power, which leads to numeric problems when the reactive power consumed by the converters is calculated. This is clearly a numerical instability which is normally overcome by choosing good initial conditions.

The AEP 14-node system [16] has been modified to incorporate two HVDC links as shown in Figure 8.5. The transmission line between nodes Nod_5 and Nod_4 has been replaced by a HVDC-link. The transmission line connecting nodes Nod_2 and Nod_4 was replaced with a second HVDC link. The parameters of both links are the same as those given in Tables 8.1 and 8.2. Three different initial conditions were given to the variables of both HVDC links. For example, the tap, ignition and extinction angles for each link changed their initial values while the other HVDC link variables remained invariable at the beginning of the iterative solution. The first test was carried out with the initial conditions given in Section 8.4.5 which is to be taken as the reference case. Two additional studies were carried out with values of $\pm 5^0$ around the reference case. Both HVDC links were given the same initial values during these tests. In each case, solutions were obtained in 4 iterations. Table 8.7 shows the settings for the DC variables as given by the solution. Tables 8.8 and 8.9 provide additional information.

Table 8.7. DC-Link control parameters for the 14-node system.

OPF Solution	V_{dR} (pu)	a_R	α_R (degrees)	V_{dI} (pu)	a_I	α_I (degrees)
HVDC-1	1.301	0.997	14.022	1.300	1.001	17.374
HVDC-2	1.324	1.011	14.978	1.323	1.012	16.073

Table 8.8. Powers at the converters.

OPF Solution	P_{dR} (MW)	Q_{dR} (MVAR)	P_{dI} (MW)	Q_{dR} (MVAR)	I_d (pu)
HVDC-1	15.041	3.496	15.037	4.468	0.116
HVDC-2	42.334	10.964	42.300	11.648	0.320

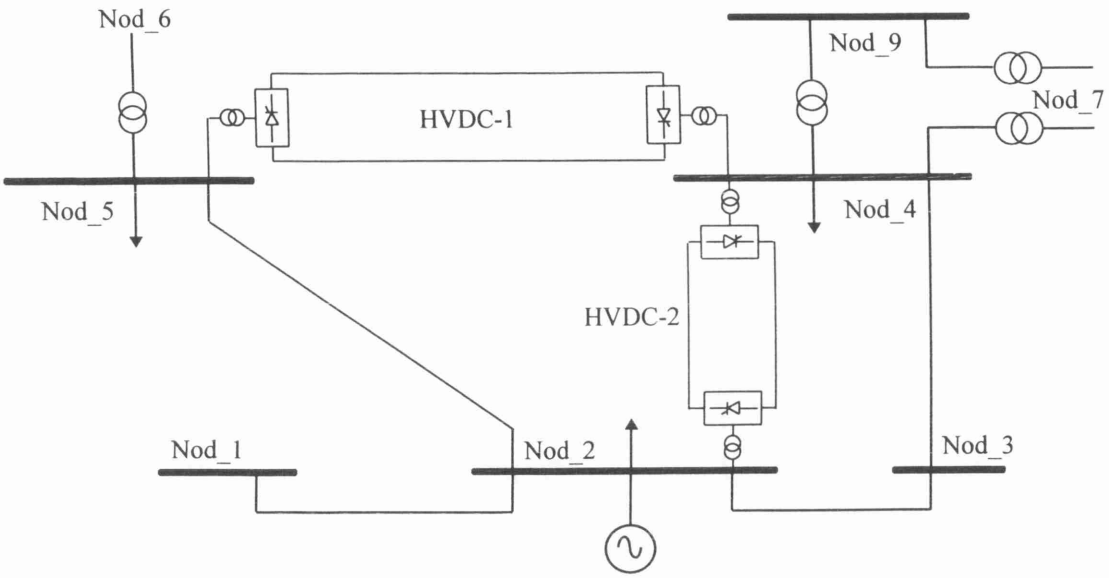

Figure 8.5. Relevant part of the upgraded AEP 14-node test system with two HVDC links.

Table 8.9. Summary of load flow solution for 14-node system.

Results	OPF Solution
Active power generation Cost ($/hr)	214.980
Active power losses (MW)	1.552
Active power generation (MW)	260.552
Reactive power generation (MVAR)	95.5535

Figures 8.6 and 8.7 show the convergence pattern for the tap positions of both transformers. It can be observed that there are no overshootings in the solution process. This type of variable is sensitive to changes in the active set and in the penalty weighting factors as shown in the Figures 8.6 and 8.7. It can also be noticed that the final values of these variables are approaching the solution until the end of the solution process. A unique solution is arrived at, in spite of the different initial conditions used.

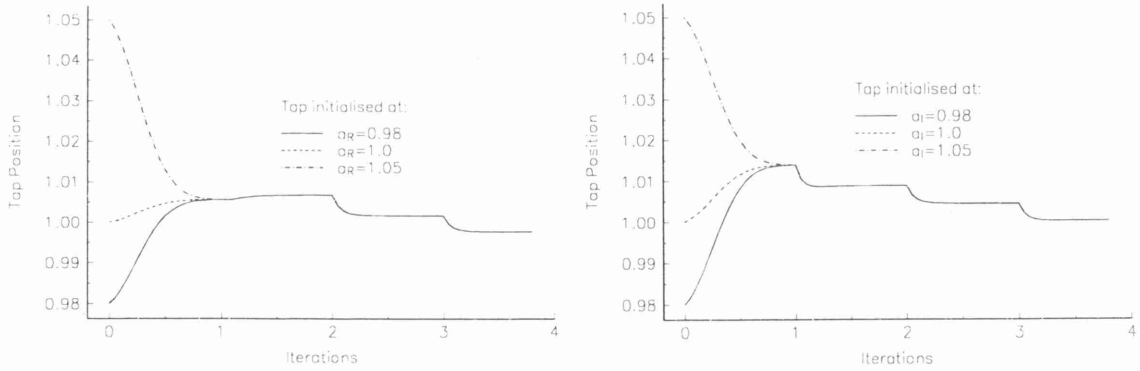

Figure 8.6. Tap position profiles for HVDC-1.

The behaviour of the ignition and extinction angles for both HVDC links is somehow irregular as shown in Figures 8.8 and 8.9. For HVDC-1, the pattern of converge seems to be insensitive to changes in the active set and does not show any overshootings. For the case of HVDC-2 link, the extinction angle is more sensitive than the firing angle. The latter reached its final value at the end of the first iteration.

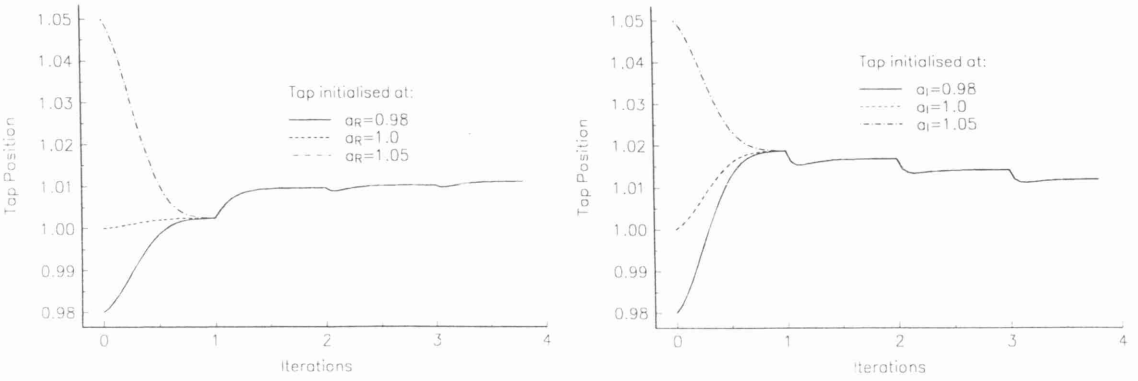

Figure 8.7. Tap position profiles for HVDC-2.

Extensive testing has shown that there are cases in which firing angles can be very sensitive to initial conditions, depending on the size of the penalty weighting factors used to enforce offending limits, and on how many variables violate their limits. Moreover, during the initial stages the solution is deeply affected if both tap positions and both control angles are modified simultaneously, i.e. four control variables would be different from the ideal initial conditions for a DC link. In some cases the solution is not reached or the active powers in the converters are too large. It should be pointed out that the DC voltages V_{dR} and V_{dI} are not changed directly. The changes are actually carried out modifying the AC voltages V_{tR} and V_{tI}. However, such changes resulted in active power converters larger than the apparent power, i.e. either an increment or decrement in the AC voltages V_{tR} and V_{tI} gave a numerical problem.

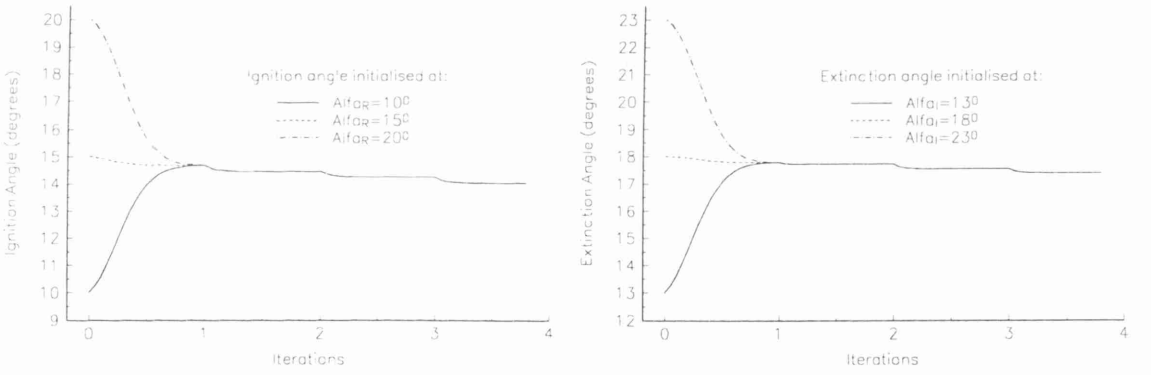

Figure 8.8. Ignition and extinction angle profiles for HVDC-1.

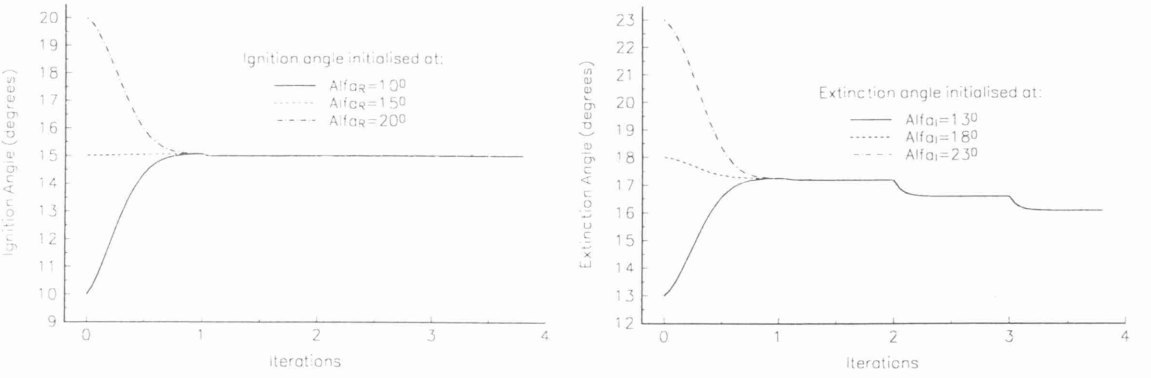

Figure 8.9. Ignition and extinction angle profiles for HVDC-2.

8.7 Power Flow Control by Using HVDC Links in a Real Power System

To show how the HVDC-OPF algorithm performs in a real life power system, the network used in previous Chapters will be modified to incorporate three HVDC links [17]. The relevant part of the network is shown in Figure 8.10 which shows the locations of the HVDC links. The transmission lines connected between nodes RIH and ROH, and MEH and TJH have been replaced by the HVDC links named as HVDC-1 and HVDC-2, respectively. Another link, named HVDC-3, was connected in series with the transmission line connecting nodes AEH and CSH. An additional node, termed AEHDC was created as shown in Figure 8.10. The parameters of the three links are the same as those given in Tables 8.1 and 8.2. The initial condition for the links were taken to be the same as those used in the 5-node and 14-node test systems. In this study, the DC systems are not maintaining a specified active power.

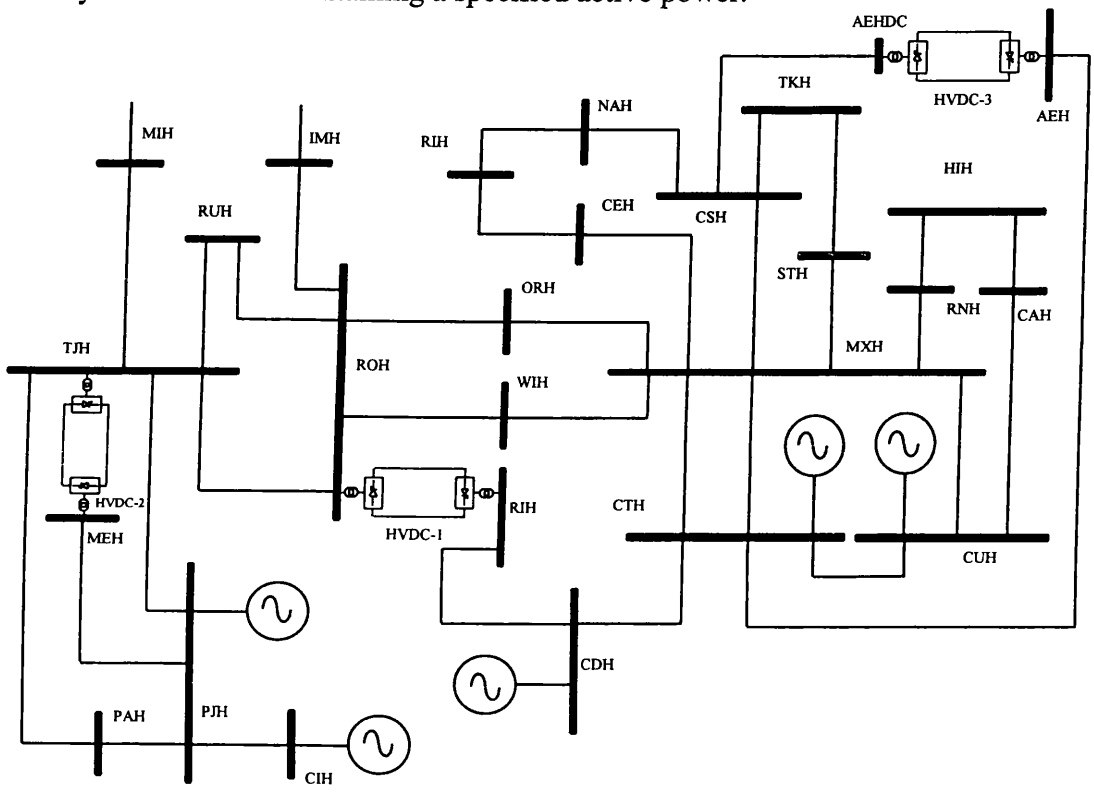

Figure 8.10. Relevant part of the 166-node test system upgraded with 3 HVDC links.

Convergence was achieved in 7 iterations. Table 8.10 shows the DC parameters obtained at the optimum solution, while Table 8.11 shows the powers associated with the HVDC links. Table 8.12 shows a summary of the relevant quantities for this system. The active power generation cost is 293.585 $/hour and the electric power losses are 20.199 MW plus 0.230 MW in the DC transmission links.

Table 8.10. DC-Link control parameters for the 14-node system.

OPF Solution	V_{dR} (pu)	a_R	α_R (degrees)	V_{dI} (pu)	a_I	α_I (degrees)
HVDC-1	1.330	1.002	13.800	1.328	1.008	17.103
HVDC-2	1.316	0.998	14.818	1.314	1.007	17.963
HVDC-3	1.309	0.971	14.902	1.309	0.997	17.600

Table 8.11. Power at the converters.

OPF Solution	P_{dR} (MW)	Q_{dR} (MVAR)	P_{dI} (MW)	Q_{dR} (MVAR)	I_d (pu)
HVDC-1	83.168	20.652	83.038	25.030	0.625
HVDC-2	68.762	18.122	68.670	21.731	0.522
HVDC-3	20.930	5.264	20.927	6.326	0.160

Table 8.12. Summary of load flow solution for 166-node system.

Results	OPF Solution
Active power generation Cost ($/hr)	293.585
Active power losses (MW)	20.199
Active power generation(MW)	2096.000
Reactive power generation (MVAR)	608.288

Figure 8.11 depicts the active power generation profile and Figure 8.12 depicts the network losses profile as a function of the iteration number. The patterns of convergence are very regular throughout the iteration process. The initial cost and network losses are higher than previous values but the process approaches the solution in a smooth fashion.

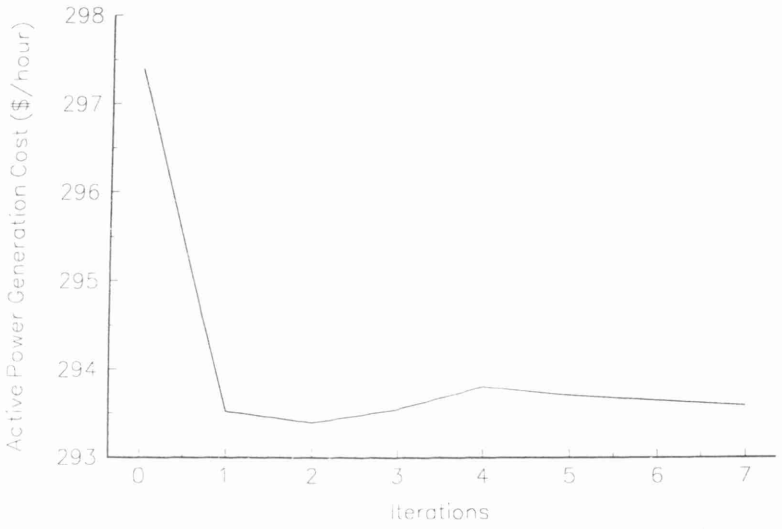

Figure 8.11. Active power generation cost profile for the 166-node system.

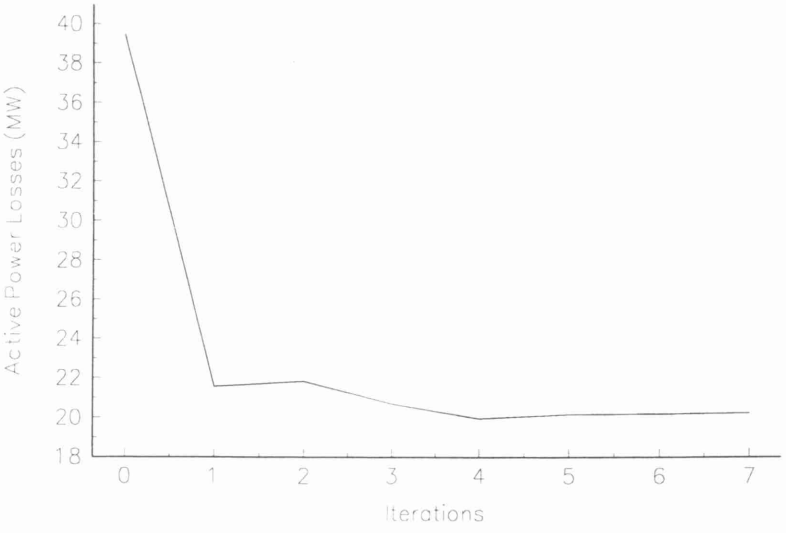

Figure 8.12. Active power losses profile for the 166-node system.

In a second test case, the HVDC links HVDC-1 and HVDC-2 are set to maintain the direct current across the HVDC links at specified values. The set value corresponds to an increase of 20% of their base power flow. Convergence was obtained in 7 iterations. The active power losses are 20.279 MW plus 0.351 MW in the HVDC links. The results for these operating conditions are presented in Tables 8.13 and 8.14.

Table 8.13. Powers at the HVDC converters.

OPF Solution	P_{dR} (MW)	Q_{dR} (MVAR)	P_{dI} (MW)	Q_{dR} (MVAR)	I_d (pu)
HVDC-1	103.000	24.681	102.611	30.912	0.800
HVDC-2	82.708	21.970	82.576	26.245	0.630
HVDC-3	15.654	3.930	15.650	4.761	0.120

Table 8.14. A summary of the load flow solution for 166-node system.

Results	OPF Solution
Active power generation Cost ($/hr)	293.605
Active power losses (MW)	20.279
Active power generation (MW)	2096.080
Reactive power generation (MVAR)	625.293

Tables 8.11 and 8.13 show that increases in active power flows across the converters result in larger amounts of reactive power absorbed by the inverters which is also reflected in the total reactive power produced by the generators. Furthermore, the active power generation cost was slightly increased when the direct currents at the links are set to specified values. Additionally, it was observed that power flow control can be carried out with ease for a wide set of values.

8.8 Power Flow Control by Using HVDC Links in a 2172-node System

An actual longitudinal power network [11] consisting of 2172 buses, 2294 transmission lines, 768 transformers, 201 of 579 generators are considered for the economic dispatch, 1259 loads, 208 fixed shunt compensators (FSC) and 10 fixed capacitive series compensators (FCSC) is used in order to show the full capabilities of the algorithm. Twelve conventional transformers were substituted by phase shifting transformers, ten FCSCs were replaced by TCSCs with four further additions. Five UPFCs and one HVDC link were also added to the network. These devices were used to maintain specified active power flows across predefined transmission paths, increasing the power transfer by more than 10%, with respect to the base case, except the phase-shifting transformers. In the UPFC, the reactive power is maintained at the base value, and the UPFC shunt converters are used to maintain the voltage magnitude at 1 pu. These FACTS controllers were embedded in the 230 and 400 KV levels. The base case converged in 9 iterations whilst the upgraded network converged in 10 iterations. All the controllable devices upheld their target values. Table 8.15 summarises the solutions for this test system.

The FACTS devices have a positive overall effect on the relevant quantities associated with this test system. From Table 8.15 it can be observed that the OPF algorithm gives the lowest production cost for the base case as opposed to the upgraded network with FACTS devices. This is because the FACTS devices were used to maintain specified

active power flows across predefined transmission paths, i.e. the solution of the system is satisfying transmission loading constraints. However, the network losses were larger for the former case than for the latter case. It should be observed that the active and reactive power generations are lower for the upgraded network than the base case. The reason for such network behaviour is that the type of FACTS devices used in the present test case, reduce the electrical distance between load and generation centres, giving reduced transmission losses

Table 8.15. Summary of load flow solution for 2172-node system.

Results	OPF solutions	
	Base case	Upgraded network
Active power load (MW)	19718.3	19718.3
Reactive power load (MVAR)	6487.59	6487.59
Active power generation Cost ($/hr)	5179.02	5215.36
Active power losses (MW)	763.654	692.557
Active power generation (MW)	20482	20410.9
Reactive power generation (MVAR)	796.945	728.417

8.9 Conclusions

An efficient and versatile HVDC system model, based on simple expressions derived from the DC link control scheme, is used to assess the steady state response of HVDC upgraded power networks. All the DC variables are combined with the nodal voltage magnitudes and angles of the power network in a single frame-of-reference for unified iterative solutions via Newton's method. The implemented OPF algorithm does not require pre-determined operating modes to decide the optimum set for the control variables. The DC variables are also regulated in order to achieve an optimal level of DC current under either condition, constrained or unconstrained current across the DC link.

Numerical examples have shown that the HVDC link model and Multipliers Method work very well in OPF. The Multipliers Method has shown to be a powerful method, which handles the HVDC link inequality constraints very well.

As expected, initial conditions far from the optimal operating point may cause the algorithm to diverge. If the initial conditions are not chosen carefully, the algorithm may experience numerical problems when performing reactive power calculations, due to the existence of large active power values in the early iterations. The conditions given in Section 8.5 provide good initial conditions for optimal iterative solutions.

The versatility of the AC-DC method is illustrated by numerical examples. Several networks of various sizes have been solved with the extended algorithm, some of them correspond to large company networks. The results clearly show the algorithm's flexibility and reliability towards the convergence.

8.10 References

[1] Sato H. and Arrillaga J.: 'Improved load-flow techniques for integrated a.c.-d.c. systems', Proceedings of IEE, Vol. 116, No. 4, April 1969, pp. 525-532.

[2] Reeve J., Fahmy G., and Stott B.: 'Versatile Load Flow Method for Multiterminal HVDC Systems', IEEE Transactions on Power Apparatus and Systems, Vol. PAS-96 , No. 3, May/June 1977, pp. 925-933.

[3] Fudeh H. and Ong M.N.: 'A Simple and Efficient AC-DC Load-Flow Method for Multiterminal DC Systems', IEEE Transactions on Power Apparatus and Systems, Vol. PAS-100, No. 11, November 1981, pp. 4389-4396.

[4] Ong M.N. and Fudeh H.: 'AC Power Flow Control with a Multiterminal DC Systems', IEEE Transactions on Power Apparatus and Systems, Vol. PAS-100, No. 11, November 1981, pp. 4686-4691.

[5] Stott B.: 'Load flow for a.c. and integrated a.c.-d.c. systems', PhD Thesis, 1971, University of Manchester.

[6] Sheble G. and Heydt G.: 'Power Flow Studies for Systems with HVDC Transmission', Proceedings of Power Industry Computer Applications Conference, New Orleans, 1975, pp. 223-228.

[7] Braunagel D.A., Kraft L.A. and Whysong J.L.: 'Inclusion of DC converter and Transmission Equations Directly in a Newton Power Flow', IEEE Transactions on Power Apparatus and Systems, Vol. PAS-95 , No. 1, January/February 1976, pp. 76-88.

[8] Arrillaga J. and Bodger P.: 'Integration of h.v.d.c. Links with fast-decoupled load flow solutions', Proceedings of IEE, Vol. 124, No. 5, May 1977, pp. 463-468.

[9] Arrillaga J. and Bodger P. 'A.C.- D.C. Load flows with realistic representation of the convertor plant', Proceedings of IEE, Vol. 125, No. 1, January 1978, pp.41-46.

[10] El-Marsafawy M.M and Mathur R.M.: 'A New, Fast Technique for Load-Flow Solution of Integrated Multi-Terminal DC/AC Systems', IEEE Transactions on Power Apparatus and Systems, Vol. PAS-99 , No. 1, January/February 1980, pp. 246-255.

[11] De Martinis U., Gagliardi F., Losi A., Mangoni V. and Rossi F.: 'Optimal Load Flow for Electrical Power Systems with multiterminal HVDC Links', IEE Proceedings, Vol. 137-C, No. 2, March 1990, pp. 139-145.

[12] Lu C.N., Chen S.S and Ong C.M.: 'The Incorporation of HVDC Equations In Optimal Power Flow Methods Using Sequential Quadratic Programming Techniques', IEEE Transactions on Power Apparatus and Systems, Vol. 3 , No. 3, August, 1988, pp. 1005-1011.

[13] Smed T., Andersson G., Sheblé G.B. and Grigsby L.L.: 'A New approach to AC/DC Power Flow', IEEE Transactions on Power Systems, Vol. 6, No. 3, August 1991, pp. 1238-1244.

[14] Sun D.I., Ashley B., Brewer B., Hughes A. and Tinney W.F.: 'Optimal Power Flow By Newton Approach', IEEE Transactions on Power Apparatus and Systems, Vol. PAS-103, No. 10, October 1984, pp. 2864-2880.

[15] Sun D.I., Hu T.I., Lin G.S., Lin C.J. and Chen C.H.: 'Experiences with Implementing Optimal Power Flow for Reactive Scheduling in the Taiwan Power System', IEEE Transactions on Power Systems, Vol. 3, No. 3, August 1988, pp. 1193-1200.

[16] Freris L.L. and Sasson A.M.: 'Investigation of the Load-Flow Problem', Proceedings of IEE, Vol. 115, No. 10, October 1968, pp. 1459-1470.

[17] Aboytes F. and Arroyo G.: 'Security Assessment in the Operation of Longitudinal Power Systems', IEEE Transactions on Power Apparatus and Systems, Vol. PWRS-1, No. 2, May 1986, pp. 225-232.

[18] Kimbark E.: 'Direct current Transmission', Vol. I, Wiley- Interscience, New-York, 1971.

[19] Kundur P.: 'Power System Stability and Control', McGraw Hill, 1994.

[20] Luenberger D.G.: 'Introduction to Linear and Nonlinear Programming', Addison-Wesley Publishing Co., Second Edition, 1984.

[21] Bertsekas D.P.: 'Constrained Optimization Lagrange Multiplier Methods', Academic Press, 1992.

[22] Stagg G.W. and El-Abiad A.H.: 'Computer Methods in Power System Analysis', McGraw-Hill, 1968.

Chapter 9

Conclusions and Suggestions for Future Research Work

9.1 General Conclusions

The FACTS concept is a new development in electrical power systems that has attracted great interest from the major manufacturers of electrical equipment, utility companies and research centres around the world.

There is widespread agreement that to determine the usefulness of this new generation of power system devices on a network-wide basis, it will become necessary to upgrade most of the analysis tools which power engineers rely upon to plan and to operate their systems. Power system application software such as:

- Load Flows.
- Optimal Power Flows.
- State Estimation.
- Transient Stability.
- Small Signal Stability.
- Electro-Magnetic Transients.
- Harmonic Analysis.

require the inclusion of comprehensive FACTS device models.

However, the provision of FACTS device modelling in power systems software intended for network-wide studies is a very challenging endeavour. For instance, in Load Flow studies, the flexibility and upgrading comes with computational problems. However at all cost, 'in-fighting' between controls should be avoided, particularly, when two or more FACTS devices are controlling network parameters at the same location. Otherwise, convergence problems will occur. Hence, it is necessary to develop complex control strategies for the efficient co-ordination of the various FACTS devices located in the power system.

Alternatively, such co-ordination schemes may be avoided by resorting to more sophisticated computational tools, such as Optimal Power Flows. These kind of tools may be used to find the static optimal operating point of an electrical power network. The solution should meet feasibility, optimality and security requirements. The

optimisation process will also automatically co-ordinate the best output of the various controllers to achieve a global optimal response.

The research work presented in this thesis has been directly oriented to develop an integrated methodology for assessing the behaviour of FACTS controllers within the framework of economic power system studies. The FACTS-OPF algorithm has been applied to solve a wide range of networks, with excellent results achieved each time. Networks with no FACTS controllers have been solved with the OPF program of a leading software vendor and with the newly developed FACTS-OPF algorithm, with both computer programs arriving at practically the same solution.

The fundamental aim of this research work has also been to provide comprehensive models for FACTS controllers. The emphasis of this research has been placed on active power flow control, however, the algorithm is quite general and can handle voltage control-related issues equally well. The Phase-Shifting and Load-Changing Transformers, Static Var Compensators, Thyristor Controlled Series Capacitors, Interphase Power Controllers, Unified Power Flow Controllers and High Voltage DC link models have been incorporated directly in the Hessian-Jacobian matrix of Newton's method, termed matrix $\boldsymbol{W}$, leading to highly robust iterative solutions.

Two models for both the TCSC and the SVC have been developed. These new models introduce the thyristor's firing angle as the control variable. The TCSC controllable reactance model has shown to behave better towards the convergence than the TCSC-FA model. However, the drawback of the former model is that the firing angle corresponding to a given compensation levels has to be determined by resorting to an additional iterative process. Referring to the SVC, both models presented in Chapter 4 are shown to be very reliable. However, the SVC total susceptance model has a similar drawback to that presented by the TCSC firing angle model.

The non-linear nature of the various FACTS controllers is incorporated with ease within the frame-of-reference provided by Newton's method. The FACTS Optimal Power Flow algorithm is capable of solving large power networks very reliably. Some test networks are available in the open literature, and others are real life power networks where hundreds of variables are adjusted to reach the best steady state operating point.

Newton's method has shown to work very well in Optimal Power Flow applications because of the structure of matrix $\boldsymbol{W}$. The matrix $\boldsymbol{W}$ has the same block sparsity structure as the nodal admittance matrix. Matrix $\boldsymbol{W}$ and the gradient vector $\boldsymbol{g}$ can be built by using superposition. The 'conventional' power system components, and the new FACTS controllers have been modelled independently and their individual contributions have been directly placed into the linearised system of equations. During the solution of the linearised set of equations, all variables involved are processed identically in every iteration.

The long standing problem of handling inequality constraints on variables and constraints on functions of variables is overcome by using the Multipliers method and the Penalty Function method, respectively. Both methods have shown to be a very effective means of achieving constrained OPF solutions. The Multipliers method works well with the regulating mechanism of the FACTS controllers within the OPF solution.

The robustness of the FACTS Optimal Power Flow towards the convergence has been rigorously studied by observing the effect of initial conditions on the various FACTS controllers. Criteria for initialising FACTS controllers are given for each one of the models developed in this research. Guidelines for FACTS initialisation have been issued

by resorting to engineering reason, extensive computational testing and simplified analytical equations, this being particularly the case of the Unified Power Flow Controller.

Extensive computational testing indicates that the FACTS Optimal Power Flow developed in this research, has real potential as a practical tool in the planning and operation of electrical power networks. Its reliability towards the convergence and solution speed are two of its strengths. Test FACTS upgraded networks, ranging from 5 to 2172 nodes have been used to demonstrate the reliability and prowess of the FACTS Optimal Power Flow.

It this generally accepted that an Optimal Power Flow program is an effective computational tool for power system analysis. It provides a realistic and effective way for minimising active power generation cost while satisfying generating units and transmission network operating limits. However, it should be remarked that in Optimal Power Flow studies, solutions cannot be guaranteed to be global minimum solutions. In this research, the initial conditions for all the nodal variables, such as voltage magnitudes and phase angles, have been selected to be as close as possible to the network rated values. It is accepted that in some cases, the starting values will not necessarily lead to a global minimum. However, the author of this thesis can rest assured that realistic operational solutions which minimise production cost are arrived at.

9.2 Future Research Work

This research work has not only given rise to a power systems tool with real potential but also to a tool which should generate further research work.

The author suggests that reactive power optimisation using a weighting reactive power injection as an objective function is feasible. This objective function is desirable because a better distribution of reactive power in the system should result in a more uniform voltage profile. It would also distribute the reactive power among the reactive power sources in proportion to their ratings. Therefore, the methodology proposed in this thesis could be applied to solve both problems, in a sequential fashion. The first solution would address the active power generation cost minimisation, including Phase-Shifting Transformers, Thyristor Controlled Series Capacitors, Interphase Power Controllers, Unified Power Flow Controllers and High Voltage DC links. The second one would deal with the minimisation of the weighting reactive power injection, including Tap-Changing Transformers, Static Var Compensators and Unified Power Flow Controllers.

A extension of the FACTS Optimal Power Flow methodology applied to the calculation of corrective actions for electric power system operating in steady state should be addressed. FACTS controllers are capable of correcting power flow violations in transmission elements, as well as nodal voltage magnitudes. An objective function which limits the number of control actions should be investigated.

The author would suggest the development of a methodology which would indicate the best place in the electric power system for the placement of FACTS controllers. The solution to this issue includes the addition of a minimum number of FACTS controller into the power network under study.

Additional work relating to the steady state modelling and analysis of FACTS devices is discussed below:

FACTS controllers generate harmonics due to the dead-band zones associated with the operating characteristics of the solid-state switches. Hence, advanced harmonic tools are going to be required to prevent harmonic voltage instabilities from taking place.

State estimation is defined as the process of assigning a value to an unknown system state variable based on measurements of the system according to a predefined criteria. The voltage magnitude and phase angle are the most popular state variables in this type of study. Measurements of voltage magnitudes, active and reactive powers are examples of information required by an estimator to produce the best estimate of the state variables. This area of study with FACTS controllers included, requires research attention.

Computer models for harmonics, transient stability and state estimation, exhibiting a good degree of validation and efficiency are not currently available to the Electricity Supply Industry. Potential users of the software would therefore benefit greatly from this new research.

Electricity companies operating under the open access transmission principles have the right to trade electrical energy from any source willing to pay prices dictated by the free market. The author suggests that a pricing strategy for the use of the FACTS upgraded transmission networks, based on sound economic principle may be developed under the concept of marginal prices supplied by OPF algorithms.

Additionally, a methodology for tracing the power output for each generator, on an individual basis, throughout the electrical power network can also be developed. The purpose is to determine which generator contributes and in what proportion to each load of the network. FACTS controllers may be used to re-direct power flows aiming at establishing well defined contract paths.

Appendix I

Hessian and Jacobian Elements for the Phase-Shifting Transformer Model

The first partial derivatives of the power flow equations with respect to the phase shifter angle in the primary winding of the transformer ϕ_{tv} are,

$$\frac{\partial P_p}{\partial \phi_{tv}} = V_p V_s (G_{ps} \sin\delta_1 - B_{ps} \cos\delta_1) \tag{I.1}$$

$$\frac{\partial Q_p}{\partial \phi_{tv}} = -V_p V_s (G_{ps} \cos\delta_1 + B_{ps} \sin\delta_1) \tag{I.2}$$

$$\frac{\partial P_s}{\partial \phi_{tv}} = -V_s V_p (G_{sp} \sin\delta_2 - B_{sp} \cos\delta_2) \tag{I.3}$$

$$\frac{\partial Q_s}{\partial \phi_{tv}} = V_s V_p (G_{sp} \cos\delta_2 + B_{sp} \sin\delta_2) \tag{I.4}$$

The second partial derivatives with respect to the phase shifter angle ϕ_{tv} and phase angles are:

$$\frac{\partial^2 P_p}{\partial \phi_{tv} \partial \delta_p} = V_p V_s (G_{ps} \cos\delta_1 + B_{ps} \sin\delta_1) \tag{I.5}$$

$$\frac{\partial^2 P_p}{\partial \phi_{tv} \partial \delta_s} = -V_p V_s (G_{ps} \cos\delta_1 + B_{ps} \sin\delta_1) \tag{I.6}$$

$$\frac{\partial^2 P_s}{\partial \phi_{tv} \partial \delta_s} = -V_s V_p (G_{sp} \cos\delta_2 + B_{sp} \sin\delta_2) \tag{I.7}$$

$$\frac{\partial^2 P_s}{\partial \phi_{tv} \partial \delta_p} = V_s V_p (G_{sp} \cos\delta_2 + B_{sp} \sin\delta_2) \tag{I.8}$$

$$\frac{\partial^2 Q_p}{\partial \phi_{tv} \partial \delta_p} = V_p V_s (G_{ps} \sin\delta_1 - B_{ps} \cos\delta_1) \tag{I.9}$$

$$\frac{\partial^2 Q_p}{\partial \phi_{tv} \partial \delta_s} = -V_p V_s (G_{ps} \sin\delta_1 - B_{ps} \cos\delta_1) \tag{I.10}$$

$$\frac{\partial^2 Q_s}{\partial \phi_{tv} \partial \delta_s} = -V_s V_p (G_{sp} \sin\delta_2 - B_{sp} \cos\delta_2) \tag{I.11}$$

$$\frac{\partial^2 Q_s}{\partial \phi_{tv} \partial \delta_p} = V_s V_p (G_{sp} \sin\delta_2 - B_{sp} \cos\delta_2) \tag{I.12}$$

The second partial derivatives with respect to the phase shifter angle ϕ_{tv} and voltages.

$$\frac{\partial^2 P_p}{\partial \phi_{tv} \partial V_p} = V_s (G_{ps} \sin\delta_1 - B_{ps} \cos\delta_1) \tag{I.13}$$

$$\frac{\partial^2 P_p}{\partial \phi_{tv} \partial V_s} = V_p (G_{ps} \sin\delta_1 - B_{ps} \cos\delta_1) \tag{I.14}$$

$$\frac{\partial^2 Q_p}{\partial \phi_{tv} \partial V_p} = -V_s (G_{ps} \cos\delta_1 + B_{ps} \sin\delta_1) \tag{I.15}$$

$$\frac{\partial^2 Q_p}{\partial \phi_{tv} \partial V_s} = -V_p (G_{ps} \cos\delta_1 + B_{ps} \sin\delta_1) \tag{I.16}$$

$$\frac{\partial^2 P_s}{\partial \phi_{tv} \partial V_p} = -V_s (G_{sp} \sin\delta_2 - B_{sp} \cos\delta_2) \tag{I.17}$$

$$\frac{\partial^2 P_s}{\partial \phi_{tv} \partial V_s} = -V_p (G_{sp} \sin\delta_2 - B_{sp} \cos\delta_2) \tag{I.18}$$

$$\frac{\partial^2 Q_s}{\partial \phi_{tv} \partial V_p} = V_s (G_{sp} \cos\delta_2 + B_{sp} \sin\delta_2) \tag{I.19}$$

$$\frac{\partial^2 Q_s}{\partial \phi_{tv} \partial V_s} = V_p (G_{sp} \cos\delta_2 + B_{sp} \sin\delta_2) \tag{I.20}$$

The second partial derivatives with respect to the phase shifter angle ϕ_{tv}.

$$\frac{\partial G_{ps}}{\partial \phi_{tv}} = \frac{T_v U_v}{A_2} (F_1 \sin\phi_1 - F_2 \cos\phi_1) \tag{I.21}$$

$$\frac{\partial B_{ps}}{\partial \phi_{tv}} = -\frac{T_v U_v}{A_2} (F_2 \sin\phi_1 + F_1 \cos\phi_1) \tag{I.22}$$

$$\frac{\partial G_{sp}}{\partial \phi_{tv}} = -\frac{T_v U_v}{A_2} (F_1 \sin\phi_2 - F_2 \cos\phi_2) \tag{I.23}$$

$$\frac{\partial B_{sp}}{\partial \phi_{tv}} = \frac{T_v U_v}{A_2}(F_2 \sin\phi_2 + F_1 \cos\phi_2) \tag{I.24}$$

$$\frac{\partial^2 P_p}{\partial^2 \phi_{tv}} = V_p V_s \left(\sin\delta_1 \frac{\partial G_{ps}}{\partial \phi_{tv}} - \cos\delta_1 \frac{\partial B_{ps}}{\partial \phi_{tv}} \right) \tag{I.25}$$

$$\frac{\partial^2 Q_p}{\partial^2 \phi_{tv}} = -V_p V_s \left(\cos\delta_1 \frac{\partial G_{ps}}{\partial \phi_{tv}} + \sin\delta_1 \frac{\partial B_{ps}}{\partial \phi_{tv}} \right) \tag{I.26}$$

$$\frac{\partial^2 P_s}{\partial^2 \phi_{tv}} = -V_s V_p \left(\sin\delta_2 \frac{\partial G_{sp}}{\partial \phi_{tv}} - \cos\delta_2 \frac{\partial B_{sp}}{\partial \phi_{tv}} \right) \tag{I.27}$$

$$\frac{\partial^2 Q_s}{\partial^2 \phi_{tv}} = V_s V_p \left(\cos\delta_2 \frac{\partial G_{sp}}{\partial \phi_{tv}} + \sin\delta_2 \frac{\partial B_{sp}}{\partial \phi_{tv}} \right) \tag{I.28}$$

The first partial derivatives of power equations with respect to the phase shifter angle in the secondary winding of the transformer ϕ_{uv} are:

$$\frac{\partial P_p}{\partial \phi_{uv}} = -V_p V_s (G_{ps} \sin\delta_1 - B_{ps} \cos\delta_1) \tag{I.29}$$

$$\frac{\partial Q_p}{\partial \phi_{uv}} = V_p V_s (G_{ps} \cos\delta_1 + B_{ps} \sin\delta_1) \tag{I.30}$$

$$\frac{\partial P_s}{\partial \phi_{uv}} = V_s V_p (G_{sp} \sin\delta_2 - B_{sp} \cos\delta_2) \tag{I.31}$$

$$\frac{\partial Q_s}{\partial \phi_{uv}} = -V_s V_p (G_{sp} \cos\delta_2 + B_{sp} \sin\delta_2) \tag{I.32}$$

The second partial derivatives with respect to the phase shifter angle ϕ_{uv} and phase angles.

$$\frac{\partial^2 P_p}{\partial \phi_{uv} \partial \delta_p} = -V_p V_s (G_{ps} \cos\delta_1 + B_{ps} \sin\delta_1) \tag{I.33}$$

$$\frac{\partial^2 P_p}{\partial \phi_{uv} \partial \delta_s} = V_p V_s (G_{ps} \cos\delta_1 + B_{ps} \sin\delta_1) \tag{I.34}$$

$$\frac{\partial^2 P_s}{\partial \phi_{uv} \partial \delta_s} = V_s V_p (G_{sp} \cos\delta_2 + B_{sp} \sin\delta_2) \tag{I.35}$$

$$\frac{\partial^2 P_s}{\partial \phi_{uv} \partial \delta_p} = -V_s V_p (G_{sp} \cos\delta_2 + B_{sp} \sin\delta_2) \tag{I.36}$$

$$\frac{\partial^2 Q_p}{\partial \phi_{uv} \partial \delta_p} = -V_p V_s (G_{ps} \sin\delta_1 - B_{ps} \cos\delta_1) \tag{I.37}$$

$$\frac{\partial^2 Q_p}{\partial \phi_{uv} \partial \delta_s} = V_p V_s (G_{ps} \sin\delta_1 - B_{ps} \cos\delta_1) \tag{I.38}$$

$$\frac{\partial^2 Q_s}{\partial \phi_{uv} \partial \delta_s} = V_s V_p (G_{sp} \sin\delta_2 - B_{sp} \cos\delta_2) \tag{I.39}$$

$$\frac{\partial^2 Q_s}{\partial \phi_{uv} \partial \delta_p} = -V_s V_p (G_{sp} \sin\delta_2 - B_{sp} \cos\delta_2) \tag{I.40}$$

The second partial derivatives with respect to the phase shifter angle ϕ_{uv} and voltages.

$$\frac{\partial^2 P_p}{\partial \phi_{uv} \partial V_p} = -V_s (G_{ps} \sin\delta_1 - B_{ps} \cos\delta_1) \tag{I.41}$$

$$\frac{\partial^2 P_p}{\partial \phi_{uv} \partial V_s} = -V_p (G_{ps} \sin\delta_1 - B_{ps} \cos\delta_1) \tag{I.42}$$

$$\frac{\partial^2 Q_p}{\partial \phi_{uv} \partial V_p} = V_s (G_{ps} \cos\delta_1 + B_{ps} \sin\delta_1) \tag{I.43}$$

$$\frac{\partial^2 Q_p}{\partial \phi_{uv} \partial V_s} = V_p (G_{ps} \cos\delta_1 + B_{ps} \sin\delta_1) \tag{I.44}$$

$$\frac{\partial^2 P_s}{\partial \phi_{uv} \partial V_p} = V_s (G_{sp} \sin\delta_2 - B_{sp} \cos\delta_2) \tag{I.45}$$

$$\frac{\partial^2 P_s}{\partial \phi_{uv} \partial V_s} = V_p (G_{sp} \sin\delta_2 - B_{sp} \cos\delta_2) \tag{I.46}$$

$$\frac{\partial^2 Q_s}{\partial \phi_{uv} \partial V_p} = -V_s (G_{sp} \cos\delta_2 + B_{sp} \sin\delta_2) \tag{I.47}$$

$$\frac{\partial^2 Q_s}{\partial \phi_{uv} \partial V_s} = -V_p (G_{sp} \cos\delta_2 + B_{sp} \sin\delta_2) \tag{I.48}$$

The second partial derivatives with respect to the phase shifter angle ϕ_{uv}.

$$\frac{\partial G_{ps}}{\partial \phi_{uv}} = -\frac{T_v U_v}{A_2} (F_1 \sin\phi_1 - F_2 \cos\phi_1) \tag{I.49}$$

$$\frac{\partial B_{ps}}{\partial \phi_{uv}} = \frac{T_v U_v}{A_2} (F_2 \sin\phi_1 + F_2 \cos\phi_1) \tag{I.50}$$

$$\frac{\partial G_{sp}}{\partial \phi_{uv}} = \frac{T_v U_v}{A_2} (F_1 \sin\phi_2 - F_2 \cos\phi_2) \tag{I.51}$$

$$\frac{\partial B_{sp}}{\partial \phi_{uv}} = -\frac{T_v U_v}{A_2} (F_1 \cos\phi_2 + F_2 \sin\phi_2) \tag{I.52}$$

$$\frac{\partial^2 P_p}{\partial^2 \phi_{uv}} = -V_p V_s \left(\sin\delta_1 \frac{\partial G_{ps}}{\partial \phi_{uv}} - \cos\delta_1 \frac{\partial B_{ps}}{\partial \phi_{uv}} \right) \tag{I.53}$$

$$\frac{\partial^2 Q_p}{\partial^2 \phi_{uv}} = V_p V_s \left(\cos\delta_1 \frac{\partial G_{ps}}{\partial \phi_{uv}} + \sin\delta_1 \frac{\partial B_{ps}}{\partial \phi_{uv}} \right) \tag{I.54}$$

$$\frac{\partial^2 P_s}{\partial^2 \phi_{uv}} = V_s V_p \left(\sin\delta_2 \frac{\partial G_{sp}}{\partial \phi_{uv}} - \cos\delta_2 \frac{\partial B_{sp}}{\partial \phi_{uv}} \right) \tag{I.55}$$

$$\frac{\partial^2 Q_s}{\partial^2 \phi_{uv}} = -V_s V_p \left(\cos\delta_2 \frac{\partial G_{sp}}{\partial \phi_{uv}} + \sin\delta_2 \frac{\partial B_{sp}}{\partial \phi_{uv}} \right) \tag{I.56}$$

Appendix II

Hessian and Jacobian Elements for the Load Tap-Changing Transformer Model

The first partial derivatives of power flow equations with respect to the tap changer in the primary winding of the transformer T_v, are,

$$\frac{\partial P_p}{\partial T_v} = \frac{2V_p^2 T_v}{A_2}\left(R_s(U_v^2 + R_1) + X_s R_2 - 2G_{pp}(R_s F_1 + X_s F_2)\right) + \frac{V_p V_s}{T_v}(G_{ps}\cos\delta_1 + B_{ps}\sin\delta_1)\left(1 - \frac{4T_v^2}{A_2}(R_s F_1 + X_s F_2)\right) + \frac{2V_p V_s T_v^2 U_v}{A_2}\left(X_s \sin(\delta_1 - \phi_1) - R_s\cos(\delta_1 - \phi_1)\right) \quad \text{(II.1)}$$

$$\frac{\partial Q_p}{\partial T_v} = \frac{2V_p^2 T_v}{A_2}\left(2B_{pp}(R_s F_1 + X_s F_2) - R_s R_2 + X_s(U_v^2 + R_1)\right) + \frac{V_p V_s}{T_v}(G_{ps}\sin\delta_1 - B_{ps}\cos\delta_1)\left(1 - \frac{4T_v^2}{A_2}(R_s F_1 + X_s F_2)\right) - \frac{2V_p V_s T_v^2 U_v}{A_2}\left(R_s \sin(\delta_1 - \phi_1) + X_s\cos(\delta_1 - \phi_1)\right) \quad \text{(II.2)}$$

$$\frac{\partial P_s}{\partial T_v} = \frac{2V_s^2 T_v}{A_2}\left(R_s(T_v^2 + R_3) + X_s R_4 + F_1 - 2G_{ss}(R_s F_1 + X_s F_2)\right) + \frac{V_s V_p}{T_v}(G_{sp}\cos\delta_2 + B_{sp}\sin\delta_2)\left(1 - \frac{4T_v^2}{A_2}(R_s F_1 + X_s F_2)\right) + \frac{2V_s V_p T_v^2 U_v}{A_2}\left(X_s \sin(\delta_2 - \phi_2) - R_s\cos(\delta_2 - \phi_2)\right) \quad \text{(II.3)}$$

$$\frac{\partial Q_s}{\partial T_v} = \frac{2V_s^2 T_v}{A_2}\left(2B_{ss}(R_s F_1 + X_s F_2) - R_s R_4 + X_s(T_v^2 + R_3) + F_2\right)$$
$$+ \frac{V_s V_p}{T_v}(G_{sp}\sin\delta_2 - B_{sp}\cos\delta_2)\left(1 - \frac{4T_v^2}{A_2}(R_s F_1 + X_s F_2)\right) \quad \text{(II.4)}$$
$$- \frac{2V_s V_p T_v^2 U_v}{A_2}\left(R_s\sin(\delta_2 - \phi_2) + X_s\cos(\delta_2 - \phi_2)\right)$$

The second partial derivatives of power flow equations with respect to the tap changer T_v and phase angles are,

$$H_{ps} = \left(G_{ps}\sin(\delta_p - \delta_s) - B_{ps}\cos(\delta_p - \delta_s)\right) \quad \text{(II.5)}$$

$$N_{ps} = \left(G_{ps}\cos(\delta_p - \delta_s) + B_{ps}\sin(\delta_p - \delta_s)\right) \quad \text{(II.6)}$$

$$H_{sp} = \left(G_{sp}\sin(\delta_s - \delta_p) - B_{sp}\cos(\delta_s - \delta_p)\right) \quad \text{(II.7)}$$

$$N_{sp} = \left(G_{sp}\cos(\delta_s - \delta_p) + B_{sp}\sin(\delta_s - \delta_p)\right) \quad \text{(II.8)}$$

$$\frac{\partial^2 P_p}{\partial T_v \partial\delta_p} = -\frac{V_p V_s H_{ps}}{T_v}\left(1 - \frac{4T_v^2}{A_2}(R_s F_1 + X_s F_2)\right)$$
$$+ \frac{2V_p V_s T_v^2 U_v}{A_2}\left(X_s\cos(\delta_1 - \phi_1) + R_s\sin(\delta_1 - \phi_1)\right) \quad \text{(II.9)}$$

$$\frac{\partial^2 P_p}{\partial T_v \partial\delta_s} = \frac{V_p V_s H_{ps}}{T_v}\left(1 - \frac{4T_v^2}{A_2}(R_s F_1 + X_s F_2)\right)$$
$$- \frac{2V_p V_s T_v^2 U_v}{A_2}\left(X_s\cos(\delta_1 - \phi_1) + R_s\sin(\delta_1 - \phi_1)\right) \quad \text{(II.10)}$$

$$\frac{\partial^2 Q_p}{\partial T_v \partial\delta_p} = \frac{V_p V_s N_{ps}}{T_v}\left(1 - \frac{4T_v^2}{A_2}(R_s F_1 + X_s F_2)\right)$$
$$- \frac{2V_p V_s T_v^2 U_v}{A_2}\left(R_s\cos(\delta_1 - \phi_1) - X_s\sin(\delta_1 - \phi_1)\right) \quad \text{(II.11)}$$

$$\frac{\partial^2 Q_p}{\partial T_v \partial\delta_s} = -\frac{V_p V_s N_{ps}}{T_v}\left(1 - \frac{4T_v^2}{A_2}(R_s F_1 + X_s F_2)\right)$$
$$+ \frac{2V_p V_s T_v^2 U_v}{A_2}\left(R_s\cos(\delta_1 - \phi_1) - X_s\sin(\delta_1 - \phi_1)\right) \quad \text{(II.12)}$$

$$\frac{\partial^2 P_s}{\partial T_v \partial\delta_s} = -\frac{V_s V_p H_{sp}}{T_v}\left(1 - \frac{4T_v^2}{A_2}(R_s F_1 + X_s F_2)\right)$$
$$+ \frac{2V_s V_p T_v^2 U_v}{A_2}\left(X_s\cos(\delta_2 - \phi_2) + R_s\sin(\delta_2 - \phi_2)\right) \quad \text{(II.13)}$$

$$\frac{\partial^2 P_s}{\partial T_v \partial \delta_p} = \frac{V_s V_p H_{sp}}{T_v}\left(1-\frac{4T_v^2}{A_2}(R_s F_1 + X_s F_2)\right) - \frac{2V_s V_p T_v^2 U_v}{A_2}\left(X_s \cos(\delta_2-\phi_2) + R_s \sin(\delta_2-\phi_2)\right) \tag{II.14}$$

$$\frac{\partial^2 Q_s}{\partial T_v \partial \delta_s} = \frac{V_s V_p N_{sp}}{T_v}\left(1-\frac{4T_v^2}{A_2}\left(R_s F_1 + X_s F_2\right)\right) - \frac{2V_s V_p T_v^2 U_v}{A_2}\left(R_s \cos(\delta_2-\phi_2) - X_s \sin(\delta_2-\phi_2)\right) \tag{II.15}$$

$$\frac{\partial^2 Q_s}{\partial T_v \partial \delta_p} = -\frac{V_s V_p N_{sp}}{T_v}\left(1-\frac{4T_v^2}{A_2}(R_s F_1 + X_s F_2)\right) + \frac{2V_s V_p T_v^2 U_v}{A_2}\left(R_s \cos(\delta_2-\phi_2) - X_s \sin(\delta_2-\phi_2)\right) \tag{II.16}$$

The second partial derivatives of power flow equations with respect to the tap changer T_v and voltages,

$$\frac{\partial^2 P_p}{\partial T_v \partial V_p} = \frac{4V_p T_v}{A_2}\left(R_s(U_v^2 + R_1) + X_s R_2 - 2G_{pp}(R_s F_1 + X_s F_2)\right) + \frac{V_s}{T_v} N_{ps}\left(1-\frac{4T_v^2}{A_2}(R_s F_1 + X_s F_2)\right) + \frac{2V_s T_v^2 U_v}{A_2}\left(X_s \sin(\delta_1-\phi_1) - R_s \cos(\delta_1-\phi_1)\right) \tag{II.17}$$

$$\frac{\partial^2 P_p}{\partial T_v \partial V_s} = \frac{V_p}{T_v} N_{ps}\left(1-\frac{4T_v^2}{A_2}(R_s F_1 + X_s F_2)\right) + \frac{2V_p T_v^2 U_v}{A_2}\left(X_s \sin(\delta_1-\phi_1) - R_s \cos(\delta_1-\phi_1)\right) \tag{II.18}$$

$$\frac{\partial^2 Q_p}{\partial T_v \partial V_p} = \frac{4V_p T_v}{A_2}\left(2B_{pp}(R_s F_1 + X_s F_2) - R_s R_2 + X_s(U_v^2 + R_1)\right) + \frac{V_s}{T_v} H_{ps}\left(1-\frac{4T_v^2}{A_2}(R_s F_1 + X_s F_2)\right) - \frac{2V_s T_v^2 U_v}{A_2}\left(R_s \sin(\delta_1-\phi_1) + X_s \cos(\delta_1-\phi_1)\right) \tag{II.19}$$

$$\frac{\partial^2 Q_p}{\partial T_v \partial V_s} = \frac{V_p}{T_v} H_{ps}\left(1-\frac{4T_v^2}{A_2}(R_s F_1 + X_s F_2)\right) - \frac{2V_p T_v^2 U_v}{A_2}\left(R_s \sin(\delta_1-\phi_1) + X_s \cos(\delta_1-\phi_1)\right) \tag{II.20}$$

$$\frac{\partial^2 P_s}{\partial T_v \partial V_s} = \frac{4V_s T_v}{A_2}\left(R_s(T_v^2 + R_3) + X_s R_4 + F_1 - 2G_{ss}(R_s F_1 + X_s F_2)\right) + \frac{V_p}{T_v} N_{sp}\left(1 - \frac{4T_v^2}{A_2}(R_s F_1 + X_s F_2)\right) + \frac{2V_p T_v^2 U_v}{A_2}\left(X_s \sin(\delta_2 - \phi_2) - R_s \cos(\delta_2 - \phi_2)\right) \quad \text{(II.21)}$$

$$\frac{\partial^2 P_s}{\partial T_v \partial V_p} = \frac{V_s}{T_v} N_{sp}\left(1 - \frac{4T_v^2}{A_2}(R_s F_1 + X_s F_2)\right) + \frac{2V_s T_v^2 U_v}{A_2}\left(X_s \sin(\delta_2 - \phi_2) - R_s \cos(\delta_2 - \phi_2)\right) \quad \text{(II.22)}$$

$$\frac{\partial^2 Q_s}{\partial T_v \partial V_s} = \frac{4V_s T_v}{A_2}\left(2B_{ss}(R_s F_1 + X_s F_2) - R_s R_4 + X_s(T_v^2 + R_3) + F_2\right) + \frac{V_p}{T_v} H_{sp}\left(1 - \frac{4T_v^2}{A_2}(R_s F_1 + X_s F_2)\right) - \frac{2V_p T_v^2 U_v}{A_2}\left(R_s \sin(\delta_2 - \phi_2) + X_s \cos(\delta_2 - \phi_2)\right) \quad \text{(II.23)}$$

$$\frac{\partial^2 Q_s}{\partial T_v \partial V_p} = \frac{V_s}{T_v} H_{sp}\left(1 - \frac{4T_v^2}{A_2}(R_s F_1 + X_s F_2)\right) - \frac{2V_s T_v^2 U_v}{A_2}\left(R_s \sin(\delta_2 - \phi_2) + X_s \cos(\delta_2 - \phi_2)\right) \quad \text{(II.24)}$$

The second partial derivatives of power flow equations with respect to the tap changer T_v,

$$\frac{\partial F_1}{\partial T_v} = 2T_v R_s, \quad \text{(II.25)}$$

$$\frac{\partial F_2}{\partial T_v} = 2T_v X_s \quad \text{(II.26)}$$

$$\frac{\partial A_2}{\partial T_v} = 4T_v^3 R_s^2 + 4T_v R_s U_v^2 R_p + 4T_v R_s R_{eq1} + 4T_v^3 X_s^2 + 4T_v X_s U_v^2 X_p + 4T_v X_s X_{eq1} \quad \text{(II.27)}$$

$$\frac{\partial K1}{\partial T_v} = \frac{\partial}{\partial T_v}\left(1 - \frac{4T_v^2}{A_2}(R_s F_1 + X_s F_2)\right) = -\left(\begin{array}{l} \frac{4T_v^2}{A_2}\left(R_s \frac{\partial F_1}{\partial T_v} + X_s \frac{\partial F_2}{\partial T_v}\right) \\ +\left(\frac{1}{A_2}\right)\left(8T_v A_2 - 4T_v^2 \frac{\partial A_2}{\partial T_v}\right)(R_s F_1 + X_s F_2) \end{array}\right) \quad \text{(II.28)}$$

$$\frac{\partial}{\partial T_v}\left(\frac{T_v}{A_2}\right) = \left(\frac{1}{A_2^2}\right)\left(A_2 - T_v \frac{\partial A_2}{\partial T_v}\right) \quad \text{(II.29)}$$

$$\frac{\partial}{\partial T_v}\left(\frac{V_p V_s}{T_v}\right) = -\frac{V_p V_s}{T_v^2} \tag{II.30}$$

$$\frac{\partial}{\partial T_v}\left(\frac{T_v^2}{A_2}\right) = \left(\frac{1}{A_2^2}\right)\left(2T_v A_2 - T_v^2 \frac{\partial A_2}{\partial T_v}\right) \tag{II.31}$$

$$\frac{\partial G_{pp}}{\partial T_v} = \left(\frac{1}{A_2^2}\right)\left(A_2\left((U_v^2 + R_1)\frac{\partial F_1}{\partial T_v} + R_2 \frac{\partial F_2}{\partial T_v}\right) - \left(F_1(U_v^2 + R_1) + F_2 R_2\right)\frac{\partial A_2}{\partial T_v}\right) \tag{II.32}$$

$$\begin{aligned}\frac{\partial N_{ps}}{\partial T_v} = &-\left(\frac{\cos\delta_1}{A_2^2}\right)\left(\begin{array}{l} A_2\left(T_v U_v\left(\cos\phi_1 \frac{\partial F_1}{\partial T_v} + \sin\phi_1 \frac{\partial F_2}{\partial T_v}\right) + U_v(F_1\cos\phi_1 + F_2\sin\phi_1)\right) \\ -T_v U_v(F_1\cos\phi_1 + F_2\sin\phi_1)\frac{\partial A_2}{\partial T_v}\end{array}\right) \\ &+\left(\frac{\sin\delta_1}{A_2^2}\right)\left(\begin{array}{l} A_2\left(T_v U_v\left(\cos\phi_1 \frac{\partial F_2}{\partial T_v} - \sin\phi_1 \frac{\partial F_1}{\partial T_v}\right) + U_v(F_2\cos\phi_1 - F_1\sin\phi_1)\right) \\ -T_v U_v(F_2\cos\phi_1 - F_1\sin\phi_1)\frac{\partial A_2}{\partial T_v}\end{array}\right)\end{aligned} \tag{II.33}$$

$$\begin{aligned}\frac{\partial^2 P_p}{\partial^2 T_v} = &2V_p^2\left(\begin{array}{l}\frac{T_v}{A_2}\left(-2G_{pp}\left(R_s\frac{\partial F_1}{\partial T_v} + X_s\frac{\partial F_2}{\partial T_v}\right) - 2(R_s F_1 + X_s F_2)\frac{\partial G_{pp}}{\partial T_v}\right) \\ +\left(R_s(U_v^2 + R_1) + X_s R_2 - 2G_{pp}(R_s F_1 + X_s F_2)\right)\frac{\partial}{\partial T_v}\left(\frac{T_v}{A_2}\right)\end{array}\right) \\ &+\frac{V_p V_s N_{ps}}{T_v}\frac{\partial K1}{\partial T_v} + \frac{V_p V_s K1}{T_v}\frac{\partial N_{ps}}{\partial T_v} + N_{ps}K1\frac{\partial}{\partial T_v}\left(\frac{V_p V_s}{T_v}\right) \\ &+2V_p V_s U_v\left(X_s\sin(\delta_1 - \phi_1) - R_s\cos(\delta_1 - \phi_1)\right)\frac{\partial}{\partial T_v}\left(\frac{T_v^2}{A_2}\right)\end{aligned} \tag{II.34}$$

$$\frac{\partial B_{pp}}{\partial T_v} = \left(\frac{1}{A_2^2}\right)\left(A_2\left(R_2\frac{\partial F_1}{\partial T_v} - (U_v^2 + R_1)\frac{\partial F_2}{\partial T_v}\right) - \left(F_1 R_2 - F_2(U_v^2 + R_1)\right)\frac{\partial A_2}{\partial T_v}\right) \tag{II.35}$$

$$\begin{aligned}\frac{\partial H_{ps}}{\partial T_v} = &-\left(\frac{\sin\delta_1}{A_2^2}\right)\left(\begin{array}{l} A_2\left(T_v U_v\left(\cos\phi_1 \frac{\partial F_1}{\partial T_v} + \sin\phi_1 \frac{\partial F_2}{\partial T_v}\right) + U_v(F_1\cos\phi_1 + F_2\sin\phi_1)\right) \\ -T_v U_v(F_1\cos\phi_1 + F_2\sin\phi_1)\frac{\partial A_2}{\partial T_v}\end{array}\right) \\ &-\left(\frac{\cos\delta_1}{A_2^2}\right)\left(\begin{array}{l} A_2\left(T_v U_v\left(\cos\phi_1 \frac{\partial F_2}{\partial T_v} - \sin\phi_1 \frac{\partial F_1}{\partial T_v}\right) + U_v(F_2\cos\phi_1 - F_1\sin\phi_1)\right) \\ -T_v U_v(F_2\cos\phi_1 - F_1\sin\phi_1)\frac{\partial A_2}{\partial T_v}\end{array}\right)\end{aligned} \tag{II.36}$$

$$\frac{\partial^2 Q_p}{\partial^2 T_v} = 2V_p^2 \left(\begin{array}{l} \frac{T_v}{A_2}\left(2B_{pp}\left(R_s\frac{\partial F_1}{\partial T_v} + X_s\frac{\partial F_2}{\partial T_v}\right) + 2(R_sF_1 + X_sF_2)\frac{\partial B_{pp}}{\partial T_v}\right) \\ +\left(X_s(U_v^2 + R_1) - R_sR_2 + 2B_{pp}(R_sF_1 + X_sF_2)\right)\frac{\partial}{\partial T_v}\left(\frac{T_v}{A_2}\right) \end{array} \right)$$

$$+ \frac{V_pV_sH_{ps}}{T_v}\frac{\partial K1}{\partial T_v} + \frac{V_pV_sK1}{T_v}\frac{\partial H_{ps}}{\partial T_v} + H_{ps}K1\frac{\partial}{\partial T_v}\left(\frac{V_pV_s}{T_v}\right) \qquad \text{(II.37)}$$

$$-2V_pV_sU_v\left(R_s\sin(\delta_1 - \phi_1) + X_s\cos(\delta_1 - \phi_1)\right)\frac{\partial}{\partial T_v}\left(\frac{T_v^2}{A_2}\right)$$

$$\frac{\partial G_{ss}}{\partial T_v} = \left(\frac{1}{A_2^2}\right)\left(A_2\left(2T_vF_1 + (T_v^2 + R_3)\frac{\partial F_1}{\partial T_v} + R_4\frac{\partial F_2}{\partial T_v}\right) - \left(F_1(T_v^2 + R_3) + F_2R_4\right)\frac{\partial A_2}{\partial T_v}\right) \text{(II.38)}$$

$$\frac{\partial N_{sp}}{\partial T_v} = -\left(\frac{\cos\delta_2}{A_2^2}\right)\left(\begin{array}{l} A_2\left(T_vU_v\left(\cos\phi_2\frac{\partial F_1}{\partial T_v} + \sin\phi_2\frac{\partial F_2}{\partial T_v}\right) + U_v(F_1\cos\phi_2 + F_2\sin\phi_2)\right) \\ -T_vU_v(F_1\cos\phi_2 + F_2\sin\phi_2)\frac{\partial A_2}{\partial T_v} \end{array} \right)$$

$$+\left(\frac{\sin\delta_2}{A_2^2}\right)\left(\begin{array}{l} A_2\left(T_vU_v\left(\cos\phi_2\frac{\partial F_2}{\partial T_v} - \sin\phi_2\frac{\partial F_1}{\partial T_v}\right) + U_v(F_2\cos\phi_2 - F_1\sin\phi_2)\right) \\ -T_vU_v(F_2\cos\phi_2 - F_1\sin\phi_2)\frac{\partial A_2}{\partial T_v} \end{array} \right) \qquad \text{(II.39)}$$

$$\frac{\partial^2 P_s}{\partial^2 T_v} = 2V_s^2 \left(\begin{array}{l} \frac{T_v}{A_2}\left(2R_sT_v + \frac{\partial F_1}{\partial T_v} - 2G_{ss}\left(R_s\frac{\partial F_1}{\partial T_v} + X_s\frac{\partial F_2}{\partial T_v}\right) - 2(R_sF_1 + X_sF_2)\frac{\partial G_{ss}}{\partial T_v}\right) \\ +\left(R_s(T_v^2 + R_3) + X_sR_4 + F_1 - 2G_{ss}(R_sF_1 + X_sF_2)\right)\frac{\partial}{\partial T_v}\left(\frac{T_v}{A_2}\right) \end{array} \right)$$

$$+ \frac{V_sV_pN_{sp}}{T_v}\frac{\partial K1}{\partial T_v} + \frac{V_sV_pK1}{T_v}\frac{\partial N_{sp}}{\partial T_v} + N_{sp}K1\frac{\partial}{\partial T_v}\left(\frac{V_pV_s}{T_v}\right)$$

$$+2V_sV_pU_v\left(X_s\sin(\delta_2 - \phi_2) - R_s\cos(\delta_2 - \phi_2)\right)\frac{\partial}{\partial T_v}\left(\frac{T_v^2}{A_2}\right) \qquad \text{(II.40)}$$

$$\frac{\partial B_{ss}}{\partial T_v} = \left(\frac{1}{A_2^2}\right)\left(A_2\left(R_4\frac{\partial F_1}{\partial T_v} - (T_v^2 + R_3)\frac{\partial F_2}{\partial T_v} - 2T_vF_2\right) - \left(F_1R_4 - F_2(T_v^2 + R_3)\right)\frac{\partial A_2}{\partial T_v}\right) \text{(II.41)}$$

$$\frac{\partial H_{sp}}{\partial T_v} = -\left(\frac{\sin\delta_2}{A_2^2}\right)\left(\begin{array}{l} A_2\left(T_v U_v\left(\cos\phi_2 \frac{\partial F_1}{\partial T_v} + \sin\phi_2 \frac{\partial F_2}{\partial T_v}\right) + U_v(F_1\cos\phi_2 + F_2\sin\phi_2)\right) \\ -T_v U_v(F_1\cos\phi_2 + F_2\sin\phi_2)\frac{\partial A_2}{\partial T_v} \end{array}\right)$$

$$-\left(\frac{\cos\delta_2}{A_2^2}\right)\left(\begin{array}{l} A_2\left(T_v U_v\left(\cos\phi_2 \frac{\partial F_2}{\partial T_v} - \sin\phi_2 \frac{\partial F_1}{\partial T_v}\right) + U_v\left(F_2\cos\phi_2 - F_1\sin\phi_2\right)\right) \\ -T_v U_v\left(F_2\cos\phi_2 - F_1\sin\phi_2\right)\frac{\partial A_2}{\partial T_v} \end{array}\right) \tag{II.42}$$

$$\frac{\partial^2 Q_s}{\partial^2 T_v} = 2V_s^2\left(\begin{array}{l} \frac{T_v}{A_2}\left(2B_{ss}\left(R_s\frac{\partial F_1}{\partial T_v} + X_s\frac{\partial F_2}{\partial T_v}\right) + 2(R_sF_1 + X_sF_2)\frac{\partial B_{ss}}{\partial T_v} + 2X_sT_v + \frac{\partial F_2}{\partial T_v}\right) \\ +\left(X_s(T_v^2 + R_3) - R_sR_4 + 2B_{ss}(R_sF_1 + X_sF_2) + F_2\right)\frac{\partial}{\partial T_v}\left(\frac{T_v}{A_2}\right) \end{array}\right)$$

$$+\frac{V_sV_pH_{sp}}{T_v}\frac{\partial K1}{\partial T_v} + \frac{V_sV_pK1}{T_v}\frac{\partial H_{sp}}{\partial T_v} + H_{sp}K1\frac{\partial}{\partial T_v}\left(\frac{V_pV_s}{T_v}\right)$$

$$-2V_sV_pU_v\left(R_s\sin(\delta_2 - \phi_2) + X_s\cos(\delta_2 - \phi_2)\right)\frac{\partial}{\partial T_v}\left(\frac{T_v^2}{A_2}\right) \tag{II.43}$$

The first partial derivatives of power flow equations with respect to the tap changer in the secondary winding U_v,

$$\frac{\partial P_p}{\partial U_v} = \frac{2V_p^2U_v}{A_2}\left(R_p(U_v^2 + R_1) + X_pR_2 + F_1 - 2G_{pp}(R_pF_1 + X_pF_2)\right)$$

$$+\frac{V_pV_s}{U_v}(G_{ps}\cos\delta_1 + B_{ps}\sin\delta_1)\left(1 - \frac{4U_v^2}{A_2}(R_pF_1 + X_pF_2)\right) \tag{II.44}$$

$$+\frac{2V_pV_sU_v^2T_v}{A_2}\left(X_p\sin(\delta_1 - \phi_1) - R_p\cos(\delta_1 - \phi_1)\right)$$

$$\frac{\partial Q_p}{\partial U_v} = \frac{2V_p^2U_v}{A_2}\left(2B_{pp}(R_pF_1 + X_pF_2) - R_pR_2 + X_p(U_v^2 + R_1) + F_2\right)$$

$$+\frac{V_pV_s}{U_v}(G_{ps}\sin\delta_1 - B_{ps}\cos\delta_1)\left(1 - \frac{4U_v^2}{A_2}(R_pF_1 + X_pF_2)\right) \tag{II.45}$$

$$-\frac{2V_pV_sU_v^2T_v}{A_2}\left(R_p\sin(\delta_1 - \phi_1) + X_p\cos(\delta_1 - \phi_1)\right)$$

$$\frac{\partial P_s}{\partial U_v} = \frac{2V_s^2 U_v}{A_2}\left(R_p(T_v^2 + R_3) + X_p R_4 - 2G_{ss}(R_p F_1 + X_p F_2)\right)$$
$$+ \frac{V_s V_p}{U_v}(G_{sp}\cos\delta_2 + B_{sp}\sin\delta_2)\left(1 - \frac{4U_v^2}{A_2}(R_p F_1 + X_p F_2)\right) \quad \text{(II.46)}$$
$$+ \frac{2V_s V_p U_v^2 T_v}{A_2}\left(X_p \sin(\delta_2 - \phi_2) - R_p \cos(\delta_2 - \phi_2)\right)$$

$$\frac{\partial Q_s}{\partial U_v} = \frac{2V_s^2 U_v}{A_2}\left(2B_{ss}(R_p F_1 + X_s F_2) - R_p R_4 + X_p(T_v^2 + R_3)\right)$$
$$+ \frac{V_s V_p}{U_v}(G_{sp}\sin\delta_2 - B_{sp}\cos\delta_2)\left(1 - \frac{4U_v^2}{A_2}(R_p F_1 + X_p F_2)\right) \quad \text{(II.47)}$$
$$- \frac{2V_s V_p U_v^2 T_v}{A_2}\left(R_p \sin(\delta_2 - \phi_2) + X_p \cos(\delta_2 - \phi_2)\right)$$

The second partial derivatives of power flow equations with respect to the tap changer U_v and phase angles

$$\frac{\partial^2 P_p}{\partial U_v \partial \delta_p} = -\frac{V_p V_s H_{ps}}{U_v}\left(1 - \frac{4U_v^2}{A_2}(R_p F_1 + X_p F_2)\right)$$
$$+ \frac{2V_p V_s U_v^2 T_v}{A_2}\left(X_p \cos(\delta_1 - \phi_1) + R_p \sin(\delta_1 - \phi_1)\right) \quad \text{(II.48)}$$

$$\frac{\partial^2 P_p}{\partial U_v \partial \delta_s} = \frac{V_p V_s H_{ps}}{U_v}\left(1 - \frac{4U_v^2}{A_2}(R_p F_1 + X_p F_2)\right)$$
$$- \frac{2V_p V_s U_v^2 T_v}{A_2}\left(X_p \cos(\delta_1 - \phi_1) + R_p \sin(\delta_1 - \phi_1)\right) \quad \text{(II.49)}$$

$$\frac{\partial^2 Q_p}{\partial U_v \partial \delta_p} = \frac{V_p V_s N_{ps}}{U_v}\left(1 - \frac{4U_v^2}{A_2}(R_p F_1 + X_p F_2)\right)$$
$$- \frac{2V_p V_s U_v^2 T_v}{A_2}\left(R_p \cos(\delta_1 - \phi_1) - X_p \sin(\delta_1 - \phi_1)\right) \quad \text{(II.50)}$$

$$\frac{\partial^2 Q_p}{\partial U_v \partial \delta_s} = -\frac{V_p V_s N_{ps}}{U_v}\left(1 - \frac{4U_v^2}{A_2}(R_p F_1 + X_p F_2)\right)$$
$$+ \frac{2V_p V_s U_v^2 T_v}{A_2}\left(R_p \cos(\delta_1 - \phi_1) - X_p \sin(\delta_1 - \phi_1)\right) \quad \text{(II.51)}$$

$$\frac{\partial^2 P_s}{\partial U_v \partial \delta_s} = -\frac{V_s V_p H_{sp}}{U_v}\left(1 - \frac{4U_v^2}{A_2}(R_p F_1 + X_p F_2)\right)$$
$$+ \frac{2V_s V_p U_v^2 T_v}{A_2}\left(X_p \cos(\delta_2 - \phi_2) + R_p \sin(\delta_2 - \phi_2)\right) \quad \text{(II.52)}$$

$$\frac{\partial^2 P_s}{\partial U_v \partial \delta_p} = \frac{V_s V_p H_{sp}}{U_v}\left(1-\frac{4U_v^2}{A_2}(R_p F_1 + X_p F_2)\right) - \frac{2V_s V_p U_v^2 T_v}{A_2}\left(X_p \cos(\delta_2 - \phi_2) + R_p \sin(\delta_2 - \phi_2)\right) \tag{II.53}$$

$$\frac{\partial^2 Q_s}{\partial U_v \partial \delta_s} = \frac{V_s V_p N_{sp}}{U_v}\left(1-\frac{4U_v^2}{A_2}(R_p F_1 + X_p F_2)\right) - \frac{2V_s V_p U_v^2 T_v}{A_2}\left(R_p \cos(\delta_2 - \phi_2) - X_p \sin(\delta_2 - \phi_2)\right) \tag{II.54}$$

$$\frac{\partial^2 Q_s}{\partial U_v \partial \delta_p} = -\frac{V_s V_p N_{sp}}{U_v}\left(1-\frac{4U_v^2}{A_2}(R_p F_1 + X_p F_2)\right) + \frac{2V_s V_p U_v^2 T_v}{A_2}\left(R_p \cos(\delta_2 - \phi_2) - X_p \sin(\delta_2 - \phi_2)\right) \tag{II.55}$$

The second partial derivatives of power flow equations with respect to the tap changer U_v and voltages,

$$\frac{\partial^2 P_p}{\partial U_v \partial V_p} = \frac{4V_p U_v}{A_2}\left(R_p(U_v^2 + R_1) + X_p R_2 + F_1 - 2G_{pp}(R_p F_1 + X_p F_2)\right) + \frac{V_s}{U_v} N_{ps}\left(1-\frac{4U_v^2}{A_2}(R_p F_1 + X_p F_2)\right) + \frac{2V_s U_v^2 T_v}{A_2}\left(X_p \sin(\delta_1 - \phi_1) - R_p \cos(\delta_1 - \phi_1)\right) \tag{II.56}$$

$$\frac{\partial^2 P_p}{\partial U_v \partial V_s} = \frac{V_p}{U_v} N_{ps}\left(1-\frac{4U_v^2}{A_2}(R_p F_1 + X_p F_2)\right) + \frac{2V_p U_v^2 T_v}{A_2}\left(X_p \sin(\delta_1 - \phi_1) - R_p \cos(\delta_1 - \phi_1)\right) \tag{II.57}$$

$$\frac{\partial^2 Q_p}{\partial U_v \partial V_p} = \frac{4V_p U_v}{A_2}\left(2B_{pp}(R_p F_1 + X_p F_2) - R_p R_2 + X_p(U_v^2 + R_1) + F_2\right) + \frac{V_s}{U_v} H_{ps}\left(1-\frac{4U_v^2}{A_2}(R_p F_1 + X_p F_2)\right) - \frac{2V_s U_v^2 T_v}{A_2}\left(R_p \sin(\delta_1 - \phi_1) + X_p \cos(\delta_1 - \phi_1)\right) \tag{II.58}$$

$$\frac{\partial^2 Q_p}{\partial U_v \partial V_s} = \frac{V_p}{U_v} H_{ps}\left(1-\frac{4U_v^2}{A_2}(R_p F_1 + X_p F_2)\right) - \frac{2V_p U_v^2 T_v}{A_2}\left(R_p \sin(\delta_1 - \phi_1) + X_p \cos(\delta_1 - \phi_1)\right) \tag{II.59}$$

$$\frac{\partial^2 P_s}{\partial U_v \partial V_s} = \frac{4V_s U_v}{A_2}\left(R_p(T_v^2 + R_3) + X_p R_4 - 2G_{ss}(R_p F_1 + X_p F_2)\right) + \frac{V_p}{U_v} N_{sp}\left(1 - \frac{4U_v^2}{A_2}(R_p F_1 + X_p F_2)\right) + \frac{2V_p U_v^2 T_v}{A_2}\left(X_p \sin(\delta_2 - \phi_2) - R_p \cos(\delta_2 - \phi_2)\right) \quad \text{(II.60)}$$

$$\frac{\partial^2 P_s}{\partial U_v \partial V_p} = \frac{V_s}{U_v} N_{sp}\left(1 - \frac{4U_v^2}{A_2}(R_p F_1 + X_p F_2)\right) + \frac{2V_s U_v^2 T_v}{A_2}\left(X_p \sin(\delta_2 - \phi_2) - R_p \cos(\delta_2 - \phi_2)\right) \quad \text{(II.61)}$$

$$\frac{\partial^2 Q_s}{\partial U_v \partial V_s} = \frac{4V_s U_v}{A_2}\left(2B_{ss}(R_p F_1 + X_s F_2) - R_p R_4 + X_p(T_v^2 + R_3)\right) + \frac{V_p}{U_v} H_{sp}\left(1 - \frac{4U_v^2}{A_2}(R_p F_1 + X_p F_2)\right) - \frac{2V_p U_v^2 T_v}{A_2}\left(R_p \sin(\delta_2 - \phi_2) + X_p \cos(\delta_2 - \phi_2)\right) \quad \text{(II.62)}$$

$$\frac{\partial^2 Q_s}{\partial U_v \partial V_p} = \frac{V_s}{U_v} H_{sp}\left(1 - \frac{4U_v^2}{A_2}(R_p F_1 + X_p F_2)\right) - \frac{2V_s U_v^2 T_v}{A_2}\left(R_p \sin(\delta_2 - \phi_2) + X_p \cos(\delta_2 - \phi_2)\right) \quad \text{(II.63)}$$

The second partial derivatives of power flow equations with respect to the tap changer U_v,

$$\frac{\partial F_1}{\partial U_v} = 2U_v R_p \quad \text{(II.64)}$$

$$\frac{\partial F_2}{\partial U_v} = 2U_v X_p \quad \text{(II.65)}$$

$$\frac{\partial A_2}{\partial U_v} = 4U_v^3 R_p^2 + 4T_v^2 R_s U_v R_p + 4U_v R_p R_{eq1} + 4U_v^3 X_p^2 + 4T_v^2 X_s U_v X_p + 4U_v X_p X_{eq1} \quad \text{(II.66)}$$

$$\frac{\partial K2}{\partial T_v} = \frac{\partial}{\partial U_v}\left(1 - \frac{4U_v^2}{A_2}(R_p F_1 + X_p F_2)\right) = -\left(\frac{4U_v^2}{A_2}\left(R_p \frac{\partial F_1}{\partial U_v} + X_p \frac{\partial F_2}{\partial U_v}\right) + \left(\frac{1}{A_2}\right)\left(8U_v A_2 - 4U_v^2 \frac{\partial A_2}{\partial U_v}\right)(R_p F_1 + X_p F_2)\right) \quad \text{(II.67)}$$

$$\frac{\partial}{\partial T_v}\left(\frac{U_v}{A_2}\right) = \left(\frac{1}{A_2^2}\right)\left(A_2 - U_v \frac{\partial A_2}{\partial U_v}\right) \quad \text{(II.68)}$$

$$\frac{\partial}{\partial T_v}\left(\frac{V_p V_s}{U_v}\right) = -\frac{V_p V_s}{U_v^2} \tag{II.69}$$

$$\frac{\partial}{\partial U_v}\left(\frac{U_v^2}{A_2}\right) = \left(\frac{1}{A_2^2}\right)\left(2U_v A_2 - U_v^2 \frac{\partial A_2}{\partial U_v}\right) \tag{II.70}$$

$$\frac{\partial N_{ps}}{\partial U_v} = -\left(\frac{\cos\delta_1}{A_2^2}\right)\left(\begin{array}{l} A_2\left(T_v U_v\left(\cos\phi_1 \frac{\partial F_1}{\partial U_v} + \sin\phi_1 \frac{\partial F_2}{\partial U_v}\right) + T_v\left(F_1\cos\phi_1 + F_2\sin\phi_1\right)\right) \\ -T_v U_v (F_1\cos\phi_1 + F_2\sin\phi_1)\frac{\partial A_2}{\partial U_v} \end{array}\right)$$
$$+\left(\frac{\sin\delta_1}{A_2^2}\right)\left(\begin{array}{l} A_2\left(T_v U_v\left(\cos\phi_1 \frac{\partial F_2}{\partial U_v} - \sin\phi_1 \frac{\partial F_1}{\partial U_v}\right) + T_v(F_2\cos\phi_1 - F_1\sin\phi_1)\right) \\ -T_v U_v (F_2\cos\phi_1 - F_1\sin\phi_1)\frac{\partial A_2}{\partial U_v} \end{array}\right) \tag{II.71}$$

$$\frac{\partial G_{pp}}{\partial U_v} = \left(\frac{1}{A_2^2}\right)\left(A_2\left(2U_v F_1 + (U_v^2 + R_1)\frac{\partial F_1}{\partial U_v} + R_2\frac{\partial F_2}{\partial U_v}\right) - \left(F_1(U_v^2 + R_1) + F_2 R_2\right)\frac{\partial A_2}{\partial U_v}\right)$$

$$\frac{\partial^2 P_p}{\partial^2 U_v} = 2V_p^2\left(\begin{array}{l} \frac{U_v}{A_2}\left(2R_p U_v + \frac{\partial F_1}{\partial U_v} - 2G_{pp}\left(R_p\frac{\partial F_1}{\partial U_v} + X_p\frac{\partial F_2}{\partial U_v}\right) - 2(R_p F_1 + X_p F_2)\frac{\partial G_{pp}}{\partial U_v}\right) \\ +\left(R_p(U_v^2 + R_1) + X_p R_2 + F_1 - 2G_{pp}(R_p F_1 + X_p F_2)\right)\frac{\partial}{\partial U_v}\left(\frac{U_v}{A_2}\right) \end{array}\right)$$
$$+\frac{V_p V_s N_{ps}}{U_v}\frac{\partial K2}{\partial U_v} + \frac{V_p V_s K2}{U_v}\frac{\partial N_{ps}}{\partial U_v} + N_{ps}K2\frac{\partial}{\partial U_v}\left(\frac{V_p V_s}{U_v}\right)$$
$$+2V_p V_s T_v\left(X_p\sin(\delta_1 - \phi_1) - R_p\cos(\delta_1 - \phi_1)\right)\frac{\partial}{\partial U_v}\left(\frac{U_v^2}{A_2}\right) \tag{II.72}$$

$$\frac{\partial H_{ps}}{\partial U_v} = -\left(\frac{\sin\delta_1}{A_2^2}\right)\left(\begin{array}{l} A_2\left(T_v U_v\left(\cos\phi_1 \frac{\partial F_1}{\partial U_v} + \sin\phi_1 \frac{\partial F_2}{\partial U_v}\right) + T_v(F_1\cos\phi_1 + F_2\sin\phi_1)\right) \\ -T_v U_v (F_1\cos\phi_1 + F_2\sin\phi_1)\frac{\partial A_2}{\partial U_v} \end{array}\right)$$
$$-\left(\frac{\cos\delta_1}{A_2^2}\right)\left(\begin{array}{l} A_2\left(T_v U_v\left(\cos\phi_1 \frac{\partial F_2}{\partial U_v} - \sin\phi_1 \frac{\partial F_1}{\partial U_v}\right) + T_v(F_2\cos\phi_1 - F_1\sin\phi_1)\right) \\ -T_v U_v (F_2\cos\phi_1 - F_1\sin\phi_1)\frac{\partial A_2}{\partial U_v} \end{array}\right) \tag{II.73}$$

$$\frac{\partial B_{pp}}{\partial U_v} = \left(\frac{1}{A_2^2}\right)\left(A_2\left(R_2\frac{\partial F_1}{\partial U_v} - (U_v^2 + R_1)\frac{\partial F_2}{\partial U_v} - 2U_v F_2\right) - \left(F_1 R_2 - F_2(U_v^2 + R_1)\right)\frac{\partial A_2}{\partial U_v}\right) \tag{II.74}$$

$$\frac{\partial^2 Q_p}{\partial^2 U_v} = 2V_p^2 \left(\begin{array}{l} \frac{U_v}{A_2}\left(2B_{pp}\left(R_p\frac{\partial F_1}{\partial U_v} + X_s\frac{\partial F_2}{\partial U_v}\right) + 2(R_pF_1 + X_pF_2)\frac{\partial B_{pp}}{\partial U_v} + 2X_pU_v + \frac{\partial F_2}{\partial U_v}\right) \\ +\left(X_p(U_v^2 + R_1) - R_pR_2 + 2B_{pp}(R_pF_1 + X_pF_2) + F_2\right)\frac{\partial}{\partial U_v}\left(\frac{T_v}{A_2}\right) \end{array} \right)$$

$$+\frac{V_pV_sH_{ps}}{U_v}\frac{\partial K2}{\partial T_v} + \frac{V_pV_sK2}{U_v}\frac{\partial H_{ps}}{\partial U_v} + H_{ps}K2\frac{\partial}{\partial U_v}\left(\frac{V_pV_s}{U_v}\right)$$

$$-2V_pV_sT_v\left(R_p\sin(\delta_1 - \phi_1) + X_p\cos(\delta_1 - \phi_1)\right)\frac{\partial}{\partial U_v}\left(\frac{U_v^2}{A_2}\right) \qquad \text{(II.75)}$$

$$\frac{\partial N_{ps}}{\partial U_v} = -\left(\frac{\cos\delta_2}{A_2^2}\right)\left(\begin{array}{l} A_2\left[T_vU_v\left(\cos\phi_2\frac{\partial F_1}{\partial U_v} + \sin\phi_2\frac{\partial F_2}{\partial U_v}\right) + T_v(F_1\cos\phi_2 + F_2\sin\phi_2)\right] \\ -T_vU_v\left(F_1\cos\phi_2 + F_2\sin\phi_2\right)\frac{\partial A_2}{\partial U_v} \end{array} \right)$$

$$+\left(\frac{\sin\delta_2}{A_2^2}\right)\left(\begin{array}{l} A_2\left(T_vU_v\left(\cos\phi_2\frac{\partial F_2}{\partial U_v} - \sin\phi_2\frac{\partial F_1}{\partial U_v}\right) + T_v(F_2\cos\phi_2 - F_1\sin\phi_2)\right) \\ -T_vU_v(F_2\cos\phi_2 - F_1\sin\phi_2)\frac{\partial A_2}{\partial U_v} \end{array} \right) \qquad \text{(II.76)}$$

$$\frac{\partial G_{ss}}{\partial U_v} = \left(\frac{1}{A_2^2}\right)\left(A_2\left((T_v^2 + R_3)\frac{\partial F_1}{\partial U_v} + R_4\frac{\partial F_2}{\partial U_v}\right) - \left(F_1(T_v^2 + R_3) + F_2R_4\right)\frac{\partial A_2}{\partial U_v}\right) \qquad \text{(II.77)}$$

$$\frac{\partial^2 P_s}{\partial^2 U_v} = 2V_s^2 \left(\begin{array}{l} \frac{U_v}{A_2}\left(-2G_{ss}\left(R_p\frac{\partial F_1}{\partial U_v} + X_p\frac{\partial F_2}{\partial U_v}\right) - 2(R_pF_1 + X_pF_2)\frac{\partial G_{ss}}{\partial U_v}\right) \\ +\left(R_p(T_v^2 + R_3) + X_pR_4 - 2G_{ss}(R_pF_1 + X_pF_2)\right)\frac{\partial}{\partial U_v}\left(\frac{T_v}{A_2}\right) \end{array} \right)$$

$$+\frac{V_sV_pN_{sp}}{U_v}\frac{\partial K2}{\partial U_v} + \frac{V_sV_pK2}{U_v}\frac{\partial N_{sp}}{\partial U_v} + N_{sp}K2\frac{\partial}{\partial U_v}\left(\frac{V_pV_s}{U_v}\right) \qquad \text{(II.78)}$$

$$+2V_sV_pT_v\left(X_p\sin(\delta_2 - \phi_2) - R_p\cos(\delta_2 - \phi_2)\right)\frac{\partial}{\partial U_v}\left(\frac{U_v^2}{A_2}\right)$$

$$\frac{\partial B_{ss}}{\partial U_v} = \left(\frac{1}{A_2^2}\right)\left(A_2\left(R_4\frac{\partial F_1}{\partial U_v} - (T_v^2 + R_3)\frac{\partial F_2}{\partial U_v}\right) - \left(F_1R_4 - F_2(T_v^2 + R_3)\right)\frac{\partial A_2}{\partial U_v}\right) \qquad \text{(II.79)}$$

$$\frac{\partial H_{sp}}{\partial U_v} = -\left(\frac{\sin\delta_2}{A_2^2}\right)\left(\begin{array}{l} A_2\left(T_v U_v\left(\cos\phi_2 \frac{\partial F_1}{\partial U_v} + \sin\phi_2 \frac{\partial F_2}{\partial U_v}\right) + T_v(F_1\cos\phi_2 + F_2\sin\phi_2)\right) \\ -T_v U_v(F_1\cos\phi_2 + F_2\sin\phi_2)\frac{\partial A_2}{\partial U_v} \end{array}\right)$$

$$-\left(\frac{\cos\delta_2}{A_2^2}\right)\left(\begin{array}{l} A_2\left(T_v U_v\left(\cos\phi_2 \frac{\partial F_2}{\partial U_v} - \sin\phi_2 \frac{\partial F_1}{\partial U_v}\right) + T_v(F_2\cos\phi_2 - F_1\sin\phi_2)\right) \\ -T_v U_v(F_2\cos\phi_2 - F_1\sin\phi_2)\frac{\partial A_2}{\partial U_v} \end{array}\right) \tag{II.80}$$

$$\frac{\partial^2 Q_s}{\partial^2 U_v} = 2V_s^2\left(\begin{array}{l} \frac{U_v}{A_2}\left(2B_{ss}\left(R_p\frac{\partial F_1}{\partial U_v} + X_p\frac{\partial F_2}{\partial U_v}\right) + 2(R_pF_1 + X_pF_2)\frac{\partial B_{ss}}{\partial U_v}\right) \\ +\left(X_p(T_v^2 + R_3) - R_pR_4 + 2B_{ss}(R_pF_1 + X_pF_2)\right)\frac{\partial}{\partial U_v}\left(\frac{U_v}{A_2}\right) \end{array}\right)$$

$$+\frac{V_sV_pH_{sp}}{U_v}\frac{\partial K2}{\partial U_v} + \frac{V_sV_pK2}{U_v}\frac{\partial H_{sp}}{\partial U_v} + H_{sp}K2\frac{\partial}{\partial U_v}\left(\frac{V_pV_s}{U_v}\right) \tag{II.81}$$

$$-2V_sV_pT_v\left(R_p\sin(\delta_2 - \phi_2) + X_p\cos(\delta_2 - \phi_2)\right)\frac{\partial}{\partial U_v}\left(\frac{U_v^2}{A_2}\right)$$

Appendix III

TCSC Fundamental Impedance

III.1 TCSC Current and Voltage Equations

The derivations are started by assuming that a loop current is trapped in the reactor-capacitor circuit and that the power system can be represented by an ideal, sinusoidal current source. Under those assumptions, the TCSC steady state voltage and current equations can be obtained from the analysis of a parallel *LC* circuit with a variable inductance. This representation is shown in Figure III.1 and the asymmetrical current pulses through the TCSC thyristors are shown schematically in Figure III.2. The original time reference (OR) is taken to be the positive-going zero-crossing of the voltage across the TCSC inductance. Also, an auxiliary time reference (AR) is taken at a time when the thyristor starts to conduct. Bold and lower case types represent complex and time domain quantities, respectively.

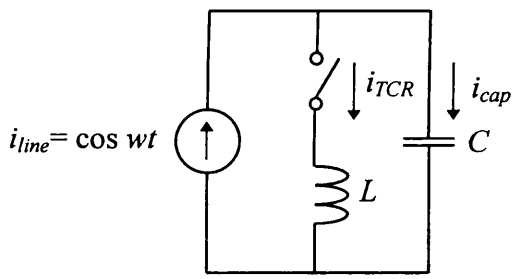

Figure III.1. Equivalent electric circuit of a TCSC module.

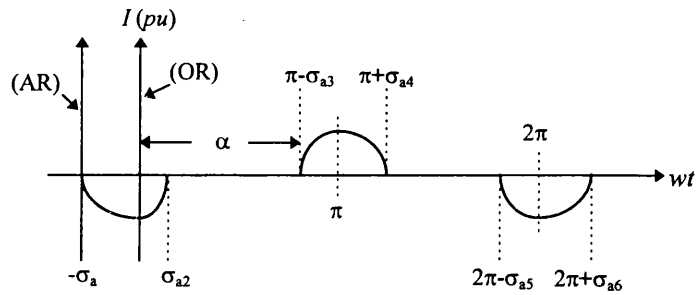

Figure III.2. Asymmetrical thyristor current.

The line current is,

$$i_{line} = \cos wt \tag{III.1}$$

or, in the AR plane,

$$i_{line} = \cos(wt - \sigma_a) = \cos wt \cos\sigma_a + \sin wt \sin\sigma_a \tag{III.2}$$

Applying Kirchhoff Current Law (KCL) to the circuit shown in Figure III.1,

$$i_{line} = i_{TCR} + i_{cap} \tag{III.3}$$

During the conduction period the voltage across the TCSC inductive and capacitive reactances coincide,

$$L\frac{di_{TCR}}{dt} = \frac{1}{C}\int i_{cap}\,dt + V_{cap}^{+} \tag{III.4}$$

where V_{cap}^{+} is the voltage across the capacitor when the thyristor turns on.

Expressing (III.2)-(III.4) in the Laplace domain,

$$I_{line}(s) = \cos\sigma_a \frac{s}{s^2 + w^2} + \sin\sigma_a \frac{w}{s^2 + w^2} \tag{III.5}$$

$$I_{line}(s) = I_{TCR}(s) + I_{cap}(s) \tag{III.6}$$

$$I_{cap}(s) = s^2 LC\, I_{TCR}(s) - CV_{cap}^{+} \tag{III.7}$$

Substituting (III.5) and (III.7) into (III.6), and solving for I_{TCR}(s),

$$\begin{aligned} I_{TCR}(s) = {} & w_o^2 \cos\sigma_a \frac{s}{(s^2 + w_o^2)(s^2 + w^2)} \\ & + w_o^2\, w \sin\sigma_a \frac{1}{(s^2 + w_o^2)(s^2 + w^2)} + \frac{w_o^2 CV_{cap}^{+}}{s^2 + w_o^2} \end{aligned} \tag{III.8}$$

where

$$w_o^2 = \frac{1}{LC} \tag{III.9}$$

From Laplace transforms tables,

$$\mathcal{L}^{-1}\left\{\frac{1}{s^2 + w_o^2}\right\} = \frac{1}{w_o}\sin w_o t \tag{III.10}$$

$$\mathcal{L}^{-1}\left\{\frac{s}{(s^2 + w_o^2)(s^2 + w^2)}\right\} = \frac{\cos wt - \cos w_o t}{w_o^2 - w^2} \tag{III.11}$$

$$\mathcal{L}^{-1}\left\{\frac{1}{(s^2 + w_o^2)(s^2 + w^2)}\right\} = \frac{w_o \sin wt - w \sin w_o t}{w_o\, w\left(w_o^2 - w^2\right)} \tag{III.12}$$

Expressing (III.8) in the time domain leads to,

$$\begin{aligned} i_{TCR} = {} & A\cos(wt - \sigma_a) - A\cos\sigma_a \cos w_o t \\ & - B\sin\sigma_a \sin w_o t + DV_{cap}^{+} \sin w_o t \end{aligned} \tag{III.13}$$

where

$$A = \frac{w_o^2}{w_o^2 - w^2} \qquad B = \frac{w_o w}{w_o^2 - w^2} \qquad D = w_o C \tag{III.14}$$

To express eq. (A.10) within the range [$-\sigma_a$, σ_{a2}], it is only necessary to shift the equation to the original time reference by adding σ_a/w to the time variable. Hence, replacing $t+\sigma_a/w$ by t into (III.13),

$$\begin{aligned} i_{thy} = A\cos\left(w\left(t+\frac{\sigma_a}{w}\right)-\sigma_a\right) - A\cos\sigma_a\cos w_o\left(t+\frac{\sigma_a}{w}\right) \\ - B\sin\sigma_a\sin w_o\left(t+\frac{\sigma_a}{w}\right) + DV_{cap}^{+}\sin w_o\left(t+\frac{\sigma_a}{w}\right) \end{aligned} \quad \text{(III.15)}$$

and performing some operations,

$$\begin{aligned} i_{TCR} &= A\cos wt \\ &+\left(-A\cos\sigma_a\cos\varpi\sigma_a - B\sin\sigma_a\sin\varpi\sigma_a + DV_{cap}^{+}\sin\varpi\sigma_a\right)\cos w_o t \\ &+\left(A\cos\sigma_a\sin\varpi\sigma_a - B\sin\sigma_a\cos\varpi\sigma_a + DV_{cap}^{+}\cos\varpi\sigma_a\right)\sin w_o t \end{aligned} \quad \text{(III.16)}$$

where

$$\varpi = \frac{w_o}{w} \quad \text{(III.17)}$$

This equation is valid for $wt \in [-\sigma_a , \sigma_{a2}]$ and contains the transient and steady state components. It must be noted that the resulting current is symmetric.

The steady state is reached when the current pulses become symmetric, i.e. $\sigma_a = \sigma_{a2}$, = ... = σ_{a6}. This condition takes place when, for a given angle, the TCSC capacitor voltage, V^{+}_{cap}, is at the same level as the coefficient of the sinusoidal term, $\sin(w_o t)$, and equal to zero. At this point the capacitor's voltage is,

$$V_{cap}^{+} = \frac{B}{D}\sin(\sigma_a) - \frac{A}{D}\cos(\sigma_a)\tan(\varpi\sigma_a) \quad \text{(III.18)}$$

The steady-state thyristor current equation is obtained by substituting eq. (III.18) into equation (III.16),

$$i_{TCR} = A\cos(wt) - A\frac{\cos(\sigma_a)}{\cos(\varpi\sigma_a)}\cos(\varpi wt) \quad \text{(III.19)}$$

where

$$\sigma_a = \pi - \alpha \quad \text{(III.20)}$$

Equation (III.20) is symmetric and it is valid in the interval $wt \in [-\sigma_a, \sigma_a]$ and $wt \in [2\pi-\sigma_a, 2\pi+\sigma_a]$.

Since the thyristor current has even and quarterly symmetry, its fundamental frequency component may be obtained by applying Fourier analysis to eq. (III.19),

$$I_{TCR(1)} = \frac{4}{\pi}\int_0^{\sigma_a}\left(A\cos(wt) - A\frac{\cos(\sigma_a)}{\cos(\varpi\sigma_a)}\cos(\varpi wt)\right)\cos(wt)d(wt) \quad \text{(III.20)}$$

Therefore, the TCR current at fundamental frequency is,

$$i_{TCR(1)} = I_{TCR(1)}\cos(wt) \quad \text{(III.21)}$$

where

$$\boldsymbol{I}_{TCR(1)} = A\left(\frac{2\sigma_a + \sin(2\sigma_a)}{\pi}\right) - \frac{4A\cos^2(\sigma_a)}{\varpi^2 - 1}\left(\frac{\varpi\tan(\varpi\sigma_a) - \tan(\sigma_a)}{\pi}\right) \quad \text{(III.22)}$$

III.2 Fundamental Impedance

The TCSC impedance at fundamental frequency is given by the following basic equation,

$$\boldsymbol{Z}_{TCSC(1)} = R_{TCSC(1)} + jX_{TCSC(1)} = \frac{\boldsymbol{V}_{TCSC(1)}}{\boldsymbol{I}_{line}} \quad \text{(III.23)}$$

where bold type indicates complex quantities. $\boldsymbol{V}_{TCSC(1)}$ is the fundamental frequency voltage across the TCSC module, $\boldsymbol{I}_{line}$ is the fundamental frequency line current and $Z_{TCSC(1)}$ is the TCSC impedance.

The voltage $\boldsymbol{V}_{TCSC(1)}$ is equal to the voltage across the TCSC capacitor and equation (III.23) can be written as,

$$\boldsymbol{Z}_{TCSC(1)} = \frac{-jX_C\boldsymbol{I}_{cap(1)}}{\boldsymbol{I}_{line}} \quad \text{(III.24)}$$

If the external power network is represented by an idealised current source, as seen from the TCSC terminals, this current source is equal to the sum of the currents flowing through the TCSC capacitor and inductor. The TCSC impedance can then be expressed as,

$$\boldsymbol{Z}_{TCSC(1)} = \frac{-jX_C(\boldsymbol{I}_{line} - \boldsymbol{I}_{TCR(1)})}{\boldsymbol{I}_{line}} \quad \text{(III.25)}$$

Substituting the expression for $\boldsymbol{I}_{TCR(1)}$, equation (III.21), into equation (III.25) and assuming,

$$\boldsymbol{I}_{line} = 1\cos\omega t \quad \text{(III.26)}$$

leads to the following expressions,

$$\boldsymbol{Z}_{TCSC(1)} = \frac{-jX_C(1\cos wt - I_{TCR(1)}\cos wt)}{1\cos wt} \quad \text{(III.27)}$$

$$\boldsymbol{Z}_{TCSC(1)} = -jX_C + jX_C I_{TCR(1)} \quad \text{(III.28)}$$

Substituting equation (III.22) into (III.28), the fundamental frequency TCSC impedance is,

$$\boldsymbol{Z}_{TCSC(1)} = -jX_C + jX_C\left(A\left(\frac{2\sigma_a + \sin(2\sigma_a)}{\pi}\right) - \frac{4A\cos^2(\sigma_a)}{k^2 - 1}\left(\frac{k\tan(k\sigma_a) - \tan(\sigma_a)}{\pi}\right)\right) \quad \text{(III.29)}$$

or,

$$\begin{aligned} X_{TCSC(1)} = &-X_C + C_1\left(2(\pi - \alpha) + \sin(2(\pi - \alpha))\right) \\ &- C_2\cos^2(\pi - \alpha)\left(\varpi\tan(\varpi(\pi - \alpha)) - \tan(\pi - \alpha)\right) \end{aligned} \quad \text{(III.30)}$$

where

$$X_{LC} = \frac{X_C X_L}{X_C - X_L} \tag{III.31}$$

$$C_1 = \frac{X_C + X_{LC}}{\pi} \tag{III.32}$$

$$C_2 = \frac{4 X_{LC}^2}{X_L \pi} \tag{III.33}$$

Appendix IV

Hessian and Jacobian Elements for the UPFC Model

IV.1 Sending Node

All first and second partial derivative terms corresponding to the sending end of the UPFC are given in this section. They are obtained by deriving equations (7.3) and (7.4) with respect to the UPFC state variables. First and second partial derivative terms for the receiving end and series and shunt sources are also given. They are derived from equations (7.5)-(7.10).

$$\begin{aligned}\frac{\partial P_s}{\partial \theta_s} = &-V_s V_r\left(G_{sr}\sin(\theta_s-\theta_r)-B_{sr}\cos(\theta_s-\theta_r)\right)\\ &-V_s V_{cR}\left(G_{sr}\sin(\theta_s-\theta_{cR})-B_{sr}\cos(\theta_s-\theta_{cR})\right)\\ &-V_s V_{vR}\left(G_{vR}\sin(\theta_s-\theta_{vR})-B_{vR}\cos(\theta_s-\theta_{vR})\right)\end{aligned} \tag{IV.1}$$

$$\frac{\partial P_s}{\partial \theta_r} = V_s V_r\left(G_{sr}\sin(\theta_s-\theta_r)-B_{sr}\cos(\theta_s-\theta_r)\right) \tag{IV.2}$$

$$\frac{\partial P_s}{\partial \theta_{cR}} = V_s V_{cR}\left(G_{sr}\sin(\theta_s-\theta_{cR})-B_{sr}\cos(\theta_s-\theta_{cR})\right) \tag{IV.3}$$

$$\frac{\partial P_s}{\partial \theta_{vR}} = V_s V_{vR}\left(G_{vR}\sin(\theta_s-\theta_{vR})-B_{vR}\cos(\theta_s-\theta_{vR})\right) \tag{IV.4}$$

$$\begin{aligned}\frac{\partial P_s}{\partial V_s} = &2V_s G_{ss}+V_r\left(G_{sr}\cos(\theta_s-\theta_r)+B_{sr}\sin(\theta_s-\theta_r)\right)\\ &+V_{cR}\left(G_{sr}\cos(\theta_s-\theta_{cR})+B_{sr}\sin(\theta_s-\theta_{cR})\right)\\ &+V_{vR}\left(G_{vR}\cos(\theta_s-\theta_{vR})+B_{vR}\sin(\theta_s-\theta_{vR})\right)\end{aligned} \tag{IV.5}$$

$$\frac{\partial P_s}{\partial V_r} = V_s\left(G_{sr}\cos(\theta_s-\theta_r)+B_{sr}\sin(\theta_s-\theta_r)\right) \tag{IV.6}$$

$$\frac{\partial P_s}{\partial V_{cR}} = V_s\left(G_{sr}\cos(\theta_s-\theta_{cR})+B_{sr}\sin(\theta_s-\theta_{cR})\right) \tag{IV.7}$$

$$\frac{\partial P_s}{\partial V_{vR}} = V_s\left(G_{vR}\cos(\theta_s - \theta_{vR}) + B_{vR}\sin(\theta_s - \theta_{vR})\right) \tag{IV.8}$$

$$\begin{aligned}\frac{\partial Q_s}{\partial \theta_s} = {} & V_s V_r\left(G_{sr}\cos(\theta_s - \theta_r) + B_{sr}\sin(\theta_s - \theta_r)\right) \\ & + V_s V_{cR}\left(G_{sr}\cos(\theta_s - \theta_{cR}) + B_{sr}\sin(\theta_s - \theta_{cR})\right) \\ & + V_s V_{vR}\left(G_{vR}\cos(\theta_s - \theta_{vR}) + B_{vR}\sin(\theta_s - \theta_{vR})\right)\end{aligned} \tag{IV.9}$$

$$\frac{\partial Q_s}{\partial \theta_r} = -V_s V_r\left(G_{sr}\cos(\theta_s - \theta_r) + B_{sr}\sin(\theta_s - \theta_r)\right) \tag{IV.10}$$

$$\frac{\partial Q_s}{\partial \theta_{cR}} = -V_s V_{cR}\left(G_{sr}\cos(\theta_s - \theta_{cR}) + B_{sr}\sin(\theta_s - \theta_{cR})\right) \tag{IV.11}$$

$$\frac{\partial Q_s}{\partial \theta_{vR}} = -V_s V_{vR}\left(G_{vR}\cos(\theta_s - \theta_{vR}) + B_{vR}\sin(\theta_s - \theta_{vR})\right) \tag{IV.12}$$

$$\begin{aligned}\frac{\partial Q_s}{\partial V_s} = {} & -2V_s B_{ss} + V_r\left(G_{sr}\sin(\theta_s - \theta_r) - B_{sr}\cos(\theta_s - \theta_r)\right) \\ & + V_{cR}\left(G_{sr}\sin(\theta_s - \theta_{cR}) - B_{sr}\cos(\theta_s - \theta_{cR})\right) \\ & + V_{vR}\left(G_{vR}\sin(\theta_s - \theta_{vR}) - B_{vR}\cos(\theta_s - \theta_{vR})\right)\end{aligned} \tag{IV.13}$$

$$\frac{\partial Q_s}{\partial V_r} = V_s\left(G_{sr}\sin(\theta_s - \theta_r) - B_{sr}\cos(\theta_s - \theta_r)\right) \tag{IV.14}$$

$$\frac{\partial Q_s}{\partial V_{cR}} = V_s\left(G_{sr}\sin(\theta_s - \theta_{cR}) - B_{sr}\cos(\theta_s - \theta_{cR})\right) \tag{IV.15}$$

$$\frac{\partial Q_s}{\partial V_{vR}} = V_s\left(G_{vR}\sin(\theta_s - \theta_{vR}) - B_{vR}\cos(\theta_s - \theta_{vR})\right) \tag{IV.16}$$

The second partial derivatives of the power flow equations are:

$$\begin{aligned}\frac{\partial^2 P_s}{\partial \theta_s^2} = {} & -V_s V_r\left(G_{sr}\cos(\theta_s - \theta_r) + B_{sr}\sin(\theta_s - \theta_r)\right) \\ & - V_s V_{cR}\left(G_{sr}\cos(\theta_s - \theta_{cR}) + B_{sr}\sin(\theta_s - \theta_{cR})\right) \\ & - V_s V_{vR}\left(G_{vR}\cos(\theta_s - \theta_{vR}) + B_{vR}\sin(\theta_s - \theta_{vR})\right)\end{aligned} \tag{IV.17}$$

$$\frac{\partial^2 P_s}{\partial \theta_s \partial \theta_r} = V_s V_r\left(G_{sr}\cos(\theta_s - \theta_r) + B_{sr}\sin(\theta_s - \theta_r)\right) \tag{IV.18}$$

$$\frac{\partial^2 P_s}{\partial \theta_s \partial \theta_{cR}} = V_s V_{cR}\left(G_{sr}\cos(\theta_s - \theta_{cR}) + B_{sr}\sin(\theta_s - \theta_{cR})\right) \tag{IV.19}$$

$$\frac{\partial^2 P_s}{\partial \theta_s \partial \theta_{vR}} = V_s V_{vR}\left(G_{vR}\cos(\theta_s - \theta_{vR}) + B_{vR}\sin(\theta_s - \theta_{vR})\right) \tag{IV.20}$$

$$\frac{\partial^2 P_s}{\partial\theta_s \partial V_s} = -V_r\left(G_{sr}\sin(\theta_s-\theta_r)-B_{sr}\cos(\theta_s-\theta_r)\right) - V_{cR}\left(G_{sr}\sin(\theta_s-\theta_{cR})-B_{sr}\cos(\theta_s-\theta_{cR})\right) - V_{vR}\left(G_{vR}\sin(\theta_s-\theta_{vR})-B_{vR}\cos(\theta_s-\theta_{vR})\right) \quad \text{(IV.21)}$$

$$\frac{\partial^2 P_s}{\partial\theta_s \partial V_r} = -V_s\left(G_{sr}\sin(\theta_s-\theta_r)-B_{sr}\cos(\theta_s-\theta_r)\right) \quad \text{(IV.22)}$$

$$\frac{\partial^2 P_s}{\partial\theta_s \partial V_{cR}} = -V_s\left(G_{sr}\sin(\theta_s-\theta_{cR})-B_{sr}\cos(\theta_s-\theta_{cR})\right) \quad \text{(IV.23)}$$

$$\frac{\partial^2 P_s}{\partial\theta_s \partial V_{vR}} = -V_s\left(G_{vR}\sin(\theta_s-\theta_{vR})-B_{vR}\cos(\theta_s-\theta_{vR})\right) \quad \text{(IV.24)}$$

$$\frac{\partial^2 P_s}{\partial\theta_r^2} = -V_sV_r\left(G_{sr}\cos(\theta_s-\theta_r)+B_{sr}\sin(\theta_s-\theta_r)\right) \quad \text{(IV.25)}$$

$$\frac{\partial^2 P_s}{\partial\theta_r \partial V_s} = V_r\left(G_{sr}\sin(\theta_s-\theta_r)-B_{sr}\cos(\theta_s-\theta_r)\right) \quad \text{(IV.26)}$$

$$\frac{\partial^2 P_s}{\partial\theta_r \partial V_r} = V_s\left(G_{sr}\sin(\theta_s-\theta_r)-B_{sr}\cos(\theta_s-\theta_r)\right) \quad \text{(IV.27)}$$

$$\frac{\partial^2 P_s}{\partial\theta_{cR}^2} = -V_sV_{cR}\left(G_{sr}\cos(\theta_s-\theta_{cR})+B_{sr}\sin(\theta_s-\theta_{cR})\right) \quad \text{(IV.28)}$$

$$\frac{\partial^2 P_s}{\partial\theta_{cR} \partial V_s} = V_{cR}\left(G_{sr}\sin(\theta_s-\theta_{cR})-B_{sr}\cos(\theta_s-\theta_{cR})\right) \quad \text{(IV.29)}$$

$$\frac{\partial^2 P_s}{\partial\theta_{cR} \partial V_{cR}} = V_s\left(G_{sr}\sin(\theta_s-\theta_{cR})-B_{sr}\cos(\theta_s-\theta_{cR})\right) \quad \text{(IV.30)}$$

$$\frac{\partial^2 P_s}{\partial\theta_{vR}^2} = -V_sV_{vR}\left(G_{vR}\cos(\theta_s-\theta_{vR})+B_{vR}\sin(\theta_s-\theta_{vR})\right) \quad \text{(IV.31)}$$

$$\frac{\partial^2 P_s}{\partial\theta_{vR} \partial V_s} = V_{vR}\left(G_{vR}\sin(\theta_s-\theta_{vR})-B_{vR}\cos(\theta_s-\theta_{vR})\right) \quad \text{(IV.32)}$$

$$\frac{\partial^2 P_s}{\partial\theta_{vR} \partial V_{vR}} = V_s\left(G_{vR}\sin(\theta_s-\theta_{vR})-B_{vR}\cos(\theta_s-\theta_{vR})\right) \quad \text{(IV.33)}$$

$$\frac{\partial^2 P_s}{\partial V_s^2} = 2G_{SS} \quad \text{(IV.34)}$$

$$\frac{\partial^2 P_s}{\partial V_s \partial V_r} = \left(G_{sr}\cos(\theta_s-\theta_r)+B_{sr}\sin(\theta_s-\theta_r)\right) \quad \text{(IV.35)}$$

$$\frac{\partial^2 P_s}{\partial V_s \partial V_{cR}} = \left(G_{sr}\cos(\theta_s-\theta_{cR})+B_{sr}\sin(\theta_s-\theta_{cR})\right) \quad \text{(IV.36)}$$

$$\frac{\partial^2 P_s}{\partial V_s \partial V_{vR}} = \left(G_{vR}\cos(\theta_s - \theta_{vR}) + B_{vR}\sin(\theta_s - \theta_{vR})\right) \tag{IV.37}$$

$$\begin{aligned}\frac{\partial^2 Q_s}{\partial \theta_S^2} = &-V_s V_r\left(G_{sr}\sin(\theta_s - \theta_r) - B_{sr}\cos(\theta_s - \theta_r)\right)\\ &-V_s V_{cR}\left(G_{sr}\sin(\theta_s - \theta_{cR}) - B_{sr}\cos(\theta_s - \theta_{cR})\right)\\ &-V_s V_{vR}\left(G_{vR}\sin(\theta_s - \theta_{vR}) - B_{sr}\cos(\theta_s - \theta_{vR})\right)\end{aligned} \tag{IV.38}$$

$$\frac{\partial^2 Q_s}{\partial \theta_s \partial \theta_r} = V_s V_r\left(G_{sr}\sin(\theta_s - \theta_r) - B_{sr}\cos(\theta_s - \theta_r)\right) \tag{IV.39}$$

$$\frac{\partial^2 Q_s}{\partial \theta_s \partial \theta_{cR}} = V_s V_{cR}\left(G_{sr}\sin(\theta_s - \theta_{cR}) - B_{sr}\cos(\theta_s - \theta_{cR})\right) \tag{IV.40}$$

$$\frac{\partial^2 Q_s}{\partial \theta_s \partial \theta_{vR}} = V_s V_{vR}\left(G_{vR}\sin(\theta_s - \theta_{vR}) - B_{vR}\cos(\theta_s - \theta_{vR})\right) \tag{IV.41}$$

$$\begin{aligned}\frac{\partial^2 Q_s}{\partial \theta_s \partial V_s} = &V_R\left(G_{sr}\cos(\theta_s - \theta_r) + B_{sr}\sin(\theta_s - \theta_r)\right)\\ &+V_{cR}\left(G_{sr}\cos(\theta_s - \theta_{cR}) + B_{sr}\sin(\theta_s - \theta_{cR})\right)\\ &+V_{vR}\left(G_{vR}\cos(\theta_s - \theta_{vR}) + B_{vR}\sin(\theta_s - \theta_{vR})\right)\end{aligned} \tag{IV.42}$$

$$\frac{\partial^2 Q_s}{\partial \theta_s \partial V_r} = V_s\left(G_{sr}\cos(\theta_s - \theta_r) + B_{sr}\sin(\theta_s - \theta_r)\right) \tag{IV.43}$$

$$\frac{\partial^2 Q_s}{\partial \theta_s \partial V_{cR}} = V_s\left(G_{sr}\cos(\theta_s - \theta_{cR}) + B_{sr}\sin(\theta_s - \theta_{cR})\right) \tag{IV.44}$$

$$\frac{\partial^2 Q_s}{\partial \theta_s \partial V_{vR}} = V_s\left(G_{vR}\cos(\theta_s - \theta_{vR}) + B_{vR}\sin(\theta_s - \theta_{vR})\right) \tag{IV.45}$$

$$\frac{\partial^2 Q_s}{\partial \theta_r^2} = -V_s V_r\left(G_{sr}\sin(\theta_s - \theta_r) - B_{sr}\cos(\theta_s - \theta_r)\right) \tag{IV.46}$$

$$\frac{\partial^2 Q_s}{\partial \theta_r \partial V_s} = -V_r\left(G_{sr}\cos(\theta_s - \theta_r) + B_{sr}\sin(\theta_s - \theta_r)\right) \tag{IV.47}$$

$$\frac{\partial^2 Q_s}{\partial \theta_r \partial V_r} = -V_s\left(G_{sr}\cos(\theta_s - \theta_r) + B_{sr}\sin(\theta_s - \theta_r)\right) \tag{IV.48}$$

$$\frac{\partial^2 Q_s}{\partial \theta_{cR}^2} = -V_s V_{cR}\left(G_{sr}\sin(\theta_s - \theta_{cR}) - B_{sr}\cos(\theta_s - \theta_{cR})\right) \tag{IV.49}$$

$$\frac{\partial^2 Q_s}{\partial \theta_{cR} \partial V_s} = -V_{cR}\left(G_{sr}\cos(\theta_s - \theta_{cR}) + B_{sr}\sin(\theta_s - \theta_{cR})\right) \tag{IV.50}$$

$$\frac{\partial^2 Q_s}{\partial \theta_{cR} \partial V_{cR}} = -V_s\left(G_{sr}\cos(\theta_s - \theta_{cR}) + B_{sr}\sin(\theta_s - \theta_{cR})\right) \tag{IV.51}$$

$$\frac{\partial^2 Q_s}{\partial \theta_{vR}^2} = -V_s V_{vR}\left(G_{vR}\sin(\theta_s - \theta_{vR}) - B_{vR}\cos(\theta_s - \theta_{vR})\right) \quad \text{(IV.52)}$$

$$\frac{\partial^2 Q_s}{\partial \theta_{vR}\partial V_s} = -V_{vR}\left(G_{vR}\cos(\theta_s - \theta_{vR}) + B_{vR}\sin(\theta_s - \theta_{vR})\right) \quad \text{(IV.53)}$$

$$\frac{\partial^2 Q_s}{\partial \theta_{vR}\partial V_{vR}} = -V_s\left(G_{vR}\cos(\theta_s - \theta_{vR}) + B_{vR}\sin(\theta_s - \theta_{vR})\right) \quad \text{(IV.54)}$$

$$\frac{\partial^2 Q_s}{\partial V_s^2} = -2B_{SS} \quad \text{(IV.55)}$$

$$\frac{\partial^2 Q_s}{\partial V_s \partial V_r} = \left(G_{sr}\sin(\theta_s - \theta_r) - B_{sr}\cos(\theta_s - \theta_r)\right) \quad \text{(IV.56)}$$

$$\frac{\partial^2 Q_s}{\partial V_s \partial V_{cR}} = \left(G_{sr}\sin(\theta_s - \theta_{cR}) - B_{sr}\cos(\theta_s - \theta_{cR})\right) \quad \text{(IV.57)}$$

$$\frac{\partial^2 Q_s}{\partial V_s \partial V_{vR}} = \left(G_{vR}\sin(\theta_s - \theta_{vR}) - B_{vR}\cos(\theta_s - \theta_{vR})\right) \quad \text{(IV.58)}$$

IV.2 Receiving Node

The first partial derivatives of the power flow equations are:

$$\frac{\partial P_r}{\partial \theta_s} = V_r V_s\left(G_{sr}\sin(\theta_r - \theta_s) - B_{sr}\cos(\theta_r - \theta_s)\right) \quad \text{(IV.59)}$$

$$\begin{aligned}\frac{\partial P_r}{\partial \theta_r} = &-V_r V_s\left(G_{sr}\sin(\theta_r - \theta_s) - B_{sr}\cos(\theta_r - \theta_s)\right)\\ &-V_r V_{cR}\left(G_{rr}\sin(\theta_r - \theta_{cR}) - B_{rr}\cos(\theta_r - \theta_{cR})\right)\end{aligned} \quad \text{(IV.60)}$$

$$\frac{\partial P_r}{\partial \theta_{cR}} = V_r V_{cR}\left(G_{rr}\sin(\theta_r - \theta_{cR}) - B_{rr}\cos(\theta_r - \theta_{cR})\right) \quad \text{(IV.61)}$$

$$\frac{\partial P_r}{\partial V_s} = V_r\left(G_{sr}\cos(\theta_r - \theta_s) + B_{sr}\sin(\theta_r - \theta_s)\right) \quad \text{(IV.62)}$$

$$\begin{aligned}\frac{\partial P_r}{\partial V_r} = &2V_r G_{rr} + V_s\left(G_{rs}\cos(\theta_r - \theta_s) + B_{rs}\sin(\theta_r - \theta_s)\right)\\ &+V_{cR}\left(G_{rr}\cos(\theta_r - \theta_{cR}) + B_{rr}\sin(\theta_r - \theta_{cR})\right)\end{aligned} \quad \text{(IV.63)}$$

$$\frac{\partial P_r}{\partial V_{cR}} = V_r\left(G_{rr}\cos(\theta_r - \theta_{cR}) + B_{rr}\sin(\theta_r - \theta_{cR})\right) \quad \text{(IV.64)}$$

$$\frac{\partial Q_r}{\partial \theta_s} = -V_r V_s\left(G_{sr}\cos(\theta_r - \theta_s) + B_{sr}\sin(\theta_r - \theta_s)\right) \quad \text{(IV.65)}$$

$$\frac{\partial Q_r}{\partial \theta_r} = V_r V_s \left(G_{sr} \cos(\theta_r - \theta_s) + B_{sr} \sin(\theta_r - \theta_s)\right) + V_r V_{cR} \left(G_{rr} \cos(\theta_r - \theta_{cR}) + B_{rr} \sin(\theta_r - \theta_{cR})\right) \quad \text{(IV.66)}$$

$$\frac{\partial Q_r}{\partial \theta_{cR}} = -V_r V_{cR} \left(G_{rr} \cos(\theta_r - \theta_{cR}) + B_{rr} \sin(\theta_r - \theta_{cR})\right) \quad \text{(IV.67)}$$

$$\frac{\partial Q_r}{\partial V_s} = V_r \left(G_{sr} \sin(\theta_r - \theta_s) - B_{sr} \cos(\theta_r - \theta_s)\right) \quad \text{(IV.68)}$$

$$\frac{\partial Q_r}{\partial V_r} = -2V_r B_{rr} + V_s \left(G_{rs} \sin(\theta_r - \theta_s) - B_{rs} \cos(\theta_r - \theta_s)\right) \quad \text{(IV.69)}$$

$$\frac{\partial Q_r}{\partial V_{cR}} = V_r \left(G_{rr} \sin(\theta_r - \theta_{cR}) - B_{rr} \cos(\theta_r - \theta_{cR})\right) \quad \text{(IV.70)}$$

The second partial derivatives of the power flow equations are:

$$\frac{\partial^2 P_r}{\partial \theta_s^2} = -V_r V_s \left(G_{sr} \cos(\theta_r - \theta_s) + B_{sr} \sin(\theta_r - \theta_s)\right) \quad \text{(IV.71)}$$

$$\frac{\partial^2 P_r}{\partial \theta_s \partial \theta_r} = V_r V_s \left(G_{sr} \cos(\theta_r - \theta_s) + B_{sr} \sin(\theta_r - \theta_s)\right) \quad \text{(IV.72)}$$

$$\frac{\partial^2 P_r}{\partial \theta_s \partial V_s} = V_r \left(G_{sr} \sin(\theta_r - \theta_s) - B_{sr} \cos(\theta_r - \theta_s)\right) \quad \text{(IV.73)}$$

$$\frac{\partial^2 P_r}{\partial \theta_s \partial V_r} = V_s \left(G_{sr} \sin(\theta_r - \theta_s) - B_{sr} \cos(\theta_r - \theta_s)\right) \quad \text{(IV.74)}$$

$$\frac{\partial^2 P_r}{\partial \theta_r^2} = -V_r V_s \left(G_{sr} \cos(\theta_r - \theta_s) + B_{sr} \sin(\theta_r - \theta_s)\right) - V_r V_{cR} \left(G_{rr} \cos(\theta_r - \theta_{cR}) + B_{rr} \cos(\theta_r - \theta_{cR})\right) \quad \text{(IV.75)}$$

$$\frac{\partial^2 P_r}{\partial \theta_r \partial \theta_{cR}} = V_r V_{cR} \left(G_{rr} \cos(\theta_r - \theta_{cR}) + B_{rr} \sin(\theta_r - \theta_{cR})\right) \quad \text{(IV.76)}$$

$$\frac{\partial^2 P_r}{\partial \theta_r \partial V_s} = -V_r \left(G_{sr} \sin(\theta_r - \theta_s) - B_{sr} \cos(\theta_r - \theta_s)\right) \quad \text{(IV.77)}$$

$$\frac{\partial^2 P_r}{\partial \theta_r \partial V_r} = -V_s \left(G_{sr} \sin(\theta_r - \theta_s) - B_{sr} \cos(\theta_r - \theta_s)\right) - V_{cR} \left(G_{rr} \sin(\theta_r - \theta_{cR}) - B_{rr} \cos(\theta_r - \theta_{cR})\right) \quad \text{(IV.78)}$$

$$\frac{\partial^2 P_r}{\partial \theta_r \partial V_{cR}} = -V_r \left(G_{rr} \sin(\theta_r - \theta_{cR}) - B_{rr} \cos(\theta_r - \theta_{cR})\right) \quad \text{(IV.79)}$$

$$\frac{\partial^2 P_r}{\partial \theta_{cR}^2} = -V_r V_{cR} \left(G_{rr} \cos(\theta_r - \theta_{cR}) + B_{rr} \sin(\theta_r - \theta_{cR})\right) \quad \text{(IV.80)}$$

$$\frac{\partial^2 P_r}{\partial \theta_{cR} \partial V_r} = V_{cR}\left(G_{rr}\sin(\theta_r - \theta_{cR}) - B_{rr}\cos(\theta_r - \theta_{cR})\right) \tag{IV.81}$$

$$\frac{\partial^2 P_r}{\partial \theta_{cR} \partial V_{cR}} = V_r\left(G_{rr}\sin(\theta_r - \theta_{cR}) - B_{rr}\cos(\theta_r - \theta_{cR})\right) \tag{IV.82}$$

$$\frac{\partial^2 P_r}{\partial V_s \partial V_r} = \left(G_{sr}\cos(\theta_r - \theta_s) + B_{sr}\sin(\theta_r - \theta_s)\right) \tag{IV.83}$$

$$\frac{\partial^2 P_r}{\partial V_r^2} = 2G_{rr} \tag{IV.84}$$

$$\frac{\partial^2 P_r}{\partial V_r \partial V_{cR}} = \left(G_{rr}\cos(\theta_r - \theta_{cR}) + B_{rr}\sin(\theta_r - \theta_{cR})\right) \tag{IV.85}$$

$$\frac{\partial^2 Q_r}{\partial \theta_s^2} = -V_r V_s\left(G_{sr}\sin(\theta_r - \theta_s) - B_{sr}\cos(\theta_r - \theta_s)\right) \tag{IV.86}$$

$$\frac{\partial^2 Q_r}{\partial \theta_s \partial \theta_r} = V_s V_r\left(G_{sr}\sin(\theta_r - \theta_s) - B_{sr}\cos(\theta_r - \theta_s)\right) \tag{IV.87}$$

$$\frac{\partial^2 Q_r}{\partial \theta_s \partial V_s} = -V_r\left(G_{sr}\cos(\theta_r - \theta_s) + B_{sr}\cos(\theta_r - \theta_s)\right) \tag{IV.88}$$

$$\frac{\partial^2 Q_r}{\partial \theta_s \partial V_r} = -V_s\left(G_{sr}\cos(\theta_r - \theta_s) + B_{sr}\sin(\theta_r - \theta_s)\right) \tag{IV.89}$$

$$\begin{aligned}\frac{\partial^2 Q_r}{\partial \theta_r^2} &= -V_r V_s\left(G_{sr}\sin(\theta_r - \theta_s) - B_{sr}\cos(\theta_r - \theta_s)\right) \\ &\quad - V_r V_{cR}\left(G_{rr}\sin(\theta_r - \theta_{cR}) - B_{rr}\cos(\theta_r - \theta_{cR})\right)\end{aligned} \tag{IV.90}$$

$$\frac{\partial^2 Q_r}{\partial \theta_r \partial \theta_{cR}} = V_r V_{cR}\left(G_{rr}\sin(\theta_r - \theta_{cR}) - B_{rr}\cos(\theta_r - \theta_{cR})\right) \tag{IV.91}$$

$$\frac{\partial^2 Q_r}{\partial \theta_r \partial V_s} = V_r\left(G_{sr}\cos(\theta_r - \theta_s) + B_{sr}\sin(\theta_r - \theta_s)\right) \tag{IV.92}$$

$$\begin{aligned}\frac{\partial^2 Q_r}{\partial \theta_r \partial V_r} &= V_s\left(G_{sr}\cos(\theta_r - \theta_s) + B_{sr}\sin(\theta_r - \theta_s)\right) \\ &\quad + V_{cR}\left(G_{rr}\cos(\theta_r - \theta_{cR}) + B_{rr}\sin(\theta_r - \theta_{cR})\right)\end{aligned} \tag{IV.93}$$

$$\frac{\partial^2 Q_r}{\partial \theta_r \partial V_{cR}} = V_r\left(G_{rr}\cos(\theta_r - \theta_{cR}) + B_{rr}\sin(\theta_r - \theta_{cR})\right) \tag{IV.94}$$

$$\frac{\partial^2 Q_r}{\partial \theta_{cR}^2} = -V_r V_{cR}\left(G_{rr}\sin(\theta_r - \theta_{cR}) - B_{rr}\cos(\theta_r - \theta_{cR})\right) \tag{IV.95}$$

$$\frac{\partial^2 Q_r}{\partial \theta_{cR} \partial V_r} = -V_{cR}\left(G_{rr}\cos(\theta_r - \theta_{cR}) + B_{rr}\sin(\theta_r - \theta_{cR})\right) \tag{IV.96}$$

$$\frac{\partial^2 Q_r}{\partial \theta_{cR} \partial V_{cR}} = -V_r\left(G_{rr}\cos(\theta_r - \theta_{cR}) + B_{rr}\sin(\theta_r - \theta_{cR})\right) \quad \text{(IV.97)}$$

$$\frac{\partial^2 Q_r}{\partial V_s \partial V_r} = \left(G_{sr}\sin(\theta_r - \theta_s) - B_{sr}\cos(\theta_r - \theta_s)\right) \quad \text{(IV.98)}$$

$$\frac{\partial^2 Q_r}{\partial V_r^2} = -2B_{rr} \quad \text{(IV.99)}$$

$$\frac{\partial^2 Q_r}{\partial V_r \partial V_{cR}} = \left(G_{rr}\sin(\theta_r - \theta_{cR}) - B_{rr}\cos(\theta_r - \theta_{cR})\right) \quad \text{(IV.100)}$$

IV.3 Series Converter

The first partial derivatives of the power flow equations are:

$$\frac{\partial P_{cR}}{\partial \theta_s} = V_{cR}V_s\left(G_{sr}\sin(\theta_{cR} - \theta_s) - B_{sr}\cos(\theta_{cR} - \theta_s)\right) \quad \text{(IV.101)}$$

$$\frac{\partial P_{cR}}{\partial \theta_r} = V_{cR}V_r\left(G_{rr}\sin(\theta_{cR} - \theta_r) - B_{rr}\cos(\theta_{cR} - \theta_r)\right) \quad \text{(IV.102)}$$

$$\begin{aligned}\frac{\partial P_{cR}}{\partial \theta_{cR}} = &-V_{cR}V_r\left(G_{rr}\sin(\theta_{cR} - \theta_r) - B_{rr}\cos(\theta_{cR} - \theta_r)\right)\\ &-V_{cR}V_s\left(G_{sr}\sin(\theta_{cR} - \theta_s) - B_{sr}\cos(\theta_{cR} - \theta_s)\right)\end{aligned} \quad \text{(IV.103)}$$

$$\frac{\partial P_{cR}}{\partial V_s} = V_{cR}\left(G_{sr}\cos(\theta_{cR} - \theta_s) + B_{sr}\sin(\theta_{cR} - \theta_s)\right) \quad \text{(IV.104)}$$

$$\frac{\partial P_{cR}}{\partial V_r} = V_{cR}\left(G_{rr}\cos(\theta_{cR} - \theta_r) + B_{rr}\sin(\theta_{cR} - \theta_r)\right) \quad \text{(IV.105)}$$

$$\begin{aligned}\frac{\partial P_{cR}}{\partial V_{cR}} = &2V_{cR}G_{rr} + V_r\left(G_{rr}\cos(\theta_{cR} - \theta_r) + B_{rr}\sin(\theta_{cR} - \theta_r)\right)\\ &+V_s\left(G_{sr}\cos(\theta_{cR} - \theta_s) + B_{sr}\sin(\theta_{cR} - \theta_s)\right)\end{aligned} \quad \text{(IV.106)}$$

The second partial derivatives of the power flow equations are:

$$\frac{\partial^2 P_{cR}}{\partial \theta_s^2} = -V_{cR}V_s\left(G_{sr}\cos(\theta_{cR} - \theta_s) + B_{sr}\sin(\theta_{cR} - \theta_s)\right) \quad \text{(IV.107)}$$

$$\frac{\partial^2 P_{cR}}{\partial \theta_s \partial \theta_{cR}} = V_{cR}V_s\left(G_{sr}\cos(\theta_{cR} - \theta_s) + B_{sr}\sin(\theta_{cR} - \theta_s)\right) \quad \text{(IV.108)}$$

$$\frac{\partial^2 P_{cR}}{\partial \theta_s \partial V_s} = V_{cR}\left(G_{sr}\sin(\theta_{cR} - \theta_s) - B_{sr}\cos(\theta_{cR} - \theta_s)\right) \quad \text{(IV.109)}$$

$$\frac{\partial^2 P_{cR}}{\partial \theta_s \partial V_{cR}} = V_s\left(G_{sr}\sin(\theta_{cR} - \theta_s) - B_{sr}\cos(\theta_{cR} - \theta_s)\right) \quad \text{(IV.110)}$$

$$\frac{\partial^2 P_{cR}}{\partial \theta_r^2} = -V_{cR}V_r\left(G_{rr}\cos(\theta_{cR}-\theta_r)+B_{rr}\sin(\theta_{cR}-\theta_r)\right) \quad \text{(IV.111)}$$

$$\frac{\partial^2 P_{cR}}{\partial \theta_r \partial \theta_{cR}} = V_{cR}V_r\left(G_{rr}\cos(\theta_{cR}-\theta_r)+B_{rr}\sin(\theta_{cR}-\theta_r)\right) \quad \text{(IV.112)}$$

$$\frac{\partial^2 P_{cR}}{\partial \theta_r \partial V_r} = V_{cR}\left(G_{rr}\sin(\theta_{cR}-\theta_r)-B_{rr}\cos(\theta_{cR}-\theta_r)\right) \quad \text{(IV.113)}$$

$$\frac{\partial^2 P_{cR}}{\partial \theta_r \partial V_{cR}} = V_r\left(G_{rr}\sin(\theta_{cR}-\theta_r)-B_{rr}\cos(\theta_{cR}-\theta_r)\right) \quad \text{(IV.114)}$$

$$\frac{\partial^2 P_{cR}}{\partial \theta_{cR} \partial \theta_s} = V_{cR}V_s\left(G_{sr}\cos(\theta_{cR}-\theta_s)+B_{sr}\sin(\theta_{cR}-\theta_s)\right) \quad \text{(IV.115)}$$

$$\frac{\partial^2 P_{cR}}{\partial \theta_{cR} \partial \theta_r} = V_{cR}V_r\left(G_{rr}\cos(\theta_{cR}-\theta_r)+B_{rr}\sin(\theta_{cR}-\theta_r)\right) \quad \text{(IV.116)}$$

$$\begin{aligned}\frac{\partial^2 P_{cR}}{\partial \theta_{cR}^2} = &-V_{cR}V_r\left(G_{rr}\cos(\theta_{cR}-\theta_r)+B_{rr}\sin(\theta_{cR}-\theta_r)\right)\\ &-V_{cR}V_s\left(G_{sr}\cos(\theta_{cR}-\theta_s)+B_{sr}\sin(\theta_{cR}-\theta_s)\right)\end{aligned} \quad \text{(IV.117)}$$

$$\frac{\partial^2 P_{cR}}{\partial \theta_{cR} \partial V_s} = -V_{cR}\left(G_{sr}\sin(\theta_{cR}-\theta_s)-B_{sr}\cos(\theta_{cR}-\theta_s)\right) \quad \text{(IV.118)}$$

$$\frac{\partial^2 P_{cR}}{\partial \theta_{cR} \partial V_r} = -V_{cR}\left(G_{rr}\sin(\theta_{cR}-\theta_r)-B_{rr}\cos(\theta_{cR}-\theta_r)\right) \quad \text{(IV.119)}$$

$$\begin{aligned}\frac{\partial^2 P_{cR}}{\partial \theta_{cR} \partial V_{cR}} = &-V_r\left(G_{rr}\sin(\theta_{cR}-\theta_r)-B_{rr}\cos(\theta_{cR}-\theta_r)\right)\\ &-V_s\left(G_{sr}\sin(\theta_{cR}-\theta_s)-B_{sr}\cos(\theta_{cR}-\theta_s)\right)\end{aligned} \quad \text{(IV.120)}$$

$$\frac{\partial^2 P_{cR}}{\partial V_s \partial V_{cR}} = \left(G_{sr}\cos(\theta_{cR}-\theta_s)+B_{sr}\sin(\theta_{cR}-\theta_s)\right) \quad \text{(IV.121)}$$

$$\frac{\partial^2 P_{cR}}{\partial V_r \partial V_{cR}} = \left(G_{rr}\cos(\theta_{cR}-\theta_r)+B_{rr}\sin(\theta_{cR}-\theta_r)\right) \quad \text{(IV.122)}$$

$$\frac{\partial^2 P_{cR}}{\partial V_{cR}^2} = 2G_{rr} \quad \text{(IV.123)}$$

IV.4 Shunt Converter

The first partial derivatives of the power flow equations are:

$$\frac{\partial P_{vR}}{\partial \theta_s} = V_{vR}V_s\left(G_{vR}\sin(\theta_{vR}-\theta_s)-B_{vR}\cos(\theta_{vR}-\theta_s)\right) \quad \text{(IV.124)}$$

$$\frac{\partial P_{vR}}{\partial \theta_{vR}} = -V_{vR}V_s\left(G_{vR}\sin(\theta_{vR}-\theta_s)-B_{vR}\cos(\theta_{vR}-\theta_s)\right) \quad \text{(IV.125)}$$

$$\frac{\partial P_{vR}}{\partial V_s} = V_{vR}\left(G_{vR}\cos(\theta_{vR}-\theta_s)+B_{vR}\sin(\theta_{vR}-\theta_s)\right) \quad \text{(IV.126)}$$

$$\frac{\partial P_{vR}}{\partial V_{vR}} = -2V_{vR}G_{vR}+V_s\left(G_{vR}\cos(\theta_{vR}-\theta_s)+B_{vR}\sin(\theta_{vR}-\theta_s)\right) \quad \text{(IV.127)}$$

The second partial derivatives of the power flow equations are:

$$\frac{\partial^2 P_{vR}}{\partial \theta_s^2} = -V_{vR}V_s\left(G_{vR}\cos(\theta_{vR}-\theta_s)+B_{vR}\sin(\theta_{vR}-\theta_s)\right) \quad \text{(IV.128)}$$

$$\frac{\partial^2 P_{vR}}{\partial \theta_s \partial \theta_{vR}} = V_{vR}V_s\left(G_{vR}\cos(\theta_{vR}-\theta_s)+B_{vR}\sin(\theta_{vR}-\theta_s)\right) \quad \text{(IV.129)}$$

$$\frac{\partial^2 P_{vR}}{\partial \theta_s \partial V_s} = V_{vR}\left(G_{vR}\sin(\theta_{vR}-\theta_s)-B_{vR}\cos(\theta_{vR}-\theta_s)\right) \quad \text{(IV.130)}$$

$$\frac{\partial^2 P_{vR}}{\partial \theta_s \partial V_{vR}} = V_s\left(G_{vR}\sin(\theta_{vR}-\theta_s)-B_{vR}\cos(\theta_{vR}-\theta_s)\right) \quad \text{(IV.131)}$$

$$\frac{\partial^2 P_{vR}}{\partial \theta_{vR}^2} = -V_{vR}V_s\left(G_{vR}\cos(\theta_{vR}-\theta_s)+B_{vR}\sin(\theta_{vR}-\theta_s)\right) \quad \text{(IV.132)}$$

$$\frac{\partial^2 P_{vR}}{\partial \theta_{vR} \partial V_s} = -V_{vR}\left(G_{vR}\sin(\theta_{vR}-\theta_s)-B_{vR}\cos(\theta_{vR}-\theta_s)\right) \quad \text{(IV.133)}$$

$$\frac{\partial^2 P_{vR}}{\partial \theta_{vR} \partial V_{vR}} = -V_s\left(G_{vR}\sin(\theta_{vR}-\theta_s)-B_{vR}\cos(\theta_{vR}-\theta_s)\right) \quad \text{(IV.134)}$$

$$\frac{\partial^2 P_{vR}}{\partial V_s \partial V_{vR}} = \left(G_{vR}\cos(\theta_{vR}-\theta_s)+B_{vR}\sin(\theta_{vR}-\theta_s)\right) \quad \text{(IV.135)}$$

$$\frac{\partial^2 P_{vR}}{\partial V_{vR}^2} = -2G_{vR} \quad \text{(IV.136)}$$

Appendix V

Hessian and Jacobian Elements for the HVDC Link Model

V.1 HVDC Link Steady State Model

All first and second partial derivative terms corresponding to equations (8.1) and (8.8) with respect to the HVDC state variables are presented below. These equations are rewritten as follows,

$$I_d = \frac{V_{dR} - V_{dI}}{R_d} \tag{V.1}$$

$$R_1 = V_{dR} - k_1 a_R V_{tR} \cos\alpha_R + k_2 \frac{V_{dR} - V_{dI}}{R_d} = 0 \tag{V.2}$$

$$R_2 = V_{dI} - k_3 a_I V_{tI} \cos\alpha_I + k_4 \frac{V_{dR} - V_{dI}}{R_d} = 0 \tag{V.3}$$

$$P_{dR} = Y_d V_{dR}^2 - Y_d V_{dR} V_{dI} \tag{V.4}$$

$$P_{dI} = Y_d V_{dI} V_{dR} - Y_d V_{dI}^2 \tag{V.5}$$

$$Q_{dR} = \sqrt{k^2 k_1^2 a_R^2 V_{tR}^2 Y_d^2 (V_{dR} - V_{dI})^2 - (Y_d V_{dR}^2 - Y_d V_{dR} V_{dI})^2} \tag{V.6}$$

$$Q_{dI} = \sqrt{k^2 k_3^2 a_I^2 V_{tI}^2 Y_d^2 (V_{dR} - V_{dI})^2 - (Y_d V_{dI} V_{dR} - Y_d V_{dI}^2)^2} \tag{V.7}$$

where,

$$k_1 = \frac{3\sqrt{2}}{\pi} np_R \tag{V.8}$$

$$k_2 = \frac{3}{\pi} X_{CR}\, np_R \tag{V.9}$$

$$k_3 = \frac{3\sqrt{2}}{\pi} np_I \tag{V.10}$$

$$k_4 = \frac{3}{\pi} X_{CI}\, np_I \tag{V.11}$$

$$Y_d = \frac{1}{R_d} \tag{V.12}$$

V.2 Rectifier Node

The first partial derivatives terms of the HVDC link equations are,

$$\frac{\partial R_I}{\partial V_{dR}} = 1 + Y_d k_2 \tag{V.13}$$

$$\frac{\partial R_I}{\partial a_R} = -k_I V_{tR} \cos\alpha_R \tag{V.14}$$

$$\frac{\partial R_I}{\partial \cos\alpha_R} = -k_I a_R V_{tR} \tag{V.15}$$

$$\frac{\partial R_I}{\partial V_{tR}} = -k_I a_R \cos\alpha_R \tag{V.16}$$

$$\frac{\partial R_I}{\partial V_{dI}} = -Y_d k_2 \tag{V.17}$$

$$\frac{\partial P_{dR}}{\partial V_{dR}} = 2Y_d V_{dR} - Y_d V_{dI} \tag{V.18}$$

$$\frac{\partial P_{dR}}{\partial V_{dI}} = -Y_d V_{dR} \tag{V.19}$$

$$\begin{aligned}\frac{\partial Q_{dR}}{\partial a_R} &= \frac{k^2 k_I^2 a_R V_{tR}^2 Y_d^2 (V_{dR} - V_{dI})^2}{\sqrt{k^2 k_I^2 a_R^2 V_{tR}^2 Y_d^2 (V_{dR} - V_{dI})^2 - (Y_d V_{dR}^2 - Y_d V_{dR} V_{dI})^2}} \\ &= \frac{v_1(a_R, V_{tR}, V_{dR}, V_{dI})}{u_1(a_R, V_{tR}, V_{dR}, V_{dI})}\end{aligned} \tag{V.20}$$

$$\begin{aligned}\frac{\partial Q_{dR}}{\partial V_{tR}} &= \frac{k^2 k_I^2 a_R^2 V_{tR} Y_d^2 (V_{dR} - V_{dI})^2}{\sqrt{k^2 k_I^2 a_R^2 V_{tR}^2 Y_d^2 (V_{dR} - V_{dI})^2 - (Y_d V_{dR}^2 - Y_d V_{dR} V_{dI})^2}} \\ &= \frac{v_2(a_R, V_{tR}, V_{dR}, V_{dI})}{u_1(a_R, V_{tR}, V_{dR}, V_{dI})}\end{aligned} \tag{V.21}$$

$$\begin{aligned}\frac{\partial Q_{dR}}{\partial V_{dR}} &= \frac{k^2 k_I^2 a_R V_{tR}^2 Y_d^2 (V_{dR} - V_{dI}) - (Y_d V_{dR}^2 - Y_d V_{dR} V_{dI})(2Y_d V_{dR} - Y_d V_{dI})}{\sqrt{k^2 k_I^2 a_R^2 V_{tR}^2 Y_d^2 (V_{dR} - V_{dI})^2 - (Y_d V_{dR}^2 - Y_d V_{dR} V_{dI})^2}} \\ &= \frac{v_3(a_R, V_{tR}, V_{dR}, V_{dI})}{u_1(a_R, V_{tR}, V_{dR}, V_{dI})}\end{aligned} \tag{V.22}$$

$$\frac{\partial Q_{dR}}{\partial V_{dI}} = \frac{-k^2 k_1^2 a_R^2 V_{tR}^2 Y_d^2 (V_{dR} - V_{dI}) + (Y_d V_{dR}^2 - Y_d V_{dR} V_{dI}) Y_d V_{dR}}{\sqrt{k^2 k_1^2 a_R^2 V_{tR}^2 Y_d^2 (V_{dR} - V_{dI})^2 - (Y_d V_{dR}^2 - Y_d V_{dR} V_{dI})^2}} = \frac{v_4(a_R, V_{tR}, V_{dR}, V_{dI})}{u_1(a_R, V_{tR}, V_{dR}, V_{dI})} \quad \text{(V.23)}$$

The second partial derivatives terms of the of HVDC link equations are,

$$\frac{\partial^2 R_1}{\partial a_R \partial V_{tR}} = -k_1 \cos\alpha_R \quad \text{(V.24)}$$

$$\frac{\partial^2 R_1}{\partial a_R \partial \cos\alpha_R} = -k_1 V_{tR} \quad \text{(V.25)}$$

$$\frac{\partial^2 R_1}{\partial \cos\alpha_R \partial V_{tR}} = -k_1 a_R \quad \text{(V.26)}$$

$$\frac{\partial^2 P_{dR}}{\partial V_{dR}^2} = 2Y_d \quad \text{(V.27)}$$

$$\frac{\partial^2 P_{dR}}{\partial V_{dR} \partial V_{dI}} = -Y_d \quad \text{(V.28)}$$

$$\frac{\partial^2 Q_{dR}}{\partial a_R^2} = u_1 \frac{\partial v_1}{\partial a_R} + v_1 \frac{\partial u_1}{\partial a_R} \quad \text{(V.29)}$$

$$\frac{\partial^2 Q_{dR}}{\partial a_R \partial V_{tR}} = u_1 \frac{\partial v_1}{\partial V_{tR}} + v_1 \frac{\partial u_1}{\partial V_{tR}} \quad \text{(V.30)}$$

$$\frac{\partial^2 Q_{dR}}{\partial a_R \partial V_{dR}} = u_1 \frac{\partial v_1}{\partial V_{dR}} + v_1 \frac{\partial u_1}{\partial V_{dR}} \quad \text{(V.31)}$$

$$\frac{\partial^2 Q_{dR}}{\partial a_R \partial V_{dI}} = u_1 \frac{\partial v_1}{\partial V_{dI}} + v_1 \frac{\partial u_1}{\partial V_{dI}} \quad \text{(V.32)}$$

$$\frac{\partial^2 Q_{dR}}{\partial V_{tR}^2} = u_1 \frac{\partial v_2}{\partial V_{tR}} + v_2 \frac{\partial u_1}{\partial V_{tR}} \quad \text{(V.33)}$$

$$\frac{\partial^2 Q_{dR}}{\partial V_{tR} \partial V_{dR}} = u_1 \frac{\partial v_2}{\partial V_{dR}} + v_2 \frac{\partial u_1}{\partial V_{dR}} \quad \text{(V.34)}$$

$$\frac{\partial^2 Q_{dR}}{\partial V_{tR} \partial V_{dI}} = u_1 \frac{\partial v_2}{\partial V_{dI}} + v_2 \frac{\partial u_1}{\partial V_{dI}} \quad \text{(V.35)}$$

$$\frac{\partial^2 Q_{dR}}{\partial V_{dR}^2} = u_1 \frac{\partial v_3}{\partial V_{dR}} + v_3 \frac{\partial u_1}{\partial V_{dR}} \quad \text{(V.36)}$$

$$\frac{\partial^2 Q_{dR}}{\partial V_{dR} \partial V_{dI}} = u_1 \frac{\partial v_3}{\partial V_{dI}} + v_3 \frac{\partial u_1}{\partial V_{dI}} \quad \text{(V.37)}$$

$$\frac{\partial^2 Q_{dR}}{\partial V_{dI}^2} = u_1 \frac{\partial v_4}{\partial V_{dI}} + v_4 \frac{\partial u_1}{\partial V_{dI}} \tag{V.38}$$

where,

$$\frac{\partial u_1}{\partial a_R} = -\frac{k^2 k_1^2 a_R V_{tR}^2 Y_d^2 (V_{dR} - V_{dI})^2}{\left(k^2 k_1^2 a_R^2 V_{tR}^2 Y_d^2 (V_{dR} - V_{dI})^2 - (Y_d V_{dR}^2 - Y_d V_{dR} V_{dI})^2\right)^{3/2}} \tag{V.39}$$

$$\frac{\partial u_1}{\partial V_{tR}} = -\frac{k^2 k_1^2 a_R^2 V_{tR} Y_d^2 (V_{dR} - V_{dI})^2}{\left(k^2 k_1^2 a_R^2 V_{tR}^2 Y_d^2 (V_{dR} - V_{dI})^2 - (Y_d V_{dR}^2 - Y_d V_{dR} V_{dI})^2\right)^{3/2}} \tag{V.40}$$

$$\frac{\partial u_1}{\partial V_{dR}} = -\frac{k^2 k_1^2 a_R^2 V_{tR}^2 Y_d^2 (V_{dR} - V_{dI}) - (Y_d V_{dR}^2 - Y_d V_{dR} V_{dI})(2Y_d V_{dR} - Y_d V_{dI})}{\left(k^2 k_1^2 a_R^2 V_{tR}^2 Y_d^2 (V_{dR} - V_{dI})^2 - (Y_d V_{dR}^2 - Y_d V_{dR} V_{dI})^2\right)^{3/2}} \tag{V.41}$$

$$\frac{\partial u_1}{\partial V_{dI}} = -\frac{-k^2 k_1^2 a_R^2 V_{tR}^2 Y_d^2 (V_{dR} - V_{dI}) + (Y_d V_{dR}^2 - Y_d V_{dR} V_{dI}) Y_d V_{dR}}{\left(k^2 k_1^2 a_R^2 V_{tR}^2 Y_d^2 (V_{dR} - V_{dI})^2 - (Y_d V_{dR}^2 - Y_d V_{dR} V_{dI})^2\right)^{3/2}} \tag{V.42}$$

$$\frac{\partial v_1}{\partial a_R} = k^2 k_1^2 V_{tR}^2 Y_d^2 (V_{dR} - V_{dI})^2 \tag{V.43}$$

$$\frac{\partial v_1}{\partial V_{tR}} = 2k^2 k_1^2 a_R V_{tR} Y_d^2 (V_{dR} - V_{dI})^2 \tag{V.44}$$

$$\frac{\partial v_1}{\partial V_{dR}} = 2k^2 k_1^2 a_R V_{tR}^2 Y_d^2 (V_{dR} - V_{dI}) \tag{V.45}$$

$$\frac{\partial v_1}{\partial V_{dI}} = -2k^2 k_1^2 a_R V_{tR}^2 Y_d^2 (V_{dR} - V_{dI}) \tag{V.46}$$

$$\frac{\partial v_2}{\partial V_{tR}} = k^2 k_1^2 a_R^2 Y_d^2 (V_{dR} - V_{dI})^2 \tag{V.47}$$

$$\frac{\partial v_2}{\partial V_{dR}} = 2k^2 k_1^2 a_R^2 V_{tR} Y_d^2 (V_{dR} - V_{dI}) \tag{V.48}$$

$$\frac{\partial v_2}{\partial V_{dI}} = -2k^2 k_1^2 a_R^2 V_{tR} Y_d^2 (V_{dR} - V_{dI}) \tag{V.49}$$

$$\frac{\partial v_3}{\partial V_{dR}} = k^2 k_1^2 a_R^2 V_{tR}^2 Y_d^2 - 6Y_d^2 V_{dR}^2 + 6Y_d^2 V_{dR} V_{dI} - Y_d^2 V_{dI}^2 \tag{V.50}$$

$$\frac{\partial v_3}{\partial V_{dI}} = -k^2 k_1^2 a_R^2 V_{tR}^2 Y_d^2 + 3Y_d^2 V_{dR}^2 - 2Y_d^2 V_{dR} V_{dI} \tag{V.51}$$

$$\frac{\partial v_4}{\partial V_{dI}} = k^2 k_1^2 a_R^2 V_{tR}^2 Y_d^2 - Y_d^2 V_{dR}^2 \tag{V.52}$$

V.3 Inverter Node

The first partial derivatives of the HVDC link equations are:

$$\frac{\partial R_2}{\partial V_{dI}} = 1 - Y_d k_4 \tag{V.53}$$

$$\frac{\partial R_2}{\partial a_I} = -k_3 V_{tI} \cos\alpha_I \tag{V.54}$$

$$\frac{\partial R_2}{\partial \cos\alpha_I} = -k_3 a_I V_{tI} \tag{V.55}$$

$$\frac{\partial R_2}{\partial V_{tI}} = -k_3 a_I \cos\alpha_I \tag{V.56}$$

$$\frac{\partial R_2}{\partial V_{dR}} = Y_d k_4 \tag{V.57}$$

$$\frac{\partial P_{dI}}{\partial V_{dR}} = Y_d V_{dI} \tag{V.58}$$

$$\frac{\partial P_{dI}}{\partial V_{dI}} = Y_d V_{dR} - 2Y_d V_{dI} \tag{V.59}$$

$$\begin{aligned}\frac{\partial Q_{dI}}{\partial a_I} &= \frac{k^2 k_3^2 a_I V_{tI}^2 Y_d^2 (V_{dR} - V_{dI})^2}{\sqrt{k^2 k_3^2 a_I^2 V_{tI}^2 Y_d^2 (V_{dR} - V_{dI})^2 - (Y_d V_{dI} V_{dR} - Y_d V_{dI}^2)^2}} \\ &= \frac{v_5(a_I, V_{tI}, V_{dR}, V_{dI})}{u_2(a_I, V_{tI}, V_{dR}, V_{dI})}\end{aligned} \tag{V.60}$$

$$\begin{aligned}\frac{\partial Q_{dI}}{\partial V_{tI}} &= \frac{k^2 k_3^2 a_I^2 V_{tI} Y_d^2 (V_{dR} - V_{dI})^2}{\sqrt{k^2 k_3^2 a_I^2 V_{tI}^2 Y_d^2 (V_{dR} - V_{dI})^2 - (Y_d V_{dI} V_{dR} - Y_d V_{dI}^2)^2}} \\ &= \frac{v_6(a_I, V_{tI}, V_{dR}, V_{dI})}{u_2(a_I, V_{tI}, V_{dR}, V_{dI})}\end{aligned} \tag{V.61}$$

$$\begin{aligned}\frac{\partial Q_{dI}}{\partial V_{dI}} &= \frac{-k^2 k_3^2 a_I^2 V_{tI}^2 Y_d^2 (V_{dR} - V_{dI}) - (Y_d V_{dI} V_{dR} - Y_d V_{dI}^2)(Y_d V_{dR} - 2Y_d V_{dI})}{\sqrt{k^2 k_3^2 a_I^2 V_{tI}^2 Y_d^2 (V_{dR} - V_{dI})^2 - (Y_d V_{dI} V_{dR} - Y_d V_{dI}^2)^2}} \\ &= \frac{v_7(a_I, V_{tI}, V_{dR}, V_{dI})}{u_2(a_I, V_{tI}, V_{dR}, V_{dI})}\end{aligned} \tag{V.62}$$

$$\begin{aligned}\frac{\partial Q_{dI}}{\partial V_{dR}} &= \frac{k^2 k_3^2 a_I^2 V_{tI}^2 Y_d^2 (V_{dR} - V_{dI}) - (Y_d V_{dI} V_{dR} - Y_d V_{dI}^2) Y_d V_{dI}}{\sqrt{k^2 k_3^2 a_I^2 V_{tI}^2 Y_d^2 (V_{dR} - V_{dI})^2 - (Y_d V_{dI} V_{dR} - Y_d V_{dI}^2)^2}} \\ &= \frac{v_8(a_I, V_{tI}, V_{dR}, V_{dI})}{u_2(a_I, V_{tI}, V_{dR}, V_{dI})}\end{aligned} \tag{V.63}$$

The second partial derivatives of the HVDC link equations are:

$$\frac{\partial^2 R_2}{\partial a_I \partial V_{tI}} = -k_3 \cos\alpha_I \tag{V.64}$$

$$\frac{\partial^2 R_2}{\partial a_I \partial \cos\alpha_I} = -k_3 V_{tI} \tag{V.65}$$

$$\frac{\partial^2 R_2}{\partial \cos\alpha_I \partial V_{tI}} = -k_3 a_I \tag{V.66}$$

$$\frac{\partial^2 P_{dI}}{\partial V_{dR} \partial V_{dI}} = Y_d \tag{V.67}$$

$$\frac{\partial^2 P_{dI}}{\partial V_{dI}^2} = -2Y_d \tag{V.68}$$

$$\frac{\partial^2 Q_{dI}}{\partial a_I^2} = u_2 \frac{\partial v_5}{\partial a_I} + v_5 \frac{\partial u_2}{\partial a_I} \tag{V.69}$$

$$\frac{\partial^2 Q_{dI}}{\partial a_I \partial V_{tI}} = u_2 \frac{\partial v_5}{\partial V_{tI}} + v_5 \frac{\partial u_2}{\partial V_{tI}} \tag{V.70}$$

$$\frac{\partial^2 Q_{dI}}{\partial a_I \partial V_{dR}} = u_2 \frac{\partial v_5}{\partial V_{dR}} + v_5 \frac{\partial u_2}{\partial V_{dR}} \tag{V.71}$$

$$\frac{\partial^2 Q_{dI}}{\partial a_I \partial V_{dI}} = u_2 \frac{\partial v_5}{\partial V_{dI}} + v_5 \frac{\partial u_2}{\partial V_{dI}} \tag{V.72}$$

$$\frac{\partial^2 Q_{dI}}{\partial V_{tI}^2} = u_2 \frac{\partial v_6}{\partial V_{tI}} + v_6 \frac{\partial u_2}{\partial V_{tI}} \tag{V.73}$$

$$\frac{\partial^2 Q_{dI}}{\partial V_{tI} \partial V_{dR}} = u_2 \frac{\partial v_6}{\partial V_{dR}} + v_6 \frac{\partial u_2}{\partial V_{dR}} \tag{V.74}$$

$$\frac{\partial^2 Q_{dI}}{\partial V_{tI} \partial V_{dI}} = u_2 \frac{\partial v_6}{\partial V_{dI}} + v_6 \frac{\partial u_2}{\partial V_{dI}} \tag{V.75}$$

$$\frac{\partial^2 Q_{dI}}{\partial V_{dI}^2} = u_2 \frac{\partial v_7}{\partial V_{dI}} + v_7 \frac{\partial u_2}{\partial V_{dI}} \tag{V.76}$$

$$\frac{\partial^2 Q_{dI}}{\partial V_{dI} \partial V_{dR}} = u_2 \frac{\partial v_7}{\partial V_{dR}} + v_7 \frac{\partial u_2}{\partial V_{dR}} \tag{V.77}$$

$$\frac{\partial^2 Q_{dI}}{\partial V_{dR}^2} = u_2 \frac{\partial v_8}{\partial V_{dR}} + v_8 \frac{\partial u_2}{\partial V_{dR}} \tag{V.78}$$

where,

$$\frac{\partial u_2}{\partial a_I} = -\frac{k^2 k_3^2 a_I V_{tI}^2 Y_d^2 (V_{dR} - V_{dI})^2}{\left(k^2 k_3^2 a_I^2 V_{tI}^2 Y_d^2 (V_{dR} - V_{dI})^2 - (Y_d V_{dI} V_{dR} - Y_d V_{dI}^2)^2\right)^{3/2}} \tag{V.79}$$

$$\frac{\partial u_2}{\partial V_{tl}} = -\frac{k^2 k_3^2 a_I^2 V_{tl} Y_d^2 (V_{dR} - V_{dI})^2}{\left(k^2 k_3^2 a_I^2 V_{tl}^2 Y_d^2 (V_{dR} - V_{dI})^2 - (Y_d V_{dI} V_{dR} - Y_d V_{dI}^2)^2\right)^{3/2}} \quad \text{(V.80)}$$

$$\frac{\partial u_2}{\partial V_{dR}} = -\frac{k^2 k_3^2 a_I^2 V_{tl}^2 Y_d^2 (V_{dR} - V_{dI})^2 - (Y_d V_{dI} V_{dR} - Y_d V_{dI}^2) Y_d V_{dI}}{\left(k^2 k_3^2 a_I^2 V_{tl}^2 Y_d^2 (V_{dR} - V_{dI})^2 - (Y_d V_{dI} V_{dR} - Y_d V_{dI}^2)^2\right)^{3/2}} \quad \text{(V.81)}$$

$$\frac{\partial u_2}{\partial V_{dI}} = -\frac{-k^2 k_3^2 a_I^2 V_{tl}^2 Y_d^2 (V_{dR} - V_{dI}) - (Y_d V_{dI} V_{dR} - Y_d V_{dI}^2)(Y_d V_{dR} - 2Y_d V_{dI})}{\left(k^2 k_3^2 a_I^2 V_{tl}^2 Y_d^2 (V_{dR} - V_{dI})^2 - (Y_d V_{dI} V_{dR} - Y_d V_{dI}^2)^2\right)^{3/2}} \quad \text{(V.82)}$$

$$\frac{\partial v_5}{\partial a_I} = k^2 k_3^2 V_{tl}^2 Y_d^2 (V_{dR} - V_{dI})^2 \quad \text{(V.83)}$$

$$\frac{\partial v_5}{\partial V_{tl}^2} = 2k^2 k_3^2 a_I V_{tl} Y_d^2 (V_{dR} - V_{dI})^2 \quad \text{(V.84)}$$

$$\frac{\partial v_5}{\partial V_{dR}} = 2k^2 k_3^2 a_I V_{tl}^2 Y_d^2 (V_{dR} - V_{dI}) \quad \text{(V.85)}$$

$$\frac{\partial v_5}{\partial V_{dI}} = -2k^2 k_3^2 a_I V_{tl}^2 Y_d^2 (V_{dR} - V_{dI}) \quad \text{(V.86)}$$

$$\frac{\partial v_6}{\partial V_{tl}} = k^2 k_3^2 a_I^2 Y_d^2 (V_{dR} - V_{dI})^2 \quad \text{(V.87)}$$

$$\frac{\partial v_6}{\partial V_{dR}} = 2k^2 k_3^2 a_I^2 V_{tl} Y_d^2 (V_{dR} - V_{dI}) \quad \text{(V.88)}$$

$$\frac{\partial v_6}{\partial V_{dI}} = -2k^2 k_3^2 a_I^2 V_{tl} Y_d^2 (V_{dR} - V_{dI}) \quad \text{(V.89)}$$

$$\frac{\partial v_7}{\partial V_{dR}} = -k^2 k_3^2 a_I^2 V_{tl}^2 Y_d^2 - 2Y_d^2 V_{dI} V_{dR} + 3Y_d^2 V_{dI}^2 \quad \text{(V.90)}$$

$$\frac{\partial v_7}{\partial V_{dI}} = k^2 k_3^2 a_I^2 V_{tl}^2 Y_d^2 - Y_d^2 V_{dR}^2 + 6Y_d^2 V_{dR} V_{dI} - 6Y_d^2 V_{dI}^2 \quad \text{(V.91)}$$

$$\frac{\partial v_8}{\partial V_{dR}} = k^2 k_3^2 a_I^2 V_{tl}^2 Y_d^2 - Y_d^2 V_{dI}^2 \quad \text{(V.92)}$$

Appendix VI

Data Test Power Systems

Data relating to the test systems using in this research are given in this appendix. Only parameter values different from zero are given. The MVA base is 100 MVA.

VI.1 5-node System

Table VI.1. Number of nodes and plant components.

Nodes	Transmission Lines	Transformers	Generators	Loads	Shunt Compensators	Slack Node
5	7	0	2	4	0	north

Table VI.2. Transmission lines.

Sending Node	Receiving Node	R (pu)	X_L (pu)	B_{TOTAL} (pu)
north	south	0.02	0.06	0.06
north	lake	0.08	0.24	0.05
south	lake	0.06	0.18	0.04
south	main	0.06	0.18	0.04
south	elm	0.04	0.12	0.03
lake	main	0.01	0.03	0.02
main	elm	0.08	0.24	0.05

Table VI.3. Loads.

Node	P_{LOAD} (MW)	Q_{LOAD} (MVAR)
south	20	10
lake	45	15
main	40	5
elm	60	10

Table VI.4. Limits of Voltage.

Type of Node	Voltage Limits (pu)	
	Min	Max
Slack node	0.9	1.5
Generator node	0.9	1.1
Load node	0.9	1.1

Table VI.5. Generators.

Node	Cost Coefficients			Active Power Limits		Reactive Power Limits	
	a ($/hr)	b ($/MWhr)	c ($/MW^{2}hr)	Min (MW)	Max (MW)	Min (MVAR)	Max (MVAR)
north	60	3.4	0.004	10	200	-500	500
souht	60	3.4	0.004	10	200	-300	300

VI.2 9-node System

Table VI.6. Number of nodes and plant components.

Nodes	Transmission Lines	Transformers	Generators	Loads	Shunt Compensators	Slack Node
9	9	0	3	3	0	nod_1

Table VI.7. Generators.

Node	Cost Coefficients			Active Power Limits		Reactive Power Limits	
	a ($/hr)	b ($/MWhr)	c ($/MW^{2}hr)	Min (MW)	Max (MW)	Min (MVAR)	Max (MVAR)
nod_1	150	5.00	0.1100	10.00	250.0	-300	300
nod_2	600	1.20	0.0850	10.00	300.0	-300	300
nod_3	335	1.00	0.1225	10.00	270.0	-300	300

Table VI.8. Transmission Lines.

Sending Node	Receiving Node	R (pu)	X_L (pu)	B_{TOTAL} (pu)
nod_1	nod_4	0.0000	0.0576	0.0000
nod_4	nod_5	0.0170	0.0920	0.1580
nod_5	nod_6	0.0390	0.1700	0.3580
nod_3	nod_6	0.0000	0.0586	0.0000
nod_6	nod_7	0.0119	0.1008	0.2090
nod_7	nod_8	0.0085	0.0720	0.1490
nod_8	nod_2	0.0000	0.0625	0.0000
nod_8	nod_9	0.0320	0.1610	0.3060
nod_9	nod_4	0.0100	0.0850	0.1760

Table VI.9. Loads.

Node	P_{LOAD} (MW)	Q_{LOAD} (MVAR)
nod_5	90	30
nod_7	100	35
nod_9	125	50

Table VI.10. Limits of Voltage.

Type of Node	Voltage Limits (pu) Min	Max
Slack node	0.9	1.1
Generator node	0.9	1.1
Load node	0.9	1.1

VI.3 11-node System

Table VI.11. Number of nodes and plant components.

Nodes	Transmission Lines	Transformers	Generators	Loads	Shunt Compensators	Slack Node
11	17	0	5	6	0	nod_1

Table VI.12. Transmission Lines.

Sending Node	Receiving Node	R (pu)	X_L (pu)	B_{TOTAL} (pu)
nod_1	nod_9	0.15	0.50	0.030
nod_1	nod_11	0.05	0.16	0.010
nod_2	nod_3	0.15	0.50	0.030
nod_2	nod_7	0.10	0.28	0.020
nod_2	nod_10	0.05	0.16	0.010
nod_3	nod_4	0.08	0.24	0.015
nod_4	nod_6	0.10	0.28	0.020
nod_4	nod_8	0.10	0.28	0.020
nod_4	nod_9	0.15	0.50	0.030
nod_5	nod_6	0.12	0.36	0.025
nod_5	nod_9	0.05	0.16	0.010
nod_7	nod_8	0.05	0.16	0.010
nod_7	nod_10	0.08	0.24	0.015
nod_8	nod_9	0.12	0.36	0.025
nod_8	nod_10	0.08	0.24	0.015
nod_8	nod_11	0.10	0.28	0.020
nod_10	nod_11	0.12	0.36	0.025

Table VI.13. Loads.

Node	P_{LOAD} (MW)	Q_{LOAD} (MVAR)
nod_6	10	2
nod_7	40	10
nod_8	90	45
nod_9	70	35
nod_10	25	5
nod_11	25	5

Table VI.14. Limits of Voltage.

Type of Node	Voltage Limits (pu) Min	Max
Slack node	1.0	1.1
Generator node	1.0	1.1
Load node	0.9	1.05

Table VI.15. Generators.

Node	Cost Coefficients a ($/hr)	b ($/MWhr)	c ($/MW^{2}hr)	Active Power Limits Min (MW)	Max (MW)	Reactive Power Limits Min (MVAR)	Max (MVAR)
nod_1	40.00	3.60	0.0050	30	120	0.00	60.0
nod_2	60.00	3.40	0.0040	30	120	0.00	60.0
nod_3	60.00	3.40	0.0040	30	120	0.00	60.0
nod_4	50.00	3.50	0.0045	30	120	0.00	60.0
nod_5	40.00	3.50	0.0045	30	120	0.00	60.0

VI.4 AEP 14-node System

Table VI.16. Number of nodes and plant components.

Nodes	Transmission Lines	Transformers	Generators	Loads	Shunt Compensators	Slack Node
14	15	5	5	11	1	nod_1

Table VI.17. Transformers.

Sending Node	Receiving Node	X_S (pu)	T_V	U_V
nod_4	nod_7	0.20912	0.978	1.0
nod_4	nod_9	0.55618	0.969	1.0
nod_5	nod_6	0.25202	0.932	1.0
nod_7	nod_8	0.17615	1.0	1.0
nod_7	nod_9	0.11001	1.0	1.0

Table VI.18. Limits of Voltage.

Type of Node	Voltage Limits (pu) Min	Max
Slack node	0.94	1.15
Generator node	0.94	1.15
Load node	0.94	1.06

Table VI.19. Transmission lines.

Sending Node	Receiving Node	R (pu)	X_L (pu)	B_{TOTAL} (pu)
nod_1	nod_2	0.01938	0.05917	0.0528
nod_1	nod_5	0.05403	0.22304	0.0492
nod_2	nod_3	0.04699	0.19797	0.0438
nod_2	nod_4	0.05811	0.17632	0.0374
nod_2	nod_5	0.05695	0.17388	0.0340
nod_3	nod_4	0.06701	0.17103	0.0346
nod_4	nod_5	0.01335	0.04211	0.0128
nod_6	nod_11	0.09498	0.19890	0.0000
nod_6	nod_12	0.12291	0.25581	0.0000
nod_6	nod_13	0.06615	0.13027	0.0000
nod_9	nod_10	0.03181	0.08450	0.0000
nod_9	nod_14	0.12711	0.27038	0.0000
nod_10	nod_11	0.08205	0.19207	0.0000
nod_12	nod_13	0.22092	0.19988	0.0000
nod_13	nod_14	0.17093	0.34802	0.0000

Table VI.20. Shunt Compensators.

Node	G (pu)	B (pu)
nod_9	0.0	0.19

Table VI.21. Loads.

Node	P_{LOAD} (MW)	Q_{LOAD} (MVAR)
nod_2	21.7	12.7
nod_3	94.2	19.0
nod_4	47.8	-3.9
nod_5	7.6	1.6
nod_6	11.2	7.5
nod_9	29.5	16.6
nod_10	9.0	5.8
nod_11	3.5	1.8
nod_12	6.1	1.6
nod_13	13.5	5.8
nod_14	14.9	5.0

Table VI.22. Generators.

Node	Cost Coefficients			Active Power Limits		Reactive Power Limits	
	a ($/hr)	b ($/MWhr)	c ($/MW^{2}hr)	Min (MW)	Max (MW)	Min (MVAR)	Max (MVAR)
nod_1	0.20	0.30	0.010	10	80	-60	80
nod_2	0.20	0.30	0.010	10	80	-40	60
nod_3	0.20	0.30	0.010	10	60	-20	40
nod_6	0.20	0.30	0.010	10	60	-20	40
nod_8	0.20	0.30	0.010	10	60	-20	40

VI.5 AEP 30-node System

Table VI.23. Number of nodes and plant components.

Nodes	Transmission Lines	Transformers	Generators	Loads	Shunt Compensators	Slack Node
30	34	7	6	21	2	nod_1

Table VI.24. Transformers.

Sending Node	Receiving Node	X_S (pu)	T_V	U_V
nod_6	nod_9	0.2080	0.978	1.0
nod_6	nod_10	0.5560	0.969	1.0
nod_9	nod_11	0.2080	1.0	1.0
nod_9	nod_10	0.1100	1.0	1.0
nod_4	nod_12	0.2560	0.932	1.0
nod_12	nod_13	0.1400	1.0	1.0
nod_28	nod_27	0.3960	0.968	1.0

Table VI.25. Limits of Voltage.

Type of Node	Voltage Limits (pu)	
	Min	Max
Slack node	0.95	1.10
Generator node	0.95	1.10
Load node	0.95	1.05

Table VI.26. Generators.

Node	Cost Coefficients			Active Power Limits		Reactive Power Limits	
	a ($/hr)	b ($/MWhr)	c ($/MW^{2}hr)	Min (MW)	Max (MW)	Min (MVAR)	Max (MVAR)
nod_1	0.00	2.00	0.0200	0	80.0	-60.00	80.0
nod_2	0.00	1.75	0.0175	0	80.0	-40.00	50.0
nod_5	0.00	1.00	0.0625	0	50.0	-20.00	40.0
nod_8	0.00	3.25	0.0083	0	55.0	-20.00	40.0
nod_11	0.00	3.00	0.0250	0	30.0	-20.00	40.0
nod_13	0.00	3.00	0.0250	0	40.0	-20.00	40.0

Table VI.27. Transmission Lines.

Sending Node	Receiving Node	R (pu)	X_L (pu)	B_{TOTAL} (pu)
nod_1	nod_2	0.0192	0.0575	0.0528
nod_1	nod_3	0.0452	0.1852	0.0408
nod_2	nod_4	0.0570	0.1737	0.0368
nod_3	nod_4	0.0132	0.0379	0.0084
nod_2	nod_5	0.0472	0.1983	0.0418
nod_2	nod_6	0.0581	0.1763	0.0374
nod_4	nod_6	0.0119	0.0414	0.0090
nod_5	nod_7	0.0460	0.1160	0.0204
nod_6	nod_7	0.0267	0.0820	0.0170
nod_6	nod_8	0.0120	0.0420	0.0090
nod_12	nod_14	0.1231	0.2559	0.0
nod_12	nod_15	0.0662	0.1304	0.0
nod_12	nod_16	0.0945	0.1987	0.0
nod_14	nod_15	0.2210	0.1997	0.0
nod_16	nod_17	0.0824	0.1923	0.0
nod_15	nod_18	0.1073	0.2185	0.0
nod_18	nod_19	0.0639	0.1292	0.0
nod_19	nod_20	0.0340	0.0680	0.0
nod_10	nod_20	0.0936	0.2090	0.0
nod_10	nod_17	0.0324	0.0845	0.0
nod_10	nod_21	0.0348	0.0749	0.0
nod_10	nod_22	0.0727	0.1499	0.0
nod_21	nod_22	0.0116	0.0236	0.0
nod_15	nod_23	0.1000	0.2020	0.0
nod_22	nod_24	0.1150	0.1790	0.0
nod_23	nod_24	0.1320	0.2700	0.0
nod_24	nod_25	0.1885	0.3292	0.0
nod_25	nod_26	0.2544	0.3800	0.0
nod_25	nod_27	0.1093	0.2087	0.0
nod_27	nod_29	0.2198	0.4153	0.0
nod_27	nod_30	0.3202	0.6027	0.0
nod_29	nod_30	0.2399	0.4533	0.0
nod_8	nod_28	0.0636	0.2000	0.0428
nod_6	nod_28	0.0169	0.0599	0.013

Table VI.28. Loads.

Node	P_{LOAD} (MW)	Q_{LOAD} (MVAR)
nod_2	21.7	12.7
nod_3	2.4	1.2
nod_4	7.6	1.6
nod_5	94.2	19.0
nod_7	22.8	10.9
nod_8	30	30
nod_10	5.8	2.0
nod_12	11.2	7.5
nod_14	6.2	1.6
nod_15	8.2	2.5
nod_16	3.5	1.8
nod_17	9.0	5.8
nod_18	3.2	0.9
nod_19	9.5	3.4
nod_20	2.2	0.7
nod_21	17.5	11.2
nod_22	0.0	0.0
nod_23	3.2	1.6
nod_24	8.7	6.7
nod_26	3.5	2.3
nod_29	2.4	0.9
nod_30	10.6	1.9

Table VI.29. Shunt Compensators.

Node	G (pu)	B (pu)
nod_10	0.0	0.19
nod_24	0.0	0.043

VI.6 AEP 57-node System

Table VI.30. Number of nodes and plant components.

Nodes	Transmission Lines	Transformers	Generators	Loads	Shunt Compensators	Slack Node
57	63	17	7	42	3	nod_1

Table VI.31. Generators.

Node	Cost Coefficients			Active Power Limits		Reactive Power Limits	
	a ($/hr)	b ($/MWhr)	c ($/MW^{2}hr)	Min (MW)	Max (MW)	Min (MVAR)	Max (MVAR)
nod_1	0.20	0.30	0.010	0	575	-200	300
nod_2	0.20	0.30	0.010	0	100	-17	50
nod_3	0.20	0.30	0.010	0	140	-10	60
nod_6	0.20	0.30	0.010	0	100	-8	25
nod_8	0.20	0.30	0.010	0	550	-140	200
nod_9	0.20	0.30	0.010	0	100	-3	9
nod_12	0.20	0.30	0.010	0	410	-150	155

Tables VI.32. Transformers.

Sending Node	Receiving Node	X_S (pu)	T_V	U_V
nod_4	nod_18	0.5550	0.970	1.0
nod_4	nod_18	0.4300	0.978	1.0
nod_21	nod_20	0.7767	1.043	1.0
nod_24	nod_25	1.1820	1.000	1.0
nod_24	nod_25	1.2300	1.000	1.0
nod_24	nod_26	0.0473	1.043	1.0
nod_7	nod_29	0.0648	0.967	1.0
nod_34	nod_32	0.9530	0.975	1.0
nod_11	nod_41	0.7490	0.955	1.0

Sending Node	Receiving Node	X_S (pu)	T_V	U_V
nod_15	nod_45	0.1042	0.955	1.0
nod_14	nod_46	0.0735	0.900	1.0
nod_10	nod_51	0.0712	0.930	1.0
nod_13	nod_49	0.1910	0.895	1.0
nod_11	nod_43	0.1530	0.958	1.0
nod_40	nod_56	1.0000	0.958	1.0
nod_39	nod_57	1.3550	0.980	1.0
nod_9	nod_55	0.1205	0.940	1.0

Table VI.33. Transmission Lines.

Sending Node	Receiving Node	R (pu)	X_L (pu)	B_{TOTAL} (pu)
nod_1	nod_2	0.0083	0.0280	0.1290
nod_2	nod_3	0.0298	0.0850	0.0818
nod_3	nod_4	0.0112	0.0366	0.0380
nod_4	nod_5	0.0625	0.1320	0.0258
nod_4	nod_6	0.0430	0.1480	0.0348
nod_6	nod_7	0.0200	0.1020	0.0276
nod_6	nod_8	0.0339	0.1730	0.0470
nod_8	nod_9	0.0099	0.0505	0.0548
nod_9	nod_10	0.0369	0.1679	0.0440
nod_9	nod_11	0.0258	0.0848	0.0218
nod_9	nod_12	0.0648	0.2950	0.0772
nod_9	nod_13	0.0481	0.1580	0.0406
nod_13	nod_14	0.0132	0.0434	0.0110
nod_13	nod_15	0.0269	0.0869	0.0230
nod_1	nod_15	0.0178	0.0910	0.0988
nod_1	nod_16	0.0454	0.2060	0.0546
nod_1	nod_17	0.0238	0.1080	0.0286
nod_3	nod_15	0.0162	0.0530	0.0544
nod_5	nod_6	0.0302	0.0641	0.0124
nod_7	nod_8	0.0139	0.0712	0.0194
nod_10	nod_12	0.0277	0.1262	0.0328
nod_11	nod_13	0.0223	0.0732	0.0196
nod_12	nod_13	0.0178	0.0580	0.0604
nod_12	nod_16	0.0180	0.0813	0.0216
nod_12	nod_17	0.0397	0.1790	0.0476
nod_14	nod_15	0.0171	0.0547	0.0148
nod_18	nod_19	0.4610	0.6850	0.0000
nod_19	nod_20	0.2830	0.4340	0.0000
nod_21	nod_22	0.0736	0.1170	0.0000
nod_22	nod_23	0.0099	0.0152	0.0000
nod_23	nod_24	0.1660	0.2560	0.0084
nod_26	nod_27	0.1650	0.2540	0.0000
nod_27	nod_28	0.0618	0.0954	0.0000
nod_28	nod_29	0.0418	0.0587	0.0000
nod_25	nod_30	0.1350	0.2020	0.0000
nod_30	nod_31	0.3260	0.4970	0.0000
nod_31	nod_32	0.5070	0.7550	0.0000
nod_32	nod_33	0.0392	0.0360	0.0000
nod_34	nod_35	0.0520	0.0780	0.0032
nod_35	nod_36	0.0430	0.0537	0.0016
nod_36	nod_37	0.0290	0.0366	0.0000
nod_37	nod_38	0.0651	0.1009	0.0020
nod_37	nod_39	0.0239	0.0379	0.0000
nod_36	nod_40	0.0300	0.0466	0.0000
nod_22	nod_38	0.0192	0.0295	0.0000
nod_41	nod_42	0.2070	0.3520	0.0000
nod_41	nod_43	0.0000	0.4120	0.0000
nod_38	nod_44	0.0289	0.0585	0.0020
nod_46	nod_47	0.0230	0.0680	0.0032
nod_47	nod_48	0.0182	0.0233	0.0000
nod_48	nod_49	0.0834	0.1290	0.0048
nod_49	nod_50	0.0801	0.1280	0.0000
nod_50	nod_51	0.1386	0.2200	0.0000
nod_29	nod_52	0.1442	0.1870	0.0000
nod_52	nod_53	0.0762	0.0984	0.0000
nod_53	nod_54	0.1878	0.2320	0.0000
nod_54	nod_55	0.1732	0.2265	0.0000
nod_44	nod_45	0.0624	0.1242	0.0040
nod_56	nod_41	0.5530	0.5490	0.0000
nod_56	nod_42	0.2125	0.3540	0.0000
nod_57	nod_56	0.1740	0.2600	0.0000
nod_38	nod_49	0.1150	0.1770	0.0060
nod_38	nod_48	0.0312	0.0482	0.0000

Table VI.34. Loads.

Node	P_{LOAD} (MW)	Q_{LOAD} (MVAR)
nod_1	55.0	17.0
nod_2	3.0	88.0
nod_3	41.0	21.0
nod_5	13.0	4.0
nod_6	75.0	2.0
nod_8	150.	22.0
nod_9	121.	26.0
nod_10	5.0	2.0
nod_12	377.	24.0
nod_13	18.0	2.3
nod_14	10.5	5.3
nod_15	22.0	5.0
nod_16	43.0	3.0
nod_17	42.0	8.0
nod_18	27.2	9.8
nod_19	3.3	0.6
nod_20	2.3	1.0
nod_23	6.3	2.1
nod_25	6.3	3.2
nod_27	9.3	0.5
nod_28	4.6	2.3
nod_29	17.0	2.6
nod_30	3.6	1.8
nod_31	5.8	2.9
nod_32	1.6	0.8
nod_33	3.8	1.9
nod_35	6.0	3.0
nod_38	14.0	7.0
nod_41	6.3	3.0
nod_42	7.1	4.4
nod_43	2.0	1.0
nod_44	12.0	1.8
nod_47	29.7	11.6
nod_49	18.0	8.5
nod_50	21.0	10.5
nod_51	18.0	5.3
nod_52	4.9	2.2
nod_53	20.0	10.0
nod_54	4.1	1.4
nod_55	6.8	3.4
nod_56	7.6	2.2
nod_57	6.7	2.0

Table VI.35. Shunt Compensators.

Node	G (pu)	B (pu)
nod_18	0.0	0.100
nod_25	0.0	0.059
nod_53	0.0	0.063

Table VI.36. Limits of Voltage.

Type of Node	Voltage Limits (pu)	
	Min	Max
Slack node	0.94	1.06
Generator node	0.94	1.06
Load node	0.94	1.06

VI.7 AEP 118-node System

Table VI.37. Number of nodes and plant components.

Nodes	Transmission Lines	Transformers	Generators	Loads	Shunt Compensators	Slack Node
118	177	9	54	118	14	nod_69

Table VI.38. Transmission Lines.

Nodes		R (pu)	X_L (pu)	B_{TOTAL} (pu)
nod_1	nod_2	0.0303	0.0999	0.0254
nod_1	nod_3	0.0129	0.0424	0.01082
nod_4	nod_5	0.00176	0.00798	0.0021
nod_3	nod_5	0.0241	0.108	0.0284
nod_5	nod_6	0.0119	0.054	0.01426
nod_6	nod_7	0.00459	0.0208	0.0055
nod_8	nod_9	0.00244	0.0305	1.162
nod_9	nod_10	0.00258	0.0322	1.23
nod_4	nod_11	0.0209	0.0688	0.01748
nod_5	nod_11	0.0203	0.0682	0.01738
nod_11	nod_12	0.00595	0.0196	0.00502
nod_2	nod_12	0.0187	0.0616	0.01572
nod_3	nod_12	0.0484	0.16	0.0406
nod_7	nod_12	0.00862	0.034	0.00874
nod_11	nod_13	0.02225	0.0731	0.01876
nod_12	nod_14	0.0215	0.0707	0.01816
nod_13	nod_15	0.0744	0.2444	0.06268
nod_14	nod_15	0.0595	0.195	0.0502
nod_12	nod_16	0.0212	0.0834	0.0214
nod_15	nod_17	0.0132	0.0437	0.0444
nod_16	nod_17	0.0454	0.1801	0.0466
nod_17	nod_18	0.0123	0.0505	0.01298
nod_18	nod_19	0.01119	0.0493	0.01142
nod_19	nod_20	0.0252	0.117	0.0298
nod_15	nod_19	0.012	0.0394	0.0101
nod_20	nod_21	0.0183	0.0849	0.0216
nod_21	nod_22	0.0209	0.097	0.0246
nod_22	nod_23	0.0342	0.159	0.0404
nod_23	nod_24	0.0135	0.0492	0.0498
nod_23	nod_25	0.0156	0.08	0.0864
nod_25	nod_27	0.0318	0.163	0.1764
nod_27	nod_28	0.01913	0.0855	0.0216
nod_28	nod_29	0.0237	0.0943	0.0238
nod_8	nod_30	0.00431	0.0504	0.514
nod_26	nod_30	0.00799	0.086	0.908
nod_17	nod_31	0.0474	0.1563	0.0399
nod_29	nod_31	0.0108	0.0331	0.0083
nod_23	nod_32	0.0317	0.1153	0.1173
nod_31	nod_32	0.0298	0.0985	0.0251
nod_27	nod_32	0.0229	0.0755	0.01926
nod_15	nod_33	0.038	0.1244	0.03194
nod_19	nod_34	0.0752	0.247	0.0632
nod_35	nod_36	0.00224	0.0102	0.00268
nod_35	nod_37	0.011	0.0497	0.01318
nod_33	nod_37	0.0415	0.142	0.0366
nod_34	nod_36	0.00871	0.0268	0.00568
nod_34	nod_37	0.00256	0.0094	0.00984
nod_37	nod_39	0.0321	0.106	0.027
nod_37	nod_40	0.0593	0.168	0.042
nod_30	nod_38	0.00464	0.054	0.422
nod_39	nod_40	0.0184	0.0605	0.01552
nod_40	nod_41	0.0145	0.0487	0.01222
nod_40	nod_42	0.0555	0.183	0.0466
nod_41	nod_42	0.041	0.135	0.0344
nod_43	nod_44	0.0608	0.2454	0.06068
nod_34	nod_43	0.0413	0.1681	0.04226
nod_44	nod_45	0.0224	0.0901	0.0224
nod_45	nod_46	0.04	0.1356	0.0332
nod_46	nod_47	0.038	0.127	0.0316

Nodes		R (pu)	X_L (pu)	B_{TOTAL} (pu)
nod_46	nod_48	0.0601	0.189	0.0472
nod_47	nod_49	0.0191	0.0625	0.01604
nod_42	nod_49	0.0715	0.323	0.086
nod_42	nod_49	0.0715	0.323	0.086
nod_45	nod_49	0.0684	0.186	0.0444
nod_48	nod_49	0.0179	0.0505	0.01258
nod_49	nod_50	0.0267	0.0752	0.01874
nod_49	nod_51	0.0486	0.137	0.0342
nod_51	nod_52	0.0203	0.0588	0.01396
nod_52	nod_53	0.0405	0.1635	0.04058
nod_53	nod_54	0.0263	0.122	0.031
nod_49	nod_54	0.073	0.289	0.0738
nod_49	nod_54	0.0869	0.291	0.073
nod_54	nod_55	0.0169	0.0707	0.0202
nod_54	nod_56	0.00275	0.00955	0.00732
nod_55	nod_56	0.00488	0.0151	0.00374
nod_56	nod_57	0.0343	0.0966	0.0242
nod_50	nod_57	0.0474	0.134	0.0332
nod_56	nod_58	0.0343	0.0966	0.0242
nod_51	nod_58	0.0255	0.0719	0.01788
nod_54	nod_59	0.0503	0.2293	0.0598
nod_56	nod_59	0.0825	0.251	0.0569
nod_56	nod_59	0.0803	0.239	0.0536
nod_55	nod_59	0.04739	0.2158	0.05646
nod_59	nod_60	0.0317	0.145	0.0376
nod_59	nod_61	0.0328	0.15	0.0388
nod_60	nod_61	0.00264	0.0135	0.01456
nod_60	nod_62	0.0123	0.0561	0.01468
nod_61	nod_62	0.00824	0.0376	0.0098
nod_63	nod_64	0.00172	0.02	0.216
nod_38	nod_65	0.00901	0.0986	1.046
nod_64	nod_65	0.00269	0.0302	0.38
nod_49	nod_66	0.018	0.0919	0.0248
nod_49	nod_66	0.018	0.0919	0.0248
nod_62	nod_66	0.0482	0.218	0.0578
nod_62	nod_67	0.0258	0.117	0.031
nod_66	nod_67	0.0224	0.1015	0.02682
nod_65	nod_68	0.00138	0.016	0.638
nod_47	nod_69	0.0844	0.2778	0.07092
nod_49	nod_69	0.0985	0.324	0.0828
nod_69	nod_70	0.03	0.127	0.122
nod_24	nod_70	0.00221	0.4115	0.10198
nod_70	nod_71	0.00882	0.0355	0.00878
nod_24	nod_72	0.0488	0.196	0.0488
nod_71	nod_72	0.0446	0.18	0.04444
nod_71	nod_73	0.00866	0.0454	0.01178
nod_70	nod_74	0.0401	0.1323	0.03368
nod_70	nod_75	0.0428	0.141	0.036
nod_69	nod_75	0.0405	0.122	0.124
nod_74	nod_75	0.0123	0.0406	0.01034
nod_76	nod_77	0.0444	0.148	0.0368
nod_69	nod_77	0.0309	0.101	0.1038
nod_75	nod_77	0.0601	0.1999	0.04978
nod_77	nod_78	0.00376	0.0124	0.01264
nod_78	nod_79	0.00546	0.0244	0.00648
nod_77	nod_80	0.017	0.0485	0.0472
nod_77	nod_80	0.0294	0.105	0.0228
nod_79	nod_80	0.0156	0.0704	0.0187
nod_68	nod_81	0.00175	0.0202	0.808

Table VI.39. Transmission lines.

Nodes		R (pu)	X_L (pu)	B_{TOTAL} (pu)
nod_77	nod_82	0.0298	0.0853	0.08174
nod_82	nod_83	0.0112	0.03665	0.03796
nod_83	nod_84	0.0625	0.132	0.0258
nod_83	nod_85	0.043	0.148	0.0348
nod_84	nod_85	0.0302	0.0641	0.01234
nod_85	nod_86	0.035	0.123	0.0276
nod_86	nod_87	0.02828	0.2074	0.0445
nod_85	nod_88	0.02	0.102	0.0276
nod_85	nod_89	0.0239	0.173	0.047
nod_88	nod_89	0.0139	0.0712	0.01934
nod_89	nod_90	0.0518	0.188	0.0528
nod_89	nod_90	0.0238	0.0997	0.106
nod_90	nod_91	0.0254	0.0836	0.0214
nod_89	nod_92	0.0099	0.0505	0.0548
nod_89	nod_92	0.0393	0.1581	0.0414
nod_91	nod_92	0.0387	0.1272	0.03268
nod_92	nod_93	0.0258	0.0848	0.0218
nod_92	nod_94	0.0481	0.158	0.0406
nod_93	nod_94	0.0223	0.0732	0.01876
nod_94	nod_95	0.0132	0.0434	0.0111
nod_80	nod_96	0.0356	0.182	0.0494
nod_82	nod_96	0.0162	0.053	0.0544
nod_94	nod_96	0.0269	0.0869	0.023
nod_80	nod_97	0.0183	0.0934	0.0254
nod_80	nod_98	0.0238	0.108	0.0286
nod_80	nod_99	0.0454	0.206	0.0546
nod_92	nod_100	0.0648	0.295	0.0472
nod_94	nod_100	0.0178	0.058	0.0604
nod_95	nod_96	0.0171	0.0547	0.01474
nod_96	nod_97	0.0173	0.0885	0.024
nod_98	nod_100	0.0397	0.179	0.0476
nod_99	nod_100	0.018	0.0813	0.0216
nod_100	nod_101	0.0277	0.1262	0.0328
nod_92	nod_102	0.0123	0.0559	0.01464
nod_101	nod_102	0.0246	0.112	0.0294
nod_100	nod_103	0.016	0.0525	0.0536
nod_100	nod_104	0.0451	0.204	0.0541
nod_103	nod_104	0.0466	0.1584	0.0407
nod_103	nod_105	0.0535	0.1625	0.0408
nod_100	nod_106	0.0605	0.229	0.062
nod_104	nod_105	0.00994	0.0378	0.00986
nod_105	nod_106	0.014	0.0547	0.01434
nod_105	nod_107	0.053	0.183	0.0472
nod_105	nod_108	0.0261	0.0703	0.01844
nod_106	nod_107	0.053	0.183	0.0472
nod_108	nod_109	0.0105	0.0288	0.0076
nod_103	nod_110	0.03906	0.1813	0.0461
nod_109	nod_110	0.0278	0.0762	0.0202
nod_110	nod_111	0.022	0.0755	0.02
nod_110	nod_112	0.0247	0.064	0.062
nod_17	nod_113	0.00913	0.0301	0.00768
nod_32	nod_113	0.0615	0.203	0.0518
nod_32	nod_114	0.0135	0.0612	0.01628
nod_27	nod_115	0.0164	0.0741	0.01972
nod_114	nod_115	0.0023	0.0104	0.00276
nod_68	nod_116	0.00034	0.00405	0.164
nod_12	nod_117	0.0329	0.14	0.0358
nod_75	nod_118	0.0145	0.0481	0.01198
nod_76	nod_118	0.0164	0.0544	0.01356

Table VI.40. Transformers.

Sending Node	Receiving Node	X_S (pu)	T_V	U_V
nod_8	nod_5	0.0267	0.985	1
nod_26	nod_25	0.0382	0.96	1
nod_30	nod_17	0.0388	0.96	1
nod_38	nod_37	0.0375	0.935	1
nod_63	nod_59	0.0386	0.96	1
nod_64	nod_61	0.0268	0.985	1
nod_65	nod_66	0.037	0.935	1
nod_68	nod_69	0.037	0.935	1
nod_81	nod_80	0.037	0.935	1

Table VI.41. Shunt compensators.

Node	G (pu)	B (pu)
nod_5	0	-0.4
nod_34	0	0.14
nod_37	0	-0.25
nod_44	0	0.1
nod_45	0	0.1
nod_46	0	0.1
nod_48	0	0.15
nod_74	0	0.12
nod_79	0	0.2
nod_82	0	0.2
nod_83	0	0.1
nod_105	0	0.2
nod_107	0	0.06
nod_110	0	0.06

Table VI.42. Limits of Voltage.

Type of Node	Voltage Limits (pu)	
	Min	Max
Slack node	0.94	1.2
Generator node	0.94	1.1
Load node	0.94	1.06

Tables VI.43. Loads.

Node	P_{LOAD} (MW)	Q_{LOAD} (MVAR)
nod_1	51	27
nod_2	20	9
nod_3	39	10
nod_4	30	12
nod_5	0	0
nod_6	52	22
nod_7	19	2
nod_8	0	0
nod_9	0	0
nod_10	0	0
nod_11	70	23
nod_12	47	10
nod_13	34	16
nod_14	14	1
nod_15	90	30
nod_16	25	10
nod_17	11	3
nod_18	60	34
nod_19	45	25
nod_20	18	3
nod_21	14	8
nod_22	10	5
nod_23	7	3
nod_24	0	0
nod_25	0	0
nod_26	0	0
nod_27	62	13
nod_28	17	7
nod_29	24	4
nod_30	0	0
nod_31	43	27
nod_32	59	23
nod_33	23	9
nod_34	59	26
nod_35	33	9
nod_36	31	17
nod_37	0	0
nod_38	0	0
nod_39	27	11
nod_40	20	23
nod_41	37	10
nod_42	37	23
nod_43	18	7
nod_44	16	8
nod_45	53	22
nod_46	28	10
nod_47	34	0
nod_48	20	11
nod_49	87	30
nod_50	17	4
nod_51	17	8
nod_52	18	5
nod_53	23	11
nod_54	113	32
nod_55	63	22
nod_56	84	18
nod_57	12	3
nod_58	12	3
nod_59	277	113

Node	P_{LOAD} (MW)	Q_{LOAD} (MVAR)
nod_60	78	3
nod_61	0	0
nod_62	77	14
nod_63	0	0
nod_64	0	0
nod_65	0	0
nod_66	39	18
nod_67	28	7
nod_68	0	0
nod_69	0	0
nod_70	66	20
nod_71	0	0
nod_72	0	0
nod_73	0	0
nod_74	68	27
nod_75	47	11
nod_76	68	36
nod_77	61	28
nod_78	71	26
nod_79	39	32
nod_80	130	26
nod_81	0	0
nod_82	54	27
nod_83	20	10
nod_84	11	7
nod_85	24	15
nod_86	21	10
nod_87	0	0
nod_88	48	10
nod_89	0	0
nod_90	78	42
nod_91	0	0
nod_92	65	10
nod_93	12	7
nod_94	30	16
nod_95	42	31
nod_96	38	15
nod_97	15	9
nod_98	34	8
nod_99	0	0
nod_100	37	18
nod_101	22	15
nod_102	5	3
nod_103	23	16
nod_104	38	25
nod_105	31	26
nod_106	43	16
nod_107	28	12
nod_108	2	1
nod_109	8	3
nod_110	39	30
nod_111	0	0
nod_112	25	13
nod_113	0	0
nod_114	8	3
nod_115	22	7
nod_116	0	0
nod_117	20	8
nod_118	33	15

Table VI.44. Generators.

Node	Cost Coefficients			Active Power Limits		Reactive Power Limits	
	a ($/hr)	*b* ($/MWhr)	*c* ($/MW^{2}hr)	Min (MW)	Max (MW)	Min (MVAR)	Max (MVAR)
nod_1	0.20	0.30	0.010	0	100	-5	15
nod_4	0.20	0.30	0.010	0	100	-300	300
nod_6	0.20	0.30	0.010	0	100	-13	50
nod_8	0.20	0.30	0.010	0	100	-300	300
nod_10	0.20	0.30	0.010	0	550	-147	200
nod_12	0.20	0.30	0.010	0	185	-35	120
nod_15	0.20	0.30	0.010	0	100	-10	30
nod_18	0.20	0.30	0.010	0	100	-16	50
nod_19	0.20	0.30	0.010	0	100	-8	24
nod_24	0.20	0.30	0.010	0	100	-300	300
nod_25	0.20	0.30	0.010	0	320	-47	140
nod_26	0.20	0.30	0.010	0	414	-1000	1000
nod_27	0.20	0.30	0.010	0	100	-300	300
nod_31	0.20	0.30	0.010	0	107	-300	300
nod_32	0.20	0.30	0.010	0	100	-14	42
nod_34	0.20	0.30	0.010	0	100	-80	240
nod_36	0.20	0.30	0.010	0	100	-80	240
nod_40	0.20	0.30	0.010	0	100	-300	300
nod_42	0.20	0.30	0.010	0	100	-300	300
nod_46	0.20	0.30	0.010	0	119	-100	100
nod_49	0.20	0.30	0.010	0	304	-85	210
nod_54	0.20	0.30	0.010	0	148	-300	300
nod_55	0.20	0.30	0.010	0	100	-8	23
nod_56	0.20	0.30	0.010	0	100	-8	15
nod_59	0.20	0.30	0.010	0	255	-60	180
nod_61	0.20	0.30	0.010	0	260	-100	300
nod_62	0.20	0.30	0.010	0	100	-20	20
nod_65	0.20	0.30	0.010	0	491	-67	200
nod_66	0.20	0.30	0.010	0	492	-67	200
nod_69	0.20	0.30	0.010	0	700	-1500	1500
nod_70	0.20	0.30	0.010	0	100	-10	32
nod_72	0.20	0.30	0.010	0	100	-100	100
nod_73	0.20	0.30	0.010	0	100	-100	100
nod_74	0.20	0.30	0.010	0	100	-60	90
nod_76	0.20	0.30	0.010	0	100	-80	230
nod_77	0.20	0.30	0.010	0	100	-20	70
nod_80	0.20	0.30	0.010	0	577	-165	280
nod_85	0.20	0.30	0.010	0	100	-8	23
nod_87	0.20	0.30	0.010	0	104	-100	1000
nod_89	0.20	0.30	0.010	0	707	-210	300
nod_90	0.20	0.30	0.010	0	100	-300	300
nod_91	0.20	0.30	0.010	0	100	-100	100
nod_92	0.20	0.30	0.010	0	100	-30	90
nod_99	0.20	0.30	0.010	0	100	-100	100
nod_100	0.20	0.30	0.010	0	352	-50	155
nod_103	0.20	0.30	0.010	0	140	-15	40
nod_104	0.20	0.30	0.010	0	100	-8	23
nod_105	0.20	0.30	0.010	0	100	-8	23
nod_107	0.20	0.30	0.010	0	100	-200	200
nod_110	0.20	0.30	0.010	0	100	-8	23
nod_111	0.20	0.30	0.010	0	136	-100	1000
nod_112	0.20	0.30	0.010	0	100	-100	1000
nod_113	0.20	0.30	0.010	0	100	-100	200
nod_116	0.20	0.30	0.010	0	100	-1000	1000